OBSERVATOIRE DE PARIS

SYSTÈMES DE RÉFÉRENCE TEMPS-ESPACE

UMR8630 / CNRS

New challenges for reference systems and numerical standards in astronomy

Nouveaux défis pour les sytèmes de référence et les constantes astronomiques

JOURNÉES 2010 ☆

SYSTÈMES DE RÉFÉRENCE SPATIO - TEMPORELS

☆ PARIS, 20-22 SEPTEMBER

OBSERVATOIRE DE PARIS

SYSTÈMES DE RÉFÉRENCE TEMPS-ESPACE

UMR 8630 / CNRS

61 avenue de l'Observatoire, F-75014 Paris, FRANCE

New challenges for reference systems and numerical standards in astronomy

Nouveaux défis pour les sytèmes de référence et les constantes astronomiques

Edited by

Actes publiés par

N. CAPITAINE

JOURNÉES 2010 ☆

SYSTÈMES DE RÉFÉRENCE SPATIO - TEMPORELS

☆ PARIS, 20-22 SEPTEMBER

Participants in the Journées 2010 in the indoor garden of Ecole Normale Supérieure

ISBN 978-2-901057-64-2

TABLE OF CONTENTS

PREFACE

The Journées 2010 "Systèmes de référence spatio-temporels", with the sub-title "New challenges for reference systems and numerical standards in astronomy", were organized from 20 to 22 September 2010 at Paris Observatory and Ecole Normale Supérieure in Paris, France. These Journées and their proceedings have been sponsored by Paris Observatory scientific council, the CNRS Institut des Sciences de l'Univers, SYRTE Department and the Ministry of Education and Research (Programme ACCES). They were the twenties conference in this series whose main purpose is to provide a forum for researchers in the fields of Earth rotation, reference frames, astrometry and time. The Journées were organized in Paris each year from 1988 to 1992, and then, since 1994, alternately in Paris (in 1994, 1996, 1998, 2000, 2004 and 2007) and other European cities, namely Warsaw in 1995 and 2005, Prague in 1997, Dresden in 1999 and 2008, Brussels in 2001, Bucharest in 2002 and St. Petersburg in 2003. Such an organization has been the result of an active and continuing cooperation between the "Systèmes de Référence Temps Espace" (SYRTE) Department of Paris Observatory and other institutions in Europe.

The scientific programme of the Journées 2010 was focused on the issues related to the recent developments and new challenges in astronomical space and time reference systems and their relativistic aspects, astrometric catalogs, Earth orientation, astronomical constants and numerical standards, planetary ephemerides and modern astrometry. There have been presentations and discussions related to the IAU Division 1 commissions and IAU Working Group "Numerical Standards for Fundamental astronomy" (NSFA), whith a WG meeting organized in association with the Journées. There has been a special session for presenting the latest developments in the solar system ephemerides and comparing details in those ephemerides. This session was organized in coordination with IAU Commission 4 with and the participation - as invited speakers - of the providers of the solar system ephemerides that are expected to be of comparable accuracy (i.e. JPL, EPM and INPOP).

There were 111 participants, coming from 19 different countries. The scientific programme included 12 invited papers, 40 oral communications and 36 posters; it was composed of the five following sessions:
Session 1: The astronomical constants, SI units and future developments in numerical standards;
Session 2: Solar system ephemerides and their comparison;
Session 3: Progress in astrometric catalogs in optical and radio wavelengths;
Session 4: Recent developments in theory and observation of Earth rotation and related reference systems;
Session 5: Pulsars timing, relativity and time transfer.

In addition to these scientific activities, the participants met for a cocktail and a conference dinner in the Salle Cassini of Paris Observatory on Monday and Tuesday evening September 20 and 21, respectively. "Best poster prizes" were awarded by the SOC to two poster authors for the quality of the scientific content and presentation. A special exhibition from archives of Paris Observatory library took place on 21 September before the dinner with documents related to the topics of these Journées (e.g. the 1896 Paris international conference on fundamental stars, Le Verrier's manuscript on Neptune, Lalande's catalogue, Danjon's astrolabe, etc.).

These Proceedings are divided into five sections corresponding to the sessions of the meeting. The Table of Contents is given on pages iii to v, the list of participants on pages viii and ix, the scientific programme and list of posters on pages x to xiv. The Postface on page 284 gives the first announcement for the "Journées" 2011 that will be held in Vienna (Austria) from 19 to 21 September 2011.

We thank here all the participants in the Journées 2010. We are very grateful to the Scientific Organizing Committee for its active role in the elaboration of the scientific programme and to all the authors of the papers for their valuable contributions. On behalf of the SOC, we thank the Local Organizing Committee, and especially its Chair, Noël Dimarcq, for the very efficient preparation of the meeting and the very good local conditions and organization. We are also very grateful to O. Becker for his efficient technical help for the publication.

This Volume is dedicated to Anne-Marie Gontier (see page vii).

Nicole CAPITAINE
Chair of the SOC
20 June 2011

In Memoriam

Anne-Marie GONTIER

(1966-2010)

Anne-Marie Gontier, our colleague and friend at Department SYRTE of Paris Observatory, passed away on 24 September, aged only 44, less than two days after the end of the Journées in which she participated.

Anne-Marie was an astronomer at Paris Observatory since 1995 and was responsible for the IVS Analysis Center of Paris Observatory since the beginning of the International VLBI Service for Geodesy and Astrometry (IVS). Anne-Marie was the mother of two young children.

Anne-Marie played a major role in the activities of our Department SYRTE within Paris Observatory, especially on VLBI analysis and processing, the maintenance of the IAU celestial reference frame and the functioning of the IERS and IVS. She was an expert in the field of Earth rotation and on the modeling, analysis and processing of VLBI observations for astrometric and geodetic applications. She was particularly active and effective in the IAU working group that developed the extragalactic celestial reference system and frame which were adopted by the IAU in 1997, as the International Celestial Reference System (ICRS) and Frame (ICRF). She developed VLBI processing and analysis systems, regularly supervising the work of students and young visitors and being involved in various scientific collaborations with astronomers and geodesists. During the period 2006-2009, as a member of the IERS/IVS working group, she actively contributed to the second realization, ICRF2, of the International Celestial Reference Frame, which was adopted by the IAU in 2009. Anne-Marie also invested much time and effort in general interest tasks for our department SYRTE, for Paris Observatory, for the French national astronomy community and more generally for the IERS and IVS communities.

All her colleagues and friends appreciated Anne-Marie for her kindness, her dedication, generosity and dynamism. She had an exceptional sense of duty and always wanted to fulfill her commitments whatever the difficulties. She has been of precious help for the organization of the Journées "Systèmes de référence spatio-temporels" for a long time. She was of great help once again in 2010, being actively involved in the local organization of the "Journees 2010" and attending all the sessions of the fist two days of the meeting until Tuesday 21 September, despite her serious health problems.

We all have been shocked by the loss of our precious colleague and friend, we miss her very much and we share the grief of her family. We especially think with great sorrow of the terrible loss that her disappearance represents for her young children.

These Proceedings are dedicated to her memory.

Nicole CAPITAINE and Noel DIMARCQ
Chairs of the SOC and the LOC

List of Participants

ACHKAR Joseph, *Observatoire de Paris - SYRTE/CNRS*, France
ALESHKINA Ekaterina, *Central (Pulkovo) Astronomical Observatory Russian Acad. Sci.*, Russia
ALTAMIMI Zuheir, *Institut Géographique National /LAREG*, France
ANDREI Alexandre, *Observatorio Nacional/MCT* Brasil; INAF-Astronomical Observatory of Turin, Italy
BAEZA Federico, *Real Instituto y Observatorio de la Armada*, Spain
BAGHBAN Golshid, *Université Pierre et Marie Curie*, France
BARACHE Christophe, *Observatoire de Paris - SYRTE/CNRS*, France
BASHAKOVA Ekaterina, *St.Petersburg State University*, Russia
BERTONE Stefano, *Observatoire de Paris - SYRTE/CNRS*, France
BIZOUARD Christian, *Observatoire de Paris - SYRTE/CNRS*, France
BOEHM Sigrid, *Vienna University of Technology Institute of Geodesy and Geophysics*, Austria
BOLOIX Tortosa Jaime, *Real Instituto y Observatorio de la Armada*, Spain
BOUCHER Claude, *Observatoire de Paris - SYRTE/CNRS*, France
BOUQUILLON Sébastien, *Observatoire de Paris - SYRTE/CNRS*, France
BOURDA Géraldine, *Laboratoire d'Astrophysique de Bordeaux*, France
BRZEZINSKI Aleksander, *Faculty of Geodesy and Cartography Warsaw*, Poland
BUCCIARELLI Beatrice, *INAF - Astronomical Observatory of Turin*, Italy
BUDNIK Frank, *ESA/ESOC*, Germany
CAPITAINE Nicole, *Observatoire de Paris - SYRTE/CNRS*, France
CHAPANOV Yavor, *Central Laboratory for Geodesy - BAS*, Bulgaria
COGNARD Ismael, *CNRS LPC2E*, France
COTTEREAU Laure, *Observatoire de Paris - SYRTE/CNRS*, France
COULOT David, *Institut Géographique National /LAREG GRGS*, France
CRIFO Francoise, *Observatoire de Paris - GEPI*, France
DAMLJANOVIC Goran, *Astronomical Observatory*, Serbia
DÉBARBAT Suzanne, *Observatoire de Paris - SYRTE/CNRS*, France
DEHANT Veronique, *Royal Observatory of Belgium*, Belgium
DELEFLIE Florent, *Observatoire de Paris-IMCE/GRGS*, France
DENG Xue-mei, *Purple Mountain Observatory*, China
DIMARCQ Noël, *Observatoire de Paris - SYRTE/CNRS*, France
DUMIN Yurii, *IZMIRAN Russian Academy of Sciences*, Russia
ESCAPA Alberto, *Dep. Applied Mathematics University of Alicante*, Spain
FEY Alan, *U.S. Naval Observatory*, USA
FIENGA Agnes, *Observatoire de Besancon ; Observatoire de Paris-IMCE*, France
FOLKNER William, *Jet Propulsion Laboratory*, USA
FOMALONT Edward, *National Radio Astronomy Observatory*, USA
FRANCOU Gerard, *Observatoire de Paris - SYRTE/CNRS*, France
GAMBIS Daniel, *Observatoire de Paris - SYRTE/CNRS*, France
GASTINEAU Mickaël, *Observatoire de Paris - IMCCE*, France
GAUME Ralph, *U.S. Naval Observatory*, USA
GERLACH Enrico, *Lohrmann Observatory Dresden Technical University*, Germany
GIORGINI Jon, *Jet Propulsion Laboratory*, USA
GONTIER Anne-Marie, *Observatoire de Paris - SYRTE/CNRS*, France
GROSS Richard, *Jet Propulsion Laboratory*, USA
GUINOT Bernard, *Observatoire de Paris*, France
GUSEV Alexander, *Kazan University*, Russia
HEFTY Jan, *Slovak University of Technology*, Slovakia
HILTON James, *U.S. Naval Observatory*, USA
HOBBS George, *CSIRO Australia Telescope National Facility*, Australia
HOHENKERK Catherine, *HM Nautical Almanac Office*, UK
IVANOVA Tamara, *Institute of Applied Astronomy of Russian Academy of Sciences*, Russia
JACOBSON Robert, *Jet Propulsion Laboratory/California Institute of Technology*, USA
JOHNSTON Kenneth, *U.S. Naval Observatory*, USA
KANJ Amale, *Observatoire de Paris - SYRTE/CNRS*, France

KOLACZEK Barbara, *Space Research Center of the PAS*, Poland
KOPEIKIN Sergei, *University of Missouri*, USA
KOROTKOVA Nadezhda, *Sternberg Astronomical Institute Moscow State University*, Russia
KOSEK Wieslaw, *Space Research Centre Polish Academy of Sciences*, Poland
KUCHYNKA Petr, *Observatoire de Paris - IMCCE*, France
KUDRYASHOVA Maria, *Royal Observatory of Belgium*, Belgium
KUDRYAVTSEV Sergey, *Sternberg Astronomical Institute Moscow State University*, Russia
LAMBERT Sebastien, *Observatoire de Paris - SYRTE/CNRS*, France
LAMINE Brahim, *Laboratoire Kastler Brossel*, France
LASKAR Jacques, *Observatoire de Paris - IMCCE*, France
LE PONCIN-LAFITTE Christophe, *Observatoire de Paris - SYRTE/CNRS*, France
MACKENZIE Ruaraidh, *ESA/ESOC*, Germany
MAIGUROVA Nadiia, *RSI Nikolaev Astronomical Observatory*, Ukraine
MALKIN Zinovy, *Central (Pulkovo) Astronomical Observatory Russian Acad. Sci.*, Russia
MANCHE Hervé, *Observatoire de Paris - IMCCE*, France
MARCETA Dusan, *Faculty of Mathematics Belgrade*, Serbia
MARCO Francisco j., *Universitat Jaume I*, Spain
MARTINEZ MARIA José, *Universidad Politécnica de Valencia*, Spain
MINAZZOLI Olivier, *Observatoire de Paris - SYRTE/CNRS*, France
MORCOV George, *Faculty of Geodesy Bucharest*, Romania
MORLEY Trevor, *ESA/ESOC*, Germany
MOURET Serge, *Lohrmann Observatory Dresden Technical University*, Germany
NASTULA Jolanta, *Space Research Centre of the Polish Academy of Sciences*, Poland
NIEDZIELSKI Tomasz, *Space Research Centre of the Polish Academy of Sciences*, Poland
NILSSON Tobias, *Vienna University of Technology Institute of Geodesy and Geophysics*, Austria
NOTHNAGEL Axel, *Institute of Geodesy and Geoinformation University of Bonn*, Germany
PASHKEVICH Vladimir, *Central (Pulkovo) Astronomical Observatory Russian Acad. Sci.*, Russia
PASNICKA Malgorzata, *Space Research Centre Polish Academy of Sciences*, Poland
PAVLOVSKAYA Natalya, *St.Petersburg State University*, Russia
PETIT Gérard, *Bureau International des Poids et Mesures*, France
PETROV Sergey, *St.Petersburg State University*, Russia
PITJEVA Elena, *Institute of Applied Astronomy of Russian Academy of Sciences*, Russia
REYNAUD Serge, *Laboratoire Kastler Brossel*, France
RICHARD Jean-Yves, *Observatoire de Paris - SYRTE/CNRS*, France
RODIN Alexander, *Pushchino Radio Astronomy Observatory*, Russia
RON Cyril, *Astronomical Institute AS CR*, Czech republic
SCHINDELEGGER Michael, *Vienna University of Technology*, Austria
SMIRNOV Sergey, *St.Petersburg State University*, Russia
SOFFEL Michael, *Lohrmann Observatory Dresden Technical University*, Germany
SOUCHAY Jean, *Observatoire de Paris - SYRTE/CNRS*, France
STAMATAKOS Nicholas, *U.S. Naval Observatory*, USA
STEFKA Vojtech, *Astronomical Institute of the Czech Republic*, Czech republic
TARIS François, *Observatoire de Paris - SYRTE/CNRS*, France
TEYSSANDIER Pierre, *Observatoire de Paris - SYRTE/CNRS*, France
TIAN Wei, *Lohrmann Observatory Dresden Technical University*, Germany
TROFIMOV Dmitry, *St.Petersburg State University*, Russia
VONDRÁK Jan, *Astronomical Institute Academy of Sciences of Czech Rep.*, Czech republic
WERATSCHNIG Julia, *HM Nautical Almanac Office*, UK
XIE Yi, *Astronomy Department of Nanjing University*, China
YAGUDINA Eleonora, *Institute of Applied Astronomy of Russian Academy of Sciences*, Russia
YAO Kunliang, *Observatoire de Paris - SYRTE/CNRS*, France
YATSKIV Yaroslav, *Main Astronomical Observatory NAS of Ukraine*, Ukraine
ZACHARIAS Norbert, *U.S. Naval Observatory*, USA
ZACHARIAS Marion, USA
ZOTOV Leonid, *Sternberg Astronomical Institute* Moscow State University, Russia

SCIENTIFIC PROGRAMME

Scientific Organizing Commitee: A. Brzeziński, Poland; N. Capitaine, France (Chair); V. Dehant, Belgium; C. Hohenkerk, UK; I. Kumkova, Russian Federation; D.D. McCarthy, USA; M. Soffel, Germany; J. Souchay, France; J. Vondrák, Czech, R; Ya. Yatskiv, Ukraine

Local Organizing Commitee: P. Baudoin, O. Becker, N. Dimarcq (Chair), D. Gambis, A.-M. Gontier, S. Lambert, M. Pailler, J.-Y. Richard

Monday 20 September 2010

(at ENS: amphithéâtre Dussane)

9:15-9:30: **Opening of the Journées 2010**

Welcome from N. Dimarcq, Director of Department SYRTE of Paris Observatory (Chair of the LOC)
Introduction to the Journées 2010 by N. Capitaine (Chair of the SOC)

9:30-11:00: **Session 1 - The astronomical constants, SI units and future developments in numerical standards** *(Chair: V. Dehant)*

Luzum B., Hilton J. and NSFA WG (invited): *IAU Working Group on Numerical Standards for Fundamental Astronomy: the second triennium*
Petit G. (invited): *The new edition of the IERS Conventions: conventional reference systems and constants*
Jacobson R., Folkner W., Taylor A., Konopliv S., Williams J. G., Brozovic M.: *Planetary System GMs in the JPL Planetary Ephemerides*
Hohenkerk C.: *SOFA - status report, a review and a look to the future*
Capitaine N., Guinot B., Klioner S.: *Proposal for the re-definition of the astronomical unit of length through a fixed relation to the SI metre*
Vondrák J., Capitaine N., Wallace P.T.: *Some new thoughts about long-term precession formula*

11:00-11:30: Coffee-break

11:30-13:00: Session 2 - Solar system ephemerides and their comparison
- Special session organized in coordination with IAU Commission 4 (Ephemerides) -
(Chair: C. Hohenkerk and J. Vondrák)

Session 2 Introductory remarks (provided by G. Kaplan, President, IAU Commission 4)
Fienga A., Manche, H., Kuchynka, P., Laskar, J., Gastineau, M. (invited): *INPOP, Intégration Numérique Planétaire de l'Observatoire de Paris*
Folkner W. (invited): *Recent developments in planetary ephemeris observations*
Pitjeva E. (invited): *EPM - Ephemerides of planets and the Moon of IAA RAS: their model, accuracy, availability*
Laskar J., Fienga A., Gastineau M., Manche H: *INPOP, a 1 Million year planetary ephemeris*
Kudryavtsev S.: *Development of long-term numerical ephemerides of major planets to analytical series*

13:00-14:00: Lunch break

14:00-16:00: Session 2 (continuation) *(Chair: C. Hohenkerk and J. Vondrák)*

Yagudina E., Krasinsky G.A., Prokhorenko S.O.:*New version of ERA-EPM Moon theory*
Manche H., Fienga A., Laskar J., Gastineau M., Bouquillon S., Francou G., Kuchynka P.: *LLR residuals of the latest INPOP solution and constraints on post-Newtonian parameters*
Dehant V., Oberst J., Nadili R.: *Geodesy instrument package on the Moon for improving our knowledge of the Moon and the realization of Reference Frames*
Pashkevich V., Eroshkin G.I: *Application of the spectral analysis methods for the investigation of the Moon rotation*
Hilton J, Hohenkerk C.: *A comparison of the high accuracy Planetary Ephemerides DE421, EPM2008, and INPOP08*

Discussion

(at Observatoire de Paris: Salle Cassini)

16:15-16:45: Coffee-break

16:45-18:30: POSTER SESSION introduced by N. Capitaine and J. Souchay

18:30-20:00: Cocktail with a Welcome from D. Egret, President of Paris Observatory

Tuesday 21 September 2010

(at ENS: amphithéâtre Dussane)

9:00-11:00: Session 3 - Progress in astrometric catalogs in optical and radio wavelengths *(Chair: K. Johnston)*

Zacharias N. & Gaume R. (invited):*UCAC and URAT: optical astrometric catalog observing programs*
Souchay J. (invited): *The Large Quasar Astrometric Catalog (LQAC) and the densification of the ICRF through the LQRF (Large Quasar Reference Frame)*
Andrei A., Bucciarelli B.: *Parallaxes of Southern Extremely Cool objects I: Targets, proper motions and first results*
Bourda G., Charlot P., Collioud R., Porcas R., Garrington S.: *Towards a VLBI catalog of optically-bright extragalactic radio sources for the alignment of the radio frame with the future Gaia frame*
Damljanovic G.: *Comparison of the proper motions in declination of four catalogues via 807 Hipparcos stars*
Yatskiv Ya, Fedorov P., Akhmetov V.: *The XPM catalogue as a realisation of the extragalactic reference system in optical and near infrared wavelengths*
Maigurova N.: *Optical positions of ICRF sources using UCAC3 reference stars*

Discussion

11:00-11:30: Coffee-break

11:30-12:30: Session 4 - Recent developments in theory and observation of Earth rotation and related reference systems *(Chair: Ya Yatskiv)*

Brzeziński A. (invited): *Diurnal excitation of Earth rotation estimated from recent geophysical models*
Gross R. (invited): *Observing and modeling long-period tidal variations in polar motion*
Altamimi Z. (invited): *Examination of ITRF2008 results*

13:00-14:00: Lunch break

14:00-15:30: Session 4 (continuation) *(Chair: A. Brzeziński)*

Petrov S., Bashakova, E., Fetisov S., Smirnov S., Trofimov D.: *Subdiurnal polar motion from GNSS observations*
Boehm S., Schuh H.: *Response of the Earth system to zonal tidal forcing examined by VLBI based dUT1 variations*
Chapanov Y., Vondrák J., Ron C.: *Centennial cycles of the solar activity and Earth rotation*
Escapa A, Getino J., Miguel D., Ferrándiz J.M.: *Influence of the inner core geopotential variations on the rotation of the Earth*
Ivanova T., Brumberg V.: *On Solution of the three-axial Earth's rotation problem*
Boucher C.: *A refined definition of the International Terrestrial Reference System*
Coulot D., Bernard E., Collilieux X.: *Influence of station referencing on the quality of EOP time series*

15:30-16:00: Coffee-break

16:00-17:45: Session 4 (continuation) *(Chair: R. Gross)*

Nastula J., Pasnicka M., Kolaczek B.: *Comparison of the hydrological excitation functions HAM of polar motion for the period 1980.0-2009.0*
Kosek W., Popski W., Niedzielski T.: *Wavelet based comparison of high frequency oscillations in the geodetic and fluid excitation functions of polar motion*
Malkin Z.: *Comparison of CPO and FCN empirical models*
Nilsson T., Boehm J., Schuh H.: *Impacts of the 2010 Chile earthquake on Earth rotation*
Pavloskaya N., Petrov S.: *Thermal S1-tide in the atmospheric angular momentum and polar motion*
Schindelegger M., Boehm J., Schuh H., Salstein D.: *High-resolution atmospheric angular momentum functions from different ECMWF data classes*
Stamatakos N., Luzum B., McCarthy D.D.: *Recent Improvements in IERS Rapid Service/Prediction Center Products*
Zotov L.: *Analysis of Chandler wobble excitation, reconstructed from observations of the Earth's polar motion*

(at Observatoire de Paris: Salle Cassini)

18:30-19:30: Exhibition from archives of Paris Observatory library

19:30-22:00: Conference dinner (Salle Cassini) and "Best Poster Award"

Wednesday 22 September 2010

(at ENS: amphithéâtre Dussane)

9:00-11:00: Session 5 - Pulsars timing, relativity and time transfer *(Chair: J. Souchay)*

Kopeikin S. (invited): *An extension of the IAU framework for reference systems*
Hobbs G. (invited): *Developing a pulsar-based time scale*
Rodin A.: *Ensemble pulsar time scale*
Korotkova N., Ilyasov Yu. P., Pshirkov M. S.: *IPTA and sensitivity of radio telescopes*
Cognard I.: *High precision pulsar timing: Nancay and the European Pulsar Timing Array*
Gusev A.: *Chandler wobble and Free Core Nutations of single pulsar*
Soffel M., Klioner S., Gerlach E.: *About the MacCullagh relations in Relativity*

11:00-11:30: Coffee-break

11:30-12:30: Session 5 (continuation) *(Chair: M. Soffel)*

Xie Y., Kopeikin S.: *Post-Newtonian mechanics of the Earth-Moon system*
Teyssandier P.: *Post-post-Newtonian light propagation without integrating geodesic equations*
Mouret S.: *Test of General Relativity with the Gaia mission*
Lamine B., Courty J.-M., Reynaud S., Jaekel M.-T.: *Testing gravity law in the solar system*

Discussion

12:30-12:45: Closing of the Journées 2010

Announcement of the Journées 2011

13:00-14:00: Lunch break
(at the canteen of Paris Observatory)

14:00-16:30: WG and task group meetings (in meeting rooms of Paris Observatory)

LIST OF POSTERS

Session 1

1.1 Débarbat S., Passeron I.: *From old weights and measures to the SI as a numerical standard for the world*
1.2 Kudryavtsev S.: *An effect in satellite motion non-modeled by the current numerical standards*

Session 2

2.1 Kaplan G.: *Session 2 Introductory remarks*
2.2 Barache C., Bouquillon S., Carlucci T., Deleflie F., Francou G., Manche H., Samain E., Torre J-M.: *Web Interface for Lunar Laser Ranging observations*
2.3 Cottereau L.: *A dynamical study of Phoebe's rotation*
2.4 Francou G., Simon J.L.: *New analytical planetary theories VSOP2010*
2.5 Giorgini J.: *Summary and Status of the Horizons Ephemeris System*
2.6 Hilton J, Hohenkerk C.: *A comparison of the high accuracy Planetary Ephemerides DE421, EPM2008, and INPOP08*
2.7 Marco F., Martnez, M.J., Lpez J.A.: *Propagation in time of errors for the mutual inclination of satellites*
2.8 Weratschnig J., Taylor D.B., Bell S.A., Hilton J., Sinclair A.T.: *Calculation of Lunar Librations in The Astronomical Almanac using JPL Lunar Ephemerides*

Session 3

3.1 Andrei A.H., Gontier A.-M. , Barache C., da Silva Neto D.N., Taris F., Bourda G. , LeCampion J.-F., Souchay J., Camargo J.I.B., Pereira Osrio J.J. , Assafin M., Vieira Martins R., Bouquillon S., Anton S.:*Gaia Initial Quasar Catalogue Updates: morphology and variability*
3.2 Yatskiv Ya., Bolotin S., Lytvyn S.: *The MAOC08a combined catalogue of radio source positions created in the course of preparation for the ICRF2 Journes 2010 "Systmes de rfrence spatio-temporels"*

Session 4

4.1 Aleshkina E.: *On correlation between variations in Earth rotation and frequency of earthquakes*
4.2 Abarca Del Rio R., Gambis, D.: *Relationship between solar activity and the Earth rotation; re-analyses*
4.3 Bizouard C., Lambert S., Remus F., Seoane L., Gambis D.: *The source of the variable Chandler wobble*
4.4 Capitaine N., Folgueira, M.: *Earth rotation based on the coordinates of the CIP in the GCRS: solution for a rigid Earth*
4.5 Chapanov Y., Gambis D.: *Variations of the Earth main moments of inertia due to glacial cycles for the last 800 Ka*
4.6 Hefty J., Gerhatova L., Burgan J.: *Combination of GPS and GLONASS in Precise Point Positioning algorithms and its effect on site coordinates determination*
4.7 Kudlay O.: *Solution and an analysis of the general celestial body rotation problem*
4.8 Kudryashova M., Lambert S., Defraigne P., Dehant V., Bruyninx C.: *Determination of nutation offsets by combining VLBI/GPS-produced normal equations*
4.9 Lambert S., Gontier A.-M., Barache C.: *Operational and research activity at the Paris Observatory VLBI analysis*
4.10 Lambert S., Gontier A.-M.: *Physical characteristics of the ICRF2 quasars*
4.11 Malkin Z.: *Using modified Allan variance for time series analysis*

4.12 Malkin Z., Miller N.: *Phase variations of the Chandler wobble from 163-yr polar motion series*
4.13 Marceta D., Segan S.: *Method for prediction of deltaT based on long-periodic terms in the Earth's rate of rotation*
4.14 Marco F., Martinez M.: *Applications of simultaneous ground-based and satellite observations*
4.15 Martinez M., Marco F.: *Delta T and tidal acceleration values from three European medieval eclipses*
4.16 Morcov G.: *About the configuration of the geoid undulations and their kinematics*
4.17 Niedzielski T., Kosek W.: *Nonlinear sea level variations in the equatorial Pacific due to ENSO*
4.18 Richard J.Y., Gambis D., Bizouard C.: *Earth rotation parameters determined over CONT08 VLBI campaign by the GRGS from the combination of space geodetic techniques*
4.19 Ron C., Vondrk J., Stefka V.: *Comparison of the various atmospheric and oceanic angular momentum series*
4.20 Stefka V.: *The recent results of non-rigorous combination method of results of space geodetic techniques*
4.21 Tian W, Brzezinski, A.: *The interpretation of the high frequency signals in the G-ring laser gyroscope*
4.22 Yao K., Capitaine, N.: *Modelling of the Earth orientation and high precision astrometric observation techniques*

Session 5

5.1 Deng X.-M., Huang T.-Y.: *2PN light propagation and measurement in the solar system*
5.2 Dumin Y.: *Perturbation of a Planetary Orbit by the Lambda-Term ("Dark Energy") in Einstein Equations*
5.3 Fienga A., Desvignes G., Cognard I., Theureau G.: *Millisecond pulsars and planetary ephemerides: frame ties and other considerations*
5.4 Kanj A., Achkar, J.: *Development of the TWSTFT Carrier-Phase technique at LNE-SYRTE*
5.5 Le Poncin-Lafitte C., Bertone S.: *Light time calculations for deep space navigation*

Session 1

THE ASTRONOMICAL CONSTANTS, SI UNITS AND FUTURE DEVELOPMENTS IN NUMERICAL STANDARDS

CONSTANTES ASTRONOMIQUES, UNITÉS SI ET DÉVELOPPEMENTS FUTURS SUR LES STANDARDS

NUMERICAL STANDARDS OF FUNDAMENTAL ASTRONOMY WORKING GROUP UPDATE

B. LUZUM, U.S. Naval Observatory, USA, N. CAPITAINE, Observatoire de Paris, France, A. FIENGA, Observatoire de Besançon, France, W. FOLKNER, Jet Propulsion Laboratory, USA, T. FUKUSHIMA, National Astronomical Observatory, Japan, J. HILTON, U.S. Naval Observatory, USA, C. HOHENKERK, HM Nautical Almanac Office, UK, G. KRASINSKY, Institute of Applied Astronomy RAS, Russia, G. PETIT, Bureau International des Poids et Mesures, France, E. PITJEVA, Institute of Applied Astronomy RAS, Russia, M. SOFFEL, Dresden Technical University, Germany, P. WALLACE, Rutherford Appleton Laboratory, UK

ABSTRACT. The Working Group (WG) for Numerical Standards of Fundamental Astronomy was initiated at the 2006 International Astronomical Union (IAU) General Assembly (GA). At the 2009 IAU GA, Resolution B2 adopted the Current Best Estimates (CBEs) assembled by the NSFA WG as the IAU (2009) System of Astronomical Constants. With the initial task completed, the WG turned its attention to other tasks of importance to its long-term success. These tasks include identifying the best methods for maintaining an IAU list of CBEs as well as setting up an archival system for past values of CBEs. Addressing these issues will standardize the maintenance of a documented list of CBEs, allowing this task to be provided as an IAU service. An update on these activities is provided. In addition, unresolved questions regarding the Gaussian gravitation constant and the use of the astronomical unit and the mass of the Sun will be discussed.

1. INTRODUCTION

The International Astronomical Union (IAU) Working Group (WG) on Numerical Standards for Fundamental Astronomy (NSFA) was tasked with updating the IAU Current Best Estimates (CBEs), conforming with the IAU Resolutions, International Earth Rotation and Reference Systems Service (IERS) Conventions and Système International d'Unités whenever possible. As part of its effort to achieve this, the WG is working in close cooperation with IAU Commissions 4 and 52, the IERS, and the Bureau International des Poids et Mesures (BIPM) Consultative Committee for Units. For a brief review of the WG, see Luzum *et al.* (2008) and Luzum *et al.* (2009).

A significant milestone was achieved at the 2009 IAU General Assembly when Resolution B2 adopted the CBEs assembled by the NSFA WG as the IAU (2009) System of Astronomical Constants. In addition to adopting a new System of Constants, the resolution also recommended:

- keeping CBEs as an electronic document;
- developing a procedure for adopting CBEs;
- that IAU Division I establish a permanent body to maintain CBEs for fundamental astronomy.

The NSFA WG is now concentrating on the first two items, namely setting up the electronic document and establishing the procedure for adopting the CBEs. The following provides the status of this work.

2. FEATURES OF THE IAU (2009) SYSTEM OF ASTRONOMICAL CONSTANTS

The IAU (2009) System of Astronomical Constants has several significant changes with respect to the IAU (1976) System of Astronomical Constants. The WG believed that the previous categories of "Defining constant," "Primary constant," "Derived constant," and "System of planetary masses" did not properly capture the structure of the new system. As a result, in addition to "Defining Constant," which was retained, more descriptive category names have been introduced to help the classification and grouping of the constants. "Natural Measurable Constant" was used to describe the constant of gravitation. The category "Body constants" contains the physical constants associated with solar system

bodies. The obliquity of the ecliptic at J2000.0 was placed in the category "Initial values at J2000.0" and "Other Constants" was used for the astronomical unit and the average value of $1 - d(TCG)/d(TCB)$.

In addition,

- eight new constants have been added to the list (L_B, TDB_0, θ_0, $\dot{\theta}$, M_S/M_{Eris}, M_{Ceres}/M_S, M_{Pallas}/M_S, and M_{Vesta}/M_S);
- two constants have been removed (τ and p);
- twelve values have been replaced by more current, accurate values (G, au, L_C, M_M/M_E, M_S/M_V, M_S/M_{Ma}, M_S/M_J, M_S/M_{Sa}, M_S/M_P, GM_S, GM_E, and ϵ_0).

The full report of the WG on the new System of Constants is expected to be finished soon (Luzum *et al.*, 2011).

3. SCIENTIFIC CONCERNS

While the establishment of the new System of Constants represents a significant milestone, it does not end the scientific efforts of the WG. As before, the WG will need to stay abreast of the improvements in the scientific community. As new values are determined by improved measurements, space missions, *etc.*, the WG will need to determine whether they should become CBEs. It will also be necessary for the WG to be cognizant of changes in other scientific areas (*e.g.* geodesy) that could be relevant to updating the CBEs.

As an example, a new value for the mass of Mercury has become available based on recently reduced MESSENGER data (Smith *et al.*, 2010). This new estimate will be used to test the procedures being established for adopting new values for CBEs.

The other long-standing concern regards the status of the Gaussian gravitation constant k and the astronomical unit au. There is a proposal being made (see Capitaine *et al.*, this volume) to redefine au, but concerns regarding these proposals have also been raised. It is expected that a resolution will be drafted to resolve this issue before the next IAU General Assembly.

4. FUNCTIONALITY CONCERNS

Two significant issues that are being addressed by the WG involve questions regarding the procedure for adopting future CBEs and the design of the CBE electronic document. Significant progress is being made in both of these areas.

What is the procedure for adopting future CBEs?

A draft procedure is being discussed within the working group that defines the procedure by which future CBEs will be adopted. The current draft calls for future CBEs to be initiated by an official proposal followed by a discussion of the merits of the proposal. Some of the points to be considered in the discussion include whether the new value is an improvement over an existing value, the length of time until a new CBE is likely to become available, and whether the new value is presented in a refereed journal article. After the discussion has concluded, a vote will take place to determine the outcome.

In addition to the formal procedure for considering new CBEs, several "bookkeeping" tasks will also need to be adopted to ensure that appropriate documentation is provided. This documentation includes providing each "version" of the constants with a unique identifier, such as a date. Old versions of the CBEs will need to be archived so that past CBE versions remain available in the future. Also, providing records or notes about significant topics of debate should be provided so that decisions of the WG can be put into the appropriate context.

What is the design of the CBE electronic document?

Initial work on designing the CBE electronic document has begun. As noted above, the document will need, in addition to the CBEs themselves, information regarding the version of CBE, archives of past values and informational notes for the values.

On a related note, the location of the home page is still a subject of discussion. It is expected that the final document will be hosted on a computer associated with an IAU-related page such as the IAU Division I page or the IAU Commission 4 page.

5. FUTURE OF NSFA WG

In order to maintain a list of CBEs into the future, the efforts of the WG will need to continue past the next IAU General Assembly, when the WG is scheduled to be dissolved. However, the current IAU bylaws do not allow for an ongoing WG. This issue is being addressed by IAU Division I which is proposing that the IAU bylaws be changed to allow for a standing working group. If this change was to be adopted and the NSFA WG becomes a standing working group, then the efforts to maintain CBEs would seamlessly be continued into the future.

6. REFERENCES

Capitaine, N., Guinot, B., Klioner, S., 2011, "Proposal for the redefinition of the astronomical unit of length (ua) through a fixed relation to the SI metre," Proc. Journées 2010 Systèmes de référence spatio-temporels, Paris, 20–22 September 2010, pp. 20–23.

Luzum, B., Capitaine, N., Fienga, A., Folkner, W., Fukushima, T., Hilton. J., Hohenkerk, C., Krasinsky, G., Petit, G., Pitjeva, E., Soffel, M., Wallace, P., 2008, "Current Status of the IAU Working Group for Numerical Standards of Fundamental Astronomy," Proc. Journées 2007 Systèmes de référence spatio-temporels, Paris, 17–19 September 2007, pp. 55–57.

Luzum, B., Capitaine, N., Fienga, A., Folkner, W., Fukushima, T., Hilton. J., Hohenkerk, C., Krasinsky, G., Petit, G., Pitjeva, E., Soffel, M., Wallace, P., 2009, "Current Status of the IAU Working Group for Numerical Standards of Fundamental Astronomy," Proc. Journées 2008 Systèmes de référence spatio-temporels, Dresden, 22–24 September 2008, pp. 37–40.

Luzum, B., Capitaine, N., Fienga, A., Folkner, W., Fukushima, T., Hilton. J., Hohenkerk, C., Krasinsky, G., Petit, G., Pitjeva, E., Soffel, M., Wallace, P., 2011, "The IAU 2009 system of astronomical constants: the report of the IAU working group on numerical standards for Fundamental Astronomy," Celest. Mech. Dyn. Astr.110, 293–304.

Smith, D. E., Zuber, M. T., Phillips, R. J., Solomon, S. C., Neumann, G. A., Lemoine, F. G., Peale, S. J., Margot, J.-L., Torrence, M. H., Talpe, M. J., Head III, J. W., Hauck, S. A., Johnson, C. L., Perry, M. E., Barnouin, O. S., McNutt Jr., R. L., Oberst, J., 2010, "The equatorial shape and gravity field of Mercury from MESSENGER flybys 1 and 2," Icarus, Vol. 209, No. 1, pp. 88–100, doi:10.1016/j.icarus.2010.04.007.

THE NEW EDITION OF THE IERS CONVENTIONS: CONVENTIONAL REFERENCE SYSTEMS AND CONSTANTS

G. PETIT

Bureau International des Poids et Mesures
92312 Sèvres France
e-mail: gpetit@bipm.org

ABSTRACT. The new reference edition of the IERS Conventions is being completed, the Conventions (2010) replacing the Conventions (2003). The paper presents the main features of this new edition for what concerns the conventional reference systems and the set of adopted constants, including associated relativistic issues. Changes in this domain vs. the Conventions (2003) will be highlighted. It is shown how the Conventions implement the framework set by the Resolutions adopted by the scientific unions (IAU, IUGG and IAG), and also try to keep consistency as much as possible with the conclusions drawn by the Unions' working groups and bodies.

1. INTRODUCTION

The International Earth Rotation and Reference Systems Service (IERS) is finalizing the new reference edition (2010) of the IERS Conventions, that describe the standard reference systems realized by the IERS and the models and procedures used for this purpose. In this paper, we focus on those parts of the Conventions that more directly relate to the reference systems and constants. Section 2 recalls the ensemble of Resolutions, adopted by the scientific Unions over the last 20 years, that make up the present framework in which the Conventions (2010) are presented. In section 3, are briefly presented the present realizations of the celestial and terrestrial reference systems. Section 4 presents a few questions that are being discussed and may become of interest for the next version of the IERS Conventions.

2. THE FRAMEWORK SET BY THE UNIONS RESOLUTIONS

In order to describe observations in astronomy and geodesy, one has to choose the proper relativistic reference systems best suited to the problem at hand. A barycentric celestial reference system (BCRS) should be used for all experiments not confined to the vicinity of the Earth, while a geocentric celestial reference system (GCRS) is physically adequate to describe processes occurring in the vicinity of the Earth. These systems have been defined in a series of Resolutions passed by scientific Unions, mostly the International Astronomical Union (IAU), in the past 20 years.

2.1 Resolutions of the International Astronomical Union

Here we briefly present the resolutions passed by the International Astronomical Union (IAU) that relate to the subject of this paper and that either are technical in nature or define the policy or methods to be used. We start this description with those passed by the 1991 General Assembly (GA), which provide the first consistent representation of coordinate systems for use in the vicinity of a body (Earth, solar system) and introduce general principles for the realization of the Celestial Reference System (CRS). IAU Resolution A4 (1991) contains nine recommendations, some of which are summarized below.

- In the first recommendation, the metric tensor for space-time coordinate systems $(t, \mathbf{x})$ centered at the barycenter of an ensemble of masses is defined. The recommended form of the metric tensor can be used, not only to describe the barycentric reference system of the whole solar system, but also to define the geocentric reference system centered in the center of mass of the Earth, now depending upon geocentric coordinates.
- In the second recommendation, the origin and orientation of the spatial coordinate grids for the barycentric and geocentric reference systems are defined.

- The third recommendation defines TCB (Barycentric Coordinate Time) and TCG (Geocentric Coordinate Time) as the time coordinates of the BCRS and GCRS, respectively.
- In the fourth recommendation, another time coordinate named TT (Terrestrial Time), is defined for the GCRS as a linear function of TCG.
- Recommendations 6 and 7 provide the basis for the realization of the CRS (see section 3.1).

At the 1997 GA, we note mostly Resolution B2 which resolves that the IAU celestial system shall be the International Celestial Reference System (ICRS) as defined by the IERS and the frame shall be the International Celestial Reference Frame (ICRF). This follows from Resolution B5 (1994). Other Resolutions of interest were passed, e.g. B6 stating that no scaling of spatial axes should be applied in any reference system, even if scaled time coordinate like TT is used for convenience of an analysis.

At the 2000 GA, following the work of the IAU WG "Relativity for astrometry and celestial mechanics" together with the BIPM-IAU Joint Committee for relativity, an extended set of Resolutions was adopted extending the IAU 1991 framework; see a more complete description in (Soffel et al., 2003).

- Resolution B1.1 describes steps towards the establishment and maintenance of the celestial reference system and frame, following Resolution B2 (1997).
- Resolution B1.6 to B1.8 introduce the IAU 2000 Precession-Nutation model, the Celestial Intermediate Pole, and the Celestial and Terrestrial Ephemeris Origins, respectively.
- Resolution B1.3 concerns the definition of the BCRS and the GCRS. The Resolution extends the form of the metric tensor given in 1991, so that its accuracy is now sufficient for all applications foreseen in the next years, including those involving accurate space clocks. For the GCRS, Resolution B1.3 also adds that the spatial coordinates are kinematically non-rotating with respect to the barycentric ones. Resolution B1.4 then provides the form of the expansion of the post-Newtonian potential of the Earth to be used with the metric of Resolution B1.3.
- Resolution B1.5 applies the formalism of Resolutions B1.3 and B1.4 to the problems of time transformations and realization of coordinate times in the solar system, based upon a mass monopole spin dipole model.
- Resolution B1.9 redefines Terrestrial Time TT, dissociating it from the geoid while maintaining continuity with the previous definition.

At the 2006 GA, we note:

- Resolution B1 that adopts the P03 precession model and a definition of the ecliptic.
- Resolution B2 which supplements the IAU (2000) resolutions on reference systems, e.g. by revising the nomenclature and specifying the default orientation of the BCRS.
- Resolution B3 which redefines Barycentric Dynamical Time (TDB) as a fixed linear transformation of TCB. TDB had been introduced by the IAU in 1976 as a dynamical time scale for barycentric ephemerides. As it had not been unambiguously defined, multiple realizations of TDB were possible.

At the 2009 GA, Resolution B2 defines the IAU 2009 system of astronomical constants as the list published by the NBFA working group (see section 3.3) and Resolution B3 resolves that the second realization of the ICRF, ICRF2, shall be the fundamental realization of the ICRS as of 1 January 2010.

2.2 Resolutions of the International Union of Geodesy and Geophysics (IUGG)

The resolutions of the International Union of Geodesy and Geophysics (IUGG) dealing with reference systems over this period consist mainly of the following two:

- Resolution 2 (1991) on "Definition of a Conventional Terrestrial Reference System" which endorsed the IAU'1991 Recommendations and explicitly based its definition of TRS on the IAU relativistic framework.
- Resolution 2 (2007) on the "Geocentric and International Terrestrial Reference Systems (GTRS and ITRS)", which aims at defining and promoting the ITRS (see section 3.2).

2.3 Recommendations of IAU working groups and commissions

The IERS Conventions also take advantage of the work of several working groups and commissions, notably the Division 1 working group "Numerical Standards in Fundamental Astronomy" (NSFA; Luzum et al., 2010), the Division 1 working group "Nomenclature in Fundamental Astronomy" (NFA; Capitaine, 2009) which acted over the period 2003-2006, and of the Commission 52 "Relativity in fundamental astronomy".

The work of the NSFA group is to update the IAU current Best Estimates, eventually defining a new official system of constants as was done with the IAU Resolution B2 (2009) defining the IAU(2009) system of astronomical constants. In doing so, it has to apply the relativistic framework defined above, and to disseminate the information on the consequences. The NSFA recommendations are passed in the IERS Conventions in many ways, apparent mostly in its chapters 1 and 3. The classes of constants, values and uncertainties are made consistent between the Conventions and the NSFA, as well as the best estimates for solar system bodies. On the other hand, no significant change appeared for the Earth constants with respect to the Conventions (2003).

A task team established by the IAU Commission 52 "Relativity in fundamental astronomy" lead to a series of recommendations on issues linked to the existence of several coordinate times (Klioner et al. 2009). In the IERS Conventions, it was attempted to follow these recommendations, notably to ensure that the notation "TXX-compatible", where TXX represents the coordinate time of interest, is used whenever needed for quantities and values.

Finally, the work of the NFA working group, see http://syrte.obspm.fr/iauWGnfa/NFA_Glossary.html, has been passed into the Conventions. The text of Chapter 5 (transformation between celestial and terrestrial systems) follows the NFA and all terms of the NFA that are relevant in the Conventions are reproduced *verbatim* in the Conventions glossary.

3. THE CELESTIAL AND TERRESTRIAL REFERENCE SYSTEMS

The IERS Conventions (2010) describe the most recent realizations of the celestial and terrestrial reference systems, i.e. the ICRF2 (IERS, 2009) for the celestial frame and ITRF2008 (Altamimi et al., 2010) for the terrestrial frame.

3.1 The celestial reference system and frame

The set of resolutions specifying the definition and realization of the celestial system stem from the IAU'1991 resolution A4, recommendations 6 and 7, which specified that lists of primary sources to define the new conventional reference frame should be established and how the coordinate axes of the new frame should be set. IAU'1997 resolution B2 then determined that, from 1/1/1998, the IAU system shall be the ICRS as defined by the IERS, and that the frame shall be the ICRF. IAU'2000 resolution B1.1 later specified the working group and procedure to maintain the ICRS. Finally, IAU'2009 resolution B3 states that, from 1/1/2010, the fundamental realization shall be the ICRF2 as defined by the IERS/IVS working group.

The following short presentation is extracted from Chapter 2 of the IERS Conventions (2010) and shows the significant improvements in the new realization ICRF2. *The generation of a second realization of the International Celestial Reference Frame (ICRF2) was constructed in 2009 by using positions of 295 new "defining" compact extragalactic radio sources selected on the basis of positional stability and the lack of extensive intrinsic source structure (IERS, 2009). Future maintenance of the ICRS will be made using this new set of 295 sources. ICRF2 contains accurate positions of an additional 3119 compact extragalactic radio sources; in total the ICRF2 contains more than five times the number of sources as in the first realization ICRF1. The position formal uncertainties of the set of positions obtained by this analysis were calibrated to render their values more realistic. The noise floor of ICRF2 is found to be only* ≈ 40 *μas, some* $5-6$ *times better than ICRF1. [....] The scatter of the rotation parameters obtained in the different comparisons indicate that the axes are stable to within 10 μas, nearly twice as stable as for ICRF1. The position stability of the 295 ICRF2 defining sources, and their more uniform sky distribution, eliminates the two largest weaknesses of ICRF1.*

3.2 The terrestrial reference system and frame

IUGG'1991 Resolution 2 introduced the Conventional TRS (CTRS) derived from a geocentric non-rotating system, as defined by the IAU Resolution A4 (1991), with the following prescriptions: use TCG as a coordinate time; have origin as the geocenter including oceans and atmosphere; show no global residual rotation with respect to horizontal motions at the Earth's surface. In 2007, IUGG Resolution 2 introduced as a new notation the GTRS, system of geocentric space-time coordinates, derived from GCRS following Resolution IAU B1.3 (2000). It then defined the ITRS as a specific GTRS.

We note that ITRF itself is not explicitly defined, which implies that it is defined by the practical realizations ITRFXXXX. However ITRS and ITRF have differences in this respect:

- ITRS is 4-dimensional (in principle) while the ITRFXXXX are 3-dimensional.
- For the scale, ITRS is TCG-compatible, ITRF is TT-compatible.
- For the origin, ITRS is geocentric (instantaneous), ITRF is "geocenter averaged over time span" (see section 4.1).
- The tide convention for ITRS is not explicitly written while ITRF realizations are *de facto* conventional tide-free (see IERS Conventions chapter 1).

Recently, the IAG created the Inter-commission WG ICGG 1-3 "Concepts and terminology related to GRS", to come up to a unified and accepted terminology. This could imply a redefinition of the ITRS.

The following short presentation is extracted from Chapter 4 of the IERS Conventions (2010) and describes the main characteristics of ITRF2008. *ITRF2008 is based on reprocessed solutions of four space geodesy techniques: VLBI, SLR, GPS and DORIS, spanning 29, 26, 12.5 and 16 years of observations, respectively. The ITRF2008 is composed of 934 stations located at 580 sites, with an imbalanced distribution between the northern (463 sites) and the southern hemisphere (117 sites). There are in total 105 co-location sites; 91 of these have local ties available for the ITRF2008 combination.*

The accuracy of ITRF2008 makes it possible to identify systematic effects present in the realization ITRF2000 of the Conventions (2003), of order 1 cm and 1 mm/yr.

4. SOME PRESENT AND FUTURE WORK IN THE IERS CONVENTIONS

In establishing the IERS Conventions (2010), some questions arose that were not fully resolved and are still being discussed. This section presents three discussion topics that are linked to the realization of reference systems. The first one is the relation between the geocenter and the origin of the frames and the associated treatment of geocenter motion. The second topic concerns models for space-time coordinates and equations of motion (chapter 10 of the Conventions) and the third one concerns the models for signal propagation (chapter 11 of the Conventions).

4.1. Geocenter motion

As exposed in section 3.2, there are practical differences between ITRS and ITRF. We here assume that the differences in the scale and the possible difference in the tide convention can be taken into account explicitly with adequate accuracy, thus they have no practical impact. On the other hand, questions linked to the difference between the origin of the frame (ITRF) and the geocenter (origin of ITRS) cannot be treated in the same way. When a phenomenon (e.g. ocean tides) causes displacements of fluid masses, the center of mass of the fluid masses moves and must be compensated by an opposite motion of the center of mass of the solid Earth. The stations, being fixed to the solid Earth, are subject to this counter motion which has components in a wide spectrum. As ITRF is presently realized with linear station motions, ITRF is geocentric only in the sense of a long-term average. Space geodesy results show that the origin translation due to geocenter motion is significant but models or series representing it have not yet been fully assessed.

This may have implications on the transformation used to relate the ITRS to the GCRS at the date t of the observation which (see chapter 5 of the IERS Conventions) can be written as:

$$[\text{GCRS}] = Q(t)R(t)W(t)\ [\text{ITRS}], \tag{1}$$

where $Q(t)$, $R(t)$ and $W(t)$ are the transformation matrices arising from the motion of the celestial pole in the celestial reference system, from the rotation of the Earth around the axis associated with the

pole, and from polar motion, respectively. Eq. (1), as well as the formulas to represent its terms, are theoretical formulations that refer to reference "systems". However, it should be clear that the numerical implementation of those formulas involves the IAU/IUGG adopted realization of those reference systems, *i.e.* the ITRF and the ICRF, respectively. It remains to be established if the Earth orientation parameters implicit in (1) are affected by this assimilation.

4.2. Models for space-time coordinates and the equations of motion

In Chapter 10 of the Conventions, the presentation of coordinate time scales now accounts for all IAU Resolutions (see section 2.1). TT and TDB having conventional definitions, the only transformations of interest are TCB−TCG and $\tau - \mathrm{TT}$, where τ is proper time.

The TCB−TCG formula may be expressed, at the geocenter, as

$$\mathrm{TCB} - \mathrm{TCG} = \frac{L_C \times (TT - T_0) + P(TT) - P(T_0)}{1 - L_B} + \mathcal{O}(c^{-4}) \tag{2}$$

where TT_0 corresponds to JD 2443144.5 TAI and where the values of L_C and L_B may be found the Conventions chapter 1. Non-linear terms denoted by $P(TT)$ have a maximum amplitude of around 1.6 ms.

In the Conventions (2003), several options were given to realize equation (2), none of which however provided a complete realization of all terms. In the Conventions (2010) one conventional transformation, XHF2002_IERS, is proposed. It is composed of the analytical formula XHF2002 based on the time ephemeris TE405 (Harada and Fukushima, 2003) complemented by an additional linear term to represent terms neglected or missing in TE405. It is expected that XHF2002_IERS is only limited by the accuracy of TE405. In this respect, Fienga et al. (2009) show that TT-TDB from TE405 and from INPOP08 display a 2×10^{-18} rate difference. The full accuracy of XHF2002_IERS is yet to be ascertained.

The transformation between proper time τ and coordinate time in the vicinity of the Earth (typically up to geosynchronous orbit or slightly above) is covered in the Conventions (2010). It is based on the IAU'1991 metric which is found to be sufficient for time and frequency applications in the GCRS in the light of present clock accuracies. When considering TT as coordinate time, the proper time of a clock located at the GCRS coordinate position $\mathbf{x}_A(t)$, and moving with the coordinate velocity $\mathbf{v}_A$, is

$$\frac{d\tau_A}{dTT} = 1 + L_G - 1/c^2 \left[\mathbf{v}_A^2/2 + U_{\mathrm{E}}(\mathbf{x}_A)\right], \tag{3}$$

where the values of L_G is given in the Conventions chapter 1 and where U_{E} denotes the Newtonian potential of the Earth at the position $\mathbf{x}_A$ of the clock in the geocentric frame. In this expression, tidal terms have been neglected as their contribution will be limited to below 1×10^{-16} in frequency and 1 ps in time amplitude up the GPS orbit. Nevertheless, some care needs to be taken when evaluating the Earth's potential U_{E} at the location of the clock as the uncertainty in U_{E} should be consistent with the uncertainty expected on (3). For example, the conventional formula used in GNSS applications uses only the first term of the Newtonian potential.

By retaining also the oblateness term (J2) of the potential, one can derive (see details and references in chapter 10 of the Conventions) a simple analytical approximation that contains an apparent relativistic clock rate and a 6-h term due to J2. The frequency instability of the passive Hydrogen maser in the Galileo satellites is expected at a few parts in 10^{15} for an averaging time of several hours. Because the 6-h J2 term is of similar magnitude, this term should be accounted for when determining and using the broadcast satellite clock model. It is known that analytical expressions may be obtained, but a conventional one has yet to be chosen.

For low Earth orbit satellites, the term in J2 is more important than at the GPS altitude and it is necessary to perform a numerical integration of Equation (3) using the term in J2 for the potential.

4.3. Models for signal propagation

The chapter 11 of the Conventions (2010) "Models for signal propagation" describes the relativistic model for the VLBI time delay and to obtain the coordinate time of propagation in ranging techniques. For these space-geodesy techniques, models have been designed to ensure an accuracy of about 1 mm.

The present VLBI model, the so-called "Consensus model" adopted at a USNO workshop in 1990, has been designed for 1 ps accuracy. It is now envisioned that future VLBI observations have a measurement

noise of order a few ps i.e. call for a model uncertainty below 1 ps. Therefore the developments done 20 years ago, e.g. as explicited in (Soffel et al. 1991), may need to be re-examined in view of the new accuracy goal.

The section on ranging techniques should cover all techniques using electromagnetic signals in the vicinity of the Earth (up to the Moon), i.e. GNSS, SLR, LLR, plus some other techniques outside the direct IERS scope e.g. radar altimetry or two-way time transfer. As it has been shown (Klioner, 2007) that post-post Newtonian terms are not required in view of the present uncertainty, no significant model change is expected.

5. CONCLUSION

The IERS Conventions (2010) are now reaching completion and are available electronically at the URL http://tai.bipm.org/iers/conv2010/conv2010.html (also at http://maia.usno.navy.mil/conv2010). The Conventions (2010) implement the framework set by the Resolutions adopted by the scientific unions and describe the standard reference systems realized by the IERS and the models and procedures used for this purpose. A reference edition represents the situation at a given moment but cannot escape the fact that several issues are not fully resolved. In this respect, the IERS Conventions are a work in progress.

6. REFERENCES

Altamimi, Z., Collilieux, X, Métivier, L., "ITRF combination: Theoretical and practical considerations and lessons from ITRF2008", Proc. IAG symposium REFAG2010, submitted.

Capitaine, N., 2009, "Nomenclature and numerical standards for IAU models and IERS Conventions for Earth rotation", Proc. Journées 2008, M. Soffel and N. Capitaine (eds.), Lohrmann-Observatorium and Observatoire de Paris, pp. 46–49.

Fey A.L., Gordon, D., and Jacobs, C.S. (eds.), 2009,"The second realization of the International Celestial Reference Frame by Very Long Baseline Interferometry", IERS TN 35, Frankfurt am Main: Verlag des Bundesamts für Kartographie und Geodäsie, 204 p.

Fienga, A., et al., 2009, "INPOP08, a 4-D planetary ephemeris: from asteroid and time-scale computations to ESA Mars Express and Venus Express contributions," A&A 507(3), pp. 1675–1686,

Harada, W., Fukushima, T., 2003, "Harmonic decomposition of time ephemeris TE405," AJ 126(5), pp. 2557–2561.

Klioner, S.A., 2007, "Relativistic aspects of the IERS Conventions", IERS Workshop on Conventions, http://www.bipm.org/utils/en/events/iers/Klioner.pdf.

Klioner, S.A., et al., 2009, "Units of relativistic time scales and associated quantities", Proc IAU Symposium 261, S. Klioner, P.K. Seidelmann and M.H. Soffel, eds., Cambridge University Press, pp. 79–84.

Luzum, B.J. et al., 2010, "The IAU 2009 system of astronomical constants: the report of the IAU Working Group on Numerical Standards for Fundamental Astronomy", Celest. Mech. Dyn. Astr. , submitted.

McCarthy, D.D., Petit, G. (eds.), 2004, "IERS Conventions (2003)", IERS TN32, Frankfurt am Main: Verlag des Bundesamts für Kartographie und Geodäsie, 127 p.

Petit, G., Luzum, B.J., (eds.), 2010, "IERS Conventions (2010)", IERS TN36, Frankfurt am Main: Verlag des Bundesamts für Kartographie und Geodäsie, in print.

Soffel M.H., Müller J., Wu, X., Xu, C., 1991, "Consistent relativistic VLBI theory with picosecond accuracy", AJ 101, pp. 2306–2310.

Soffel M.H. et al., 2003, "The IAU2000 resolutions for astrometry, celestial mechanics and metrology in the relativistic framework: explanatory supplement", AJ 126(6), pp. 2687–2706.

PLANETARY SYSTEM GMS IN THE JPL PLANETARY EPHEMERIDES

R. A. JACOBSON[1], W. M. FOLKNER[2], A. H. TAYLOR[3], A. S. KONOPLIV[4], J. G. WILLIAMS[5], M. BROZOVIC[6]

[1] Jet Propulsion Laboratory, California Institute of Technology
4800 Oak Grove Drive, Pasadena, CA 91109
e-mail: robert.jacobson@jpl.nasa.gov

[2] Jet Propulsion Laboratory, California Institute of Technology
4800 Oak Grove Drive, Pasadena, CA 91109
e-mail: william.folkner@jpl.nasa.gov

[3] KinteX, Inc.
Simi Valley, CA 93065
e-mail: tony.taylor@kinetx.com

[4] Jet Propulsion Laboratory, California Institute of Technology
4800 Oak Grove Drive, Pasadena, CA 91109
e-mail: alexander.konopliv@jpl.nasa.gov

[5] Jet Propulsion Laboratory, California Institute of Technology
4800 Oak Grove Drive, Pasadena, CA 91109
e-mail: james.williams@jpl.nasa.gov

[6] Jet Propulsion Laboratory, California Institute of Technology
4800 Oak Grove Drive, Pasadena, CA 91109
e-mail: marina.brozovic@jpl.nasa.gov

ABSTRACT. Fundamental to JPL planetary ephemeris development are the values of the planetary system GMs. Currently, all but the GM of the Pluto system have been determined with data obtained from spacecraft. This article gives an overview of the sources of the GM values in previous and current ephemerides.

1. INTRODUCTION

The GMs of the planetary systems within the solar system are fundamental constants needed for the development of the planetary ephemerides or more correctly the ephemerides of the planetary system barycenters. Except for Mercury and Venus, the GMs of the systems are the sum total of the planet and the planetary satellite GMs. The basic method for determining the GMs is the measurement of the gravitational effects produced by the planets and satellites on the motion of other bodies in the solar system. Prior to the advent of interplanetary spacecraft, the other bodies were planets, satellites, and asteroids. After the 14 December 1962 flyby of Venus by Mariner 2, spacecraft were added to the list of bodies. With the exception of the dwarf planet Pluto, the determination of the GMs of all planetary systems incorporate spacecraft data. The primary type of this data is Earthbased Doppler tracking of the spacecraft near a planet or satellite.

2. MERCURY

The Mariner 10 spacecraft had three flybys of Mercury: March 1974, September 1974, and March 1975. Howard et al. (1974a) determined the GM using tracking from the first flyby. The second flyby produced no usable data. Anderson et al. (1987) combined the data from the first and third flybys to improve the GM estimate. The Messenger spacecraft on its way to enter orbit about Mercury in 2011 has also had three flybys: January and October 2008, September 2009. Smith et al. (2010) analyzed tracking from the first 2 flybys to obtain a GM value. Taylor (2009) estimated the GM using the data from all 3 flybys.

3. VENUS

The Mariner 2 flyby of Venus in 1962 was the first successful planetary encounter by a spacecraft. Anderson et al. (1964) fit the Doppler acquired during the flyby to obtain a GM estimate; crude processing procedures were used but a rather reasonable result was obtained. Data from subsequent flybys by Mariner 5 in 1967 and Mariner 10 in 1974 were also analyzed to produce GM estimates (Anderson et al., 1967; Anderson and Efron, 1969; Howard et al., 1974b). With the arrival of Pioneer Venus Orbiter (PVO) in 1978, work on the development of a gravity field model for Venus began. Sjogren et al. (1990) used the PVO Doppler tracking to estimate the GM. Later Konopliv and Sjogren (1994) combined the PVO data with tracking from the Magellan orbiting spacecraft to develop a 60 degree and order gravity field and obtain an associated GM. Konopliv and Sjogren (1996) extended the gravity field to degree and order 180 and revised the GM estimate.

4. EARTH-MOON

Estimates of the Earth and Moon GMs are found during development of the gravitational field models of those bodies from tracking of Earth and lunar orbiters. The current best estimate of the Earth GM is quite accurate (Ries et al., 1992); note that because the Ries value was determined in the geocentric metric, it must be converted to the barycentric metric before it can be used with the planetary ephemerides. Konopliv et al. (2001) obtained an estimate of the Moon GM along with an estimate of the lunar gravity field from the orbiting Lunar Prospector spacecraft. The accuracy of that GM and gravity field, however, is limited because of lack of tracking data over the far side of the Moon.

The Earth-Moon system GM is found together with the lunar orbit using Lunar Laser Ranging (LLR) measurements (Williams et al., 2009; Williams, 2010). This system GM is currently more accurate than the sum of the separate Earth and Moon GMs from the gravity field work. The Earth-Moon mass ratio is determined as one of the parameters when fitting ephemerides of solar system bodies from observations which include ranging data. These data are sensitive to the motion of the Earth about the Earth-Moon system barycenter. Konopliv et al. (2002) obtained a value as part of their work on the gravity field and orbit of the asteroid Eros using data from the NEAR spacecraft. Relying on radar range to Mercury and Venus and ranging to several spacecraft at Mars, Folkner et al. (2008) improved the mass ratio during the development of the DE421 planetary ephemerides. The mass ratio combined with the system GM yields the GMs of the individual bodies.

5. MARS

Doppler tracking of Mariner 4 during its 1964 flyby of Mars yielded the first Martian GM estimate based on spacecraft data (Null, 1969). Following the 1971 insertion of Mariner 9 into Martian orbit, Born (1974) found the Mars GM and a low order and degree gravity field from the tracking. Konopliv and Sjogren (1995) followed by developing a 50 degree and order gravity field and associated Mars GM from the combination of Mariner 9 and Viking Doppler. They also estimated the GMs of the satellites thus producing a true system GM estimate. Yuan et al. (2001) extended the gravity field to 75th degree and order using the Mariner 9, Viking, and Mars Global Surveyor (MGS) data, and Konopliv et al. (2006) developed a 95 degree and order gravity field model from the MGS and Mars Odyssey tracking data. Recently, Konopliv et al. (2010) added data from the Mars Reconnaissance Orbiter to that from the MGS and Mars Odyssey to improve the gravity field reaching degree and order 110.

6. JUPITER

The Pioneer 10 and Pioneer 11 flybys of Jupiter in 1973 and 1974, respectively, provided Doppler tracking to estimate the GM of the Jovian system including the GMs of the Galilean satellites (Null, 1976). Campbell and Synnott (1985) added the 1979 Voyager 1 and Voyager 2 tracking to that from the Pioneers to update the GMs. Jacobson (2005) extended Campbell and Synnott's work to include tracking from the 1992 Ulysses flyby and the Galileo orbiting spacecraft to revise the system and Galilean satellite GMs. A GM for Amalthea was also determined, but its value is less than the uncertainty in the total system GM.

7. SATURN

The first spacecraft to visit Saturn was Pioneer 11 in 1979. Null et al. (1981) used the Doppler tracking to get the GMs of the system and Rhea, Titan, and Iapetus; GMs for the other satellites were taken from Kozai (1976). Campbell and Anderson (1989) added the tracking from the 1980 and 1981 Voyager 1 and Voyager 2 encounters to that from Pioneer and determined the system, Rhea, Titan, and Iapetus GMs; again the Kozai GMs were assumed for the other satellites. Jacobson et al. (2006) extended Campbell and Anderson's work by adding data from the Cassini orbiting spacecraft and Earth-based observations of Saturn's Lagrangian satellites to obtain the system GM as well as the GMs of all of the major satellites.

8. URANUS AND NEPTUNE

The Voyager 2 flybys of Uranus in 1986 and Neptune in 1989 provide the data to determine the GMs in those planetary systems. Jacobson et al. (1992) estimated the Uranian system and major satellite GMs from the Voyager tracking, the Voyager satellite imaging, and Uranian satellite astrometry over the period 1960–1985. Jacobson (2007) updated the analysis with improved data processing techniques and and an extension of the astrometry to cover 1911–2006. In a procedure analogous to that used for Uranus, Jacobson et al. (1991) obtained the Neptune and Triton GMs from an analysis of Voyager tracking, Voyager imaging, and satellite astrometric observations from 1847 to 1988. Jacobson (2009) extended that earlier work by improving the data processing, adding astrometry through 2008, including the satellite Proteus in the system, and incorporating all available observations of Proteus.

9. PLUTO

No spacecraft have yet visited the Pluto system; the New Horizons spacecraft is planned to arrive in 2015. Consequently, the GMs of the bodies in the system must be determined from observations of the motions of Pluto's satellites. Prior to the discovery of Nix and Hydra in 2005, analysis of the motion of Charon produced estimates of the system GM (Harrington and Christy, 1981; Tholen, 1985; Null and Owen, 1996; Olkin et al., 2003). Subsequent to the Nix and Hydra discovery, observations of all three satellites have been used (Tholen et al., 2008, 2010; Brozovic and Jacobson, 2010).

The research described in this publication was carried out at the Jet Propulsion Laboratory, California Institute of Technology, under a contract with the National Aeronautics and Space Adminstration.

10. REFERENCES

Anderson, J. D. et al., 1987, "The mass, gravity field, and ephemeris of Mercury", Icarus, 71, 337–349.

Anderson, J. D., Efron, L., 1969, "The mass and dynamical oblateness of Venus", BAAS 1 (3), 231–232.

Anderson, J. D., Null, G. W., Thorton, 1964, Progress in Astronautics and Aeronautics, Vol. 14. Academic Press, Inc., New York, pp. 131–155.

Anderson, J. D. et al., 1967, "Celestial mechanics experiment", Science, 158, 1689–1690.

Born, G. H., 1974, "Mars physical parameters as determined from Mariner 9 observations of the natural satellites and Doppler tracking", J. Geophys. Res., 79, 4837–4844.

Brozovic, M., Jacobson, R. A., 2010, "Preliminary orbits and masses for the satellites of Pluto", Presented at Nix and Hydra: Five Years after Discovery Workshop, STScI, Baltimore, MD.

Campbell, J. K., Anderson, J. D., 1989, "Gravity field of the Saturnian system from Pioneer and Voyager tracking data", AJ, 97, 1485–1495.

Campbell, J. K., Synnott, S. P., 1985, "Gravity field of the Jovian system from Pioneer and Voyager tracking data", AJ, 90, 364–372.

Folkner, W. M., Williams, J. G., Boggs, D. H., 2008, "The Planetary and Lunar Ephemeris DE421", Interoffice Memo. 343R-08-003 (internal document), Jet Propulsion Laboratory, Pasadena, CA.

Harrington, R. S., Christy, J. W., 1981, "The satellite of Pluto. III", AJ, 86, 442–443.

Howard, H. T. et al., 1974a, "Mercury: results on mass, radius, ionosphere, and atmosphere from Mariner 10 dual-frequency radio signals", Science, 185, 179–180.

Howard, H. T. et al., 1974b, "Venus: mass, gravity field, atmosphere, and ionosphere as measured by the Mariner 10 dual-frequency radio system", Science, 183, 1297–1301.

Jacobson, R. A., 2005, "Jovian satellite ephemeris – JUP230", private communication.

Jacobson, R. A., 2007, "The gravity field of the Uranian system and the orbits of the Uranian satellites and rings", BAAS, 39 (3), 453.
Jacobson, R. A., 2009, "The orbits of the Neptunian satellites and the orientation of the pole of Neptune", AJ, 137, 4322–4329.
Jacobson, R. A. et al., 2006, "The gravity field of the Saturnian system from satellite observations and spacecraft tracking data", AJ, 132 (6), 2520–2526.
Jacobson, R. A. et al., 1992, "The masses of Uranus and its major satellites from Voyager tracking data and Earth-based Uranian satellite data", AJ, 103 (6), 2068–2078.
Jacobson, R. A., Riedel, J. E., Taylor, A. H., 1991, "The orbits of Triton and Nereid from spacecraft and Earthbased observations", A&A, 247, 565–575.
Konopliv, A. S. et al., 2001, "Recent gravity models as a result of the Lunar Prospector Mission", Icarus, 150, 1–18.
Konopliv, A. S. et al., 2010, "Mars high resolution gravity fields from MRO, Mars seasonal gravity, and other dynamical parameters", to appear in Icarus.
Konopliv, A. S., Sjogren, W. L., 1994, "Venus spherical harmonic gravity model to degree and order 60", Icarus, 112, 42–54.
Konopliv, A. S., Sjogren, W. L., 1995, "The JPL Mars gravity field, Mars50c, based upon Viking and Mariner 9 Doppler tracking data", JPL Publication 95-5, Jet Propulsion Laboratory, Pasadena, CA.
Konopliv, A. S., Sjogren, W. L., 1996, "Venus gravity handbook", JPL Publication 96-2, Jet Propulsion Laboratory, Pasadena, CA.
Konopliv, A. S. et al., 2002, "A global solution for the Gravity Field, Rotation, Landmarks, and Ephemeris of Eros", Icarus, 160, 289–299.
Konopliv, A. S. et al., 2006, "A global solution for the Mars static and seasonal gravity, Mars orientation, Phobos and Deimos masses, and Mars ephemeris", Icarus, 182, 23–50.
Kozai, Y., 1976, "Masses of satellites and oblateness parameters of Saturn", Pub. Astron. Soc. Japan, 28, 675–691.
Null, G. W., 1969, "A solution for the mass and dynamical oblateness of Mars using Mariner-IV Doppler data," BAAS, 1 (4), 356.
Null, G. W., 1976, "Gravity field of Jupiter and its satellites from Pioneer 10 and Pioneer 11 tracking data", AJ, 81, 1153–1161.
Null, G. W. et al., 1981, "Saturn gravity results obtained from Pioneer 11 tracking data and Earth-based Saturn satellite data", AJ, 86, 456–468.
Null, G. W., Owen, Jr., W. M., 1996, "Charon/Pluto mass ratio obtained with HST CCD observations in 1991 and 1993", AJ, 111, 1368–1381.
Olkin, C. B., Wasserman, L. H., Franz, O. G., 2003, "The mass ratio of Charon to Pluto from Hubble Space Telescope astrometry with the fine guidance sensors", Icarus, 164, 254–259.
Ries, J. C. et al., 1992, "Progress in the determination of the gravitational coefficient of the Earth", Geophys. Res. Letters, 19 (6), 529–531.
Sjogren, W. L., Trager, G. B., Roldan, G. R., 1990, "Venus: a total mass estimate", Geophys. Res. Letters, 17 (10), 1485–1488.
Smith, D. E. et al., 2010, "The equatorial shape and gravity field of Mercury from MESSENGER flybys 1 and 2", Icarus, 209, 88–100.
Taylor, A. H., 2009, "The mass of Mercury from the 3 Messenger flybys", personal communication.
Tholen, D. J., 1985, "The orbit of Pluto's satellite", AJ, 90, 2353–2359.
Tholen, D. J., Buie, M. W., Grundy, W. M., 2010, "Improved masses of Nix and Hydra", BAAS, 42 (4), 984.
Tholen, D. J. et al., 2008, "Masses of Nix and Hydra", AJ, 135, 777–784.
Williams, J. G., 2010, "Earth+Moon GM from lunar laser ranging", personal communication.
Williams, J. G., Turyshev, S. G., Boggs, D. H., 2009, "Lunar laser ranging test of the equivalence principle with the Earth and Moon", International Journal of Modern Physics, D 18 (7), 1129–1175.
Yuan, D. N. et al., 2001, "Gravity field of Mars: A 75th degree and order model", J. Geophys. Res., 106 (E10), 23377–23401.

SOFA—A STATUS REPORT, REVIEW AND LOOK TO THE FUTURE

C.Y. HOHENKERK
HM Nautical Almanac Office
UK Hydrographic Off ice, Taunton, TA1 2DN
e-mail: Catherine.Hohenkerk@ukho.gov.uk

ABSTRACT. Standards of Fundamental Astronomy (SOFA) is an International Astronomical Union (IAU) service that provides accessible and authoritative algorithms and procedures that implement standard models used in fundamental astronomy. SOFA consists of a dedicated web site from which the SOFA Software Collections may be downloaded and a Board that provides and checks the material. At present this IAU Division 1 activity reports to IAU Commission 19; however the members of the international Board are selected from various Commissions. This presentation looks at SOFA's development, in particular over the last few years. For the future we consider what SOFA needs to provide and its place within the IAU.

1. SOFA — A REVIEW

SOFA is an IAU initiative started by Division 1, that has the task of establishing and maintaining an accessible and authoritative set of algorithms and procedures that implement standard models used in fundamental astronomy.

SOFA provides a collection of routines, a library, in both Fortran and ANSI C, which form a basis, the building blocks, to enable users to write their own applications, using authoritative methods. For example, there are routines that calculate precession and nutation angles, and the transformation matrix between the celestial and terrestrial reference systems that support IAU Resolutions.

To do this successfully there is a Board of experts that produces and validates the material and a web site from where the libraries may be obtained. The current Board members are John Bangert (US Naval Observatory, USA), Steve Bell (Webmaster, HM Nautical Almanac Office (UKHO), UK), Mark Calabretta (Australia Telescope National Facility, Australia), Anne-Marie Gontier[1] (Observatoire de Paris, France), George Hobbs, (Australia Telescope National Facility, Australia), Catherine Hohenkerk (Chair, HM Nautical Almanac Office, UK), Wen-Jing Jin (Shanghai Observatory, China), Brian Luzum (IERS, US Naval Observatory, USA), Zinovy Malkin (Pulkovo Observatory, Russia), Jeffrey Percival (University of Wisconsin, USA), Patrick Wallace (Rutherford Appleton Laboratory, UK). The Board represents, from IAU Division 1, Commissions on Ephemerides (4), Astrometry (8), Earth Rotation (19), Time (31) and Relativity (52). This includes members of the current working group on Numerical Standards for Fundamental Astronomy (NFSA). From Division XII we also represent Commission 5, and the Working Groups on FITS and Astronomical Data.

SOFA was initially set up by the IAU in 1994 under the Division 1 Working Group on Astronomical Standards (WGAS). Patrick Wallace was appointed as the first Chair of the SOFA Board in February 1996, a position he held for the Board's first 15 years. Work really began after the first Board meeting, in October of 1996. The first Fortran release was made in 2001 March, while the first ANSI C release was achieved in February 2009. The latest release, in January 2010, made available the seventh Fortran release and the second ANSI-C release. On March 20th of this year, Patrick Wallace stepped down and the Board elected Catherine Hohenkerk as the new Chair. The whole Board were pleased that Wallace wished to continue as a member of the Board and intended to continue providing the various routines.

The SOFA Centre is its web site (www.iausofa.org). It is the public face of SOFA. From this web site users navigate to each routine and view or copy the source code for that individual routine. Alternatively either of the current libraries, Fortran or ANSI C, may be downloaded. It also is an archive where

[1]It is with great sadness that we record the untimely death of Anne-Marie Gontier on September 24th 2010, just after the Journées in which she participated. Anne-Marie had been a member of the board almost from the beginning, which provided a strong link with the Observatoire de Paris that has been to SOFA's great benefit.

previous releases may be obtained. Over the last three years, for which statistics are available, the site receives about 800 unique visitors each month from over 100 countries.

2. SOFA'S CURRENT SOFTWARE COLLECTION

There are at present 113 astronomy routines that cover categories for:

- calendars (7),
- time scales (2),
- Earth rotation and sidereal time (15),
- ephemerides (2),
- fundamental arguments (14),
- geocentric/geodetic transformations (5),
- precession/nutation/polar motion (60),
- star space motion (2),
- star catalogue conversions (6).

Those that support IAU resolutions, such as those on precession and nutation angles, are designated as canonical routines, as are those for the fundamental arguments used for nutation. There are also the 52 utility (support) routines that perform the basic vector/matrix manipulations, conversion of degrees to radians, etc.

There are two types of documentation. There are the introductory comments to the code giving detailed information, such as what the routine does and how it is used. This includes information on the input and output arguments, the accuracy of the algorithm, as well as the references that it is based on. These preambles to each routine are pulled together into the manual. This type of information is terse and although fully specifies the routine, is not aimed at the beginner. The manual is supplied both as an ASCII (.lis) file and an Adobe Acrobat (.pdf) file. It has also been split up into smaller more useful sections; title, board members, copyright information, vector-matrix library (vml), astronomy library (lib), etc., so users need only look at what is relevant to them.

The other type of documentation are Cookbooks, each of which contains more descriptive material and includes examples, with code and intermediary results. The first cookbook, *SOFA Tools for Earth Attitude*, deals with both the equinox based and CIO based methods of transformations from the Geocentric Celestial Reference System (GCRS) to the International Terrestrial Reference System (ITRS). Included is the complete Fortran program that computes the transformation, which demonstrates five methods viz:

1. IAU 1976/1980/1982/1994 (equinox based),
2. IAU 2000A, CIO based using classical angles,
3. IAU 2000A, equinox based, using classical angles,
4. IAU 2006/2000A, CIO based using classical angles, and
5. IAU 2006/2000A, CIO based, using X, Y series.

Before the SOFA library is used it is very important to ensure that on your computer system things are working as expected. SOFA provides a tool, a validation program, for both the Fortran (`t_sofa_f.for`) and ANSI C (`t_sofa_c.c`) that is run during the compilation process (`make test`), which does this check. This is not an exhaustive test, but the validation program does call all the routines and checks the calculated results against stored values to some specified precision. The stored values have been produced independently using quadruple precision. At the end of the process a message will be displayed. Note: Users who encounter a failure of the validation program are encouraged to contact the Board

(sofa@ukho.gov.uk), noting details of the system (i.e., compiler, operating system, and hardware) upon which the failure took place.

3. LATEST RELEASE OF SOFA

In January of this year (the latest release), the SOFA web site was moved to www.iausofa.org, a web site hosted at the United Kingdom Hydrographic Office (UKHO). Since its address is independent of the host institution, in theory, if the webmaster needs to move the web site, then this will not affect users. At the same time the web site was given a new design. All the previous features are included, but the presentation has been streamlined. At present requests to the older web sites are being forwarded, however, at the next release these older sites will be removed.

A new feature allows users to register their e-mail address so that they may receive news about errors and updates. This also gives the Board some idea of how SOFA is being used.

The latest routines to be added to SOFA in the January release were for transformations between geocentric and geodetic coordinates. There are two routines, GD2GCE and GC2GDE that, given the parameters for an ellipsoid, (a, f), will convert from geodetic to geocentric coordinates and geocentric to geodetic coordinates, respectively. There is a canonical routine (EFORM) that gives the parameters, equatorial radius (a) and flattening (f), for three standard reference ellipsoids; (1) WGS84, (2) GRS80 and (3)WGS72. Lastly two routines, GD2GC and GC2GD, are provided, which are equivalent to GD2GCE and GC2GDE, but uses one of the specified standard ellipsoids.

4. LOOK TO THE FUTURE

The next tranche of routines to be added to SOFA are for transformation between time scales. At present SOFA includes two routines in this category. These routines, DAT and DTDB, do not transform between time scales, but give the differences between two particular time scales, that is between TAI and UTC, and an approximation to TT−TDB, respectively.

SOFA recognizes seven time scales, namely TAI, UTC, UT1, TT, TCG, TDB, and TCB. The strategy is to provide routines that link adjacent pairs of time scales. This gives the user the option to select those needed to construct the required chain, and importantly provide supplementary quantities such as ΔT and UT1−UTC, which either cannot be predicted or for which there are model choices. This was agreed as the simplest scheme that gives the user the most flexibility. Table 1 lists the sixteen linking routines.

Name	*Transformation*	*Date/Time Arguments*
`TAIUTC`	TAI ⇒ UTC	`TAI1, TAI2, UTC1, UTC2`
`UTCTAI`	UTC ⇒ TAI	`UTC1, UTC2, TAI1, TAI2`
`UTCUT1`	UTC ⇒ UT1	`UTC1, UTC2, DUT, UT1, UT2`
`UT1UTC`	UT1 ⇒ UTC	`UT1, UT2, DUT, UTC1, UTC2`
`TAIUT1`	TAI ⇒ UT1	`TAI1, TAI2, DTA, UT1, UT2`
`UT1TAI`	UT1 ⇒ TAI	`UT1, UT2, DTA, TAI1, TAI2`
`TTUT1`	TT ⇒ UT1	`TT1, TT2, DT, UT1, UT2`
`UT1TT`	UT1 ⇒ TT	`UT1, UT2, DT, TT1, TT2`
`TAITT`	TAI ⇒ TT	`TAI1, TAI2, TT1, TT2`
`TTTAI`	TT ⇒ TAI	`TT1, TT2, TAI1, TAI2`
`TTTCG`	TT ⇒ TCG	`TT1, TT2, TCG1, TCG2`
`TCGTT`	TCG ⇒ TT	`TCG1, TCG2, TT1, TT2`
`TTTDB`	TT ⇒ TDB	`TT1, TT2, DTR, TDB1, TDB2`
`TDBTT`	TDB ⇒ TT	`TDB1, TDB2, DTR, TT1, TT2`
`TDBTCB`	TDB ⇒ TCB	`TDB1, TDB2, TCB1, TCB2`
`TCBTDB`	TCB ⇒ TDB	`TCB1, TCB2, TDB1, TDB2`

Table 1: The SOFA time scale transformation routines. Argument pairs `TAI1, TAI2` *etc.* are the encoded times produced by the DTF2D routine and decoded using D2DTF.

The routines use SOFA's two-argument Julian date convention. Thus the two routines DTF2D and D2DTF handle the conversion between civil date and time, i.e., year, month, day, hour, minute and

seconds and the two-part Julian date (or in the case of UTC, quasi-JD) and vice versa. This includes dealing with, in the case of UTC, leap seconds and the rare but crucial cases when it is correct to print out more than 59.... seconds. Importantly, the routines take care to preserve precision by ensuring that the tiny differences are added to (or subtracted from) the smaller of the two date arguments.

To help the user there will be a cookbook called *Time Scale & Calendar Tools*, and although the Fortran and C version of the cookbook are identical, they will have different program code.

We hope to make the next release available soon after the time scale routines are independently tested by George Hobbs (Australia Telescope National Facility) who has been co-opted onto the Board on behalf of Commission 31 (Time).

For the future there are the transformations between the Barycentric Celestial Reference System (BCRS) and the Geocentric Celestial Reference System (GCRS) which include the effects of parallax, light-time, light-deflection and aberration. These effects will involve positions of the Sun and planets. A few of the SOFA Board are on the Commission 4 Working Group that has just been set up with the mission to provide universal access to the various high-precision ephemerides of solar system bodies.

The present structure of the IAU is to have groups that last for a fixed period of time. SOFA, due to the very nature of its mandate, does not conform to this. Thus Division I has requested the IAU Executive Committee to consider a change in the IAU by-laws that would permit the IAU to create service organizations and standing committees. If this proposal is accepted, then it is suggested that SOFA would be a service organization.

Acknowledgements. The work of SOFA gets done by good will and this is an appropriate place and time to put on record some acknowledgments.

The Board would like to thank the UK Hydrographic Office for hosting the SOFA web site.

Thanks are due not only to the webmaster (who is now a Board member) but also to all the Board members for all their efforts, and to their host institutions.

Finally, during the process of electing a new Chair earlier this year, it was made abundantly clear that the Board would like to record and acknowledge the leadership of Patrick Wallace over its first fifteen years during his chairmanship. The Board also acknowledges the huge contribution that he has made and is still making to SOFA and the wider astronomical community.

5. REFERENCES

Fukushima, T., 1995, "Report of the IAU WGAS Subgroup on Standard Procedures", Highlights of Astronomy, 10.

Wallace, P. T., 1996,"The IAU SOFA Initiative", Astronomical Society of the Pacific Conference Series, 101, pp 207-210.

Wallace, P. T., 1998,"SOFA: Standards of Fundamental Astronomy", Highlights of Astronomy, 11, p 191.

Wallace, P., 2000, "SOFA Software Progress Report", Proceedings of IAU Colloquium 180: Towards Models and Constants for Sub-Microarcsecond Astrometry", pp 353-362.

Wallace, P., 2000, "SOFA", IAU Joint Discussion, 2.

Wallace, P., 2002, "Update to SOFA Report", Highlights in Astronomy, 12, p 128.

Wallace, P.T., 2002, "Software for Implementing the IAU 2000 Resolutions", IERS Technical Note No. 29, pp 65-69.

Wallace, P. T., 2004, "SOFA software support for IAU 2000", Bulletin of the American Astronomical Society, 36, p 694.

Wallace, P. T., 2009, "Recent SOFA Developments", Proceedings of the Journées 2008 Systèmes de référence spatio-temporels, pp 50-53.

SOFA's web site is at http://www.iausofa.org

PROPOSAL FOR THE RE-DEFINITION OF THE ASTRONOMICAL UNIT OF LENGTH THROUGH A FIXED RELATION TO THE SI METRE

N. CAPITAINE[1], B. GUINOT[1], S.A. KLIONER[2]

[1]SYRTE, Observatoire de Paris, CNRS, UPMC
61, avenue de l'Observatoire, 75014 – Paris, France
e-mail: n.capitaine@obspm.fr; guinot.bernard@wanadoo.fr

[2]Lohrmann Observatory,
Dresden Technical University, 01062 Dresden, Germany
e-mail: Sergei.Klioner@tu-dresden.de

ABSTRACT. As already suggested before the 2009 IAU General assembly (Klioner 2008; Capitaine & Guinot 2009), it is proposed to re-define the ua as a fixed number of SI metres through a defining constant. Such a change of status for the ua would limit its role to that of a unit of length of "convenient" size for some applications. Consequently, $GM_{\rm Sun}$ which would cease to have a "fixed" value in astronomical units and will have to be determined experimentally, which is shown to be desirable for modern dynamics of the solar system. The defining number to be adopted for the conventional definition of the ua should be, for continuity reason, the value for the current best estimate of the ua in m as adopted by IAU 2009 Resolution B2 (i.e. ua = 1.495 978 707 00 x 10^{11} m) (Luzum et al. 2011). Such a change of status of the ua would be a great simplification for the users of the astronomical constants, would let possible variations of the mass of the Sun (and/or G) appear directly, and would avoid an unnecessary deviation from the SI.

1. THE ASTRONOMICAL UNITS

The current System of astronomical constants includes three astronomical units as defined in the IAU 1976 System:

- The astronomical unit of time is a time interval of one day (D) of 86 400 s. It provides a unit of time of "convenient" size for astronomy, which is related to the SI by a defining number.
- The astronomical unit of length (ua) is a specific astronomical unit for expressing distances in the solar system. Its definition is based on the Gaussian gravitational constant k and its value in SI has to be determined experimentally.
- The astronomical unit of mass is the mass of the Sun, $M_{\rm Sun}$. It is a specific astronomical unit for expressing masses; its value in SI has to be derived from the SI values of (1) the heliocentric gravitational constant, $GM_{\rm Sun}$, and (2) the gravitational constant G (which has a current relative uncertainty of 10^{-4}, cf. CODATA 2006). The value of $GM_{\rm Sun}$ in SI is obtained from the SI values for the ua and the day. Therefore, the value in SI of the astronomical unit of mass depends on the ua.

2. DEFINITION AND ROLE OF THE ASTRONOMICAL UNIT OF LENGTH (UA)

In the IAU 1976 System of astronomical constants, the astronomical unit of length has been defined as "that length (A) for which the Gaussian gravitational constant (k) takes the value of 0.017 202 098 95 when the units of measurements are the astronomical units of length, mass and time. The dimensions of k^2 are those of the constant of gravitation (G), i.e., $L^3\ M^{-1}\ T^{-2}$. The term "unit distance" is also for the length A."

In the SI brochure (cf. Table 7 entitled "Non-SI units whose values in SI units must be obtained experimentally"), which is intended to non-astronomers, the astronomical unit is defined as "approximately

equal to the mean Earth-Sun distance. It is the radius of an unperturbed circular Newtonian orbit about the Sun of a particle having infinitesimal mass, moving with a mean motion of 0.017 202 098 95 radians per day (known as the Gaussian constant)."

For any planet, the mean motion n is measured in SI (i.e. rad/s) and can be trivially converted into astronomical units (i.e. rad/D); its semi major axis can be expressed as $a^3 = k^2/n^2$ (if perturbations are neglected). Hence the distances to other planets are in ua and the accuracy of the time measurements is transferred into the relative distances. This definition of the ua was explained by the lack of precise measures of distances in the solar system, while it provides accurate relative distances. It let open the problem of precise scaling of the solar system in the SI.

The status of the ua in the IAU 1976 System of astronomical constants and the IERS Conventions 2003 is such that k is a "defining constant"; the scale distance in the solar system is provided by the value A of the ua in metre as fitted to a planetary ephemeris.

In the IAU 1976 System of astronomical constants, the uncertainty in the estimated ua was of 2 km; The heliocentric gravitational constant was a "derived constant", such that: $GM_{Sun} = k^2A^3/D^2$. In the IERS Conventions 2003, the uncertainty in the ua, as derived from the JPL ephemerides DE403 (Standish 1995) was of 6 m, i.e. more than 2 orders of magnitude better than its IAU 1976 value.

3. RECENT EVOLUTION AND NEW SITUATION

There have been a number of changes and improvements in various contexts since the ua was defined as described in the previous section.

1. The recent IAU Resolutions (1991, 2000, 2006) have specified the definition of the celestial reference systems in the General Relativity framework; in addition, they have recommended improvements in the concepts and models. The definition of the ua should be adapted to comply with this new context.

2. Modern observations in the solar system are based on ranging to planets, spacecraft observations, Very Long Baseline Interferometry (VLBI), etc, which are high accuracy observations. Therefore, ranging observations are so accurate that there is no longer a reason to have a scale-invariant description of the solar system as provided by the current definition of the ua.

3. Recent ephemerides of solar system objects are such that:
- the primary determination of the GM_i of the planets have been obtained directly in $\mathrm{km^3 s^{-2}}$ (TDB-compatible values) and then converted into values in astronomical units in order to comply with the IAU unit distance (Folkner et al. 2008);
- the direct estimation of GM_{Sun} has been tested in the INPOP08 ephemerides (Fienga et al. 2009).

This shows that, in the context of modern ephemerides, the ua appears as an intermediate unit only used for historical purposes.

4. The decrease of the solar mass is expected to be detectable in a near future, i.e. when the accuracy has been improved by a factor 10. With the current definition of the ua, time dependence of M_{Sun} immediately leads to time-dependent astronomical units for length and mass. To investigate the dynamical effects of the time-dependence of M_{Sun} using such time-dependent units is a non-sense.

All these reasons make clear that the status of the ua and GM_{Sun} should be reformed to be more in agreement with the modern context (Klioner 2008, Capitaine & Guinot 2009).

Yet, in the IAU 2009 System of astronomical constants (Luzum et al. 2011) that was recently adopted by the IAU as a replacement of the IAU 1976 System, the ua is still defined from the Gaussian gravitational constant k, which is called an "auxiliary defining constant". However, the numerical values provided for the ua and GM_{Sun} in the table associated with that system have been obtained from the following procedure: (i) the TDB-compatible value of the ua is an average (Pitjeva & Standish 2009) of recent estimates of the ua defined by k, (ii) the TDB-compatible value of GM_{Sun} has been derived from the ua fitted to the DE 421 ephemerides (Folkner et al. 2008). This value of GM_{Sun} is consistent, within uncertainties, with the IAU 2009 value for the ua but has not been directly derived from that value. This shows that the historical definition of the ua is no longer required for modern ephemeris. Note that TDB- and TCB-compatible values are provided for GM_{Sun}.

4. THE RELATIVISTIC FRAMEWORK

If the historical status of the ua were to be kept, it would be necessary to extend its definition to General relativity. Several options have been considered (Guinot 1995, Capitaine & Guinot 1995, Brumberg & Simon 2004, Standish 2005, Pitjeva 2005, Klioner 2008).

First, it would be necessary to extend the Gaussian gravitational constant to the GR framework; there are several possible options, but the geometrical interpretation through the motion around the Sun would be more delicate. Second, it would be necessary to take into account the use of TCB or TDB, i.e. the scaling factor $F = 1 - L_B$ between values of a quantity associated to the use of TCB and TDB; there are several options, such as scaling only the units, scaling only the values, or scaling both, out of which the two most logical possibilities would be:

- option 1: $k^2 = GM_{\rm Sun}$ has the same value with both TCB and TDB, which requires scaling the units of time and length; thus, we would have:
  . for the "unit distance": $\mathrm{ua_{TDB}} = F^{1/3}\ \mathrm{ua_{TCB}}$,
  . for the distance: TDB-compatible value in $\mathrm{ua_{TDB}}$ $=$ $F^{2/3}\times$ TCB-compatible value in $\mathrm{ua_{TCB}}$,
  which would be very confusing because of the unusual scaling;
- option 2: $\mathrm{ua_{TDB}}$ =$\mathrm{ua_{TCB}}$; this requires:
  . for the distance in astronomical units: TDB-compatible value = $F\times$ TCB-compatible value,
  but then $GM_{\rm Sun}$ in astronomical units is no longer k^2 either with TDB or with TCB, which kills the uniqueness of the Gaussian constant k.

This shows that relativity makes the usual definition of the ua even trickier. It would then be better to avoid extending that definition to the GR framework.

5. THE PROPOSAL FOR THE RE-DEFINITION OF THE UA

As already suggested before the 2009 IAU General assembly (Klioner 2008; Capitaine & Guinot 2009), it is proposed to re-define the ua as a fixed number of SI metres through a defining constant.

This would mean:

- dropping the k constant and abandoning the experimental determination of the ua in SI unit,
- determining experimentally $GM_{\rm Sun}$.

Such a change of status for the ua would limit its role to that of a unit of length of "convenient" size for some applications.

Note that defining the ua as a conventional number of metres is in accordance with the adopted way (Klioner et al. 2009) to use the SI units for the relativistic time scales and associated quantities, so that for distances in astronomical units one simply has: TDB-compatible value = $F\times$ TCB-compatible value.

The defining number to be adopted for the conventional definition of the ua should be, for continuity reason, the value for the current best estimate of the ua in m as adopted by IAU 2009 Resolution B2 (i.e. ua = 1.495 978 707 00 x 10^{11} m exactly).

Note also that the CCU declared (CCU 2009) its support to move to a fixed relationship to the SI metre through a defining number determined by continuity.

6. CONCLUSION

A re-definition of the ua is necessary in the modern context in order to make the system of astronomical constants best compliant with modern dynamical astronomy. From the point of view of the principles, the important point is the change of status for the astronomical unit of length (and not the value of its defining number).

Such a change of status of the ua:

- would be a great simplification for the users of the astronomical constants,
- will let possible variations of the mass of the Sun (and/or G) to appear directly (which is the option that has the most physical meaning), and would avoid an unnecessary deviation from the SI.

This should be largely discussed within the astronomical community in order to be proposed at the next IAU GA (2012).

7. REFERENCES

Brumberg, V. A., Simon, J.-L., 2004, Proceedings of the Journées 2003 "Systèmes de référence spatio-temporels", A. Finkelstein & N. Capitaine (eds), pp. 302–313.

Capitaine, N., Guinot, B., 1995, "Astronomical units and constants in a relativistic framework", Highlights of Astronomy, Vol 10, IAU, 1994, I. Appenzeller (ed), 201.

Capitaine, N., Guinot, B., 2009, "The astronomical units, Proceedings of the "Journées 2008 Systèmes de référence spatio-temporels", M. Soffel and N. Capitaine (eds.), Lohrmann-Observatorium and Observatoire de Paris, pp 73–74.

CCU 2009: Report of the 19th meeting (26-28 May 2009) to the International Committee for Weights and Measures Comitínternational des poids et mesures (`http://www.bipm.org/en/committees/cc/ccu/publications_cc.html`).

CODATA, (`http://physics.nist.gov/cuu/Constants/index.html`, (2006).

Fienga, A., Laskar, J., Morley, T., Manche, H. et al., 2009, "INPOP08: a 4D-planetary ephemeris", A&A 507, 3, 1675–1686.

Folkner W.M., Williams J.G., Boggs D.H., 2008, Memorandum IOM 343R-08-003, Jet Propulsion Laboratory.

Folkner, W.M., 2008, e-mails NFSA WG discussion (04/06/2008).

Guinot B., 1995, "Le système international d'unités (SI) et les unités astronomiques", Proc. Journées 1994 "Systèmes de référence spatio-temporels", N. Capitaine (ed), 21–30.

Huang T.-Y., Han C.-H., Yi Z.-H., Xu B.-X., 1995, "What is the astronomical unit of length?", A&A 298, 629–633.

IERS Conventions (2003), IERS Technical Note 32, D.D. McCarthy and G. Petit (eds), Frankfurt am Main: Verlag des Bundesamts für Kartographie und Geodäsie, 2004.

Klioner S., 2008, "Relativistic scaling of astronomical quantities and the system of astronomical units", A&A 478, 951–95.

Klioner, S. A., Capitaine, N., Folkner, W. M., Guinot, B., Huang, T.-Y., Kopeikin, S. M., Pitjeva, E. V., Seidelmann, P. K., Soffel, M. H., "Units of relativistic time scales and associated quantities", in Relativity in Fundamental Astronomy: Dynamics, Reference Frames, and Data Analysis, Proceedings of the IAU Symposium, Volume 261, p. 79-84.

Luzum, B., Capitaine, N., Fienga, A., Folkner, W., Fukushima, T., Hilton. J., Hohenkerk, C., Krasinsky, G., Petit, G., Pitjeva, E., Soffel, M., Wallace, P., 2011, "The IAU 2009 system of astronomical constants: the report of the IAU Working Group on Numerical Standards for Fundamental Astronomy," Celest. Mech. Dyn. Astr. 110, 293–304.

Pitjeva, E.V., 2005, "High-Precision Ephemerides of Planets EPM and Determination of Some Astronomical Constants", Solar System Research, Volume 39, Issue 3, pp. 176–186.

Pitjeva, E.V. and Standish, E.M., "Proposals for the masses of the three largest asteroids, the Moon-Earth mass ratio and the astronomical unit," Celest. Mech. Dyn. Astr., 103, pp. 365–372, doi: 10.1007/s10569-009-9203-8, (2009).

Standish E.M. 1995, "Report of the IAU WGAS Sub-Group on Numerical Standards", Highlights of Astronomy, Vol 12, IAU 1994, Appenzeller, I. (ed), 180.

Standish E.M., 2005, "The Astronomical Unit now", in "Transits of Venus, New views of the Solar System and Galaxy", Proc. IAU Coll. 196, D.W. Kurtz (ed), pp. 163–179.

SOME NEW THOUGHTS ABOUT LONG-TERM PRECESSION FORMULA

J. VONDRÁK[1], N. CAPITAINE[2], P. WALLACE[3]

[1]Astronomical Institute, Acad. Sci. Czech Rep.
Boční II, 141 31 Prague 4, Czech Republic
e-mail: vondrak@ig.cas.cz

[2] Observatoire de Paris, SYRTE/UMR8630-CNRS
61, Ave. de l'Observatoire, 75014 Paris, France
e-mail: n.capitaine@obspm.fr

[3] STFC / Rutherford Appleton Laboratory
Harwell Science and Innovation Campus, Didcot, Oxfordshire OX11 0QX, UK
e-mail: patrick.wallace@stfc.ac.uk

ABSTRACT. In our preceding study (Vondrák et al. 2009) we formulated developments for the precessional contribution to the CIP X, Y coordinates suitable for use over long time intervals. They were fitted to IAU 2006 close to J2000.0 and to the numerical integration of the ecliptic (using the integrator package Mercury 6) and of the general precession and obliquity (using Laskar's solution LA93) for more distant epochs. Now we define the boundary between precession and nutation (both are periodic) to avoid their overlap. We use the IAU 2006 model (that is based on the Bretagnon's solution VSOP87 and the JPL planetary ephemerides DE406) to represent the precession of the ecliptic close to J2000.0, a new integration using Mercury 6 for more distant epochs, and Laskar's LA93 solution to represent general precession and obliquity. The goal is to obtain new developments for different sets of precession angles that would fit to modern observations near J2000.0, and at the same time to numerical integration of the translatory-rotatory motions of solar system bodies on scales of several thousand centuries.

1. INTRODUCTION

This is a continuation of our preceding study (Vondrák et al. 2009) in which we demonstrated that all models of precession in use, including the most recent one, IAU 2006 (Capitaine et al. 2003, Hilton et al. 2006), lose their accuracy rapidly in time, being expressed in terms of polynomial development, no matter which precession parameters are used. The IAU 2006 model is very accurate, but usable only for a limited time interval (several centuries around the epoch J2000.0); its errors however rapidly increase with longer time spans. In reality, precession is a complicated, very long-periodic process, with periods of hundreds of centuries. This can be seen in numerically integrated equations of motion of the Earth in the solar system and of its rotation.

Here we assume that precession covers all periods longer than 100 centuries; shorter ones are included in the nutation. In this connection, it is necessary to mention that the IAU 2000 model of nutation includes several terms with longer periods: 105 cy, 209 cy for the luni-solar terms and 933 cy, 150 cy, 129 cy, 113 cy for the planetary terms. The amplitudes of these terms are however very small (lower than 4 mas for one term and lower than 0.1 mas for the others).

The goal of the present study is to find relatively simple expressions for different precession parameters, with accuracy comparable to the IAU 2006 model near the epoch J2000.0, and useful accuracy outside the interval ±10 cy (a few arcminutes at the extreme epochs ±2000 cy).

2. NUMERICAL INTEGRATIONS

Here we use the following numerical integrations as a basis for all subsequent calculations:

- For the precession of the ecliptic (parameters $P_A = \sin\pi_A \sin\Pi_A$, $Q_A = \sin\pi_A \cos\Pi_A$) the new integration of the solar system motion, using the package Mercury 6 (Chambers 1999), in interval

±2000 cy from J2000.0, with 1-day steps. The elements of the Earth's orbit are then smoothed and interpolated with 1-cy steps.

- For the general precession and obliquity (parameters p_A, ϵ_A) the integration LA93 by Laskar et al. (1993) in the interval ±1 million years, with 10-cy steps, interpolated in 1-cy steps. Additional corrections are applied to account for: slightly different values of the dynamical ellipticity (compatible with the IAU 2006 model) and its secular change $\dot{J}_2$, constant and secular tidal change of the obliquity.

In both cases, inside the interval ±10 cy around J2000.0 the integrated values are replaced with the values computed from the IAU 2006 model which, in turn, is based on Bretagnon's semi-analytical theory VSOP87 (Bretagnon 1987) and JPL DE406 (Standish 1998) ephemerides.

The relations of the four above mentioned angles to other parameters describing precession are shown in Fig. 1. To calculate different precession parameters, we obtain first the auxiliary angles α, β, γ from the triangle $\Upsilon\Upsilon_o$N, and then the angles φ, δ by solving the triangle $\Upsilon\Upsilon_o P_t$ (see Vondrák et al. 2009).

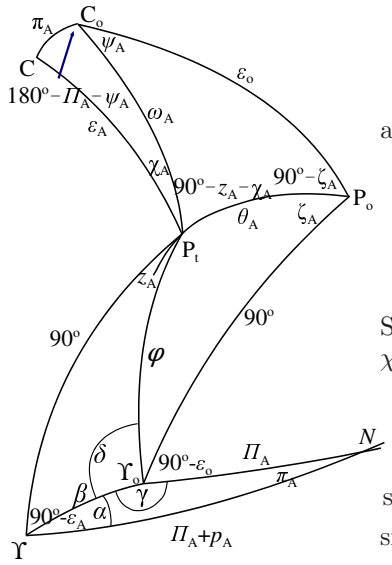

From the triangle $\Upsilon_o P_t P_o$ follow precession parameters θ_A, ζ_A

$$\begin{aligned} \cos\theta_A &= -\sin\varphi\sin(\gamma+\delta-\varepsilon_\circ) \\ \sin\theta_A\sin\zeta_A &= -\sin\varphi\cos(\gamma+\delta-\varepsilon_\circ) \\ \sin\theta_A\cos\zeta_A &= \cos\varphi, \end{aligned} \tag{1}$$

and the triangle $P_o P_t C_o$ then yields precession parameters ω_A, ψ_A:

$$\begin{aligned} \cos\omega_A &= \cos\varepsilon_\circ\cos\theta_A + \sin\varepsilon_\circ\sin\theta_A\sin\zeta_A \\ \sin\omega_A\sin\psi_A &= \sin\theta_A\cos\zeta_A \\ \sin\omega_A\cos\psi_A &= \sin\varepsilon_\circ\cos\theta_A - \cos\varepsilon_\circ\sin\theta_A\sin\zeta_A. \end{aligned} \tag{2}$$

Solving the triangles $P_t C C_o$, $P_o P_t C_o$ we finally obtain the parameters χ_A, z_A:

$$\begin{aligned} \sin\varepsilon_A\sin\chi_A &= P_A\cos\psi_A + Q_A\sin\psi_A \\ \sin\varepsilon_A\cos\chi_A &= \cos\pi_A\sin\omega_A - (P_A\sin\psi_A - Q_A\cos\psi_A)\cos\omega_A \\ \sin\theta_A\sin(z_A+\chi_A) &= \sin\omega_A\cos\varepsilon_\circ - \cos\omega_A\sin\varepsilon_\circ\cos\psi_A \\ \sin\theta_A\cos(z_A+\chi_A) &= \sin\varepsilon_\circ\sin\psi_A. \end{aligned} \tag{3}$$

Figure 1: Precession parameters

We used these formulas to calculate all above defined precession parameters in the interval ±2000 cy with 1-cy steps. Since the pole coordinates X, Y are referred to the GCRS rather than the mean equator and equinox of J2000.0, they require small additional corrections to account for displacements of the celestial pole and equinox (see Eq.(3) in Vondrák et al. 2009).

3. ANALYTICAL APPROXIMATION

To find the long-term analytical approximation of precession parameters, we apply the following steps:

- Spectral analysis of integrated values is done, using a modified Vaníček method (Vondrák 1977);
- Periods found are identified with those found by Laskar et al. (1993, 2004). In positive cases, Laskar's values are adopted;
- Sine/cosine amplitudes of the terms found in preceding step, plus cubic parabola, are fitted to the numerical integration. The weights used in the fit are very high close to J2000.0, and they decrease quadratically with time;
- Small additional corrections are applied to the constant, linear and quadratic terms, so that the function value and first two derivatives are identical with those of the IAU 2006 model.

Here we show long-term expressions for only some of the precession parameters and their comparison with both integrated values and the IAU 2006 model. In these examples, T is the time in Julian centuries, running from J2000.0, and periodic terms have the general form $\sum(C_i \cos 2\pi T/P_i + S_i \sin 2\pi T/P_i)$.

Table 1: Periodic terms in ψ_A, ω_A

term	C/S	ψ_A[″]	ω_A[″]	P[cy]
$p+\nu_6$	C_1	-22420.160932	1314.679626	402.90
	S_1	-3354.740507	-8658.248888	
p	C_2	12364.867916	1698.164478	256.75
	S_2	-3953.468853	5359.936261	
	C_3	-1855.311803	-2946.745615	292.00
	S_3	7053.538527	-717.285550	
$p+s_6$	C_4	2501.910635	691.170703	537.22
	S_4	-1895.196678	931.408851	
$p+g_2-g_5$	C_5	111.451479	-14.110991	241.45
	S_5	143.109393	-12.736900	
	C_6	70.863565	-534.673649	375.22
	S_6	1343.619428	-6.985495	
$2p+s_3$	C_7	389.332023	-356.790963	157.87
	S_7	1727.488574	77.098670	
	C_8	2128.481251	-142.160739	275.90
	S_8	316.951469	846.285243	
	C_9	368.139198	256.137565	203.00
	S_9	-1217.037602	83.329986	
	C_{10}	-785.264907	162.716848	445.90
	S_{10}	-407.953884	-324.406028	
	C_{11}	-927.251157	95.138364	170.72
	S_{11}	-441.696960	-193.842226	
	C_{12}	35.623831	-332.752312	713.37
	S_{12}	-87.277001	-5.493032	
	C_{13}	-521.921176	124.581532	313.90
	S_{13}	-295.259639	-240.668180	
	C_{14}	66.351105	82.685046	128.38
	S_{14}	-422.734446	18.984123	

Long-term expressions for the precession angles ψ_A, ω_A, are given as

$$\begin{aligned} \psi_A &= 8472.888973 + 5042.8012257T - \\ &- 0.00740773T^2 + 285\times10^{-9}T^3 + \textstyle\sum_\psi \\ \omega_A &= 84283.366108 - 0.4449631T + \\ &+ 0.00000068T^2 + 150\times10^{-9}T^3 + \textstyle\sum_\omega, \end{aligned} \qquad (4)$$

where the cosine/sine amplitudes of the periodic parts $\sum_\psi$, $\sum_\omega$ are given in Table 1. The comparison of the long-term model of precession angles ψ (reduced by a conventional rate $5045''$/cy, in order to see more details) and obliquity, $\psi_A - 5045''T$ (top), ω_A (bottom) is shown in Fig. 2a, in which the vertical scale is in arcseconds.

The curves representing the new model and integrated values in Fig. 2 (full and dotted lines, respectively) are very close so that they are graphically indistinguishable. The IAU 2006 precession model (dashed line) fits well to both integrated values and new model near the epoch J2000.0, but it diverges rapidly from both of them for more distant epochs.

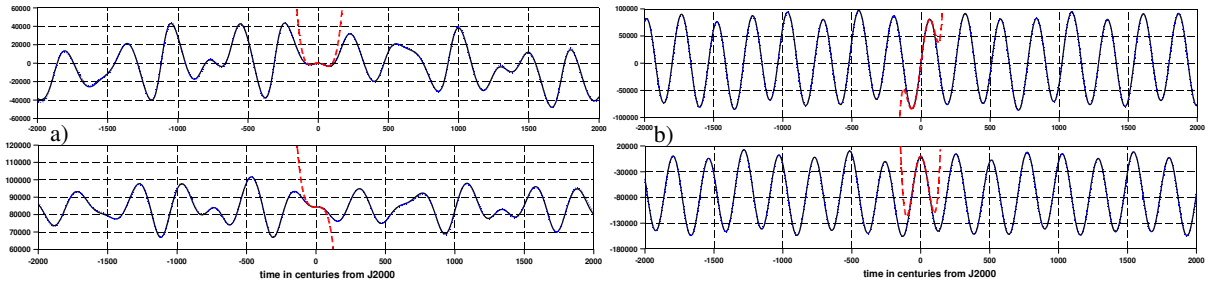

Figure 2: Long-term models of parameters a) ψ_A, ω_A, b) X, Y

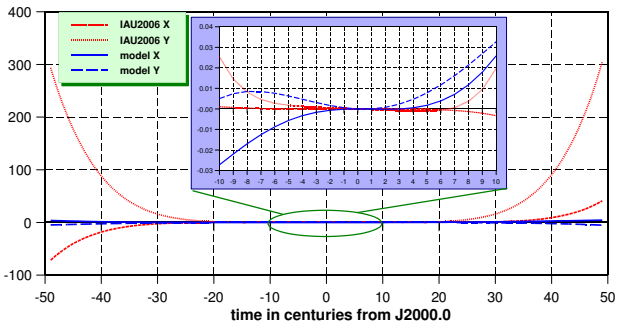

Closeups of the differences between the IAU 2006 and long-term models from the integrated values are depicted in Fig. 3; differences in X, Y of the IAU 2006 model are shown as short dashed and dotted lines, the differences of the long-term model as full and long dashed lines. The vertical scales are again in arcseconds.

Figure 3: Comparison of X, Y values - closeups

Table 2: Periodic terms in X, Y

term	C/S	$X[''']$	$Y[''']$	P[cy]
p	C_1	-819.946005	75004.345355	256.75
	S_1	81491.288050	1558.521633	
σ_3	C_2	-8444.676986	624.033815	708.15
	S_2	787.162943	7774.939774	
$p - g_2 + g_5$	C_3	2600.009737	1251.136728	274.20
	S_3	1251.296938	-2219.533890	
$p + g_2 - g_5$	C_4	2755.175572	-1102.213989	241.45
	S_4	-1257.951746	-2523.969336	
s_1	C_5	-167.659179	-2660.663565	2309.00
	S_5	-2966.800362	247.850562	
s_6	C_6	871.855033	699.292008	492.20
	S_6	639.744569	-846.485543	
$p + s_4$	C_7	44.769702	153.167261	396.10
	S_7	131.600315	-1393.123929	
$p + s_1$	C_8	-512.313270	-950.865460	288.90
	S_8	-445.040719	368.526188	
$p - s_1$	C_9	-819.415456	499.756007	231.10
	S_9	584.524115	749.044958	
	C_{10}	-538.071710	-145.189989	1610.00
	S_{10}	-89.756178	444.704321	
	C_{11}	-189.793616	558.115977	620.00
	S_{11}	524.429711	235.934536	
$2p + s_3$	C_{12}	-402.922967	-23.923094	157.87
	S_{12}	-13.549103	374.049112	
	C_{13}	179.516279	-165.405552	220.30
	S_{13}	-210.157617	-171.329809	
	C_{14}	-9.814377	9.344900	1200.00
	S_{14}	-44.920033	-22.899576	

Long-term expressions for the precession angles X, Y, are given as

$$\begin{aligned} X &= 5453.270624 + 0.4252850T - \\ &- 0.00037173T^2 - 152 \times 10^{-9}T^3 + \sum_X \\ Y &= -73750.937353 - 0.7675456T - \\ &- 0.00018725T^2 + 231 \times 10^{-9}T^3 + \sum_Y, \end{aligned} \quad (5)$$

where the cosine/sine amplitudes of the periodic parts X, Y are given in Table 2. The comparison of the long-term model of precession angles X (top) and Y (bottom) is shown in Fig. 2b, in arcseconds.

4. CONCLUSIONS

The present study demonstrates the possibility of constructing a new model of precession that is equivalent to the most recent IAU model of precession in a short-term sense (up to several centuries around J2000.0) and, at the same time, fitting well to modern long-term numerical integrations of the motions of the solar system bodies. The accuracy of this solution is improved, with respect to Vondrák et al. (2009), mainly in the long-term precession of the ecliptic. The long-term expressions are valid only in the interval ±2000 cy from J2000.0; outside this interval their validity rapidly deteriorates. This limitation not only reduces the necessary number of periodic terms, but also avoids the problem of resonances in the solar system mentioned by Laskar et al. (2004). We also derived the expressions for all other precession parameters that are not presented here due to the page limit, but they are available on request from the first author.

Acknowledgements. This study was supported by the grant LC506 awarded by the Ministry of Education, Youth and Sports of the Czech Republic.

5. REFERENCES

Capitaine, N., Wallace, P.T. and Chapront, J., 2003, "Expressions for IAU 2000 precession quantities", A&A , 412, pp. 567–586.

Chambers, J.E., 1999, "A hybrid symplectic integrator that permits close encounters between massive bodies", MNRAS , 304, pp. 793-799.

Bretagnon, P. and Francou, G., 1988, "Planetary theories in rectangular and spherical variables. VSOP87 solutions.", A&A , 202, pp. 309-315.

Hilton, J., Capitaine, N., Chapront, J., Ferrándiz, J.M., Fienga, A., Fukushima, T., Getino, J., Mathews, P., Simon, J.-L., Soffel, M., Vondrák, J., Wallace, P., Williams, J., 2006, "Report of the International Astronomical Union Division I Working Group on Precession and the Ecliptic", Celest. Mech. Dyn. Astr. , 94, pp. 351-367.

Laskar, J., Joutel, F. and Boudin, F., 1993, "Orbital, precessional, and insolation quantities for the Earth from −20 Myr to +10 Myr", A&A , 270, pp. 522-533.

Laskar, J., Robutel, P., Joutel, F., Gastineau, M., Correia, A.C.M. and Levrard, B., 2004, "A long-term numerical solution for the insolation quantities of the Earth", A&A , 428, pp. 261–285.

Standish, E.M., 1998, "JPL Planetary and Lunar Ephemerides, DE405/LE405", JPL IOM 312, F-98-048.

Vondrák, J., 1977, "The rotation of the Earth between 1955.5 and 1976.5", Studia Geopys. Geod. 21, pp. 107-117.

Vondrák, J., Capitaine, N., Wallace, P.T., 2009, "Towards a long-term parametrization of precession", in: M. Soffel, N. Capitaine (eds.) Journées 2008 Systèmes de référence spatio-temporels, Lohrmann Observatorium Dresden and Observatoire de Paris, pp. 23-26.

FROM OLD WEIGHTS AND MEASURES TO THE SI AS A NUMERICAL STANDARD FOR THE WORLD

S. DÉBARBAT, I. PASSERON, F. LAUNAY

SYRTE, Observatoire de Paris, CNRS, UPMC,
61, avenue de l'Observatoire, 75014 – Paris, France
e-mail: suzanne.debarbat@obspm.fr; irene.passeron@obspm.fr; francoise.launay@obspm.fr

ABSTRACT. After the efforts made by Charlemagne to unify weights on the one hand, and measures on the other hand, Picard was most probably the first in France to submit a proposal for a new system based on a unit linking up length and time through the second-pendulum. Despite further proposals, it was not before the end of the 18th century, one century after Picard, that the *Système métrique décimal* was adopted, with the *Mètre* as a fundamental standard. Almost one more century later, by 1960, the SI was decided at the international level and, by 1983, a new definition of the metre was decided, eventually linking up length and time.

1. AT THE BEGINNING: A DESIRE OF STANDARDIZATION

Pondere, numero et mensura "with weight, number and measure": this formulation often introduces a rational explanation of the world. But it also shows a will for political and economical power over the world through the control of possessions, human activities and exchanges. The desire to speak the same language grew with centralization and intensification of commercial exchanges.

Charlemagne was most probably among the firsts to attempt to unify weights and measures (789), due to his position in Europe: *Roi des Francs* (768) and finally *Empereur d'Occident* (800). He has put his name to the *pié de Charlemagne* for measuring lengths (human standards like the foot have been used from the beginning of metrology) and to the *pile de Charlemagne* for measuring weights.

Colbert (1619-1683) tried in vain to standardize weights and measures in all French ports. He founded the *Académie Royale des Sciences* of Paris whose main purpose was to measure the territory of France.

One of its members, Jean Picard (1620-1682), who had taken part in determining the dimensions of the Earth using astronomical observations and a one-second pendulum clock, suggested that the very length of the pendulum of this clock become the new standard for measuring lengths in France.

1669-1670: Picard designed a portable quadrant and used it for geodesic measurements along the recently fixed *Méridien of the Observatoire Royal* founded by Louis XIV in 1667. The measurements of a part of this meridian provided him the dimensions of the Earth. This meridian was measured later by the Cassinis with a better precision. It was chosen for the expedition of Delambre and Méchain, which gave eventually the length adopted in 1799 for the "*Mètre étalon*".

1720: Another French astronomer, Jacques Cassini (1677-1756), suggested linking the unit of length to the measurement of the Earth by creating the *pied géométrique*, which was equal to one hundredth of the length of an arc of 1" of the meridian, and was not affected by the gravity, as the period of the pendulum was.

Two expeditions were sent by Louis XV, one to Lapland (1736-37), close the North Pole, and the other to Ecuador (1735-1744), to determine the length of the meridian of the Earth, a universal measurement, by astronomical and geodesic observations.

The *Encyclopédie ou Dictionnaire raisonné des sciences, des arts et des métiers* (Diderot et D'Alembert, 1751-1765, established after the model of the English *Cyclopædia*) was the greatest editorial venture of the Age of Enlightenment; it intended to be the best compilation of the products of reason and human ingenuity. The entries for "Mesure" and "Poids" show the diversity of length and weight measures used in different places and times. On the other hand, throughout his mathematical articles, D'Alembert showed the power of geometry and analysis, especially for measuring the figure of the Earth ("Figure de la Terre" entry).

2. THE REVOLUTION

All these considerations explain why, together with domestic and foreign trade difficulties, the French Revolution succeeded in promoting the "mètre" as the fundamental unit for the "Système métrique décimal", its major quality being its decimal character. After discussion, in 1791 March 30, the ten-millionth part of a quarter of meridian was chosen by the French Academy of Sciences, as more universal than the other proposals.

The successive values of the length of the "mètre étalon" (standard meter) able to represent $1/10^7$ of a quarter of a terrestrial meridian are now given with some important dates:

1799 December 10: After the expedition led by Delambre and Méchain to obtain more accurate measurements, the *mètre* was definitely fixed as being equal to "3 pieds 11 lignes deux cent quatre-vingt-seize millièmes" of the *Toise du Pérou* (i.e. 443.296 *lignes* since there were 6 *pieds* in a *Toise*, and 144 lignes in a *pied*), a little more than half a French *Toise* (1.9484m). The yard was 0.914m.

1812: Going backwards, a Napoleonic decree set that *1 toise = 2 mètres*; *1 aune = 1.20 mètre*; there were thus 3 *pieds* in a *mètre*. What a confusion!

1837: a law enjoined to have the metric system as a unique and legal one from 1840 January 1. Victor Hugo was then able to make jokes in "*argot légal*" (legal slang).

3. THE STANDARDIZATION

1875 May 28: The *Conférence diplomatique du mètre* leading to the *Convention du mètre* and the *Bureau international des poids et mesures* (BIPM) was installed in 1876 in the Pavillon de Breteuil, at Sèvres (south-west of Paris). The "mètre international étalon" (90% platinum, 10% iridium), with an X section, was made. The original was left at the BIPM, while replicas were provided to all the participating countries for their national depots. The length of reference was the distance between the gravity centres of three lines etched on both ends of the metallic pieces at a small distance from the edges. Several institutions were successively created: Commission for the System of Units, ancestor of the *Comité consultatif des unités* (CCU), *Comité international des poids et mesures* (CIPM), *Conférence générale des poids et mesures* (CGPM), the highest authority in the field.

1960 October 14: The *Système international d'unités* (SI) was fixed; it was based on the "Système métrique décimal" created during the French Revolution. All the successive realizations of the "mètre étalon" had to be consistent with the 1799 value. In the SI system, the length of the *Mètre* is equal to 1 650 763.73 vacuum wavelengths of the orange-red emission line in the electromagnetic spectrum of the krypton-86 atom.

1983 October 20: "*Le mètre est la longueur du trajet parcouru dans le vide par la lumière pendant la durée de 1/299 792 458 seconde*" (the distance covered by light in vacuum in ...). The *Laboratoire primaire du temps et des fréquences* (nowadays the LNE/SYRTE), is one of the five laboratories which has contributed to the value chosen for the velocity of light. This decision relates time and length similarly to Picard's proposal.

2010: Fifty years later, there are still people saying that the length of the *Mètre étalon* is in error when compared to the value obtained from measurements of the distance Dunkerque-Barcelona made nowadays, with GPS. Such a false consideration has a long story, dating back to the decision taken by the end of the 18th century. Since that time, each time a new measurement is made, with more accurate instruments, methods or techniques, it is said that the "mètre" is based on some error, from calculations or measurements. It must not be forgotten than the length of the "mètre" is a convention decided in 1799, based on a will of standardization framed by a symbolic search of universality. It was then decided, and this decision was confirmed by the Bureau des longitudes (the French Board of Longitudes) by mid-19th century, that the 1799 length of the *mètre* will never change, having been fixed according to the *Toise du Pérou*, which is nowadays preserved in the collections of the Observatoire de Paris, as an historical and material proof.

AN INERTIAL EFFECT IN SATELLITE MOTION NOT DESCRIBED BY THE CURRENT IERS CONVENTIONS

S.M. KUDRYAVTSEV

Sternberg Astronomical Institute of Moscow State University
13, Universitetsky Pr., Moscow, 119992, RUSSIA
e-mail: ksm@sai.msu.ru

ABSTRACT. We recall a known inertial effect in satellite motion caused by the indirect acceleration of the center of integration (the central planet) due to the oblateness of the planet and an attracting third-body. As estimated, the effect leads to perturbations in satellite motion to be well detectable by the modern tools of measuring the satellite orbital parameters. However, the effect is not described by the current IERS Conventions (2003); we suggest to include it to the future IERS Conventions (2010).

1. FORMULATION OF THE EFFECT

Let's consider the motion of an artificial satellite T_1 in the gravitational fields of the oblate central planet T_0 and an attracting oblate third-body T_2. The gravitational potential between T_0 and T_2 is

$$U_{02} = f \iiint_{T_0} dm_0 \iiint_{T_2} \frac{dm_2}{r''_{20}}, \tag{1}$$

where r''_{20} is the distance between an elementary mass dm_2 of the body T_2 and an elementary mass dm_0 of the body T_0, and f is the gravitational constant.

The Eq. (1) can be expanded as follows

$$\begin{aligned} U_{02} &= f\frac{M_0 M_2}{r_{02}}\left\{1 + \sum_{n=2}^{\infty}\sum_{m=0}^{n}\left(\frac{R_0}{r_{02}}\right)^n P_{nm}(\sin\phi_{02})\left[C^{(0)}_{nm}\cos m\lambda_{02} + S^{(0)}_{nm}\sin m\lambda_{02}\right]\right. \\ &+ \left.\sum_{n=2}^{\infty}\sum_{m=0}^{n}\left(\frac{R_2}{r_{20}}\right)^n P_{nm}(\sin\phi_{20})\left[C^{(2)}_{nm}\cos m\lambda_{20} + S^{(2)}_{nm}\sin m\lambda_{20}\right] + O\left(C^{(2)}_{20}\frac{R_2^2 R_0}{r_{20}^3}\right)\right\}, \end{aligned} \tag{2}$$

where hereafter r_{ij}, ϕ_{ij}, λ_{ij} are spherical coordinates of the mass center of body T_j in the reference frame of body T_i; $C^{(i)}_{nm}$ and $S^{(i)}_{nm}$ are the coefficients of the expansion of gravitational potential of body T_i in spherical functions; M_i, R_i are the mass and mean equatorial radius of body T_i; P_{nm} are associated Legendre polynomials, and $i, j = 0, 1, 2$.

Then the motion equations of the artificial satellite T_1 in an inertial reference frame are as follows.

$$\ddot{x}_{01} \equiv \ddot{x}_1 - \ddot{x}_0 = -fM_0\frac{x_{01}}{r_{01}^3} + fM_2\left(\frac{x_{02}-x_{01}}{r_{21}^3} - \frac{x_{02}}{r_{20}^3}\right) + \frac{\partial R_{01}}{\partial x_{01}} + \frac{\partial R_{21}}{\partial x_{21}} + \frac{\partial R_{02}}{\partial x_{02}} - \frac{\partial R_{20}}{\partial x_{20}}, \tag{3}$$

where

$$R_{01} \equiv fM_0\frac{1}{r_{01}}\left\{\sum_{n=2}^{\infty}\sum_{m=0}^{n}\left(\frac{R_0}{r_{01}}\right)^n P_{nm}(\sin\phi_{01}) \times \left[C^{(0)}_{nm}\cos m\lambda_{01} + S^{(0)}_{nm}\sin m\lambda_{01}\right]\right\}, \tag{4}$$

$$R_{21} \equiv fM_2\frac{1}{r_{21}}\left\{\sum_{n=2}^{\infty}\sum_{m=0}^{n}\left(\frac{R_2}{r_{21}}\right)^n P_{nm}(\sin\phi_{21}) \times \left[C^{(2)}_{nm}\cos m\lambda_{21} + S^{(2)}_{nm}\sin m\lambda_{21}\right]\right\}, \tag{5}$$

$$R_{02} \equiv fM_2\frac{1}{r_{02}}\left\{\sum_{n=2}^{\infty}\sum_{m=0}^{n}\left(\frac{R_0}{r_{02}}\right)^n P_{nm}(\sin\phi_{02}) \times \left[C^{(0)}_{nm}\cos m\lambda_{02} + S^{(0)}_{nm}\sin m\lambda_{02}\right]\right\}, \tag{6}$$

$$R_{20} \equiv fM_2 \frac{1}{r_{20}} \left\{ \sum_{n=2}^{\infty} \sum_{m=0}^{n} \left(\frac{R_2}{r_{20}} \right)^n P_{nm} (\sin \phi_{20}) \times \left[C_{nm}^{(2)} \cos m\lambda_{20} + S_{nm}^{(2)} \sin m\lambda_{20} \right] \right\}, \quad (7)$$

and x_i is Cartesian x-coordinate of body T_i in the inertial reference frame; $x_{ij} \equiv x_j - x_i$.

The last two summands in the right-hand side of Eq. (3) describe the inertial terms in satellite motion caused by the additional accelerations of the central planet due to oblateness of the planet and that of the third-body, respectively. The corresponding expressions for accelerations $\ddot{y}_{01}$ and $\ddot{z}_{01}$ of the other two Cartesian coordinates of the satellite are similar to Eq. (3). Also, from Eq. (6) one can conclude that the inertial term caused by the Moon attraction on the oblate Earth is some 10^3 times more than a similar term caused by the Sun attraction.

2. DISCUSSION OF THE EFFECT

Table 1 presents the effect of the considered inertial terms in Keplerian elements of the LAGEOS and ETALON geodynamical satellites over one year interval. The effect is periodic; variations of maximum amplitude has a period close to that of the lunar orbital motion. Here a, e, ω are the semimajor axis, eccentricity and argument of satellite perigee, respectively; $(e\cos\omega, e\sin\omega)$ is the eccentricity vector.

Satellite	Start of time interval	$\Delta e \times a$ [cm]	$e\Delta\omega \times a$ [cm]	$\frac{\partial}{\partial t}(e\cos\omega)$ [mas/yr]	$\frac{\partial}{\partial t}(e\sin\omega)$ [mas/yr]
LAGEOS-1	1988/01/07	3	6	28	29
LAGEOS-2	1993/01/01	7	5	30	29
ETALON-1	1992/06/01	15	25	32	41
ETALON-2	1992/06/01	27	13	38	44

Table 1: Maximum variations in satellite Keplerian elements due to the inertial effect.

One sees the discussed effect is large enough to be detectable by the current tools of measuring the satellite orbital parameters, e.g. by laser technique. This "indirect oblateness effect" is known in the satellite dynamics in that or another form since the beginning of spaceflights (Sturms 1964, Moyer 1971). However, the current IERS Conventions (McCarthy and Petit 2004) do not describe the corresponding inertial terms. The online documentation of the advanced GEODYN II system for satellite orbit determination (Pavlis et al. 2010) does not mention the discussed terms as well, although the software itself does take them into account (Rowlands 2010, private communication).

The IERS Conventions are very detailed in describing the satellite force model, and for long time are deservedly a standard for developers of satellite dynamics software. The absence of the inertial terms in this standard might mislead its potential users, therefore we suggest to include a description of these terms to the future IERS Conventions (2010).

Acknowledgements. Research supported in part by the Russian Foundation for Basic Research under grant no. 10-02-00234-a. A travel grant provided to the author by the LOC of the Journées 2010 and the French Ministry of Research (MESR) in the framework of the programme ACCES is sincerely appreciated.

3. REFERENCES

McCarthy, D.D., Petit, G. (eds.), "IERS Conventions (2003)", 2004, IERS Technical Note 32, Frankfurt am Main: Verlag des Bundesamts für Kartographie und Geodäsie.

Moyer, T.D., 1971 "Mathematical Formulation of the Double-Precision Orbit Determination Program (DPODP)" Technical Report 32-1527, Jet Propulsion Laboratory, Pasadena, CA.

Pavlis, D.E., Rowlands, D.D., et al., 2010, "GEODYN II Systems Description", Vol.1, NASA Goddard, Greenbelt, MD. http://terra.sgt-inc.com/geodyn.

Sturms, F.M., Jr., 1964, "Equations of Motion for a Double-Precision Trajectory Program", in Supporting Research and Advanced Development, Space Programs Summary 37-29, Vol. IV, pp. 1-6, Jet Propulsion Laboratory, Pasadena, CA.

Session 2

SOLAR SYSTEM EPHEMERIDES AND THEIR COMPARISON

EPHÉMÉRIDES DU SYSTÈME SOLAIRE ET LEUR COMPARAISON

INTRODUCTORY REMARKS FOR SESSION 2

G. H. KAPLAN
President, IAU Commission 4 (Ephemerides)
e-mail: gk@gkaplan.us

ABSTRACT. Three institutions are now providing high-quality fundamental solar system ephemerides to the astronomical community. This session presents some important new information on how the ephemerides from all three groups are constructed, and how they compare with each other. These kinds of comparisons are essential in improving solar system ephemerides generally and understanding their limitations.

Since the 1960s, there has been a continuing need to develop ever more accurate representations of the motions of the planets, their satellites, and the Moon, due to the requirements of spacecraft navigation and the continued development of high-precision observational techniques like radar ranging, LLR, pulsar timing, and VLBI. Indeed, the accuracy of the best observations currently exceeds our modeling capabilities — we simply don't have good mass estimates for the huge number of small bodies in the solar system — so that new ephemerides must be constantly recomputed to meet the latest requirements.

We have come a long way just over the course of my career. When I started at the U.S. Nautical Almanac Office 39 years ago, we were still using Newcomb's developments extensively, and progress seemed to be defined by ever more complicated general planetary theories similar to Newcomb's, that is, analytical developments for a planet's position based on a series expansion of the disturbing function. The most sophisticated theories at that time were probably Clemence's Theory of Mars, published in 1961, and Eckert's Improved Lunar Ephemeris, published in 1954, the latter based on Brown's 1919 theory. The group of planetary and lunar theories developed by Bretagnon, Chapront, Deprit, Krasinski, and collaborators in the last few decades of the 20th century are part of this important branch of celestial mechanics.

Fundamental Solar System Ephemerides
Used in *The Astronomical Almanac*
(and predecessor publications)
Over the Past 50 Years

1960 to 1983

Mercury – Earth: Newcomb (1895) theories
Mars: Newcomb (1898) theory with Ross (1917) corrections
Jupiter – Pluto: *Coordinates of the Five Outer Planets, 1653-2060* (Eckert, Brouwer & Clemence 1951) *
Moon: Improved Lunar Ephemeris (Eckert 1954)

1984 to 2002

JPL DE200/LE200 (Standish 1982, 1990) *

2003 to present

JPL DE405/LE405 (Standish 1998) *

* N-body numerical integrations
(others are analytical theories)

N-body numerical integrations become practical after World War II due to the commercialization of electronic computers and their steady increase in speed, especially after the introduction of solid-state circuitry. In fact, some of the first applications of automated computing technology to scientific problems involved the calculation of ephemerides. A landmark in this field was the completion of the *Coordinates of the Five Outer Planets, 1653–2060*, by Eckert, Brouwer, and Clemence, published in 1951, which were calculated on one of the first stored-program electronic computers, IBM's SSEC, with 12,500 electron tubes. In the introduction to this ephemeris, it was noted that each integration step took "less than two minutes." Its descendents included, in the U.S., integration programs developed in Fortran at MIT and JPL in the 1960s, and similar integrators written elsewhere, for example, at the Institute of Theoretical Astronomy in Leningrad.

Figure 1: IBM's SSEC computer in its New York City location. IBM photo from *Columbia University Computing History* at http://www.columbia.edu/acis/history/ (used with permission).

The JPL planetary and lunar ephemerides have been the recognized state of the art for three decades (and counting). These ephemerides have been developed under the leadership of Myles Standish and now Bill Folkner, with significant contributions from Jim Williams, Skip Newhall, and others. The quality of the product is due not only to the increasing sophistication of the perturbation model, but also to the inclusion of spacecraft and other high-precision observations in increasing numbers and kinds, along with careful post-solution analysis. This work requires meticulous attention to detail, and the need to continually incorporate new types of observations undoubtedly discouraged other groups with fewer resources from trying to compete. Even Bretagnon's analytical theories were fit to JPL's DE200/LE200 ephemeris rather than to individual observations.

So it is very exciting that now we have two other institutions, the Institute for Applied Astronomy in St. Petersburg, and the Institut de Mécanique Céleste et de Calcul des Ephémérides here in Paris, that have produced independent ephemerides for general use, fit to a large number and variety of observations, that are comparable in quality to those produced by JPL. This session provides some important new information on how the ephemerides from all three institutions are constructed, and how they compare with each other. These kinds of comparisons are essential in improving solar system ephemerides generally and understanding their limitations.

One last note: IAU Commission 4 has established a Working Group on Standardizing Access to Ephemerides, to suggest standard software or data formats that would allow users to easily obtain ephemeris data and to switch seamlessly (if possible) among the available sources. James Hilton (jms.l.hilton@gmail.com or james.hilton@usno.navy.mil) is the working group's chair, and he welcomes input from everyone.

PLANETARY AND LUNAR EPHEMERIDES INPOP10A

A. FIENGA[1], H. MANCHE[2], P. KUCHYNKA[2], J. LASKAR[2], M. GASTINEAU[2]

[1] Institut UTINAM-CNRS 6213
41 bis avenue de l'observatoire, 25000 Besançon,
e-mail: agnes.fienga@obs-besancon.fr

[2] Astronomie et Systèmes Dynamiques, IMCCE-CNRS UMR8028
77 avenue Denfert-Rochereau, 75014 Paris

ABSTRACT. The INPOP10a planetary and lunar ephemeris has several improvements compared to the previous INPOP solutions. No big change was brought in the dynamics but improvements were implemented in the fitting process, the data sets used in the fit and in the general features of the solution. A specific characteristic of INPOP10a is the fit of the mass of the Sun instead of the astronomical unit. Determinations of PPN parameters as well as adjustments of the Sun J_2 and of asteroid masses are also presented. As for INPOP08, INPOP10a provides to the user, positions and velocities of the planets and of the Moon and TT-TDB Chebychev polynomials at `http://www.imcce.fr/inpop`.

1. THE DATA SETS

A detailed description of the data set used for the construction of INPOP10a can be found in (Fienga et al. 2010). Several data sets have been added since INPOP08. The global distribution of the data used for the INPOP fit has changed its balance compared to INPOP06: now, more than 56% of the planetary observations are deduced from the tracking data of spacecrafts including range, VLBI angular positions and flyby normal points. The statistics of the obtained postfit residuals as well as the number of points and their distribution in time are presented in table 1.

For Mercury, two normal points deduced from the Mariner tracking data in 1974 and 1975 have been provided by JPL (Folkner 2010) and three corrections to Mercury positions have been obtained during the Messenger flybys of Mercury in 2008 and 2009. These five points change drastically our knowledge of the Mercury orbit. Until now, only direct radar ranging on the Mercury surface were available with an accuracy of about 800 meters. For Mars and Venus, like with INPOP08, tracking data of MEX and VEX missions provided by ESA (Morley 2009, Morley 2010) are used in the fit as described in Fienga et al. (2009). To the Saturn Cassini normal points provided by JPL over the 2005 to 2007 period and used in INPOP08, are added VLBI observations of the spacecraft (Jones et al. 2010) with an accuracy better than few milliarcseconds (mas). Flybys data of Jupiter, Uranus and Neptune obtained during several missions (Pioneer 10 and 11, Viking 1 and 2, Ulysses and Cassini) are also added, provided by Folkner (2009). These observations improve the estimations of the geocentric distances to the outer planets while no observation of that type were used in INPOP06 and INPOP08 adjustments. New optical data obtained from 2000 to 2008 with the Flagstaff Astrometric Scanning Transit Telescope are also added for Uranus, Neptune and Pluto. Stellar occultations (Sicardy 2009) are taken into account in INPOP10a by the use of measured offsets in topocentric (α, δ).

A detailed description of the fit procedure for the Moon orbit and libration and of the Lunar Laser Ranging observations used for the fit is presented by (Manche et al. 2010) in this volume.

2. FITTING PROCEDURE

In INPOP10a, the value of the AU is fixed to the value given in the IERS2003 convention. The GM of the Sun is fitted to the observations with the initial conditions of planets, the densities of the asteroids and the oblateness coefficient J_2 of the Sun. Values of the fitted parameters are given in table 2. (Konopliv et al. 2010) presents also a value of the GM of the Sun fitted on Mars data only when the value obtained with INPOP10a is fitted over all the available data including flyby points of Mercury. This difference explains the bigger uncertainty of (Konopliv et al. 2010) estimation. The two estimations are however consistent at 2 sigmas.

The selection of asteroids modeled in INPOP10a is based on Kuchynka et al. (2010).

Table 1: Statistics of the INPOP10a and INPOP08 postfit residuals.C.n.p stands for Cassini normal points, Mess. for Messenger mission and all the residuals in angular quantities are given in milliarcseconds.

Planet Type of Data		INPOP08 mean ± 1σ	INPOP10a mean ± 1σ	Planet Type of Data		INPOP08 mean ± 1σ	INPOP10a mean ± 1σ
Mercury				Saturn			
Direct range [m] (462)	1965-2000	30 ± 842	7 ± 866	C.n.p. ra (31)	2004-2007	1.5 ± 4	0.7 ± 4
Mariner range [m] (2)	1974-1975	-1000 ± 305	-28 ± 85	C.n.p. de (31)	2004-2007	7.0 ± 7	6.5 ± 7
Mess. ra (3)	2008-2009	1.1 ± 0.7	0.4 ± 1.2	C.n.p. range [m]	2004-2007	0.5 ± 22	0.0 ± 17
Mess. de (3)	2008-2009	2.0 ± 1.9	1.9 ± 2.1	VLBI ra (10)	2004-2009	0.3 ± 0.7	0.0 ± 0.6
Mess. range [m] (3)	2008-2009	52 ± 619	-0.6 ± 1.9	VLBI de (10)	2004-2009	-1.2 ± 2.0	0.1 ± 0.4
Venus				Opt. ra (7824)	1914-2008	-16 ± 305	-16 ± 305
Direct range [km] (489)	1965-2000	0.5 ± 2.3	0.5 ± 2.2	Opt. de (7799)	1914-2008	-7 ± 276	-9 ± 276
VEX range [m] (22145)	2006-2010	1.6 ± 4.4	-0.2 ± 3.9	Uranus			
VLBI (22)	1990-2007	2 ± 2	2 ± 2.5	flybys ra (1)	1986	-90	-30
Mars				flybys de (1)	1986	-36	-7
MGS range [m] (10474)	1998-2008	-0.9 ± 1.6	0.5 ± 1.9	range [km] (1)	1986	1139	0.080
MEX range [m] (24262)	2006-2010	-3.5 ± 2.0	0.0 ± 1.7	Opt. ra (4145)	1914-2008	-44 ± 278	-27 ± 290
Path range [m] (90)	1997	6.8 ± 12.5	-5.0 ± 5.0	Opt. de (4130)	1914-2008	-38 ± 339	-11 ± 338
Vkg range [m] (1256)	1976-1982	-27.4 ± 19.0	-5.7 ± 35.0	Neptune			
VLBI (96)	1989-2007	0.5 ± 0.5	-0.0 ± 0.4	flybys ra (1)	1989	-88	-11
Jupiter				flybys de (1)	1989	-48	-10
flybys ra (5)	1974-2000	48.0 ± 40.0	6 ± 5	range [km] (1)	1989	2305	0.004
flybys de (5)	1974-2000	-10.0 ± 50	-13 ± 18	Opt. ra (4340)	1914-2008	-32 ± 282	2 ± 281
range [km] (5)	1974-2000	-27± 55	-0.6 ± 1.6	Opt. de (4320)	1914-2008	-36 ± 335	2 ± 330
VLBI (24)	1996-1997	4 ± 11	0.2 ± 11	Pluto			
Opt. ra (6216)	1914-2008	20 ± 304	-26 ± 304	occ. ra (13)	2005-2009	-6 ± 46	-1 ± 47
Opt. de (6082)	1914-2008	-44 ± 313	-54 ± 303	occ. de (13)	2005-2009	16 ± 30	-2 ± 19
				Opt. ra (2449)	1914-2008	353 ± 926	38 ± 629
				Opt. de (2463)	1914-2008	-22 ± 524	17 ± 536

Table 2: Values of planetary ephemerides parameters. The (F) indicates a fixed value. The equivalent value of AU deduced from the estimation of the GM$\odot$ in INPOP10a and (Konopliv et al. 2010) are given in the line labelled "AU from GM$\odot$". Only the three biggest asteroid masses fitted in INPOP10a are given in this table.

	INPOP08	INPOP10a	(Konopliv et al. 2010)
EMRAT	(81.30054 ± 0.00005)	(81.3005700 ± 0.0000010)	(81.3005694 ± 0.0000015)
$J_{2\odot}$	(1.82 ± 0.47) × 10^{-7}	(2.40 ± 0.25) × 10^{-7}	
GM$\odot$ [km^3. s^{-2}]	132712440017.98700 ± 50 (F)	132712440055 ± 1	132712440042 ± 10
AU [m]	149597870699.2 ± 0.11	149597870691.0 (F)	
AU [m] from GM$\odot$		149597870704.9 ± 0.3	149597870700.0 ± 3

	INPOP08	INPOP10a	(Konopliv et al. 2010)	Baer (2010)
Ceres [$10^{12} \times M_\odot$]	465.8 ± 4.5	475.836 ± 2.849	467.900 ± 3.250	475.500 ± 4.755
Pallas [$10^{12} \times M_\odot$]	107.6 ± 10.0	111.394 ± 2.808	103.440 ± 2.550	106.000 ± 1.060
Vesta [$10^{12} \times M_\odot$]	139.2 ± 15.0	133.137 ± 1.683	130.970 ± 2.060	133.070 ± 0.266

PPN parameter fixed	PPN estimated	INPOP08	INPOP10a	(Konopliv et al. 2010)
(γ -1) = 0	(β -1) × 10^{-4}	(0.75 ± 1.25)	(-0.5 ± 1.5)	
(γ -1) = (0.21 ± 0.23) × 10^{-4}	(β -1) × 10^{-4}		(-0.1 ± 1.9)	(0.4 ± 2.4)
(β -1) = 0	(γ -1) × 10^{-4}		(0.6 ± 1.0)	(1.8 ± 2.6)

$\dot{\varpi}_{\rm sup}$	INPOP08	INPOP10a	Pitjeva 2009	Pitjeva 2010
Mercury [mas.cy^{-1}]	-10 ± 30	0.2 ± 3	-3.6 ± 5	-4 ± 5
Saturn [mas.cy^{-1}]	-10 ± 8	0 ± 2	-6 ± 2	-10 ± 15

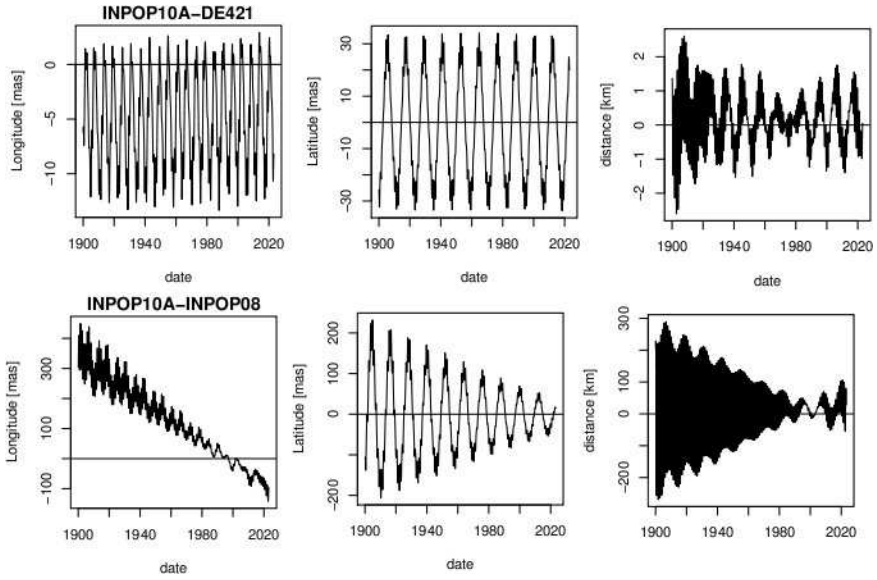

Figure 1: Comparison of Jupiter geocentric longitudes, latitudes and distances estimated with INPOP10a, DE421, INPOP08

The perturbations of 24635 asteroids have been taken into account using for most of them an averaging of their perturbations by a ring with fixed physical characteristics and for 161 of them, individual perturbations (see Kuchynka et al. 2010). Based on a study of the correlations between the asteroids, we found 30 asteroids among the most perturbing objects highly correlated with each others. In order to decrease the uncertainties on the mass estimations, we fixed 15 asteroid masses to values well determined by other methods (close encounters, binary) extracted from Baer (2010). Besides these fixed values, we estimate 146 asteroid masses using a BVLS algorithm (Lawson and Hanson, 1995) with large constraints on the densities.

We used the mass of planets provided by the IAU 2009 CBE lists (Luzum 2010).

The Moon orbit and libration are fitted over LLR observations. See in this volume (Manche et al. 2010) for more details. The final version of INPOP10a was obtained after an iterative process between planetary fit and Moon fit.

3. RESULTS AND APPLICATIONS

The table 1 gives the planetary postfit residuals obtained with INPOP08 and INPOP10a. Some of the data sets used in INPOP10a were not used in the INPOP08 adjustment: this explains some differences between the two columns of table 1. Furthermore, we obtain with INPOP10a an important improvement of the Jupiter orbit compared to INPOP08, as one can see on Figure 1. The addition of the flyby points of outer planets in the data used for the fit helps to reduce the differences between INPOP and the JPL DE ephemerides.

In Figure 2 are presented the asteroid masses obtained with INPOP10a compared to values found in the literature, ranked by their impact on the Earth-Mars distances over the 1990 to 2010 period. The major sources of comparisons are the values obtained with DE421 (Folkner et al. 2008), DE423 (Konopliv et al. 2010) and other type of estimations gathered in Baer (2010) with realistic errorbars estimated by Kuchynka (2010). It then appears clearly that the estimations for the most perturbing objects are quite consistent when the estimations of the weak perturbing objects show bigger discrepancies. For the asteroids inducing perturbations up to 10 meters, the differences in GMs are usually below 1-sigma or very close to 1-sigma except for 52 Europa. For this asteroid, which induced a maximum of 10 meters on the Earth-Mars distances, the errorbars are very large for all the determinations based on planetary ephemerides: we thus conclude to a bad determination of this mass based on the present interval of available data.

Table 3: Angles of rotation deduced from adjustment of rotation matrices following equations 1 and 2. The angles are given in mas and the uncertainties are the formal 1-sigma deduced from the least squares. [1] stands for (Folkner et al. 1994) and [2] for (Standish 1998)

	θ	η	ζ
	mas	mas	mas
DE405 → ICRF	6 ± 5	15 ± 11	-4 ± 6
INPOP08 → ICRF	4 ± 5	15 ± 11	-2.5 ± 6
INPOP10a → ICRF	4 ± 5	15 ± 11	-3.0 ± 6
DE200 → ICRF	6 ± 5	28 ± 11	9 ± 6
DE200 → ICRF [1]	2 ± 2	12 ± 3	6 ± 3
DE200 → DE405 [2]	1 ± 2	14 ± 3	10 ± 3

Table 2 gives the obtained values for the mass of the Sun, the Sun J_2, the Earth-Moon mass ratio and the three biggest asteroid masses and the interval of sensitivity of data to modifications of PPN β with γ equal to 1 or with γ equal to the value obtained by the Cassini experiment (Bertotti et al. 2000), and of PPN γ with β equal to 1. The results obtained for both modified parameters are presented on Figure 3. Supplementary advances in the Mercury and Saturn perihelia have also been tested. These results were obtained based on the method presented in Fienga et al. (2010). We computed several fits for different values of the PPN parameters (β, γ or both) or supplementary advances in perihelia with a simultaneous fit of initial conditions of planets, mass of the Sun and asteroid densities. The given intervals correspond to values of parameters inducing changes in the postfit residuals below 5% compared to INPOP10a postfit residuals. For the advances of perihelia, the estimations based on INPOP10a show the clear incompatibility of a significant supplementary advance in Mercury or Saturn orbits and the observations used in the INPOP10a adjustment. This conclusion is due to the densification of very accurate Cassini observations around Saturn and to the Mercury flybys points used in INPOP10a. As one can see in table 2, the obtained PPN intervals are compatible with each other with a better accuracy of INPOP10a due to the use of Messenger normal points. On the plots of the Figure 3, are plotted the PPN (β,γ) zones for which postfit residuals have been estimated. On the left hand side, each square is a planetary solution fitted to observations as INPOP10a but built with the corresponding values of (β, γ). In the center, the red area limits the region of (β, γ) for which all the postfit residuals have variations to INPOP10a residuals smaller than 5 %. In the gray zone, all but the Mercury flyby residuals have residuals smaller than 5 %. Then limits with specific denominations are given in order to specify which observations have their residuals modified by more than 5 % from their INPOP10a values. The right hand side plot is a zoomed and densified representation of the left hand plot. As it appears clearly on Figure 3, each type of data used in the fit gives indeed different limits for the (β, γ) variations. These limits reflect more the weighting of the data than the real sensitivity of these data to (β, γ). However, it is interesting to note the strong constraint brought by the Mercury flybys data on the right hand side plot. In the dark read area, the possible variations acceptable for all the residuals including the Mercury points are compatible with the best estimations found in the literature and obtained with different methods (LLR, Cassini experiment, VLBI astrometry).

In this volume will be presented in details the method implemented to use millisecond pulsar observations, radio timing and VLBI, for reference frame ties. Based on radio timing data obtained at the NRT (Desvignes 2010) and VLBI astrometry extracted from (Chatterjee et al. 2009) and (Deller et al. 2009), rotation matrices between the JPL DE200, DE405, INPOP08 and INPOP10a frames and the ICRF were estimated and presented in table 3. These estimations are consistent with values obtained for DE200 (Folkner et al. 1994) and DE405 (Standish 1998). The uncertainties are indeed important and are induced by a lack of sources with a mas-level accuracy. Only four pulsars observed by the NRT have at the present time the mas level astrometry for both techniques, VLBI and radio timing. Thanks to new VLBI observations of millisecond pulsars planned for next months for the FERMI mission follow-up, the sample should be increased rapidly.

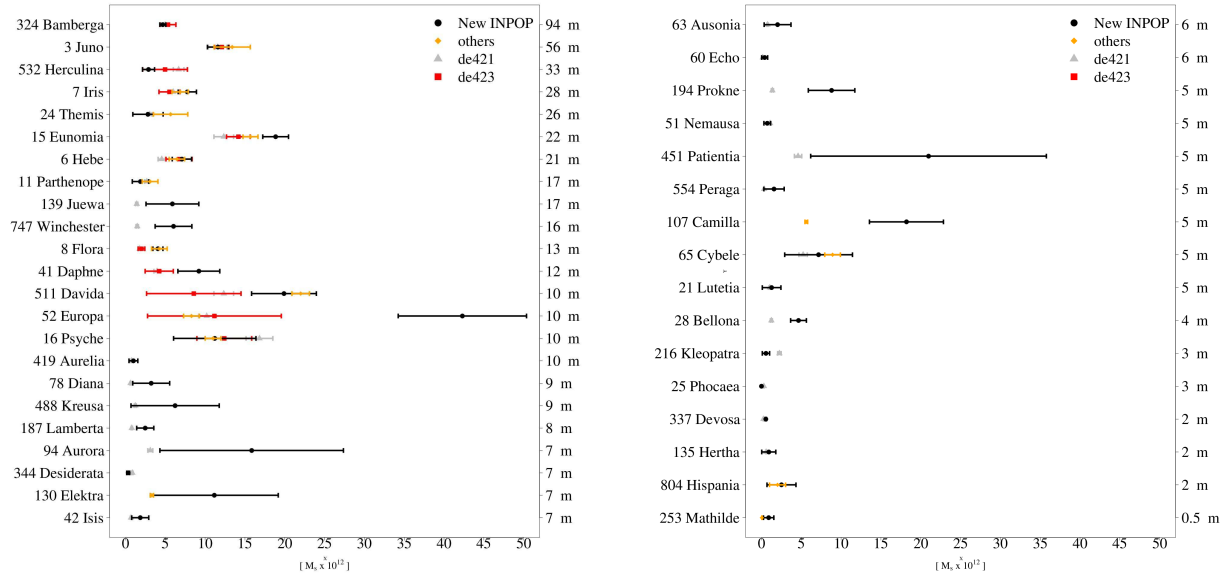

Figure 2: Comparisons of the first 23 asteroid masses given in 10^{12} solar mass (x-axis) estimated by different authors and ranked by their impact on the Earth-Mars distances over 1990 to 2010 (y-axis). The mass estimations of the 3 biggest asteroids and perturbers Ceres, Pallas and Vesta are given in table 2. "others" stands for estimations gathered by Baer (2010).

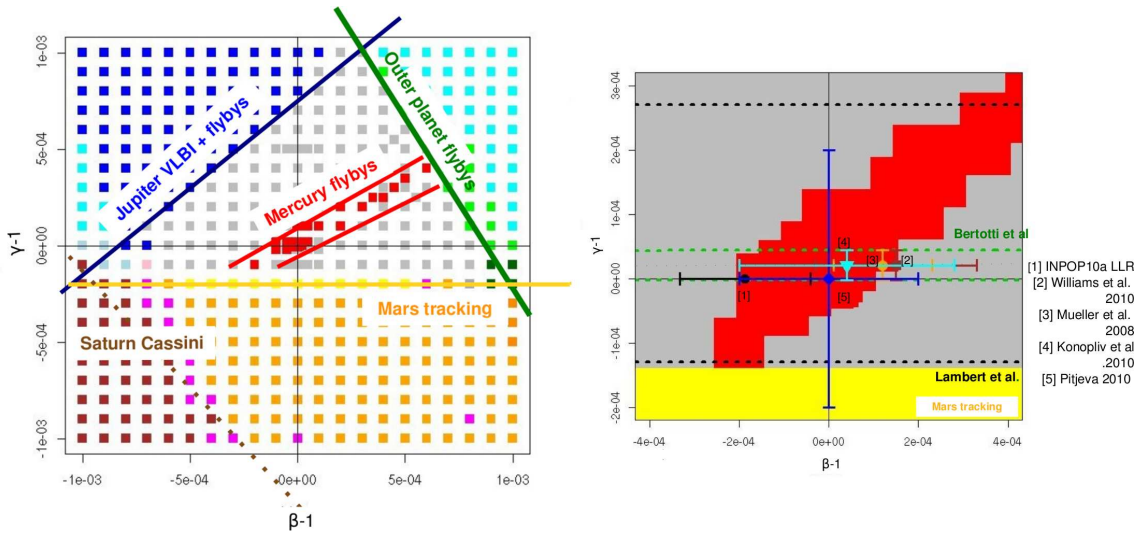

Figure 3: Variations of postfit residuals obtained for different values of PPN β (x-axis) and γ (y-axis). References on the right hand side plot label values of (β, γ) obtained in the literature.

4. REFERENCES

Baer, J., 2010, http://home.earthlink.net/ jimbaer1/astmass.txt.

Baer, J.; Milani, A.; Chesley, S.; Matson, R. D, 2008, "An Observational Error Model, and Application to Asteroid Mass Determination", American Astronomical Society, DPS meeting 40, 52.09; Bulletin of the American Astronomical Society, Vol. 40, p.493.

Chatterjee, S., Brisken, W.F., Vlemmings, W. H. T., Goss, W. M., Lazio, T. J. W., Cordes, J. M., Thorsett, S. E., Fomalont, E. B., Lyne, A. G., Kramer, M., 2009, "Precision Astrometry with the Very Long Baseline Array: Parallaxes and Proper Motions for 14 Pulsars", The Astrophysical Journal, Volume 698.

Deller, A. T.; Tingay, S. J.; Bailes, M.; Reynolds, J. E., 2009," Precision Southern Hemisphere VLBI Pulsar Astrometry. II. Measurement of Seven Parallaxes", The Astrophysical Journal, Volume 701

Fienga, A., Laskar, J., Morley, T., Manche, H., Kuchynka, P., Le Poncin-Lafitte, C., Budnik, F., Gastineau, M., Somenzi, L., 2009, "INPOP08, a 4-D planetary ephemeris: from asteroid and time-scale computations to ESA Mars Express and Venus Express contributions", Astronomy and Astrophysics, 507, 1675.

Fienga, A., Laskar, J., Kuchynka, P., Le Poncin-Lafitte, C., Manche, H., Gastineau, M., 2010a, "Gravity tests with INPOP planetary ephemerides", Proceedings of the IAU Symposium "Relativity in Fundamental Astronomy: Dynamics, Reference Frames, and Data Analysis", Volume 261, p. 159-169.

Fienga, A., Manche, H., Kuchynka, P., Laskar, J., Gastineau, M., 2010b, "INPOP10a", arxiv

Folkner, W.M., 2010, private communication.

Folkner, W.M., 2009, private communication.

Folkner, W.M., Williams, J.G., Boggs, D.H., 2008, "The planetary and lunar ephemerides DE421", IOM 343R-08-003

Folkner, W.B., Charlot, P., Finger, M. H., Williams, J. G., Sovers, O. J., Newhall, Xx, Standish, E. M., Jr., 1994, "Determination of the extragalactic-planetary frame tie from joint analysis of radio interferometric and lunar laser ranging measurements", Astronomy and Astrophysics , 287, 279

Jones, Dayton L.; Fomalont, E., Dhawan, V., Romney, J., Lanyi, G., Border, J., Folkner, W., Jacobson, R., 2010, "Astrometric Observations of Cassini with the VLBA: The First Eight Epochs", American Astronomical Society, AAS Meeting 215, 448.13; Bulletin of the American Astronomical Society, Vol. 42, p.456.

Konopliv, A.S., Asmar, S.W., Folkner, W. M., Karatekin, O., Nunes, D.C., Smrekar, S.E., Yoder, C.F., Zuber, M.T., 2010, "Mars High Resolution Gravity Fields from MRO, Mars Seasonal Gravity, and Other Dynamical Parameters", Icarus, in press.

Konopliv, A. S., Asmar, S. W., Carranza, E., Sjogren, W. L., Yuan, D. N., 2001, "Recent Gravity Models as a Result of the Lunar Prospector Mission", Icarus, 150, p. 1-18

Kuchynka, P., Laskar, J., Fienga, A., Manche, H., 2010., "A ring as a model of main-belt in planetary ephemerides.", Astronomy and Astrophysics, 514, A96.

Lawson, C., Hanson, R., 1995, in "Solving Least Squares Problems, Revised edition,", eds. SIAM

Luzum, B.J., 2010, "System of Astronomical Constants", Proceedings of the IAU Symposium "Relativity in Fundamental Astronomy: Dynamics, Reference Frames, and Data Analysis", Volume 261, p. 878.

Manche, H., Fienga, A., Laskar, J., Bouquillon, S., Francou, G., Gastineau, M., 2010, "LLR residuals of INPOP10a and constraints on post-Newtonian parameters", in this volume.

Morley, T., 2010, private communication.

Morley, T., 2009, private communication.

Pitjeva, E., 2010, Proceedings of the IAU Symposium "Relativity in Fundamental Astronomy: Dynamics, Reference Frames, and Data Analysis", Volume 261, p. 878.

Pitjeva, E., 2009, Proceedings of the Jounees2008 "Astrometry, Geodynamics and Astronomical Reference Systems"

Sicardy, B., 2009, private communication.

Standish, E.M., 1998, "Linking the Dynamical Reference Frame to the ICRF", Hightlights of Astronomy, 11, 37

UNCERTAINTIES IN THE JPL PLANETARY EPHEMERIS

W.M. FOLKNER
Jet Propulsion Laboratory, California Institute of Technology
4800 Oak Grove Drive, Pasadena, CA 91109
e-mail: william.m.folkner@jpl.nasa.gov

ABSTRACT. The numerically integrated planetary ephemerides by JPL, IMCCE, and IPA are largely based on the same observation set and dynamical models. The differences between ephemerides are expected to be consistent within uncertainties. Uncertainties in the orbits of the major planets and the dwarf planet Pluto based on recent analysis at JPL are described.

1. INTRODUCTION

Numerically integrated ephemerides of the planets have been used to support planetary spacecraft missions since the first missions to Mars in the 1960s [Peabody et al. 1964]. The accuracy of the ephemerides has improved dramatically over time, due to improvements in the definition of the celestial reference frame, advanced models for Earth's orientation, CCD images of planets and natural planetary satellites from observatories, laser ranging to retro-reflectors on the Moon and measurements of radio signals from spacecraft in proximity to planets. The accuracy of the ephemerides is an important factor for planetary spacecraft missions. Near-term missions with a need for accurate planetary ephemerides include the MESSENGER mission to Mercury, with orbit insertion in March 2011; the Mars Science Laboratory planned for launch in November 2011 and arrival at Mars in August 2012; and the New Horizons mission to Pluto with arrival in the summer of 2015.

The accuracy of the planetary ephemerides is generally assessed for each mission, which requires characterizing the observation accuracy and the possible systematic errors. Systematic errors may be assessed by comparing orbit estimates based on non-overlapping or partial data sets. In a recent accuracy analysis of JPL ephemerides for near-term planetary encounters, it has been found that scaling the formal uncertainty (sigma) by a factor of two gives a reasonable measure of the variation in estimated orbits based upon partial or non-overlapping data sets.

The observations in current planetary ephemerides are generally as described in Folkner et al. [2009]. Additional data used for the uncertainties given below are described for each planet. VLBI observations of spacecraft at Mars, Saturn, and Venus serve to align the planetary ephemeris with the International Celestial Reference Frame [Fey et al., 2009].

2. PLANETARY EPHEMERIS UNCERTAINTIES

Figures 1-8 show the uncertainty in right ascension, declination, and distance of the major planets and the dwarf planet Pluto with respect to Earth over the time period 1950 to 2050. For planets with natural satellites the uncertainty is for the system barycenter.

The Mercury orbit estimate is based on radar ranging to the planet's surface, range measurements from two encounters by the Mariner 10 spacecraft, and VLBI and range measurements for three encounters of the MESSENGER spacecraft. The uncertainty is dominated by an overall rotation uncertainty of $\sim 0.001''$, with a slow growth in uncertainty in right ascension and distance due to uncertainty in the semi-major axis. After the MESSENGER spacecraft goes in to orbit, radio range measurements are expected to improve the Mercury orbit accuracy by a factor of three.

The Venus orbit estimate is dominated by range measurements to the Venus Express spacecraft, as evidenced by the minimum in distance uncertainty over the observation period from 2006 to 2010. The Venus Express range data serve to indirectly tie the Venus orbit orientation to the ICRF through VLBI observations of spacecraft in orbit about Mars.

The Mars orbit estimate is based on range and VLBI observations of spacecraft in orbit about Mars and range measurements to the Viking landers. The uncertainty in the Mars orbit for a one-year prediction is about 300 m, as required for the Mars Science Laboratory mission, but grows rapidly for times before and after the spacecraft observation time span due to the influence of asteroids with orbits near that of Mars. The predicted orbit and uncertainty depend greatly on the asteroid model used. For the uncertainty given here, the mass parameters for the 67 asteroids with greatest influence on the orbit of Mars were estimated along with planetary orbital parameters [Konopliv et al. 2010].

The Jupiter orbit estimate is based on analysis of radio signals for spacecraft passing by Jupiter, by VLBI observations of the Galileo spacecraft in orbit about Jupiter, and by modern optical observations of the Galilean satellites. No range measurements were made to the Galileo spacecraft because the high-gain antenna failed to open. Significant improvement in the Jupiter ephemeris is expected from ranging measurements from the Juno mission, planned for launch in October 2011 and arrival at Jupiter in 2016.

The Saturn orbit estimate is dominated by range and VLBI observations of the Cassini spacecraft. The VLBI observations made using the Very Long Baseline Array [Jones et al. 2010] are the most accurate angular observations of planets available. The current data set covers the time period 2004 to 2010, less than one quarter of the orbital period, which results in the periodic signature seen in the uncertainty in right ascension and declination. Additional measurements should be available through 2017.

The orbits of Uranus, Neptune, and Pluto are dominated by astrometric observations, with only a small fraction of an orbit for each planet covered with modern observations made using ICRF-based star catalogs. Encounters by the Voyager 2 spacecraft with Uranus and Neptune are evident in the minima for the respective orbit uncertainties. The uncertainty in the distance to Pluto is an important factor for planning observations during the New Horizons mission encounter in 2015.

Acknowledgements. The planetary ephemeris development is dependent on high quality observations. Tony Taylor and colleagues at Kinetx Inc. provided Mercury position estimates for the three MESSENGER spacecraft encounters. Trevor Morley and colleagues at the Europeans Space Operations Center provided range measurements to the Venus Express and Mars Express spacecraft. Alex Konopliv of JPL provided normalized range measurements for Mars Global Surveyor, Mars Odyssey, and Mars Reconnaissance Obiter. Jim Border of JPL provided VLBI measurement support for spacecraft at Mars and Venus. Bob Jacobson of JPL provided range and direction measurements derived from spacecraft encounters with Jupiter, Uranus and Neptune and for the Cassini spacecraft about Saturn. Dayton Jones of JPL and Ed Fomalont of NRAO provided VLBI observations of the Cassini spacecraft. Hugh Harris and Alice Monet at the US Naval Observatory, and Bill Owen of JPL provided astrometric observations of the outer planets. The research described in this publication was carried out at the Jet Propulsion Laboratory, California Institute of Technology, under a contract with the National Aeronautics and Space Administration.

3. REFERENCES

Fey, A., Gordon, D., Jacobs, C., eds, 2009, "The second realization of the International Celestial Reference Frame by very long baseline interferometry", IERS Technical Note 35, International Earth Rotation and Reference Systems Service

Folkner, W. M., Williams, J. G., and Boggs, D. H., 2009, "The planetary and lunar ephemeris DE 421", Interplanetary Network Progress Report 42-178, Jet Propulsion Laboratory, California Institute of Technology, http://ipnpr.jpl.nasa.gov.

Jones, D. L., Fomalont, E., Dhawan, V., Romney, J., Folkner, W. M., Lanyi, G., Border, J., and Jacobson, R., 2010, "VLBA astrometric observations of the Cassini spacecraft at Saturn", Astronomical Journal (in press).

Konopliv, A. S., Asmar, S., Folkner, W. M., Karatekin, O., Nunes, D. C., Smrekar, S. E., Yoder, C. F., Zuber, M. T., 2010, "Mars High Resolution Gravity Fields from MRO, Mars Seasonal Gravity, and Other Dynamical Parameters", Icarus (in press)

Peabody, P. R., Scott, J. F., and Orozco, E. G., 1964, "JPL Ephemeris Tapes E9510, E9511, and E9512", Technical Memorandum 33-167, Jet Propulsion Laboratory, California Institute of Technology.

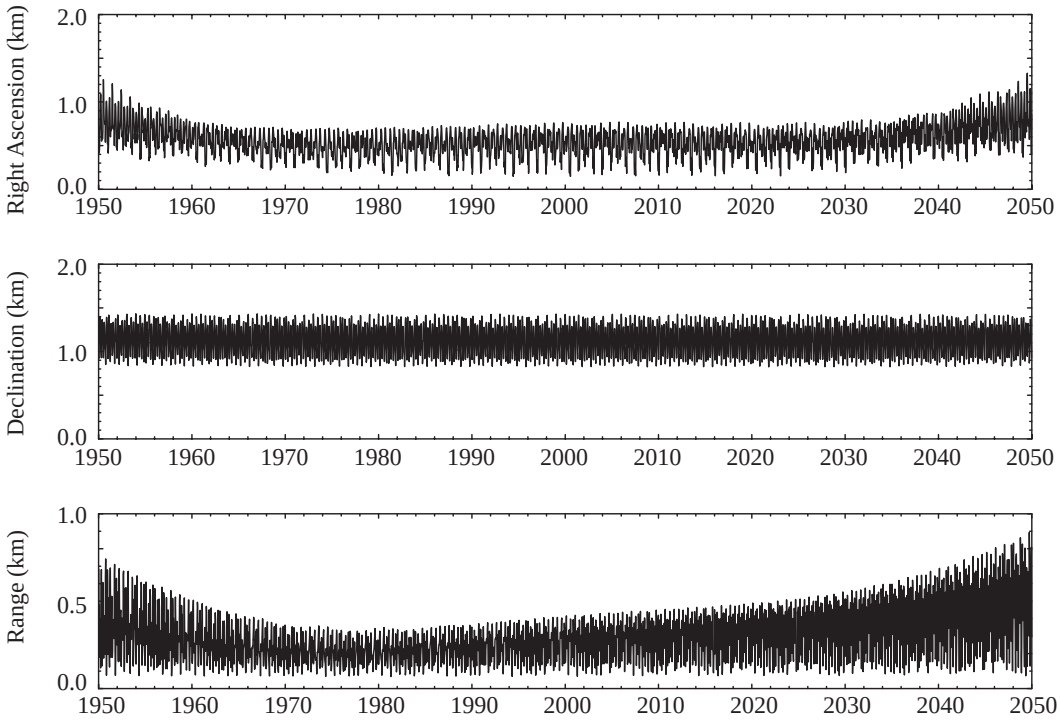

Figure 1: Mercury orbit uncertainty with respect to Earth

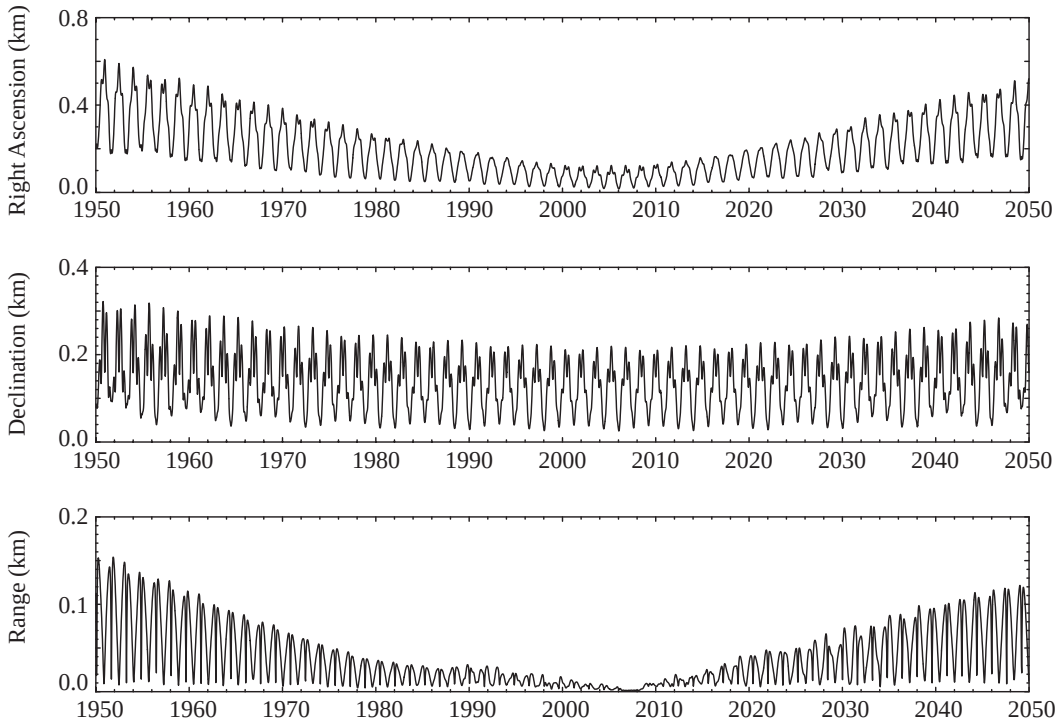

Figure 2: Venus orbit uncertainty with respect to Earth

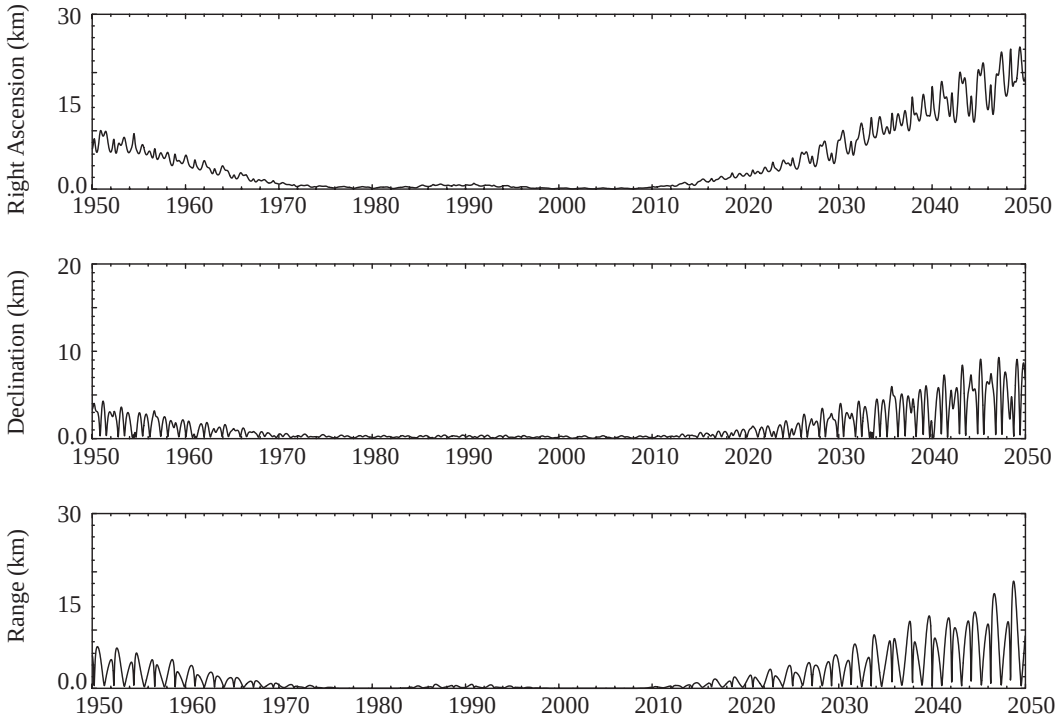

Figure 3: Mars orbit uncertainty with respect to Earth

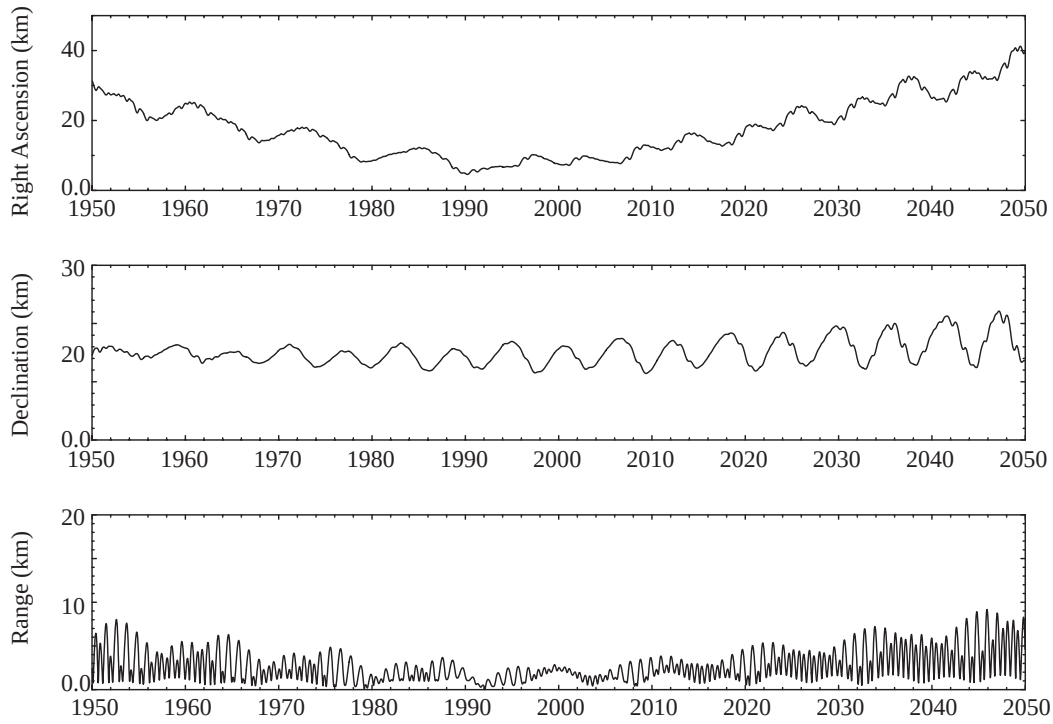

Figure 4: Jupiter orbit uncertainty with respect to Earth

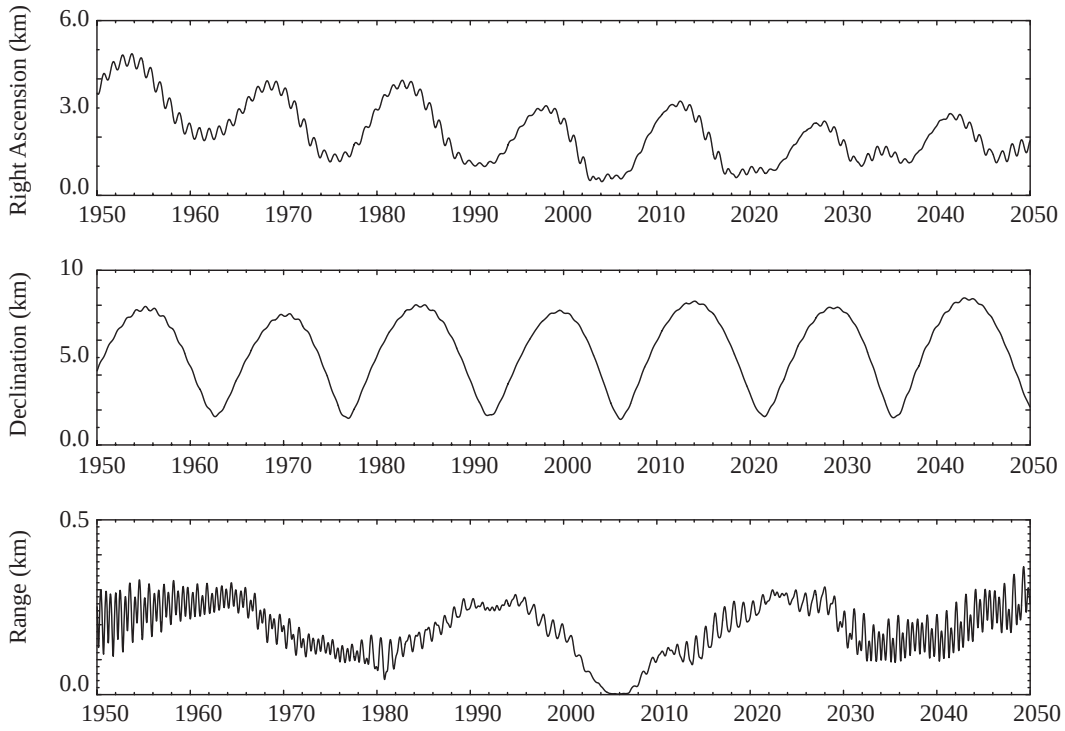

Figure 5: Saturn orbit uncertainty with respect to Earth

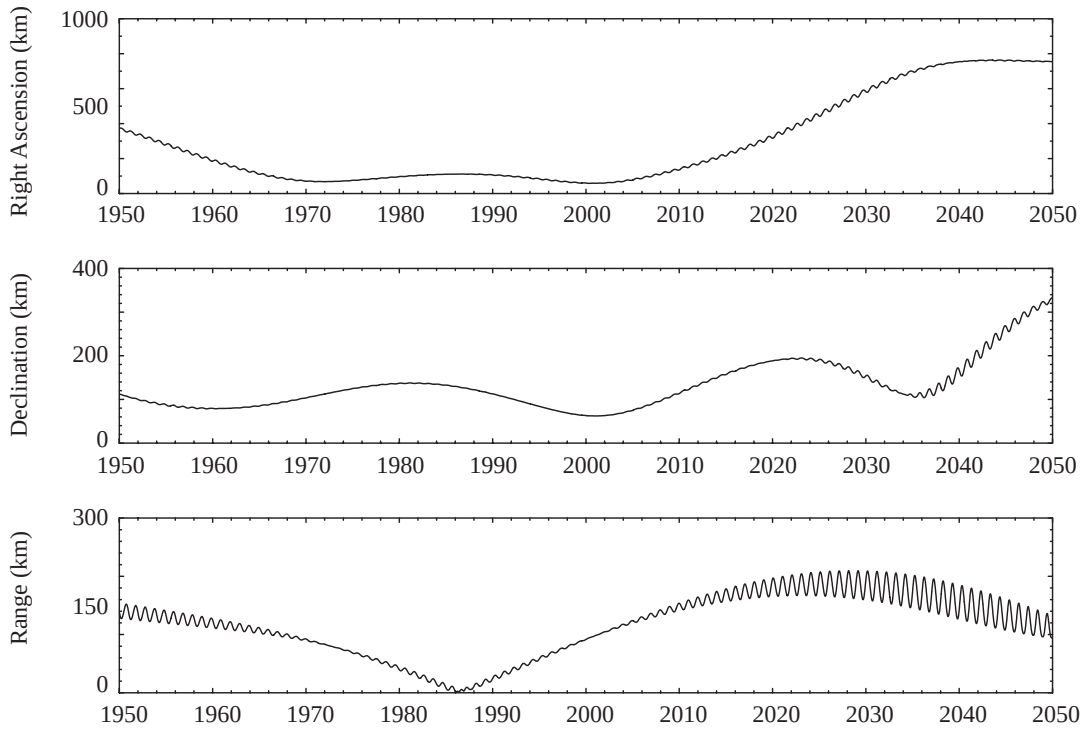

Figure 6: Uranus orbit uncertainty with respect to Earth

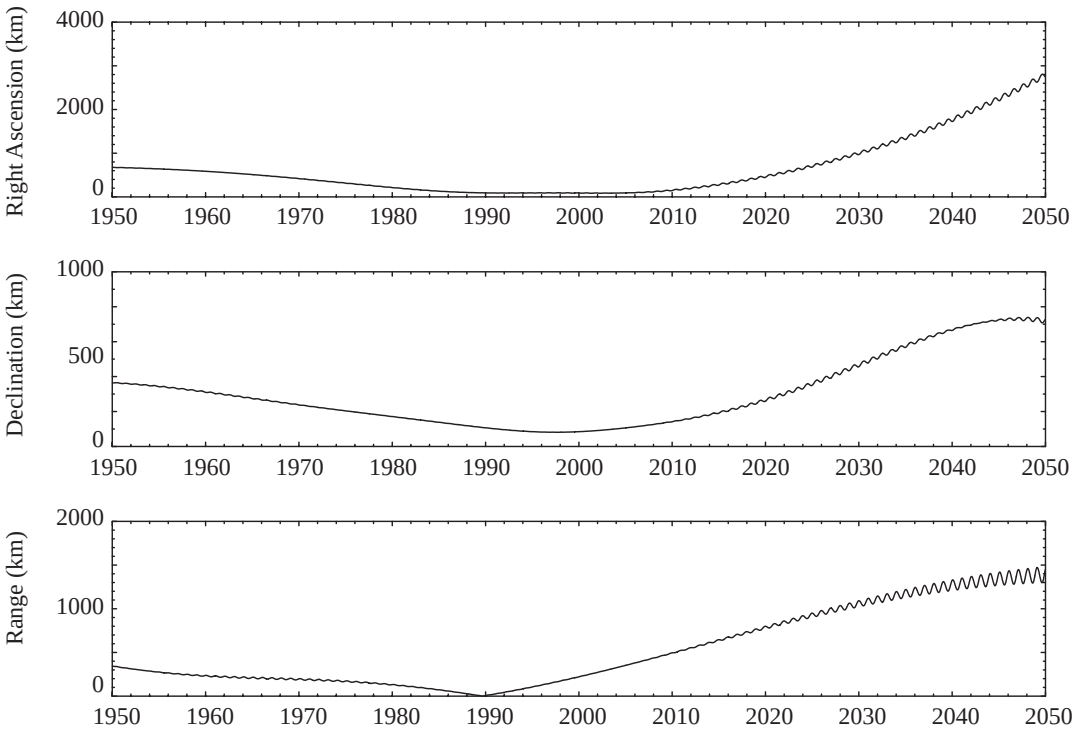

Figure 7: Neptune orbit uncertainty with respect to Earth

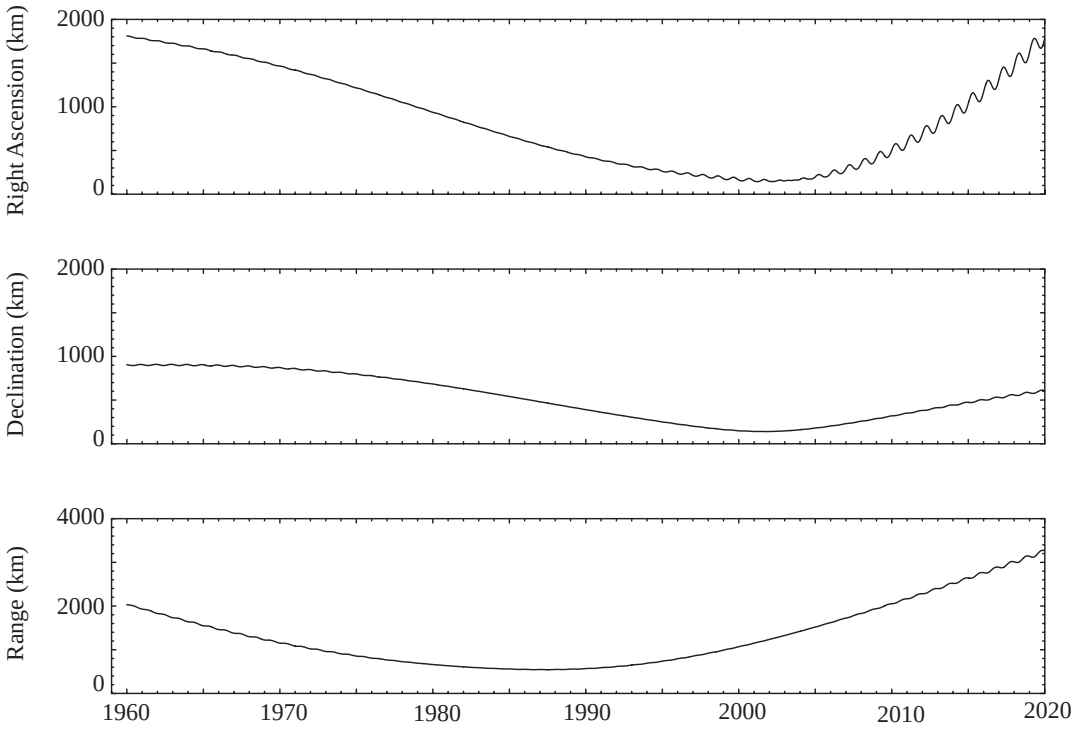

Figure 8: Pluto orbit uncertainty with respect to Earth

EPM – EPHEMERIDES OF PLANETS AND THE MOON OF IAA RAS: THEIR MODEL, ACCURACY, AVAILABILITY

E.V. PITJEVA, O.A. BRATSEVA, V.E. PANFILOV

Institute of Applied astronomy RAS
Kutuzov Quay 10, 191187 St.-Petersburg
e-mail: evp@ipa.nw.ru; olga-brat@yandex.ru; panfilov777@sibmail.com

ABSTRACT. The current state of the last version of the planet part of EPM's ephemerides of IAA RAS (EPM2010) integrated in the PPN metric over the 1800 - 2200 time interval is presented. The updated dynamical model includes perturbations from all Trans-Neptunian Objects at the mean distance of 43 AU in addition to the perturbations from the major planets, the Moon, the Sun, and asteroids of the main belt. EPM2010 ephemerides have resulted from a least square adjustment to observation data totaling about 620000 position observations of different types. EPM2010 have been oriented onto the ICRF by the inclusion of all VLBI spacecraft observations into the fitting. The uncertainty of EPM ephemerides is controlled by comparison with a prior accuracy of observations and the independent DE421 ephemeris. The differences between the times TT and TDB have been constructed for EPM2004 (that is the basis for the Russian Astronomical Yearbook) and EPM2008 ephemerides. The access to these ephemerides with their TT-TDB are available via ftp://quasar.ipa.nw.ru/incoming/EPM/. This package allows a competent user to obtain the rectangular coordinates of the Sun, Moon, and nine major planets by means of a subroutine written in standard languages Fortran, C, Pascal, Java. Moreover this package gives a possibility to obtain access to ephemerides of Ceres, Pallas, Vesta, Eris, Haumea, Makemake, Sedna constructed simultaneously with the main EPM ephemerides.

1. RENEWAL OF EPM EPHEMERIDES: CONSTANTS, MODEL, DATA

The EPM ephemerides (**E**phemerides of **P**lanets and the **M**oon) of IAA RAS originated in the seventies of the last century and have been developed since that time. These ephemerides are based upon relativistic equations of motion for celestial bodies and light rays, as well as relativistic time scales. The numerical integration of the equations of celestial bodies motion has been performed in the Parameterized Post–Newtonian metric for General Relativity in the TDB time scale. EPM ephemerides are computed in the barycentric coordinate frame of J2000.0 by Everhart method over the 400 years interval (1800–2200) using the program package ERA-7 (ERA: **E**phemeris **R**esearch in **A**stronomy) developed to support scientific research in dynamical and ephemeris astronomy (Krasinsky & Vasilyev, 1997). This paper concerns a planetary part of the EPM ephemerides, a lunar part of the EPM ephemerides is presented in another paper (Krasinsky et al., 2010) of the same publication.

The updated model of EPM2010 includes the new values of planet masses adopted by the XXVI GA IAU and other constants, the improved dynamical model with Trans–Neptunian Objects (TNO) and the expanded database (1913–2009). The dynamical model includes perturbations from the 21 largest TNO and a massive ring of all other TNO being at the mean distance of 43 AU, in addition to the perturbations from the major planets, the Moon, the Sun, and asteroids of the main belt (the 301 largest asteroids and the massive asteroid ring).

2. OBSERVATIONS, THEIR REDUCTION, TT-TDB

Database, to which EPM2010 have been adjusted (more 620000 measurements) includes, in addition to previous observations since 1913, the recent spacecraft measurements, namely, ranging to Venus Express (VEX, 2006 – 2009), VLBI data of Odyssey, MRO and VEX (2006–2010), three-dimensional normal point observations of Cassini (2004 – 2006), along with CCD Flagstaff and TMO data of the outer planets and their satellites (1995 – 2009), as well as the new VLBI Cassini points (right ascension and declination) 2004 – 2010 (Jones et al., 2010). These measurements have resulted in a significant improvement of planet orbits, especially for Venus and Saturn and the orientation of the EPM2010 ephemerides to ICRF.

All the new data from spacecraft have been obtained due to the kindness of William Folkner and Agnes Fienga.

Three main factors that influence the accuracy of the constructed ephemerides and the estimated parameters are

1) dynamical models of planet motion,

2) observational data proper,

3) reductions of the observational data.

The main reductions of optical observations of planets are the correction to the additional phase effect (the main phase corrections were made by observers themselves) and the corrections of referencing to the ICRF reference frame. The most precise optical data of the outer planets and their satellites, obtained at Flagstaff, Nikolaev, La Palma, Table Mountain Observatory have already been referenced to the ICRF by observers themselves. The remaining optical observations, referenced to different catalogues, at first were transformed to the FK4 systems by Sveshnikov. Then they were referenced to the FK5 using known formulae (Standish), and were finally transformed to the ICRF using the values of the three angles of rotation from the HIPPARCOS to FK5 catalogues, J2000 in mas (Mignard and Froeschle, 2000):

$\varepsilon_x = -19.9,\ \varepsilon_y = -9.1,\ \varepsilon_z = 22.9.$

The observations of satellites of outer planets are of great importance, as they are more accurate than the observations of their parent planets and are practically free from the phase effect.

The reduction of the radar measurements maintains all the relevant corrections. Observations have been reduced to relativistic corrections, the effects of propagation of electromagnetic signals in the Earth troposphere and in the solar corona. The largest delay is in the plasma of the solar corona near superior solar conjunctions. The following model was used for the solar corona reduction:

$N_e(r) = \frac{A}{r^6} + \frac{B+\dot{B}t}{r^2}$,

where $N_e(r)$ is the electron density. The parameters B and $\dot{B}$ determined from observations were different for different solar conjunctions. The correction of observations of Venus and Mars for their topography has been carried out by means of using modern hypsometric maps of surfaces of these planets and the representation of the global topography by an expansion of spherical functions of 16 – 18 degrees; the topography of Mercury has been represented by Legendre functions to the second order with estimating the expansion coefficients from radar observations.

For the transition from the time of observations (UTC) to Barycentric Dynamical Time (TDB), time for construction of modern planet ephemerides, it is necessity to have transition between Terrestrial Time (TT) and TDB.

$$TT = TAI + 32.184s, \quad UTC = TAI + \mathbf{c}(i).$$

For relation TT – TDB the differential equation from paper by the Klioner (2008) has been used:

$$\frac{\mathrm{d}(TT - TDB)}{\mathrm{d}TDB} = \left(L_B + \frac{1}{c^2}\alpha'\right)(1 + L_B - L_G) - L_G + \frac{1}{c^4}\beta' \tag{1}$$

where $L_B = 1.550519768 \cdot 10^{-8}$, $L_G = 6.969290134 \cdot 10^{-10}$, c is the speed of light in vacuum, α' and β':

$$\alpha' = -\frac{1}{2}v_E^2 - \sum_{A \neq E} \frac{GM_A}{r_{EA}},$$

$$\beta' = -\frac{1}{8}v_E^4 + \frac{1}{2}\left[\sum_{A \neq E} \frac{GM_A}{r_{EA}}\right]^2 + \sum_{A \neq E} \frac{GM_A}{r_{EA}} \left\{ 4\mathbf{v}_A \cdot \mathbf{v}_E - \right.$$

$$\left. -\frac{3}{2}v_E^2 - 2v_A^2 + \frac{1}{2}\mathbf{a}_A \cdot \mathbf{r}_{EA} + \frac{1}{2}\left(\frac{\mathbf{v}_A \cdot \mathbf{r}_{EA}}{r_{EA}}\right)^2 + \sum_{B \neq A} \frac{GM_B}{r_{AB}} \right\}.$$

The equation (1) was integrated with positions and velocities of the planets from EPM2004 and EPM2008 over the time intervals on which these ephemerides were constructed. The results of comparison of the obtained differences (TT-TDB) for EPM2004 and EPM2008 over the interval from 1880 to 2020 are shown in Figure 1.

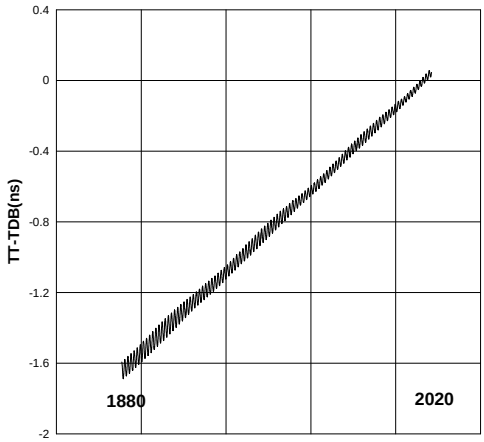

Figure 1: Differences between the difference (TT-TDB) for ephemerides EPM2004 and EPM2008 in ns.

Planet	Type of data	Time interval	N	$< O - C >$	σ
VENUS	VEX τ [m]	2006–2009	1288	0.0	3.6
MARS	spacecraft VLBI [mas]	1989–2010	136	0.0	0.6

Table 1: Mean values and rms residuals for some radiometric observations.

3. THE SOLUTION PARAMETERS

More than 260 parameters have been determined while improving the planetary part of EPM2010 to about 620000 data:

- the orbital elements of all the planets and 18 satellites of the outer planets whose observations were used to improve the orbits of these planets;
- the value of the Astronomical Unit in m;
- three orientation angles of the ephemerides relative to the International Celestial Reference Frame (ICRF) and their velocities;
- 13 rotation parameters of Mars and the coordinates of the three landers on the martian surface;
- masses of the ten asteroids that perturb Mars most strongly, mean densities for three taxonomic classes of asteroids (C, S, M), the mass and the radius of the asteroid ring;
- the mass of the a massive ring of TNO in the ecliptic plane with the radius of 43 AU;
- the mass ratio of the Earth and the Moon;
- the solar quadrupole moment (J_2) and 21 parameters of the solar corona for different conjunctions with the Sun;
- eight coefficients of Mercury's topography and the corrections to the surface levels of Venus and Mars;
- five coefficients of the phase effect correction of the outer planets;
- constant bias for spacecraft and some radar planet observations, that were interpreted as calibration errors of the instruments or as systematic errors of unknown origin;
- the post-model parameters (β, γ, $\dot{G}/G$, $\dot{G}M_\odot/GM_\odot$, secular trends of the planet perihelia and semi-major axes).

Mean values and rms residuals of observations added to the paper (Pitjeva, 2009) are presented in Tables 1, Tables 2 and on Figure 2, where the VEX data are shown. The data residuals do not exceed their a priori accuracies. The rms residuals of ranging for Viking are 8.8 m, for Pathfinder 2.8 m, for MGS and Odyssey 1.2–1.4 m, for Cassini (Saturn) 3.0 m, for VEX 3.6 m.

EPM2010 have been oriented to ICRF with the accuracy better than 1 mas by including into the total solution the 196 ICRF-base VLBI measurements of spacecraft (Magellan, Phobos, MGS, Odyssey, Venus Express, Mars Reconnaissance Orbiter, Cassini) 1989 - 2010 near Venus, Mars, Saturn (see Table 3 and Figure 3).

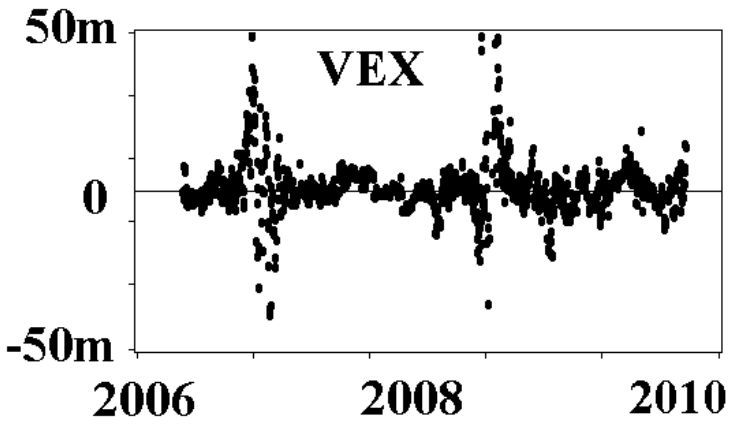

Figure 2: VEX range residuals

Planet	N	$< O-C >_\alpha$	σ_α	$< O-C >_\delta$	σ_δ
VENUS*	4	1.5	2.0	1	6.5
JUPITER	13038	10	184	-29	197
JUPITER*	16	0.0	1.9	-4.9	8.0
SATURN	16246	-2	153	-1	146
SATURN*	92	0.1	0.4	0.0	0.4
URANUS	11692	3.7	172	0.8	204
URANUS*	2	-43	9	-26	12
NEPTUNE	11342	4.9	155	6.4	198
NEPTUNE*	2	-9	3.5	-14	4.0
PLUTO	5470	0.4	141	3	142

Table 2: Mean values and rms residuals for optical observations and spacecraft encounters*, α and δ in mas, 1913–2009

The differences between various ephemerides are useful to know since they are indicative of the realistic accuracies of the ephemerides. The comparison of our recent EPM2008 ephemeris with the standard DE405 and the recent DE421 ephemerides has been made (Table 4). The differences of heliocentric distances for the inner planets between EPM2008 and DE405 or DE421 are small. Table 4 shows a significant progress in agreement (and in reduction of the uncertainties) of the orbits of all the planets, especially due to the VEX (Venus) and Cassini (Saturn). The adjusted value of several parameters are further presented. The obtained values of parameters are shown with their real uncertainties estimated by comparing the values obtained in dozens of different test LS solutions, as well as by comparing parameter values produced by independent groups, or the uncertainties equal 5–10 σ of the formal errors of the WRMS method.

Two parameters that characterize the ring modeling the effect from small asteroids (its mass M_{ring} and radius R_{ring}) have been determined:

$$M_{ring} = (0.87\pm0.35)\cdot 10^{-10} M_\odot, \;\; R_{ring} = (3.13\pm0.05) \text{ AU}.$$

Time interval	Number of obs.	ε_x mas	ε_y mas	ε_z mas
1989–1994	20	4.5±0.8	−0.8±0.6	−0.6±0.4
1989–2003	62	1.9±0.1	−0.5±0.2	−1.5±0.1
1989–2007	118	-1.528±0.062	1.025±0.060	1.271±0.046
1989–2010	196	-0.099±0.047	-0.052±0.056	0.045±0.030

Table 3: The rotation angles for the orientation of EPM onto ICRF

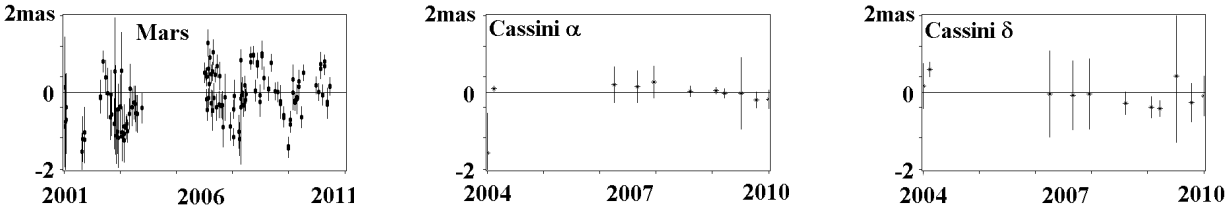

Figure 3: The VLBI residuals of the different Mars spacecraft and Cassini

Planet	DE405–EPM2008	DE421–EPM2008
Mercury	384 m	185 m
Venus	53.7 m	4.6 m
Earth	26.8 m	11.9 m
Mars	272 m	233 m
Jupiter	19.7 km	4.8 km
Saturn	29.3 km	0.4 km
Uranus	864 km	310 km
Neptune	6100 km	848 km
Pluto	29000 km	1800 km

Table 4: Maximum differences in the heliocentric distances of planets for DE and EPM ephemerides, 1950–2050

The estimation of the total mass of the main belt asteroids represented by the sum masses of the 301 largest asteroids and the asteroid ring is:

$$\mathrm{M}_{belt}=(13 \pm 2)\cdot 10^{-10} M_\odot \text{ (about 3 Ceres mass).}$$

The mass value of the ring of TNO has been obtained:

$$\mathrm{M}_{TNOring}=(498 \pm 14)\cdot 10^{-10} M_\odot \ (5\sigma).$$

Thus, the total mass of all TNO including Pluto, the 21 largest TNO and the TNO ring of other TNO objects with the 43 AU radius is:

$$\mathrm{M}_{TNO}=775\cdot 10^{-10} M_\odot \text{ (about 164 } \mathrm{M}_{Ceres} \text{ or 2 } \mathrm{M}_{Moon}).$$

The obtained value of the Moon-Earth mass ratio is

$$M_{Earth}/M_{Moon} = 81.3005676 \pm 0.0000030$$

The quadrupole moment of the Sun J_2 and the values of PPN parameters are:

$$J_2 = (2.0 \pm 0.5) \cdot 10^{-7},\ |\beta - 1| < 0.0002,\ |\gamma - 1| < 0.0002.$$

The value $GM_\odot$ in the physical system of units $[m^3 s^{-2}]$ may be estimated from fitting ephemerides to observations. However, according to the present definition of the Astronomical Unit, this value may be calculated from an entirely equivalent process – that of adjusting the AU value, obtained in meters while fitting planet ephemerides, by the relation,

$$GM_\odot[m^3 s^{-2}] = k^2 \cdot AU[m]^3/86400[s]^2,$$

where k=0.01720209895 is Gaussian gravitational constant.

The two estimations of $GM_\odot$ have been obtained A) from the estimated value of AU, B) the direct estimation of $GM_\odot$ if the value of AU is fixed:

A) AU=(149597870696.2±0.4)m (10 σ), then $\mathrm{GM}_\odot$=(132712440031.9±0.1) $\mathrm{km}^3/\mathrm{s}^2$ (10 σ);

B) fixed AU=149597870696.4 m, obtained $\mathrm{GM}_\odot$=(132712440032.7±0.7) $\mathrm{km}^3/\mathrm{s}^2$ (10 σ).

In the second case (B) the formal error of WRMS is significantly larger than in case A due to strong correlation of $GM_\odot$ with the orbital elements of the inner planets, especially with their major semi-axes; whereas the AU correlation with all the estimated parameters is considerably less. Thus, the present AU definition does not prevent the estimation of $GM_\odot$, $G\dot{M}_\odot$, AU and gives the possibility to estimate $GM_\odot$ more accurately.

4. SOFTWARE SUPPORT FOR EPHEMERIDES EPM

A new program package Calc_Eph containing IAA Planetary and Moon Ephemerides (EPM2004, EPM2008) along with associated reading and interpolating routines has been recently created. Routines of this package allow a competent user to obtain the rectangular coordinates of the Sun, the Moon, and nine major planets, three asteroids (Ceres, Pallas, Vesta) and four TNO (Eris, Haumea, Makemake, Sedna), the so called "dwarf planets", as well as TT-TDB differences. The program package affords an opportunity to get the rectangular coordinates of the Sun, the Moon, and nine major planets with respect to different centers (barycentric, geocentric, heliocentric and planetocentric) and barycentric (Solar System) coordinates of the dwarf planets. Routines included in the package support ephemeris EPM2004, as well as EPM2008. They support polynomial approximation for both binary and ASCII ephemeris files. Source code of the package Calc_Eph is free and available for outside users by FTP:
ftp://quasar.ipa.nw.ru/incoming/EPM/. The package is implemented in four standard languages: Fortran (Intel Fortran), ANSI C, Pascal, Java. The software package consists of a main test program ("Demo") and a module which contains reading and interpolating routines ("Calc_Eph") The interface of the calculating routines is unified with the other well known software products: DE, INPOP. The list of the subroutines contained in Calc_Eph are of primary interest to the user:

- InitBin, InitBinD, InitBinT: Read binary ephemeris or TT-TDB files;
- InitTxt, InitTxtD, InitTxtT: Read ASCII ephemeris or TT-TDB files;
- Calc_EPM, Calc_EPD: Calculate position and velocity (in AU, AU/day) of specified object with respect to specified center at the specified date;
- Calc_TDB: Calculate differences (in s) between TT and TDB times.

The initializing routines download the whole ephemeris in RAM without bufferization. The program package Calc_Eph is made for multiple call of interpolating routine in one program. User can obtain ephemerides of big planets, the "dwarf planets" or TT-TDB differences either in one program in any sequence, or one group at a time.

Clac_Eph is actually being supported and renovated. The package is accompanied by a manual. The routines of the package are easy to use, can be embedded in the user's software and can be called together with the existing products (DE, INPOP). At the present time, within the framework of the Working Group on Standardizing Access to Ephemerides activity, the unified ephemerides representation format and software are being developed.

5. REFERENCES

Jones D.L., Fomalont E., Dhawan V., Romney J., Lanyi G., Border J., Folkner W., Jacobson R., 2010, "Astrometric observations of Cassini with the VLBA: the first eight epochs", BAAS 42, p. 456.

Klioner S.A., 2008, "Relativistic astrometry and astrometric relativity", Giant Step: from Milli- to Micro-arcsecond Astrometry, Proc. IAU Symposium 248, pp. 356–362, doi: 10.1017/S174392130801956X.

Krasinsky G. A., Vasilyev M. V., 1997, "Era: knowledge base for ephemeris and dynamical astronomy", in I.M. Wytrzyszczak, J.H. Lieske & R.A. Feldman (eds.), Dynamics and Astrometry of Natural and Artificial Celestial Bodies, Proc. IAU Colloquium 165 (Dordrecht: Kluwer Academic Publishers), pp. 239–244.

Krasinsky G. A., Prokhorenko S.O., Yagudina, E.I., 2010, "New version of EPN-ERA lunar theory", this volume.

Mignard F., Froeschlé M., 2000, "Global and local bias in the FK5 from the HIPPARCOS data", A&A 354, pp. 732–739.

Pitjeva E.V., 2009, "Ephemerides EPM2008: the updated model, constants, data", Proceedings of the "Journees 2008 Systemes de reference spatio-temporels, M. Soffel and N. Capitaine (eds.), Lohrmann-Observatorium and Observatoire de Paris, pp. 57–60.

INPOP, A MILLION YEAR EPHEMERIS

J. LASKAR[1], A. FIENGA[2], M. GASTINEAU[1], H. MANCHE[1]

[1] IMCCE, UMR8028, Observatoire de Paris, UPMC
77 avenue Denfert-Rochereau, 75014 Paris, France

[2] Observatoire de Besançon
41 bis avenue de l'Observatoire, BP 1615, 25010 Besançon cedex, France

ABSTRACT. In the INPOP ephemeris, we integrate the Earth spin evolution at the same time as the planetary orbits. This allows to extend the ephemeris over extended time span. We present here some of the preliminary results obtained over 1 Myr.

1. MOTIVATION

The reasons for extending the planetary ephemerides over several Myr arise from the correlation that is established between the variation of insolation daily received on Earth and its climatic response that is recorded in various forms in the ice caps or in the sediments (Imbrie and Imbrie, 1979). Since several decades, our group has been involved in the construction of reference solutions for paleoclimate computations .The various solutions La93, La2004, La2010 (resp. Laskar et al., 1993, 2004, 2011) that have been constructed correspond to increasing accuracy. In La93, the equations of motion and of precession were averaged. In La2004, the equations of motion were no longer averaged, and the initial conditions were obtained by a fit to DE406 over its range ($[-5000, +1000]$ yr from the present) (Standish, 1998). The length of validity of La2004 was estimated to be around 40 Myr (Laskar et al., 2004), but in order to extend further the length of validity of this long term solution, it was necessary to extend also the duration of the short time ephemeris of reference.

This was in fact one of the motivation for the construction of the INPOP ephemerides. The goal was to obtain a full scale planetary ephemeris that could be extended over at least 1 Myr, and that could then be used as a target solution for the less accurate long time ephemeris. We have thus removed in INPOP all constraints that would limit the time validity of the solution. In particular, we have not used an external polynomial formula for precession, but we have integrated the precession equations of the Earth together with its orbital elements (Fienga et al., 2008). The numerical integrator has also been specifically designed in order to reduce the roundoff error during long time integrations.

2. INPOP NUMERICAL ERRORS OVER 1 MYR

The estimate of the error in Longitude in INPOP08 (Fienga et al., 2009) is obtained by integrating INPOP one way and back over 1 Myr. Each way is about 3 months of CPU time. The results are displayed in Table 1 (left) with the differences over 10, 100, and 1000 kyr. This error that comes from the numerical integration as well as from some instability of the system can be compared to the difference of the integration of INPOP06 and INPOP08 over the same time intervals (Table 1, right). It can be observed in Table 1 that over 10 kyr, the numerical error is much smaller than the model difference (INPOP06-INPOP08). This is still true over 100 kyr.

Over 1 Myr, the situation is more involved. Indeed, for the outer planets, the numerical error (Table 1) is much smaller than the model error (Table 2), and this is also the case for the Moon. This is also the case in a lesser extent for the inner planets, except for Mars where the numerical error is larger than the model error.

This is probably due to some instability resulting from the asteroidal motions. In that case, in both computations on INPOP06 and INPOP08, this instability is present and induces a large amplification of the initial differences of model. It is then understandable that the final difference over one way and back

	Differences in INPOP08 one way and back			Differences INPOP06 − INPOP08		
	10 kyr	100 kyr	1 Myr	10 kyr	100 kyr	1 Myr
Mercury	$< 1E-6$	0.004452	0.543	0.7	6	39
Venus	0.000107	0.117994	75.552	0.2	4	699
EMB	0.007642	0.834716	375.493	0.2	8	952
Mars	0.003620	20.916387	3905.538	0.4	42	694
Jupiter	$< 1E-6$	0.000514	1.214	32.6	326	3304
Saturn	$< 1E-6$	0.000116	0.466	8.1	80	769
Uranus	$< 1E-6$	0.000102	0.669	16.0	162	1718
Neptune	$< 1E-6$	0.000111	0.028	7.1	75	735
Pluto	$< 1E-6$	0.000124	0.030	94.8	378	5129
Moon	0.005105	0.779816	290.251	96.1	12678	1245609

Table 1: Maximum difference in longitude (in arcsec) in INPOP08 over 10 kyr, 100 ky and 1 Myr after one way and back (left) and differences in longitude (in arcsec) between INPOP06 and INPOP08 over 10 kyr, 100 ky and 1 Myr (right). EMB is the Earth-Moon barycenter

in INPOP08, or between INPOP06 and INPOP08 are in the same range. Because of these suspected instabilities, the errors in Table 1 are somewhat larger than what could be extrapolated from Table 1 of (Fienga et al., 2008). This is largely because the step size adopted for the long integrations is here 0.09375 days, about twice larger than the step size of 0.0553409090... days retained for the short time INPOP ephemerides. Although in most cases, the model error is still much larger than the numerical error, for a better consistency, we should adopt in further computation the same step size of 0.0553409090... days for short term and long term ephemerides. The price to pay will be to double the integration time.

Acknowledgements. This work was supported by ANR-ASTCM. It benefited from support from INSU-CNRS, PNP-CNRS, and CS, Paris Observatory.

3. REFERENCES

Fienga, A., Laskar, J., Morley, T., Manche, H., Kuchynka, P., Poncin-Lafitte, C. L., Budnik, F., Gastineau, M., and Somenzi, L. (2009). INPOP08, a 4-D planetary ephemeris: from asteroid and time-scale computations to ESA mars express and venus express contributions. A&A 507:1675–1686.

Fienga, A., Manche, H., Laskar, J., and Gastineau, M. (2008). Inpop06: a new numerical planetary ephemeris. A&A 477:315–327.

Imbrie, J. and Imbrie, K. P. (1979). Ice Ages: Solving the Mystery.

Laskar, J., Fienga, A., Gastineau, M., and Manche, H. (2011). La2010: A new orbital solution for the long term motion of the earth. http://adsabs.harvard.edu/abs/2011arXiv1103.1084L.

Laskar, J., Joutel, F., and Boudin, F. (1993). Orbital, precessional, and insolation quantities for the earth from -20 MYR to +10 MYR. A&A 270:522–533.

Laskar, J., Robutel, P., Joutel, F., Gastineau, M., Correia, A. C. M., and Levrard, B. (2004). A long-term numerical solution for the insolation quantities of the earth. A&A 428:261–285.

Standish, E. M. (1998). JPL Interoffice Memorandum, page 98.

DEVELOPMENT OF LONG-TERM NUMERICAL EPHEMERIDES OF TELLURIC PLANETS TO ANALYTICAL SERIES

S.M. KUDRYAVTSEV

Sternberg Astronomical Institute of Moscow State University
13, Universitetsky Pr., Moscow, 119992, RUSSIA
e-mail: ksm@sai.msu.ru

ABSTRACT. We develop numerical ephemerides of telluric planets to compact analytical series valid over 3000BC–3000AD. The long-term planetary ephemerides DE406 are used as the source; a spectral analysis of tabulated values for the heliocentric mean longitude of every telluric planets is made. For that purpose we used our modification of the spectral analysis method which allows one to develop the tabulated values directly to Poisson series where both amplitudes and arguments of the series' terms are high-degree polynomials of time. As a result, the maximum difference between the mean longitudes of the telluric planets given by the numerical ephemerides DE406 and the new analytical series is less than 0.07 arcsec over the total time interval of 6,000 years. The number of Poisson terms in every development is less than 950.

1. MODERN REPRESENTATIONS OF PLANETARY/LUNAR COORDINATES

There are three major approaches for development and representation of the planetary and lunar coordinates:

1. **Numerical ephemerides.** The following ephemerides of the major planets and the Moon are known as the most accurate now:

   - DE-series (Jet Propulsion Laboratory NASA, USA); the latest ephemerides of this series are DE423 (Konopliv et al., 2010);
   - EPM-series (Institute of Applied Astronomy RAS, Russia); the latest ephemerides of this series are EPM2010 (Pitjeva et al. 2010);
   - INPOP-series (IMCCE, Observatoire de Paris, France); the latest ephemerides of this series are INPOP10a (Fienga et al. 2010).

   An advantage of the numerical ephemerides is usually their high-accuracy, but a certain disadvantage is that they run up to hundreds megabytes and are often not cross-platform.

2. **Analytical/semi-analytical motion theories.** Historically, it was the first and for long time the only way for representation of the celestial bodies' coordinates. Last years the most advanced analytical motion theories of the major planets and the Moon are being developed at the BDL/IMCCE, France; the latest analytical theory of the planetary motion is VSOP2010 (Francou and Simon 2010).

   Advantages of the analytical/semi-analytical theories of planetary and lunar motion are their compactness and computer platform independence. In particular, this was one of the reasons why the BDL/IMCCE–based analytical series for lunar and planetary coordinates have replaced the JPL–based numerical ephemerides within all key elements of the ground software systems used for Hubble Space Telescope mission support (McCuttcheon 2003). However, it is relatively difficult to develop and improve analytical motion theories. As a consequence, the accuracy of the available analytical theories of the major planets' and Moon's motion is not so high as that of the modern numerical ephemerides of these bodies.

3. **Frequency analysis of planetary/lunar numerical ephemerides.** It is a "mixed" approach. First, numerical ephemerides are used for tabulating coordinates of celestial bodies over a certain interval of time. Then, by using a spectral analysis method, some analytical series approximating

the tabulated values are built. In particular, such an approach was used by Chapront (1995, 2000) for analytical representation of numerical ephemerides of the major planets and by Kudryavtsev (2007) for harmonic development of the lunar ephemeris.

In this way the advantages of the first and second approaches can be merged. The approximating series are usually compact and cross-platform. Moreover, the analytical series obtained with help of modern spectral analysis methods can be of accuracy compatible to that of numerical ephemerides (Kudryavtsev 2007, Kudryavtsev and Kudryavtseva 2009). A known disadvantage of any spectral analysis method is a problem of "close frequencies". However, it can be solved (or at least essentially diminished) by using, as the source, the long-term numerical ephemerides of the Moon and major planets which cover thousands of orbital periods of these bodies. To analytically represent numerical ephemerides over such a long-term interval, one should rather employ Poisson series, where both amplitudes and arguments of the series' terms are high-degree polynomials of time, than pure Fourier series. For that, a corresponding modification of the spectral analysis method was developed (Kudryavtsev 2004, 2007). The next section briefly presents the method.

2. SPECTRAL ANALYSIS OF PLANETARY EPHEMERIDES TO POISSON SERIES

Let $f(t)$ be a function tabulated by its numerical values over an interval of time $[-T, T]$ with a small sampling step. Over the same interval we build an analytical representation of the function by a finite h-order Poisson series of the following form

$$f(t) \approx \sum_{k=0}^{N} \Big[\big(A^c_{k0} + A^c_{k1} t + \cdots + A^c_{kh} t^h\big) \cos \omega_k(t) + \big(A^s_{k0} + A^s_{k1} t + \cdots + A^s_{kh} t^h\big) \sin \omega_k(t) \Big] \tag{1}$$

where $A^c_{k0}, \cdots, A^s_{kh}$ are constants and $\omega_k(t)$ are some pre-defined arguments which are assumed to be q-degree polynomials of time t, and

$$\omega_0(t) \equiv 0, \qquad \omega_k(t) = \nu_k t + \nu_{k2} t^2 + \cdots + \nu_{kq} t^q \quad \text{if } k > 0. \tag{2}$$

In order to obtain such an expansion, we first find the projections of $f(t)$ on a basis generated by functions

$$\mathbf{c}_{kl}(t) \equiv t^l \cos \omega_k(t), \quad \mathbf{s}_{kl}(t) \equiv t^l \sin \omega_k(t); \quad k = 0, 1, \cdots, N;\ l = 0, 1, \cdots, h$$

through numerical computation of the following scalar products

$$A^c_{kl} = < f, \mathbf{c}_{kl} > \equiv \frac{1}{2T} \int_{-T}^{T} f(t) t^l \cos \omega_k(t) \chi(t)\, dt, \tag{3}$$

$$A^s_{kl} = < f, \mathbf{s}_{kl} > \equiv \frac{1}{2T} \int_{-T}^{T} f(t) t^l \sin \omega_k(t) \chi(t)\, dt \tag{4}$$

where $\chi(t) = 1 + \cos \frac{\pi}{T} t$ is the Hanning filter chosen as the weight function. The proper choice of arguments $\omega_k(t)$ depends on the specific task. In the present study the polynomial arguments of the resulting Poisson series are various combinations of multipliers of the planetary mean mean longitudes, where the latter are defined by Simon et al. (1994).

However, the basis functions $\mathbf{c}_{kl}$, $\mathbf{s}_{kl}$ are not usually orthogonal. Therefore, at the second step we perform an orthogonalization process over the expansion coefficients in order to improve the quality of representation and avoid superfluous terms [see details in Kudryavtsev (2004, 2007)].

In the present study we use this method in order to develop the planetary numerical ephemerides to compact Poisson series. There are several options for the planetary variables to be represented by analytical series:

- rectangular (Cartesian) coordinates;
- spherical coordinates: distance, latitude, longitude;
- osculating orbital (e.g. Keplerian) elements;
- differences of osculating orbital elements from their mean values.

After some tests we have chosen the latter option. The heliocentric mean longitude of a planet is represented as follows

$$\lambda(t) = \bar{\lambda}(t) + \sum_{k=1}^{N} \big[A_{k0} \sin\big(\omega_k(t) + \varphi_{k0}\big) + A_{k1} t \sin\big(\omega_k(t) + \varphi_{k1}\big) + A_{k2} t^2 \sin\big(\omega_k(t) + \varphi_{k2}\big) \big], \qquad (5)$$

where $\bar{\lambda}(t)$ is the mean mean longitude of the planet as defined by Simon et al. (1994).

We made harmonic development of the mean longitude of four telluric planets: Mercury, Venus, Earth-Moon barycenter (EMB) and Mars. We started with tabulating numerical values for the difference between the osculating heliocentric mean longitude of every considered planet and the corresponding planetary mean mean longitude on every day within 3000BC–3000AD. The most long-term planetary ephemerides DE406 (Standish 1998) are used as a source. Then the tabulated values were processed by a new modification of the spectral analysis method as described above, and compact Poisson series representing the planetary mean longitude in form (5) are built. Table 1 presents the main characteristics of these series.

Planet	Maximum difference from DE406	Number of terms, N
Mercury	0.014”	331
Venus	0.035”	450
EMB	0.022”	568
Mars	0.068”	948

Table 1: Expansion of heliocentric mean longitude of telluric planets over 3000BC–3000AD.

The accuracy of the new development is compatible to that obtained by Chapront (2000) in his representation of planetary mean longitudes from DE406 over the same interval of time. A better approximation accuracy by Chapront (2000) is reached in case of Mercury and Venus, a better accuracy by us is reached in case of EMB and Mars. However, Chapront (2000) made his expansion for the difference between the planetary mean longitudes from DE406 and those provided by the VSOP87 analytical theory of planetary motion (Bretagnon and Francou 1988). Therefore, the series by Chapront (2000) should be completed by the corresponding terms from VSOP87. As a result, the total number of terms necessary to represent the planetary mean longitude is there essentially more than that in our solution.

The current version of the VSOP2010 analytical theory approximates the DE406 mean longitudes of the telluric planets with a maximum error of a few 0.1 arcsec over 6,000 years (Francou and Simon 2010). However, these values might be not the final ones, because the work on this exceptional theory is being continued.

Acknowledgements. Research supported in part by the Russian Foundation for Basic Research under grant no. 10-02-00234-a. A travel grant provided to the author by the LOC of the Journées 2010 and the French Ministry of Research (MESR) in the framework of the programme ACCES is sincerely appreciated.

3. REFERENCES

Bretagnon, P., Francou, G., 1988, “Planetary theories in rectangular and spherical variables”, A&A , 202, pp.309–315.

Chapront, J., 1995, “ Representation of planetary ephemerides by frequency analysis. Application to the five outer planets” A&AS , 109, pp.181–192.

Chapront, J., 2000, “Improvement of planetary theories over 6000 years”, Celest. Mech. Dyn. Astr. , 78, pp.75–82,

Fienga, A., Manche, H., Kuchuynka, P., Laskar, J., Gastineau, M., 2010, “INPOP10a”, arxiv:1011.4419v1 [astro-ph.EP] 19 November 2010.

Francou, G., Simon, J.L., 2010, “New analytical planetary theories VSOP2010”, Poster at the Journées 2010, Observatoire de Paris, 20–22 September 2010.

Konopliv et al. 2010, “DE423”, ftp://ssd.jpl.nasa.gov/pub/eph/planets/ascii/de423/. Accessed 11 December 2010.

Kudryavtsev, S.M., 2004, “Improved harmonic development of the Earth tide generating potential”, J. Geodesy, 77, pp.829–838, doi: 10.1007/s00190-003-0361-2.

Kudryavtsev, S.M., 2007, “Long-term harmonic development of lunar ephemeris”, A&A , 471, pp.1069–1075, doi: 10.1051/0004-6361:20077568.

Kudryavtsev, S.M., Kuryavtseva, N.S., 2009, “Accurate analytical representation of Pluto modern ephemeris”, Celest. Mech. Dyn. Astr. , 105, pp.353–360, doi: 10.1007/s10569-009-9236-z.

McCuttcheon, R.A., 2003, “A platform-independent solar-lunar-planetary package for flight dynamics applications based on methods from the Bureau des Longitudes”, Preprint of Institute of Applied Mathematics RAS, N 32, p.7.

Pitjeva, E., Bratseva, O., Panfilov, V., 2010, “EPM–ephemerides of planets and the moon of IAA RAS: their model, accuracy, availability”, Book of Abstracts of the Journées 2010, Observatoire de Paris, 20–22 September 2010, p.7.

Simon, J.L., Bretagnon, P., Chapront, J., Chapront-Touzé, M., Francou, G., Laskar, J., 1994, “Numerical expressions for precession formulae and mean elements for the Moon and planets”, A&A , 282, pp.663–683.

Standish, E.M., 1998, “JPL planetary and lunar ephemerides DE405/LE405”, Technical Report 312.F–98–048, JPL Interoffice Memorandum.

NEW VERSION OF EPM-ERA LUNAR THEORY

G.A. KRASINSKY, S.O. PROKHORENKO, E.I. YAGUDINA
Institute of Applied Astronomy, Acad. Sci., Russia
10, Kutuzov quay, 191187-St-Petersburg, Russia
e-mail: kra@ipa.nw.ru; prs@ipa.nw.ru; eiya@ipa.nw.ru

ABSTRACT. The numerical Lunar theory EPM-ERA has been developed in IAA RAS (Krasinsky 2002, Aleshkina et al.1996). In the paper (Yagudina 2008) 16320 LLR data (1970-2008) have been included for the process of improving the Moon ephemeris and obtaining some selenodynamical parameters. A new version of ERA-EPM Lunar theory was corrected by the improved model of dissipative effect of the lunar rotation by integrating the orbital and rotational motions with the retarded argument. The comparison of the improved dynamical model with 17131 LLR data from 1970 till 2010 has been made. This version has been compared with three versions of DE ephemerides.

1. INTRODUCTION

The lunar part of EPM ephemerides of IAA RAS is called EPM-ERA. In the paper, a new version of EPM-ERA2010 is presented. This version differs from the previous ones by the following:

1. Tidal perturbations in the orbital Lunar motion (due to the tidal dissipation on the Earth's body), as well as in the rotational motion of the Moon (due to tidal dissipation on the Moon's body) are computed by a more complicated model with the retarded argument (compare with the previous EPM-ERA2008);

2. In the processing of LLR observations 17131 were used instead of 16320 LLR observations in the previous version;

3. The new version was transformed in the new ERA-Windows. The previous versions were calculated in DOS version (Krasinsky and Vasiliev, 1996).

2. MODEL AND ESTIMATED PARAMETERS

A dynamical model has been developed by the simultaneous numerical integration of the orbital and rotational motion of the Moon, major planets and biggest asteroids. The potential of the Moon is calculated up to 4-th order of the zonal index. The potential of the Earth includes the 2-th order harmonics C_{20}, C_{22}. Tidal perturbation in the lunar orbital motion (due to tidal dissipation on the Earth's body) and also in rotational Lunar motion (due to tidal dissipation on the Moon's body) was computed by a model with a retarded argument. Method of integration is Everhart's method with the constant step of integration. Partials of lunar ranging with respect to the dynamical parameters of the

N	Parameters estimated
1-6	Lunar orbital state vector for the epoch JD 2446000.5
7-12	Euler's angles and their time derivatives for the same epoch
13-18, 22-24	Coordinates of reflectors A11, A14, L2
20	X coordinate for reflector Apollo 15 (A15)
25-42	Coordinates of 6 observational stations
44	Lag of Earth's body tides
48-51	Secular trends in sidereal angles of the Earth and Moon
55	Lag of Moon's body tides
52-54, 59-63	Harmonics of lunar potential from C_{20} to S_{33}
56-58	Lunar Love numbers k_2, h_2, l_2
64-65	Secular trends of the corrections to the parameters of Earth's equator

Table 1: Parameters determined

orbital and rotational model of the Moon are computed by the integration of variational equations; in few cases, they were obtained by integration of a rigorous system of equations with slightly varying values of the parameter (k_2). The set of parameters includes the lunar initial coordinates and velocities, libration angles and their velocities, harmonics of lunar potential from C20 to S33, Lunar Love numbers k_2, h_2, l_2, the coordinates of reflectors, observational stations and others (Table 1). In LLR analysis, a number of parameters appeared to be strongly correlated and may only be estimated because four reflectors could be observed. Unfortunately, such disparity of the observation distribution deteriorates the estimate reliability of a number of selenodynamical parameters. As lunar rangings are invariant relatively to the rotation of the Earth-Moon system as a whole, the whole set of the orientation parameters of this system cannot be determined simultaneously. Due to this reason, two coordinates of the most frequently observable reflector Apollo 15 were fixed (longitude and latitude). The values of these two parameters were obtained from a simplified solution made as the first step, in which lunar libration was not improved. The LLR observations are sensitive to the Earth's gravitational constant Gm_E. The investigation shows that the observable effect cannot be reliably separated from corrections to X coordinate of the reflectors. Thus, the Gm_E value has not been included in the list of parameters.

3. OBSERVATIONS

In the present analysis, 17131 LLR observations have been included in the processing. They were carried out mainly at McDonald (Texas), where at different epochs three different sites were activated as McDonald observatory, MLRS1 and MLRS2; Cerga station (France) and a set of observations of the two years duration made at Haleakala Observatory (Hawai) and 643 observations were made in Apache station (mm accuracy). The number of observations at each site is shown in Table 2. Four reflectors could be observed: 1-Apollo 11, 2-Apollo 14, 3-Apollo 15, 4-Lunahod2. The number of ranging to Apollo 11, Apollo 14, Apollo 15, Lunahod2 are 1723, 1670, 13231 and 486, respectively.

Station	Time interval	Number of LLR observations
McDonald	1970 Mar - 1985 Jun	3440
MLRS1	1985 Jan - 1988 Jan	275
MLRS2	1988 Aug - 1900 August	3066
HALEAKALA	1989 Nov - 2010 March	694
CERGA	1985 Jan - 2010 March	9013
APACHE	2006 August - 2009 June	643
TOTAL	1970 Mar- 2010 April	17131

Table 2: Distribution of LLR observations caption

4. ANALYSIS OF RESULTS

Using the derivatives from EPM-ERA, all the calculations have been made with the three versions of DE ephemerides: DE403, DE405, DE421. The O-C, post-fit residuals (wrms), the number of included and rejected LLR observations by the processing of DE ephemerides along with EPM are given in Table 3. Because the EPM-ERA model was been implemented by the obtained corrections, the post-fit residuals practically coincide with the O-C difference computed with the improved model equal (6.8 cm).

Ephemeris	O-C Wrms (cm)	Residuals Wrms (cm)	Number of observations	Number of deleted observations
DE403	22.2	5.2	16827	304
DE405	258.2	5.6	16837	294
DE421	561.8	5.7	16833	298
EPM-ERA2010	6.8	6.8	16821	310

Table 3: O-C and residuals for DE ephemerides compared with EPM-ERA2010

For the current version of EPM-ERA, the post-fit residuals and O-C coincide. For DE ephemerides, a similar work could not be carried out on the full scale and only corrections to reflector coordinates and observational stations were incorporated.

wrms (cm) O-C	wrms(cm) residuals	number of observations	Observational stations	Interval of observations
39.5	30.3	3411	McDonald	19700415.0 - 19850630.0
10.7	7.2	275	MLRS1	19850301.0 - 19880127.1
16.4	4.1	8996	CERGA	19840407.2 - 20100121.2
14.3	7.2	694	Haleakala	19841113.1 - 19900830.1
17.6	5.6	2808	MLRS2	19880229.0 - 20100405.1
39.5	3.4	643	Apache	20060407.1 -20090615.1
22.2	5.2	16827	All stations	19700415.0 -20100405.1

Table 4: DE403 ephemeris, statistics of residuals

wrms (cm) O-C	wrms(cm) residuals	number of observations	Observational stations	Interval of observations
267.9	28.9	3416	McDonald	19700415.0 - 19850630.0
227.6	7.5	275	MLRS1	19850301.0 - 19880127.1
246.9	4.5	8996	CERGA	19840407.2 - 20100121.2
133.8	7.6	694	Haleakala	19841113.1 - 19900830.1
215.0	5.8	2811	MLRS2	19880229.0 - 20100405.1
348.6	4.7	643	Apache	20060407.1 -20090615.1
258.2	5.6	16837	All stations	19700415.0 -20100405.1

Table 5: DE405 ephemeris, statistics of residuals

wrms (cm) O-C	wrms(cm) residuals	number of observations	Observational stations	Interval of observations
577.7	29.5	3411	McDonald	19700415.0 - 19850630.0
533.9	6.5	275	MLRS1	19850301.0 - 19880127.1
535.7	4.6	8999	CERGA	19840407.2 - 20100121.2
288.8	8.3	694	Haleakala	19841113.1 - 19900830.1
483.2	6.1	2811	MLRS2	19880229.0 - 20100405.1
750.4	3.9	643	Apache	20060407.1 -20090615.1
561.8	5.7	16833	All stations	19700415.0 -20100405.1

Table 6: DE421 ephemeris, statistics of residuals

Tables 4, 5, 6, 7 demonstrate the post-fit residuals and O-C (cm wrms, the number of observations for 6 stations, the observational interval at each station and the same parameters for all the stations together for all DE ephemerides (DE403, De405, DE421) and for EPM-ERA2010. The plots of Fig. 1, Fig. 2, Fig. 3, Fig. 4 show us the statistics of residuals for all ephemerides.

5. CONCLUSION

The investigation shows that the inner accuracy of DE ephemerides (5.4-5.7cm) is slightly better than that of EPM-ERA2010 (6.8 cm). But the accuracy of DE ephemerides cannot be used by an independent researcher because it is not possible to feed back the corrected values of the parameters. In the current version of EPM-ERA2010 ephemeris, an attempt to improve the model of the tidal perturbations in the rotational motion of the Moon (due to dissipation in Moon's body) has been carried out. The expansion of the retarded function in a power series of delay is used. This part of the model needs small further improvements.

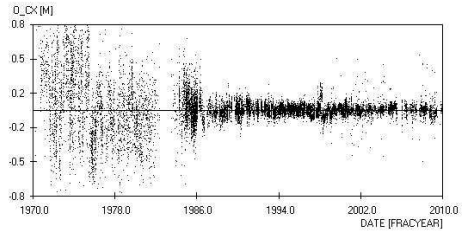

Figure 1: DE403

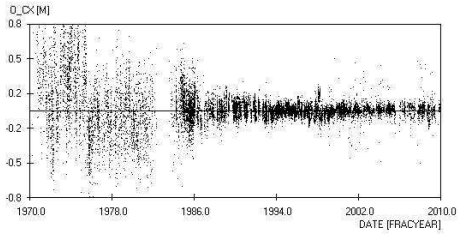

Figure 2: DE405

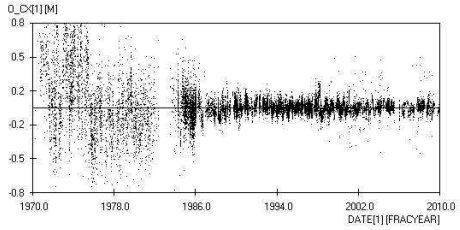

Figure 3: DE421

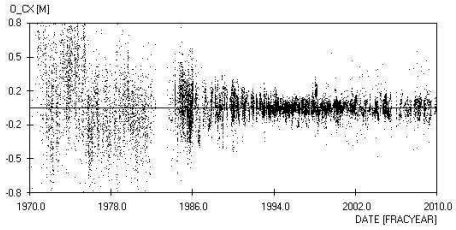

Figure 4: EPM-ERA2010

wrms (cm) O-C	wrms(cm) residuals	number of observations	Observational stations	Interval of observations
31.5	31.5	3399	McDonald	19700415.0 - 19850630.0
12.2	12.2	275	MLRS1	19850301.0 - 19880127.1
5.1	5.1	8996	CERGA	19840407.2 - 20100121.2
13.6	13.7	694	Haleakala	19841113.1 - 19900830.1
6.7	6.7	2808	MLRS2	19880229.0 - 20100405.1
5.7	5.7	643	Apache	20060407.1 -20090615.1
6.8	6.8	16821	All stations	19700415.0 -20100405.1

Table 7: EPM-ERA2010 ephemeris, statistics of residuals

6. REFERENCES

Krasinsky G.A.,2002, "Selenodynamical parameters from analysis of LLR observations of 1970-2001", Communications of the IAA RAS, N 148, pp.1–27.

Aleshkina E.Yu., KrasinskyG.A., Vasiliev M.V .1996, "Analysis of LLR data by the program ERA", Proceedings of IAU Colloquium 165, Poznan, Poland, pp. 228–232.

Yagudina E.I., 2008. "Numerical Lunar Theory EPM2008 from Analysis of LLR data", Book of abstracts Journées, Dresden, 22-24 September, pp11.

Krasinsky G.A., Vasiliev M.V.1996, "ERA: knowledge base for Ephemeris and dynamical astronomy", Proceedings of IAU Colloquium 165, Poznan, Poland, pp.239–244.

LLR RESIDUALS OF INPOP10A AND CONSTRAINTS ON POST-NEWTONIAN PARAMETERS

H. MANCHE[1], A. FIENGA[2], J. LASKAR[1], S. BOUQUILLON[3], G. FRANCOU[3], M. GASTINEAU[1]

[1] IMCCE, UMR8028, Observatoire de Paris, UPMC
77 avenue Denfert-Rochereau, 75014 Paris
e-mail: manche@imcce.fr

[2] Observatoire de Besançon
41 bis avenue de l'Observatoire, BP 1615, 25010 Besançon cedex

[3] SYRTE, Observatoire de Paris, CNRS, UPMC
61 avenue de l'Observatoire, 75014 Paris

ABSTRACT. Among all parameters involved in Lunar Laser Ranging computations (dynamical and reduction model), only some of them can be fitted to observations. Following is presented the method of their selection used for INPOP solutions and the residuals obtained. Then, adding the parameterized post-Newtonian parameters β and γ to the list of fitted parameters gives some constraints on their values and uncertainties.

1. SELECTION OF THE PARAMETERS FITTED TO LLR OBSERVATIONS

A planetary and lunar solution depends on:

- a dynamical model, describing how all bodies are interacting together
- a model of data reduction; for LLR observations, the model describes the light propagation from emission (on the Earth) to reflection (on the Moon) and reception (back on the Earth)
- a set of parameters, whose values are determined by a least square fit to observations

A total of 188 parameters are involved in LLR computations. They are listed in table 1, but all of them are not independent. For example, a modification of the position of Haleakala's emission station can be compensated by changing the position of the reception one; thus, they can not be fitted together. Other parameters are better determined by planetary observations (like the Earth-Moon mass ratio and the initial conditions for the Earth-Moon barycenter) or other techniques (velocities of stations by VLBI). Eventually, most of the offsets taken into account by J. Williams (private communication) are up to now ignored, because further investigation is needed about their relevance.

Parameter	Number
selenocentric positions of reflectors	12
geocentric positions and velocities of the 7 stations	42
initial conditions for the Earth-Moon vector (position and velocity)	6
initial conditions for Moon's librations (Euler's angles and their derivatives)	6
initial conditions for the Earth-Moon barycenter vector (position and velocity)	6
Earth's zonal coefficients of potential up to 4^{th} degree	3
Moon's zonal and tesseral coefficients of potential up to 4^{th} degree	18
Moon's principle moment of inertia C	1
time delays and Love numbers involved in tides effects (Earth and Moon)	10
ratio and sum of the masses of the Earth and the Moon	2
post-Newtonian parameters β and γ	2
offsets (constant and linear terms) applied to LLR measurements for some periods	40×2

Table 1: List of the 188 parameters involved in the reduction of LLR observations

Removing all these kinds of parameters leads to fit only 74 ones. But some of them remain badly determined, with important formal error compared to the fitted value: for example, the Moon's potential

coefficient S_{43} is fitted to $(-2.0 \pm 13.5) \times 10^{-6}$.

To select which parameters are to be fitted to LLR observations, an iterated process is used by removing at each step the one with the greatest ratio between the formal error and the value. Removing degrees of freedom induces a weak increase of residuals to observations, as shown in table 2 with Grasse (3), Mc Donald, MLRS2 or Apollo data. On the other hand, fixing the value of a parameter may decrease the formal error of an another one if they are strongly correlated. For example, it is the case for the Moon's coefficient of potential C_{33}, which formal error decreases from 6.8×10^{-7} when 74 parameters are fitted, to 3.3×10^{-8}, 6.3×10^{-9}, 5.2×10^{-9} and 4.6×10^{-9} when only 65, 59, 55 and 51 parameters are fitted.

The INPOP10a solution, that is S059, is chosen so that the formal errors of all parameters represent less than 5% of the fitted values. Its Chebychev representation is available at `www.imcce.fr/inpop` and its LLR residuals are shown in table 2.

The R423 column of table 2 shows residuals obtained with our own reduction process, applied to the latest JPL's solution DE423, and by fitting only parameters involved in the reduction (positions of stations and reflectors, some offsets). Residuals shown here are thus not the ones obtained directly by the JPL, which could be much lower: for instance, less than 2 cm for Apollo station (Williams, private communication). One can see that they are better than INPOP10a ones (except for MLRS2 from 1988 to 1999), maybe because DE423 takes into account a lunar core.

	Solution:	S074	...	S065	...	S059	...	S055	...	S051	R423
	Maximum ratio	750%	...	9%	...	3.6%	...	1.2%	...	0.3%	
Station	Period	σ(cm)	...	σ(cm)	...	σ(cm)	...	σ(cm)	...	σ(cm)	σ(cm)
Grasse (1)	1984-1986	15.9	...	15.9	...	16.0	...	15.6	...	16.2	14.7
Grasse (2)	1987-1995	6.3	...	6.3	...	6.4	...	6.0	...	8.2	5.9
Grasse (3)	1995-2010	3.7	...	3.7	...	4.0	...	5.4	...	6.9	3.9
Mc Donald	1969-1985	31.2	...	31.4	...	31.8	...	36.1	...	50.0	29.8
MLRS1 (1)	1982-1985	73.3	...	73.0	...	73.3	...	72.5	...	71.7	70.3
MLRS1 (2)	1986-1988	8.0	...	7.5	...	7.3	...	7.4	...	9.8	6.1
MLRS2 (1)	1988-1999	4.3	...	4.3	...	4.3	...	4.3	...	6.5	4.7
MLRS2 (2)	1999-2008	4.6	...	4.6	...	4.8	...	4.9	...	6.5	4.6
Haleakala	1984-1992	8.1	...	8.2	...	8.1	...	8.4	...	11.6	8.1
Apollo	2006-2009	4.8	...	4.9	...	4.9	...	5.3	...	7.1	4.7

Table 2: Evolution of LLR residuals during the selection of fitted parameters process. For each solution Sxxx (where xxx is the number of parameters fitted) is given the greatest ratio between the formal error and the fitted value for the parameters. σ is the standard deviation of residuals for each station and epoch, expressed in centimeters. INPOP10a corresponds to the solution S059, with 59 parameters fitted.

2. TESTS OF POST-NEWTONIAN PARAMETERS β AND γ

The post-Newtonian parameters β and γ are involved at several steps in the building of a planetary and lunar solution, both in the dynamical and reduction parts:

- in the computation of Einstein-Infeld-Hoffmann acceleration vectors of bodies (see for instance Newhall, 1983)
- in the computation of the additional geodesic torques upon the Earth and the Moon (see for instance Misner et al., 1973)
- in the time scale transformation between TT and TDB (see Fienga et al., 2009 or Klioner et al, 2010)
- in the time delay due to the relativistic light deviation (see Williams et al., 1996).

Changing their values with respect to the general relativity ones (β=γ=1) will have consequences on LLR computations. They thus can be fitted together with the same 59 parameters as for INPOP10a. Three kinds of adjustments have been conducted:

- fit of β and the same 59 parameters as INPOP10a, with γ fixed to 1 (that is 60 fitted parameters).
- fit of γ and the same 59 parameters as INPOP10a, with β fixed to 1 (that is 60 fitted parameters).
- fit of γ, β and the same 59 parameters as INPOP10a (that is 61 fitted parameters).

For each type of adjustment, the uncertainties at 3σ (where σ is the formal error provided by the least square fit) are given in table 3. They are smaller than in (Müller et al., 2008), but fitted values are not always consistent with the general relativity.

Parameters fitted	$\beta - 1$	$\gamma - 1$	Correlation
(59)+β	$(-0.2 \pm 0.4) \times 10^{-3}$	0 (fixed)	$[\beta, X] = 0.35$
(59)+γ	0 (fixed)	$(-1.1 \pm 0.76) \times 10^{-3}$	$[\gamma, X] = 0.33$
(59)+β+γ	$(5.1 \pm 1.6) \times 10^{-3}$	$(-9.7 \pm 2.8) \times 10^{-3}$	$[\beta, \gamma] = 0.96$

Table 3: Fitted values and uncertainties (at 3σ) of post-Newtonian parameters β and γ. [β,X] (respectively [γ,X]) is the maximum correlation between β (respectively γ) and one of the 59 other parameters.

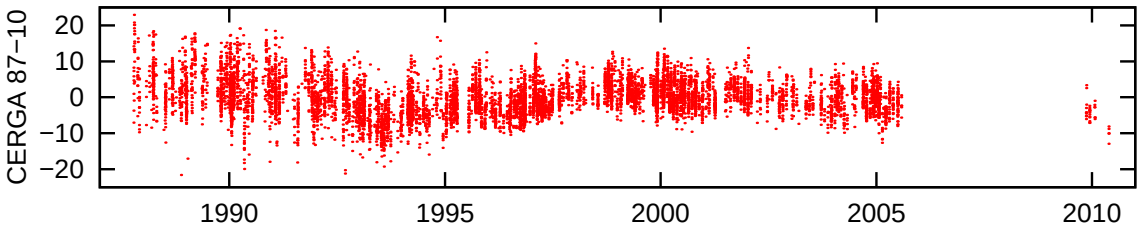

Figure 1: INPOP10a's LLR residuals (in cm) for the CERGA station, between 1987 and 2010.

These bad results could come not only from a big correlation (0.96) between β and γ, but also from the remaining signal on residuals for CERGA's observations, shown on figure 1. This latter is characteristic of a problem in modeling, that adjustment of parameters tries to compensate, and potentially leads to biased values. This signal has always been present in our LLR computations, including the R423 reduction previously described. The potential problem is thus not in the dynamical part, because INPOP's and DE423's modelings are independent. The signal is also present in the S2000 solution of (Chapront et al., 2001), where both dynamical and reduction modelings differ from INPOP's ones.

Other tests have been made by computing a map of (β,γ). More than 1600 couples of values (β,γ) are fixed in $[0.95, 1.05]^2$. For each one, a solution is built by fitting the same 59 parameters as in INPOP10a; then, the χ^2 and R functions are evaluated:

$$\chi^2(\beta,\gamma) = \sum_i \rho_i^2 (O-C)_i^2 \text{ and } R(\beta,\gamma) = \sqrt{\frac{\chi^2}{\chi_0^2}} - 1 \qquad (1)$$

In these expressions, $(O-C)_i$ are the residuals (differences between the measurement and the computation), (ρ_i) are the ponderations applied to the observations, $\chi_0^2 = \chi^2(\beta_0, \gamma_0)$, where β_0 and γ_0 are the values where χ^2 is minimum, that is the ones from the last line of tab. 3. The R function is representative of the increase of residuals when β and γ differ from the "optimal" values (β_0,γ_0). Its contour lines are shown on figure 2.

First, one can notice that the shapes of ellipses confirm the strong correlation between β and γ. The best determined combination seems to be according the $2\beta - 11\gamma$ direction. It is different from the Nordtvedt parameter $\eta = 4\beta - \gamma - 3$, maybe because for LLR computations, post-Newtonian parameters are involved not only in the Lunar orbit around the Earth, but also in the light propagation with the Shapiro's deviation.

Second, one can notice that the general relativity values (blue dot) are not so far away from the ones where χ^2 is minimum (green dot), with a degradation limited to less than $R = 0.5\%$. For instance, LLR residuals for the CERGA's station between 1995 and 2010 grow from 3.98 cm to 4.0 cm when β and γ are both fixed to 1. This weak increase is not significant and is smaller than variations induced by changing the ponderations, the preliminary solution first fitted to planetary observations, ...

In the end, the constraints on post-Newtonian parameters obtained with LLR do not seem to be as good as the ones obtained by adjustment to planetary observations, exposed in this volume by (Fienga et al, 2010, figure 4). This point of view has to be balanced by the fact that LLR residuals computed directly at JPL by J. Williams are much lower than the ones of INPOP10a. Even if these latter are consistent with (Chapront et al.,2001), (Aleshkina, 2002) or solutions actually developed at SYRTE by S. Bouquillon and G. Francou, an improvement of the reduction modeling seems to be possible.

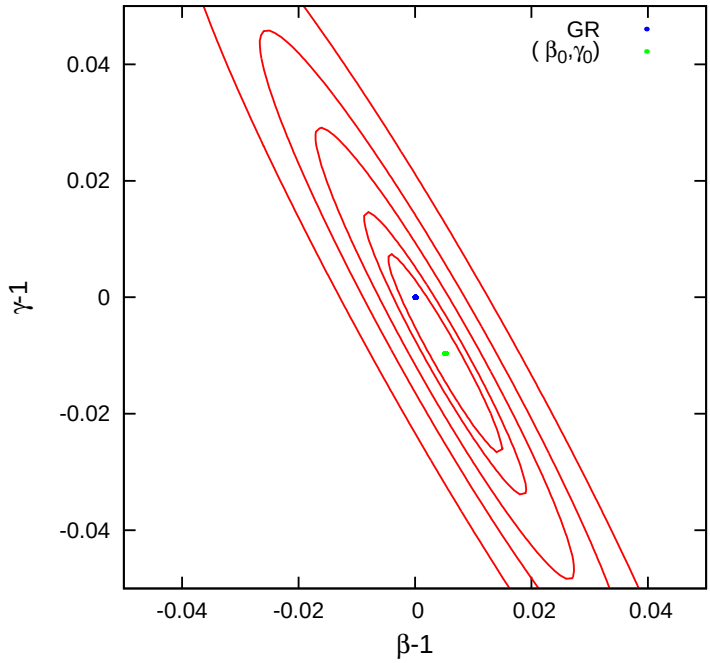

Figure 2: Contour lines (1%, 2%, 5%, 10% and 20%) for the R function. The blue dot corresponds to the general relativity values (β=γ=1), the green dot corresponds to the values of β and γ where χ^2 is minimum (see the last line of table 3).

3. REFERENCES

Aleshkina, E. Y., 2002, "Lunar numerical theory and determination of parameters k_2, δ_M from analysis of LLR data", A&A , 394, pp. 717-721

Chapront, J., Chapront-Touzé, M., and Francou, G. 2001, "Contribution of LLR to the reference systems and precession", in Journées 2000 - Systèmes de référence spatio-temporels, ed. N. Capitaine, pp. 96-101

Fienga, A., Laskar, J., Morley, T., Manche, H., Kuchynka, P., Le Poncin-Laffitte, C., Budnik, F., Gastineau, M., and Somenzi, L., 2009, "INPOP08, a 4-D planetary ephemeris : from asteroid and time-scale computations to ESA Mars Express and Venus Express contributions", A&A , 507, 1675

Fienga, A., Laskar, Manche, H., Kuchynka, P., and Gastineau, M., 2010, "Planetary and lunar ephemerides INPOP10a", in this volume

Klioner, S. A., Gerlach, E., and Soffel, M. H., 2010, "Relativistic aspects of rotational motion of celestial bodies", in IAU Symposium, Vol. 261, IAU Symposium, ed. S. A. Klioner, P. K. Seidelmann, and M. H. Soffel, pp. 112–123

Misner, C. W., Thorne, K. S., and Wheeler, J. A., 1973, "Gravitation", ed. Misner, C. W., Thorne, K. S., and Wheeler, J. A.

Müller, J., Williams, J. G., and Turyshev, S. G., 2008, "Lunar Laser Ranging Contributions to Relativity and Geodesy", in Astrophysics and Space Science Library, Vol. 349, Lasers, Clocks and Drag-Free Control : Exploration of Relativistic Gravity in Space, ed. H. Dittus, C. Lammerzahl, and S. G. Turyshev, pp. 457-472

Newhall, X. X., Standish, E. M., and Williams, J. G., 1983, "DE 102 - A numerically integrated ephemeris of the moon and planets spanning forty-four centuries", A&A , 125, pp. 150–167

Williams, J. G., Newhall, X. X., and Dickey, J. O., 1996, "Relativity parameters determined from lunar laser ranging", Phys. Rev. D, 53, 6730

GEODESY INSTRUMENT PACKAGE ON THE MOON FOR IMPROVING OUR KNOWLEDGE OF THE MOON AND THE REALIZATION OF REFERENCE FRAMES

V. DEHANT[1], J. OBERST[2], R. NADALINI[3]
[1] Royal Observatory of Belgium
3 avenue Circulaire, B1180 Brussels, Belgium
e-mail: v.dehant@oma.be
[2] Technical University Berlin and DLR-Berlin, Germany
e-mail: oberst@igg.tu-berlin.de
[3] Active Space Technologies GmbH, Berlin, Germany
e-mail: riccardo.nadalini@activespacetech.com

ABSTRACT. The use of passive Laser reflectors on the lunar surface appeared to be the most attractive in the Apollo era, but the next generation of LLR experiment should therefore aim at a substantial improvement thanks to a one way ranging concept. A particular strength of this proposed experiment is given when several stations are ranging to the Moon simultaneously and/or when several geodetic stations on the Moon are used simultaneously, as this is expected to improve the modeling geometry and data quality. The proposed experiment may well initiate the installation of new observing stations on Earth - perhaps within the infrastructure of existing astronomical observatories. In the case of the beacon mode, only passive optical receivers are needed on the ground. We explore the requirements for the instrumentation of such a ground station. We propose to deploy and operate a microwave receiver/transmitter with precisely known mechanical local ties to the Laser beacon/receiver, which will permit observations of the tangential position of the moon with respect to the celestial frame. We propose to include a GNSS microwave transmitter into the proposed equipment realizing a "GPS/Galileo satellite on the Moon" that is tracked together with GNSS satellites by receivers on the ground and possibly on the future generation of GNSS satellites. The ultimate objectives of our proposal are twofold, the improvement of the reference frames for the Earth and a better understanding of the Moon's interior.

1. OBJECTIVES

Owing to technological advances over the years, one can expect that the future geodetic measurement resolution will be improved by more than an order of magnitude. This step is nevertheless presently still limited by the instrumental precision level and by the geometry involved in the present measurement reference frames. We propose the deployment of a set of geodetic instruments on the Moon in order to improve the reference frame realizations for the Earth. In addition, the proposed set-up shall improve the ranging and Doppler measurements to the Moon, and thus the knowledge about the interior of the Moon. Applications to the moons of Mars and to lander on the Martian surface shall provide wonderful opportunities to dedicated science there and also to reference frame improvements.

2. STATE OF THE ART AND NEXT DESIGN

Presently there are only passive Laser reflectors on the lunar surface. These reflectors are targeted by the Earth Lunar Laser Ranging (LLR) ground stations and the round-trips of photons are used for measuring the Earth-Moon distance in the line of sight. There are presently five retroreflectors on the Moon surface.

A few decade ago, it was conceivable to make range measurements to the Moon by several alternative techniques. However, the use of passive Laser reflectors on the Lunar surface appeared to be the most attractive in the Apollo era for simple reasons: while the retroreflector arrays which had to be taken to the Moon were reasonably compact and very robust against failure, all the technologically complex instrumentation remained on Earth. In fact, owing to technological advances over the years, the measurement resolution could be improved by more than one order of magnitude, which is the basis of many

scientific results that were achieved.

Unfortunately, the Laser link budget for ranging is very marginal, and even today, only very few terrestrial stations have the sophisticated technical equipment required to participate in Lunar ranging campaigns. As a consequence, a limited number of measurements have been collected in the past, and the distribution of measurements within the lunar cycle is strongly biased. A next generation LLR experiment should therefore aim at a substantial improvement of the link budget, so that the technique can cope e.g. with both a close proximity of the solar light background (new moon) and maximum brightness around the lunar target (full moon).

In parallel to this, it is highly desirable to complement the lunar laser ranging measurements with Very Long Baseline Interferometry (VLBI) measurements to the Moon as well as with the use of compact and precise radio transponders at the location of the landing sites on the Moon surface.

At the same time it is highly desirable to combine all the currently available high precision space geodetic techniques i.e. VLBI and Global Navigation Satellite System (GNSS) on Earth to match the currently available equipment at geodetic observatories. On Earth, the most commonly used precise positioning technique is indeed performed by GNSS observations. The GNSS satellite orbits are monitored from the ground and the inertial frame is provided by the observation of radiosources using VLBI. Similarly for the DORIS (Détermination d'Orbite et Radiopositionnement Intégrés par Satellite, or, in English, Doppler Orbitography and Radiopositioning Integrated by Satellite) observation, the Doppler and ranging measurements involved are used for obtaining positions and velocities of the beacon and of the spacecraft. In this context, it is very difficult to obtain precise inertial orbits for the GNSS constellation or for the DORIS system. Attempts are presently performed for a better precision of the orbits and of the Earth Orientation Parameters through combinations of the techniques. However it is very difficult to decontaminate the ground station tracking of the orbits from their own motion in space, inducing mapping of unmodeled effects in the orbits, which are changing with time.

As the Moon dynamics can be better followed than spacecraft undergoing wheel desaturation or maneuvers, we propose a new instrumental suite of technique combination on the Moon to obtain better ties between all reference frames in inertial space. This will provide in addition as very important objective the possibility to better understand the interior of the Moon. The suite involves a GNSS emitter, a microwave transponder, and an active laser system (see Figure 1).

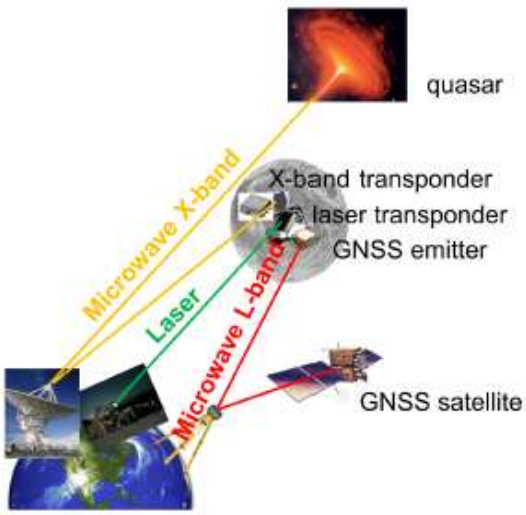

Figure 1: New proposed suite of instruments for a lander on the Moon.

This suite incorporates thus:

- An advanced Laser beacon / Laser receiver experiment to improve the Laser link budget substantially: while in the reflector case, the signal strength decreases with lunar distance r to the fourth power ($1/r^4$), for transponders, signal strength decreases with only $1/r^2$;
- A microwave receiver/transmitter (a coherent transponder); the down-link beacon (from the Moon to the Earth) will resemble quasar emission and can, thus, be observed in sequence with quasars in a differential mode;

- A GNSS microwave transmitter (P-code); we practically realize a "GPS/Galileo satellite on the Moon" that is tracked together with GNSS satellites by receivers on the ground; the GPS/Galileo type of transmitter would make the Moon in its drag-free orbit a "natural GPS satellite" within the global navigation satellite system;
- A space qualified Cesium clock which will be the frequency reference for the whole suite, including the laser beacon generation and the GNSS or microwave;
- and additionally, one needs precisely known mechanical local ties between all the instrument and in particular to the Laser beacon.

3. AIMS

With the co-location of several geodetic techniques on the Moon, it is of course easier to understand the links between the techniques and to achieve better combinations of instruments. The results expected concerning the Moon position will be better. The combination will not only be distance observation and observation of velocity in the line-of-sight, but as well observations of the tangential position of the Moon with respect to the celestial frame. The system will not only allow better links between the techniques but as well allow to improve the modeling geometry and data quality. The proposed instrumentation realizes a "GPS/Galileo satellite on the Moon that is tracked together with GNSS satellites by receivers on the ground and possibly on the future generation of GNSS satellites.

The objectives will be summarized in the following:

- improvement of the reference frames for the Earth,
- better understanding of the Moons interior.

With this suite of instruments we are co-locating three different space geodetic techniques on the Moon. Each of these techniques is self-contained and draws on a different set of infrastructure on the Earth. The maximum benefit is expected when all the observations are coordinated between the techniques. Furthermore it may turn out that due to limitations of the available sensor block voltage supply the observations need to be scheduled by remote control for the optimum turnaround. An operation concept of the instrument set will be developed, and potential and limits of the experiment will be fully explored.

A Laser transponder on the Moon will greatly increase our knowledge on the variation of Lunar range. More measurements at higher accuracy, from observatories in both, Northern and Southern Hemisphere, without observational bias will be available. The new range data are the basis for comprehensive models of the dynamics of the Earth/Moon system and will give stronger determinations of Lunar ephemeris, rotation, and tidal deformation. They will also contribute to much better realizations of the various reference systems, i.e. the terrestrial and selenocentric frame, but also the dynamic realization of the celestial reference system. New reflectors on the Moon will provide additional accurate surface positions for cartographic control, and they also will contribute significantly to research in fundamental and gravitational physics.

The microwave transmitter/transponder will permit us to carry out observations of the tangential motion of the Moon in the quasi-inertial space with an accuracy in the range of 100 - 300 microarcseconds (which translates to the sub-meter level). It will also permit us to measure relative velocity of the Moon with respect to the Earth at better than a few hundredths of mm/s. Together with the radial information from Laser ranging, the tangential component from VLBI will push the insight into the Moon's orbital behavior including its libration to as yet unknown frontiers and there with obtain information on the core of the Moon). With the inclusion of a GNSS microwave transmitter in the package, three of the major space geodetic techniques will be co-located on the Lunar surface supporting the efforts for a rigorous combination of these techniques. This will eventually allow us to define a unified reference frame rather than a measurement-biased frame as today.

A "GPS/Galileo satellite on the Moon" or the "Moon as a natural GPS/Galileo satellite" that is linked to VLBI will make it possible to directly reference the GNSS satellite constellations (and thus GNSS-determined station coordinates) to the ICRF (International Celestial Reference Frame). This will allow us to measure UT1, i.e., the rotation angle of the Earth, as well as components of nutation with high temporal resolution (and there with obtain information on the deep interior of the Earth) while today GNSS is capable to provide only mean rates of Earth orientation and nutation.

A "local tie" between GNSS and VLBI on the Moon would allow for a consistent interpolation of VLBI derived UT1 data with high rate GNSS derived values. A link to the Moon may also improve

the sensitivity of GNSS to components of the geocenter. The identification and monitoring of possible geocenter variations by GNSS is currently limited by satellite radiation pressure modeling deficiencies, a restriction that does not apply to the Earth's natural neighbor.

The possibility for continuous tracking of Lunar targets, independent of weather conditions and observation scheduling of LLR stations or large VLBI telescopes, is one of the major advantages of a GNSS transmitter on the Moon as well as of a microwave transmitter/transponder. It will provide additional independent comparisons, support calibration of measurements, and allow interpolation of SLR and VLBI results. In addition, such an instrument would allow for a continuous precise monitoring of the space clock.

These additional laser ranging measurements to the Moon will also allow better accuracy on the determination of the geophysical parameters such as the core dimension determined from libration and tidal displacements (Rambaux and Williams, 2010).

4. CONCLUSIONS

A GPS/Galileo satellite on the Moon or the Moon as a natural GPS/Galileo satellite that is linked to VLBI will make it possible to directly refer the GNSS satellite constellations (and thus GNSS-determined station coordinates) to the ICRF (International Celestial Reference Frame). Three of the major space geodetic techniques will be co-located on the lunar surface supporting the efforts for a rigorous combination of these techniques. The propose suite of instruments allows to combine all the currently available high precision space geodetic techniques, like VLBI, microwave at X-band, and GNSS at the location of the landing sites on the Moon, to match the currently available equipment at geodetic observatories on the Earth. With this approach, a unified reference frame will be computed rather than a measurement-biased frame.

Together with the radial information from Laser ranging (the position and velocity of the Moon with respect to the Earth will be determined at a never-reached precision of the sub-cm level and a few hundredths of mm/s), the tangential component from VLBI will push the insight into the Moon's orbital behaviour including its libration to as yet unknown frontiers and there with obtain information on the core of the Moon. This conclusion is further strengthened in the context the recent reprocessing of lunar seismic data and the findings related to a liquid core, a partial melting boundary layer, and a solid inner core inside the Moon.

Constraining the detailed structure of the lunar core is necessary to improve our understanding of the present-day thermal structure of the interior and the history of a lunar dynamo, as well as the origin and thermal and compositional evolution of the Moon.

5. PERSPECTIVES; APPLICATION TO MARS

The described system design developed for the Moon, can be adapted to Phobos and Deimos, the two moons of Mars, or to landers on Mars. Particular efforts will have to be performed for respecting the link budgets. Geodetic experiments in the Mars system will allow us to constrain the interiors of Mars and its moons, study the origin of the Mars satellite system, and even testing relativity theory. There are presently two mission proposed respectively for the Exploration Programme and Science Programme of ESA: the Mars-GeO and GETEMME.

1. Mars-GeO (for Mars Geophysical Observatories) mission to Mars (with an orbiter and landers in order to study the interior of Mars); this proposal is now considered for Exploration Programme and not for the Science Programme anymore; Veronique Dehant PI.

2. GETEMME (Gravity, Einstein's Theory, and Exploration of the Martian Moons' Environment) proposal (aiming at precise relative position of Phobos and Deimos in order to solve the question of their interior structure and origin); this proposal has been sent in with laser and radioscience instruments; Juergen Oberst PI.

6. REFERENCES

Rambaux, N., Williams J.G., 2010, The Moon's physical librations and determination of their free modes, Celestial Mechanics and Dynamical Astronomy, DOI: 10.1007/s10569-010-9314-2.

APPLICATION OF THE SPECTRAL ANALYSIS METHODS FOR THE INVESTIGATION OF THE MOON ROTATION

V.V. PASHKEVICH[1], G.I. EROSHKIN[2]

Central (Pulkovo) Astronomical Observatory of the Russian Academy of Science
Pulkovskoe Shosse 65/1, 196140, St. Petersburg, Russia
[1] e-mail: pashvladvit@yandex.ru
[2] e-mail: eroshkin@gao.spb.ru

ABSTRACT. Dynamics of the rotational motion of the Moon is investigated numerically by using Rodrigues-Hamilton parameters over 418.9 year time interval. The results of the numerical solution of the problem are compared with the composite semi-analytical theory of the Moon rotation (SMR), consisting of Cassini relations and the semi-analytical solutions of the lunar physical libration problem (Eckhardt D.H., 1981), (Moons M., 1982), (Moons M., 1984), (Pešek I., 1982). The initial conditions of the numerical integration are taken from SMR. The investigation of the discrepancies is carried out by the optimal spectral analysis methods for the Newtonian case. All the periodic terms representing the behavior of the residuals are interpreted as corrections to SMR semi-analytical theory. As a result, the Moon Rotation Series (MRS2010) are constructed, which are dynamically adequate to the DE200/LE200 ephemeris over 418.9 year time interval. A numerical solution for the Moon rotation is obtained anew with the new initial conditions calculated by means of MRS2010. The discrepancies between the new numerical solution and MRS2010 do not surpass 20 mas over 418.9 year time interval. The result of the comparison demonstrates that MRS2010 series are more accurately represent the Moon rotation than SMR series.

1. MATHEMATICAL MODEL OF THE PROBLEM

The numerical solution of the problem is obtained by solving the Lagrange differential equations of the second kind for the Moon rotation with respect to the fixed ecliptic and equinox of epoch J2000. The mathematical model of the problem is described in detail in the paper (Eroshkin G.I., Pashkevich V.V., 1997).

The semi-analytical solutions of the lunar physical libration problem include four solutions:

a) MP500 is the 3rd degree solution for the force function (Moons M., 1982);

b) Additional solution for the 4th degree perturbations of the force function (Eckhardt D.H., 1981);

c) Effect of planetary perturbations (Moons M., 1984);

d) Effect of the Earth's flattening (Pešek I., 1982).

As a result of compilation, a semi-analytical theory of the Moon rotation is constructed with respect to the ecliptic and equinox of date. Then the semi-analytical theory is reduced to the fixed ecliptic J2000.0.

The orbital motions of the disturbing bodies are defined by the DE200/LE200 ephemeris. The high-precision numerical integration method (Belikov, 1990) with a number of modifications (Eroshkin et al., 1993) was applied.

2. ALGORITHMS AND RESULTS

The result of the comparison between the numerical solution and semi-analytical solution SMR is studied by means of two variants of the spectral analysis schemes (Figure 1).

Numerical solution of the Moon rotation is implemented with the quadruple precision of the calculations. The initial conditions are computed by the semi-analytical theory of the Moon rotation (SMR), which corresponds to the fixed ecliptic J2000.0. The Moon rotation series SMR consist of 380 periodical terms with the periods from 5.648 days to 84541.30 years. The discrepancies between the numerical

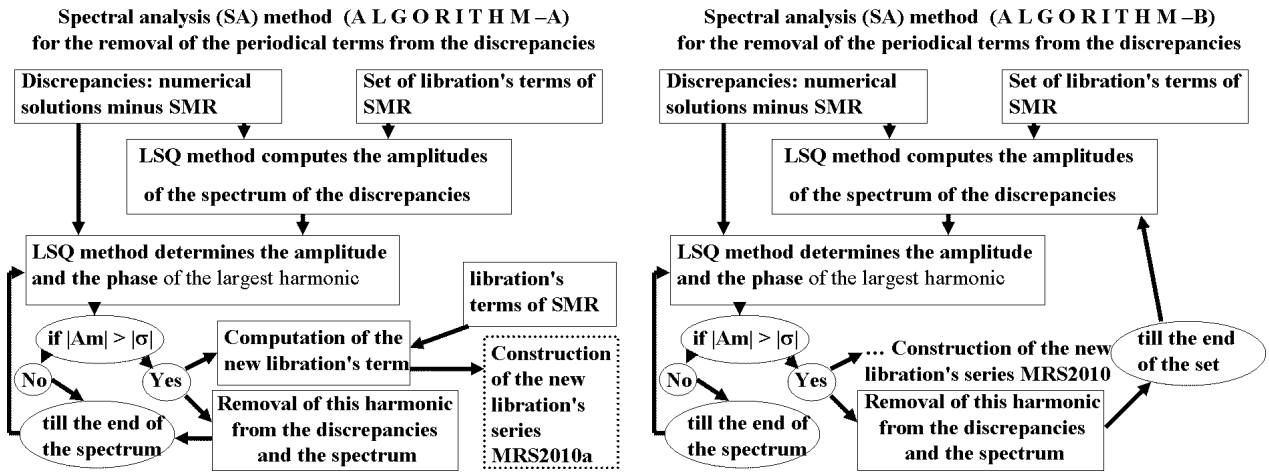

Figure 2: Two types of Algorithms

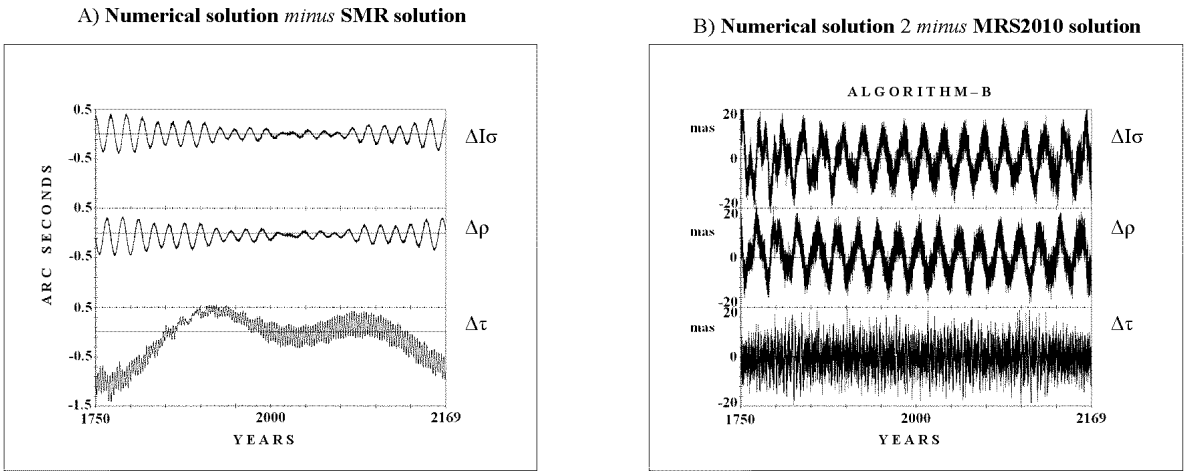

Figure 3: Discrepancies between the numerical and semi-analytical solutions of the Moon rotation

solution and SMR are obtained in Euler angles over 418.9 year time interval with one day spacing (Figure 2A).

The investigation of the discrepancies is carried out by the least squares method (LSQ) and by the spectral analysis method (SA). The set of the frequencies of SMR theory is used without a change. Only the coefficients of the periodic terms are improved.

SA method - A: The spectrum of the discrepancies between the numerical solution and SMR is constructed only once (Figure 3, ALGORITHM - A). Every coefficient of the new periodic term equals the sum of the calculated periodic term coefficient and the coefficient of the corresponding periodic term of SMR. The found new harmonic is removed from the discrepancies and from the spectrum. Starting from the maximum term of the spectrum the procedure is accomplished successively up to its least term. The new periodic and Poisson terms representing the new series MRS2010A are determined.

SA method - B: The spectrum of the discrepancies is constructed anew after the removal of every largest residual harmonic from the discrepancies. Each constructed spectrum is used for the determination of the new coefficient of the periodic term as in SA method - A. This procedure is performed for every harmonic of the set. The new periodic and Poisson terms representing the new series MRS2010 are determined.

The compilation of the power spectrum of the discrepancies between the numerical and semi-analytical SMR solutions for ALGORITHM - B is constructed, beginning from the largest of the residual harmonics, step by step (Figure 3, ALGORITHM - B).

The power spectra represented in Figure 3 are restricted by the terms with the periods from 5.648

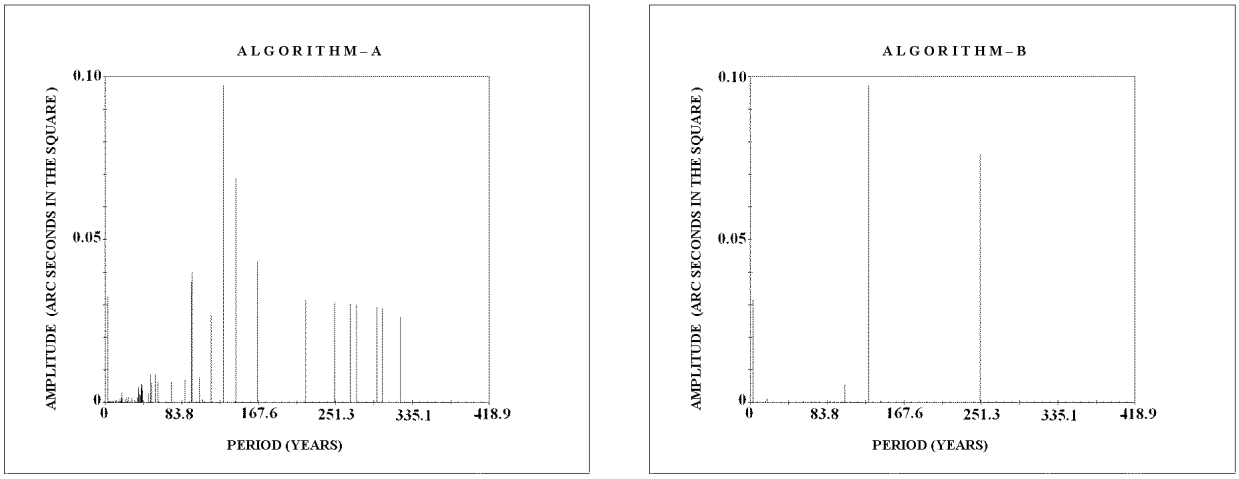

Figure 4: Spectrum of the discrepancies between the numerical and SMR solutions for $\Delta\tau$

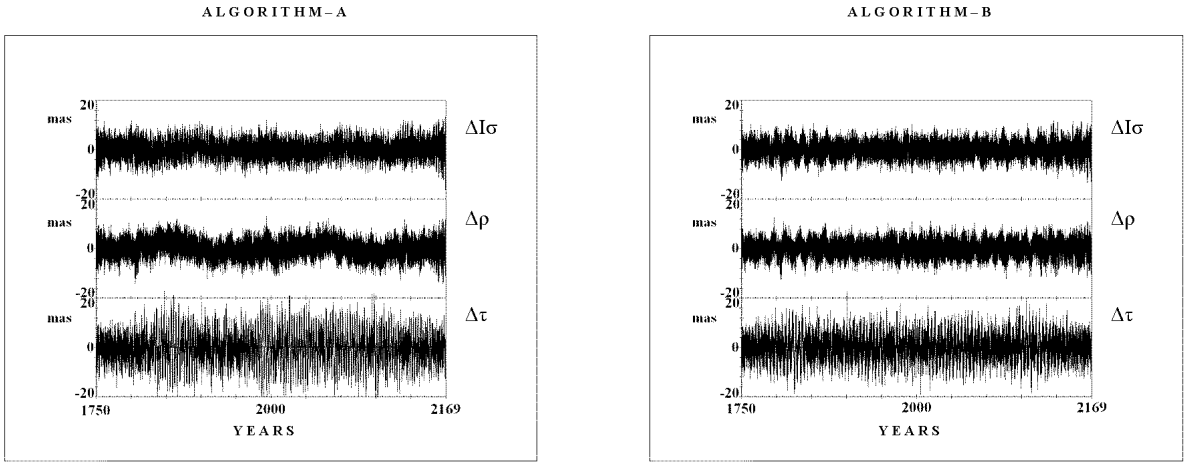

Figure 5: Residuals after the formal removal of 351 periodical terms from the discrepancies between the numerical and semi-analytical (SMR) solutions

days to 418.9 years. Therefore the set of the frequencies of SMR theory, which is used in SA methods, is restricted only by 351 periodical terms.

Figure 3 demonstrates that the composed power spectrum of the discrepancies between the numerical and semi-analytical SMR solutions for ALGORITHM - B is preferential than the power spectrum for ALGORITHM - A, because the close harmonics distinguish better from each other (Figure 3, ALGORITHM - B).

Figure 4 demonstrates that the residuals, after the formal removal of 351 periodical terms from the discrepancies between the numerical and semi-analytical SMR solutions, for ALGORITHM - B are less than the ones for ALGORITHM - A.

This investigation demonstrates that ALGORITHM - B is more accurate than ALGORITHM - A . Thus MRS2010 is better than MRS2010A.

Then the numerical solution for the Moon rotation is constructed anew with the new initial conditions calculated by means of MRS2010, which includes 1433 periodical and Poisson terms. The appearance of Poisson terms in the harmonics is the main difference between MRS2010 series and SMR series.

The results of the comparison of the new numerical integration of the lunar rotation with the new MRS2010 are presented in Figure 2B. The residuals do not reveal secular trends. The behavior of the residuals can be described by the superposition of the harmonics representing both the forced physical libration and the fictive free physical libration. The most essential harmonics of the residuals are the periodic harmonics of the fictive free physical libration with the period of 2.9 years in the longitude ($\Delta\tau$),

with the periods of 27.2 days and of 24 years in the inclination ($\Delta\varrho$) and in the node longitude ($\Delta I\sigma$). The appearance of the harmonics of the fictive free physical libration in the numerical solution is explained by the errors of the initial conditions, which are defined by the not enough precise semi-analytical solutions.

Figure 2 demonstrates that the discrepancies of the comparison in the libration angles decrease 25 times for both $\Delta I\sigma$ and $\Delta\varrho$ and 75 times for $\Delta\tau$, after the construction of the new more accurate MRS2010 semi-analytical solution.

The discrepancies of the comparison between the numerical solutions and MRS2010 do not surpass 20 mas over 418.9 year time interval (Figure 2B). It means an essentially better consistency of MRS2010 series with the DE200/LE200 ephemeris.

3. CONCLUSION

It was found that ALGORITHM - B, in which the spectrum is constructed anew after the removal of every largest residual harmonic from the discrepancies, is more accurate than ALGORITHM - A, in which the spectrum is constructed only one time.

ALGORITHM - B is very time-consuming. Hence it is not suitable for the investigation of the long time series, as follows from our previous investigation of the Earth rotation (V.V.Pashkevich and G.I.Eroshkin, 2005). However ALGORITHM - B is very suitable for the investigation of the short time series (the Moon rotation).

The new more accurate series MRS2010, dynamically adequate to the DE200/LE200 ephemeris over 418.9 year time interval, is constructed. MRS2010 includes about 1433 periodical and Poisson terms.

The discrepancies between the numerical solution and MRS2010 do not surpass 20 mas over 418.9 year time interval.

Acknowledgements. The investigation was carried out at the Central (Pulkovo) Astronomical Observatory of the Russian Academy of Science and the Space Research Centre of the Polish Academy of Science, under a financial support of the Cooperation between the Polish and Russian Academies of Sciences, Theme No 38 and the grant of Polish Academy of Science, No 52603732/3972.

4. REFERENCES

Belikov, M.V., 1993, "Methods of numerical integration with uniform and mean square approximation for solving problems of ephemeris astronomy and satellite geodesy", Manus. Geod., 15, No 4, pp. 182–200.

Eckhardt, D.H., 1981, "Theory of Libration of the Moon", The Moon and the planets, 25, pp.3–49.

Eroshkin, G.I., Taibatorov, K.A., Trubitsina, A.A., 1993, "Constructing the specialized numerical ephemerides of the Moon and the Sun for solving the problems of the Earth's artificial satellite dynamics", ITA RAS Preprint No 31, (in Russian).

Eroshkin, G.I., Pashkevich, V.V., 1997, "Numerical Simulation of the Rotational Motion of the Earth and Moon", Dynamics and Astrometry of Natural and Artificial Celestial Bodies, IAU Colloquium 165 (I.M.Wytrzyszczak, J.H.Lieske, R.A.Feldman, eds), Kluwer, Dordrecht, pp.275–280.

Moons, M., 1982, "Physical Libration of the Moon", Celest. Mech. 26, pp.131–142.

Moons, M., 1984, "Planetary Perturbations on the Libration of the Moon", Celest. Mech. 34, pp.263–273.

Pashkevich, V.V., Eroshkin, G.I., 2005, "Choice of the optimal spectral analysis scheme for the investigation of the Earth rotation problem", in Proc. of Journees 2005: Earth dynamics and reference systems: five years after the adoption of the IAU 2000 Resolutions (Space Research Centre of Polish Academy of Sciences, Warsaw, Poland, 19-21 September 2005), pp. 105–109.

Pešek, I., 1982, "An Effect of the Earth's Flattening on the Rotation of the Moon", Bull. Astron. Inst. Czechosl., 33, pp.176–179.

A COMPARISON OF THE HIGH ACCURACY PLANETARY EPHEMERIDES DE421, EPM2008, and INPOP08

J.L. HILTON[1] and C.Y. HOHENKERK[2]

[1] U.S. Naval Observatory
3450 Massachusetts Ave., NW, Washington, DC 20392, USA
e-mail: james.hilton@usno.navy.mil

[2] HM Nautical Almanac Office, UKHO
Admiralty Way, Taunton, TA1 2DN, England
e-mail: Catherine.Hohenkerk@UKHO.gov.uk

ABSTRACT. At the heart of many astronomical applications lies a planetary ephemeris. Since the 1980s the *de facto* world standard has been the Jet Propulsion Laboratory's DE (Development Ephemeris) series ephemerides. Recently, ephemerides from the Paris Observatory (Intégrateur Numérique Planétaire de l'Observatoire de Paris, or INPOP) and the Institute of Applied Astronomy in St. Petersburg (Ephemerides Planets-Moon, or EPM) have become available. These two ephemerides now provide accuracies similar to those from JPL. Here we compare the constants, initial conditions, and planetary positions produced by DE421, INPOP08, and EPM2008, the most recent ephemerides released for general use from these three groups. Ultimately, the true test of any ephemeris is how well its predictions compare with actual observations. Other considerations, such as availability, shall be discussed as well.

1. INTRODUCTION

Recently, two series of planetary ephemerides, the Ephemerides Planets-Moon (EPM) from the Institute for Applied Astronomy (Pitjeva 2009, Yagudina 2009) and the Intégrateur Numérique Planétaire de l'Observatoire de Paris (INPOP) from the Paris Observatory (Fienga et al. 2009) have become widely available. These two ephemerides provide positions and velocities with accuracies comparable to the well established Development Ephemerides (DE) from the *Jet Propulsion Laboratory*, JPL, (Standish 1998). The availability of these three high accuracy ephemerides prompts the question: How do they compare to one another? The ultimate test of any ephemeris is how well it actually predicts the future positions of the bodies included in it.

In particular, this paper is an initial comparison of the DE421, EPM2008, and INPOP08 ephemerides to the DE405 ephemerides, which is currently used in *The Astronomical Almanac*. The final report, including all comparisons and graphs, will be made available at the IAU Commission 4: Ephemerides web site[1]. There is no attempt here to determine which ephemeris is 'best'. Such a judgement is left for the user to make based on the data provided and his application of the ephemerides.

2. AVAILABILITY AND SOFTWARE

All three ephemerides, software to read them, and documentation are available on the internet. The DE421 ephemeris files are available by ftp[2] from the Solar System Dynamics group at JPL. The EPM2008 ephemeris files are available by ftp[3] from the Laboratory of Ephemeris Astronomy at the Institute for Applied Astronomy. And the INPOP08 ephemeris files are available by http[4] from the Insitut de mécanique céleste et de calcul de éphémérides. The ephemeris files are all available as ASCII text. Both EPM2008 and INPOP08 are available in binary versions as well, while JPL provides a Fortran program to convert DE421 from ASCII to binary format.

The data in all three ephemerides store their data as series Chebyshev polynomials using Barycentric Dynamical Time (TDB) as the independent variable. DE421 and INPOP08 store the coefficients for all

[1] *http://iaucom4.org/*
[2] *ftp://ssd.jpl/nasa.gov*
[3] *ftp://quasar.ipa.nw.ru/incoming/EPM2008/*
[4] *http://www.imcce.fr/inpop/calceph*

the body's positions in a single file while EPM2008 stores the velocity coefficients in individual body files.[5] Except for Uranus, Neptune, and Pluto in EPM2008, the segment length of the Chebyshev polynomials is an integer number of days.

All the ephemerides provide Barycentric Celestial Reference System (BCRS) positions of the Sun, planets, and Pluto, and geocentric equatorial positions for the Moon. Each also has a lunar rotation ephemeris. EPM2008, however, does not currently make its lunar rotation ephemeris available. The INPOP08 ephemeris includes an ephemeris of the difference between TDB and Terrestrial Time as well.

3. SUMMARY OF THE MODELS

A summary of the parameters used in modeling the three ephemerides is given in Table 1. No comprehensive summary is available for any of the ephemerides, so the data in this table is the best available estimate gathered from a variety of sources including the headers of the ephemeris files and the available papers and memos published describing them.

	DE405	DE421	EPM2008	INPOP08
Year Produced	1995	2007/08	2009	2009
Span	1600-2200	1900-2050	1800-2197	$1900-2100$ $1000-3000$
Parameters	156	228	> 260	402
Main Belt Objects	300	343	301 + ring	303 + ring
Trans-Neptunian Objects	Pluto	Pluto	Pluto + 20	Pluto

Table 1: A summary of the parameters used for each of the ephemerides.

All of the ephemerides are based on the numerical integration of a parameterized post-Newtonian gravitation model accurate to at least the second order in c^{-1}, where c is the speed of light, and fit to a set of observations similar to those described in Folkner et al. (2008). A subset of the parameters, varying between ephemerides, were adjusted using partial differential equations describing the link between the parameters and the observed values.

Probably the greatest difference in the models was the treatment of small solar system bodies not included in the ephemerides themselves. DE421 includes the Newtonian forces of the dwarf planet (1) Ceres, along with 342 main belt asteroids that had been previously determined to be the greatest perturbers of Mars. EPM2008 includes the integration of Ceres, 300 asteroids, and 21 trans-Neptunian objects (TNOs) including Pluto. In addition, the mass of the remainder of the main belt asteroids was represented by a ring with a mass, $(0.87 \pm 0.35) \times 10^{-10}\,\mathrm{M}_\odot$, and radius, $3.13 \pm 0.05\,\mathrm{AU}$. INPOP08 uses Ceres and 302 independently integrated main belt asteroids determined to be the most likely to produce significant perturbations over the time span of the ephemerides. Like EPM2008, a ring at 3.147 AU with a mass of $(1.0 \pm 0.3) \times 10^{-10}\,\mathrm{M}_\odot$ is used to represent the remaining mass of the main asteroid belt.

4. INITIAL COMPARISON

The ephemerides, DE421, EPM 2008 and INPOP08 are compared to DE405. Coordinates compared were the heliocentric range, longitude, and latitude of the planets and Pluto, while for the Moon geocentric coordinates were used, from 1900 through 2050, the period common to all the ephemerides. In general, the differences of the three ephemerides with respect to DE405 and with respect to each other increase with the increasing semimajor axis of the body. The maximum absolute differences with respect to DE405 over this time period are given in Table 2.

Fig. 1, for example, plots of differences for Jupiter and shows a significant difference for INPOP08. This is due to the fact that INPOP08 did not include the Galileo spacecraft observations for the position of Jupiter, while the others do. These observations have subsequently been included in INPOP10A[6] (Fienga 2010, private communication).

The dominant difference in the longitudes, e.g. Fig. 1, middle panel, for each of the objects is a secular trend arising from small differences in the mean motion of each of the objects. The difference in the mean motion also results in a gradual increase over time in the range differences of the planets giving those plots a "bow tie" aspect to them, Fig. 1, left panel.

[5]The relationship between the integral and derivative of the dependent variable in a Chebyshev polynomial is relatively simple. Thus, there is no penalty for storing either velocities or positions.

[6]INPOP10A became available about four weeks before prior to Journées 2010.

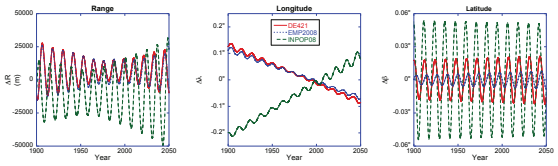

Figure 1: The difference in the heliocentric range, longitude, and latitude of Jupiter for DE421, EPM2008, and INPOP08 with respect to DE405.

Object	DE421			EPM2008			INPOP08		
	ΔR (AU)	ΔLong. (″)	ΔLat. (″)	ΔR (AU)	ΔLong. (″)	ΔLat. (″)	ΔR (AU)	ΔLong. (″)	ΔLat. (″)
Mercury	3.1×10^{-9}	0.011	0.006	2.6×10^{-9}	0.007	0.007	5.1×10^{-9}	0.016	0.009
Venus	3.9×10^{-10}	0.001	0.002	3.6×10^{-10}	0.001	0.002	4.1×10^{-10}	0.002	0.002
Earth	2.2×10^{-10}	0.001	0.002	1.8×10^{-10}	0.002	0.001	4.1×10^{-10}	0.004	0.002
Mars	3.7×10^{-9}	0.005	0.002	4.8×10^{-9}	0.008	0.001	7.7×10^{-9}	0.013	0.002
Jupiter	1.8×10^{-7}	0.137	0.022	1.8×10^{-7}	0.123	0.008	3.3×10^{-7}	0.213	0.054
Saturn	2.0×10^{-6}	0.144	0.044	2.0×10^{-6}	0.144	0.045	2.0×10^{-6}	0.142	0.048
Uranus	6.4×10^{-6}	0.249	0.050	6.4×10^{-6}	0.229	0.010	5.4×10^{-6}	0.199	0.022
Neptune	3.5×10^{-5}	0.568	0.046	4.0×10^{-5}	0.650	0.026	2.0×10^{-5}	0.337	0.056
Pluto	0.00025	1.399	0.242	0.00026	1.364	0.285	0.00010	2.166	0.538
Barycenter	6.2×10^{-9}	1.635	0.136	9.7×10^{-7}	93.104	50.396	4.4×10^{-9}	0.375	0.077
Moon*	2.4×10^{-11}	0.023	0.008	4.2×10^{-11}	0.052	0.013	4.1×10^{-11}	0.025	0.006

*The lunar differences are geocentric rather than heliocentric.

Table 2: The maximum heliocentric absolute differences with respect to DE405.

The dominant difference in latitude for each of the objects is a periodic component with the period of its orbital period, Fig. 1, right panel. This difference can arise from a difference in the orientation of the planetary reference system, a difference in the object's inclination, or a difference in the position of the nodes of the orbits. For all of the bodies in each of the ephemerides, the combined difference from all three of these sources is small; an indication of the basic soundness of the ephemerides.

Fig. 2 shows the EPM2008 offset in the barycenter is two orders of magnitude greater than for the other ephemerides. This offset is a result of including TNOs other than Pluto in its model. To first order, the motions of the additional TNOs are slow enough that their contribution to position to the solar system barycenter can be considered a fixed offset from the center of mass of the Sun and other solar system bodies. Moreover, Jupiter's contribution to the position of the barycenter dominates over that of the other planets. Thus, the position of the EPM2008 barycenter, which includes the TNOs, is offset with respect to the barycenters of the other ephemerides, which do not include the other TNOs. This offset gives EPM2008 a barycentric position that moves with respect to the others with a periodic motion with approximately Jupiter's sidereal period.

There is an offset of approximately 76″ between the rotation angle around the lunar pole of rotation, between DE421 and INPOP08. The most likely reason for this difference is a difference in the rotation about the polar axis between the mean-Earth mean-lunar pole of rotation (ME) reference system and the lunar principal moments of inertia (PMI) reference system. Lunar laser observations used to determine the position and orientation of the Moon are made in the ME reference system, while the rotation angle is given in the natural system for solving the lunar rotation equation of motion, the PMI reference system. The offset rotation between these two reference systems must be solved for in determining the lunar rotation parameters. Thus, as long as the offset rotations between the two reference systems are published, the difference between the two ephemerides should be of no concern to the observer. Yagudina (2010, private communication) has stated that current lack of an offset rotation between the lunar ME and PMI reference systems is the reason that EPM2008 does not currently make its lunar rotation ephemeris available.

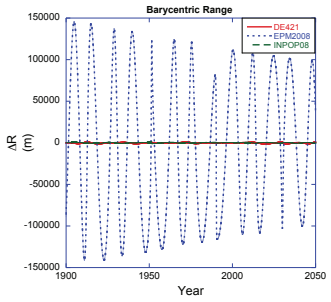

Figure 2: The difference in barycenter range of the Sun with respect to DE405.

5. DISCUSSION & FUTURE WORK

All three of the high accuracy solar system planetary ephemerides, DE421, EPM2008, and INPOP08, provide high quality models of the positions and velocities of the Sun, Moon, planets, and Pluto. Three significant differences were found: (1) A difference in the position of Jupiter in INPOP08. (2) The barycentric positions produced by EPM2008 differ. (3) A constant offset in the value of the lunar rotation angle between DE421 and INPOP08. These differences show how important it is for the user to understand what data have been used and the choice of models and parameters.

Further comparisons are planned. The first will be to replace DE405 as a standard with DE421, and INPOP08 with INPOP10A. Then, there are more quantitative numerical tests, such as determining the constant of integration, the angular momentum and energy. All the ephemeris generating groups hold some observations in reserve to check their accuracies. This check is the most important test of the ephemerides. Thus, comparison of each of the ephemerides with a uniform set of observations, including observations made after the construction of the ephemerides, is planned.

6. REFERENCES

Fienga, A. Laskar, J. Morley, T., Manche, H. Kuchynka, P., Le Poncin-Lafitte, C., Budnik, F., Gastineau, M. & Somenzi, L. 2009, "INPOP08 a 4-D Planetary Ephemeris: From Asteroid and and Time-Scale Computations to ESA Mars Express and Venus Express Contributions," Astron. Astrophys., 507, 1675–1686

Folkner, W.M., Williams, J.G. & Boggs, D.H. 2008, "The Planetary and Lunar Ephemeris DE421," Jet Propulsion Laboratory Memorandum IOM 343R-08-003

Pitjeva, E.V. 2009, "Ephemerides EPM2008: The Updated Model, Constants, Data," in Proceedings of Journées 2008 "Systèmes de référence spatio-temporels", M. Soffel & N. Capitaine (eds.), (Lohrmann-Observatorium & Observatoire de Paris), 57–60

Standish, E.M. 1998, "JPL Planetary and Lunar Ephemerides, DE405/LE405," Jet Propulsion Laboratory Memorandum IOM 312.F-98-048

Yagudina, E.I. 2009, "Lunar Numerical Theory EPM2008 from Analysis of LLR Data," Proceedings of Journées 2008 "Systèmes de référence spatio-temporels", M. Soffel & N. Capitaine (eds.), Lohrmann-Observatorium & Observatoire de Paris, 61–64

WEB INTERFACE FOR LUNAR LASER RANGING OBSERVATIONS

(http://polac.obspm.fr/PaV/)

C. BARACHE[1], S. BOUQUILLON[1], T. CARLUCCI[1], F. DELEFLIE,[2,3], D. FERAUDY[3], G. FRANCOU[1], H. MANCHE[2], E. SAMAIN[3], J.-M. TORRE[3] *(in alphabetical order)*

[1] SYRTE/Observatoire de Paris, 61 Avenue de l'Observatoire, Paris, France

[2] IMCCE/Observatoire de Paris, 61 Avenue de l'Observatoire, Paris, France

[3] GeoAzur/Observatoire de la Côte dAzur, 2130 Route de l'Observatoire, Saint-Vallier-de-Thiey, France

ABSTRACT. We report the current development of a web interface for the preparation and the validation of Lunar Laser Ranging (LLR) observations. With this service which is not yet completely implemented at the time of this presentation, distant LLR observers will be able to easily run some Paris observatory tools used for the lunar motion. It will allow them to compute predictions of geocentric and topocentric coordinates of lunar targets (as retro-reflectors and craters) and predictions of round-trip times of laser-pulses between terrestrial stations and lunar retro-reflectors. It will also allow them to compare their own LLR observations with computations (lunar solutions and reduction models), in terms of rms, and with a real-time access.

1. INTRODUCTION

The address of the web site is *http://polac.obspm.fr/PaV/*. It is divided into two main web-pages : a first one for the computation of predictions of LLR observations and a second one for the validations of LLR observations. Each one of these pages is divided into two frames : the left frame is dedicated to the user requests while the right frame is used to display the results of user requests. The next two sections of this proceeding give more details about the "prediction" web-page and the "validation" web-page respectively.

2. PREDICTION OF LLR OBSERVATIONS

The user of this web interface can choose between two lunar solutions for computing predictions. Each one of these lunar solutions uses distinct lunar ephemerides and distinct reduction models.

With the first lunar solution that we named ELP96 Solution, the ephemerides are given by an improved version of the analytical solution of the Moon ELP2000-82B (Chapront-Touzé & Chapront, 1988, 1996). Initially, the lunar coordinates given by this solution are referred to the dynamical mean ecliptic. The change to the equatorial frame of the Celestial Ephemeris Pole is carried out by analytical expressions of the precession-nutation. This solution is fitted to the Lunar Laser Ranging observations made from 1972 until 2002 (Chapront & Francou, 2002).

With the second lunar solution that we named INPOP Solution, the ephemerides come from the last available version of the numerical integration INPOP (10A) which are fitted on planetary and lunar observations (Fienga et al., 2008, 2009). They are available at *http://www.imcce.fr/inpop/*. LLR observations are reduced with a model consistent with IERS Conventions 2003, including tectonic plate motion, solid tides effects, ocean and atmospheric loading, polar tide, relativistic light deviation and tropospheric time delay. This second lunar solution is not yet implemented at the time of this presentation.

With both lunar solutions, the most recent values for the "Earth Orientation Parameters" (EOP) are needed to compute accurate predictions for the preparation of future LLR observations. To do that, a daily automatic update has been implemented to download the latest EOP series and the latest EOP predictions computed by the Earth Orientation Center of IERS.

The users can also choose the following requests :
- the LLR station on Earth,
- the lunar target (retro-reflectors or craters),
- the initial date and time of the first prediction,
- the step size between two successive predictions (in second or minute),
- the number of steps,
- the weather conditions,
- the wavelenght of the laser used.

The results are displayed in the right part of the screen. By default, the display format of this prediction is a format we developed recently and named TPF (for Topocentric Prediction Format). This format gives for each instant chosen by the user and for the selected lunar target seen from the selected station the corresponding :
- apparent equatorial rectangular coordinates in meter,
- round-trip light time in second,
- right ascension and declination in degree,
- azimuth and zenith distance in degree.

The prediction can also be computed with the format CPF (acronym for Consolidated Laser Ranging Prediction Format) which has been created by the ILRS Predictions Formats Study Group for satellite laser ranging and lunar laser ranging. An explanation of this format can be found in:
http://ilrs.gsfc.nasa.gov/products formats procedures/predictions/.

3. VALIDATION OF LLR OBSERVATIONS

To validate his LLR observations, the user of this web interface can choose between one of the two lunar solutions described above.

To submit LLR observations, the user selects and copies his own LLR observations data from a file and then pastes them into the "users data capture area" in the left part of the screen. The available formats for users data submission are:
- the format MINI (explanation at: *http://www.physics.ucsd.edu/∼tmurphy/apollo/norm_pts.html*),
- the format CSTG (explanation at: *http://ilrs.gsfc.nasa.gov/products_formats_procedures/*),
- the format CRD (explanation at: *http://ilrs.gsfc.nasa.gov/docs/crd_v1.01.pdf*).

The results of validation process are displayed in the right part of the screen. For each LLR observation, a line of results is given. This line contains:
- the number of processed observations,
- the station identification,
- the reflector number,
- the date and time of the observation,
- the observed round-trip light time in second,
- the difference between the observed light time and the computed light time in nanosecond and its equivalent in meter for the distance station-reflector.

These results can be downloaded as an ASCII file or as a Virtual Observatory table. The bias and the standard deviation of residuals are given for the retro-reflectors all together and for each one of them. Graphs of residuals are also available according to the stations, the reflectors, the time and residuals units.

4. REFERENCES

Chapront-Touzé, M., Chapront, J., 1988, *A&A*, 190, 342.
Chapront-Touzé, M., Chapront, J., 1996, *Celest.Mech.*, 66, 31.
Chapront, J., Francou G., 2002, *A&A*, 387, 700.
Fienga, A., et al., 2008, *A&A*, 477, 315.
Fienga, A., et al., 2009, *A&A*, 507, 1675.

A DYNAMICAL STUDY OF PHOEBE'S ROTATION

L. COTTEREAU
Observatoire de Paris, Systèmes de Référence Temps Espace (SYRTE), CNRS/UMR8630
61 avenue de l'Observatoire, 75014 Paris, France
e-mail: laure.cottereau@obspm.fr

ABSTRACT. With a fast non synchronous rotation, Phoebe is a particular satellite in the Saturnian system (most of the satellites are synchronously rotating) and must show a very different rotational evolution. We propose for the first time to determine the combined motion of the precession and nutation of Phoebe considered as a rigid body by numerical and analytical integration. We further compare our results with those obtained by Kinoshita for the Earth (1977), emphasizing their astonishing similarities (obliquity, value of the precession, nutation amplitudes and arguments). Moreover we show that a pure analytical accurate model of the nutation is not easy to construct due to the fact that the orbital motion of Phoebe is far from being Keplerian. At last we present the prospect for future studies among which are the effect of the Sun, Titan and the dynamical ellipticity of Saturn on the precession-nutation motion.

1. PHOEBE A NON KEPLERIAN MOTION

One of the important steps in our study was to describe the orbital motion of Phoebe by fitting the curves of the temporal variations of the orbital elements a, e, M and L_s (Emelyanov, 2007) in the same way as in Simon et al.(1994) for the planets. for the Earth, the semi-major axis is nearly constant with relative variation about 10^{-5}. In comparison, for Phoebe, approximating a by a constant is not a good approximation. The semi major axis of the satellite shows periodic variations with a relative amplitude of 10^{-3} around a mean value of $a = 0.0864273$. The presence of the relatively large periodic components on the mean elements of Phoebe shows that the motion of this satellite is not close to a Keplerian one, as it is the case for the planets of the Solar system. This departure may be due to the attraction of the Sun, Jupiter and the other satellites of Saturn on Phoebe. The individual study of the other orbital elements confirms this result. Indeed, the residuals obtained after subtraction of a polynomial functions at 6th order fitted to the mean anomaly, the mean longitude and the eccentricity, have periodic components which reach an amplitude of 4° for the mean anomaly.

2. PRECESSION NUTATION OF PHOEBE : NUMERICAL AND ANALYTICAL RESULTS

Applying the theoretical framework already used by Kinoshita (1977) for the Earth, the precession and the nutation motion of Phoebe are determined both analytically and from numerical integration of the equations of motion. We found that the precession-nutation motion of Phoebe undergoing the gravitational perturbation of Saturn is quite similar to that the Earth undergoing the gravitational effect of both the Moon and the Sun. Thus our value for the precession of Phoebe, that is to say 5580".65 cy, is very close to the corresponding value for the Earth (5081"/cy) and the nutation in longitude and in obliquity (see Figs.) of Phoebe with peak to peak variations of 26" and 8" are of the same order of amplitude as the nutation of the Earth (respectively 36" and 18" peak to peak). Moreover Phoebe obliquity (23°.95) is roughly the same as the Earth's one (23°.43). Notice that the physical dissymmetry characterized by the large value of the dynamical flattening 0.06465 and of the triaxiality −0.0111 (Aleshkina, 2010) and the large eccentricity of Phoebe which directly increase the amplitude of the precession and the nutation is compensated by its slow revolution and fast rotation (0.386d) (Bauer et al., 2004).

We also investigated the possibility to construct analytical tables of Phoebe nutation, as was done for the Earth. After fitting the curves of temporal variations of the orbital elements given by Emelyanov (2007) with linear expressions and replacing them in the equations motion (Cottereau et al, 2010), the precession-nutation of Phoebe is determined by analytical integration. Although the amplitude of the

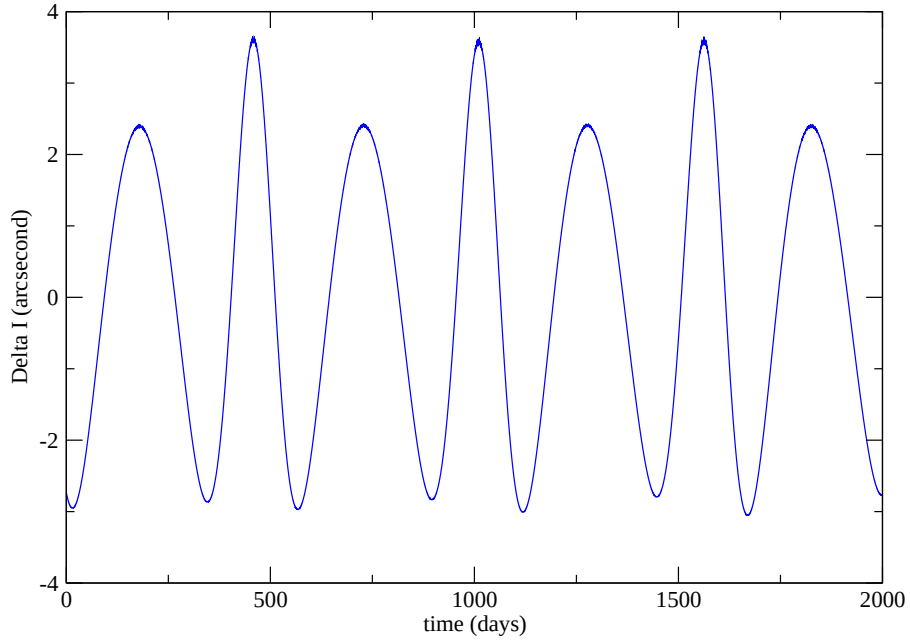

Figure 1: Nutation of Phoebe in obliquity for 2000 days time span (Cottereau et al., 2010).

nutation motion is close to the Earth one, we demonstrated that the analytical model used by Kinoshita (1977) for the Earth does not describe the nutation motion of a disturbed body like Phoebe with the same accuracy (10^{-5} for the Earth). This analytical model does not take into account the large perturbing effects of the celestial bodies on the orbit of the satellite. To describe the nutation motion of Phoebe a FFT approach is better than a pure analytical integration done with linear expressions for e, M and L_s. The FFT analysis is better fitted to describe the periodic variations characterizing the nutation signals of Phoebe. For the calculation of the precession, the discrepancies between the two models is decreased because these periodic variations are averaged.

To conclude we have shown that the analytical model set by Kinoshita (1977) gives a good first approximation of the precession-nutation of Phoebe but further analytical developments are needed to reach the same accuracy than for the terrestrial planets. We think that this work can be a starting point for further studies such as the elaboration of another very precise analytical model of the rotation of Phoebe by taking into account effects ignored in this paper, as the direct effects of the Sun, of Titan and of Saturn dynamical flattening. Such a model is required to develop the long term ephemerides of Phoebe's rotation, which should require long term orbital ephemerides, not still available.

3. REFERENCES

Aleshkina, E. Y., Devyatkin, A. V., & Gorshanov, D. L. 2010, IAU Symposium, 263, 141
Bauer, J. M., Buratti, B. J., Simonelli, D. P., & Owen, W. M., Jr. 2004, ApJ, 610, L57
Cottereau, L., Souchay, J., & Aljbaae, S. 2010, A &A, 515, A9
Cottereau, L., Aleshkina, E., & Souchay, J. 2010, A &A, 523, A87
Emelyanov, N. V. 2007, A &A, 473, 343
Kinoshita H. 1977, Celestial Mechanics, 15, 277
Simon J. L., Bretagnon P., Chapront J., Chapront-Touze M., Francou G., & Laskar J. 1994, A &A, 282, 663

NEW ANALYTICAL PLANETARY THEORIES VSOP2010

G. FRANCOU, J.-L. SIMON
(SYRTE and IMCCE), Observatoire de Paris, France

ABSTRACT. The planetary theories VSOP are essentially issued from the research works of P. Bretagnon. After the last version, VSOP2000, he began to make some improvements, but, unfortunately, he did not have time to complete his work. We took up again this work introducing various changes and complements and build two versions : VSOP2010A fitted to DE405 (numerical integration of the JPL) and VSOP2010B, not yet finished, fitted to INPOP08A (numerical integration of the IMCCE at Paris observatory). Over the time interval [1890,2000], the estimated precision is 3 to 10 times better than that of VSOP2000. Over the time interval [-4000,8000], the gain in precision is about 5 times better for the telluric planets and 10 to 50 times better for the outer planets in comparison with VSOP2000.

1. INTRODUCTION

The VSOP theories are analytical solutions for the motion of the planets of the solar system. They are based on the integration of Lagrange differential equations for the elliptic elements : a, semi-major axis, λ mean longitude, $k = \mathrm{e} \cos \varpi$, $h = \mathrm{e} \sin \varpi$, $q = \sin i/2 \cos \Omega$, $p = \sin i/2 \sin \Omega$ where the time is expressed in TDB and e, ϖ, i, and Ω are respectively the eccentricity, the longitude of the perihelion, the inclination and the longitude of the ascending node.

2. HISTORICAL REVIEW

• VSOP82 (Bretagnon, 1982) : Perturbations developed up to the 3rd order of the masses and iterative method up to the power 5 of time in the Poisson series for the 4 outer planets; Perturbations of the Earth-Moon barycenter by the Moon; Relativity introduced by the Schwarzschild problem; Fitted to the numerical integration of the JPL DE200 (Standish, 1982).

• VSOP87 (Bretagnon, 1988) : Extension of VSOP82 in several versions: rectangular or spheric variables, ecliptic reference frame J2000 or of the date, heliocentric or barycentric coordinates.

• VSOP2000 (Moisson and Bretagnon, 2001) : Perturbations developed up to the 3rd order of the masses and iterative method up to the power 7 of time in the Poisson series for the 8 planets; Perturbations by the 5 big asteroids introduced during the iterations; Perturbations by the Moon on the telluric planets; Fitted to the numerical integration DE403 (Standish 1995).

3. MAIN CHARACTERISTICS

3.1. *The last improvements of P. Bretagnon*

- Additional iterations up to the power 12 of time in the Poisson series.
- Numerical precision 10 times better than VSOP82.
- Orbits of the 8 planets and the 5 big asteroids analytically computed during the same process.
- Perturbations of the Moon on the 8 planets introduced during the iterations.
- Relativistic corrections included as for the solution VSOP2000.

3.2. *Our new changes and complements*

• For the theories VSOP2010 we have kept a form similar to the solution VSOP2000, i.e., Poisson series where the arguments are : the mean mean longitudes of the planets $\bar{\lambda_p} = \lambda_p^0 + n_p^0$ t where t is the time (TDB), λ_p^0 is the integration constant of the mean longitude λ and n_p^0 the integration constant of the mean motion, the Delaunay angles of the Moon D, F, l, and the argument μ (defined hereunder).

• VSOP2010A is fitted to the numerical integration DE405 (Standish, 1998) which is the bases of The Astronomical Almanac since 2003.

• VSOP2010B (not yet finished), is fitted to the recent numerical integration INPOP08A (Fienga et al., 2009) which is the new standard reference for the planetary ephemerides published by IMCCE.

• We have computed the perturbations due to the $J2$ of the Sun on the telluric planets.

• We have introduced the perturbations of asteroids (295 in the case of VSOP2010A, 298 in the case of VSOP2010B) under the form of Poisson series of μ (see hereunder).

• We have improved the precision of the theories of Jupiter and Saturn over a large time-span by improving up to the power 20 of time the Poisson developments of some long period arguments starting from the solutions TOP (Simon, 2010). In TOP solutions, the motion of the outer planets and Pluto are computed under the form of Poisson series of only one angular argument μ, linear function of time t given by : $\mu = (n_5\text{-}n_6)\ t\ /\ 880$ where n_5 and n_6 are the mean motions of Jupiter and Saturn respectively.

• We have added the perturbations of Pluto over the outer planets at the first order of the masses under the form of Poisson series of μ.

• We have introduced a complete solution of the motion of Pluto issued from TOP (not yet finished for VSOP2010B).

4. RESULTS AND PRECISION

In VSOP2010A and VSOP2010B, each element (a, λ, k, h, q, p) of each planet has the form of Poisson series developed up to the power 12 of time (power 20 for a et λ of Jupiter and Saturn) where a is expressed in au, λ is expressed in radian and the time is expressed in thousand of years.

Over the interval [1890;2000], the precision of the solutions VSOP2000, VSOP2010A and VSOP2010B can be estimated by their maximum differences with the numerical integrations DE403, DE405 and INPOP08A respectively on the mean longitude λ (see the table hereunder).

λ : maximum differences analytical theory - numerical integration over [1890;2000]. Unit is mas.

Planet	VSOP2000-DE403	VSOP2010A-DE405	VSOP2010B-INPOP08A
Mercury	0.27	0.07	0.04
Venus	0.29	0.08	0.03
Earth-Moon Barycenter	0.35	0.06	0.04
Mars	2.89	2.01	1.13
Jupiter	0.47	0.20	0.06
Saturn	1.75	0.19	0.13
Uranus	1.49	0.86	0.77
Neptune	1.86	0.27	0.10

We can see that the gain in precision related to VSOP2000 is more important for VSOP2010B than for VSOP2010A. That is essentially due to our computation of the perturbations by the asteroids which is closer between VSOP2010B and INPOP08A than in the case of VSOP2010A and DE405.

Over a greater interval [-4000,+8000] a comparison with an internal numerical allows to say that the solutions VSOP2010 are about 5 times better than VSOP2000 for the telluric planets and 10 to 50 times better for the outer planets.

5. REFERENCES

Standish, E.M., 1982, *A&A*, 114, 297.
Bretagnon, P., 1982, *A&A*, 114, 278.
Bretagnon, P., Francou G., 1988, *A&A*, 202, 309.
Simon, J.L., et al., 1992, *A&A*, 265, 308.
Standish, E.M., et al, 1995, *JPL IOM*, 314, 10, 127.
Standish, E.M., 1998, *JPL IOM*, 312.F, 98.
Moisson, X., Bretagnon, P., 2001, *Celest.Mech.*, 80, 205.
Simon, J.L., 2003, *IMCCE*, Note S081, 53.
Fienga, A., et al., 2009, *A&A*, 507, 1675.
Simon, J.-L., 2010, *private communication*.

SUMMARY AND STATUS OF THE HORIZONS EPHEMERIS SYSTEM

J. GIORGINI
Jet Propulsion Laboratory/California Institute of Technology
4800 Oak Grove Drive, Pasadena, CA 91109, USA
e-mail: jon.d.giorgini@jpl.nasa.gov

ABSTRACT

Since 1996, the Horizons system has provided searchable access to JPL ephemerides for all known solar system bodies, several dozen spacecraft, planetary system barycenters, and some libration points. Responding to 18,400,000 requests from 300,000 unique addresses, the system has recently averaged 420,000 ephemeris requests per month.

Horizons is accessed and automated using three interfaces: interactive telnet, web-browser form, and e-mail command-file.

Asteroid and comet ephemerides are numerically integrated from JPL's database of initial conditions. This small-body database is updated hourly by a separate process as new measurements and discoveries are reported by the Minor Planet Center and automatically incorporated into new JPL orbit solutions. Ephemerides for other objects are derived by interpolating previously developed solutions whose trajectories have been represented in a file. For asteroids and comets, such files may be dynamically created and transferred to users, effectively recording integrator output. These small-body SPK files may then be interpolated by user software to reproduce the trajectory without duplicating the numerically integrated n-body dynamical model or PPN equations of motion.

Other Horizons output is numerical and in the form of plain-text observer, vector, osculating element, or close-approach tables, typically expected be read by other software as input. About one hundred quantities can be requested in various time-scales and coordinate systems. For JPL small-body solutions, this includes statistical uncertainties derived from measurement covariance and state transition matrices. With the exception of some natural satellites, Horizons is consistent with DE405/DE406, the IAU 1976 constants, ITRF93, and IAU2009 rotational models.

PROPAGATION IN TIME OF ERRORS FOR THE MUTUAL INCLINATION OF SATELLITES

F.J. MARCO[1], M.J. MARTINEZ[2], J.A. LOPEZ[1]

[1] Universidad Jaume I
Dept. Matematicas, Institut de Matematiques I, Aplicacions de Castello, Catellon, Spain
e-mail: marco@mat.uji.es; lopez@mat.uji.es

[2] Universidad Politecnica de Valencia
Dept. Matematica Aplicada, Valencia, Spain
e-mail: mjmartin@mat.upv.es

ABSTRACT

1. In the context of Keplerian elements, the inclination is a metric element and therefore a dynamic element. Variation in mass will produce a $(\Delta i_{mass}(t))$ variation.
2. Infinitesimal errors in the reference induce errors in all elements and, in particular, a $(\Delta i_{ref}(t))$
3. The question is how to distinguish the source (mass or reference) of error for a given $\Delta i(t)$.
4. Let us consider in the first place the minor planet Pallas, with different masses $M_p = 108e-12M_{Sun}$ and $m_p = 398e-12M_{Sun}$ (See [2])
5. We take the values ϵ_x, ϵ_y, ϵ_z given by [3] between Hipparcos and FK5. In both cases we show the evolution of $(\Delta i_{ref}(t)))$. It is clear that we find "crossed correlations" for $(\Delta i_{mass}(t))$ as well as for $(\Delta i_{ref}(t))$ and other variations such as $(\Delta i_{ref}(t))$, $(\Delta\Omega_{mass}(t))$ respectively. (See Fig 1)
6. For a long period of observation we can determine the kind of error. We apply the same principle to the mutual inclination of satellites. We take an example from [1] (See Figs 2, 3)
6a. We consider an ideal case of two bodies around a central body. We have modified their masses taking $m_1 = 2e-5, 2e-4, 4e-4$ and $m_2 = 1e-5, 1e-4, 2e-4$.
6b. We have considered a rotation of 5 min in the three coordinate axes, which means an uncertainty in the third decimal value.
6c. In Fig. 4 we show the difference between Δi_{ref} and Δi_{mass} for a long period of time.

1. CONCLUSION

There is a degree of uncertainty when we want to determine the values of the masses, because from the analysis of the differences between the elements we can deduct an uncertainty in their determination, with values under $2e-4$

There are clear relationships of affinity between certain variations of the elements with respect of the mass and others with respect to infinitesimal rotations in the reference. These relationships appear as symmetries or antisymmetries when they are plotted.

The mutual inclination of the two bodies shows a clear dependence with their mutual distance, getting a sudden increment when the bodies are near a close encounter, as expected.

It is important to have observations for long periods of time to be compared with the computed positions near the time when several close encounters between satellites are expected.

Acknowledgements. Part of this work was supported by grant P1-1B2009-07 from Fundacio Caixa Castello BANCAIXA and a grant GV/2009/027 from Generalitat Valenciana

2. REFERENCES

[1] Kinoshita H., 1993, Cel. Mech. 57.
[2] Krasinsky G.A., Pitjeva E.V. et al., 2001, "Estimating Masses of Asteroids", 3.Russian Academy of Sciences, Institute of Applied Astronomy, 139.
[3] Mignard F. & Froeschle M., 2000, A&A 354.

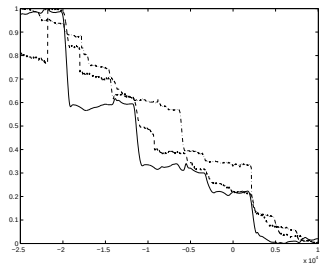

Figure 1: Pair Δi, $\Delta\Omega$ The solid line is $[\Delta i_{ref}]$, the dashed and dashed-dotted line are $[\Delta\Omega_{mass}]$ for the two masses considered.

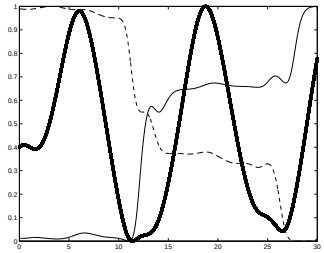

Figure 2: Comparison among the mutual differences in inclination $(i_{m1} - i_{m2})_{ref}$, (thin solid line), the distance between the bodies (thick solid line) and the $\Delta\Omega_{mass}$ for the first body (dashed line))

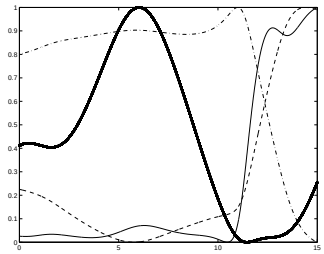

Figure 3: Comparison among the mutual differences in inclination $(i_{m1} - i_{m2})_{mass}$ (thin solid line), the distance between the bodies (thick solid line) and the a_{ref} for both bodies (a_{m1} is the dashed line and a_{m2} the dashed-dotted line)

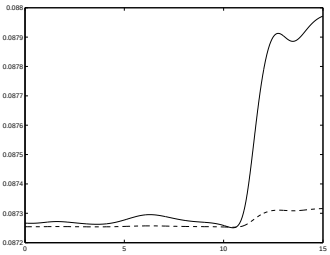

Figure 4: Comparison among the mutual differences in inclination $(i_{m1} - i_{m2})_{mass}$ (solid line), and $(i_{m1} - i_{m2})_{ref}$ (dashed line)

COMPUTATION OF THE QUANTITIES DESCRIBING LUNAR LIBRATIONS IN THE ASTRONOMICAL ALMANAC

J.M. WERATSCHNIG[1], D.B. TAYLOR[1], S.A. BELL[1], J.L. HILTON[2], A.T. SINCLAIR[1]

[1] HMNAO, UKHO, Admiralty Way, Taunton, TA1 2DN, UK
e-mail: hmnao@ukho.gov.uk

[2] Astronomical Applications Department, USNO
3450 Massachusetts Ave, NW, Washington, DC 20392-5420, USA
e-mail: james.hilton@usno.navy.mil

ABSTRACT. This paper provides a summary of HM Nautical Almanac Office Technical Note 74, on which the poster presented at the Journees 2010 is based. We briefly describe the method used for calculating lunar librations as they are presented in Section D of The Astronomical Almanac. The Euler angles from the JPL DE403/LE403 ephemerides are used to calculate improved lunar librations, beginning with the 2011 edition. Implementation of this ephemeris data supersedes the analytical theory of Eckhardt (1981, 1982) used since 1985.

1. INTRODUCTION

Cassini's laws describe general properties of the Moon's motion: the descending node of the Moon's equator coincides with the ascending node of the Moon's orbit on the ecliptic, the equator maintains a constant inclination to the ecliptic and the rotation rate is such that on average the same side is always facing the Earth. The rotation rate is equal to the rate of motion of the Moon's mean longitude. Dynamical perturbations cause small (of order of a few arcseconds) periodic variations from this mean state, i.e. physical librations. Overlaid are the much larger (of order of several degrees) optical librations which are caused by variations in the rate of the Moon's orbital motion and the inclination of the Moon's equator to its orbital plane. The mean central meridian of the side facing the Earth is specified as the prime meridian to define the rotational state of the Moon. Its direction in space differs by 180° from the mean longitude of the Moon (see Figure 1).

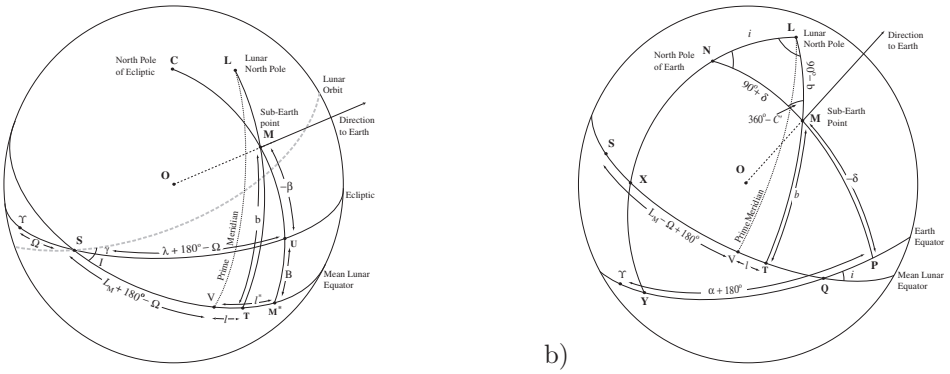

Figure 1: Selenocentric sphere: a) lunar orbit and relationships between sub-Earth point, M, the mean lunar equator and the ecliptic. S is the descending node of the lunar equator on the ecliptic. b) relationships between the sub-Earth point M, the mean lunar equator and the Earth's equator.

2. IMPLEMENTATION OF JPL LUNAR ROTATION ANGLES

The JPL DE403 ephemeris includes an ephemeris for the rotation of the Moon. The Euler angles describing the rotation of the Moon, defined relative to the ICRS equator and equinox, are ϕ, θ and ψ (see Table 1 and Figure 2, also Newhall and Williams, 1997) and describe the orientation of the principal

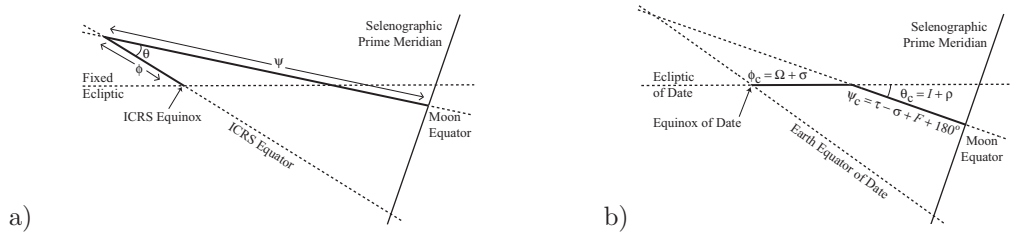

Figure 2: a) the reference frame in the principal moment of inertia (PA) system; b) the reference frame in the mean Earth/rotation axis (ME) system. Description of the angles is given in Table 1.

Table 1: Euler angles as used in Figure 2:

ϕ	Angle along ICRS equator, from ICRS X-axis to ascending node of the lunar equator	ϕ_C	Angle from equinox of date to descending node of lunar equator on ecliptic of date
θ	Inclination between lunar equator and ICRS equator	θ_C	Inclination between lunar equator and ecliptic of date
ψ	Angle along lunar equator from node to lunar prime meridian	ψ_C	Angle along lunar equator from descending node on ecliptic to the lunar prime meridian

axes of inertia of the Moon (PA system, see Figure 2a). Angles given in this system can be transformed to give the Euler angles ϕ_C, θ_C and ψ_C, defined relative to the ecliptic and equinox reference frame of date. They describe the orientation of a slightly different lunar axis system (ME system, see Figure 2b). These quantities are used to compute Ω, I and L_M which are needed to calculate the total librations l_T, b_T and the position angle C_T. For details, see Technical Note 74 and references therein.

3. OVERVIEW OF THE ALGORITHM

First, apparent positions for the Moon (α, δ, d) and the Sun $(\alpha_S, \delta_S, d_S)$ at time t (where α is the right ascension, δ the declination and d the distance) are obtained; as well as the nutation in longitude $(\Delta\psi)$ and obliquity $(\Delta\epsilon)$, also the true obliquity (ϵ). The apparent equatorial coordinates are rotated around the X-axis by the angle ϵ to determine the apparent ecliptic positions of the Sun(λ_S, β_S) and Moon (λ, β). Also $\tau = d/c$, the light time correction for the Moon, is needed (c is the speed of light). The inclination I_m at time $t - \tau$ and the fundamental arguments Ω and L_M (see Simon et al, 1994) are evaluated. From $(\lambda - \Omega - \Delta\psi)$, β, I, and L_M the optical (geometric) librations l_o and b_o are calculated. In order to obtain the position angle of the axis of rotation (C'_o), Ω' and i are determined. Using Euler angles from the ephemeris and applying the transformations needed to go from Figure 2a to Figure 2b, the new Euler angles $(\phi_C, \theta_C, \psi_C)$ are obtained: this transforms from the system of the ephemeris to the true date system by substituting ϕ_C for Ω, θ_C for I, $\psi_C + \phi_C - 180^\circ$ for L_M. This determines the total librations l_T, b_T and C'_T. By subtracting the optical from the total librations, the physical librations δl_p and δb_p are calculated. The quantity $\delta C'_p = C'_o - C'_T$ is obtained as well. These values are tabulated in Section D of The Astronomical Almanac. A detailed step-by-step example of this method can be found in Technical Note 74.

4. REFERENCES

D.B. Taylor, S.A. Bell, J.L. Hilton, A.T. Sinclair, HMNAO Technical Note 74, http://www.hmnao.com/data/tn/naotn74.pdf

Konopliv, A.S., Asmar, S.W., Carranzo, E., Sjogren, W.L., Yuan, D.N., 2001, Icarus, 150, 1.

Newhall, X.X., Williams, J.G., 1997, Cel. Mech. and Dyn. Ast., 66, 21.

Seidelmann, P.K., et al., 2007, Report of the IAU/IAG Working Group on Cartographic Coordinates and Rotational Elements: 2006, Cel. Mech. and Dyn. Ast., 98, 155.

Simon, J.L., et al., 1994, A&A , 282, 663.

Session 3

PROGRESS IN ASTROMETRIC CATALOGS IN OPTICAL AND RADIO WAVELENGTHS

PROGRÈS SUR LES CATALOGUES ASTROMÉTRIQUES OPTIQUES ET RADIO

UCAC AND URAT: OPTICAL ASTROMETRIC CATALOG OBSERVING PROGRAMS

N. ZACHARIAS, R. GAUME
U.S. Naval Observatory
3450 Mass.Ave. NW, Washington, DC 20392, USA
nz@usno.navy.mil
gaume@usno.navy.mil

ABSTRACT. The third USNO CCD Astrograph Catalog (UCAC3) all-sky catalog was released in August 2009. The final release, UCAC4, is in preparation and will include corrections and improvements to positions and proper motions, as well as publication of intermediate data. Properties of UCAC products are presented.

The USNO Robotic Astrometric Telescope (URAT) project uses the optics of the UCAC telescope with a new, wide-field camera to cover 28 sq.deg per exposure. A new all-sky survey to R $\approx$ 18 mag will begin in 2011 from Arizona and be continued from Chile. Neutral density spots on the single bandpass filter allow observations of bright stars. URAT will be able to directly link Hipparcos stars and extragalactic sources of the International Celestial Reference Frame (ICRF). Multiple sky overlaps per year will give mean positions, proper motions and parallaxes from these CCD observations. An accuracy level of 10 mas is expected for high signal-to-noise stellar observations.

1. INTRODUCTION

The goal of the astrometric observing programs described here is to provide many millions of accurate, all-sky, optical reference stars fainter than Hipparcos and Tycho-2 stars, at current epochs, including positions and proper motions. These star catalogs are aiming at a densification of the optical reference frame on the coordinate system of the defining radio frame (ICRF2, Fey et al. 2009). Due to errors in the proper motions of star catalogs the predicted positions at a future epoch degrade with time. Only new observations can improve the quality of the positions and proper motions.

name of catalog	ground space	proper motion	mag range	numb stars	pos.err (mas)	catalog release	remark
ICRF2	G	QSO	radio	3414	0.3	2009	VLBI
Hip.	S	yes	$\leq$ 12	100 K	1.0	1997	ESA
Tycho-2	G/S	yes	$\leq$12	2.5 M	10..100	2000	ESA,USNO
UCAC3	G	yes	8..16	100 M	20.. 70	2009	first CCD survey
2MASS	G	no	IR	500 M	90	2003	1 epoch
USNO-B	G	yes	12..21	1000 M	200	2003	Schmidt plates
PanSTARRS	G	yes	17..23	2000 M	$\leq$30	$\geq$2011	Hawaii
SkyMapper	G	yes	16..22	1000 M	?	$\geq$2011	Australia
SST	G	yes	17..23	2000 M	?	$\geq$2011	DARPA
URAT1	G	yes	8..18	500 M	10..30	2012	USNO,NOFS,CTIO
LSST	G	yes	18..24	3000 M	?	$\geq$2015	NOAO
nano-JASMINE	S	yes	near IR	2 M	3.0	$\geq$2013	Japan
JMAPS	S	yes	0..14	30 M	1.0	2018	USNO
Gaia	S	yes	6..20	1000 M	0.025	$\geq$2015	ESA
SIM	S	yes	0..20	20,000	0.004	on hold	NASA,JPL

Table 1: Comparison of current and future (nearly) all-sky survey observing projects significant for astrometry.

Table 1 provides an overview about current and future, astrometric, global catalog observing programs from the ground and space. The UCAC program is essentially complete, pending a final data release, while the URAT program is a ground-based follow-up to UCAC to begin in 2011 with improved accuracy and reaching even fainter magnitudes with first results expected to be released in 2012. Contrary to other ground-based sky survey projects, URAT uses a small-aperture, dedicated astrometric telescope for highest positional accuracy of stars in the mid-magnitude range, bridging the gap between the current optical reference frame and deeper surveys.

2. UCAC

The USNO CCD Astrograph Catalog project observations were completed in 2004. Operating in a bandpass between V and R, over 278,000 exposures of 1 sq.deg each were obtained in a 2-fold all-sky overlap pattern with each field having a long (125 sec) and a short (25 sec) exposure. After the UCAC1 early data release (Zacharias et al. 2000), the widely used UCAC2 catalog (Zacharias et al. 2004) was released, covering declinations $-90°$ to about $+50°$ for over 48 million stars.

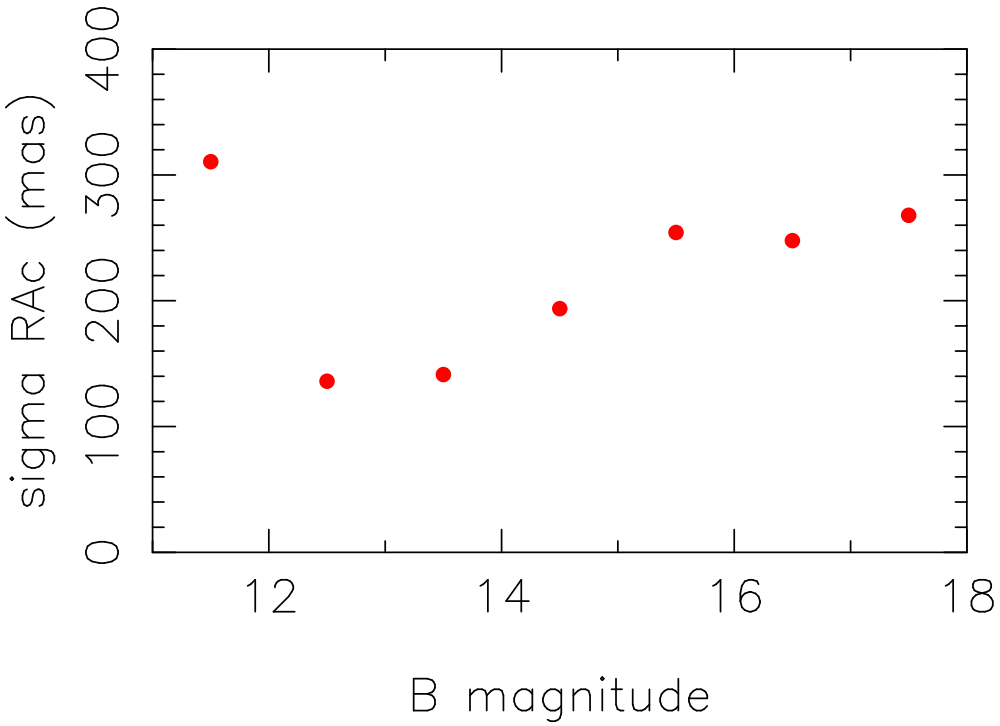

Figure 1: Precision of re-reduced NPM first epoch data. The standard error for the RA*cos(Dec) coordinate is shown as a function of NPM blue magnitude (Girard 2010). Results for the Dec coordinate are similar.

UCAC2 is a relatively "clean" reference star catalog, having cut out all identified "problem" cases (like blended images), while the UCAC3 released in 2009 is the first all-sky catalog in this series (Zacharias et al. 2010), aiming at a high degree of completeness and thus also includes a relatively large number of problem cases and unreliable low S/N sources. Details about the astrometric reductions of UCAC3 can be found elsewhere (Finch et al. 2010).

UCAC3 was put together within a given deadline and lacks high-quality proper motions for faint stars north of declination $-30°$. Uncorrected SuperCosmos data of Schmidt plate scans were widely used. This resulted in systematic errors in UCAC3 proper motions as function of the Schmidt plate pattern of up to about 10 mas/yr in some areas (Zacharias et al. 2010, Röser et al. 2010).

Most stars brighter than about V=12.5 and many others brighter than V=14 have high-quality proper motions in UCAC3 due to the use of early epoch astrograph plates. Over 5000 plates from the AGK2 (epoch close to 1931), as well as from the Hamburg Zone astrograph and USNO Black Birch twin-astrograph programs, have been scanned on the StarScan machine (Zacharias et al. 2008) and reduced

for UCAC. All other faint stars to the limit of UCAC and south of $\delta = -30°$ also have high-quality proper motions thanks to the Southern Proper Motion (SPM) program and re-reductions in a joint USNO/Yale effort, which provided SPM 1st epoch data in time for the UCAC3.

The proper motion problems of UCAC3 north of $\delta = -30°$ and software bugs causing for example some stars (about 1% of all stars in the catalog) to be listed twice and others not at all, will be resolved in the upcoming, final, UCAC4 release. In a collaboration between USNO and Yale University, the Northern Proper Motion (NPM) Lick astrograph plates (which were also scanned on the PMM machine at NOFS, like the SPM plates) were re-processed to provide a new, highly accurate star catalog at a mean epoch of about 1950 covering all sky north of the SPM data. Fig. 1 shows the random errors of the NPM 1st epoch data and combined with the ≈ 50 year epoch difference to UCAC CCD observing, proper motion errors of 3 to 5 mas/yr are expected with remaining systematic errors estimated to be on the 2 mas/yr level. In addition to a compiled catalog of about 100 million stars, individual CCD observed positions will become available with the UCAC4 release in 2011.

3. OPTICAL REFERENCE FRAME TODAY

About 20 years after the central epoch of observations the positional accuracy of individual Hipparcos stars has degraded to typically 20 mas per coordinate (1 σ). The coordinate axes of the Hipparcos reference frame are still aligned to the ICRF with errors not larger than 2.7 mas and system rotations not larger than 0.55 mas/yr; limits set by a recent investigation of 46 radio stars (Boboltz et al. 2007).

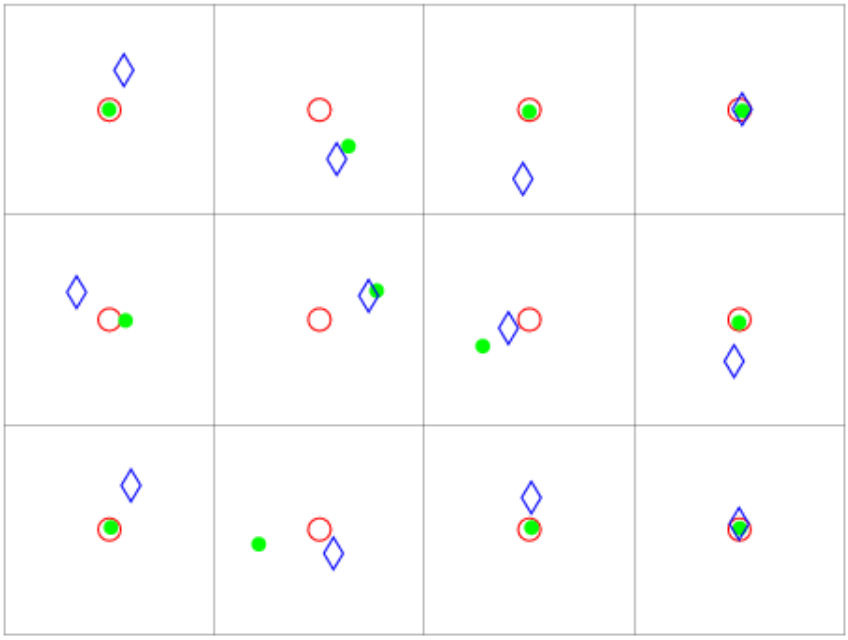

Figure 2: 2-dim (RA,Dec) position discrepancies of selected Hipparcos stars. A red, open circle represents the new Hipparcos reduction position, while a green, filled circle shows the original Hipparcos catalog position relative to that and the blue diamond indicates the location of the UCAC CCD observation as obtained near the 2000 epoch. The respective Hipparcos catalogs position, proper motion and parallax data was used to derive a position at the UCAC epoch for this comparison. The size of the box for each star is 1 arcsec = 1000 mas.

However, some Hipparcos stars can have much larger positional errors at current epochs. During the UCAC3 construction about 1500 stars (random sample) were excluded as reference stars and the observed CCD-based positions (at about epoch 2000) compared with the original (ESA 1997) and re-reduced (van Leeuwen 2007) Hipparcos catalog positions at that epoch. For about 1 to 2 % of the stars large discrepancies were found (Zacharias et al. 2009) up to several 100 mas (Figure 2). Sometimes the CCD data agree with the original but not the new reductions and vice versa, and sometimes all 3 data

points are not consistent with estimated errors by large margins.

Limits of the Tycho-2 reference frame begin to become visible as well. Systematic radio-optical extragalactic reference frame source position differences are seen in the 30 mas range for some areas, which may be due to remaining Tycho-2 systematic errors (Zacharias & Zacharias 2009). Small magnitude equations of Tycho-2 positions are seen in UCAC3 data (Zacharias et al. 2010) and in work with the SPM (Girard, private communication) as function of declination zones.

Going to fainter stars, systematic errors of star positions at current epochs are at least 20 mas just from the expected error propagation of proper motion errors in UCAC type catalogs. For Schmidt plate data, these local systematic errors reach 200 to 400 mas, as seen in many external comparisons.

4. URAT

The USNO Robotic Astrometric Telescope (URAT) project uses the same astrograph "red lens" as was used for the UCAC program. A completely new tube assembly has been built in the USNO Instrument Shop and electronic upgrades of its B&C mount are in progress. For the first time, on September 9, 2010, the new mount system was operated under computer control to point at stars and track.

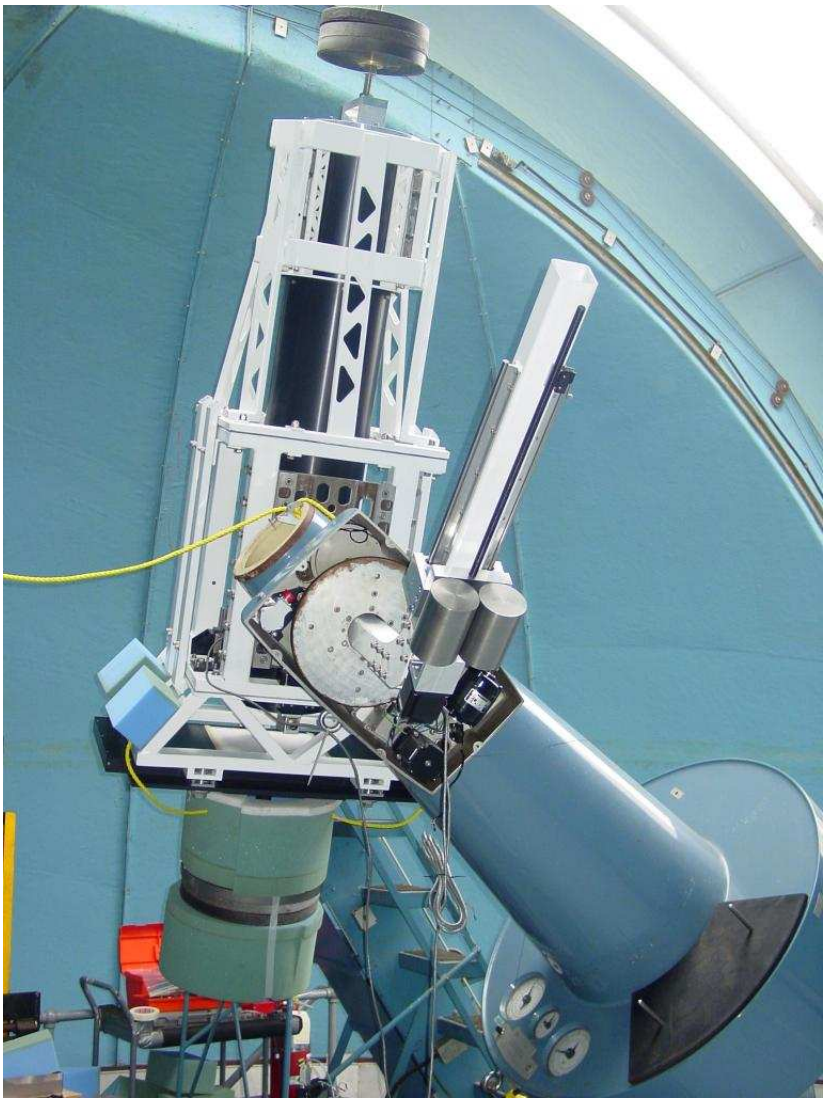

Figure 3: The new tube assembly of the USNO astrograph in 2009 after completion of the mechanical work. The camera dewar has a mass of ≈ 140 kg and the change in mass due to evaporating LN_2 requires a movable counterweight on the opposite side to balance this relatively small telescope on its mount.

telescope aperture	20	cm
bandpass	670–750	nm
pixel scale	0.905	arcsec/pixel
pixel size	9.0	μm
field of single detector	2.65 x 2.65	degree
number of imaging detectors	4	STA1600
number of guide/focus det.	3	2k by 5k each
sky area per exposure	28	sq. degree
survey expos.time	4	min
magnitude range	8 – 18	mag
survey begin at NOFS	2011	

Table 2: Properties of the URAT program.

A summary of the URAT project properties is given in Table 2. The detector design and electronics allow for clocked anti-blooming operations which extend the usable dynamic range for astrometry by about 3 magnitudes at the bright end (beyond saturation). The dewar has a 300 mm clear aperture window which also serves as the filter. It contains also 2 neutral density spots (5 and 7.5 mag attenuation, respectively) to allow stars as bright as about R = 1 be observed relative to surrounding stars of magnitude 8 or fainter in a large area of sky. A prototype camera with a single, front-side illuminated 10k detector was successfully operated in 2007/2008. A "4-shooter" camera for URAT was funded in 2008. The 4 thinned STA16000 detectors of 10,560 by 10,560 pixels each (Figure 3) image 28 square degrees of sky in a single exposure. On 3 sides of the 2 by 2 array of main detectors, there are additional 2k by 5k CCDs with 8 μm pixel size used for guiding and focus control.

Figure 4: Flat field image of a successfully thinned 10k detector for the URAT camera. Pixel data of the 16 outputs are shown with overscans. The cosmetic quality is excellent with only 2 column defects on the entire 111 million pixel area.

After test and commissioning the entire instrument will be moved to the USNO Flagstaff, Arizona station (NOFS) in 2011 to begin a new sky survey. The shipping container also serves as control room.

After 2 to 3 years of operation, the instrument will likely be moved to the Cerro Tololo Interamerican Observatory (CTIO) to observe the southern hemisphere. Due to the large field of view, several complete sky overlaps per year will be obtained of the accessible hemisphere to derive mean positions, proper motions and parallaxes on the 10 to 30 mas level, depending on the brightness of stars.

The URAT survey will be able to directly link many ICRF optical counterparts to the Hipparcos reference frame. A successful Gaia mission of course will supersede most of the URAT data; however, a significant improvement of the optical reference frame and data for galactic dynamics studies are expected from URAT in several releases beginning in 2012. URAT will also provide excellent reference stars for the other ongoing or planned very deep surveys until then.

For the latest update on UCAC and URAT, see
http://www.usno.navy.mil/usno/astrometry/optical-IR-prod .

5. REFERENCES

Boboltz, D. A., Fey, A. L., Puatua, W., Zacharias, N., Claussen, M. J., Johnston, K. J., Gaume, R. A., 2007, "VLA+PT Astrometry of 46 Radio Stars" AJ 133, pp. 906

ESA 1997, "The Hipparcos Catalogue", ESA SP-1200

Fey, A., Gordon, D., Jacobs, C.S. (Eds.), 2009, "The second realization of the international celestial reference frame by very long baseline interferometry", IERS Technical Note No. 35, Frankfurt

Finch,C., Zacharias,N., Wycoff,G., 2010, "UCAC3 astrometric reductions", AJ 139, 2200–2207

Girard, T., 2010, private communication.

Röser, S., Demleitner, M., Schilbach, E., 2010, "The PPMXL catalog of positions and proper motions on the ICRF", AJ 139, pp. 2440

van Leeuwen, F. 2007, "Hipparcos, the new reduction of the raw data", A&A 474, pp. 653

Zacharias, M.I., Zacharias, N., 2009, "Significant radio-optical reference frame offsets from CTIO data", poster paper IAU General Assembly, Rio de Janeiro

Zacharias,N., Urban,S.E., Zacharias,M.I., Hall,D.M., Wycoff,G.L., Rafferty,T.J., Germain,M.E., Holdenried,E.R., Pohlman,J.W., Gauss,F.S., Monet,D.G., Winter,L., 2000, "The first US Naval Observatory CCD Astrograph Catalog", AJ 120, pp. 2131

Zacharias,N., Urban,S.E., Zacharias,M.I., Wycoff,G.L., Hall,D.M., Monet,D.G., Rafferty,T.J., 2004, "The Second US Naval Observatory CCD Astrograph Catalog (UCAC2)", AJ 127, pp. 3043–3059

Zacharias,N., Winter,L, Holdenried,E.R., De Cuyper,J.-P., Rafferty,T.J., Wycoff,G.L., 2008, "The StarScan plate measuring machine: overview and calibrations", PASP 120, pp. 644

Zacharias, N., Finch,C., Wycoff,G., Hartkopf,W., 2009, "Improving Hipparcos Proper Motions with UCAC", DDA meeting, Virginia Beach, BAAS 41 No.2, p. 910, abstract 16.03

Zacharias,N., Finch,C., Girard,T., Hambly,N., Wycoff,G., Zacharias,M.I., et al. 2010, "The Third US Naval Observatory CCD Astrograph Catalog (UCAC3)", AJ 139, pp. 2184–2199

THE LARGE QUASAR ASTROMETRIC CATALOGUE (LQAC) AND THE DENSIFICATION OF THE ICRF THROUGH THE LQRF (LARGE QUASAR REFERENCE FRAME)

J. SOUCHAY
SYRTE, Observatoire de Paris, CNRS, UPMC
61 avenue de l'Observatoire, 75014 Paris, France
e-mail: Jean.Souchay@obspm.fr

ABSTRACT. As quasars are generally considered as ideal objects for astrometry, for they are supposed to materialize quasi-inertial directions in space, it looks interesting to compile all the existing quasars catalogues in a single one, emphasizing the astrometric quality of the objects according to the catalogue they are coming from. This is the purpose of the LQAC (Large Quasar Astrometric Catalogue) achieved by Souchay et al. (2009). In this paper we explain in some details the basic principles of the construction of the LQAC, as well as the prospects of a new version of this catalogue, and the link with the establishment of the Large Quasar Reference Frame (Andrei et al. 2009).

1. THE LQAC: AN EXHAUSTIVE COMPILATION OF THE VARIOUS QUASARS CATALOGUES

The quasars are playing a fundamental role in astrometry, because they are supposed to indicate quasi-inertial directions in space. As a consequence the primary reference frame for all astronomers is the ICRF (International Celestial Reference Frame) (Ma et al. 1998) with its recent up-date the ICRF2 (Boboltz et al. 2010), based on a set of 3414 radio loud extragalactic objects, mainly quasars, observed via the VLBI, presently the most accurate technique for the measurements of celestial coordinates, at the level of a few μas (microarcseconds). If the quality of optical observations, typically of the order of a few mas (milliarcseconds) at best, is by two orders worse than VLBI, no doubt that in the near future, with the improvement of optical techniques and the up-come of space missions as GAIA, the gap between the two kinds of techniques will be shortened. Moreover the number of optically recorded quasars is roughly 30 times larger than the ICRF2 sample ($\approx$ 110,000 objects instead of 3,500 ones). This overwhelming advantage in density of "optical quasars" counterbalances in some way their lack of accuracy with respect to radio-loud quasars. In fact, in order to construct the LQAC, we gathered the 12 largest quasar catalogues, 4 from radio interferometry programs and 8 from optical surveys.

One of the important steps consisted in carrying out the cross-identification between these catalogues. For that purpose we adopted an archiving strategy giving priority to the *a priori* most accurate catalogues (in fact the 4 radio ones), with a letter as a flag for each one. The list of the catalogues concerned is given in table 1. The most accurate catalogue was obviously the ICRF-Ext2 (Fey et al. 2004) (because it was not still superseded by the ICRF2 during the construction of the LQAC) which naturally was labelled with flag "A". It was followed by the three other VLBI catalogues, the VLBA (Fomalont et al. 2003) which contains 3357 sources with a milliarcsecond accuracy (flag "B") , the VLA (flag "C") and the JVAS (flag "D") catalogues which complete the radio quasars sample. At optical wavelengths the largest quasars catalogue was by far the fifth version of the SDSS (Sloan Digital Sky Survey) by Adelman-Mc.Carthy et al. (2007) containing 74 868 objects, followed by the 2-degree Field (2dF) Quasar Redshift Survey quoted as 2QZ (Croom et al. 2004) and including 22 971 objects. The FIRST radio survey (Gregg et al. 1996) and the Hewitt and Burbridge (1993) catalogue complete the list. Notice that for the LQAC we also took into account other optical catalogues as 2MASS (Cutri et al. 2003), the USNO B1.0 catalogue (Monet et al. 2003) and the GSC2.3 catalogue (Lasker et al. 2008). In fact the purpose of including these last three catalogues was not to include other quasars, but to complete significantly the photometric data after cross-identification with the quasars of the catalogues already mentioned before.

Table 1: Characteristics of the catalogues participating in the LQAC (Large Quasar Astrometric Catalogue) compilation.

Catalogue	Flag	Wavelength	No. quasars	Accuracy arcsec	Search radius arcsec
ICRF-Ext2	A	radio	717	0.001	1
VLBA	B	radio	3 357	0.001	1
VLA-015	C	radio	1 701	0.015	1
JVAS	D	radio	2 118	0.2	1
SDSS	E	optical	74 868	0.2	1
2QZ	F	optical	22 971	0.2	1
FIRST	G	radio	969	0.5	2
VLA+015	H	radio	157	0.2	2
HB	I	optical+radio	7 245	1.5	2-5-30*
2MASS	J	infrared	-	0.2	1
GSC2.3	K	optical	-	0.2	1
B1.0	L	optical	-	0.2	1
VV06	M	optical+radio	85 189	1.0	2-5-10*

*Three different search radii have been considered for the cross-identification.

For all the catalogues, except the Hewitt and Burbridge (1993), quoted in the following as HB, the positions of the objects are accurate at the level of $1''$ (arcsecond). Therefore the cross-identifications of quasars between these catalogues do not present any difficulty when adopting a $1''$ search radius. This is due to the fact that the probability to find two different quasars in one arcsecond circle is quasi-null. Things are becoming more complicated when one of the catalogues, which is the case of the sole HB one, contains objects with large positioning uncertainty. In the particular case of the HB catalogue, the search radius must be extended up to $30''$, for the uncertainty in position of the sources can reach this amount. Thus the probability of mismatch is rather big, but fortunately the redshift is a helpful criteria to discriminate the case of a simple or double object. In the case the redshift is roughly the same ($\Delta z < 0.1$, the object is considered as the same in the two catalogues. In the opposite case the two objects are considered to be different. This is illustrated in Fig. 1, where we can observe that the differentiation between the two cases is rather easy.

2. ADVANTAGES OF THE LQAC

The work consisting in compiling all the recorded quasars with a periodical up-date has been done for the last two decades in a very systematic, regular and complete manner by Véron-Cetty and Véron as in their recent version (Véron-Cetty and Véron 2006). Nevertheless the LQAC, whose the acronym implies that it is directed towards astrometric quality, brings some further improvements with respect to the compilation above : (i) it aims at being larger by including new quasars; (ii) it gives the most accurate determination of the celestial positions of the objects; (iii) it contains more information concerning their photometric properties; (iv) for the sake of homogeneity it systematically privileges large surveys to small catalogues; (v) by using a system of flag it gives directly a clear information about the cross-identification between the twelve catalogues in the compilation; (vi) it is based on a compilation strategy which ranges the catalogues by decreasing order of accuracy; (vii) it proposes a determination of the absolute magnitudes of the quasars in bands r and i by using up-to-date models of galactic extinction mapping (Schlegel et al. 1998) and new values of cosmological parameters (Spergel et al. 2007).

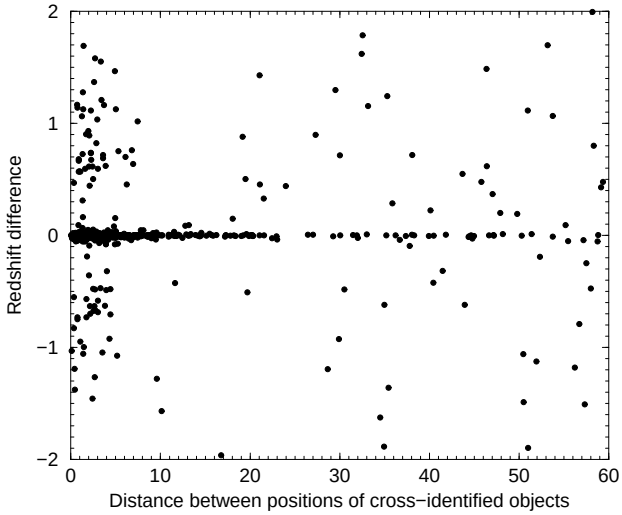

Figure 1: Comparisons of redshifts between common objects of the Hewitt and Burbridge catalogue and of the pre-compiled A-H catalogue, with respect to the angular distance of the objects. The quasars ranged horizontally corresponds *a priori* to a single object whereas those clearly out of the horizontal line correspond to a double object.

3. THE LQRF AND THE FUTURE UPDATE OF THE LQAC

Following the construction of the LQAC, the Large Quasar Reference Frame (LQRF) was built by Andrei et al. (2009) in order to give the positions of the LQAC quasars with an optimized accuracy with respect to the original catalogues, the care of avoiding incorrect matches of its constituents quasars, the homogenization of the astrometry from different catalogues and the aim of obtaining a milli-arcsecond global alignment with the ICRF, as well as typical individual source position accuracies higher than 100 mas (milliarcseconds).

The methodology for building the LQARF is the following one: starting from the updated and presumably complete Large Quasar Astrometric Catalog (LQAC) list of QSOs, the initial optical positions of the quasars were taken from the USNO B1.0 catalogue (Monet et al. 2003), the GSC2.3 catalogue (Lasker et al. 2008), and from the SDSS Data Release 5 (Adelman-McCarthy et al. 2007). Then, the initial positions were placed onto UCAC2-based reference frames (Zacharias,2006), followed by an alignment with the ICRF, to which were added the most precise sources from the VLBA calibrator list and the VLA calibrator list (when reliable optical counterparts exist). Finally, the LQRF axes were inspected through spherical harmonics, to define right ascension, declination and magnitude terms. In its first version (Andrei et al. 2009) the LQRF contains 100.165 quasars, represented with a rather homogeneous spatial density across the sky, from -83° to +88.5° in declination. For these reasons it can be considered as a good densification of the ICRF, the average angular distance between adjacent elements being roughly 10 arcmins.

Following all these efforts towards densification and accuracy, an up-dated version of the LQAC, called LQAC-2, is presently in preparation. The improvements with respect to the first version (Souchay et al. 2009) will be both quantitative and qualitative. On the quantitative side the quasars recently discovered will be included, in particular those coming from the last up-date of the SDSS quasars catalogue. Thus the expected total number of objects will be increased from roughly 110 000 to at least 140,000. On the qualitative side, in addition to the column giving the celestial coordinates as taken directly from the original catalogues participating at the compilation, another column with the coordinates (*a priori* more accurate) computed for the LQRF (Andrei et al. 2009) will be given. Moreover each object will

have an identification number directly associated with its celestial coordinates (α, δ).A significant new information will concern the compacity of the objects, a fundamental point to determine their ability to serve as a point-like source. A compacity index will be given, numbered from 1 to 10, according to its profile. At last the ambiguity concerning the HB quasars positions mentioned in Section 1 will be eliminated after clear recognition of the HB objects and positioning at the level of $1''$.

4. REFERENCES

Adelman-McCarthy, J.K., Agüeros, M.A., Allam, S.S., et al. = 2007, ApJS, 172, 634
Andrei,A.H., Souchay, J., Zacharias, N. et al.,2009, AA 505,385A
Boboltz, D.A, Gaume,R.A., Fey A.L., et al., AAS 2154690B
Croom, S.M., Smith, R.J., Boyle, B.J., et al. 2004, MNRAS, 349, 1397
Cutri, R.M., Skrutskie, M.F., van Dyk, S., et al. 2003, NASA/IPAC Infrared Science Archive, http://irsa.ipac.caltech.edu/applications/Gator/=20
Fey, A.L., Ma, C., Arias, E.F., et al. 2004, AJ, 127, 3587
Fomalont, E.B., Petrov, L., MacMillan, D.S., et al. 2003, AJ, 126, 2562
Gregg, M.D., Becker, R.H., White, R.L., et al. 1996, AJ, 112, 407
Hewitt, A., & Burbidge, G. 1993, ApJS, 87, 451=20
Lasker, B. M., Lattanzi, M. G., McLean, B. J., et al. 2008, AJ, 136, 735
Ma, C., Arias, E.F., Eubanks, T.M., et al. 1998, AJ, 116, 516
Monet, D.G., Levine, S.E., Canzian, B., et al. 2003, AJ, 125, 984
Schlegel, D.J., Finkbeiner, D.P., & Davis, M. 1998, ApJ, 500, 525
Schneider, D.P., Hall, P.B., Richards, G.T., et al. 2005, AJ, 130, 367
Spergel, D.N., Bean, R., Doré, O., et al. 2007, ApJS, 170, 377=20
Souchay, J.,Andrei, A.H., Barache, C. et al., 2009, AA 494,799
Véron-Cetty, M.-P., & Véron, P. 2006, A&A, 455, 773
Zacharias N. Urban, S.E, Zacharias, M., et al.,2004, AJ127,3043Z

ABSOLUTE PARALLAXES AND PROPER MOTIONS FROM THE PARSEC PROGRAM

B. BUCCIARELLI[1], A.H. ANDREI[1,2,3], R.L. SMART[1], M.G. LATTANZI[1], U. SCHIROSI[1], J.L. PENNA[2], M. DAPRÁ[1], T.G. de MOURA ESTEVÃO[3], V.A. d'ÁVILA[2], J.I.B. CAMARGO[2], M.T. CROSTA[1], B. GOLDMAN[4], H.R.A. JONES[5], L. NICASTRO[6], D.N. da SILVA NETO[7], R. TEIXEIRA[8]

[1] OATo-INAF, Strada Osservatorio 20, Pino Torinese TO, Italy; e-mail: bucc@oato.inaf.it
[2] ON/MCT Brazil, [3] OV/UFRJ Brazil, [4] MAX PLANCK, Heidelberg Germany, [5] CARST, University of Hertfordshire UK, [6] IASFC-INAF Italy, [7] UEZO-RJ Brazil, [8] IAG-USP Brazil

ABSTRACT. The PARallaxes of Southern Extremely Cool objects (PARSEC) program is designed to measure trigonometric parallaxes of 150 confirmed brown dwarfs in the southern hemisphere with the aim of using distances as fundamental calibrators for the investigation of star formation and evolution in the very low-mass regime. A scientifically useful addition to the primary scope of the project is the derivation of stellar proper motions, by combining observations from the full field of view, linked to the UCAC2 catalogue, with first-epoch data from 2MASS. To date, a proper motion catalogue of about 200,000 objects has been compiled. Tailored reduction techniques allow to attain milliarcsecond accuracy in the derived astrometric parameters, as validated by external comparisons.

1. OBSERVATIONAL STRATEGY

PARSEC observations are carried out with the Wide Field Imager on the ESO 2.2 m telescope at La Silla. The detector is a mosaic of 8 CCDs sized 2k x 4k 15μm pixels, providing a scale of 0.2″/pixel and a total field of view of 0.3 square degrees. All images are taken in the z filter (central wavelength 964.8 nm), a suitable compromise between the optimal QE of the system in the I band and the expected brightness of the targets, whose $(I-z)$ is typically larger than 1.5. Exposure times are indicatively 150 s and 300 s for bright ($z < 18$) and faint ($z \geq 18$) objects respectively; during nights with particularly poor seeing ($> 1.5''$), times are adjusted to obtain a highest-pixel signal of > 100 counts above the background.

With earliest observations dating back to April 2007, a frequency of 3-4 observing runs per year and an envisaged time span of the program of 4 years, the parallax ellipse is optimally sampled for almost all the targets. The end points of the ellipse's major axis correspond to the most crucial observations, which occur when the so-called parallax factor F reaches its highest numerical value. In fact, the star's apparent displacement in right ascension, due to its annual parallax, is adequately given by $\Delta\alpha cos\delta = F\pi$, where π is the trigonometric parallax and $F \equiv (Ycos\alpha - Xsin\alpha)$ is a function of the star's right ascension α and the Sun's geocentric equatorial coordinates $(X, Y) = (cos\lambda_\odot, sin\lambda_\odot cos\epsilon)$, ϵ being the inclination between the equatorial and ecliptic planes. It is clear that, having fixed the measurement error on the stellar displacement, a larger value of F would result in a smaller error on the estimated parallax. It can be shown that $|F|$ is maximum when the geocentric angle between the Sun and the star is 90°. When planning our observations, we also require that the target be near the meridian (+/- 20 min) in order to minimize differential refraction effects; these two conditions are simultaneously best met at evening/morning twilight, when stars crossing the meridian are approximately perpendicular to the direction of the setting/rising sun. Therefore, twilight hours bear the most relevance to our observing program.

Targets are picked from the nightly schedule according to a priority flag which reflects the observing history of each object and which is updated at every run. Finally, after an initial acquisition, the pointing is refined to move the target always in the same (x, y) position, which falls in the top third of CCD#7. For all the subsequent parallax reductions we only use data from this portion of the detector: this is sufficiently large that we have enough reference objects for a transformation to a common system and sufficiently small to assume that a variation in astrometric distortion over the observational campaign would be smaller than the errors of a linear transformation.

Once the raw CCD data are pre-reduced using the prescriptions illustrated in Andrei et al. (2010),

the stellar density profiles are fitted with a bi-dimensional Gaussian model giving an estimation of the objects' *centroiders* $(x(t), y(t))$ at the time of observation, which are our basic astrometric measurements.

2. THE DERIVATION OF PARALLAXES

The target's relative parallax and its relative-to-absolute correction are derived following the methods discussed in TOPP (Smart et al. 2003, 2007). These have been extensively tested and successfully used to produce the first PARSEC results (Andrei et al. 2010), i.e., preliminary parallaxes for 10 brown dwarfs, 2 of which within 10 parsecs, with a median *rms* error of 4.2 milliarcseconds.

In this contribution we focus on some aspects concerning the problem of rank deficiency intrinsic to the task of parallax determination with small-field astrometry. Let's consider n frames taken at different observing times $t_\nu; \nu = 1, ..., n$ and m stars observed in each of those frames. For any star μ; $\mu = 1, .., m$, assuming that the change in position is only due to parallax and proper motion effects, its longitudinal *standard coordinate* on the tangential plane, identified by the intersection of the telescope optical axis with the celestial sphere, can be modelled as:

$$\xi_\mu(t_\nu) \equiv \xi_{\nu\mu} = \xi_{0\mu} + \Delta t_\nu \mu_\nu + F_\nu \pi_\mu \tag{1}$$

where ξ_0 is the tangential position at a chosen reference epoch t_0 and $\Delta t_\nu = t_\nu - t_0$; μ, π are the star's *proper motion* in right ascension and its *parallax*, and F is the parallax factor defined in the previous section.[1] On the other hand, the $\xi_\mu(t_\nu)$ are functions of the true values of the measured coordinates $x_{\nu\mu}$, which we assume to be well represented by the linear transformation:

$$\xi_{\nu\mu} = x_{\nu\mu} + A_\nu x_\mu + B_\nu y_\mu + C_\nu \tag{2}$$

where the A_ν, B_ν, C_ν are the so-called *plate parameters*. Equations 1 and 2 can be trivially combined to obtain the *observation equation* for star μ on frame ν. We introduce now vector $\mathbf{l^T} = (\mathbf{l_1^T}, ..., \mathbf{l_n^T})$ where $\mathbf{l_\nu^T} = (x_{\nu 1}, ...x_{\nu m})$ is the vector of measurements of all the stars on frame ν. Moreover, let's $\mathbf{p^T} = (A_1, B_1, C_1, ..., A_n, B_n, C_n, \xi_1, \mu_1, \pi_1, ..., \xi_m, \mu_m, \pi_m)$ be the vector of instrumental and astrometric unknowns. With this formalism, the final system of equations can be expressed in matricial form as:

$$\mathbf{X} \cdot \mathbf{p} = -\mathbf{l} \tag{3}$$

The explicit form of $\mathbf{X}$ is given by:

$$\mathbf{X} = \begin{pmatrix} \mathbf{M_1} & & & -\mathbf{I} & -\Delta t_1 \mathbf{I} & -F_1 \mathbf{I} \\ & \mathbf{M_2} & & -\mathbf{I} & -\Delta t_2 \mathbf{I} & -F_2 \mathbf{I} \\ & & \ddots & \vdots & \vdots & \vdots \\ & & \mathbf{M_n} & -\mathbf{I} & -\Delta t_n \mathbf{I} & -F_n \mathbf{I} \end{pmatrix}$$

where $\mathbf{I}$ is the identity matrix, Δt_i and F_i are defined as in equation 2, and the matrices

$$\mathbf{M_i} = \begin{pmatrix} x_{i1} & y_{i1} & 1 \\ x_{i2} & y_{i2} & 1 \\ \vdots & \vdots & \vdots \\ x_{im} & y_{im} & 1 \end{pmatrix}$$

differ from each other inasmuch as the measurements of stellar positions in a given field of view change in value from one frame to another. The number of columns of matrix $\mathbf{X}$ is $3m + 3n$, but its rank is only $3(m + n) - 3$, meaning that some a-priori known position, proper motion and parallax must be used in order to solve the system of equations 3. If we assume that the plate parameters are small ($<< 1$), which is generally the case provided that the CCD axes are properly aligned and the scale factor well known, the matrices $\mathbf{M_i}$ will be nearly identical, and can therefore be approximated by a unique matrix $\mathbf{M}$ by choosing, e.g., $\mathbf{M} = \mathbf{M_1}$. With this substitution, the dimension of the null space of $\mathbf{X}$ becomes equal to 9 (Eichhorn 1988). If no approximations are made, only 3 *singular values* of $\mathbf{X}$ are exactly equal to zero, and the *rank deficiency* of the problem decreases mathematically to 3; however, 6 of the remaining

[1] Analogous formulae hold for the ζ component in latitude, which is neglected in this treatment. We note that the parallax factor in declination is sensibly smaller than the one in right ascension, bearing therefore much less weight into the estimation process

singular values are *nearly* zero; therefore, in a numerical sense, the singularity of the problem is still equal to 9. The physical meaning of such indeterminacy relies in the impossibility of distinguishing, solely based on the measurements, whether an observed translation, rotation, or scale factor are accountable to instrumental effects as opposed to some global astrometric behaviour of the stellar field.

To solve equation 3 in the least-square sense, one must determine a particular solution out of the infinite solutions of the associated normal system. Two different approaches are considered: the first one is to add to matrix $\mathbf{X}$ nine linearly independent constraint equations in order to eliminate the rank deficiency; the second one consists in finding a *minimum norm* solution using, e.g., the singular value decomposition method, which allows to construct an orthonormal set of vectors spanning the *range* of $\mathbf{X}$.

In the first approach, a suitable choice of constraints, as suggested by Eichhorn (1988) and subsequently analysed by Rapaport (1998), is represented by the set of equations

$$\mathbf{M}^T \mathbf{P}_s = \mathbf{C}$$

with $\mathbf{M}^T$ defined above;

$$\mathbf{P}_s = \begin{pmatrix} \xi_{01} & \mu_1 & \pi_1 \\ \xi_{02} & \mu_2 & \pi_2 \\ \vdots & \vdots & \vdots \\ \xi_{0m} & \mu_m & \pi_m \end{pmatrix}$$

being the unknown astrometric parameters of the *reference* stars, and $\mathbf{C}$ an arbitrary 3x3 matrix. While for the constraint equations involving stellar positions, the elements of $\mathbf{C}$ can be calculated using *reference* stars' catalogue values, this is not the case for the ones concerning parallaxes and proper motions, which are not usually available. A suitable choice is to put all the other elements of $\mathbf{C}$ equal to zero, which means fixing at zero the barycenter of parallaxes and proper motions of the reference stars, plus adding an orthogonalization condition with respect to the plate measurements.

Both the described approaches should be equivalent, as in principle one can fully recover one solution from the other by noticing that the so-called *general solution*, i.e., the one generating the complete set of solutions of system 3, is given by the sum of a *particular* solution and a linear combination of the orthonormal vectors spanning the null space of $\mathbf{X}$. However, as already stated, the rank deficiency of the problem is not exactly 9, and solutions obtained with different set of constraints are not exactly equivalent. The method adopted in TOPP is an iterative one, naturally converging to a minimum-norm-type solution without the necessity of adding extra conditions. We are currently investigating the extent to which the choice of different constraints can influence the final determination of the relative-to-absolute parallax correction.

3. THE DERIVATION OF PROPER MOTIONS

The raw data from the entire field of view of the ESO Wide Field Imager have been used to compute proper motions of anonymous objects down to the magnitude limit of an average CCD exposure, i.e., $I \simeq 19$. To this end, independently for each CCD and each observing time, we have determined an astrometric reduction relative to the Second US Naval Observatory CCD Astrograph Catalog (UCAC2, Zacharias et al. 2004). With an average number of reference stars per CCD equal to 20, polynomial fits of degree 2 or 3, depending on the actual number of UCAC2 stars available, were used to transform the (x, y) measurements onto equatorial coordinates (α, δ). Then, each object was matched to the Two Micron All Sky Survey (2MASS, Skrutskie et al. 2006) point source catalogue. We employed a nearest-neighbor match, which should be sufficient to avoid mismatches even in the presence of high proper motions, given that the epoch difference between 2MASS and PARSEC observations is small and that our targets are clear of the Galactic disk. However, we are developing a more robust matching algorithm making use of GSC2.3 positions at different epochs.

In Andrei et al. (2010), results for 197,500 sources are analysed by means internal and external comparisons showing that our proper motions are well behaved, with a median *rms* error of 5 mas/year, both for right ascension and declination. Figure 1 is a plot of the reduced proper motion $H(K) = K + 5log(\mu_{tot}) + 5$, as a function of the $z - K$ color for all objects in the PARSEC proper motion catalogue. The z magnitudes come from a zero-point correction to the instrumental magnitudes of the first observations while K are 2MASS magnitudes. It can be seen that brown dwarf objects, which are marked with diamonds, are well segregated in this diagram.

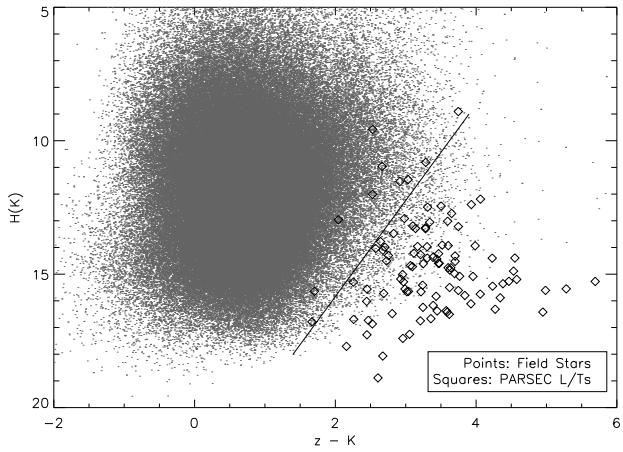

Figure 1: A reduced proper motion diagram ($H(k)$ versus $z-K$) of the 197,500 objects in the PARSEC proper motion catalogue. The region of possible brown dwarf candidates is delimited by the solid line

4. CONCLUSIONS

The PARSEC program has been successfully using ESO 2.2m Wide Field Camera observations to derive parallaxes of selected brown dwarfs, as well as proper motions of field stars at the milliarcsecond level accuracy, with direct astrophysical applications. Different methods for overcoming the rank deficiency inherent to the parallax derivation are being investigated. The PARSEC proper motion catalog, which to-date counts $\simeq 200,000$ objects, can be exploited to identify new brown dwarf candidates via the reduced proper motion diagram, for spectroscopic follow-up.

5. REFERENCES

Andrei, A.H., Smart, R.L., Penna, J.L., d'Avila, V.A., Bucciarelli, B., Camargo, J.I.B., Crosta, M.T., Dapr, M., Goldman, B., Jones, H.R.A., Lattanzi, M.G., Nicastro, L., da Silva Neto, D.N., and Texeira, R., 2010, "Parallaxes of Southern Extremely Cool objects I: Targets, Proper motions and first results", AJ accepted.

Eichhorn, H., 1988, "A General Explicit Solution of the Central Overlap Problem", ApJ, 334, pp. 465–469.

Rapaport, M., 1998, "Some new results on the central overlap problem in astrometry", A&A 335, pp.769–773.

Skrutskie, M.F., Cutri, M.R., Stiening, R., Weinberg, M.D., Schneider, S., Beichman, C., Capps, R., Chester, T., Elias, J., Huchra, J., Liebert, J., Lonsdale, C., Monet, D.G., Price, S., Seitzer, P. et al., 2006, "The Two Micron All Sky Survey (2MASS)", AJ 131, 1163–1183.

Smart, R.L., Lattanzi, M.G., Bucciarelli, B., Massone, G., Casalegno, R., Chiumiento, G., Drimmel, R., Lanteri, L. Marocco, F., Spagna, A., 2003, "The Torino Observatory Parallax Program: White dwarf candidates", A&A 404, pp. 317–323.

Smart, R.L., Lattanzi, M.G., JareiB, H., Bucciarelli, B., Massone, G., 2007, "Nearby ctar candidates in the Torino observatory parallax program", A&A 464, pp. 787–791

Zacharias, N., Urban, S.E., Zacharias, M.I., Wycoff, G.L., Hall, D.M., Monet, D.G., and Rafferty, T.J., 2004, "The Second US Naval Observatory CCD Astrographic Catalog (UCAC2)." AJ 127, pp.3043–3059

TOWARDS A VLBI CATALOG OF OPTICALLY-BRIGHT EXTRAGALACTIC RADIO SOURCES FOR THE ALIGNMENT OF THE RADIO FRAME WITH THE FUTURE GAIA FRAME

G. BOURDA[1], A. COLLIOUD[1], P. CHARLOT[1], R. PORCAS[2], S GARRINGTON[3]

[1] Université de Bordeaux, Observatoire Aquitain des Sciences de l'Univers
CNRS-UMR5804, Laboratoire d'Astrophysique de Bordeaux
2 rue de l'Observatoire, BP 89, F-33271 Floirac Cedex, France
e-mail: bourda@obs.u-bordeaux1.fr

[2] Max-Planck-Institut für Radioastronomie
Auf dem Hügel 69, 53121 Bonn, Germany

[3] University of Manchester, Jodrell Bank Observatory
Macclesfield, Cheshire SK11 9DL, UK

ABSTRACT. The space astrometry mission Gaia will construct a dense optical QSO-based celestial reference frame. For consistency between optical and radio positions, it will be important to align the Gaia and VLBI frames with the highest accuracy. In this respect, it was found that only 70 sources from ICRF were suitable to establish this link, either because they are not bright enough at optical wavelengths or because they show extended radio emission which precludes reaching the highest astrometric accuracy. In order to improve the situation, we initiated a multi-step VLBI observational project, dedicated to finding additional suitable radio sources for aligning the two frames. The sample consists of about 450 optically-bright radio sources, typically 20 times weaker than the ICRF sources, which have been selected by cross-correlating optical and radio catalogs. The initial observations, aimed at checking whether these sources are detectable with VLBI, and conducted with the European VLBI Network in 2007, showed an excellent 90% detection rate. This paper reports on global VLBI observations carried out in March 2008 to image 105 from the 398 previously detected sources. All sources were successfully imaged, revealing point-like VLBI structures for about half of them, which is very promising for the future. While the remaining ∼300 detected sources from our initial sample will be imaged in the same way, the next step, dedicated to measuring accurately the position of these sources, will be engaged in the near future.

1. CONTEXT

During the past decade, the IAU (International Astronomical Union) fundamental celestial reference frame was the ICRF (International Celestial Reference Frame; Ma et al. 1998, Fey et al. 2004), composed of the VLBI (Very Long Baseline Interferometry) positions of 717 extragalactic radio sources, measured from dual-frequency S/X observations (2.3 and 8.4 GHz). Since 1 January 2010, the IAU fundamental celestial reference frame has been the ICRF2 (IERS Technical Note 35), successor of the ICRF. It includes VLBI coordinates for 3 414 extragalactic radio sources, with a floor in position accuracy of 40 μas and an axis stability of 10 μas.

The European space astrometry mission Gaia, to be launched in 2012, will survey all stars and QSOs (Quasi Stellar Objects) brighter than apparent optical magnitude 20 (Perryman et al. 2001). Optical positions with Gaia will be determined with an unprecedented accuracy, ranging from a few tens of μas at magnitude 15–18 to about 200 μas at magnitude 20 (Lindegren et al. 2008). Unlike Hipparcos, Gaia will permit the realization of the extragalactic celestial reference frame directly at optical bands, based on the QSOs that have the most accurate positions. A preliminary Gaia catalog is expected to be available by 2015 with the final version released by 2020.

In this context, aligning VLBI and Gaia frames will be crucial for ensuring consistency between the measured radio and optical positions. This alignment, to be determined with the highest accuracy, requires several hundreds of common sources, with a uniform sky coverage and very accurate radio and optical positions. Obtaining such accurate positions implies that the link sources must be brighter than optical magnitude 18 (Mignard 2003), and must not show extended VLBI structures.

In a previous study, we investigated the potential of the ICRF for this alignment and found that only 70 sources (10% of the catalog) are appropriate for this purpose (Bourda et al. 2008). This highlights the need to identify additional suitable radio sources, which is the goal of a VLBI program that we initiated four years ago (Bourda et al. 2010a). This program has been devised to observe 447 optically-bright extragalactic radio sources extracted from the NRAO VLA Sky Survey, a dense catalog of weak radio sources (Condon et al. 1998). The observing strategy to detect, image, and measure accurate VLBI positions for these sources is described in Bourda et al. (2010a).

The initial observations, whose goal was to assess the VLBI detectability of the targets, were conducted with the European VLBI Network (EVN) in 2007. These showed an excellent 90% detection rate (Bourda et al. 2010a). Proceeding further with our program, we now report on global VLBI imaging observations carried out in March 2008 to image 105 of the 398 previously detected sources.

2. OBSERVATIONS AND DATA REDUCTION

The observations were performed during a 48-hour experiment (hereafter designated as GC030), on 7–9 March 2008, with a global VLBI array recording at 512 Mb/s in a dual-frequency S/X mode. This network was composed of 5 telescopes from the EVN (Effelsberg, Medicina, Noto, Onsala-20m and Hartebeesthoek), the DSN 70-m Robledo telescope for part of the time, and 9 antennas of the VLBA (Very Long Baseline Array). Sixteen 8 MHz-wide sub-bands were recorded, with 8 contiguous bands at each of S- and X-band. On average, a total of three to four 5-minute long scans were scheduled on each of the 105 target sources. In addition, we observed a sample of 10 well distributed ICRF sources, for use as calibrators. In all, about 80% of the allocated time was spent on source, while the rest was used for slewing.

The correlation of GC030 was done with the VLBA correlator at the Array Operations Center in Socorro (New Mexico, USA). The correlated data were then calibrated using the Astronomical Image Processing System (AIPS[1]). An initial amplitude calibration for each sub-band was accomplished using system temperature measurements taken during the observations combined with gain curves supplied for each telescope. Prior to fringing the targets, phase offsets between the sub-bands were determined by fringing a short calibrator scan, and then applied to all data. This allowed us to combine all sub-bands together when fringing, thereby increasing the signal-to-noise-ratio and maximizing chances of detection for these weak targets. Calibrators were used in a second stage to estimate amplitude correction factors for each station, each band (S and X), and each sub-band. These corrections, at the level of less than 10% on average, were applied to the calibrated data, which were then exported as FITS files.

The remaining data reduction was conducted with the Caltech DIFMAP[2] software-package which was used for imaging. Visibility data for each frequency band were selfcalibrated, Fourier inverted, and CLEANed following the hybrid-mapping technique (Pearson & Readhead 1984), using DIFMAP in an automatic mode. A point-source model was used as a starting model for the iterative procedure in all cases. Uniform weighting and, after several iterations, natural weighting, were applied to derive the final images.

3. RESULTS

Based on the analysis described above, VLBI maps at X- and S-bands were successfully produced for each of the 105 target sources observed during GC030. These images have the following characteristics:

- The typical beam has a size of about 1.2×0.5 mas at X-band and 4.2×2.0 mas at S-band.
- The dynamic range (defined as the ratio of the first plotted contour level to the peak brightness) is generally ∼1:100.
- The typical image noise rms is 0.080 mJy/beam at X-band and 0.117 mJy/ beam at S-band. This compares well with the theoretical image thermal noise at X- and S-bands, which are 0.050 and 0.082 mJy/beam, respectively.

When considering all 105 targets, the total flux density ranges from 23 mJy to 222 mJy at X-band, with a median value of 61 mJy, and from 22 mJy to 397 mJy at S-band with a median value of 65 mJy. Based on the X-band and S-band flux densities, the spectral index α (defined as $S \propto \nu^{\alpha}$, where S is the source flux density and ν is the frequency) has also been determined. In this definition, the sources with a

[1] http://www.aips.nrao.edu
[2] http://www.astro.caltech.edu/∼tjp/citvlb/index.html

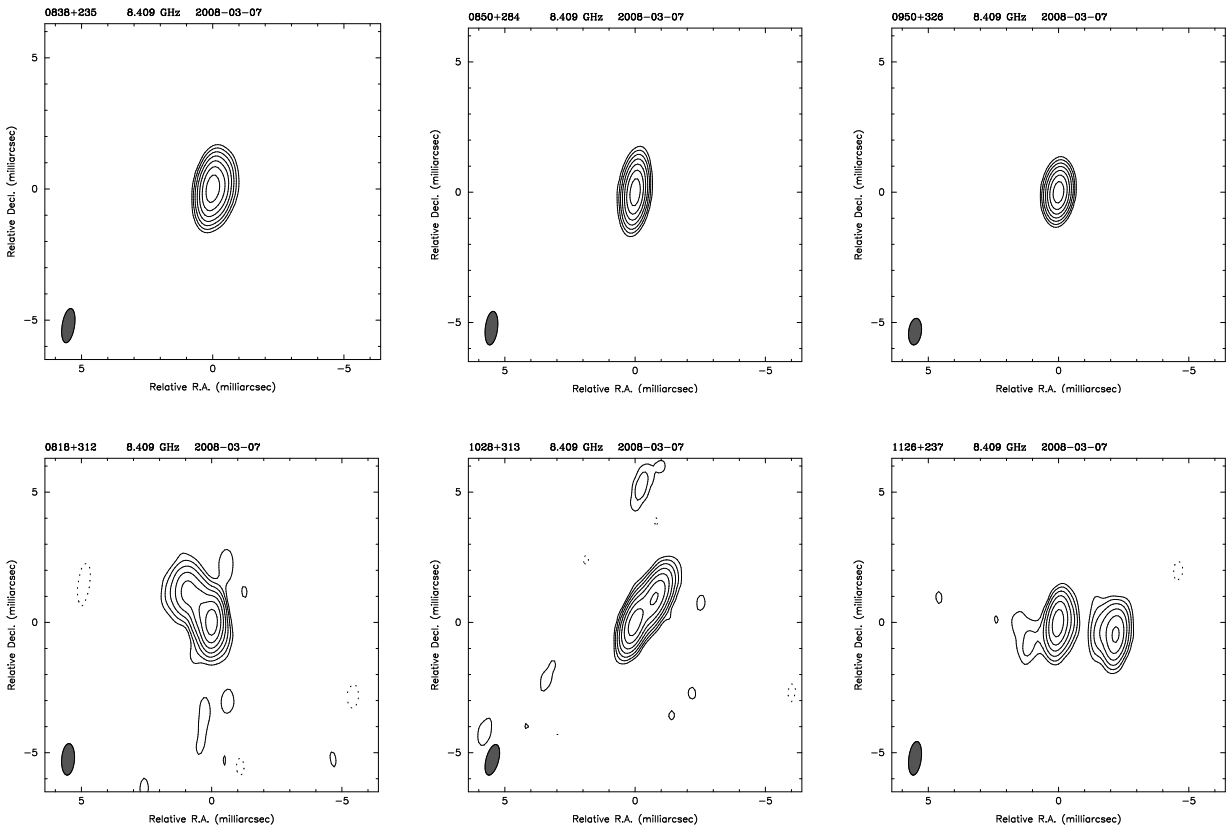

Figure 1: Examples of X-band VLBI maps for sources observed during GC030. *Upper panel*: Three sources suitable for the alignment with Gaia (point-like sources): 0838+235, 0850+284, 0950+326. *Lower panel*: Three sources not suitable for this alignment (sources with extended VLBI structures): 0818+312, 1028+313, 1126+237. The first contour level is typically 1% of the peak brightness, with successive contours increasing by a factor of 2. The FWHM (Full Width at Half Maximum) Gaussian restoring beam applied to the images is shown as an ellipse in the lower left of each panel.

dominating compact core are expected to have $\alpha > -0.5$. The median value of α for the sources observed during GC030 is -0.05, with $\alpha > -0.5$ for more than 90% of the targets (97 sources out of 105 sources imaged).

The images derived from GC030 show a variety of morphologies, ranging from point-like sources to extended or even double sources (e.g. see Fig. 1). In order to identify the most point-like ones, suitable for the Gaia link, we used the so-called "structure index" (SI) as an indicator of astrometric quality (Fey & Charlot 1997; Fey & Charlot 2000). Accordingly, only sources with SI < 3.0 should be used, since one wants to determine the link with the highest accuracy.

Analysis of the structure index values at X- and S-bands for all 105 sources observed during GC030 indicates that about half of them (47 sources) show point-like or compact structures at X-band (SI < 3.0), whereas the other half show extended structures. The resulting list of suitable sources is given in Bourda et al. (2010b) and can be accessed online[3].

4. FUTURE PROSPECTS

From now on, 50% of the remaining 293 detected sources from our initial sample have been observed in 2010, and the 25% still remaining will be observed in March 2011. These sources will be imaged in the same way. Assuming similar statistics, we expect another 150 suitable link sources to be identified. The final stage of this project, dedicated to measuring accurately the VLBI position of those sources, will be

[3]http://www.obs.u-bordeaux1.fr/BVID/GC030

engaged during the year 2011. While making the Gaia link possible, these new VLBI positions will also serve in the future to densify the VLBI frame at the same time.

Acknowledgements. The authors would like to thank the VLBI friends at the EVN and VLBA observing stations. This work has benefited from research funding from the European Community's sixth Framework Programme under RadioNet R113CT 2003 5058187. The EVN is a joint facility of European, Chinese, South African and other radio astronomy institutes funded by their national research councils. The VLBA is part of the National Radio Astronomy Observatory (NRAO), which is operated by Associated Universities, Inc., under cooperative agreement with the National Science Foundation.

5. REFERENCES

Bourda, G., Charlot, C., Le Campion, J.-F., 2008, "Astrometric suitability of optically-bright ICRF sources for the alignment with the future Gaia celestial reference frame", A&A 490, pp. 403–408.

Bourda, G., Charlot, P., Porcas, R., Garrington, S., 2010a, "VLBI observations of optically-bright extragalactic radio sources for the alignment of the radio frame with the future Gaia frame. I. Source detection", A&A 520, A113.

Bourda, G., Collioud, A., Charlot, P., Porcas, R., Garrington, S., 2010b, "VLBI observations of optically-bright extragalactic radio sources for the alignment of the radio frame with the future Gaia frame. II. Imaging candidate sources", A&A (online).

Condon, J., Cotton, W., Greisen, E., Yin, Q., Perley, R., et al., 1998, "The NRAO VLA Sky Survey", AJ 115, pp. 1693–1716.

Fey, A., Charlot, P., 1997, "VLBA Observations of Radio Reference Frame Sources. II. Astrometric Suitability Based on Observed Structure", ApJS 111, pp. 95–142.

Fey, A., Charlot, P., 2000, "VLBA Observations of Radio Reference Frame Sources. III. Astrometric Suitability of an Additional 225 Sources", ApJS 128, pp. 17–83.

Fey, A., Ma, C., Arias, E., Charlot, P., Feissel-Vernier, M., et al., 2004, "The Second Extension of the International Celestial Reference Frame: ICRF-EXT.1", AJ 127, pp. 3587–3608.

IERS Technical Note 35, 2009, "The Second Realization of the International Celestial Reference Frame by Very Long Baseline Interferometry", A. Fey, D. Gordon & C. Jacobs (eds.), Frankfurt am Main: Verlag des Bundesamts für Kartographie und Geodäsie.

Lindegren, L., Babusiaux, C., Bailer-Jones, C., Bastian, U., Brown, A., et al., 2008, "The Gaia mission: science, organization and present status", In: Proceedings of IAU Symposium 248, "A Giant Step: from Milli- to Micro-arcsecond Astrometry", W. Wenjin, I. Platais & M. Perryman (eds.), Cambridge University Press, pp. 217–223.

Ma, C., Arias, E., Eubanks, T., Fey, A., Gontier, A.-M., et al., 1998, "The International Celestial Reference Frame as Realized by Very Long Baseline Interferometry", AJ 116, pp. 516–546.

Mignard, F., 2003, "Future Space-Based Celestial Reference Frame", In: Proceedings of IAU General Assembly XXV, Joint Discussion 16: "The International Celestial Reference System: Maintenance and Future Realization", R. Gaume, D. McCarthy & J. Souchay (eds.), pp. 133–140.

Pearson, T., Readhead, A., 1984, "Image Formation by Self-Calibration in Radio Astronomy", ARA&A 22, pp. 97–130.

Perryman, M., de Boer, K., Gilmore, G., Hog, E., Lattanzi, M., et al., 2001, "GAIA: Composition, formation and evolution of the Galaxy", A&A 369, pp. 339–363.

COMPARISON OF THE PROPER MOTIONS IN DECLINATION OF FOUR CATALOGUES VIA 807 HIPPARCOS STARS

G. DAMLJANOVIC

Astronomical Observatory
Volgina 7, 11060 Belgrade 38, Serbia
e-mail: gdamljanovic@aob.bg.ac.rs

ABSTRACT. A comparison of four astrometric catalogues with the use of μ_δ for 807 Hipparcos stars is done. Pairwise differences of μ_δ from the catalogues PZT, EOC-2, Hipparcos and new Hipparcos were used to determine their random and systematic errors. The latitude part of ten Photographic Zenith Tubes (PZT data made at 6 observatories) were useful to combine them with the Hipparcos data and to construct the PZT catalogue with μ_δ for 807 stars, which are some of results of PhD thesis (Damljanović, 2007). During last few years, the new Hipparcos, EOC-2 and PZT catalogues have appeared. The Hipparcos one was published in 1997. Also, as a combination of the ground-based and Hipparcos satellite data, many other astrometric catalogues have appeared (TYCHO-2, ARIHIP, etc.) to check and improve the Hipparcos data or to make the densification of data. Usually, the task was to get more accurate coordinates and proper motions of stars than the Hipparcos ones. The useful and big set of data (about 4.4 million optical observations made during last century) are the astrometric observations of latitude and universal time variations; the observed stars are referred to Hipparcos catalogue. Originally, these data were made to determine the Earth Orientation Parameters (EOP), but nowadays for the opposite task (to get the improved coordinates and proper motions of some Hipparcos stars which were observed from the ground over many decades); the EOC-2 catalogue is based on these data. During comparison of four mentioned catalogues, the proper motion differences as a function of coordinates (α, δ), magnitudes and color indices were investigated; determined random and systematic errors of catalogues are relatively small and close to each other.

1. INTRODUCTION

The epoch of the Hipparcos catalogue is 1991.25, and after publishing (ESA, 1997) some other catalogues appeared, as the ARIHIP (Wielen et al., 2001), TYCHO-2 (Høg et al., 2000), EOC-2 (the Earth Orientation Catalogue) (Vondrák, 2004), PZT (Damljanović and Pejović, 2008), re-reduced Hipparcos data (van Leeuwen, 2007), etc.

The interval of Hipparcos satellite data was less than 4 years, and it is not enough for a good accuracy (which is about 1 mas/yr) of proper motions (of double/multiple stars); also, there are some other problems (Vondrák et al., 1998; Vondrák, 2004; van Leeuwen, 2007; Damljanović and Pejović, 2010).

It was clear that combination of Hipparcos/Tycho data with ground-based ones can check and improve the positions and proper motions of common stars. Also, the PZT catalogue is based on more than 0.9 million ground-based observations (made during the time interval 1915.8 – 1992.0) of 807 common PZT/Hipparcos stars (Damljanović, 2007; Damljanović and Pejović, 2008); the accuracy is close to or better than the Hipparcos one.

To check the quality of data, the differences of μ_δ (between PZT, EOC-2, Hipparcos and new Hipparcos) were investigated as a function of coordinates, magnitudes and color indices; all four catalogues have relatively small random and systematic errors which are close to each other (Damljanović and Pejović, 2010).

2. DATA AND RESULTS

Main about the proper motion μ of the star (tangential part on the sphere), μ_α (along the α) and μ_δ (along the δ) is possible to read in the book (Eichhorn, 1974). It is of importance here that the error ϵ_{μ_δ} of μ_δ is proportional to $1/t$ (with long time interval t of ground-based observations it is possible to get good accuracy ϵ_{μ_δ}, better than the Hipparcos one).

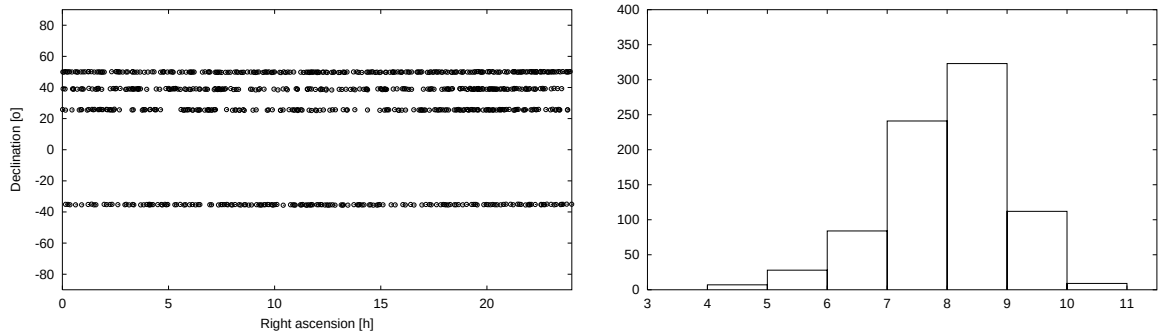

Figure 1: Distribution of 807 stars on the celestial sphere, and distribution of their magnitudes

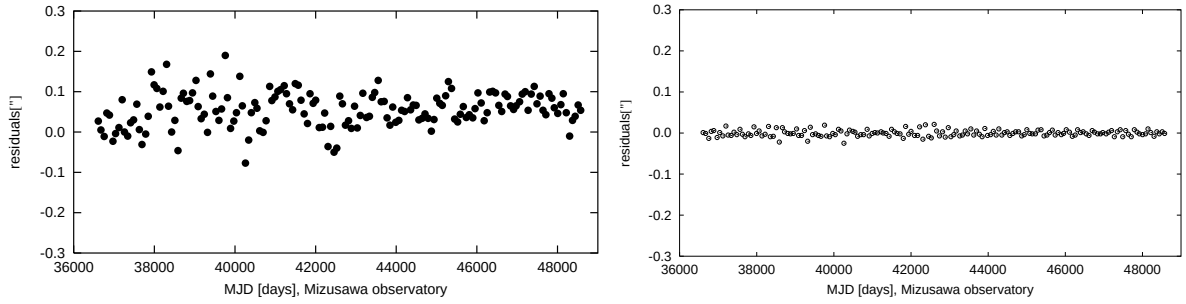

Figure 2: Mean residuals r_i (left) and r_i' (right) in bins of 0.2 years vs. time in MJD; Mizusawa

To construct the PZT catalogue, the latitude variations of optical observations made by 10 PZT instruments (at 6 observatories: Mizusawa, Mount Stromlo, Ondřejov, Punta Indio, Richmond and Washington) together with the Hipparcos data were used (Damljanović, 2005; Damljanović and Pejović, 2005; Damljanović and Pejović, 2010; Damljanović et al., 2006).

Fig. 1 shows the distribution of 807 stars on the celestial sphere (zenith zones of PZT instruments). Also, the distribution of their magnitudes (PZT stars are mostly between 6 mag and 10 mag).

Fig. 2 displays the mean residuals $r_i = -(\varphi_i - \Delta\varphi_i)$ and $r_i' = r_i - se_i$ (in bins of 0.2 years) vs. time in MJD for Mizusawa observatory. The polar motion effect $\Delta\varphi_i$ (calculated by using Kostinski's formula (Kulikov, 1962)) was removed from received data of latitude variations φ_i (Damljanović and Pejović, 2008; Damljanović and Pejović, 2010). The systematic effects se_i removed very well from the values r_i (see Fig. 2, Mizusawa example) to get r_i'.

From PZT observations, the latitude can be calculated by using McCarthy's (1970) formula. If the stars have sufficiently long periods of observations (more than 20 years), the PZT data have got good quality (Damljanović and Pejović, 2008; Damljanović and Pejović, 2010) and good formal errors (close to EOC-2 and new Hipparcos ones, see Fig. 4).

From Fig. 3 (mean differences between PZT data and EOC-2, Hipparcos and new Hipparcos ones, as

catalogue	s_0	p_1	p_2	p_3
PZT-EOC2	168	1 ± 9	-7 ± 6	6 ± 13
PZT-HIP	209	5 ± 12	-5 ± 7	3 ± 16
PZT-NHIP	215	11 ± 12	-3 ± 7	7 ± 17
EOC2-HIP	110	4 ± 6	1 ± 4	-3 ± 8
EOC2-NHIP	132	10 ± 7	4 ± 4	1 ± 10
NHIP-HIP	81	-6 ± 5	-2 ± 3	-4 ± 6

Table 1: Comparison of μ_δ of 807 stars, from Hipparcos, re-reduced Hipparcos (NHIP), PZT and EOC-2, to get formal and systematic errors (in 0.01 mas/yr).

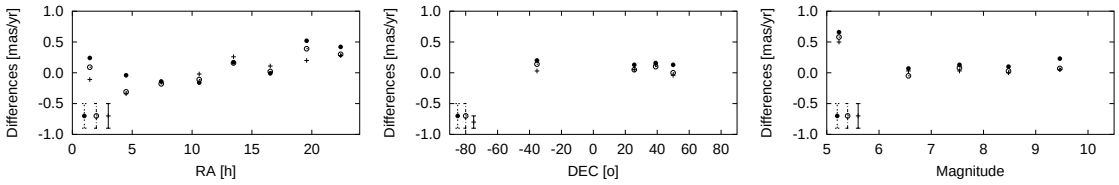

Figure 3: Mean proper motion differences (with a typical mean error bars) of 807 stars, as a function of α, δ and magnitude, between PZT data and: the re-reduced Hipparcos (solid circle), Hipparcos (open circle) and EOC-2 ones (+)

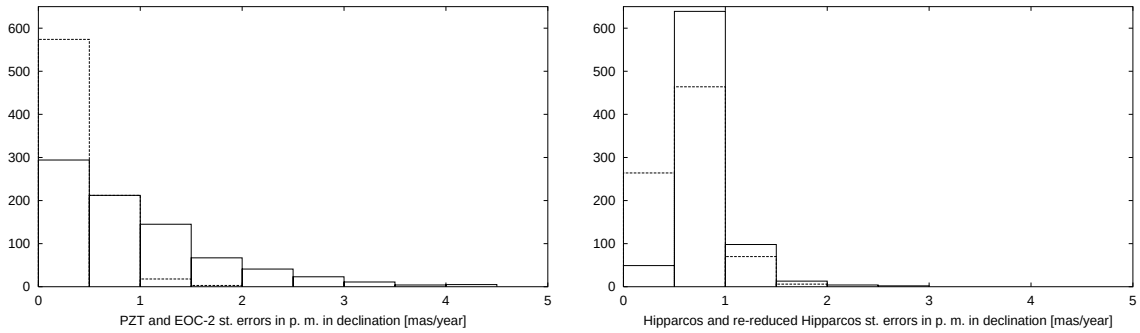

Figure 4: Distribution of standard errors in proper motions in declination for 807 stars: PZT (solid lines), EOC-2 (doted lines), Hipparcos (solid lines) and re-reduced Hipparcos (doted lines)

the function of coordinates and magnitude) is evident that PZT results are on the average very close to those of the three other catalogues (Damljanović and Pejović, 2010). A typical mean error bars of mean values, but not standard deviations in the bins, are shown. The values of standard deviations are close to the values s_0 (see in Table 1), respectively.

The formula $p_1 + p_2(m - m_0) + p_3(B - V) = \Delta$ (according to Ivanov and Yatsenko (2003)) and LSM (the Least Squares Method) were used to determine random and systematic errors of four catalogues. The calculated values of p_1, p_2 and p_3 (which describe the systematic part of differences Δ) are presented in Table 1, m are the magnitudes and $B - V$ color indices. s_0 is the random part of Δ (the sum of random errors of both of the two treated catalogues) and the error of unit weight of the solution of the system given by last equation.

The values of Table 1 are small. It means, the random and systematic errors of values Δ are very small, and μ_δ data of all four catalogues are close to each other (μ_δ data have got a high accuracy). So, there is no significant relationship between Δ and $m - m_0$ (or $B - V$).

3. CONCLUSIONS

It is possible to satisfy the requirements of the modern astrometry by using some of ground-based data, as it was the case of PZT observations to construct the PZT catalogue. And to check the present reference frame (Ron and Vondrák, 2001); the Hipparcos catalogue data materialize that frame.

The PZT catalogue data, the values of μ_δ for 807 stars (Damljanović and Pejović, 2008), were compared with the EOC-2, Hipparcos and new Hipparcos data. The consistency is good.

The procedure of determining random and systematic errors for 807 common stars of four catalogues by pairs (PZT, EOC-2, Hipparcos and new Hipparcos), according to Ivanov and Yatsenko (2003), shows that it is not find a significant relationship between the differences Δ (of μ_δ) and magnitudes and color indices. So, all catalogues have high accuracy of μ_δ. The random and systematic errors of μ_δ are small and close to each other. Also, it is an independent checking of μ_δ from the catalogues EOC-2, Hipparcos and new Hipparcos.

The PZT catalogue data are available at the URL:http://saj.matf.bg.ac.rs/177/pdf/Table2.dat.

Acknowledgements. Author performed his work as a part of the Projects No 146004 “Dynamics of celestial

bodies, systems and populations" supported by the Ministry of Science and Technological Development of R. Serbia.

4. REFERENCES

Damljanović, G., 2005, "Photographic zenith tubes observations to improve Hipparcos proper motions in declination of some stars", Serb. Astron. J., 170, pp. 127–132.

Damljanović, G., 2007, "Improvement of accuracy of proper motions of Hipparcos Catalogue stars using optical latitude observations", PhD Thesis, Belgrade Univ.

Damljanović, G., Pejović, N., 2005, "Improved proper motions in declination of some Hipparcos stars via long–term classical observations", in: Z. Knežević, A. Milani (eds.), Dynamics of Populations of Planetary Systems, IAU Coll., 197, pp. 471–474.

Damljanović, G., Pejović, N., 2008, "Corrections to the Hipparcos proper motions in declination for 807 stars", Serb. Astron. J., 177, pp. 109–113.

Damljanović, G., Pejović, N., 2010, "Error analysis of proper motions in declination obtained for 807 Hipparcos stars from PZT observations over many decades", Astron. Nachr., 331(8), pp. 843–851.

Damljanović, G., Pejović, N., Jovanović, B., 2006, "Improvement of Hipparcos proper motions in declination", Serb. Astron. J., 172, pp. 41–51.

Eichhorn, H., 1974, "Astronomy of star positions", Frederick Ungar Publishing Co., New York.

ESA, 1997, "The Hipparcos and Tycho Catalogues", ESA SP-1200, ESA Publications Division, Noordwijk.

Høg, E., Fabricius, C., Makarov, V.V. et al., 2000, A&A, 355, L27.

Ivanov, G., Yatsenko, A., 2003, "A comparison of some astrometric catalogues with the use of stars with large proper motions", Kinematika i fizika nebesnykh tel, 19(5), pp. 477–480.

Kulikov, K.A., 1962, "Izmenyaemost' shirot i dolgot", Moskva (in Russian).

McCarthy, D.D., 1970, "Reduction method and star positions for Washington and Richmond Photographic Zenith Tube", Master's Thesis, University of Virginia.

Ron, C., Vondrák, J., 2001, Proc. of the Journées 2000 – Systèmes de Référence Spatio-Temporels, N. Capitaine (ed.), pp. 201.

van Leeuwen, F., 2007, "Hipparcos, the new reduction of the raw data", Dordrecht: Springer.

Vondrák, J., 2004, "Astrometric star catalogues as combination of Hipparcos/Tycho catalogues with ground-based observations", Serb. Astron. J., 168, pp. 1–7.

Vondrák, J., Pešek, I., Ron, C., Čepek, A., 1998, "Earth orientation parameters 1899.7–1992.0 in the ICRS based on the HIPPARCOS reference frame", Astron. Inst. of the Academy of Sciences of the Czech R., Publ. No. 87.

Wielen, R., Schwan, H., Dettbarn, C. et al., 2001, Veröff. Astron. Rechen–Inst. Heidelberg No. 40.

THE XPM CATALOGUE AS A REALISATION OF THE EXTRAGALACTIC REFERENCE SYSTEM IN OPTICAL AND NEAR INFRARED WAVELENGHS

P.N. FEDOROV[1], V.S. AKHMETOV[1], Ya.S.YATSKIV[2].

[1] Institute of Astronomy of Kharkiv National University
Sumska 35, 61022 Kharkiv, Ukraine
e-mail: pnfedorov@gmail.com

[2] Main Astronomical Observatory NAS of Ukraine
Akademika Zabolotnogo 27, 03680 MSP Kiev, Ukraine
e-mail: yatskiv@mao.kiev.ua

ABSTRACT. The analysis of the absolute proper motions of the XPM catalogue is shortly presented in this article. It is shown that coordinate axes, given by the XPM catalogue, have ambiguities of rotations relative to the LQAC quasars and ICRF2 sources less than 0.2 mas/yr. In our opinion the XPM catalogue is the independent as to proper motions realization of the ICRS system in optical and near infrared ranges of wavelengths. The XPM star proper motions were compared with those from modern catalogues UCAC-3 and PPMXL. It is concluded that the proper motions of stars in these modern catalogues have considerable random and systematic errors.

1. INTRODUCTION

The final version of the XPM catalogue compiled on the basis of 2MASS (Skrutskie et al. 2006) and USNO 2.0 (Monet D. et al. 1998) catalogues is presented. The XPM catalogue (Fedorov et al. 2009, 2010) contains positions and absolute proper motions of about 300 million objects covering the whole sky in the magnitude range $10^m < B < 22^m$ as well as the standard J, H, K, B and R magnitudes. Positions in the XPM are referred to the HCRF (Kovalevsky et al. 1997) for the 2000 epoch. The Catalogue contains proper motions over the whole sky without gaps. In the fields, which cover the zone of avoidance or which contain less than of 25 galaxies the so-called quasi absolute calibration was performed. The proper motion errors are varying from 3 to 10 mas/yr depending on a field under consideration. The zero-point of the absolute proper motion frame (the absolute calibration) was derived by using more than 1.1 million galaxies from 2MASS and USNO-A2.0. The mean formal error of absolute calibration is less than 1 mas/yr. The XPM Catalogue will be available via CDS in Strasbourg in 2010.

2. THE INVESTIGATION OF ABSOLUTE PROPER MOTIONS STARS IN THE XPM

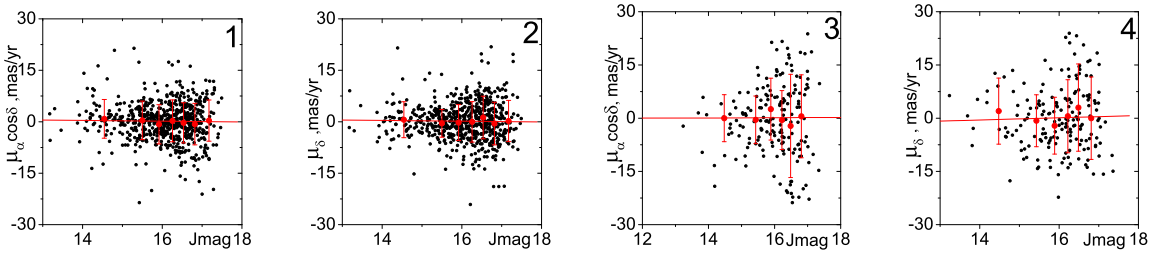

Figure 1: Scatter of individual formal proper motions of optical counterparts of ICRF2 sources as a function of magnitude J. 1, 2 - Northern hemisphere, 3, 4 - Southern hemisphere.

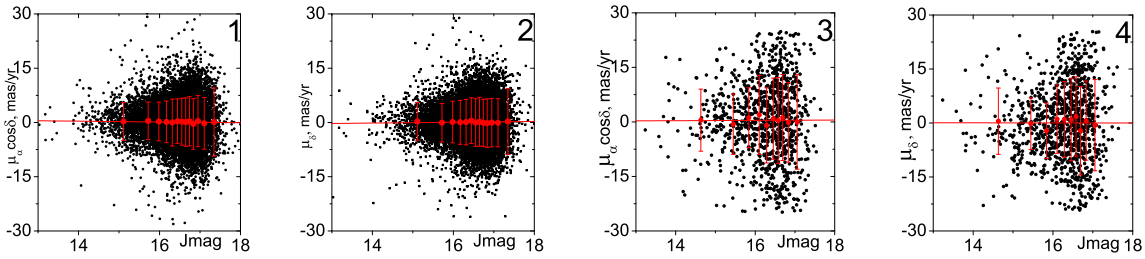

Figure 2: Scatter of individual formal proper motions of LQAC quasars as a function of magnitude J. 1, 2 - Northern hemisphere, 3, 4 - Southern hemisphere.

Below we present some results of investigations of the XPM catalogue and brief information for possible users of the Catalogue. For analysis of quality of the proper motions of the XPM stars the different tests have been made. About 1000 optical counterparts of ICRF2 (Arias et al. 2009) sources and a few tens thousands LQAC (Souchay et al. 2009) quasars were identified among the XPM catalogue objects. These objects were not used in procedure of the absolute calibration of proper motions. Therefore formal proper motions were obtained for them in the same way as for stars. So far as these objects are the extragalactic point sources we expect that their mean proper motion should be zero. The analysis was made for northern and south hemisphere separately since the initial data for them are given by different surveys. Scatters of individual formal proper motions of optical counterparts of ICRF2 sources and LQAC quasars as a function of magnitude J are shown in Fig. 1 and Fig. 2. The red solid circles and lines show the mean values and standard deviations respectively. The mean value of formal proper motions of ICRF2 sources and LQAC quasars are less than 0.2 mas/yr. The standard deviations for ICRF2 sources are estimated to be approximately from 4-8 mas/yr (north) to 6-10 mas/yr (south) and for LQAC quasars are estimated to be approximately from 3-8 mas/yr (north) to 7-12 mas/yr (south).

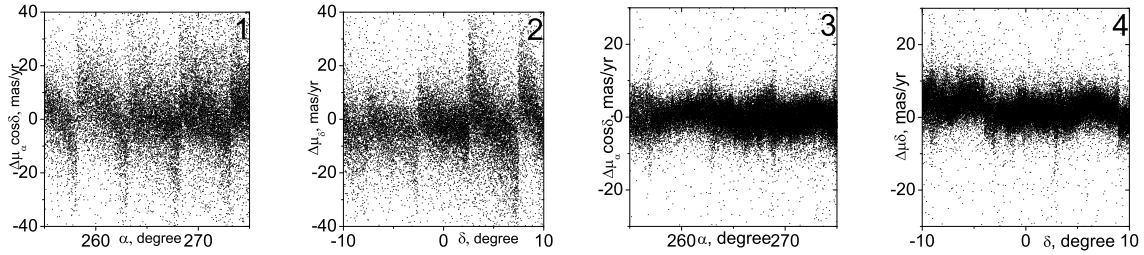

Figure 3: The individual differences of proper motions of stars (XPM - UCAC-3.0; 1, 2) and (XPM - PPMXL; 3, 4) in selected fields as a function of RA end Dec

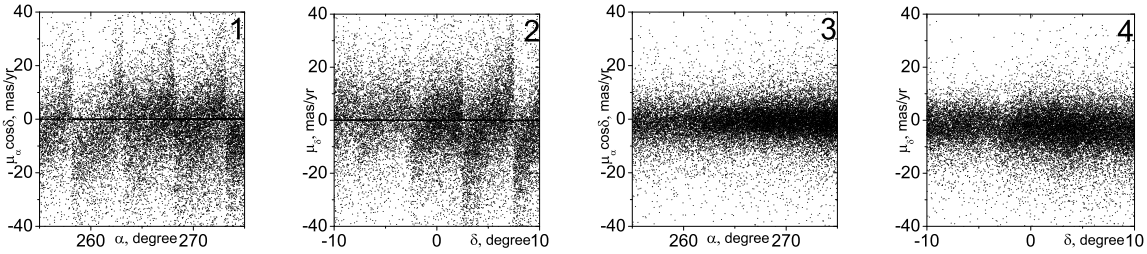

Figure 4: The proper motions of stars UCAC-3.0 (1, 2) and XPM (3, 4) in selected fields as a function of RA end Dec

Any difference of mean value of formal proper motions of extragalactic sources from zero we regard as

the residual rotation of coordinate axes given by the XPM. The dispersions of formal proper motions of extragalactic sources characterize the random errors of proper motions of point sources in corresponding magnitude range. Performed tests definitely indicate that the coordinate axes, given by the positions of XPM catalogue for fixed epoch are non-rotating with respect to distant extragalactic objects to within ± 0.20 mas/yr. Thus we can conclude that the coordinates and the derived absolute proper motions of the XPM stars materialize the ICRS (Arias et al. 1995) in optical and near infrared ranges of wavelengths.

3. COMPARISON OF XPM WITH OTHER CATALOGUES OF PROPER MOTIONS

1. The individual differences of proper motions of stars (XPM - UCAC3 and XPM - PPMXL) in the selected fields were calculated. We have found, that proper motions of the UCAC-2, UCAC-3 catalogues (Zacharias et al. 2004, 2010) are distorted by the appreciable systematic errors. Although the mean proper motions from field to field behaves quite smoothly, the breaks at the borders of fields are very large and reach a value 40 mas/yr (Fig. 3). One can see also that proper motions of the PPMXL catalogue (Roeser et al. 2010) also contain the breaks which are considerably less than in the UCAC-3 and reach about 5-10 mas/yr.

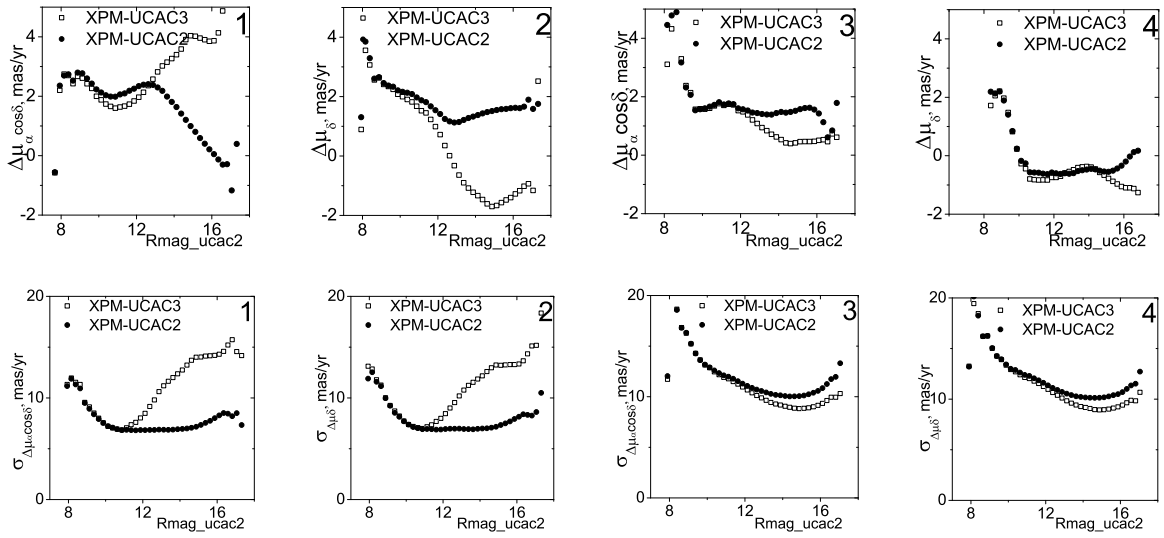

Figure 5: The systematic differences of proper motions (XPM-UCAC2) and (XPM-UCAC3) (top panel) as well as their dispersions (bottom panel), depending on the magnitude R of UCAC2. 1, 2 - Northern hemisphere, 3, 4 - Southern hemisphere

The noted facts should be taking into account in course of kinematical investigations as well as in astrometric applications. Since the majority of modern high-precision observations are executing with CCD in the fields with size about several tens arc minutes the results obtained from these observations due to breaks can be erroneous. For the comparison the UCAC-3 and the XPM proper motions as a function of the coordinates for the same fields are presented in Fig. 4. As can see the XPM proper motions have not considerable distortions.

2. The systematic differences of proper motions (XPM-UCAC2), (XPM-UCAC3) and (XPM-PPMXL) as well as their dispersions, depending on the magnitude were computed.

The systematic differences of proper motions between the UCAC-2.0, UCAC-3.0, PPMXL and the XPM catalogues are shown in Figs. 5 and 6 for the Northern and Southern hemispheres, respectively. Undoubtedly, the systematic differences of proper motion (UCAC-2.0-UCAC-3.0) for the Northern and Southern hemispheres are the most intriguing feature. It could be a result of using the early epoch the Schmidt plate data from the SuperCOSMOS project.

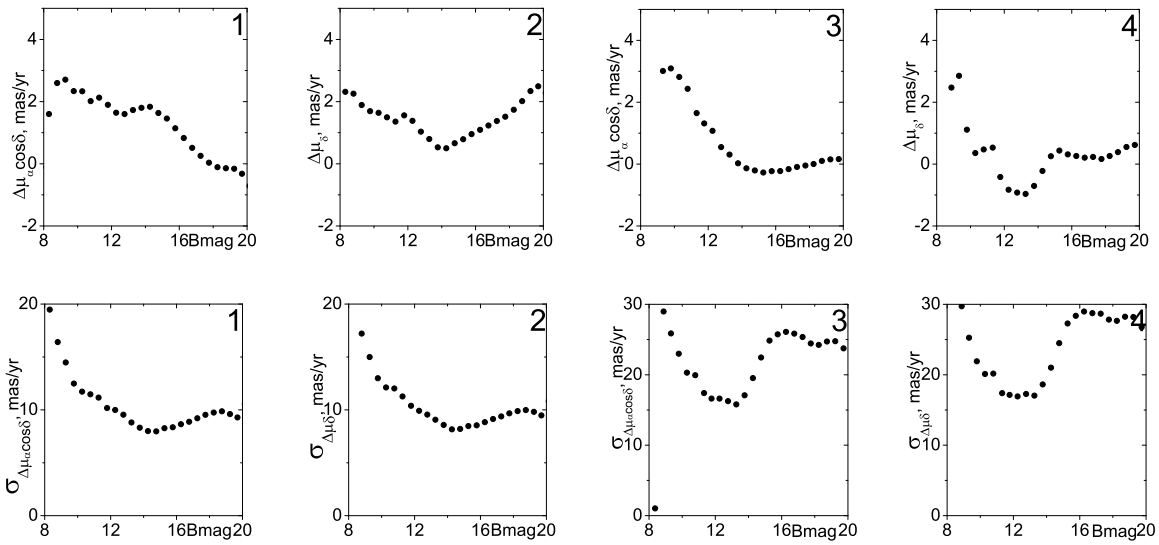

Figure 6: The systematic differences of proper motions (XPM-PPMXL) (top panel) as well as their dispersions (bottom panel), depending on the magnitude B of PPMXL. 1, 2 - Northern hemisphere, 3, 4 - Southern hemisphere.

4. SUMMARY

In our opinion the XPM catalogue is very important for astrometry as it makes possible to realize the global quasi-inertial coordinate system in the magnitude range $10^m < B < 22^m$. The coordinates and proper motions of the XPM sources are referred to the International Celestial Reference System in optical and near infrared ranges of wavelengths. The reached accuracy of determination of the residual rotation of the XPM system is about $\pm$ 0.20 mas/yr. In addition to astrometry, the data of this catalogue could be used for determining the kinematical parameters of the Galaxy, for example, in the framework of the OgorodnikovMilne model.

5. REFERENCES

Arias E. F., Charlot P., Feissel M., Lestrade J.-F., 1995, "The extragalactic reference system of the International Earth Rotation Servise, ICRS", A&A , 303, pp. 604-608.

Arias E. F. et al., 2009, "The Second Realization of the International Celestial Reference Frame by Very Long Baseline Interferometry", IERS Technical Note No. 35.

Fedorov P.N., Myznikov A.A., Akhmetov V.S., 2009, "The XPM Catalogue: absolute proper motions of 280 million stars", MNRAS , 393, pp. 133-138.

Fedorov P.N., Akhmetov V.S., Bobylev V.V. and Bajkova A.T., 2010 "An investigation of the absolute proper motions of the XPM catalogue", MNRAS , 406, 1734-1744

Kovalevsky J. et al., 1997,"The Hipparcos Catalogue as a realisation of the extragalactic reference system", A&A 323, p. 620-633

Monet, D., 1998, The 526,280,881 Objects In The USNO-A2.0 Catalog, A&AS Bulletin of the American Astronomical Society, Vol. 30, p.1427

Roeser S, M. Demleitner and Schilbach E, 2010, The PPMXL Catalog of Positions and Proper Motions on the ICRS. Combining USNO-B1.0 and the Two Micron All Sky Survey (2MASS), AJ 139 p. 2440-2447

Skrutskie M.F. et al., 2006, "The two Micron All Sky Survey (2MASS)", AJ , 131, 1163

Souchay J., et al., 2009, "The construction of the large quasar astrometric catalogue (LQAC)", A&A 494, p. 799-815

Zacharias N., et al., 2004, "The Second US Naval Observatory CCD Astrograph Catalog (UCAC2)", AJ 127 p. 3043-3059

Zacharias N., et al., 2010, "The Third US Naval Observatory CCD Astrograph Catalog (UCAC3)", AJ 139 p. 2184-2199.

OPTICAL POSITIONS OF ICRF SOURCES USING UCAC3 REFERENCE STARS

N. MAIGUROVA, M. MARTYNOV, G. PINIGIN
RSI "Nikolaev Astronomical Observatory"
1, Observatorna St., Mykolaiv, Ukraine, 54030
e-mail: nadija@mao.nikolaev.ua

ABSTRACT. Optical positions for 171 extragalactic radio sources (ERS) were derived using UCAC3 as a reference catalogue. The extragalactic sources are located in the range of declinations from -40 to +80 degrees. The observations of the optical counterparts of the extragalactic radio sources were performed using 1.5m Russian-Turkish Telescope (Turkey) and 1m Telescope YAO (Kunming, China) during 2000-2003 years. The fields around the extragalactic sources have sizes $4' \times 3'$, $6.5' \times 6.5'$ and $8' \times 8'$. We have used UCAC3 catalogue because it is all-sky catalogue contained enough reference stars for the astrometric reduction of the most part of our fields. The standard error of one optical position is about 40 mas for both coordinates. The mean optical positions of the ERS were compared with ICRF radio positions. Additionally, the results obtained with UCAC3 as a reference catalogue were compared with the previous ones obtained with UCAC2 and 2MASS catalogues.

1. STATEMENT OF PROBLEM

To align the radio and optic realization of the ICRS with the highest accuracy, it is desirable to have observations of common objects with uniform sky coverage and accurate optical positions. Therefore till astrometric space missions will not produce scientific results, ground based astrometric observations of ERS are very important. For resolving of this task observations of the optical counterparts of the ICRF radio sources were carried out mostly during 2000-2003 years in frame of the International Project between astronomical observatories from China, Turkey, Russia and Ukraine (Aslan et al., 2005).The previous astrometric reductions of these observations were made using UCAC2 and 2MASS reference catalogues (Aslan et al., 2010). The UCAC3 catalogue (Zacharias et al., 2010) was used as reference catalogue for calculation of the optical positions of ERS in this work because it covers all our zone of declination and has enough stellar density for astrometric reductions in small fields.

2. OBSERVATIONS AND REDUCTIONS

The observations of optical counterparts of the ICRF radio sources were carried out using two telescopes equipped with CCD-cameras. There were Russian-Turkish telescope (1500/11620) and telescope of Yunnan Observatory (1000/13250). The more detailed information about telescopes, detectors and reductions are given in (Aslan et al., 2010). The observations were completed for the declination range of -40 to +80 degrees. We have tried to have uniform distribution in available declination zone on the celestial sphere but there was a gap in zone between 10 and 12 hours in right ascension because part of observational data was unusable for proceeding by reason of small field of view. Figure 1 plots the distribution of the observed optical counterparts of the ERS in celestial sphere. The range of stellar V-magnitudes of observed ERS is from 13 to 20. (V-magnitudes were taken from (Archinal et al., 1997) Two-dimensional elliptical Gaussian model was applied to the image profile fits. And then linear six-parameter mode was used for transformation the measured coordinates to tangential. Unweighted least -squares method was performed for standard reductions with available reference stars if number of stars in the frame was more than 4. Figure 2 shows the average optical minus catalogue ((O-C)) differences and absolute average (O-C) differences in both coordinates against UCAC3 magnitudes for UCAC3 stars. Every point is the average from 30 to 200 UCAC3 reference stars. There are no magnitude equation in range of reference stars and significant systematic errors. The average (O-C) absolute differences show that internal mean error of stars is about 35 mas for the stellar magnitudes range from 10 to 15.5 and deteriorates on faint end.

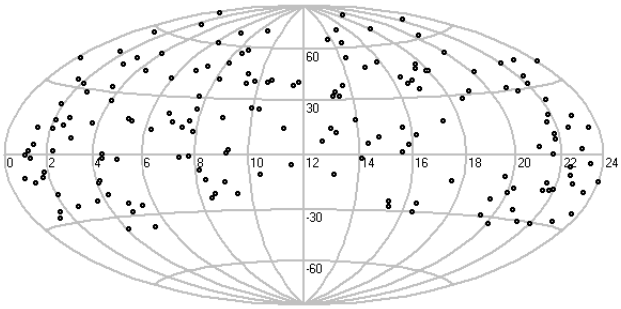

Figure 1: Distribution of observed optical counterpart of ERS over celestial sphere

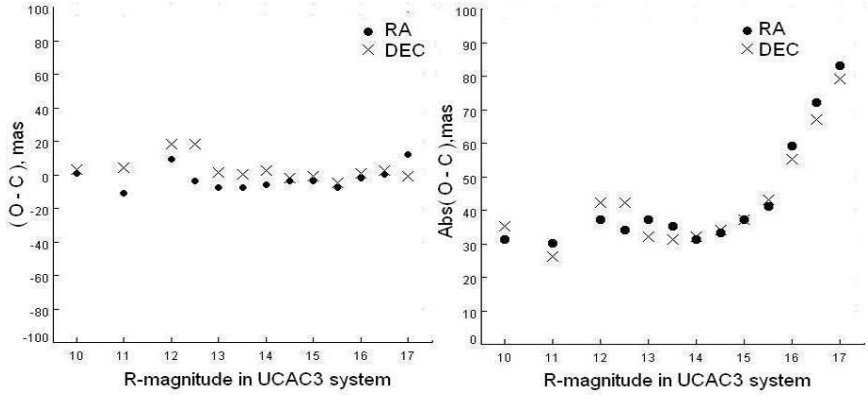

Figure 2: (O - C) (right) and absolute (O - C) (left) differences of the UCAC3 reference stars in both coordinates against UCAC3 magnitudes, filled circles - right ascension, crosses - declination

3. RESULTS

Optical positions of 171 optical counterparts of ERS were obtained using UCAC3 reference stars. The unweighted mean of optical positions and optical minus radio position differences (O - R) are calculated from the scatter of the individual optical positions. The average number of frames per source was about 6. The mean values of optical minus radio positions differences are -6 ± 4 mas and $11 \pm 4 mas$ for right ascension and declination, respectively. From the 171 final optical positions 15 lie beyond 150 mas from radio positions. The final statistics of the comparison this results with previous reductions using 113 common ERS is given in Table 1. The Figure 3 displays the averaged (O - R) position differences with respect to the UCAC3, UCAC2 and 2MASS catalogues as function of right ascension and declination. The figure displays no significant zonal systematic differences between catalogues on their accuracy levels, with the exception perhaps a difference between UCAC3 and 2MASS catalogues in high declination zone. Further study may clarify whether these zonal differences are significant. The parameters of relative orientation between optical and radio frames have been calculated using (O - R) position differences with respect to the UCAC3 and UCAC2 catalogues following the method used by (Arias et al., 1988). Table 2 shows the mean values of rotation angles and their standard errors obtained by least squares procedure.

Table 1: Mean values of (O-R) differences with their errors

Reference Catalogue	$\Delta\alpha cos\delta, mas$	$\Delta\delta, mas$	σ_α, mas	σ_δ, mas	N_{ERS}
UCAC2	-7 ± 4	13 ± 4	39	38	113
UCAC3	-9 ± 5	15 ± 4	57	57	113
2MASS	-8 ± 6	33 ± 7	87	88	113

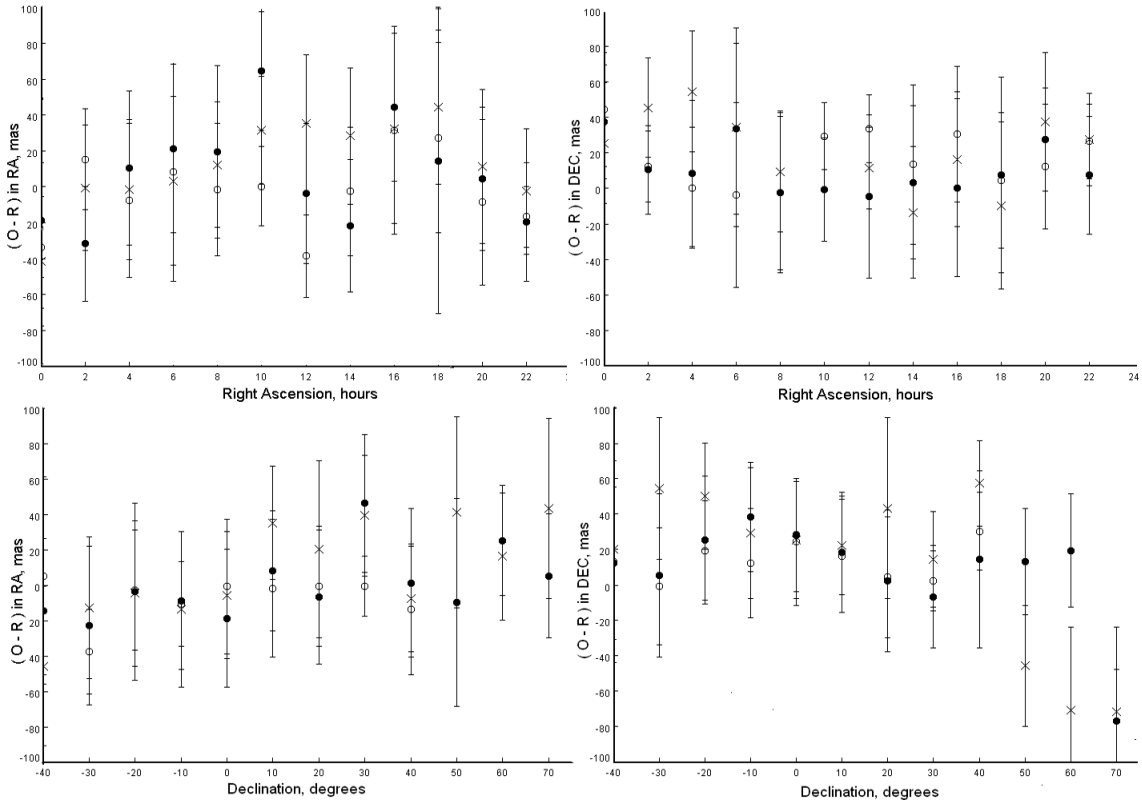

Figure 3: Averaged (O - R) differences as function of right ascension (up) and declination (down) for 171 ERS, filled circles - UCAC3 catalogue, open circles - UCAC2 catalogue, cross - 2MASS catalogue

Table 2: Optical-radio rotational parameters

Reference Catalogue	ϖ_x, mas	ϖ_y, mas	ϖ_z, mas	N	σ, mas
UCAC2	-0.2 ± 5.8	7.2 ± 5.5	7.0 ± 4.5	130	43
UCAC3	-0.1 ± 6.1	6.4 ± 5.8	-1.8 ± 2.4	152	57

4. CONCLUSIONS

Astrometric positions for optical counterparts of 171 ERS from the ICRF list were obtained using reference stars from the UCAC3 catalog in declination zone from −40 to +80 degrees. Though accuracy of the UCAC3 catalogue is a little worse than UCAC2, it is a good all-sky densification of Hipparcos reference frame and can be used as reference catalogue for astrometric reductions in small fields.

5. REFERENCES

Archinal, B.A., Arias, E.F., Gontier, A.-M., Mercuri-Moreau, C., 1997, "Physical characteristics of radio sources", IERS Technical Note 23, pp.III-11 - III-25.

Arias, F., Feissel, M., Lestrade, J.F., 1988, "Comparison of VLBI celestial reference frames", Astronomy and Astrophysics, Vol.199, pp.357-363.

Aslan, Z., Gumerov, R., Jin, W., Khamitov, I., Maigurova, N., Pinigin, G., Protsyuk, Yu., Shulga, A., Tang, Z., Wang, S., 2005, "Results of Joint project on linking opticalradio reference frames", Kinematics and Physics of Celestial Bodies Suppl. Ser., vol.5, pp. 333-337.

Aslan, Z., Gumerov, R., Jin, W., Khamitov, I., Maigurova, N., Pinigin, G., Tang, Z., Wang, S., 2010, "Optical counterpart positions of extragalactic radio sources and connecting optical and radio reference frames", Astronomy and Astrophysics, vol.510, A10.

Zacharias, N., Finch, C., Girard, T., Hambly, N., Wycoff, G., Zacharias, M.I., Castillo, D., Corbin, T.,

DiVittorio, M., Dutta, S., Gaume, R., Gauss, S., Germain, M., Hall, D., Hartkopf, W., Hsu, D., E. Holdenried, V. Makarov, M. Martines, B. Mason, D. Monet, T. Rafferty, A. Rhodes, T. Siemers, Smith, D., Tilleman, T., Urban, S., Wieder, G., Winter, L. and Young, A., 2010, "The Third US Naval Observatory CCD Astrograph Catalog (UCAC3)", Astronomical Journal, vol.139, pp. 2184-2199.

GAIA INITIAL QUASAR CATALOGUE - UPDATES: MORPHOLOGY AND VARIABILITY

A.H. ANDREI[1,2,7], A.-M. GONTIER[3], C. BARACHE[3], D.N. da SILVA NETO[4], F. TARIS[3], G. BOURDA[5], J.-F. Le CAMPION[5], J. SOUCHAY[3], J.I.B. CAMARGO[1], J.J. PEREIRA OSÓRIO[6], M. ASSAFIN[7], P. CHARLOT[5], R. VIEIRA MARTINS[1], S. BOUQUILLON[3], S. ANTON[6]

[1]ON/MCT; [3]SYRTE/OP; [4]UEZO/RJ; [5]Observatoire de Bordeaux; [6]CICGE/FCUP; [7]OV/UFRJ
[2]OATo/INAF, Strada del Osservatorio 2, Pino Torinese (TO), 10024, Italy
e-mail: oat1@on.br

ABSTRACT. The present version of the GAIA Initial QSO catalogue (GIQC_III) contains 174,744 sources, divided in 3 categories: defining (full reliability, 123,880 sources), candidate (lacking full confirmation of redshift or magnitude or pointlikeness, 24,229 sources), and other (pending confirmation of two or more characteristics, 26,235 sources). The GIQC_III now includes morphological indexes, as derived from the study of the target's PSF from DSS R, B, and I plates, in comparison with at least 6 well imaged neighbor stars. A study was also made on the relationship between optical flux long term variability and the centroid's random walk. For that, classes of objects most prone to exhibit such relationship can be discussed.

1. LATEST IMPLEMENTATIONS

In recent years there was a significant increase of number of optically bright quasars for which an ICRF related astrometric position can be derived, along with an improvement of the evenness of their sky distribution (Véron-Cetty & Véron, 2006; Souchay et al., 2008). This enabled to build an optical representation of the ICRS, the LQRF (Andrei et al., 2009) formed by 100,165 QSOs all-sky distributed.

This answers to the requirements such as from micro and macro lensing, binaries, and space density counts, as well as the requirements of space astronomy missions. In particular, for the forthcoming GAIA mission an Initial Quasar Catalogue is being compiled. The workpackage is formed by the authors of this contribution. A.-M. Gontier belonged to this workpackage and her absence will be sorrowly felt.

RA (deg)	DEC (deg)	MAG	z	Rshr	Rsrn	Rgrn	Bshr	Bsrn	Bgrn	Ishr	Isrn	Igrn	Class
0.000000	-0.032778	19.40	1.560										C P
0.002083	-0.450833	20.09	0.250										O F
0.005291	-2.033269	19.29	1.356	0.75	0.10	0.13							D
0.005735	-30.607458	19.18	1.143	0.20	0.01	0.91							D
0.007326	-31.373790	19.74	1.331	0.73	0.44	0.00				1.82	1.14	1.37	D
0.011279	-25.193609	21.56	1.314										O F
0.012178	-35.059062	17.09	0.508	0.59	0.20	0.27				0.39	0.80	0.07	D
0.022792	-27.419533	19.11	1.930	0.12	1.01	0.41							D
0.027500	0.515278	20.37	1.823										D S
0.033333	-63.593333	17.00	0.136										C A
0.034167	0.276389	20.03	1.837										D S
0.038604	15.298477	19.40	1.199	0.92	0.02	0.30	0.36	0.92	0.08	1.11	1.51	1.46	D S
0.039089	13.938450	18.29	2.240	0.59	0.23	0.14	0.63	0.91	0.09	2.07	0.16	1.43	D S

Figure 1: The first lines of the GAIA Initial Quasar Catalogue - GIQC_III. RA and DEC are self-explanatory. And so is the redshift (z) on the 4th column. MAG is V whenever available. When it is not g, r, or the weighted average of the available colors. It follows 3 groups (from the DSS R, B, and I plates) of 3 PSF estimators (SHARP, SROUND, and GROUND) for which the closer to 0, the more stellar-like is the QSO PSF (in the local photometric standard). The first Class column is either **D**efining, **C**andidate, or **O**ther. The second Class column is **S**DSS source (for **D**s); either **I**CRF source, optically point-like **A**GN, or **P**oor observational history (for **C**s); and either **E**mpty field, low precision **R**adio position, **U**nreliable detection, or optically **F**aint (for **O**s).

The latest version of the GAIA Initial Quasar Catalogue (GIQC_III) contains 174,744 sources, divided in 3 categories: defining (full reliability, 123,880 sources), candidate (lacking full confirmation of redshift or magnitude or pointlikeness, 24,229 sources), and other (pending confirmation of two or more characteristics, 26,235 sources). The GIQC_III includes morphological indexes, as derived from the study of the target's PSF from DSS R, B, and I plates, in comparison with at least 6 well imaged neighbor stars. It also includes the most reliable positions, magnitudes, and redshifts. Figure 1 presents an extract of the GIQC_III. The catalogue may be consulted on demand to oat1@on.br (A.Andrei)

2. THE MORPHOLOGICAL INDEXES

The morphological indexes were determined from 5x5 arcmin cuts of B, R, I DSS images. At least 6 well imaged are retained as comparison to the quasar's PSF. The IRAF measures SHARP (probing skewness), SROUND (probing roundness), and GROUND (probing normalness) define the indexes. The robustness of the morphological indexes was verified by a trial bench on 1,343 R images for which also the SDSS DR7 images (0.396arcsec/px) were retrieved. The results show that the PSF analysis reproduces well the SDSS star/galaxy separator and that the DSS plates perform much alike to the SDSS frames. The excess (rate of objects beyond 2 σ) of non-stellar quasars is significant as given by all the indicators, on both the DSS2 and DR7 images, measured either against the field stars or the SDSS classified stars.

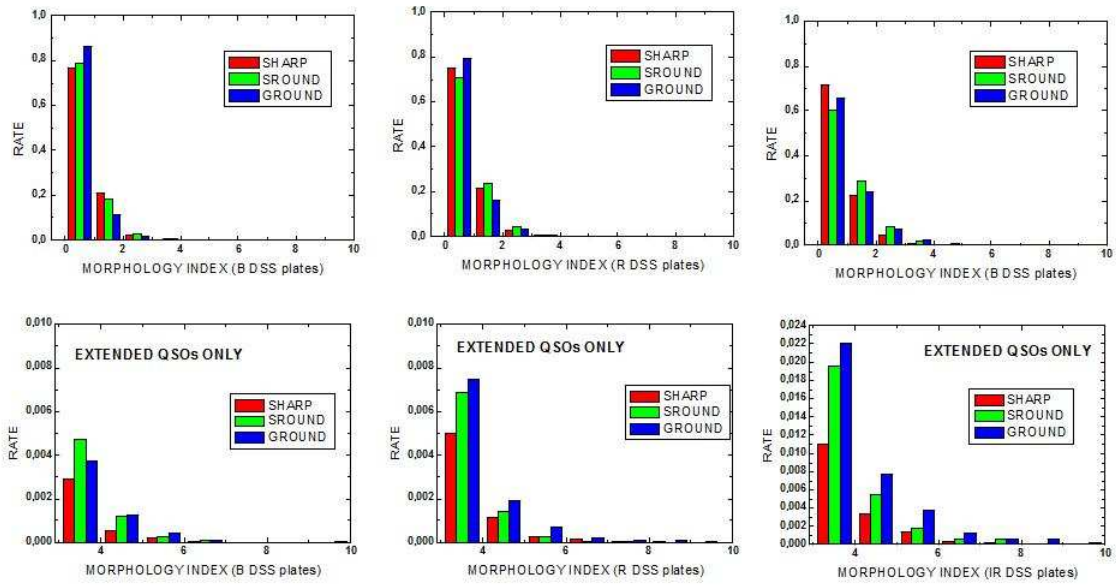

Figure 2: Histograms of the morphological indexes are shown on the upper row. The second row zooms the histograms into the region of non-pointlikeness. It is evident that the degree of non-pointlikeness varies along the spectrum. The bluer the QSO is looked to, the deeper into the power force it is perused, and the more pointlike it looks. Notice that the atmosphere transparency works right against this.

Acknowledgements. We acknowledge the use of the Digitized Sky Surveys (DSS) and of the Sloan Digital Sky Survey (SDSS-DR7) data, and their funding institutions. AHA thanks the PARSEC International Incoming Fellowship and IPERCOOL International Research Staff Exchange Scheme within the Marie Curie 7th European Community Framework Programme, and CNPq grant PQ-307126/2006-0.

3. REFERENCES

Véron-Cetty, M.-P., Véron, P., 2006, A&A, 455, 773.

Souchay, J., Andrei, A.H., Barache, C., Bouquillon, S., Suchet, D., Baudin, M., Gontier, A.-M., Lambert, S., Le Poncin-Lafitte, C., Taris, F., Arias F.E., 2008, A&A, 485, 299.

Andrei, A.H., Souchay, J., Zacharias, N., Smart, R.L., Vieira Martins, R., da Silva Neto, D.N., Camargo, J.I.B., Assafin, M., Barache, C., Bouquillon, S., Penna, J.L., Taris, F., 2009, A&A, 505, 385.

MAO C 08A COMBINED CATALOGUE OF RADIO SOURCE POSITIONS CREATED IN THE COURSE OF PREPARATION FOR THE ICRF2

Ya.S. YATSKIV[1], S.L. BOLOTIN[2], S.O. LYTVYN[1]

[1] Main Astronomical Observatory of the NAS of Ukraine
27 Ak. Zabolotny St., 03680, Kiev, Ukraine
e-mail: yatskiv@mao.kiev.ua; slytvyn@mao.kiev.ua

[2] NVI, Inc./NASA GSFC
Greenbelt, code 698, USA, MD20771
e-mail: sergei.bolotin@nasa.gov

ABSTRACT. Twelve combined catalogues of radio source positions were created at the Main Astronomical Observatory of the NAS of Ukraine (the acronym "GAOUA" was used by the IERS) with the Kiev arc length method since 1991. In the course of preparation for the second realization of the ICRF we created the new combined catalogue (designated as maoC08a) on the basis of individual solutions provided by the IVS Working Group on the ICRF2. In this paper, the method of combining the individual catalogues as well as the results of comparison of the maoC08a and individual catalogues are briefly discussed.

1. INTRODUCTION

Ya. Yatskiv and A. Kuryanova (1990) have proposed and realized new method for combination of individual catalogues of radio source (RS) positions. By using this method a series of combined catalogues of radio sources positions designated "RSC(GAOUA) YY C" in 1997-2005 and "RSC(MAO) 08 C 01" in 2008 were created at the Main Astronomical Observatory of NAS of Ukraine (see O. Molotaj, V. Telnuk-Adamchuk and Ya. Yatskiv, 2000, A. Kurjanova and Ya. Yatskiv, 1993, Ya. Yatskiv and A. Kuryanova, 1993, Ya. Yatskiv, A. Kurjanova and S. Lytvyn, 2005).

2. INITIAL CATALOGUES USED FOR CREATION OF THE MAO C08a

General information on individual catalogues of RS positions is given in Table 1.

Table 1: General characteristics of CRF solutions

Catalogue	Number of sources		Software	Analysis center
aus007a	1564	1516	OCCAM 6.2	GA
bkg001a	3019	2978	CALC 10.00, SOLVE 2007.10.31	BKG
gsf007b	3414	3378	CALC 10.00, SOLVE 2008.12.05	GSFC
iaa08c	2961	2918	QUASAR	IAA
mao008a	3555	3512	StellBreeze	MAO
opa008b	3244	3214	CALC 10.00, SOLVE 2008.12.05	OP
usn010b	3414	3380	CALC 10.00, SOLVE 2007.11.08	USNO
maoC08a	3572	3572	Combined	MAO

In the column "Number of sources" the numbers of all sources in catalogues and the numbers of sources used for creation of the combined catalogue are given. From 212 defining RS eight sources were excluded: seven from them were suspected in lack of stability and their coordinates were estimated as local parameters in individual solutions and one source (1903-802), which was missed in bkg001a solution.

3. MAO C08a COMBINED CATALOGUE AND ITS COMPARISON WITH INDIVIDUAL ONES

MAO C08a catalogue which consists of 3572 RS was compared with individual catalogues in the following way:

– parameters of transformation model between two catalogues were estimated with the LS method,
– the model was applied to coordinates of one of catalogues and weighted root means squares residuals (RMSR) for right ascensions and declinations were calculated,
– based on comparison of three catalogues (the combined and two individual ones) the so-called external uncertainties were evaluated.

The results of comparison are discussed in S. Bolotin and S. Lytvyn (2010). Here we present the RMSR for various pairs of catalogues (see Table 2).

Table 2: RMS of weighted post-fit residuals ($\Delta\alpha\cos\delta$ and $\Delta\delta$) in μas

ID	aus007a		bkg001a		gsf007b		iaa008c		mao008a		opa008b		usn010b	
maoC008a	155	208	39	37	27	30	45	42	43	54	27	39	27	41
aus007a			137	200	141	218	139	204	139	238	141	229	135	221
bkg001a					40	39	47	46	59	61	42	42	42	69
gsf007b							49	64	41	46	15	15	24	29
iaa008c									59	52	46	40	49	49
mao008a											41	46	46	55
opa008b													24	28

Note: First number is RMSR for $\Delta\alpha\cos\delta$ and second number is RMSR for $\Delta\delta$.

One can see that RMSR for all catalogues except aus007a are the same order. For estimation of so-called "external uncertainties" of catalogues ($\sigma_1, \sigma_2, \sigma_3$) we have used coordinate differences of two individual catalogues and combined one (see Table 3). Addition information on this evaluation of catalogues one can find in S. Bolotin, S. Lytvyn (2010).

Table 3: Comparison of catalogues: estimation of external uncertainties (in μas)

Coordinate	Index		σ_1,	σ_2,	σ_3,
	1	2	μas	μas	μas
α	bkg001a	gsf007b	88	23	10
δ	bkg001a	gsf007b	115	30	7
α	gsf007b	mao008a	26	55	12
δ	gsf007b	mao008a	33	62	10
α	gsf007b	usn010b	24	25	11
δ	gsf007b	usn010b	29	41	9

4. CONCLUSIONS

Based on results of our study we can conclude that

– systematic random error differences between individual catalogues (except aus007a) and combined one are small (about 50 μas).
– upper limit of precision of the maoC08a catalogue is on the level of 50 μas.

5. REFERENCES

Bolotin S., Lytvyn S., 2010, "Individual and combined solution of celestial reference frame". Proc. of the 6th Orlov Conference, pp. 55-63.

Molotaj O., Tel'nuk-Adamchuk V., and Yatskiv Ya., 200, "The GAO UA series of compiled celestial reference frame", Kinematika i Fizika Nebesnykh Tel, Suppl. 3, pp. 55-58.

Kur'yanova A., Yatskiv Ya., 1993, "The compiled catalog of positions of extragalactic radio sources RSC (GAO UA) 91 C 01", Kinematics and Physics of Celestial bodies, 9, No.2, pp. 15-25.

Yatskiv Ya., Kur'yanova A., Lytvyn S., 2005, "New combination solution for RS positions RSC (GAO UA) 05 C03", 2005, Proc. Journees 2005, Warsow. pp. 19-20.

Yatskiv Ya., Kur'yanova A., 1989, "A new approach to the construction of a compiled catalogue of positions of extragalactic radio sources", Inertial coordinate system of sky: IAU symp. 141, pp. 295-296.

Session 4

RECENT DEVELOPMENTS IN THEORY AND OBSERVATION OF EARTH ROTATION AND RELATED REFERENCE SYSTEMS

DÉVELOPPEMENTS RÉCENTS SUR LA THÉORIE ET L'OBSERVATION DE LA ROTATION DE LA TERRE ET LES SYSTÈMES DE RÉFÉRENCE ASSOCIÉS

DIURNAL EXCITATION OF EARTH ROTATION ESTIMATED FROM RECENT GEOPHYSICAL MODELS

A. BRZEZIŃSKI[1,2]

[1] Faculty of Geodesy and Cartography, Warsaw University of Technology, Warsaw, Poland
[2] Space Research Centre, Polish Academy of Sciences, Warsaw, Poland
e-mail: alek@cbk.waw.pl

ABSTRACT. Nearly diurnal variations in the atmospheric and nontidal oceanic angular momenta (AAM, OAM) contribute at measurable level to all components of Earth rotation. The estimated contributions to nutation have amplitudes over 0.1 milliarcsecond (mas), while in case of polar motion and UT1 the amplitudes are up to 0.04 mas. However, there are still significant discrepancies between the contributions estimated from different geophysical models as well as between those derived from geophysical models and geodetic data. Here we use a new consistent set of 20-year time series of AAM and OAM based on the ERA-Interim reanalysis fields and the corresponding simulation from the ocean model OMCT, to extract the diurnal component and to estimate the influence on Earth rotation. Results are compared to the earlier estimates using the AAM series from the NCEP-NCAR reanalysis model and the OAM series from the barotropic ocean model, derived by Brzeziński et al. (2004). The estimated geophysical contributions are also compared to the available results derived from the space geodetic observations of Earth rotation.

1. INTRODUCTION

Nearly diurnal variations in distribution of the atmospheric and oceanic masses and in the pattern of winds and ocean currents, associated with the daily cycle in solar heating, change the angular momentum of these two media (AAM, OAM). Diurnal variations of AAM and OAM excite small, below 1 milliarcsecond (mas), but already well detectable variations in all components of Earth rotation including precession-nutation, polar motion and the axial component of rotation expressed by the Universal Time UT1 or changes in the length of day LOD. Understanding this effect is important for modeling global dynamics of the solid Earth and its external fluid layers at daily and subdaily periods. A general description of the perturbations of Earth rotation caused by diurnal thermal tides in the atmosphere and in the oceans was given by Brzeziński et al. (2002), Brzeziński (2008).

Diurnal excitation of Earth rotation can be estimated from the AAM and OAM data only in case when the sampling period of the excitation time series is shorter than 12 hours. This condition is satisfied by most of the AAM series which are available from the International Earth Rotation and Reference Systems Service (IERS) Special Bureau for the Atmosphere (SBA) because the standard sampling interval is 6 hours. Of particular importance are the AAM series derived from the reanalyzes of the Atmospheric Global Circulation Models (AGCM) extending over decades. Unfortunately, all the OAM time series which are available from the IERS Special Bureau for the Oceans (SBO) have daily and longer sampling rates therefore are not useful for studying the diurnal and subdiurnal effects. The OAM series with subdaily resolution are still produced only occasionally and have experimental character.

A first successful attempt to estimate the diurnal component of atmospheric excitation was done by Bizouard et al. (1998) based on the 6-hourly AAM series from the U.S. National Center for Environmental Prediction, National Center for Atmospheric Research (NCEP-NCAR) reanalysis AGCM (Kalnay et al., 1996). They used the approach developed by Brzeziński (1994). By applying the so-called complex demodulation procedure they could extract the diurnal retrograde component of excitation, designated "celestial effective angular momentum" (CEAM) function, which was then used to estimate the atmospheric contribution to nutation. They considered the harmonic components of excitation which contribute to the periodical components of the conventional precession-nutation model, but also devoted much space to the nonharmonic component contributing to the nutation residuals expressed by the time series of the celestial pole offsets. Brzeziński et al. (2002) used the same AAM data and similar methodology to estimate the atmospheric contributions to prograde diurnal and retrograde/prograde semidiurnal components of polar motion, as well as to diurnal and semidiurnal components of UT1/LOD. In case of

semidiurnal components, the 6-hourly sampling of AAM did not allow resolving the spectrum therefore only rough overall estimate could be given.

Brzeziński et al. (2004) used a hourly OAM time series spanning 1993.0–2000.5, derived from the barotropic Ocean Global Circulation Model (OGCM), to estimate the non-tidal oceanic contribution to nutation, prograde diurnal and retrograde/prograde semidiurnal polar motion. They also re-estimated the atmospheric contributions over the same 7.5-year period in order to compare them to the oceanic effect and to estimate the aggregated contribution to nutation and polar motion from the dynamically coupled atmosphere-ocean system.

Here we will estimate the diurnal atmospheric and nontidal oceanic contributions to precession-nutation, prograde polar motion and UT1/LOD, using a new consistent set of 20-year excitation time series produced by the IERS Associated Product Centre Deutsches GeoForschungsZentrum (GFZ) Potsdam, Germany (courtesy of Henryk Dobslaw). Amplitudes of the main harmonic terms will be compared to the earlier results of Brzeziński et al. (2004). We will also compare the estimated geophysical perturbations of Earth rotation to the determinations from the space geodetic observations.

2. DATA ANALYSIS

We used in the analysis a new set of geophysical excitation series: AAM, OAM and the hydrological angular momentum (HAM). The AAM series is based on the ERA Interim re-analysis from the European Center for Medium Weather Forecasts (ECMWF) (Uppala et al., 2008) with $1^\circ \times 1^\circ$ regular grids and 37 vertical pressure levels. The HAM estimate is computed from output of the hydrological model LSDM (Dill, 2008) with $0.5^\circ \times 0.5^\circ$ spatial resolution. The model is forced by precipitation, evaporation and 2m-temperatures. The OAM series is computed from the Ocean Model for Circulation and Tides (OMCT) (Dobslaw and Thomas, 2007). Discretized on a regular $1.875^\circ \times 1.875^\circ$ grid with 13 vertical layers, the model is forced by wind stress, atmospheric pressure, 2m-temperatures, and freshwater fluxes from both atmosphere and continental hydrosphere. Further details about these data sets and the underlying models can be found in (Dobslaw et al., 2010) and the references therein. We note only here that the new set of geophysical excitation series is consistent in a sense of mass conservation in the corresponding models.

We ignore in our analysis the HAM series because of its daily sampling rate. More generally, it is expected that the contribution of HAM can be important in the excitation balance of Earth rotation at seasonal frequencies but is negligible at high frequencies including diurnal and subdiurnal bands. The AAM and OAM series span the period between 1989.0 and 2009.0 with 6-hourly sampling which is sufficiently short for resolving the diurnal frequency band. The pressure term of AAM is given with the inverted barometer (IB) correction and the OAM series is referred to the IB ocean model. Consequently, the aggregated atmospheric and oceanic influence on Earth rotation is expressed just by the sum AAM+OAM. This representation of new AAM and OAM series is also consistent with that of the series used by Brzeziński et al. (2004) which enables direct comparisons of the estimated contributions to Earth rotation.

We process all terms of the AAM and OAM series in a similar way as Brzeziński et al. (2004) and by applying the procedure described in details by Brzeziński (2000) and Brzeziński et al. (2004). First, we express the axial component of excitation χ_3 in the units of LOD. Next, we compute the complex demodulate of the equatorial component of excitation $\chi = \chi_1 + i\chi_2$, with $i = \sqrt{-1}$ being the imaginary unit, at frequencies $-\Omega$ (contributing to nutation) and $+\Omega$ (contributing to prograde diurnal polar motion), and of the axial component χ_3 at frequency $+\Omega$. Here Ω denotes the diurnal sidereal frequency equal to 1 cycle per sidereal day (cpsd). Each demodulated series is then smoothed by a Gaussian low-pass filter with full width at half maximum equal to 10 days and re-sampled at equidistant 5-days intervals. That gives 1457 data points starting from modified Julian date (MJD) 47540.0.

The demodulated series are spectrally analyzed by applying the maximum entropy method (MEM) algorithm developed by Brzeziński (1995). The demodulated series and the corresponding power spectral density (PSD) functions are shown in Figures 1, 2 and 3. Note that the demodulated series are different than the original once, in particular that of χ_3 is the complex quantity. On the other hand, the PSD functions have only been shifted along the frequency axis in such a way that the demodulation frequency becomes 0. The tidal code used to label the spectral lines in the PSD plots of Figures 1 to 3 refers to the original AAM and OAM series, with the superscripts "$-/+$" denoting the retrograde/prograde variations.

Finally, we estimate for each of the demodulated series the best least-squares fit of the model which is a sum of the first order polynomial and the complex sinusoids with periods ± 1 year, $\pm 1/2$ year and

Table 1: Main periodical components of the atmospheric and nontidal oceanic contributions to nutation. VLBI estimate is taken from the MHB 2000 model (Mathews et al., 2002). Units are μas.

Excit. term	Brzeziński et al., 2004				This study			
	in-phase		out-of-phase		in-phase		out-of-phase	
	excitation: ψ_1^- component, nutation: retrograde annual							
A presIB	51.8	±27.2	51.3	±27.2	50.5	±6.4	−43.6	±6.4
A wind	6.9	±2.3	9.2	±2.3	7.2	±1.7	2.6	±1.7
O mass	3.1	±39.9	124.0	±39.9	−5.3	±31.1	8.9	±31.1
O veloc.	−0.6	±0.7	0.8	±0.7	0.2	±0.3	1.5	±0.3
A-IB+O	**61.2**	**±48.3**	**185.3**	**±48.3**	**52.6**	**±31.8**	**−30.6**	**±31.8**
	excitation: S_1^- component, nutation: prograde annual							
A presIB	−40.8	±2.1	−44.0	±2.1	27.7	±0.4	−53.2	±0.4
A wind	−7.1	±0.7	−26.9	±0.7	−2.4	±0.5	−21.1	±0.5
O mass	−68.6	±4.3	−22.3	±4.3	39.8	±1.7	−6.4	±1.7
O veloc.	3.4	±0.3	−2.9	±0.3	−4.5	±0.2	−3.2	±0.2
A-IB+O	**−113.1**	**±4.8**	**−96.1**	**±4.8**	**+60.6**	**±1.8**	**−83.9**	**±2.8**
VLBI	10.4		−108.2		10.4		−108.2	
	excitation: P_1^- component, nutation: prograde semiannual							
A presIB	−11.3	±0.9	4.7	±0.9	4.7	±0.3	−17.7	±0.3
A wind	−6.2	±0.6	−38.9	±0.6	−12.9	±0.6	−43.1	±0.5
O mass	16.4	±2.7	2.2	±2.7	37.4	±1.3	6.8	±1.2
O veloc.	−0.6	±0.2	0.1	±0.2	−0.7	±0.2	2.1	±0.2
A-IB+O	**−1.7**	**±2.9**	**−31.9**	**±2.9**	**31.5**	**±1.5**	**−51.9**	**±1.3**

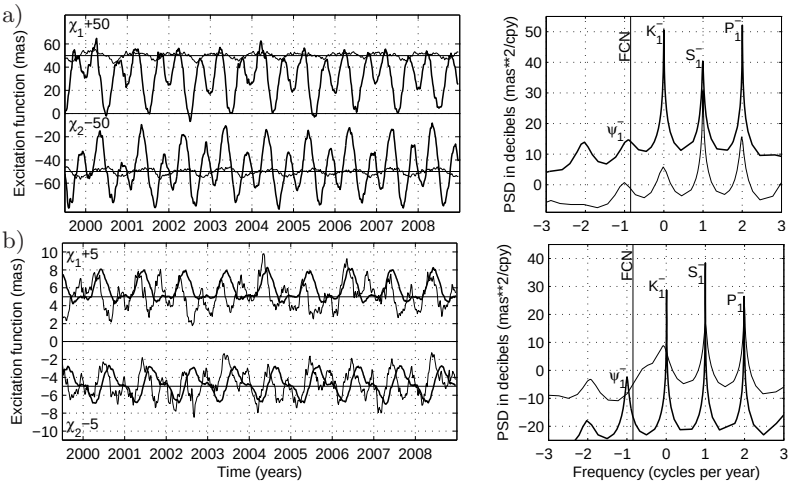

Figure 1: Equatorial effective angular momentum functions of the atmosphere (AAM – thick line) and ocean (OAM – thin line) demodulated at frequency −1 cpsd: a) motion term, b) mass term. On the right-hand side shown are the MEM power spectra estimated over the entire 20-year period. Period of analysis 1989.0–2009.0.

±1/3 year. Such a model comprises all terms which could be detected by the spectral analysis, on the other hand each component of the model has a physical explanation either as being excited by the S_1 thermal tide, or as expressing its seasonal modulations, annual – (K_1, P_1), semiannual – (ψ_1, π_1). The estimated parameters are convolved with the theoretical transfer function (Brzeziński, 1994) in order to estimate the corresponding terms of nutation, polar motion and UT1/LOD.

Results of estimation are shown in Tables 1, 2 and 3. In case of nutation (Table 1) we apply the same convention for representation of the in-phase and out-of-phase coefficients of the circular nutation terms as Bizouard et al. (1998), which may differ from the conventions applied by other investigators. For instance, Mathews et al. (2002) described each circular term of nutation by the pair of coefficients (real, imaginary) which are exactly opposite in sign to our pair (in-phase, out-of-phase). In case of prograde diurnal polar motion $p = x_p - iy_p$ (Table 2) the parametrization is

$$x_p = x^{sin}\sin(arg) + x^{cos}\cos(arg),$$
$$y_p = y^{sin}\sin(arg) + y^{cos}\cos(arg),$$

and in case of diurnal UT1 variation (Table 3)

$$\mathrm{UT1} = \mathrm{UT1}^{sin}\sin(arg) + \mathrm{UT1}^{cos}\cos(arg),$$

where the argument is expressed as $arg = (\mathrm{GMST} + \pi) + k_1 l_m + k_2 l_s + k_3 F + k_4 D + k_5 \hat{\Omega}$, and l_m, l_s, F, D, $\hat{\Omega}$ are the fundamental arguments used in the nutation theory; GMST denotes Greenwich mean sidereal time, and $k_1, \ldots, k_5$ is a set of integer coefficients identifying the quasi-harmonic component of perturbation. Table 2 shows only the coefficients x^{sin} and x^{cos} because for the prograde harmonics of polar motion the following relationships hold $y^{sin} = -x^{cos}$, $y^{cos} = x^{sin}$.

The estimated coefficients of the main periodical components of perturbation are compared in the tables to the results of Brzeziński et al. (2004). Note that the last paper was entirely devoted to the equatorial components of Earth rotation, hence when comparing the UT1/LOD results in Table 3 the reference (Brzeziński et al., 2004) means only the same excitation data sets while the estimated coefficients are published here for the first time. We shown also in the tables the coefficients estimated from the Very

Long Baseline Interferometry (VLBI) measurements of Earth rotation. This is done for only one term of perturbation corresponding to the S_1 term of excitation. The reason, discussed by Brzeziński (2008), is that the other diurnal terms are dominated by the ocean tide contributions and the uncertainty of their amplitudes is at the same level as the nontidal contributions expressed by AAM and OAM. Finally, we note that several other estimates of the perturbation by the S_1 tide, including those from the alternative reanalysis AAM data, from the operational AAM series and from the hydrodynamic ocean model of Ray and Egbert (2004), can be found in (Brzeziński, 2008).

3. RESULTS AND CONCLUSIONS

Analysis of a new set of 20-year time series of atmospheric and nontidal ocean angular momenta confirmed several features which could be either deduced from the physics or detected from earlier investigations using alternative data sets. The spectral structure of excitation is similar in all three cases considered: it consists of the S_1 component driven by the thermal (radiational) atmospheric tide and its side lobes shifted in frequency by ±1 and ±2 cycles per year. The side lobes are caused by seasonal modulations of the S_1 tide. In case of the retrograde diurnal equatorial component of excitation contributing to nutation, there is much greater power in the wind term of AAM than in the pressure term. However, this discrepancy of power is largely counterbalanced by the opposite discrepancy of the transfer coefficients used to convert the amplitudes of geophysical excitation to the amplitudes of nutation. Spectral analysis of the residuals obtained after removal of the polynomial-harmonic model (not shown here) revealed that in all three cases the S_1 term of diurnal excitation contains the random component which could not be expressed by the harmonic model. A proper representation of this component is in the time domain therefore the atmospheric-oceanic excitation considered here needs to be monitored on regular basis.

From the comparison with earlier results of Brzeziński et al. (2004) and with the VLBI estimate it can be seen a rough agreement in size of the estimated atmospheric and nontidal oceanic contributions to nutation, diurnal polar motion and diurnal UT1/LOD variation, nevertheless the differences are in most cases

Table 2: Main periodical components of the atmospheric and nontidal oceanic contributions to prograde diurnal polar motion. VLBI estimates are taken from (Gipson, 1996) – G96, and from (Bolotin and Brzeziński, 2006) – BB06. Units are μas.

Excitation term	Brzeziński et al., 2004				This study			
	x-sin		x-cos		x-sin		x-cos	
	P_1^+ component, period 1.0027454 day							
A presIB	0.3	±0.1	0.8	±0.1	0.1	±0.1	−0.6	±0.1
A wind	−0.5	±0.2	0.3	±0.2	0.0	±0.1	2.2	±0.1
O mass	−1.0	±0.3	−1.4	±0.3	−3.0	±0.1	−0.1	±0.1
O veloc.	1.3	±0.2	0.3	±0.2	2.6	±0.1	−0.3	±0.1
A-IB+O	**0.1**	**±0.4**	**0.0**	**±0.4**	**−0.3**	**±0.2**	**1.2**	**±0.2**
	S_1^+ component, period 0.9999999 day							
A presIB	−0.7	±0.1	−3.8	±0.1	−3.2	±0.1	0.6	±0.1
A wind	5.2	±0.1	−0.1	±0.1	1.9	±0.1	2.7	±0.1
O mass	7.2	±0.3	−3.5	±0.3	4.0	±0.1	0.1	±0.1
O veloc.	−3.4	±0.3	4.0	±0.3	−0.8	±0.1	−0.1	±0.1
A-IB+O	**8.3**	**±0.4**	**−3.4**	**±0.4**	**1.9**	**±0.2**	**3.3**	**±0.2**
VLBI – G96	7		−28		7		−28	
VLBI – BB06	27		−13		27		−13	
	K_1^+ component, period 0.9972696 day							
A presIB	−0.5	±0.1	−0.2	±0.1	0.1	±0.1	0.4	±0.1
A wind	0.4	±0.2	−0.2	±0.2	0.1	±0.1	−0.6	±0.1
O mass	0.9	±0.4	1.2	±0.4	2.5	±0.1	1.8	±0.1
O veloc.	−0.9	±0.3	−0.3	±0.3	−1.9	±0.1	−0.2	±0.1
A-IB+O	**−0.1**	**±0.5**	**0.5**	**±0.5**	**0.8**	**±0.2**	**1.4**	**±0.2**

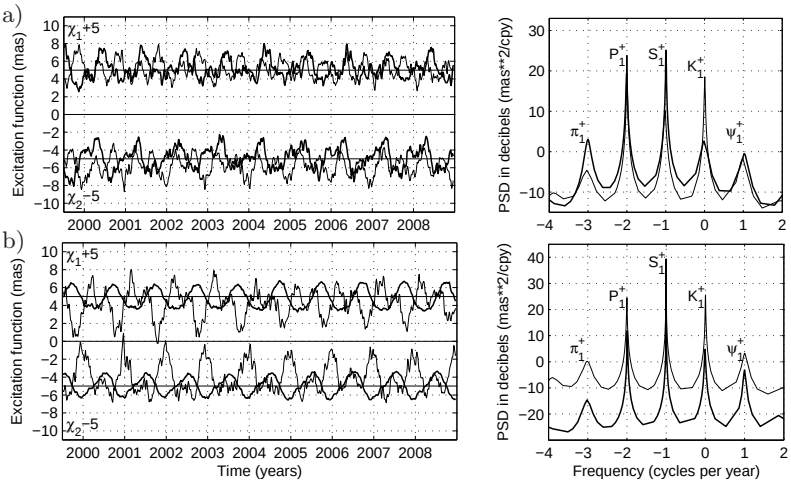

Figure 2: Same as in Figure 1 but the demodulation period is +1 cpsd.

Table 3: Main periodical components of the atmospheric and nontidal oceanic contributions to diurnal UT1 variation. VLBI estimates are taken from (Gipson, 1996) – G96, and from (Bolotin and Brzeziński, 2006) – BB06. Units are μas. (Note: 1 μs of UT1 corresponds to 15 μas.)

Excitation term	Brzeziński et al., 2004		This study	
	UT1-sin	UT1-cos	UT1-sin	UT1-cos
	P_1 component, period 1.0027454 day			
A presIB	2.2 ±0.3	−0.6 ±0.1	−0.4 ±0.1	0.5 ±0.1
A wind	−1.5 ±0.2	−1.7 ±0.2	0.6 ±0.1	−6.4 ±0.5
O mass	−0.6 ±0.3	0.0 ±0.1	22.5 ±0.3	−21.8 ±0.3
O veloc.	1.4 ±0.1	2.5 ±0.2	0.0 ±0.1	1.1 ±0.1
A-IB+O	**1.5 ±0.5**	**0.3 ±0.3**	**22.7 ±0.3**	**−26.6 ±0.6**
	S_1 component, period 0.9999999 day			
A presIB	0.9 ±0.1	−4.6 ±0.3	−7.5 ±0.1	1.5 ±0.1
A wind	14.4 ±0.2	−3.4 ±0.1	1.2 ±0.5	0.3 ±0.1
O mass	−5.3 ±0.2	−2.5 ±0.1	6.3 ±0.4	1.0 ±0.1
O veloc.	−7.4 ±0.2	5.0 ±0.1	−10.8 ±0.1	8.0 ±0.1
A-IB+O	**2.6 ±0.4**	**−5.6 ±0.3**	**−10.7 ±0.7**	**10.9 ±0.2**
VLBI – G96	−32	17	−32	17
VLBI – BB06	−25	7	−25	7
	K_1 component, period 0.9972696 day			
A presIB	−0.8 ±0.4	0.5 ±0.3	0.3 ±0.1	−0.7 ±0.1
A wind	2.7 ±0.3	−0.5 ±0.2	−0.2 ±0.3	−3.0 ±0.4
O mass	0.5 ±0.3	0.9 ±0.3	19.0 ±0.2	−28.2 ±0.2
O veloc.	−0.7 ±0.2	0.2 ±0.2	1.2 ±0.1	−0.3 ±0.1
A-IB+O	**1.7 ±0.6**	**1.0 ±0.5**	**20.3 ±0.4**	**−32.2 ±0.5**

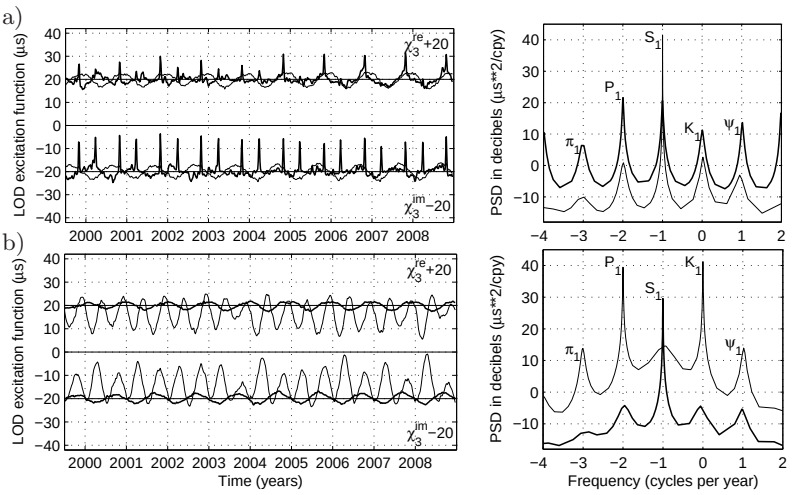

Figure 3: Same as in Figure 1 but for the axial component of excitation and the demodulation period of +1 cpsd.

still significantly larger than the estimated formal uncertainties. In case of the prograde annual nutation, which is the only nutation component where comparison of AAM and OAM with the VLBI estimate is possible, there is considerable improvement of agreement between the model and observation in the in-phase amplitude but a slight increase of discrepancy in the out-of-phase amplitude. For prograde diurnal polar motion the estimated geophysical contribution is at the level of only 4 μas, which is 2 times less than found previously. The amplitude of the S_1^+ component is almost 10 times smaller than estimated from VLBI observations. This large discrepancy between the modeled and observed amplitudes, noted already in previous works, clearly needs further investigations. In case of diurnal UT1/LOD variation the estimated geophysical contribution to the S_1 component is at the level of 10 μas, about 2 times larger than in the previous estimation but still 3 times less than derived from VLBI data. Another feature is the large size of the side lobes P_1 and K_1 of the OAM mass term and the anomalous behavior of the AAM wind term, not seen in the previous data.

Acknowledgements. The author expresses his sincere thanks for the grant provided by Paris Observatory, which covered travel expenses and the costs of participation in Journées 2010.

4. REFERENCES

Bizouard, Ch., Brzeziński, A., and Petrov, S. D., 1998, "Diurnal atmospheric forcing and temporal variations of the nutation amplitudes", J. Geodesy, 72, pp. 561–577.

Bolotin, S., and Brzeziński, A., 2006, "A search for geophysical signals in diurnal and semidiurnal polar motion from analysis of the routine VLBI observations", Geophys. Res. Abstracts, Vol.8, abstract No. EGU06-A-01665.

Brzeziński, A., 1994, "Polar motion excitation by variations of the effective angular momentum function, II: extended model", manuscripta geodaetica, 19, pp. 157–171.

Brzeziński, A., 1995, "On the interpretation of maximum entropy power spectrum and cross-power spectrum in earth rotation investigations", manuscripta geodaetica, 20, pp. 248–264.

Brzeziński, A., 2000, "The CEP and geophysical interpretation of modern Earth rotation observations", in. Proc. IAU Colloquium 178, Conf. Ser., vol. 208, eds. S. Dick, D. McCarthy, and B. Luzum, Astron. Soc. of the Pacific, San Francisco, Calif., pp. 585–594.

Brzeziński, A., 2008, "On the influence of diurnal atmospheric tides on Earth rotation", Proc. Journées Systèmes de Référence Spatio-Temporels 2007, ed. N. Capitaine, Observatoire de Paris, pp. 180–183.

Brzeziński, A., Bizouard, Ch., and Petrov, S. D., 2002, "Influence of the atmosphere on Earth rotation: what new can be learned from the recent atmospheric angular momentum estimates?", Surveys in Geophysics, 23, pp. 33–69.

Brzeziński, A., Ponte, R. M., and Ali, A. H., 2004, "Nontidal oceanic excitation of nutation and diurnal/semidiurnal polar motion revisited", J. Geophys. Res., 109(B11), doi: 10.1029/2004JB003054.

Dill, R., 2008, "Hydrological model LSDM for operational earth rotation and gravity field variations". Sci. Tech. Report 08/09, Helmholtz Centre Potsdam, Deutsches GeoForschungsZentrum GFZ, Potsdam, Germany, 37 pp.

Dobslaw, H., and Thomas, M., 2007, "Simulation and observation of global ocean mass anomaly", J. Geophys. Res., 112(C05040), doi: 10.1029/2006JC004035.

Dobslaw, H., Dill, R., Grötzsch, A., Brzeziński, A., and Thomas, M., 2010, "Seasonal polar motion excitation from numerical models of atmosphere, ocean, and continental hydrosphere", J. Geophys. Res., 115 (B10), doi: 10.1029/2009JB007127.

Gipson, J. M., 1996, "Very long baseline interferometry determination of neglected tidal terms in high-frequency Earth orientation variations", J. Geophys. Res., 101(B12), pp. 28,051–28,064.

Kalnay, E., et al., 1996, "The NMC/NCAR 40-year reanalysis project", Bull. Amer. Met. Soc. 77(3), pp. 437–471.

Mathews, P. M., Herring, T. A., and Buffet B. A., 2002, "Modeling of nutation-precession: New nutation series for nonrigid Earth, and insights into the Earth's interior", J. Geophys. Res., 107(B4), doi: 10.1029/2001JB000390.

Ray, R. D., and Egbert, G. D., 2004, "The Global S_1 Tide", J. Phys. Oceanogr. 34, pp. 1922–1935.

Uppala, S., Dee, D., Kobayashi, S., Berrisford, P., and Simmons, A., 2008, "Towards a climate data assimilation system: status update of ERA Interim", ECMWF newsletter, 115, pp. 12–18.

OBSERVING AND MODELING LONG-PERIOD TIDAL VARIATIONS IN POLAR MOTION

R.S. GROSS[1], S.R. DICKMAN[2]

[1] Jet Propulsion Laboratory, California Institute of Technology
4800 Oak Grove Drive, Pasadena, CA 91109, USA
e-mail: Richard.Gross@jpl.nasa.gov

[2] Department of Geological Sciences and Environmental Studies
Binghamton University, Binghamton, NY 13902, USA
e-mail: dickman@binghamton.edu

ABSTRACT. By exchanging angular momentum with the solid Earth, ocean tides cause the Earth's rotation to change. While hydrodynamic tide models have been used to study the effect of ocean tides on polar motion, it is shown here that none of the published models can fully account for the observed variations. An empirical ocean tide model is therefore determined by fitting periodic terms at the tidal frequencies to polar motion excitation observations spanning 1980.0−2010.4 from which atmospheric and non-tidal oceanic effects were removed. While the empirical ocean tide model does fully account for all of the observed tidal power, tests indicate that the model may not have completely converged. So better models of the effects of ocean tides on polar motion are still needed, both dynamical and empirical.

1. INTRODUCTION

Because the long-period tide raising potential is symmetric about the Earth's polar axis it cannot cause an axisymmetric Earth to wobble. But because the oceans are irregularly distributed on the surface of the Earth, ocean tides can and do cause the Earth to wobble. Therefore, observations of the ocean tide-induced wobbles of the Earth can potentially be used to assess the accuracy of ocean tide models. This potential is explored here by comparing models of long-period ocean tidal variations in polar motion excitation to observations. It is shown than none of the currently available dynamic ocean tide models are able to fully account for the observed long-period tidal variations. So following Gross (2009), an empirical model for the effect of the monthly (27.56-day), fortnightly (13.66-day), and termensual (9.13-day) ocean tides on polar motion excitation is determined and its convergence properties examined.

2. OBSERVED TIDAL VARIATIONS IN POLAR MOTION EXCITATION

The observed polar motion excitation series used in this study is that determined from the polar motion and polar motion rate values of the COMB2009 Earth orientation series (Ratcliff and Gross 2010). COMB2009 is a combination of Earth orientation measurements determined from data acquired by the techniques of lunar and satellite laser ranging (LLR and SLR), very long baseline interferometry (VLBI), and the global positioning system (GPS). Because of the corrupting influence on the recovered polar motion rate estimates of errors in the subdaily tide model that is used when reducing the Earth orientation data acquired by these techniques, polar motion rate estimates are generally unreliable and hence were not used when generating COMB2009. Instead, the COMB2009 polar motion rate values were determined numerically from the polar motion measurements as part of the state estimation process of the Kalman filter that was used to generate COMB2009. The polar motion excitation series determined from the COMB2009 polar motion and polar motion rate values consists of daily midnight values spanning 20 January 1962 to 28 May 2010. Figure 1a is a power spectrum of that portion of the COMB2009 polar motion excitation series spanning 25 March 1995 to 28 May 2010. Just visible above the background power is a spectral peak at the prograde fortnightly tidal frequency of +27 cycles per year (cpy).

Removing atmospheric and non-tidal oceanic effects from the observed polar motion excitation observations will lower the level of the background power evident in Figure 1a and enhance the signal-to-noise ratio of the observed tidal signals. Wind and atmospheric surface pressure effects, assuming an inverted

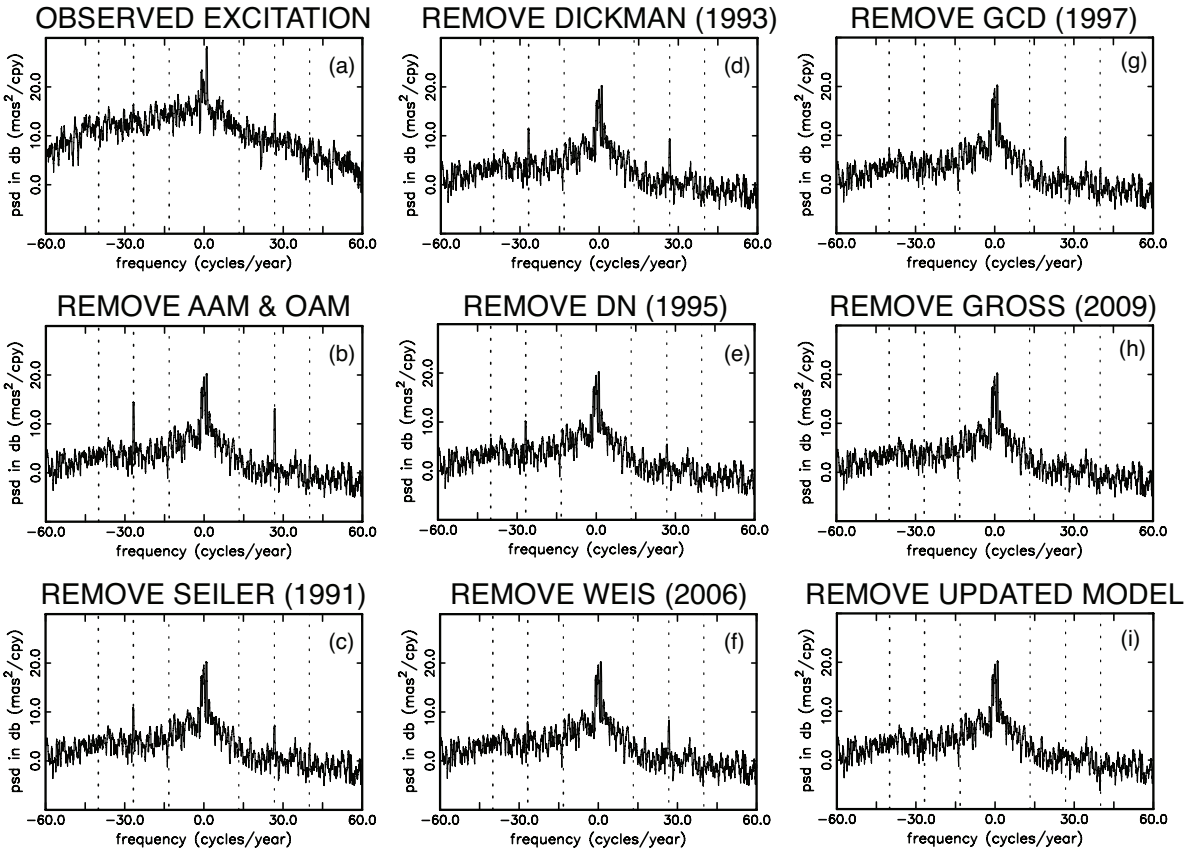

Figure 1: Power spectral density (psd) estimates in decibels (db) computed by the multitaper method from time series spanning 25 March 1995 to 28 May 2010 of the: (a) observed COMB2009 polar motion excitation functions; (b) residual excitation functions formed by removing atmospheric and non-tidal oceanic effects from the observations; (c) residual excitation functions formed by additionally removing the dynamical ocean tide model of Seiler (1991) as reported by Gross (1993); (d) residual excitation functions formed by instead removing the dynamical ocean tide model of Dickman (1993) as reported by Gross et al. (1997); (e) residual excitation functions formed by instead removing the dynamical ocean tide model of Dickman and Nam (1995) as reported by Dickman and Gross (2010); (f) residual excitation functions formed by instead removing the dynamical ocean tide model of Weis (2006) as reported by Gross (2009); (g) residual excitation functions formed by instead removing the empirical ocean tide model of Gross et al. (1997); (h) residual excitation functions formed by instead removing the empirical ocean tide model of Gross (2009); and (i) residual excitation functions formed by instead removing the empirical ocean tide model determined here. Vertical dashed lines indicate the prograde and retrograde frequencies of the monthly (±13 cpy), fortnightly (±27 cpy), and termensual (±40 cpy) tidal terms. The retrograde component of polar motion excitation is represented by negative frequencies, the prograde component by positive frequencies.

barometer response of the oceans to the surface pressure variations, were removed from the polar motion excitation observations using atmospheric angular momentum values computed from products of the National Centers for Environmental Prediction (NCEP) / National Center for Atmospheric Research (NCAR) reanalysis project by the International Earth Rotation and Reference Systems Service (IERS) Global Geophysical Fluids Center (GGFC) Special Bureau for the Atmosphere (Salstein 2003). Current and oceanic bottom-pressure effects were removed from the polar motion excitation observations using oceanic angular momenta values computed by the IERS GGFC Special Bureau for the Oceans (Gross 2003) from products of the kf080 data assimilating version of the oceanic general circulation model run at the Jet Propulsion Laboratory (JPL) as part of their participation in the Estimating the Circulation and Climate of the Oceans (ECCO) consortium (Stammer et al. 2002). Figure 1b shows the power spectrum of the observed polar motion excitation series from which atmospheric and non-tidal oceanic effects have been removed. As can be seen, peaks at both the retrograde and prograde fortnightly tidal frequencies of ±27 cpy are now both very prominent, and a small peak at the prograde termensual frequency of +40 cpy is now also visible.

3. DYNAMICAL OCEAN TIDE MODELS

One of the first dynamical ocean tide models to be used to study ocean tidal effects on the Earth's rotation was that of Brosche (1982), later updated by Seiler (1991). Figure 1c is a spectrum of the result of removing the Seiler (1991) long-period ocean tide model as reported by Gross (1993) from the residual polar motion excitation series whose spectrum is shown in Figure 1b. As can be seen, while the amplitudes of the fortnightly tides at ±27 cpy are reduced, there is still some residual power evident at these frequencies. And since the Seiler (1991) model includes only the fortnightly, monthly, and semi-annual long-period tides, the peak at the prograde termensual frequency of +40 cpy is left unchanged.

Dickman (1993) used his spherical harmonic ocean tide model to study the effect of 10 long-period tidal constituents on the Earth's rotation, including the fortnightly and termensual tides. Figure 1d shows the effect of removing the Dickman (1993) ocean tide model as reported by Gross et al. (1997) from the residual polar motion excitation series whose spectrum is shown in Figure 1b. While the Dickman (1993) model eliminates the observed power at the prograde termensual tidal frequency, it reduces but does not eliminate the observed power at the fortnightly tidal frequencies.

Dickman and Nam (1995) revised the Dickman (1993) tide model by altering the values of the frictional parameters used in the model. The bottom friction and lateral turbulent dissipation parameters in the revised model were determined by maximizing the agreement between the model and the observations at the fortnightly tidal frequency. Figure 1e shows the effect of removing the Dickman and Nam (1995) ocean tide model as reported by Dickman and Gross (2010) from the residual polar motion excitation series whose spectrum is shown in Figure 1b. Like the Dickman (1993) model, the Dickman and Nam (1995) model eliminates the observed power at the prograde termensual tidal frequency. And while the Dickman and Nam (1995) model accounts for more of the observed fortnightly tidal power than does the Dickman (1993) model, it does not completely eliminate it.

Most recently, Weis (2006) developed a high-resolution, global ocean tide model and used it to study the effects of 12 long-period tidal constituents on the Earth's rotation, including the fortnightly and termensual tides. Figure 1f shows the effect of removing the Weis (2006) ocean tide model as reported by Gross (2009) from the residual polar motion excitation series whose spectrum is shown in Figure 1b. Like the Dickman (1993) and Dickman and Nam (1995) tide models, the Weis (2006) model completely accounts for the observed prograde termensual tidal power. And while it accounts for more of the observed retrograde fortnightly tidal power than do the Seiler (1991), Dickman (1993), and Dickman and Nam (1995) models, it accounts for less of the observed prograde fortnightly tidal power than do either the Seiler (1991) or the Dickman and Nam (1995) models.

4. EMPIRICAL OCEAN TIDE MODELS

Figure 1 shows that none of the dynamical ocean tide models discussed here are able to fully account for the observed fortnightly tidal power. Recognizing this, a number of studies have developed empirical tide models by least-squares fitting periodic terms at the tidal frequencies to polar motion observations. For example, Gross et al. (1997) determined an empirical ocean tide model by fitting a mean, trend, seasonal, and periodic terms at the monthly, fortnightly, and termensual tidal frequencies to polar motion excitation observations from which atmospheric effects had been removed. Figure 1g shows the effect of removing the Gross et al. (1997) empirical ocean tide model from the residual polar motion excitation series whose spectrum is shown in Figure 1b. As can be seen, while the Gross et al. (1997) model does a good job of removing the observed retrograde fortnightly tidal power, it does not completely remove either the observed prograde fortnightly or the observed prograde termensual tidal power.

When determining their model, Gross et al. (1997) included separate periodic terms for the two principal fortnightly tides (*Mf* and *mf*) and the two principal termensual tides (*Mtm* and *mtm*). Since the frequencies of the two principal fortnightly tides differ by only 1/18.6 cpy, as do the frequencies of the two principal termensual tides, the oceans and hence the Earth's rotation should have the same relative response to the tidal potential at these two nearby frequencies. That is, the phase of the two principal fortnightly tidal terms in polar motion excitation should be the same and the ratio of their amplitudes should be the same as the ratio of the amplitudes of these two terms in the tidal potential. However, Gross et al. (1997) found that their results for the two principal fortnightly tidal terms did not have this property, nor did their results for the two principal termensual terms. This inconsistency in their empirical tide model may explain why it does not fully explain the prograde fortnightly and prograde termensual tidal power that is observed during 25 March 1995 to 28 May 2010 (Figure 1g). So

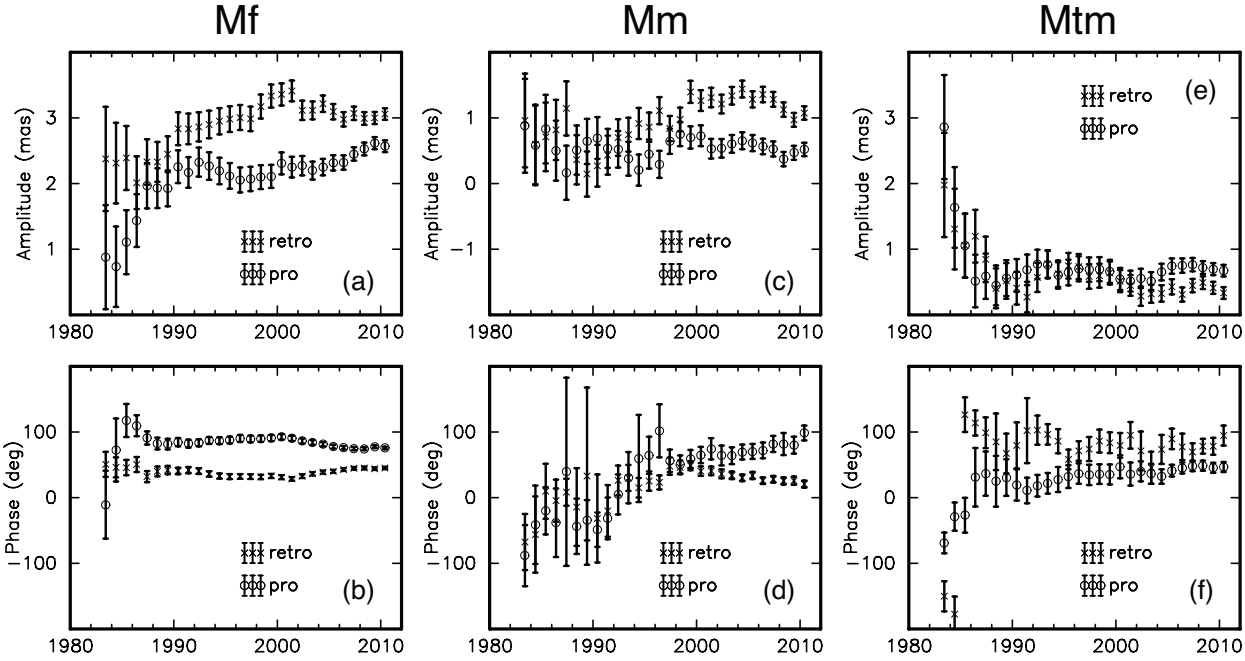

Figure 2: Test of the convergence of the updated empirical ocean tide model determined here. The amplitudes (a, c, e) in milliarcseconds (mas) and phases (b, d, f) in degrees (deg) of the retrograde (retro, crosses) and prograde (pro, circles) components of the fortnightly *Mf*, monthly *Mm*, and termensual *Mtm* tidal terms are plotted as a function of the epoch of the last measurement included in the fit. The ±1-sigma formal uncertainties of the recovered amplitudes and phases are indicated by the error bars.

Gross (2009) determined an empirical ocean tide model by constraining the phases of the two principal fortnightly tidal terms to be the same and constraining their relative amplitudes to be the same as that of the tidal potential. Similar constraints were applied to the two principal termensual tidal terms. Figure 1h shows the effect of removing the Gross (2009) empirical ocean tide model from the residual polar motion excitation series whose spectrum is shown in Figure 1b. This empirical model, which was determined by fitting observations spanning 2 January 1980 to 8 September 2006, is seen to fully account for the fortnightly and termensual tidal power that is observed during 25 March 1995 to 28 May 2010.

By studying the convergence properties of his empirical tide model, Gross (2009) became concerned that it had not converged because the amplitudes and phases of the recovered fortnightly tidal terms continued to change as additional observations were included in the fit. So a new empirical ocean tide model was determined here by taking the same approach as Gross (2009) but by fitting observations spanning 2 January 1980 to 28 May 2010, an additional 3.7 years. The coefficients of this updated empirical tide model are given in Table 1 (the entries labeled "This paper") along with the coefficients of the Dickman (1993), Dickman and Nam (1995), and Weis (2006) dynamical ocean tide models and of the Gross (2009) empirical ocean tide model. Figure 1i shows the effect of removing the updated Gross (2009) empirical ocean tide model from the residual polar motion excitation series whose spectrum is shown in Figure 1b. Like the Gross (2009) empirical tide model, the updated model determined here also fully accounts for the fortnightly and termensual tidal power that is observed during 25 March 1995 to 28 May 2010. But also like the Gross (2009) empirical tide model, the updated model may still not have converged because the amplitudes and phases of the recovered tidal terms continue to change as additional data is included in the fit, particularly for the monthly tide (see Figure 2).

Table 1: Long-Period Ocean Tidal Variations in Polar Motion Excitation

Tide Model	Tidal Argument					Period	Prograde		Retrograde	
	l	l'	F	D	Ω	(days)	amp (μas)	phase (degrees)	amp (μas)	phase (degrees)
mtm										
Dickman (1993)	1	0	2	0	1	9.12	130.38	72.73	213.45	15.05
Dickman & Nam (1995)	1	0	2	0	1	9.12	205.83	67.21	269.95	21.17
Weis (2006)	1	0	2	0	1	9.12	248.17	−21.16	182.26	−137.16
Gross (2009)	1	0	2	0	1	9.12	180.15	51.26	80.18	−26.98
This paper	1	0	2	0	1	9.12	278.91	46.69	138.08	94.61
Mtm										
Dickman (1993)	1	0	2	0	2	9.13	315.24	72.89	517.67	15.17
Dickman & Nam (1995)	1	0	2	0	2	9.13	497.59	67.27	652.59	21.14
Weis (2006)	1	0	2	0	2	9.13	857.20	35.84	535.91	102.84
Gross (2009)	1	0	2	0	2	9.13	434.55	51.26	193.41	−26.98
This paper	1	0	2	0	2	9.13	672.76	46.69	333.05	94.61
mf										
Dickman (1993)	0	0	2	0	1	13.63	521.36	99.93	713.09	7.85
Dickman & Nam (1995)	0	0	2	0	1	13.63	841.32	88.42	1002.12	13.15
Weis (2006)	0	0	2	0	1	13.63	887.43	25.83	766.26	82.84
Gross (2009)	0	0	2	0	1	13.63	880.22	73.88	1205.93	39.27
This paper	0	0	2	0	1	13.63	1065.30	75.78	1268.09	45.16
Mf										
Dickman (1993)	0	0	2	0	2	13.66	1257.22	100.08	1716.11	7.82
Dickman & Nam (1995)	0	0	2	0	2	13.66	2028.73	88.53	2414.94	13.11
Weis (2006)	0	0	2	0	2	13.66	3071.79	47.83	3107.14	70.84
Gross (2009)	0	0	2	0	2	13.66	2123.44	73.88	2909.16	39.27
This paper	0	0	2	0	2	13.66	2569.90	75.78	3059.11	45.16
MSf										
Dickman (1993)	0	0	0	2	0	14.77	105.46	105.26	135.32	6.21
Dickman & Nam (1995)	0	0	0	2	0	14.77	168.13	92.70	194.74	11.60
Weis (2006)	0	0	0	2	0	14.77	474.74	134.83	422.74	−13.15
Mm										
Dickman (1993)	1	0	0	0	0	27.56	465.13	135.86	283.75	−6.50
Dickman & Nam (1995)	1	0	0	0	0	27.56	643.61	123.13	520.16	−1.06
Weis (2006)	1	0	0	0	0	27.56	681.12	102.83	838.55	8.85
Gross (2009)	1	0	0	0	0	27.56	567.37	68.42	1391.36	34.62
This paper	1	0	0	0	0	27.56	520.12	98.49	1075.23	20.63
MSm										
Dickman (1993)	−1	0	0	2	0	31.81	83.17	140.41	39.25	−10.77
Dickman & Nam (1995)	−1	0	0	2	0	31.81	111.62	128.72	79.23	−4.36
Weis (2006)	−1	0	0	2	0	31.81	134.44	102.83	161.31	5.85
Ssa										
Dickman (1993)	0	0	2	−2	2	182.62	107.85	162.21	397.94	172.16
Dickman & Nam (1995)	0	0	2	−2	2	182.62	118.56	159.42	336.32	175.46
Weis (2006)	0	0	2	−2	2	182.62	55.97	−59.28	399.43	−28.11
Sa										
Dickman (1993)	0	1	0	0	0	365.26	3.15	163.17	355.33	169.47
Dickman & Nam (1995)	0	1	0	0	0	365.26	3.33	161.60	332.53	170.51
Weis (2006)	0	1	0	0	0	365.26	26.39	−32.02	39.64	−80.09
Mn										
Dickman (1993)	0	0	0	0	1	−6798	221.54	167.34	174.03	167.12
Dickman & Nam (1995)	0	0	0	0	1	−6798	221.43	166.88	175.07	166.68

amp, amplitude; μas, microarcseconds; see Gross (2009) for definition of tabulated amplitudes & phases

5. SUMMARY

The Earth's rotation responds to changes in the tidal height and also, because the tides are not in equilibrium, to changes in the tidal currents. While many hydrodynamic models of the ocean tides exist, relatively few include both the tidal height and the tidal current components that are needed for Earth rotation studies. Those that do and that have been used previously to study the effects of ocean tides on polar motion have been examined here to test the degree to which they can explain the tidal variations that are observed to occur during 25 March 1995 to 28 May 2010. Since none of them can fully account for the observed tidal variations, an updated empirical model for the effects of long-period ocean tides on polar motion excitation was determined by fitting periodic terms at the tidal frequencies to observations spanning 2 January 1980 to 28 May 2010 from which atmospheric and non-tidal oceanic effects had been removed. While this empirical model does fully account for the tidal variations that are observed to occur during 25 March 1995 to 28 May 2010 (the time spanned by the second half of the data used to determine the empirical tide model), tests indicate that at least some of the tidal terms have not yet converged. So better models of the effects of ocean tides on polar motion are still needed, both dynamical and empirical.

Acknowledgements. The work of RSG described in this paper was performed at the Jet Propulsion Laboratory, California Institute of Technology, under contract with the National Aeronautics and Space Administration. Support for that work was provided by the Earth Surface and Interior Focus Area of NASA's Science Mission Directorate. The JPL supercomputers used in this investigation were provided by funding from the JPL Office of the Chief Information Officer.

6. REFERENCES

Brosche, P., 1982, "Oceanic tides and the rotation of the Earth", in Sun and Planetary System, edited by W.G. Fricke and G. Teleki, pp. 179–184, Reidel.

Dickman, S.R., 1993, "Dynamic ocean-tide effects on earth's rotation", Geophys. J. Int. , 112, pp. 448–470.

Dickman, S.R., Gross, R.S., 2010, "Rotational evaluation of a long-period spherical harmonic ocean tide model, J. Geod., 84, pp. 457–464, doi:10.1007/s00190-010-0383-5.

Dickman, S.R., Nam, Y.S., 1995, "Revised predictions of long-period ocean tidal effects on earth's rotation rate", J. Geophys. Res., 100(B5), pp. 8233–8243.

Gross, R.S., 1993, "The effect of ocean tides on the Earth's rotation as predicted by the results of an ocean tide model", Geophys. Res. Lett., 20(4), pp. 293–296.

Gross, R.S., 2003, "The GGFC Special Bureau for the Oceans: Past progress and future plans", in IERS Technical Note 30: Proceedings of the IERS Workshop on Combination Research and Global Geophysical Fluids, edited by B. Richter, W. Schwegmann, and W.R. Dick, pp. 131–138, Bundesamts für Kartographie und Geodäsie, Frankfurt, Germany.

Gross, R.S., 2009, "An improved empirical model for the effect of long-period ocean tides on polar motion", J. Geod., 83(7), pp. 635–644, doi:10.1007s00190-008-0277-y.

Gross, R.S., Chao, B.F., Desai, S., 1997, "Effect of long-period ocean tides on the Earth's polar motion", Prog. Oceanogr., 40, pp. 385–397.

Ratcliff, J.T., Gross, R.S., 2010, "Combinations of Earth orientation measurements: SPACE2009, COMB2009, and POLE2009", Jet Propulsion Laboratory Publ. 10-22, 29 pp., Pasadena, Calif.

Salstein, D.A., 2003, "The GGFC Special Bureau for the Atmosphere of the International Earth Rotation and Reference Systems Service", in IERS Technical Note 30: Proceedings of the IERS Workshop on Combination Research and Global Geophysical Fluids, edited by B. Richter, W. Schwegmann, and W.R. Dick, pp. 121–124, Bundesamts für Kartographie und Geodäsie, Frankfurt, Germany.

Seiler, U., 1991, "Periodic changes of the angular momentum budget due to the tides of the world ocean", J. Geophys. Res., 96(B6), pp. 10287–10300.

Stammer, D., Wunsch, C., Fukumori, I., Marshall, J., 2002, "State estimation improves prospects for ocean research", Eos Trans. AGU, 83(27), pp. 289–295.

Weis, P., 2006, "Ocean Tides and the Earth's Rotation – Results of a High-Resolving Ocean Model Forced by the Lunisolar Potential", Ph.D. thesis, Universität Hamburg.

EXAMINATION OF SOME ITRF2008 RESULTS

Z. ALTAMIMI, X. COLLILIEUX
Institut Géographique National, LAREG
6-8 Avenue Blaise Pascal, 77455 Marne-la-Vallée, France
zuheir.altamimi@ign.fr, xavier.collilieux@ign.fr

ABSTRACT. Following the procedure already used for the ITRF2005 formation, the ITRF2008 uses as input data time series of station positions and Earth Orientation Parameters (EOPs) provided by the four space geodetic techniques (VLBI, SLR, GPS and DORIS). The integration of these techniques together in the ITRF construction crucially requires co-location sites where two or more techniques are (were) operated and where local ties between the instrument reference points are available. The paper summarizes briefly the main features and results of the ITRF2008, with a particular emphasis on the quality assessment of the estimated quantities: station positions, velocities and Polar motion. For more details regarding the ITRF2008 description and results the reader may refer to Altamimi et al. (2011).

1. INTRODUCTION

ITRF2008 was generated following the same strategy adopted for the ITRF2005. It is a refined version of the International Terrestrial Reference Frame (ITRF) based on reprocessed solutions of the four space geodetic techniques: VLBI, SLR, GPS and DORIS, spanning 29, 26, 12.5 and 16 years of observations, respectively. We recall here that the two steps used for the ITRF2008 construction are: (1) stacking the individual time series to estimate a long-term solution per technique comprising station positions at a reference epoch, velocities and daily EOPs; and (2) combining the resulting long-term solutions of the four techniques together with the local ties in co-location sites. A full description of the procedure used for the ITRF2008 computation as well as a detailed discussion of the results are published in Altamimi et al. (2011). For the purpose of this paper we examine the quality of ITRF2008 station positions, velocities and Polar Motion.

2. QUALITY ASSESSMENT OF ITRF2008 STATION POSITIONS, VELOCITIES AND POLAR MOTION

We evaluate the quality of the ITRF2008 determination of station positions and velocities by comparing the associated spherical errors to past ITRF solutions. The spherical errors correspond, for each point position and velocity, to the square root of the square sum of the formal errors along the three components. Figure 1 shows these errors (computed at the epochs of minimum variances following Altamimi et al. (2002)) in station positions and velocities indicating the precision gain of ITRF2008, compared to ITRF2005 and ITRF2000.

In order to assess the quality of the ITRF2008 associated polar motion estimates, we compared the corresponding two components (x and y) to the IGS reprocessed time series called Repro 1. Figure 2 illustrates the differences in milli-arc-seconds between the two series and Table 1 summarizes the statistics of the comparison showing that the consistency between the two series is at the level of 10 milli-arc-seconds.

	Bias	Drift	WRMS
Xpole	5.3	4.36	9.2
Ypole	15.8	-2.00	10.6

Table 1: Bias (at epoch 2005.0), drift and WRMS of polar motion difference between ITRF2008 and IGS Repro1 solution in micro-arc-seconds

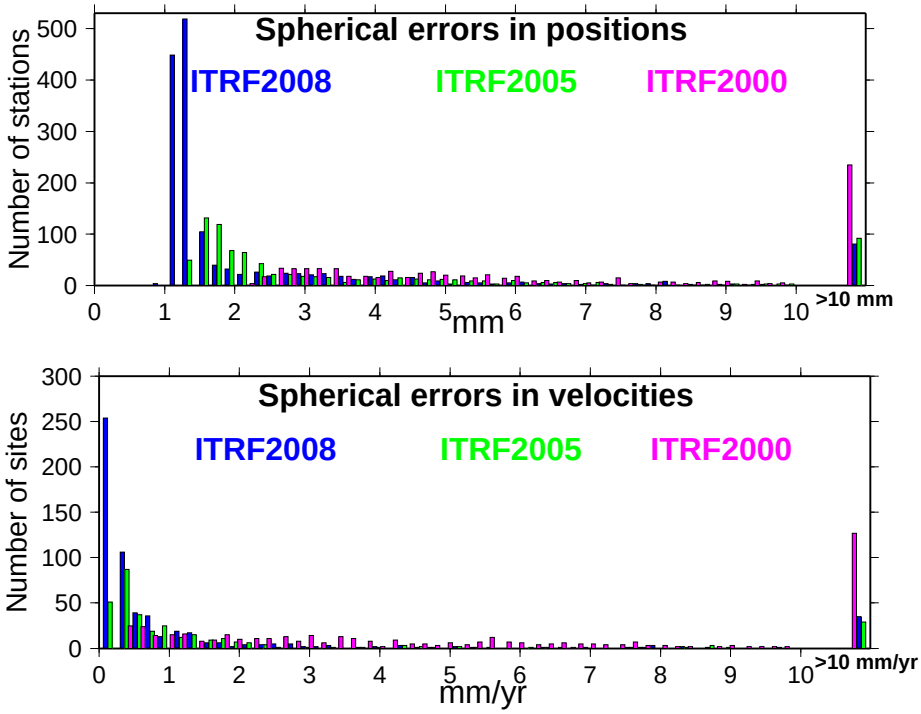

Figure 1. Spherical errors of station positions and velocities of three successive ITRF solutions

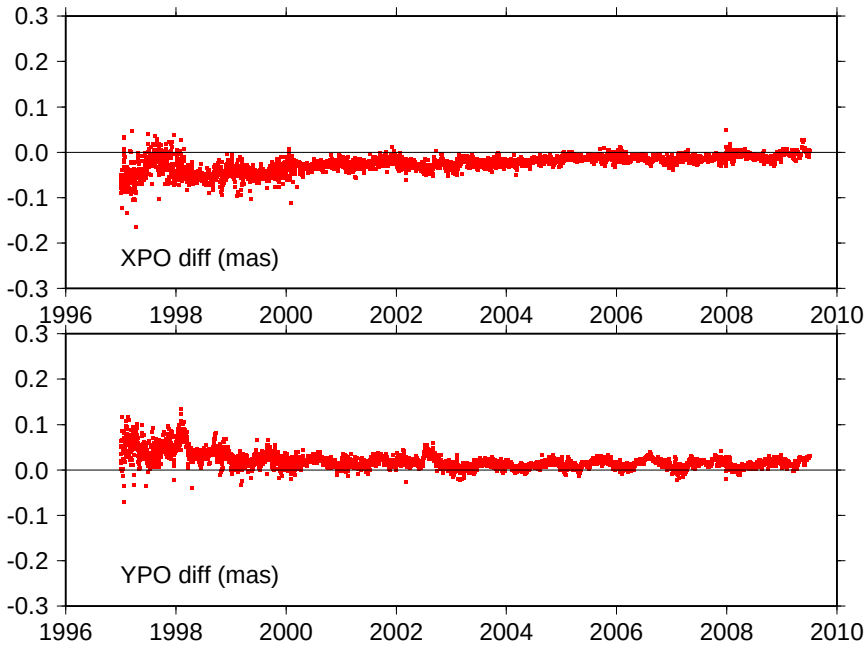

Figure 2. Polar motion difference between ITRF2008 and IGS Repro1 solution

3. REFERENCES

Altamimi, Z., Sillard, P., Boucher, C. 2002, ITRF2000: A New Release of the International Terrestrial Reference Frame for Earth Science Applications, J. Geophys. Res.(Solid Earth), 107(B10):2214, doi:10.1029/2001JB000561.

Altamimi, Z., Collilieux, X., Métivier, L., 2011, ITRF2008: an improved solution of the International Terrestrial Reference Frame, Journal of Geodesy, submitted.

RESPONSE OF THE EARTH SYSTEM TO ZONAL TIDAL FORCING EXAMINED BY VLBI BASED dUT1 VARIATIONS

S. BÖHM, H. SCHUH

Institute of Geodesy and Geophysics, Advanced Geodesy
Vienna University of Technology
Gußhausstraße 27-29, 1040 Vienna, Austria
e-mail: sigrid.boehm@tuwien.ac.at

ABSTRACT. The VLBI group at the Institute of Geodesy and Geophysics of Vienna University of Technology is developing the software VieVS (Vienna VLBI software) for the analysis of geodetic VLBI data. VieVS incorporates the most recent models recommended by the IERS Conventions and in contrast to other VLBI software uses a parameterization with piece-wise linear offsets at integer hours. Thus it provides more flexibility for combination or comparison with time series from other space geodetic techniques or of geophysical origin. We employed this new software to re-process all available geodetic VLBI sessions from 1984 till 2010, suitable for the determination of the Earth rotation parameters (ERP), i.e. dUT1 (UT1–UTC) and the polar motion coordinates x_p and y_p. Zonal tidal signals with periods from 5 to 35 days in the derived dUT1 long-time series were then used to estimate the so-called zonal response coefficient κ defined by Agnew and Farrell (1978). The frequency dependent zonal response coefficient is an extension to the concept of the Love number k_2 which allows for a response of the Earth to tidal forcing, deviating from purely elastic behaviour and thus taking into account effects of ocean tides, a fluid core and mantle anelasticity. A tidally induced change of the rotation rate of the Earth and consequently of dUT1 is proportional to the tide-generating potential through the zonal response coefficient κ. The values estimated for κ for different tidal frequencies from VLBI observations of dUT1 were compared to theory and to the results of previous determinations of κ from observations of space geodetic techniques.

1. dUT1 TIME SERIES FROM VieVS ANALYSIS

A new software for the analysis of geodetic VLBI observation data, called VieVS (shortly for Vienna VLBI Software) is developed at the Institute of Geodesy and Geophysics of the Vienna University of Technology (Boehm et al., 2009). The recent, fully operational release of the software is available free of charge for registered users (refer to VieVS webpage for further information). VieVS is written in Matlab and consists of several main programs (i.e. Matlab-scripts) which are usually executed in a pre-defined sequence but can be processed independently from each other as well, if the necessary input information has already been created in a previous run. The following table provides a sketch of the VieVS structure:

VIE_SETUP	processing setup (choosing the data, storage folders...)
VIE_INIT	data reading (observation data in NGS-format)
VIE_MOD	calculation of observed–computed, partial derivatives
VIE_LSM	least squares adjustment (Gauss-Markov-Model)
VIE_GLOB	module for global solution (multi-year solution)
VIE_SIM	tool for the simulation of VLBI measurements

Table 1: VieVS structure

VieVS differs from other VLBI software packages, which use least squares adjustment, in a slightly different way of parameterization. All estimable parameters (this holds also for station coordinates) can be estimated as piecewise linear offsets at integer hours (like 12:00 or 18:00 UTC) or integer minute fractions of integer hours (like 12:20, 12:40 UTC). Traditionally, i.e. in other VLBI software packages, the parameters are modelled as piecewise linear functions where the first offset is estimated at the epoch

of the first observation, which is usually not taken at an exact full minute time point. The alternative parameterization used in VieVS facilitates the allocation of estimated parameters at the same epochs as they result from other space geodetic techniques and thus provides a good starting basis for the combined estimation of the parameters from observation data of different techniques. The delay model implemented in the software adheres to the latest IERS recommendations including the transformation from celestial to terrestrial reference frame using the concept of the non-rotating origin.
In order to generate a long-time series of dUT1 we re-processed all 24 hours sessions from 1984 to 2010 with an adequate global station distribution. dUT1 was estimated with six hours resolution whereas the other Earth orientation parameters (polar motion, nutation/precession) were set up in daily intervals. Station positions were calculated sessionwise applying no-net-rotation and no-net-translation conditions on the coordinates of the VLBI terrestrial reference frame VTRF2008. The coordinates of the radio sources were fixed to the second realisation of the international celestial reference frame, ICRF2.

2. DETERMINATION OF THE ZONAL RESPONSE COEFFICIENT κ

For a perfectly elastic, spherically symmetric Earth without oceans the zonal tidal potential of degree two would induce a change δLOD in the length of day (LOD) (Moritz and Mueller, 1987):

$$\frac{\delta LOD}{LOD_0} = -k_2 \frac{2}{3} \frac{R^3}{GC} a_{20} \tag{1}$$

where LOD_0 corresponds to the nominal length of day of 86400 seconds, C is the axial moment of inertia, G is the gravitational constant and R stands for the mean Earth radius. k_2 denotes the Love number for degree two which usually is used as a proportionality factor to express a change of the gravitational potential of the Earth due to a perturbing potential such as the tidal potential. The zonal tidal potential can be represented using Legendre polynomials as $V_{20} = a_{20} P_{20}\,(cos\theta)$, with the tidal potential amplitude a_{20}.
To allow for a more realistic Earth behaviour considering also mantle anelasticity, dynamic oceans and a fluid core, Agnew and Farrell (1978) introduced a kind of extension of the Love number concept which they called the zonal response coefficient of the Earth-ocean system κ. The zonal response coefficient is frequency dependent and complex-valued, thus permitting a retarded response of the Earth system to the acting force. We exchange the Love number k_2 in the above-mentioned equation with κ and express the change of the Earth's rotation speed in terms of universal time instead of LOD (i stands for the complex unit):

$$\delta UT1(\omega) = -\kappa(\omega) \frac{1}{i\omega} \frac{2}{3} \frac{R^3}{GC} a_{20}(\omega) \tag{2}$$

Depending on the presumed Earth model we can give some possible values for κ. According to Chao et al. (1995), for a spherically symmetric Earth without oceans κ would have the value of the (static) Love number $k_2 = 0.3$. An equilibrium ocean would increase the value by 16%, whereas a completely decoupled fluid core would decrease it by about 11%, leading to a total theoretical value of $\kappa = 0.315$. If the oceans are additionally considered to have a dynamic response and furthermore time dependent core-mantle coupling and mantle anelasticity are assumed then the zonal response coefficient becomes frequency dependent and a phase lag is introduced, making it complex-valued. Equation (2) could be used to introduce values for κ derived from theoretical considerations and deduce modelled variations of universal time. The other option is to calculate the UT1 variations from measurements of space geodetic techniques and estimate the corresponding κ values for each tidal frequency ω. In this study we chose the second option and estimated the zonal response coefficient, within a period range from 5–35 days, from dUT1 variations observed by VLBI.
Since equation (2) merely holds for tidally induced changes in universal time a certain pre-processing has to be applied in order to reduce the observed dUT1, containing all kinds of signal, to $\delta UT1$, which denotes purely tidal variations. The dominating sources of excitation within the investigated frequency bands besides tidal excitation are strong zonal winds and to a moderate extent also atmospheric pressure variations. The atmospheric excitation can be modeled with atmospheric angular momentum functions (AAMF) which are calculated from numerical weather model data. We used so called effective AAMF from NCEP/NCAR reanalyses to account for dUT1 variations induced by the atmosphere. These functions are provided by the Special Bureau for the Atmosphere of the IERS Global Geophysical Fluids Center (Salstein and Rosen, 1997) and were computed from reanalysis data of the National Centers for

Environmental Prediction (NCEP) and the National Center for Atmospheric Research (NCAR). The axial AAMF χ_3 mass and motion terms were in a first step converted to length of day variations and subsequently integrated to derive variations of universal time. The atmospheric UT1 variations were then subjected to a high-pass filtering to eliminate signal with periods beyond 40 days. The same filtering was applied to the dUT1 time series calculated with VieVS. We derived the final tidal $\delta UT1$ time series by subtracting the filtered atmospheric UT1 variations from the filtered observed dUT1 time series. Equation (3) served as a functional model for the estimation of κ in a least squares adjustment using $\delta UT1(t)$ as pseudo-observations:

$$\delta UT1(t) = \sum_j -\kappa(\omega_j)\frac{1}{i\omega_j}\frac{2}{3}\frac{R^3}{GC}a_{20}(\omega_j t) \tag{3}$$

The amplitudes a_{20} were taken from the HW95 tidal potential catalogue (Hartmann and Wenzel, 1995). We estimated κ for a total of 41 tidal frequencies ω_j. The resulting values including error bars for the nine terms with the largest tidal amplitudes are shown in Figure 1 in terms of κ magnitudes and phases. In addition to the values obtained from the VieVS dUT1 time series the picture shows resulting

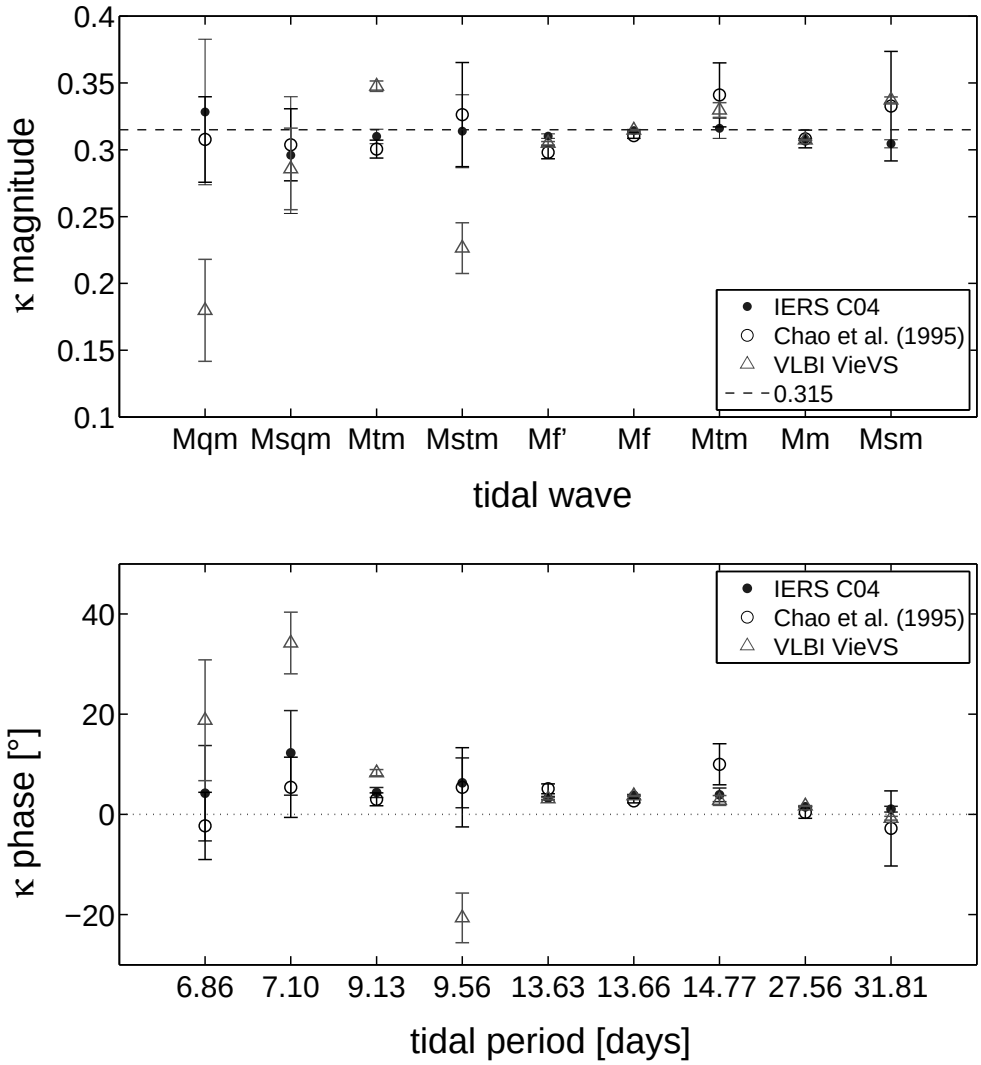

Figure 1: Amplitudes (top) and phases (bottom) of the zonal response coefficient κ

κ for the IERS C04 dUT1 series (IERS webpage) and the estimates given in Chao et al. (1995) for comparison. The IERS C04 κ values were obtained by applying the same estimation procedure as for

the VieVS dUT1 times series to the C04 dUT1 time series from 1984-2010, which are provided by the IERS with daily resolution. Chao et al. (1995) used 13 years (1980–1992) of LOD data for their study. The LOD series was derived from a universal time series (with daily sampling) stemming from a Kalman filter combination of different space geodetic measurements of Earth rotation.

3. DISCUSSION OF THE RESULTS

We used the new VLBI analysis software VieVS for the determination of dUT1 time series with six hours resolution from selected 24 hours sessions of the years 1984 to 2010. The time series was cleaned from UT1 variations stemming from atmospheric excitation and filtered for periods longer than 40 days. The remaining zonal tidal signals were introduced to a least squares adjustment as pseudo-observations in order to estimate the complex zonal response coefficient κ for 41 tidal periods from 5–35 days.
The results for the nine main tidal periods are represented as magnitudes and phases in Figure 1. For comparison the figure also contains the κ values calculated from the IERS C04 dUT1 series and the numerical estimates from a study by Chao et al. (1995). We would actually expect a more precise estimation of κ from the VieVS dUT1 time series because of the much longer time interval and higher resolution. This assumption turns out to be true for the periods longer than ten days, where the VieVS results also agree well with the IERS C04 results and have continuously smaller error bars than the estimates from Chao et al. (1995). In the higher frequency bands around seven and nine days we can see partially large deviations of the VieVS based κ values w.r.t. the two reference results, accompanied also by comparably large error bars. It is somewhat surprising that the VieVS estimates also do not agree with the IERS C04 estimates, although they were calculated from the same time interval and the C04 dUT1 series are primarily based on VLBI observations. The main differences between the VieVS dUT1 and C04 dUT1 series are the temporal resolution, which is six hours in the first and 24 hours in the second case, and the continuity. The C04 series is continuous, while the VieVS series has gaps at days where there was no observing session. To which extend these differences are able to influence the estimation of the zonal response coefficient needs to be further investigated. Concerning the larger error bars in the higher frequency bands we should note that they are coherent with smaller amplitudes of these terms in the tidal potential and thus are most probably a consequence of the worse signal-to-noise ratio.

4. CONCLUDING REMARKS

The κ results of this study have to be regarded as preliminary and will not be consulted for further geophysical interpretation before the unexplained discrepancies in the higher frequencies have been clarified. However, the very distinct and precise results for the longer periods show that it is definitely promising and worthwhile to investigate the zonal response of the Earth by means of now accessible long-time series of dUT1 or LOD.

5. REFERENCES

Agnew, D.C., Farrell, W.E., 1978, "Self-consistent equilibrium ocean tides", Geophys. J. R. Astron. Soc. 55, Issue 1, pp. 171–181.

Boehm, J., Spicakova, H., Plank, L., Teke, K., Pany, A., Wresnik, J., Englich, S., Nilsson, T., Schuh, H., Hobiger, T., Ichikawa, R., Koyama, Y., Gotoh, T., Kubooka, T., Otsubo, T., 2009, "Plans for the Vienna VLBI Software VieVS", Proceedings of the 19th European VLBI for Geodesy and Astrometry Working Meeting, G. Bourda, P. Charlot and A. Collioud (eds.), Bordeaux, pp. 161–164.

Chao, B.F., Merriam, J.B., Tamura, Y., 1995, "Geophysical analysis of zonal tidal signals in length of day", Geophys. J. Int. 133, Issue 3, pp. 765–775.

IERS webpage: http://www.iers.org/

Hartmann, T., Wenzel, H., 1995, "The HW95 tidal potential catalogue", Geophys. Res. Lett., 22(24), pp. 3553-3556.

Moritz, H., Mueller, I.I., 1987, "Earth Rotation - Theory and Observation", Ungar Publishing Company, New York, p. 196.

Salstein, D.A., Rosen, R.D., 1997, "Global momentum and energy signals from reanalysis systems", 7th Conf. on Climate Variations, American Meteorological Society, Boston, MA, pp. 344–348.

VieVS webpage: http://vievs.hg.tuwien.ac.at/

CENTENNIAL CYCLES OF THE SOLAR ACTIVITY AND EARTH ROTATION

Ya. CHAPANOV[1], J. VONDRÁK[2], C. RON[2]

[1] National Institute of Geophysics, Geodesy and Geography of Bulgarian Academy of Sciences
Acad. G. Bonchev Str., Bl.1, Sofia 1113, Bulgaria,
e-mail: chapanov@clg.bas.bg

[2] Astronomical Institute, Academy of Sciences of Czech Republic
Boční II, 141 31 Prague, Czech Republic
email: vondrak@ig.cas.cz, ron@ig.cas.cz

ABSTRACT. The centennial variations of the Universal Time UT1 and Length of Day LOD are investigated by means of long historical observational series of UT1 and LOD variations, which cover time span more than 3 centuries long. The correlation between the centennial cycles of the Earth rotation, climate and Total Solar Irradiance TSI is determined using the time series of North America temperature ($2.2Ka$) and precipitation ($8Ka$), Mean Sea Level MSL variations at Stockholm tide gauge station since 1774 and reconstructed TSI variations since 843. The model of the solar influences on the centennial and decadal cycles of the Earth rotation is based on a main centennial cycle and harmonics, ending by oscillation with period around $9a$. The value of the dominating period of the main centennial cycle of this model is determined among $171.44a$, $178.7a$ (Jose cycle), $210a$ and $230a$ (de Vries cycle) by looking for the minimum residuals of UT1, LOD, TSI and MSL approximation.

1. INTRODUCTION

The irregular and long-term variations of the Earth rotation are mainly caused by the displacements of matter in different parts of the planet which excitation mechanism is the influence of the Sun and solar activity cycles. The solar cycles can drive great number of geodynamical processes connected with the convections of the Earth fluids on the surface and inside the Earth. Many of climate and weather parameters are affected directly by the variations of the solar activity.

The time series of universal time UT1 and climatic variations give good opportunity to study the long-term oscillations of UT1, corresponding to the sunspots, magnetic and equatorial solar asymmetry cycles of the solar activity with periods of about 11, 22 and 45 years (Chapanov et al., 2008a, b, c; 2009c).

It has been shown that the delayed 11.2-year oscillations of UT1 are highly-correlated with the sunspot cycles (Wolf's numbers Wn for the period 1753.5-1950.5 with correlation coefficients 0.64 and linear regression $\mathrm{UT1} - \mathrm{TT} = 0.66Wn + 29.67$ [ms] (Chapanov et al., 2008c). Similar results are obtained in (Chapanov 2006; Chapanov and Gambis, 2008a) by means of the solution C04 of the IERS for the EOP. The time series of UT1 variations reveal strong correlation between the 11-year and 22-year cycles of the Earth rotation and the Mean Sea Level (MSL) (Chapanov and Gambis, 2009a, 2009b). A model of the Earth rotation excitation, based on the global water redistribution, is suggested in (Chapanov and Gambis, 2009b).

The existing long climatic and astronomical time series with centennial and millennial time spans are useful to study interconnection between the centennial cycles of the solar activity and Earth rotation.

2. TIME SERIES AND SPECTRA OF EARTH ROTATION AND CLIMATIC DATA

The available data of Earth rotation, solar activity and climatic parameters consist of time series with duration from centuries to several millennia:

- LOD and UT1–TT for the period 1623-2005 (Fig.1, a, b);
- Smoothed Wolf's numbers for the period 1700-2010 (Fig.1, c);
- Total solar Irradiance TSI for the period 1610-2010 (Lean et al., 1995, Lean 2000) and for the period 843-1961 (Bard et al., 2000, Fig.1, d);

- $2.2Ka$ time series of North America temperature (Salzer and Kipfmueller, 2005, Fig.2, a);
- $8Ka$ time series of North America precipitation for the period (Hughes and Graumlich, 2000, Fig.2, b);
- Mean sea level at Stockholm for the period 1774-2002 (Ekman, 2003, Fig.2, c, d)

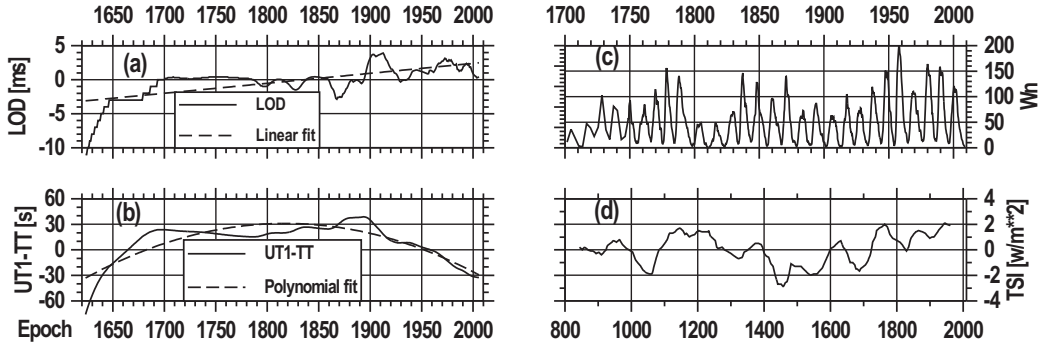

Figure 1: Time series of Lenght of Day LOD (a), the difference between the Universal Time UT1 and Terrestrial Time TT (b), Wolf's numbers (c) and Total Solar Irradiance TSI, according Bard et al. solution (2000) - (d).

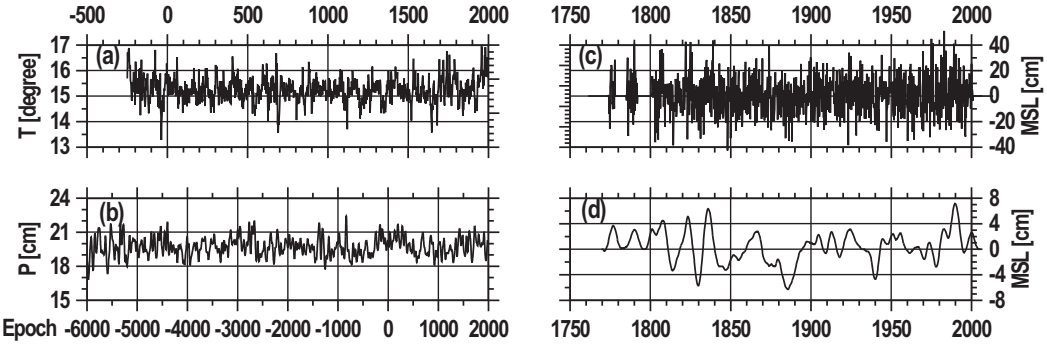

Figure 2: Time series of North America temperature (a) and precipitation (b), detrended Mean Sea Level (MSL) at Stockholm (c) and 5-year averaged MSL (d).

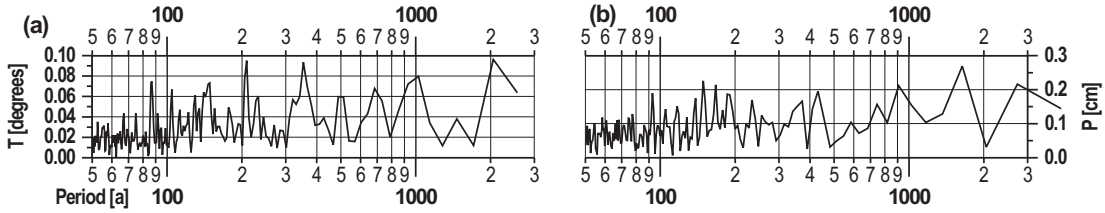

Figure 3: Amplitude spectra of North America temperature (a) and precipitation (b).

Jose (1965) points out a repeating solar system configuration of the 4 outer planets with period of 178.7 years. He suggests this configuration modulates the solar cycles. Sharp (2010) suggests other value - 171.44 years, which is the synodic period of Uranus and Neptune. The amplitude spectra of North America temperature and precipitation show a millennial long-periodical oscillation with period between 2000 and 3000 years (Fig,3, a, b). This long-periodical oscillation is known as Hallstatt cycles with period, estimated between 2300 and 2400 years in scientific papers. The North America temperature spectrum contains significant oscillations with periods 210 and 230 years, which appear as the 10-th and 11-th harmonics of 2300-year Hallstatt cycle. So, the candidates of the main centennial cycles of climatic

variations, driven by the solar activity are four oscillations with periods of 171.44, 178.7, 210 and 230 years.

3. MODELS OF CENTENNIAL OSCILLATIONS

The model of the centennial cycles of the Earth rotation and solar activity is

$$F = f_0 + f_1(t - t_0) + \sum_{j=1}^{N_k} a_j \sin j\frac{2\pi}{P_k}(t - t_0) + b_j \cos j\frac{2\pi}{P_k}(t - t_0), \quad (1)$$

where t_0 is the mean epoch of observations F, N_k - the harmonics number of the frequencies $\omega_k = 2\pi/P_k$, which correspond to different centennial periods P_k. We will examine four centennial models with main periods P_k =171.44, 178.7, 210 and 230 years. The number of the harmonics N_k should be greater or equal to $P_k/11 + 1$, which includes all solar frequencies with periods from 11 years to P_k years.

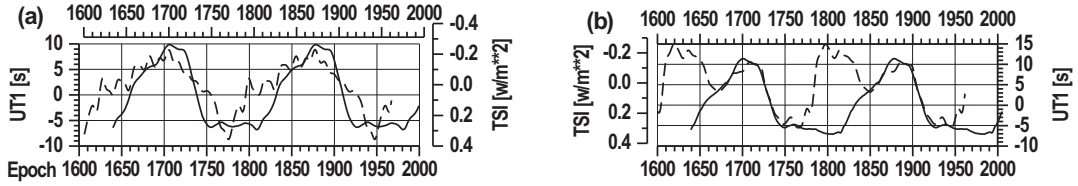

Figure 4: Comparison between UT1 and TSI centennial cycles, determined by 171.44-year model (a) and 178.7-year model (b).

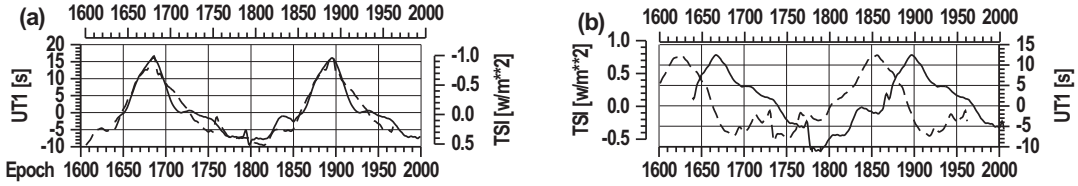

Figure 5: Comparison between UT1 and TSI centennial cycles, determined by 210-year model (a) and 230-year model (b).

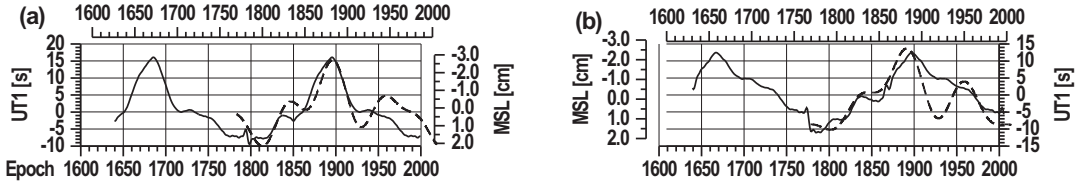

Figure 6: Comparison between UT1 and MSL centennial cycles, determined by 210-year model (a) and 230-year model (b).

The centennial cycles of UT1 variations are compared with corresponding TSI cycles from the solution of Bard et al. (2000), which provide more smooth curve than other solar indices. The 172-year model yields poor agreement between the UT1 and TSI variations (Fig.4, a). Partial correlation between the UT1 and negative TSI variations exists in the case of 178.7-year model (Fig.4, b), which points out that this oscillation and its harmonics are presented in the centennial solar-terrestrial influences, but it is not the dominating period. The same conclusion is valid for 230-year model (Fig.5, b), where the TSI and UT1 cycles are significantly shifted. The 210-year model yields almost exact match between the UT1 and negative TSI cycles (Fig.5, a), so the dominating period of the centennial solar-terrestrial influences is with value of about 210 years. A relatively good agreement between the UT1 and negative MSL

centennial cycles exists (Fig.6), so the probable source of Earth rotation centennial variations is cooling effects of the solar grand minima and corresponding increasing of the polar ice thickness.

4. CONCLUSIONS

The best agreement between the centennial cycles of the TSI and UT1 is achieved by 210a model.

The dependence between the TSI and UT1 centennial variations is negative, so the Earth rotation acceleration is connected with the decrease of the MSL, due to cooling effects of solar grand minima and corresponding increasing of the polar ice thickness.

Partial correlation exists between the 180- and 230-year cycles of the time series of solar and climatic indices, UT1 and LOD. The solar grand minima are irregular in time and the time intervals between them are not multiple by the examined periods, so the appropriative model of the centennial cycles of the Earth rotation should combine 180a, 210a, 230a oscillations and their harmonics.

Acknowledgement. The paper was supported by the contract DO02-275 with the Bulgarian NSF and the Grant Agency of the Academy of Sciences of the Czech Republic under the project IAA300130702.

5. REFERENCES

Bard, E., G. Raisbeck, F. Yiou, and J. Jouzel, 2000, "Solar irradiance during the last 1200 years based on cosmogenic nuclides", TELLUS B, vol. 52 (3), pp. 985-992.

Chapanov, Ya., 2006, "On the long-periodical oscillations of the Earth rotation", Proc. Journées 2005 "Systèmes de référence spatio-temporels"', Warsaw, 2006, 129-130.

Chapanov Ya., Gambis D., 2008a, "Correlation between the solar activity cycles and the Earth rotation", Proc. Journées 2007 "Systèmes de référence spatio-temporels", Paris. 2008, 206-207.

Chapanov Ya., Vondrák J., Ron C., 2008b, "22-year Oscillations of UT1, Core Angular Momentum and Geomagnetic Field", Proc. Journées 2008 "Systèmes de référence spatio-temporels", Dresden, 22-24 September 2008, 182-185.

Chapanov Ya., Vondrák J., Ron C., 2008c, "Decadal Oscillations of The Earth Rotation", AIP. Conf. Proc. Vol. 1043 "Exploring the Solar system and the Universe", Bucharest, 14-20 April, 2008. 2008, 197-200.

Chapanov Ya., Gambis D. 2009a, "Change of the Earth moment of inertia during the observed UT1 response to the 11-year solar cycles", Proc. Journées 2008 "Systèmes de référence spatio-temporels", Dresden, 2009, P.131-132.

Chapanov Ya., Gambis D., 2009b, "Solar-terrestrial energy transfer during sunspot cycles and mechanism of Earth rotation excitation", Proc. IAU Symposium 264, 2009.

Chapanov Ya., Vondrák J., Ron C., 2009c, "Common 22-year cycles of Earth rotation and solar activity", Proc. IAU Symposium 264, 2009.

Chapanov Ya., Gambis D., 2010a, "A model of global water redistribution during solar cycles, derived by astronomical data", Conf. BALWOIS-2010, Ohrid, 2010.

Chapanov Ya., Gambis D., 2010b, "Long-periodical variations of Earth rotation, determined from reconstructed millennial-scale glacial sea level", Conf. BALWOIS-2010, Ohrid, 2010.

Ekman, M, 2003, "The world's longest sea level series and a winter oscillation index for northern Europe 1774 - 2000", Small Publications in Historical Geophysics, 12, 31 pp.

Hughes, M. K. and L. J. Graumlich, 2000, "Multi-Millennial Nevada Precipitation Reconstruction". International Tree-Ring Data Bank. IGBP PAGES/World Data Center-A for Paleoclimatology Data Contribution Series #2000-049. NOAA/NGDC Paleoclimatology Program, Boulder CO, USA.

Jose, P., 1965, "Sun's motion and sunspots", Astronomical Journal, 70, pp. 193 - 200.

Lean, J., Beer, J., & Bradley, R., 1995, "Reconstruction of Solar Irradiance Since 1610: Implications for Climate Change", Geophys. Res. Let., 22, No. 23, pp. 3195-3198

Lean, J., 2000, "Evolution of the Sun's Spectral Irradiance Since the Maunder Minimum", Geophys. Res. Let, 27, No. 16, pp. 2425-2428

Salzer, M.W. and K.F. Kipfmueller, 2005, "Reconstructed Temperature and Precipitation on a Millennial Timescale from Tree-Rings in the Southern Colorado Plateau", U.S.A. Climatic Change, 70, No 3, pp. 465 - 487

Sharp, G., 2010, "Are Uranus & Neptune responsible for Solar Grand Minima and Solar Cycle Modulation?", arXiv:1005.5303v3 [physics.geo-ph], 15pp.

INFLUENCE OF THE INNER CORE GEOPOTENTIAL VARIATIONS ON THE ROTATION OF THE EARTH

A. ESCAPA[1], J. GETINO[2], D. MIGUEL[2] & J. M. FERRÁNDIZ[1]

[1] Department of Applied Mathematics, University of Alicante
PO Box 99, E-03080 Alicante, Spain
e-mail: alberto.escapa@ua.es

[2] Department of Applied Mathematics, University of Valladolid
E-47011 Valladolid, Spain

ABSTRACT. In this investigation we determine a new contribution to the rotation of a three layer Earth model composed by an axial–symmetric mantle, a fluid core, and an axial–symmetric inner core. This contribution emerges as a consequence of the variation of the geopotential induced by the differential rotation of the solid inner core. Within the framework of the Hamiltonian theory of the rotation of the non–rigid Earth, and following the same guidelines as those described in Escapa et al. (2001, 2008), we discuss the influence of this effect on the motion of the Earth figure axis. We also provide numerical estimations for the amplitudes of the nutational motion of this axis.

1. INTRODUCTION

The accurate modeling of the Earth rotational motion requires to consider a three layer structure that reproduces, to some extent, the Earth interior configuration. It is the case, for example, of the last theory of the Earth nutational motion adopted by the International Astronomical Union (IAU), based on the work by Mathews et al. (2002). This three layer structure (Figure 1) is composed of an external solid (mantle) that encloses a fluid (fluid outer core) containing another solid (inner core). In addition, rotational studies also assume that the barycenters of the three constituents are always located in the same point O.

The presence of the inner core introduces three additional degrees of freedom in the description of the system. They are necessary to take into account the possible rotation of the inner core with respect to the mantle. We will refer to this possible rotation as the differential rotation of the inner core. It affects the rotational dynamics of the Earth in different ways. For example, it originates new mechanical interactions of hydrodynamical, gravitational, electromagnetic, or viscous nature. These interactions influence the evolution of the mantle, the fluid, and the inner core itself, and are absent in one or two layer models.

At the same time, the existence of the solid inner core also changes the Earth response to model–independent perturbations like, for example, to the main contribution of the gravitational torque exerted on the Earth by the Moon and the Sun. This perturbation is the same for one, two, or three layer models. However, the response, i.e. the rotational motion, is different according to the particular model under consideration. From the perspective of the dynamical modeling, this change is related with the modification of the nutational normal modes of the Earth (e.g. Moritz & Mueller 1987). The inclusion of the inner core implies the appearance of two new nutational normal modes with respect to the two layer case: the Prograde Free Core Nutation and the Inner Core Wobble (e.g. Escapa et al. 2001).

Among the contributions of the solid inner core to the rotation of the Earth there is one specially peculiar, because it has no equal in one or two layer models. The differential rotation of the inner core modifies the outer gravitational field generated by the Earth. In other words, there exists a variation in the geopotential due to the differential rotation of the inner core. This situation arises even for the models involving rigid layers and an homogeneous fluid. From a mechanical point of view its origin is clear, since a differential rotation of the inner core entails a redistribution of mass inside of Earth. In turn, this redistribution modifies the geopotential.

This effect has been considered previously in some investigations (e.g. Greiner–Mai et al. 2000, 2001, Escapa et al. 2008), but, as far as we know, its influence in the rotational motion of the Earth has not

been explicitly evaluated. Due to the minute size of the inner core with respect to the whole Earth and its quasi–sphericity, the numerical values induced by this mechanism should be small. However, some of the current studies of the Earth rotation provide improvements that are at the level of the microarcsecond (Dehant et al. 2008). Hence, in addition to the theoretical interest, it can be also relevant to discuss qualitatively this contribution from the point of view of establishing accurate numerical standards.

2. ANALYTICAL MODELING

We will sketch the main guidelines to evaluate the contribution of the variations of the geopotential to the rotation of the Earth, these variations stemming from the differential rotation of the inner core. For a comprehensive exposition, we refer the reader to Escapa et al. (2011). Since the influence of this effect is expected to be small, it will be enough to consider a simplified three layer Earth model. In particular, we will assume that the Earth is composed of three quasi–spherical, ellipsoidal layers: an axial–symmetrical rigid mantle, a fluid outer core, and an axial–symmetrical rigid inner core.

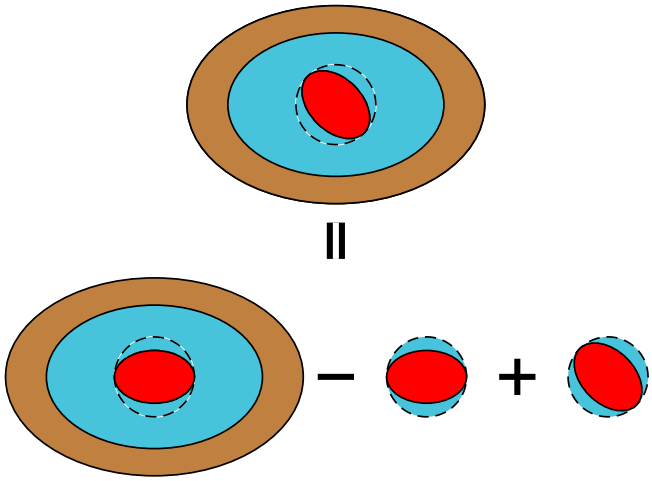

Figure 1: Three layer Earth model.

The rotational dynamics of this system is determined by the hydrodynamical and gravitational interactions. They provide its evolution through the differential equations of motion. We will establish these equations with the help of Analytical Dynamics. Within this framework, it is necessary to construct the rotational kinetic energy and the potential energy of the system. The kinetic energy, $\mathcal{T}$, accounts for the hydrodynamical interaction of the fluid with the solid layers. The potential energy is composed of two terms. One term, $\mathcal{V}_i$, is included to describe the internal gravitational torques among the layers. These torques are consequence of the stratification of the model (e.g. Ramsey 1940). The other one, $\mathcal{V}_e$, is related with the gravitational perturbations caused on the Earth by the external bodies, particulary by the Moon and the Sun.

We will focus our discussion on $\mathcal{V}_e$, since it is the function linked with the geopotential. Usually, it is expanded in a series of spherical harmonics, the main contribution coming from the second degree term. This term can be divided in two parts, accordingly their dependence on the differential rotation of the inner core. Although other approaches are possible (e.g. Escapa et al. 2008), a convenient way to obtain this division is with the aid of MacCullagh's formula

$$\mathcal{V}_e = G\frac{m}{2r^5}\left[3\begin{pmatrix} x \\ y \\ z \end{pmatrix}^t \Pi \begin{pmatrix} x \\ y \\ z \end{pmatrix} - \text{trace}\,(\Pi)\, r^2\right]. \tag{1}$$

Here, G represents the gravitational constant. The symbol m denotes the mass of the perturber; r its distance to O; and x, y, and z its coordinates relative to the T_m reference system, whose vectorial basis is constituted by the principal axes of the mantle and with origin at O. The matrix Π is the matrix of inertia of the whole Earth.

Therefore, the expression providing the variation of the geopotential can be constructed once we have determined the matrix of inertia of the Earth. The form of this matrix is derived by considering the decomposition given in Figure 1 (see also Escapa et al. 2001). We get

$$\begin{aligned}\Pi &= A\begin{pmatrix}1&0&0\\0&1&0\\0&0&1+e\end{pmatrix}+A_s\,(e_s-\delta)\begin{pmatrix}k_1^2&k_1k_2&k_1k_3\\k_1k_2&k_2^2&k_2k_3\\k_1k_3&k_2k_3&k_3^2-1\end{pmatrix}= \\ &= \Pi_0+\Delta\Pi.\end{aligned} \tag{2}$$

In this equation A, A_s are the smallest principal moments of inertia of the Earth and the inner core, and e, e_s their ellipticities. The parameter δ is related with the ellipticity of a thin fluid layer surrounding the solid inner core (Escapa et al. 2001). The quantities k_1, k_2, and k_3 are the co–ordinates of the figure axis of the inner core in the mantle reference system T_m. As a consequence of the differential rotation they are functions of time, in contrast to the other parameters appearing in Eq. (2).

In this way, the matrix of inertia depends on the differential rotation through the term $\Delta\Pi$. This dependence is inherited by the geopotential, as it can be shown by substituting Eq. (2) into Eq. (1). Thus, the variation of the geopotential induced by the differential rotation can be derived from

$$\begin{aligned}\mathcal{V}_e &= G\frac{1}{2}\frac{m}{r^5}\left[3\begin{pmatrix}x\\y\\z\end{pmatrix}^t\Pi_0\begin{pmatrix}x\\y\\z\end{pmatrix}-\ \mathrm{trace}\,(\Pi_0)\ r^2\right]+\frac{3}{2}G\frac{m}{r^5}\begin{pmatrix}x\\y\\z\end{pmatrix}^t\Delta\Pi\begin{pmatrix}x\\y\\z\end{pmatrix}= \\ &= \mathcal{V}_2+\Delta\mathcal{V}_2,\end{aligned} \tag{3}$$

since $\mathrm{trace}(\Delta\Pi)=0$. This formula shows that the order of magnitude of the new contribution $\Delta\mathcal{V}_2$ relative to the main part of second degree term $\mathcal{V}_2$ is $A_s(e_s-\delta)/(Ae)$, whose value is about 10^{-5}. Indeed this quantity is small, but it might be not enough to neglect its influence at the microarcsecond level.

3. DISCUSSION

To analyze the influence of $\Delta\mathcal{V}_2$ on the rotational motion of the Earth, we will employ the Hamiltonian formalism (e.g. Getino & Ferrándiz 2001). In our situation the Hamiltonian of the system, given by the sum of the kinetic and potential energies, turns out to be

$$\mathcal{H}=\mathcal{T}+\mathcal{V}_i+\mathcal{V}_2+\Delta\mathcal{V}_2. \tag{4}$$

The equations of motion are obtained by formulating this Hamiltonian in terms of an Andoyer–like set of canonical variables (Escapa et al. 2001, 2008). Then, it is possible to obtain an analytical solution of these equations by employing a perturbation algorithm developed by Hori (1966). At the first order, this method allows us to separate the contributions due to $\Delta\mathcal{V}_2$ from that originated by $\mathcal{V}_2$.

Following this approach, we have obtained analytical expressions for the the rotational motion of the figure axis. This motion is usually decomposed in two parts (e.g. Kinoshita 1977). The first part is given by the motion of the angular momentum axis. The nutation in longitude and obliquity of the plane perpendicular to this axis is named Poisson terms. The second one represents the motion of the figure axis with respect to the angular momentum axis, in this case the associated nutation is referred as Oppolzer terms.

Specifically, within our order of approximation we have obtained (Escapa et al. 2011) that the motion of the angular momentum axis is not affected by the perturbation $\Delta\mathcal{V}_2$. It means that the Poisson terms are zero. In addition, this fact also implies that the precession of the Earth is not influenced by this perturbation. In contrast, the motion of the figure axis relative to the angular momentum axis is affected, i.e. the Oppolzer terms are different from zero. In this way, the perturbation $\Delta\mathcal{V}_2$ induces a periodic motion in the figure axis. The frequencies of this motion are the same as those derive when considering the $\mathcal{V}_2$ perturbation, that is to say, the induced motion contributes to the long–period nutations.

The numerical representation of this motion is given by providing the amplitudes of the nutation in longitude, $\Delta\psi$, and in obliquity, $\Delta\epsilon$, of the plane perpendicular to the figure axis. They are displayed in Table 1, and have been computed from the numerical values given in Kinoshita (1977), and those reported in Mathews et al. (1991) for the Preliminary Reference Earth Model (PREM). Since at this

stage our purpose is to obtain an estimation of the contribution, we have only evaluated the amplitudes of the ten main terms in the trigonometric expansion of the orbital motion of the Moon and the Sun. In this regard, let us point out that the values of the amplitudes can be altered by the particular choice of some parameters of the rheological model, although the order of magnitude is kept.

As it can be seen in Table 1, the amplitudes of the new contributions are above the order of the microarcsecond for many nutational arguments. In particular, the values in the annual and semi–annual band are specially significant. It shows the need of incorporating the influence of the variation of the geopotential induced by the differential rotation of the inner core in the actual standards and models of the Earth rotation.

Argument					Period	Figure axis (μas)	
l_M	l_S	F	D	$\overline{\Omega}$	Days	$\Delta\psi$	$\Delta\epsilon$
+0	+0	+0	+0	+1	-6793.48	2.79	-0.31
+0	+0	+0	+0	+2	-3396.74	0.00	-0.01
+0	+1	+0	+0	+0	365.26	14.95	9.29
+0	-1	+2	-2	+2	365.25	-1.78	0.48
+0	+0	+2	-2	+2	182.63	44.61	-19.92
+0	+1	+2	-2	+2	121.75	1.64	-0.72
+1	+0	+0	+0	+0	27.55	-2.22	0.02
+0	+0	+2	+0	+2	13.66	7.17	-3.08
+0	+0	+2	+0	+1	13.63	1.22	-0.63
+1	+0	+2	+0	+2	9.13	0.96	-0.41

Table 1: Numerical estimation of the nutations of the figure axis due to the influence of the inner core in the geopotential.

Acknowledgements. AE's contribution was carried out thanks to a sabbatical leave from the University of Alicante at the National Astronomical Observatory of Japan (NAOJ), supported by the Spanish Ministerio de Educación, project PR2009-0379, within the Programa Nacional de Movilidad de Recursos Humanos I-D+i 2008-2011. The generous hospitality of the NAOJ staff is gratefully acknowledged. This work has been partially supported by the Spanish projects I+D+I AYA2010-22039-C02-01, AYA2010-22039-C02-02, and by the International Teams program, project 172, of the International Space Science Institute (ISSI) at Bern, Switzerland.

4. REFERENCES

Dehant, V., Lambert, S., Folgueira, M., Koot, L., & Rambaux, N., 2008, Proceedings of the Journées 2007. Ed. N. Capitane, Observatoire de Paris, 82–87.

Escapa, A., Getino, J., & Ferrándiz, J. M., 2001, J. Geophys. Res., 106, 11387–11397.

Escapa, A., Getino, J., & Ferrándiz, J. M., 2008, Proceedings of the Journées 2007. Ed. N. Capitane, Observatoire de Paris, 113–114.

Escapa, A., Getino, J., Miguel, D., & Ferrándiz, J. M., 2011 (to be submitted).

Getino, J. & Ferrándiz, J. M., 2001, MNRAS , 322, 785–799.

Greiner-Mai, H., Jochmann, H., & Barthelmes, F., 2000, Phys. Earth Planet. Inter., 117, 81–93.

Greiner-Mai, H. & Barthelmes, F., 2001, Geophys. J. Int. , 144, 27–36.

Hori, G., 1966, Publ. Astron. Soc. Japan, 18, 287–296.

Kinoshita, H., 1977, Celest. Mech. Dyn. Astr. , 15, 277–326.

Mathews, P. M., Buffet, B.A., & Herring T.A., 2002, J. Geophys. Res., 107, 10.1029.

Mathews, P. M., Bufett, B.A., Herring, T.A., & Shapiro, I.I., 1991, J. Geophys. Res., 96, 8243–8257.

Moritz, H. & Mueller, I., 1987, Earth Rotation, Frederic Ungar, New York.

Ramsey, A. S., 1940, An Introduction to the theory of Newtonian attraction, Cambridge University Press, Cambridge.

ON SOLUTION OF THE THREE–AXIAL EARTH'S ROTATION PROBLEM

V. A. BRUMBERG, T. V. IVANOVA
Institute of Applied Astronomy
10, Kutuzov quay, St. Petersburg, 191187, Russia
e-mail: itv@ipa.nw.ru

ABSTRACT. The three–axial rigid–body Earth's rotation problem is treated in the form compatible with the General Planetary Theory GPT. This paper completes the results of (Brumberg and Ivanova, 2007, 2010).

1. THE SYSTEM OF THE EQUATIONS FOR THE PLANETARY AND LUNAR MOTIONS AND THE EARTH'S ROTATION

The complete system of the equations for the planetary and lunar motions and the Earth's rotation was derived in (Brumberg and Ivanova, 2010). It has the form

$$\dot{X} = \mathrm{i}\,\mathcal{N}[PX + R(X,t)] \tag{1}$$

where

$$X = (a,\, \bar{a},\, b,\, \bar{b},\, X_{37}, \ldots, X_{43}), \quad R = (R_1, \ldots, R_4,\, R_{37}, \ldots, R_{43}) \tag{2}$$

are vectors with 43 components (eccentric and oblique Laplace–type variables of the planets and the Moon a, b and R_i for $i = 1, 2, 3, 4$ are 9–vectors, $X_{36+\kappa}$ and $R_{36+\kappa}$ for $\kappa = 1, 2, \ldots, 7$ are connected with the Earth's rotation and depend on four Euler parameters (replacing three classical Euler angles) and three components of the Earth's rotation angular velocity.

$\mathcal{N}$ and P are 43×43 diagonal matrices of the structure

$$\mathcal{N} = \mathrm{diag}(N, N, N, N, n, n, n, n, n, n, n)\,,$$

$$P = \mathrm{diag}(E_{(9)}, -E_{(9)}, E_{(9)}, -E_{(9)}, 1,\, -1,\, 1,\, -1, -4\sqrt{k_1 k_2}\,, 4\sqrt{k_1 k_2}\,, 0)$$

where N is 9×9 diagonal matrix of mean motions n_i, $E_{(9)}$ is unitary matrices of dimension 9×9, k_1, k_2 and n are determined by

$$k_1 = \frac{I_3 - I_1}{2I_2}\,, \qquad k_2 = \frac{I_3 - I_2}{2I_1}\,, \qquad n = -\frac{\Omega}{2}\,,$$

$\Omega = 7.292115 \cdot 10^{-5}$ rad/s being the mean Earth's rotation velocity and $I_i (i = 1, 2, 3)$ being principal inertia moments.

2. THE SECULAR SYSTEM

Our aim is to reduce (1) to the secular system. For that, the system (1) is subjected to a number of the normalizing Birkhoff and the linear transformations. As a result, the secular system describing the evolution of the Earth's rotation (depending on the planetary and lunar evolution) is presented by

$$\dot{p}_1 = \mathrm{i}\, n(p_1 + F_{37}), \tag{3}$$

$$\dot{p}_3 = \mathrm{i}\, n(p_3 + F_{39}), \tag{4}$$

$$\dot{p}_5 = \mathrm{i}\, n(-4\sqrt{k_1 k_2}\, p_5 + F_{41}), \tag{5}$$

$$\dot{p}_7 = \mathrm{i}\, n\, F_{43} \tag{6}$$

with conjugate equations for p_1, p_3, p_5. Our computations show that the right–hand members F consist of two parts, i.e.

$$F_{36+\kappa} = U_\kappa^{*(1)} + U_\kappa^{*(2)}\,, \qquad \kappa = 1, \ldots, 7 \tag{7}$$

with

$$U_\kappa^{*(1)} = p_\kappa(1-\delta_{\kappa 7}) \sum\nolimits^{*} U_{iklm}^{(\kappa,s)} (p_1p_2)^{s_2}(p_3p_4)^{s_4}(p_5p_6)^{s_6} p_7^{s_7} \times (w_N\overline{w}_N)^{s_4} \prod_{j=1}^{9} (z_j\overline{z}_j)^{k_j}(w_j\overline{w}_j)^{m_j}\,, \tag{8}$$

$$U_\kappa^{*(2)} = (1-\delta_{\kappa 7}) p_5^{\delta_{\kappa 5}} p_6^{\delta_{\kappa 6}} \sum\nolimits^{*} U_{iklm}^{(\kappa,s)} \left(\prod_{j=1}^{4} p_j^{s_j}\right) (p_5p_6)^{\min\{s_5,s_6\}} p_7^{s_7} \times$$

$$\times (w_N\bar{w}_N)^{\max\{s_3-\delta_{\kappa 3},\, s_4-\delta_{\kappa 4}\}} \prod_{j=1}^{9} (z_j\overline{z}_j)^{k_j}(w_j\overline{w}_j)^{m_j} \tag{9}$$

with numerical coefficients $U_{iklm}^{(\kappa,s)}$. δ_{ij} is the Kronecker symbol. $p_2 = \overline{p}_1, p_4 = \overline{p}_3, p_6 = \overline{p}_5$. It is seen from (8)–(9) that F_{43} is equal to 0 and, therefore, the equation (6) can be omitted ($p_7 = const$).

Equations (3)–(6) with the right–hand members (7)–(9) admit three first integrals

$$p_1p_2 + (w_N\bar{w}_N)p_3p_4 = C_1, \qquad p_5p_6 = C_2, \qquad p_7 = C_3 \tag{10}$$

with real constants $C_1\,, C_2\,, C_3$.

The secular system describing the evolution of the planetary and lunar orbits (independent of the Earth's rotation) may be presented in the form

$$\dot{z}_\sigma = \mathrm{i}(\mu_\sigma z_\sigma + n_\sigma U_{1\sigma}^{*}), \qquad \dot{w}_\sigma = \mathrm{i}(\nu_\sigma w_\sigma + n_\sigma U_{3\sigma}^{*}) \tag{11}$$

with

$$U_{\kappa\sigma}^{*} = (z_\sigma\delta_{\kappa 1} + w_\sigma\delta_{\kappa 3}) \sum\nolimits^{*} U_{iklm}^{(\kappa,\sigma)} (z_j\overline{z}_j)^{k_j}(w_j\overline{w}_j)^{m_j}\,, \quad \kappa = 1,3\,, \quad \sigma = 1,2,\ldots,9\,,$$

μ_j and ν_j being the planetary ($j = 1,2,\ldots,8$) and lunar ($j = 9$) motions of pericentres and nodes, respectively and ν_N being 0 (in our computations $N = 5$). This system admits the first integrals

$$z_j\overline{z}_j = \mathrm{const}\,, \qquad w_j\overline{w}_j = \mathrm{const} \tag{12}$$

leading to straightforward integration.

3. SOLUTION OF THE EARTH'S ROTATION SECULAR SYSTEM

Designating $p_1 = g,\ p_3 = h,\ p_5 = f$ one may present the secular system for the Earth's rotation in the form

$$\begin{aligned}
\dot{g} &= \mathrm{i}\,n\big[gG(g\overline{g},\, h\overline{h},\, z_j\overline{z}_j,\, w_j\overline{w}_j) + \Phi(g,\,\overline{g},\,h,\,\overline{h},\,z_j\overline{z}_j,\,w_j\overline{w}_j)\big]\,,\\
\dot{h} &= \mathrm{i}\,n\big[hH(g\overline{g},\, h\overline{h},\, z_j\overline{z}_j,\, wj\overline{w}_j) + \Psi(g,\,\overline{g},\,h,\,\overline{h},\,z_j\overline{z}_j,\,w_j\overline{w}_j)\big]\,,\\
\dot{f} &= \mathrm{i}\,n\big[fF(g\overline{g},\, h\overline{h},\, z_j\overline{z}_j,\, w_j\overline{w}_j) + \Theta(g,\,\overline{g},\,h,\,\overline{h},\,z_j\overline{z}_j,\,w_j\overline{w}_j)\big]
\end{aligned} \tag{13}$$

where

$$gG = g + U_1^{*(1)}\,, \quad hH = h + U_3^{*(1)}\,, \quad fF = -4\sqrt{k_1k_2}\,f + U_5^{*(1)}\,, \tag{14}$$

$$\Phi = U_1^{*(2)}\,, \qquad \Psi = U_3^{*(2)}\,, \qquad \Theta = U_5^{*(2)}\,. \tag{15}$$

The third equation of (13) is separated from the first two. Hence, these equations may be treated analytically in much the same manner as in (Brumberg and Ivanova, 2007). It is seen from (8)–(9) that the planetary and lunar coordinates enter in every part as the functions of the first integrals (12), i.d. they enter as the constants. Therefore, with taking into account the first integrals (10) the first parts $U_\kappa^{*(1)}$ of the right–hand members are ready to integrate (13), the second parts $U_\kappa^{*(2)}$ are of more general form but they are less significant than the first parts. Our computations show that within the linear theory with respect to small parameters depending on the dynamical flattenings and C_3

$$G = 1 + (g\overline{g} - h\overline{h}\,w_N\overline{w}_N)h\overline{h}\,w_N\overline{w}_N\,\Sigma_1 + C_0\,, \tag{16}$$

$$H = 1 - (g\overline{g} - h\overline{h}\, w_N\overline{w}_N) g\overline{g}\, \Sigma_1 + C_0\,, \tag{17}$$

$$F = -4\sqrt{k_1 k_1} - 4\sqrt{k_1 k_2} C_3 + (C_1^2 - 6g\overline{g}h\overline{h}\, w_N\overline{w}_N)\, \Sigma_1'\,, \tag{18}$$

$$\Phi = \overline{h}\, w_N\overline{w}_N \left\{ \left[g^3\overline{g} - 3g^2 h\overline{h}\, w_N\overline{w}_N - 3g\overline{g}\, h^2\, w_N\overline{w}_N + h^3\overline{h}\, (w_N\overline{w}_N)^2 \right] \Sigma_2 + \right.$$
$$\left. + (\overline{g}h^3\, w_N\overline{w}_N - g^3\overline{h})\, w_N\overline{w}_N \Sigma_2' \right\}, \tag{19}$$

$$\Psi = -\overline{g} \left\{ \left[[g^3\overline{g} - 3g^2 h\overline{h}\, w_N\overline{w}_N - 3g\overline{g}h^2\, w_N\overline{w}_N + h^3\overline{h}\, (w_N\overline{w}_N)^2 \right] \Sigma_2 + \right.$$
$$\left. + (\overline{g}h^3\, w_N\overline{w}_N - g^3\overline{h})\, w_N\overline{w}_N \Sigma_2' \right\}, \tag{20}$$

$$\Theta = -f\, w_N\overline{w}_N (g\overline{g} - h\overline{h}\, w_N\overline{w}_N)(g\overline{h} + \overline{g}h)\Sigma_2'' \tag{21}$$

where the constants $\Sigma_1, \Sigma_1', \Sigma_2, \Sigma_2', \Sigma_2''$ are the functions of the first integrals (12), C_0 depends on k_1, k_2 and two first integrals (10).

To solve (13) the method of the variation of the arbitrary constants is used. Neglecting temporarily the second parts one gets the trigonometrical solution

$$g = g_0 \exp \mathrm{i}\,\xi\,, \quad h = h_0 \exp \mathrm{i}\,\eta\,, \quad f = f_0 \exp \mathrm{i}\,\zeta\,,$$
$$\xi = n\Delta t + \xi_0\,, \quad \eta = n\sigma t + \eta_0\,, \quad \zeta = n\chi t + \zeta_0 \tag{22}$$

with real constants g_0, h_0, f_0, ξ_0, η_0, ζ_0 and the frequency factors

$$\Delta = G\,, \qquad \sigma = H\,, \qquad \chi = F\,. \tag{23}$$

The amplitudes g_0, h_0 of the trigonometrical solution (22) are determined from (23)

$$g_0^4 = \frac{(1 + C_0 - \sigma)^2}{[2(1 + C_0) - \Delta - \sigma]\Sigma_1}\,, \quad h_0^4 w_N^2 \overline{w}_N^2 = \frac{(\Delta - 1 - C_0)^2}{[2(1 + C_0) - \Delta - \sigma]\Sigma_1}\,.$$

The amplitude $f_0 = \sqrt{C_2}$. By combining three frequencies n, $n\Delta$, $n\sigma$ one can restore the fundamental frequencies of the classical solution.

$$n(\Delta + \sigma) = \dot{\varphi}\,, \qquad n(\Delta - \sigma) = \dot{\psi}\,. \tag{24}$$

The frequency χ corresponds to the Euler period of the Earth's rotation.

To evaluate the influence of Φ, Ψ, Θ one may retain the form (22) with constant Δ, σ, χ and slowly change g_0, h_0, f_0, ξ_0, η_0, ζ_0. By substituting (22) into (13) one gets the rates of changing these variables

$$\mathrm{i}\, g\dot{\xi}_0 + g g_0^{-1}\dot{g}_0 = \mathrm{i}\, n[\Phi + g(G - \Delta)], \tag{25}$$

$$\mathrm{i}\, h\dot{\eta}_0 + h h_0^{-1}\dot{h}_0 = \mathrm{i}\, n[\Psi + h(H - \sigma)], \tag{26}$$

$$\mathrm{i}\, f\dot{\zeta}_0 + f f_0^{-1}\dot{f}_0 = \mathrm{i}\, n[\Theta + f(F - \chi)], \tag{27}$$

By combining these equations with their conjugates one obtains at once

$$2g_0\dot{g}_0 = \mathrm{i}\, n(\overline{g}\Phi - g\overline{\Phi}) \equiv \mathrm{i}\, n\, (g\overline{h} - \overline{g}h) w_N\overline{w}_N \left[D\Sigma_2 - C_1\Sigma_2'(g\overline{h} + \overline{g}h) w_N\overline{w}_N \right]\,, \tag{28}$$

$$2h_0\dot{h}_0 = \mathrm{i}\, n(\overline{h}\Psi - h\overline{\Psi}) \equiv -\mathrm{i}\, n\, (g\overline{h} - \overline{g}h) \left[D\Sigma_2 - C_1\Sigma_2'(g\overline{h} + \overline{g}h) w_N\overline{w}_N \right]\,, \tag{29}$$

$$2f_0\dot{f}_0 = \mathrm{i}\, n(\overline{f}\Theta - f\overline{\Theta}) \equiv 0 \tag{30}$$

with $D = g^2\overline{g}^2 - h^2\overline{h}^2\, (w_N\overline{w}_N)^2$. With the use of

$$g\overline{h} - \overline{g}h = 2\,\mathrm{i}\, g_0 h_0 \sin(\xi - \eta), \qquad g\overline{h} + \overline{g}h = 2g_0 h_0 \cos(\xi - \eta) \tag{31}$$

one gets

$$\dot{g}_0 = n h_0 w_N\overline{w}_N \left\{ D\Sigma_2 \sin(\eta - \xi) - g_0 h_0 w_N\overline{w}_N C_1\Sigma_2' \sin[2(\eta - \xi)] \right\}, \tag{32}$$

$$\dot{h}_0 = -n g_0 \left\{ D\Sigma_2 \sin(\eta - \xi) - g_0 h_0 w_N\overline{w}_N C_1\Sigma_2' \sin[2(\eta - \xi)] \right\}, \tag{33}$$

$$\dot{f}_0 = 0\,. \tag{34}$$

4. NUMERICAL ESTIMATES

To get the approximate numerical estimates of the constants of our solution by comparing it with the classical SMART97 solution we use the same techniques as in (Brumberg and Ivanova, 2007). In accordance with the SMART97 solution the initial (for the epoch J2000) values of the Euler angles and their derivatives are

$$\begin{aligned} \psi^{(0)} &= -0.00006\,78954\,609\,, \qquad \dot\psi^{(0)} = 0.70105\,4959\cdot 10^{-6}/d\,, \\ \theta^{(0)} &= 0.40906\,46190\,715\,, \qquad \dot\theta^{(0)} = -0.09606\,7366\cdot 10^{-6}/d\,, \\ \varphi^{(0)} &= 4.89489\,89303\,002\,, \qquad \dot\varphi^{(0)} = 6.30038\,8130/d \end{aligned} \tag{35}$$

(the angles ψ , ω , φ of SMART97 correspond to our angles $-\psi$, $-\theta$, φ, respectively). Starting with these initial values and the value $n = -3.1501\,9368/d$ we get the initial values (for the epoch J2000) for

$$g_0^{(0)} = -\sin\frac{\theta^{(0)}}{2} = -0.2031\,0924\,, \quad h_0^{(0)} = \frac{1}{\sqrt{w_N\overline{w}_N}}\cos\frac{\theta^{(0)}}{2} = 70.7495\,9950\,, \tag{36}$$

$$f_0^{(0)} = \frac{1}{2\Omega}\sqrt{\frac{\omega_1^2}{k_2}+\frac{\omega_2^2}{k_1}} = .0000\,0058 \tag{37}$$

where ω_1 and ω_2 are the components of the vector of the Earth rotation angular velocity referred to rotating Earth–fixed coordinate system. Then we obtain the numerical values for the first integrals of the secular system of the Earth's rotation

$$C_1 = 1.0000000000000, \qquad C_2 = .0000000000003, \qquad C_3 = .0000000201237 \tag{38}$$

and the values for

$$\Delta = 1.0000\,0022\,, \qquad \sigma = 1.0000\,0001\,, \qquad \chi = -.0065\,6895\,, \tag{39}$$

$$n(\Delta+\sigma) = -6.3003\,8810/d\,, \qquad n(\Delta-\sigma) = -.0000\,0067/d\,, \qquad n\chi = .0206\,9345. \tag{40}$$

Our results in $\dot\varphi$ and $\dot\psi$ coincide with the SMART97 solution up to $10^{-7}/d$. Then

$$\xi_0^{(0)} = -\frac{\psi^{(0)}+\varphi^{(0)}}{2} = -2.4474\,1552\,, \qquad \eta_0^{(0)} = \frac{\pi}{2}+\psi^{(0)}-\gamma = 2.5467\,0110 \tag{41}$$

where $\gamma = -3.4233\,8818$ was obtained in (Brumberg and Ivanova, 2007).

$\dot\zeta_0$ is determined from (27) with taking into account (31) and (34) and admitting for the approximate estimates $F-\chi = 0$ in (27)

$$\dot\zeta_0 = n\sqrt{w_N\overline{w}_N}\,\sin\theta\,\frac{\Delta-\sigma}{C_1\Sigma_1}\,\Sigma_2''\cos(\eta-\xi)\,. \tag{42}$$

The initial value (for the epoch J2000) for $\zeta_0^{(0)}$ is determined by

$$\zeta_0^{(0)} = -\frac{1}{2}n\sqrt{w_N\overline{w}_N}\,\frac{\Delta-\sigma}{C_1\Sigma_1}\,\Sigma_2''\left[\frac{\cos(\theta^{(0)}+\eta_0^{(0)}-\xi_0^{(0)})}{\dot\theta^{(0)}-n\Delta+n\sigma}+\frac{\cos(\theta^{(0)}-\eta_0^{(0)}+\xi_0^{(0)})}{\dot\theta^{(0)}+n\Delta-n\sigma}\right] = -.0313\,8315\,. \tag{43}$$

Six constants $g_0^{(0)}$, $h_0^{(0)}$, $f_0^{(0)}$, $\xi_0^{(0)}$, $\eta_0^{(0)}$, $\zeta_0^{(0)}$ are arbitrary constants of the trigonometrical solution of the Earth's rotation secular system.

5. CONCLUSION

The technique of this paper allows to construct a general theory of motion and rotation of the solar system bodies.

6. REFERENCES

Brumberg V., Ivanova T., 2007,"Precession/nutation solution consistent with the general planetary theory", Celest. Mech. Dyn. Astr. , vol. 97, pp. 189–210.

Brumberg V., Ivanova T., 2010,"On constructing the general Earth's rotation theory", Celest. Mech. Dyn. Astr. , submitted.

A REFINED DEFINITION OF THE INTERNATIONAL TERRESTRIAL REFERENCE SYSTEM

C. BOUCHER
Observatoire de Paris - SYRTE

ABSTRACT. Recent discussions have shown the need to upgrade and refine the definition of the International Terrestrial Reference System (ITRS). This presentation reviews the various issues, in particular related to the scale and origin. It also looks at the impact on IERS activities (ITRF and conventions), on the need to modify the related IUGG resolution, as well as the ongoing ISO standard related to ITRS.

1. BACKGROUND

Terrestrial Reference Systems (TRS) refer to an important domain of Geodesy, involving both theoretical and applied aspects, as well as deep connections with Astronomy, Earth Sciences and Geo-information. The concept of TRS designates any mathematical reference frame co-moving with the Earth in space, which immediately implies several visions for TRS:

- An astronomical vision, using TRS to study translational and rotational motion of the Earth in inertial space
- An Earth Science vision, using TRS to build physical models of the Earth system, and its various components (solid earth, oceans, atmosphere, hydrosphere)
- A metrological vision, using TRS together with suitable coordinate systems (geographical coordinates, map projections) to define geographical position of objects in the Earth's vicinity

The need to define and adopt a unique preferred TRS is widely recognized both for scientific, technical and societal reasons.

During the last thirty years, astronomers and geodesists developed a series of joint activities in this field, starting with the MERIT and COTES projects at the beginning of 80's, followed by the creation of the International Earth Rotation and Reference Systems Service (IERS) in 1988, jointly by the International Astronomical Union (IAU) and the International Union of Geodesy and Geophysics (IUGG) . IERS is in charge to propose a detailed definition of such a unique and prefered system, designated under the name of International Terrestrial Reference System (ITRS). IERS is also in charge to determine a series of primary realizations of ITRS, designated as International Terrestrial Reference Frames (ITRF), in addition to a comprehensive description of relevant conventions, known as IERS Conventions (Petit, Luzum, 2010)

Meantime IAU adopted the IAU 2000 system, and established an action to modernize the nomenclature in Fundamental Astronomy, to which IAG took part, in order to develop consistent definitions between astronomical and geodetic communities.This led IAG to propose to get a more formal definition of ITRS, officially adopted by the IUGG through its Resolution 2 of the Perugia General Assembly (2007). Considering the need to promote these results in a consistent way within the whole geodetic community, the International Association of Geodesy (IAG) like IAU did, expressed the need for a unified and accepted terminology related to basic TRS-related concepts and consequently established an intercommission working group (ICWG 1-3) on "Concepts and terminology related to Geodetic Reference Systems".

Presently, some issues are raised upon the necessity to refine the present definition of ITRS.

2. WHY TO REFINE THE DEFINITION OF ITRS ?

Following the three faces mentioned before for TRS, we can mention several of these issues:

On an astronomical view, the main current problem is to establish a rigorous definition of ITRS within the framework of the background relativistic model presently adopted by IAU (Soffel et al 2003). Such a definition must be in particular consistent with currently used time scales and the transformation formula to celestial system.

On a geophysical view, it is important to have a very precise definition which can be embedded into geophysical models. One can mention some of the relevant topics:

- motion of the geocenter
- sea level variations
- global rotation of tectonic plates (NNR, hot spots...)

On a metrological view, the adopted definition for ITRS must be tridimensional and consistent with the Terrestrial Time (TT)

3. DISCUSSION ISSUES

- **dimension of ITRS**

  The current situation is inconsistent. The IUGG resolution explicitly consider ITRS as a specific Global Terrestrial Reference System (GTRS) which is a local coordinate system in the relativistic framework, and therefore 4-dimensional. The IAG WG recommends ITRS to be tridimensional. This is the present proposed choice.

- **scale of ITRS**

  As specific GTRS, the ITRS scale is consistent with TCG. Most people who already gave an opinion about this point are in favor of a scale consistent with TT. The new definition should then follow this choice, if this preferred opinion is confirmed.

- **origin of ITRS**

  Two main options are considered for the origin :

  - either the center of mass of the whole Earth system, including atmosphere, ocean and continental water, which is the current option
  - or to choose an origin linked to the solid Earth, such as its center of mass, or a center of figure

  The pro and contra of these options are presently under investigation.

  Additional discussion could also be raised concerning the ITRS orientation, including its time evolution.

4. CONCLUDING REMARKS

Further contributions are expected to fix the choice for each item. These choices must be then translated into a relativistic definition of ITRS, following the present IAU formalism. Finally an new IUGG resolution will be required to publicize this.

5. REFERENCES

Petit G, Luzum B, 2010, IERS Conventions (2010), IERS Technical Note 36

Soffel M et al, 2003, The IAU 2000 resolutions for Astrometry, Celestial Mechanics and Metrology in the relativistic framework

INFLUENCE OF STATION REFERENCING ON THE QUALITY OF EOP TIME SERIES

D. COULOT[1], E. BERNARD[1 2] X. COLLILIEUX[1]

[1]LAREG, Institut Géographique National, GRGS
6 et 8 Avenue Blaise Pascal, Cité Descartes Marne la Vallée cedex 2
77455 Champs sur Marne, France
e-mail: david.coulot@ign.fr; etienne.bernard@ign.fr; xavier.collilieux@ign.fr

[2]CMLS - Ecole Polytechnique, 91128 Palaiseau cedex, France

ABSTRACT

EOP series (at a daily sampling) are computed together with (weekly) station positions. The definition of the terrestrial frames (TF) underlying these position series affects the accuracy of the estimated EOP series. The goal of this work is to evidence this influence for Satellite Laser Ranging (SLR) network, from two points of view.

In the first case study, the station referencing is realized through minimum constraints which align the orientation of the weekly TF with respect to a given Terrestrial Reference Frame (TRF). The weekly station networks over which these constraints are applied have a significant influence on the stability of the EOP series. To get the best stability, we thus search for weekly core networks with optimization methods. The WRMS of the so-computed EOP series shows a 25 μas improvement compared to the standard approach recommended by the analysis working group of the International Laser Ranging Service (ILRS).

In the second approach, the station referencing with respect to a given TRF is realized through the computation of weekly Helmert transformations. The EOP series consistent with the so-obtained station position series are directly computed by adding the estimated rotations. The results provided by an optimization (on the basis of a stochastic algorithm) of this approach will be compared to the results above.

COMPARISON OF THE HYDROLOGICAL EXCITATION FUNCTIONS HAM OF POLAR MOTION FOR THE PERIOD 1980.0-2007.0

J. NASTULA[1], M. PASNICKA[1], B. KOLACZEK[1]

[1] Space Research Center Polish Academy of Sciences
ul. Bartycka 18A, 00-716 Warsaw
e-mail: nastula@cbk.waw.pl
e-mail: mpasnicka@cbk.waw.pl
e-mail: kolaczek@cbk.waw.pl

ABSTRACT. In this study we compared contributions of polar motion excitation determined from hydrological models and harmonic coefficients of the Earth gravity field obtained from Gravity Recovery and Climate Experiment (GRACE). Hydrological excitation function (hydrological angular momentum - HAM) has been estimated from models of global hydrology, based on the observed distribution of surface water, snow, ice and soil moisture. All of them were compared with observed Geodetic Angular Momentum (GAM), excitations of polar motion. The spectra of these excitation functions of polar motion and residual geodetic excitation function G-A-O obtained from GAM by elimination of atmospheric and oceanic excitation functions were computed too. Phasor diagrams of the seasonal components of the polar motion excitation functions of all HAM excitation functions as well as of two GRACE solutions: CSR, CNES were determined and discussed.

1. ANALYSIS AND RESULTS

Hydrological angular momentum have been estimated from several models of global hydrology: NCEP/NCAR (National Centers for Environmental Prediction/National Centers for Atmospheric Research), CPC (Climate Prediction Centre), GLDAS (Global Land Assimilation Data System), NOAA (National Oceanic and Atmospheric Association). They are available in the Special Bureau of Hydrology of Global Geophysical Fluids Center (GGFC) of the International Earth Rotation and Reference Frame Service (IERS). The HAM GFZ (GeoForschungZentrum) and WGHM CRU (WaterGAP Global Hydrology Model Climate Research Unit) were delivered by personal communication.

In recent years many studies on the impact of land hydrology on the polar motion excitation were carried on (Shuanggen et al. 2010, Brzezinski et al. 2009, Chen and Wilson, 2005; Nastula et al. 2007; Seoane et al. 2009). Investigations of influence of HAM on the polar motion in different part of spectra show that consideration of the HAM data not improve agreement of the geophysical excitation of polar motion containing contributions from atmosphere, oceans and hydrology with geodetic excitation function GAM (Nastula and Kolaczek, 2005).

Since 2002 satellite GRACE (Gravity Recovery and Climate Experiment) mission has delivered precise data of time gravimetric variations and has allowed to determined mass-gravimetric polar motion excitation function. Due to the GRACE mission and in a lesser extent LAGEOS missions, the geophysical fluids mass variability can be determined from gravity field observations. The coefficients of the second degree and of the first order of the Earth gravity field are proportional to variations of equatorial components χ_1, χ_2 of the series of gravimetric excitation function of polar motion. This gravimetric function can be compared with the mass term of geodetic excitation function of polar motion. Several centers, GeoforschungZentrum (GFZ), Center for Space Research (CSR), the Jet Propulsion Laboratory (JPL), Centre National d'Etudes Spatiales /the Groupe de Recherche en Géodésie Spatiale (CNES/GRGS) computed coefficients of series of time variable gravitation and of adequate layer of water storage (Brzezinski et al. 2009, Chen and Wilson, 2005; Nastula et al. 2007; Seoane et al. 2009).

Hydrological excitation functions were computed by the following formula (Eubanks, 1993):

$$\begin{bmatrix}\chi_1^{mass}\\ \chi_2^{mass}\end{bmatrix} = -\frac{1.098R_e^2}{C-A}\iint \Delta q(\phi,\lambda,t)sin(\phi)cos(\phi)\begin{bmatrix}cos(\lambda)\\ sin(\lambda)\end{bmatrix}dS \quad (1)$$

where $\Delta q(\phi, \lambda, t)$ represents the changes in water storage in unit area (in kgm^{-2}), R_e is the Earth's mean radius, dS is the surface elements area, C and A are the Earth's principal moments of inertia.

The gravimetric excitation of polar motion was computed from harmonic coefficient of the Earth gravity field based on formula (Chen and Wilson, 2005):

$$\begin{bmatrix} \chi_1^{mass} \\ \chi_2^{mass} \end{bmatrix} = -\frac{1}{(1+k_2')\sqrt{\frac{3}{5}}\frac{C-A}{1.098R_e^2M}} \begin{bmatrix} \Delta C_{21} \\ \Delta S_{21} \end{bmatrix} \tag{2}$$

where M and R_e are the mass and mean radius of the Earth, respectively, C and A are the Earth's principal moments of inertia, is the degree-2 Love number (-0.301) accounting for elastic deformational effects on gravitational change. ΔC_{21}, ΔS_{21} are Stokes coefficients of the gravity field.

The IERS provides time series of Geodetic Angular Momentum (GAM) with one day sampling, the series are available for the period 1962-2010 from the IERS website. The geodetic excitation function is obtained from the IERS C04 series of polar motion (Bizouard, Gambis, 2007).

Comparison of the equatorial components of GRACE gravimetric excitation polar motion functions with the geodetic residuals excitation function G-A-O and hydrological ones CPC and NCEP/NCAR are shown in Fig. 1. The gravimetric excitation functions are fairly consistent with the geodetic residuals excitation function. Some compatibility of the CPC data with GRACE CNES and CSR can be seen at the Fig. 1, but only for χ_2.

Spectra of the complex-valued components of (χ=χ_1 + iχ_2) of hydrological excitation functions as well as of geodetic residuals G-A-O using Fourier Transform Band Pass Filter (FTBPF) (Kosek, 1995) in the broad band with 200 and 600 days cutoff were computed (Fig. 2). The spectra of all these considered models show oscillations with annual, semiannual and 120 day periods both in the prograde and retrograde band, but the annual oscillations are the strongest ones. It is easy to see that amplitudes of the spectra of these models are different in different models. Subtracting from geodetic excitation function GAM the impact of the atmosphere and ocean does not remove the annual and semiannual oscillations (Fig.2). Retrograde annual oscillations of the NOAA and NCEP/NCAR functions have similar amplitude to those of the geodetic residuals G-A-O. Annual oscillations of the CPC data are stronger than those of geodetic residuals G-A-O.

In order to check agreement of activity of the hydrological and gravimetric excitation functions of polar motion we computed also the prograde and retrograde components of annual and semiannual oscillations of complex polar motion excitation functions, for each hydrological excitation functions and for geodetic residuals G-A-O using LSQ method (Brzezinski, 1992, Brzezinski et al. 2009). The model comprising the second order polynomial and a sum of complex sinusoids with periods 365.25 and 180 days was computed by LSQ method. Amplitudes and phases of these oscillation are presented in terms of phasor diagrams shown in Figure 3. On the basis of phasor diagrams shown in Figure 3, can be concluded, that the hydrological excitation functions have different amplitudes and phases, furthermore, no function is close to the geodetic residuals in prograde and retrograde annual oscillations. In retrograde annual oscillations three hydrological functions have a similar phases: GFZ, CPC, NOAA, and the GFZ and CPC have similar amplitudes. Errors of phases and amplitudes, which are drawn as a circle, have different sizes. In the case of the annual prograde and annual retrograde oscillations errors are smaller than the determined vectors. But in semiannual prograde and semiannual retrograde oscillations errors for GLDAS excitation function exceeded determine vectors.

Figure 3 shows, that the phasor diagrams of the GRACE gravimetric excitation functions of polar motion computed by CNES and CSR show disagreement of amplitudes and phases of their vectors as well as of G-A-O and NCEP/NCAR, CPC vectors. In prograde annual oscillations the phase and amplitude for the vectors of GRACE excitation functions and for CPC excitation function are similar (Fig. 3). For the retrograde annual oscillation only the vector of GRACE CNES excitation function follows in the same direction as the vector of CPC excitation function.

2. CONCLUSIONS

Phasor diagrams of annual and semiannual oscillations of polar motion show that different models of HAM excitation functions differ significantly in amplitudes and phases and temporal characteristics in their spectra. None of the HAM functions do close the budget of the needed global geophysical excitation function of polar motion. The gravimetric excitation functions of polar motion based on GRACE data also do not close this budget.

Spectra of seasonal oscillations of geophysical fluids excitation functions mainly annual and semiannual are different too. The annual oscillation is the strongest one. Prograde annual and semiannual oscillations of geophysical fluids excitation functions are smaller than those of geodetic ones.

The models of land hydrology are still under development. At present it is difficult to say, which hydrological model is the best for improvement the agreement with geodetic excitation function GAM.

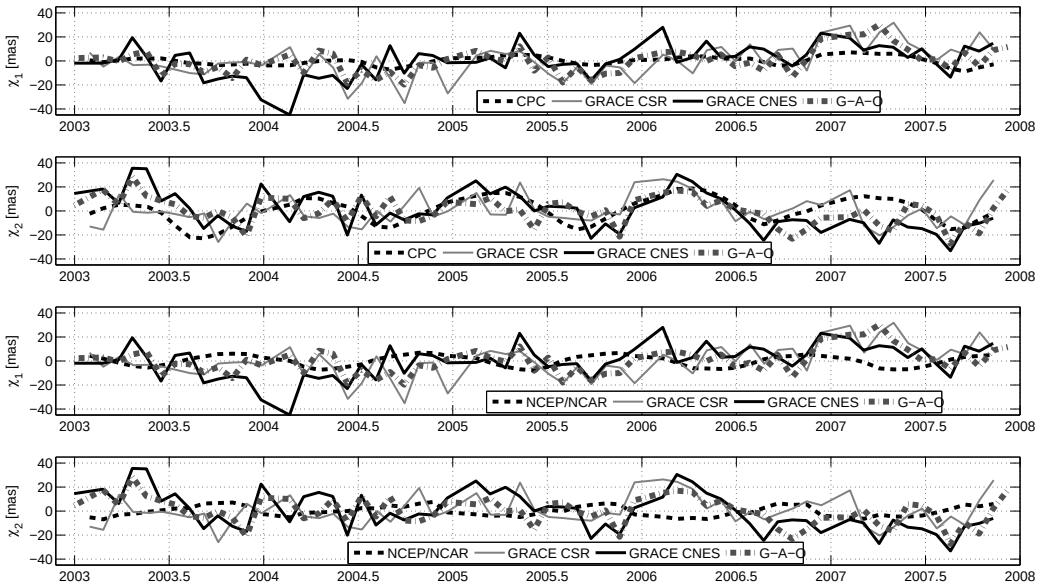

Figure 1: Comparison of χ_1, χ_2 components of: gravimetric excitation polar motion (GRACE CNES, GRACE CSR), residuals of the geodetic excitation function G-A-O and hydrological excitation functions CPC and NCEP/NCAR.

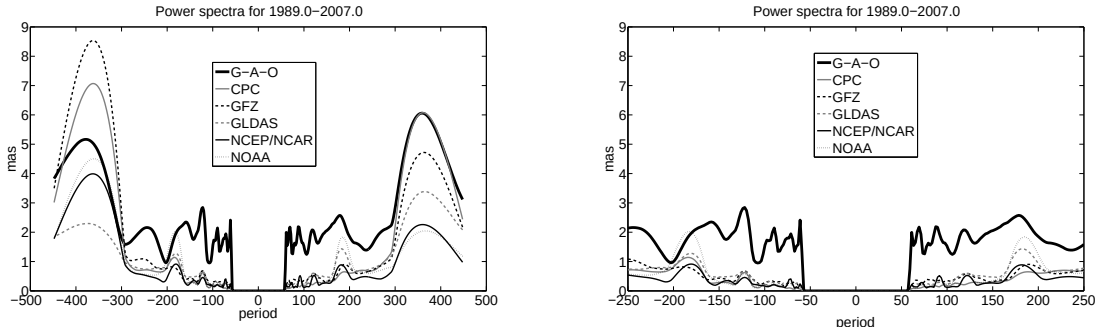

Figure 2: FTBPF amplitude spectra of the different complex geophysical excitation functions of the polar motion.

3. REFERENCES

Bizouard, C. and D. Gambis, 2007, "The combined solution C04 for Earth Orientation Parameters consistent with International Terrestrial Reference Frame 2005", Technical Note of IERS Earth Orientation Centre, http://hpiers.obspm.fr/iers/eop/eopc04 05/C04 05.guide.pdf

Brzezinski, A., 1992, "Polar motion excitation by variations of the effective angular momentum functions: considerations concerning deconvolution problem", Manuscr. Geodet, 17,3-20.

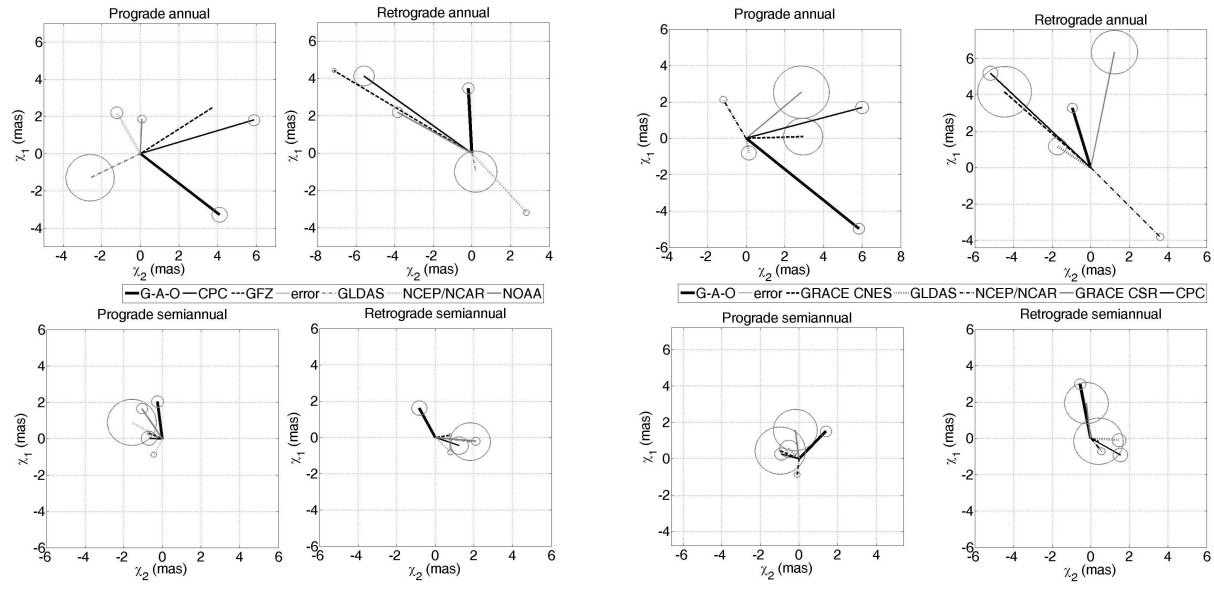

a) b)

Figure 3: Phasor diagrams of the seasonal components of the residual of the **a)** geodetic excitation function (G-A-O) and different hydrological excitation functions (CPC, GFZ, GLDAS, NCEP/NCAR, NOAA); analysis is done over the period 1989.0-2007.0 (at left) and **b)** phasor diagrams of the seasonal components of the residual of geodetic excitation function (G-A-O), gravimetric excitation functions GRACE CNES and GRACE CSR and different hydrological excitation function. Analysis is done over the period 2003.0-2008.0 (at right)

Brzezinski, A., J. Nastula, B. Kolaczek, 2009, "Seasonal excitation of polar motion estimated from recent geophysical models and observations", Journal of Geodynamics, 48, 235-240

Chen, J. L. and C. R. Wilson, 2005, "Hydrological excitation of polar motion, 1993-2002", J. Geophys. Int. 160, 833-839, doi: 10.1111/j.1365-246X.2005.02522.x

Eubanks, T. M., 1993, "Variations in the orientation of the Earth, in Contributions of Space Geodesy to Geodynamics: Earth Dynamisc", Geodyn. Ser., 24, edited by D. E. Smith and D. L. Turcotte, pp. 1-54, AGU, Washington

Kosek, W., 1995, "Time Variable Band Pass Filter Spectrum of real and complex-valued polar motion series", Artificial Satellites, Planetary Geodesy, 30, 283-299

Nastula, J. and B. Koaczek, 2005, "Analysis of Hydrological Excitation of Polar Motion, proceedings of the Workshop: Forcing of polar motion in the Chandler frequency band: a contribution to understanding interannual climate variations", Centre Européen de Géodynamique et de Seismologie, Luxembourg, 149-154.

Nastula, J., 2007, "Comparison of polar motion excitation series derived from GRACE and from analyses of geophysical fluids ", Geophysical Research Letters, 34, L11306, 6 PP., doi:10.1029/2006GL028983

Shuanggen, J., D. P. Chambers, Byyron D. Tapley, 2010, "Hydrological and oceanic effects on polar motion from GRACE and models", Journal of Geophysical Research, 115, doi:10.1029/2009JB006635

Seoane, L., J. Nastula and D. Cambis, 2009, "The use of gravimetric data from GRACE mission in the understanding of polar motion variations", Geophys. J. Int. p. L11306 10.1111/j.1365-246X.2009.04181.x.

Wilson, C. R., 1985, "Discrete polar motion equations", Geophys. J. R. Astron. Soc., 80, 551-554

WAVELET BASED COMPARISON OF HIGH FREQUENCY OSCILLATIONS IN THE GEODETIC AND FLUID EXCITATION FUNCTIONS OF POLAR MOTION

W. KOSEK[1,2], W. POPIŃSKI[1], T. NIEDZIELSKI[1,3]

[1]Space Research Centre, Polish Academy of Sciences, Warsaw, Poland
e-mail: kosek@cbk.waw.pl

[2]Environmental Engineering and Land Surveying, University of Kraków, Poland

[3]Oceanlab, University of Aberdeen, Scotland, UK

ABSTRACT. It has been already shown that short period oscillations in polar motion, with periods less than 100 days, are very chaotic and are responsible for increase in short-term prediction errors of pole coordinates data. The wavelet technique enables to compare the geodetic and fluid excitation functions in the high frequency band in many different ways, e.g. by looking at the semblance function. The wavelet-based semblance filtering enables determination the common signal in both geodetic and fluid excitation time series. In this paper the considered fluid excitation functions consist of the atmospheric, oceanic and land hydrology excitation functions from ECMWF atmospheric data produced by IERS Associated Product Centre Deutsches GeoForschungsZentrum, Potsdam. The geodetic excitation functions have been computed from the combined IERS pole coordinates data.

1. INTRODUCTION

Chaotic oscillations in Earth Orientation Parameters (EOP), driven by exchange of angular momentum between the solid Earth and geophysical fluids, are main causes of increase in their short-term prediction errors (Kosek et al. 2009; Kosek 2010). The EOP predictions are necessary for real time transformation between the terrestrial and celestial reference frames, however the prediction estimates of x, y pole coordinates and UT1-UTC data are still not satisfactory. To increase the EOP prediction accuracy the international cooperation have led to the EOPPCC (Earth Orientation Parameters Prediction Comparison Campaign) in 2005-2008 (Kalarus et al. 2010), IERS Working Group on Prediction in 2006-2009 and recently Earth Orientation Parameters Combination Prediction Pilot Project which started in October 2010. The wavelet coefficients related to translation and scale parameters, computed for any time series, describe its non-stationary character. As a result of using them, it is possible to compare two time series in time-frequency domain (Kosek 2010) and it is also feasible to filter common signals in the two time series using wavelet semblance filtering (Cooper and Cowan 2008; Cooper 2009). In this paper, the semblance function based on the wavelet transform coefficients is applied to show (1) time-frequency similarities in pole coordinates data and pole coordinates model data as well as (2) common oscillations in geodetic and fluid excitation functions which consists of the atmospheric, ocean and land hydrology excitation functions.

2. DATA

The following data sets were used in the analysis: (1) equatorial components of the effective angular momentum functions of the atmosphere (AAM), ocean (OAM) and land hydrology (HAM) from ECMWF atmospheric data produced by IERS Associated Product Centre Deutsches GeoForschungsZentrum (GFZ) Potsdam, from 1 January 1989 to 31 December 2009 (Dill 2008; Dobslaw and Thomas 2007); (2) IERS pole coordinates data x, y EOPC04_IAU2000.62-now, between 1962 and 2010 (IERS 2010).

3. COMPARISON OF POLE COORDINATES DATA AND THEIR FLUID EXCITATION FUNCTIONS

In order to show how fluid excitation functions excite polar motion, the geodetic excitation functions can be computed from pole coordinates data or the model pole coordinates data can be calculated from

fluid excitation functions. The geodetic excitation functions were computed from the IERSC04 pole coordinates data using the time domain, Wilson and Haubrich (1976), deconvolution formula, in which the Chandler period was equal to 435 days and the quality factor $Q = 100$. The pole coordinates model data were computed from the equatorial components of fluid excitation functions using the trapezoidal rule of numerical integration (Kosek et al. 2009). The fluid excitation functions consist of the AAM or the sums of AAM+OAM and AAM+OAM+HAM excitations.

A comparison of the pole coordinates data and the pole coordinates model data computed from fluid excitation functions was done using the semblance functions. The semblance function of the order r between two complex-valued time series $x(t)$ and $y(t)$ is computed by the following formula:

$$\hat{\vartheta}^r_{xy}(a) = \hat{S}_{xy}(a) cos^r(\Delta\hat{\phi}_{xy}(a))/\sqrt{\hat{S}_{xx}(a)\hat{S}_{yy}(a)} \tag{1}$$

where $\hat{S}_{xy}(a) = \sum_{b=0}^{n-1} \hat{X}(b,a)\overline{\hat{Y}(b,a)}$ is the wavelet cross-spectrum between $x(t)$ and $y(t)$ time series, $\hat{S}_{xx}(a) = \sum_{b=0}^{n-1} |\hat{X}(b,a)|^2$ and $\hat{S}_{yy}(a) = \sum_{b=0}^{n-1} |\hat{Y}(b,a)|^2$ are the wavelet spectra of $x(t)$ and $y(t)$, respectively, and

$$\Delta\hat{\phi}_{xy}(a) = arg\left[\frac{1}{n}\sum_{b=0}^{n-1}[\hat{X}(b,a)\overline{\hat{Y}(b,a)}]/[|\hat{X}(b,a)||\hat{Y}(b,a)|]\right] \tag{2}$$

is the phase synchronization function between $x(t)$ and $y(t)$ time series. The wavelet transform coefficients of $x(t)$ (or $y(t)$) are computed by the following formula:

$$\hat{X}(b,a) = \sqrt{|a|}/n \sum_{\nu=-n/2+1}^{n/2} \hat{x}(\nu)\overline{\varphi}(a2\pi\nu/n)\exp(i2\pi b\nu/n)\ , \tag{3}$$

where $a \neq 0$ and $b = 0, 1, \ldots, n-1$, are dilation and translation parameters, respectively, $\hat{x}(\nu)$ is the Discrete Fourier Transform of $x(t)$, $t = 0, 1, \ldots, n-1$, $\tilde{\varphi}(\omega)$ is the Continuous Fourier Transform of the Morlet wavelet function $\varphi(t) \approx \exp(-t^2/2)\exp(i2\pi t)/\sqrt{2\pi}$ (Goupillaud et al. 1984).

Figure 1 shows the Wavelet Transform semblance functions of the orders 0 and 3 between the considered geodetic and fluid excitation functions. The semblance functions increase when ocean excitation is added to the atmospheric one, and become still greater when the land hydrology excitation is taken into account. Moreover, adding hydrology excitation function to the sum of atmospheric and ocean terms improves the phase agreement between the geodetic and fluid excitation in the annual frequency band. This is because the semblance function of the order 3 attains higher values in the aforementioned frequency band after including land hydrology excitation.

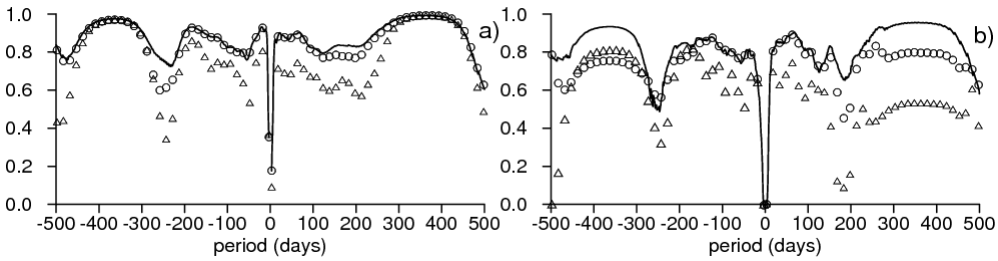

Figure 1: The semblance functions of the orders "0" a) and "3" b) between the geodetic and fluid excitation functions AAM (triangles), AAM+OAM (circles) and AAM+OAM+HAM (solid line).

4. WAVELET BASED SEMBLANCE FILTERING

The wavelet semblance function of two discrete complex-valued signals $x(t), y(t)$, $t = 0, 1, ..., n-1$, where $n = 2^p$, is defined for scale index j and translation index k as

$$\vartheta^{xy}_{j,k} = cos(\theta) = Re\big[S^x_{j,k}S^y_{j,k}/(|S^x_{j,k}||S^y_{j,k}|)\big], \tag{4}$$

where $S^x_{j,k} = \sum_{t=0}^{n-1} x(t)\overline{\varphi}_{j,k}(t)$, $S^y_{j,k} = \sum_{t=0}^{n-1} y(t)\overline{\varphi}_{j,k}(t)$ are the wavelet transform coefficients of $x(t)$, $y(t)$ time series, respectively, θ is interpreted as the angle between $S^x_{j,k}$ and $S^x_{j,k}$ in a complex plane,

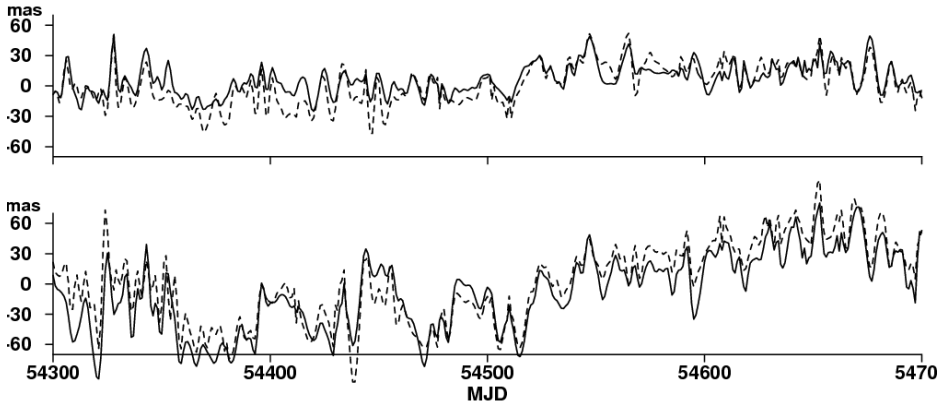

Figure 2: An example of common oscillations in the equatorial components (ψ_1/χ_1 - upper graph, ψ_2/χ_2 - lower graph) of geodetic (solid line) and fluid AAM+OAM+HAM (dashed line) excitation functions, computed using wavelet based semblance filtering with threshold value equal to 0.90.

$\varphi_{j,k}(t)$ is the discrete Shannon wavelet function (Frazier and Torres 1994). For a fixed lowest frequency index $0 \le j_o \le p-2$ and time index $k = -2^{j_o}, -2^{j_o}+1, ..., 2^{j_o}-1$, the Shannon wavelet function is given by:

$$\varphi_{j_o}(t) = exp[-i\pi(t-n/2)/n]\frac{sin[2^{j_o+1}\pi(t-n/2)/n]}{n \cdot sin[\pi(t-n/2)/n]}, \qquad \varphi_{j_o}(n/2) = 2^{j_o+1}/n, \tag{5}$$

and for higher frequency index $j = j_o+1, j_o+2, ..., p-1$, and time index $k = -2^{j-1}, -2^{j-1}+1, ..., 2^{j-1}-1$, this function is given by:

$$\varphi_j(t) = exp[-i\pi(t-n/2)/n]\frac{sin[2^j\pi(t-n/2)/n]\{2cos[2^j\pi(t-n/2)/n]-1\}}{n \cdot sin[\pi(t-n/2)/n]}, \qquad \varphi_j(n/2) = 2^j/n. \tag{6}$$

The semblance function varies in the interval $< -1, 1 >$ and detects oscillations in two time series, which are out of phase (-1) and in phase (1). Semblance filtering is performed by keeping in the reconstruction formulas of both time series $x(t) = \sum_{j=j_o}^{p-1}\sum_{k=-2^{j-1}}^{2^{j-1}-1} S^x_{j,k}\varphi_{j,k}(t)$, $y(t) = \sum_{j=j_o}^{p-1}\sum_{k=-2^{j-1}}^{2^{j-1}-1} S^x_{j,k}\varphi_{j,k}(t)$ only the wavelet transform coefficients $\widetilde{S}^x_{j,k}$, $\widetilde{S}^y_{j,k}$ for which the semblance $\vartheta^{xy}_{j,k}$ exceeds a given threshold (e.g. equal to 0.90 or 0.99). Other wavelet transform coefficients of both time series, for which the semblance is below the adopted threshold, are set to zero. The common signals in $x(t)$ and $y(t)$ are computed using the following reconstruction formulas:

$$\widetilde{x}(t) = \sum_{j=j_o}^{p-1}\sum_{k=-2^{j-1}}^{2^{j-1}-1} \widetilde{S}^x_{j,k}\varphi_{j,k}(t)\,, \qquad \widetilde{y}(t) = \sum_{j=j_o}^{p-1}\sum_{k=-2^{j-1}}^{2^{j-1}-1} \widetilde{S}^y_{j,k}\varphi_{j,k}(t). \tag{7}$$

Using semblance filtering, with the discrete Shannon wavelet functions, it is possible to filter from both time series the variations which are characterized by a good phase agreement. Such an approach enables determination of common oscillations in all possible frequency bands in two complex-valued time series. Figure 2 shows an example of the common oscillations in the geodetic and fluid excitation functions which consist of the sum of atmospheric, ocean and land hydrology excitations. The results of wavelet semblance filtering indicate that the filtered common oscillations in the geodetic and fluid excitation functions in all frequency bands behave very similarly.

Table 1 shows the correlation coefficients in 1989.0-2009.0 between the geodetic and fluid excitation functions, computed using wavelet based semblance filtering for threshold values equal to 0.00, 0.90 and 0.99. When the threshold value is equal to zero, then the excitation functions data are not filtered. It can be noticed that increase in the threshold values increases the correlation coefficients. In addition, correlation coefficients become greater when the fluid excitation function is composed of more components.

threshold	0.00		0.90		0.99	
Fluid excitation	ψ_1/χ_1	ψ_2/χ_2	ψ_1/χ_1	ψ_2/χ_2	ψ_1/χ_1	ψ_2/χ_2
AAM	0.441	0.642	0.773	0.856	0.828	0.866
AAM+OAM	0.553	0.710	0.823	0.895	0.868	0.942
AAM+OAM+HAM	0.562	0.728	0.830	0.909	0.883	0.926

Table 1: Correlation coefficients in 1989-2009 between the geodetic ψ_1, ψ_2 and fluid χ_1, χ_2 excitation functions, computed using wavelet based semblance filtering for threshold values equal to 0.0, 0.9 and 0.99.

5. CONCLUSIONS

Wavelet based techniques allow one to perform a time-frequency comparison of the geodetic and fluid excitation functions. These functions become the most similar when the fluid excitation function is composed of the atmospheric, ocean and land hydrology excitation functions. Higher order semblance function reveals that addition of hydrology angular momentum to the sum of atmospheric and oceanic ones improves the phase agreement between the geodetic and fluid excitation functions in the annual frequency band. The common oscillations in the geodetic and fluid excitation functions can be detected using wavelet based semblance filtering. Increase in the threshold value in the semblance filtering of the geodetic and fluid excitation functions increases the correlation coefficients values between filtered common oscillations.

Acknowledgements. The research was supported by Polish Ministry of Science and Higher Education, grant no. N N526 160136 under leadership of Dr Tomasz Niedzielski. Attendance of W. Kosek and T. Niedzielski at the Journées 2010 in Paris was supported by the conference grant.

6. REFERENCES

Cooper G.R.J. and D.R. Cowan 2008, Comparing time series using wavelet-based semblance analysis, Computers and Geosciences 34, 95–102.

Cooper G.R.J. 2009, Wavelet based semblance filtering, Computers and Geosciences 35, 1988–1991.

Dill R. 2008, Hydrological model LSDM for operational Earth rotation and gravity field variations. Scientific Technical Report STR08/09, GFZ, Potsdam, Germany, 35p.

Dobslaw H., Thomas M. 2007, Simulation and observation of global ocean mass anomalies. J. Geophys. Res., 112, C05040, doi:10.1029/2006JC004035.

Frazier M. and Torres R. 1994, The sampling theorem, S-transform, and Shannon wavelets for R, Z, T and Z_N, in Benedetto J.J., Frazier M.W., (eds.), Wavelets - Mathematics and Applications, CRC Press, Boca Raton, 221–245.

Goupillaud P., Grossman A., and Morlet J. 1984, Cycle-Octave and Related Transforms in Seismic Signal Analysis. Geoexploration, 23: 85–102.

IERS 2010, http://hpiers.obspm.fr/iers/eop/eopc04_05/.

Kalarus M., H. Schuh, W. Kosek, O. Akyilmaz, Ch. Bizouard, D. Gambis, R. Gross, B. Jovanovic, S. Kumakshev, H. Kutterer, L. Ma, P. J. Mendes Cerveira, S. Pasynok, L. Zotov 2010, Achievements of the Earth Orientation Parameters Prediction Comparison Campaign, Journal of Geodesy 84: DOI: 10.1007/s00190-010-0387-1, 587–596.

Kosek, W., Rzeszótko A., Popiński W. 2009, Contribution of wide-band oscillations excited by the fluid excitation functions to the prediction errors of the pole coordinates data., Proc. Journées 2008 "Systèmes de référence spatio-temporels" and X. Lohrmann-Kolloquium, M Soffel and N. Capitaine (eds.). Lohrmann–Observatorium Technische Universitat Dresden, Germany and Observatoire de Paris Systèmes de Référence Temps-Espace UMR8630/CNRS, Paris, FRANCE, 168–171.

Kosek W. 2010, Causes of prediction errors of pole coordinates data, Proc. the 6th Orlov's Conference, "The study of the Earth as a planet by methods of geophysics, geodesy and astronomy ", June 22-24, 2009, MAO NAS of Ukraine, Kiev, Ukraine. (ed. Ya. Yatskiv) 96–103.

Wilson C.R. and Haubrich R.A. 1976, Geophys. J. R. Astron. Soc. 46, 707–743.

COMPARISON OF CPO AND FCN EMPIRICAL MODELS

Z.M. MALKIN
Central Astronomical Observatory at Pulkovo of RAS
Pulkovskoe Ch. 65, St. Petersburg 196140, Russia
e-mail: malkin@gao.spb.ru

ABSTRACT. In this presentation, several publicly available empiric models of the celestial pole offset (CPO) and free core nutation (FCN), included those developed by the author, are investigated and compared each other from different points of view, such as representation of the observation data, FCN parameters variation, prediction accuracy. Based on this study, some practical recommendations are proposed.

1. INTRODUCTION

The motion of the celestial pole (CP) is one of the principal constituents of the Earth rotation, and its accurate modelling is needed for many applications. However, even the most accurate modern theory IAU2003/2006 provides the accuracy of the CP position at a level of about 0.5 mas, which is not sufficient for many practical tasks. CPO includes free core nutation (FCN) oscillation with period of about 430 days, other periodic and quasi-periodic terms, and trends. This complicated CPO structure can be clearly seen in Fig 1, where the differences between the CP coordinates observed by very long baseline interferometry (VLBI) and the IAU model are shown. For VLBI, the IVS (International VLBI Service for Geodesy and Astrometry) combined solution was used (Böckmann et al. 2010).

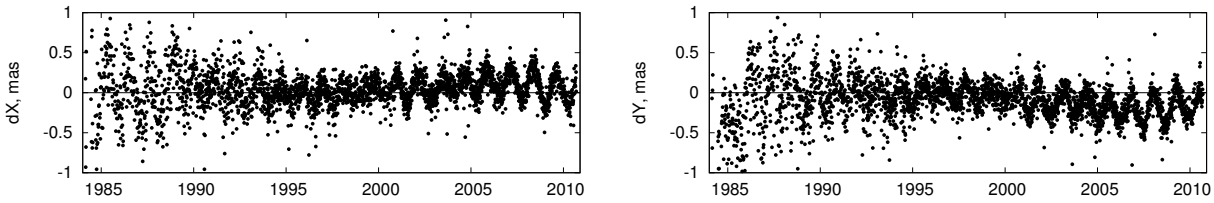

Figure 1: IVS combined CPO solution.

The FCN is often thought to be the largest component of the CPO. However, one can see that both FCN signal and sum of other CPO components are of similar value of about 0.2–0.3 mas in our days. Thus the FCN is only a part of the CPO, even not prevailing, but sometimes they are mixed in practical use, e.g. it seems to be the case for the IERS Conventions (McCarthy & Petit 2004) that recommends using an FCN model for accurate coordinate transformation between celestial and terrestrial reference systems.

It seems reasonable and practical to use FCN models for geophysical studies, such as core-mantle coupling or inner Earth's rheological structure, and use CPO models for applications related to astronomy, in particular for coordinate transformation between terrestrial and celestial systems.

2. CPO AND FCN MODELS COMPARISON

In practice, three CPO and two FCN models are available for user's choice:
— OPA/IERS C04 CPO series (IERS AR 2007, ftp://hpiers.obspm.fr/iers/eop/eopc04_05/)
— NEOS/IERS CPO series (IERS AR 2007, ftp://maia.usno.navy.mil/ser7/)
— Pulkovo ZM2 CPO series (Malkin 2007, http://www.gao.spb.ru/english/as/persac/index.htm)
— OPA/IERS SL FCN series (Lambert 2009, http://syrte.obspm.fr/ lambert/fcn/)
— Pulkovo ZM1 FCN series (Malkin 2007, http://www.gao.spb.ru/english/as/persac/index.htm)

In fact, only the SL model has a parametric representation, others are given in the form of dX and dY time series. However, we refer to them also as models, non-parametric though, because they are a result of data processing as well.

Also, two other FCN models are known: MHB (Herring et al. 2002) and GVS (Gubanov 2010). However, the MHB model is not supported anymore, and, in fact, is replaced by the SL model constructed in a way close to MHB. The GVS model is not publicly available in parametric or time series form either. So, these models were not used in this study.

All the CPO and FCN models are results of approximation of CPO time series observed by VLBI. IERS C04 CPO solution is a combination of almost all VLBI series available including both individual solutions from IVS Analysis Centers and IVS combined solution (IERS AR 2007). In turn, C04 series is used to evaluate SL model (Lambert 2009). NEOS CPO series is constructed using several selected VLBI series (IERS AR 2007). ZM2 series is constructed using combining IVS CPO series (Malkin 2007).

One of the most important application of CPO in space geodesy is its use in coordinate transformation between terrestrial and celestial frames. In principle, only full CPO models C04, NEOS and ZM2 should be compared from this point of view. However, we also include SL model in this analysis because in is recommended by IERS as a replacement for CPO (McCarthy & Petit 2004). Figure 2 shows the representation of the actual CP motion as observed by VLBI and all four models for 2010.

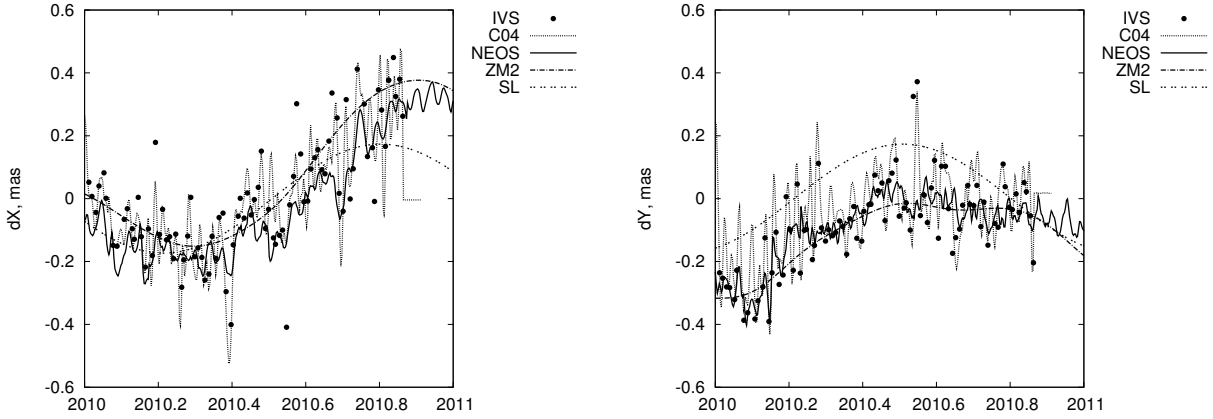

Figure 2: IVS combined CPO solutions and models.

Some features of compared models are clearly visible in the plots. SL model shows substantial bias wit respect to VLBI data and other models, which directly follows from the method of construction of this model. C04 models evidently includes high frequency components, may be not corresponding to the actual CP movement; this model also does not include prediction, which makes is unsuitable for near real-time data processing. NEOS model is much closer to IVS series but sometimes is biased, which can be explained by using of different time series. ZM2 shows the best representation of the IVS combined solution, which we consider as the IERS standard for dX and dY data.

As mentioned above, FCN observations and modelling allows us to gain knowledge of properties of the inner Earth. In particular, important conclusions can be derived from the FCN amplitude and phase variations. As was shown previously (Malkin 2007) MHB, SL, and ZM1 models show similar behavior of the FCN amplitude and phase. Updated results for SL and ZM1 models are depicted in Fig 3. One can see from this comparison that both models reveal very similar variations in the FCN amplitude and phase, except the amplitude in the beginning of the interval, where VLBI results have relatively low accuracy as it can be seen in Fig. 1. As to the phase variations, SL model provides better time resolution and cover longer time interval including prediction. Similar results were obtained for the GVS model (Gubanov 2010). It can be mentioned here that the method used for construction of the ZM1 model allows one to compute the FCN series with any desirable time resolution just adjusting the wavelet parameter (Malkin 2007). Detailed discussion on physical reasons of observed phase and amplitude changes is beyond of the scope of this paper. For example, one of interesting observation is correlation between the FCN phase jumps and geomagnetic jerks (Shirai et al. 2005)

Since VLBI CPO results are available with delay 1-2 weeks for rapid EOP sessions, CPO prediction is needed for applications requiring real-time and forecast CPO values. Prediction accuracy of different CPO models was assessed in (Malkin 2010), and result is shown in Fig. 4

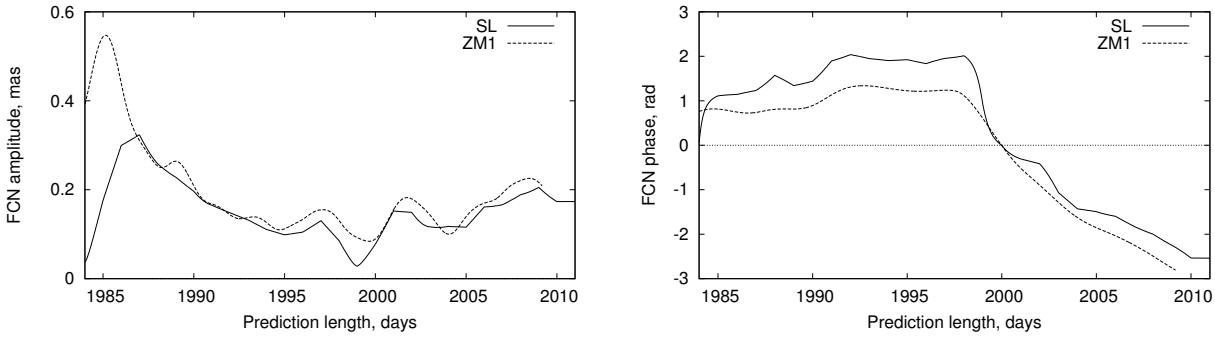

Figure 3: FCN amplitude and phase variations.

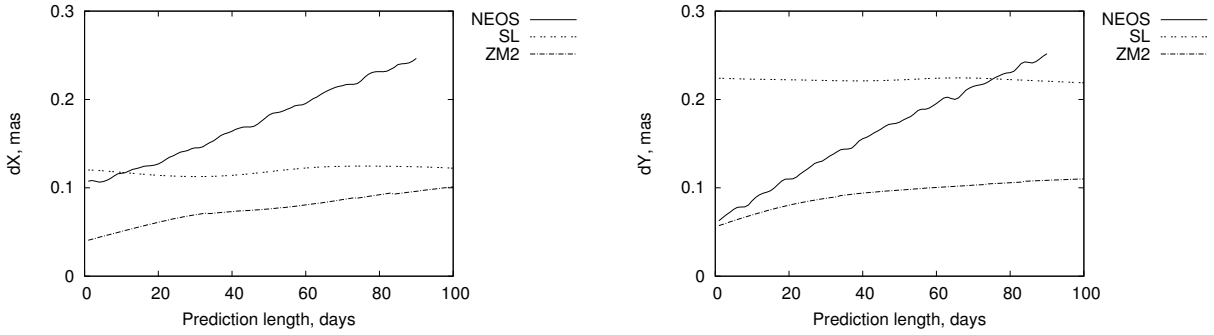

Figure 4: CPO prediction errors, see (Malkin 2010) for details.

A practical impact of different CPO modelling on UT1 estimates obtained from VLBI Intensives series. These observations are performed on restricted network of 2-3 stations during short session duration In Fig. 5, differences are shown between UT1 estimates obtained with given CPO model and without CPO modelling (zero model). As shown above, in our days, FCN contribution to CPO is at a level of 50-60%. In correspondence with this fact, UT1 estimates obtained with SL (FCN) model lie between UT1 estimates obtained with NEOS and ZM2 (CPO) and with zero models.

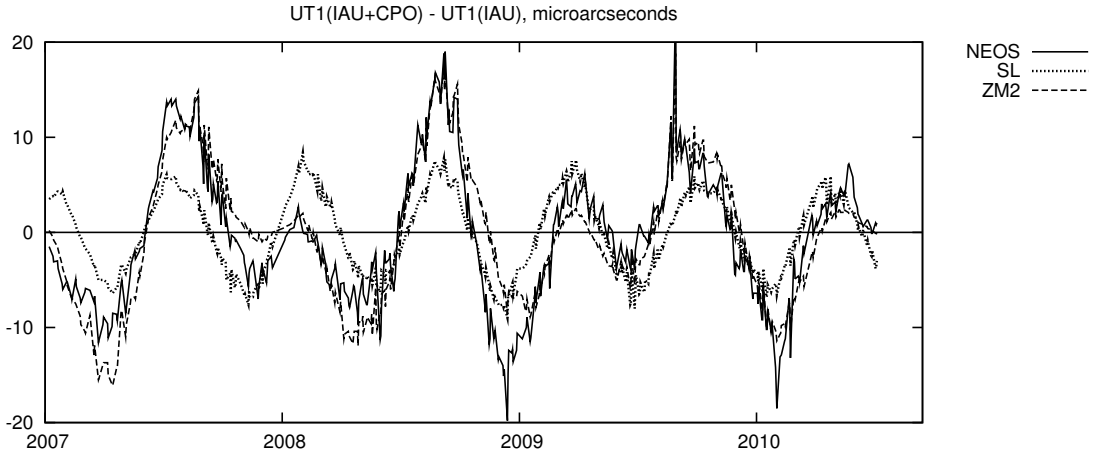

Figure 5: Results of UT1 Intensives processing with different CPO models.

3. CONCLUSIONS

Modelling of the CPO is necessary for highly accurate applications in astronomy, geodesy, navigation and other fields, particularly required transformation between terrestrial and celestial coordinate systems with accuracy better than several tenths of milliarcsecond. Currently, several CPO and FCN models are available, and all of them are used by different users. Some of them are the FCN models, which represent only a part of the CPO impact on the CP motion. These models have been compared in this work.

The FCN models are most suitable for geophysical studies. Two models compared here, ZM1 developed in the Pulkovo observatory and SL developed in the Paris observatory show similar FCN amplitude and phase variations, and hence they are nearly equivalent from this point if view. However, it is not the case for CPO modelling. Using different models for space geodesy data processing can lead to substantial biases and systematic differences in results, as was shown, for example, for VLBI UT1 Intensives.

Unfortunately, there is no generally accepted option to account for the CPO in various applications, in particular in space geodesy data processing. The SL model recommended by the IERS Conventions (McCarthy & Petit 2004) is not an CPO model and can compensate only about a half of the full effect. It seems advisable that IERS consider another model more close to the actual CIP motion to recommend it in the Conventions. A new model should also provide accurate CPO prediction for several weeks.

The simplest way to eliminate the main deficiencies of the IERS (SL) model would be to include bias removed during the model construction (Lambert 2009). However, it still is perhaps too smoothed. Besides it is updated only once a year (Lambert, personal communication).

NEOS model show much better approximation of the VLBI data, but has poor prediction (Malkin 2010).

The ZM2 model seems to be preferable as providing the best approximation of the VLBI results and CPO prediction.

Acknowledgements. The author is grateful to the organizers of the conference for the travel support.

4. REFERENCES

Böckmann, S., Artz, T., Nothnagel, A., Tesmer, V. International VLBI Service for Geodesy and Astrometry: Earth orientation parameter combination methodology and quality of the combined products. 2010, J. Geophys. Res., 115(B4), B04404.

Gubanov, V.S., 2010, "New estimates of retrograde free core nutation parameters", Astron. Letters, 36(6), pp. 444–451.

Herring, T.A., Mathews, P.M., Buffett, B.A., 2002, "Modelling of nutation-precession: Very long baseline interferometry results", J. Geophys. Res., 107(B4), pp. 2069–2080.

IERS Annual Report 2007, 2009, Verlag des Bundesamts für Kartographie und Geodäsie, Frankfurt am Main.

Lambert, S.B., 2009, "Empirical Model of the Free Core Nutation (Technical Note)", http://syrte.obspm.fr/∼lambert/fcn/notice.pdf

Malkin, Z.M., 2007, "Empiric Models of the Earth's Free Core Nutation", Solar System Research, 41(6), pp. 492–497.

Malkin, Z.M., 2010, "Analysis of the Accuracy of Prediction of the Celestial Pole Motion", Astronomy Reports, 54(11), pp. 1053-1061.

McCarthy, D.D., Petit, G. (eds), 2004, "IERS Conventions (2003)", IERS Technical Note 32, Verlag des Bundesamts für Kartographie und Geodäsie, Frankfurt am Main.

Shirai, T., Fukushima, T., Malkin Z., 2005, "Detection of phase disturbances of free core nutation of the Earth and their concurrence with geomagnetic jerks", Earth Planets Space, 57(2), pp. 151–155.

IMPACTS OF THE 2010 CHILE EARTHQUAKE ON EARTH ROTATION

T. NILSSON, J. BÖHM, H. SCHUH
Vienna University of Technology, Institute of Geodesy and Geophysics
Gußhausstraße 27-29, 1040 Vienna, Austria
e-mail: tobias.nilsson@tuwien.ac.at

ABSTRACT. We investigate the impact of the 2010 Chile Earthquake on the geometry and rotation of the Earth. We find that the Earthquake moved the city Concepción 310 cm towards West and 65 cm towards South. The Earthquake should also have increased the length of day by 0.3–0.5 μs and moved the figure axis of the Earth by 2.5–3 mas, however these changes are too small to be confirmed by measurements.

1. INTRODUCTION

The impact of Earthquakes on the rotation of the Earth has been a topic of research since the 1960's (Mansinha and Smylie, 1967, Dahlen, 1971, 1973, Chao and Gross, 1987, Gross and Chao, 2006). Theoretically, an Earthquake should change both the rotation speed of the Earth and the figure axis. However, the effect has still not been observed. The reason is that the change in Earth rotation caused by an Earthquake is usually very small. Only very strong Earthquakes (magnitude $\gtrsim$9) can cause changes in the Earth rotation large enough to get be observed with current space geodetic techniques.

On February 27, 2010, at 06:34 UTC a magnitude 8.8 Earthquake occurred in Chile about 155 km NNE of the city Concepción. This has been the strongest Earthquake in recent years. In this work we investigate the displacements and changes in Earth rotation due to this Earthquake.

2. DISPLACEMENT OF TIGO CONCEPCION

In Concepción there is a VLBI (Very Long Baseline Interferometry) radio telescope, TIGO, which regularly participates in IVS (International VLBI Service for Geodesy and Astrometry, Schlüter and Behrend (2007)) geodetic VLBI sessions. It survived the Earthquake relatively well and was able to start observing again about 2.5 weeks after the Earthquake. Sessions with TIGO before and after the Earthquake were analysed with the Vienna VLBI software (VieVS) (Böhm et al., 2010) in order to determine how much this station was moved by the Earthquake. The results can be seen in figure 1. As comparison, the results from GPS are shown, obtained from the IGS (International GNSS Service, Dow et al. (2009)) weekly solutions. We can see that TIGO was moved about 310 cm to the West, 65 cm to the South, and about 4–5 cm downwards. The results from VLBI and GPS are in good agreement.

3. EFFECT ON EARTH ROTATION

An Earthquake causes displacements of masses inside the Earth, i.e. the moment of inertia will change. Thus, due to the conservation of angular momentum, the rotation of the Earth will also change. The change in the pole coordinates ($p = p_x - i\,p_y$) can be calculated using the Euler-Liouville equation:

$$p(t) + \frac{i}{\sigma_{ch}}\frac{dp}{dt} = \chi(t) \tag{1}$$

where σ_{ch} is the frequency of the Chandler Wobble and $\chi = \chi_x + i\,\chi_y$ is the polar motion excitation function. The change in χ due to an Earthquake, $\Delta\chi$, is related to the change in the moment of inertia, ΔI, by (Gross and Chao, 2006):

$$\Delta\chi = \frac{1.61}{C - A}\Delta I \tag{2}$$

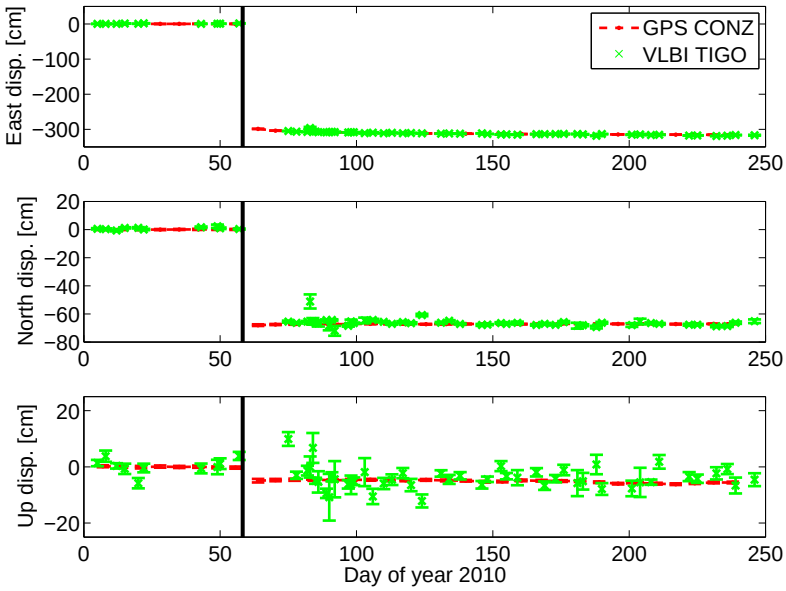

Figure 1: Displacement of Concepción measured by GPS (red) and VLBI (green).

	LOD [μs]	χ_x [mas]	χ_y [mas]
Global CMT	0.3	-0.1	2.5
USGS	0.5	-0.4	2.8

Table 1: Predicted changes in the Length of Day (LOD) and polar motion excitations (χ) due to the 2010 Chile Earthquake

where C and A are the axial and equatorial moment of inertia, and $\Delta I = \Delta I_{xz} + i\,\Delta I_{yz}$. Assuming that the change in the moment of inertia can be described by a step function, it can be shown that the change in p is:

$$\Delta p(t) = \frac{1.61 \Delta I}{C - A} \left[1 - e^{i\sigma_{ch}(t-t_0)}\right] \tag{3}$$

where t_0 is the time epoch of the Earthquake. We can easily see from this equation that the effect of the Earthquake is a change in the mean position of the pole (the figure axis) and in the amplitude of the Chandler Wobble. The instantaneous change in the pole coordinates ($\Delta p(t_0)$) will however be almost zero. Thus, when trying to detect the impact of the Earthquake on the Earth rotation, we should investigate the polar motion excitation function rather than the polar motion directly.

Similarly the change in Length of Day (LOD), $\Delta\Lambda$, can be related to the change in the axial moment of inertia, ΔI_{zz}, through (Gross and Chao, 2006):

$$\Delta\Lambda = \frac{\Lambda_0}{C_m} \Delta I_{zz} \tag{4}$$

where Λ_0 is the nominal LOD (86400 s) and C_m is the axial moment of inertia of the crust and the mantle.

In order to calculate $\Delta\chi$ and $\Delta\Lambda_0$ we need to know the change in the moment of inertia of the Earth. Using elastic dislocation theory, Dahlen (1971, 1973) presented a model for this change expressing it as a function of the Earthquake location (latitude θ, longitude ℓ, and depth h), and seismic parameters for the Earthquake (seismic moment M_0, strike angle α, dip angle δ, and rake angle λ):

$$\Delta I_{jz} = M_0 \sum_{k=1}^{3} \Gamma_k(h) g_{jk}(\theta, \ell, \alpha, \delta, \lambda) \tag{5}$$

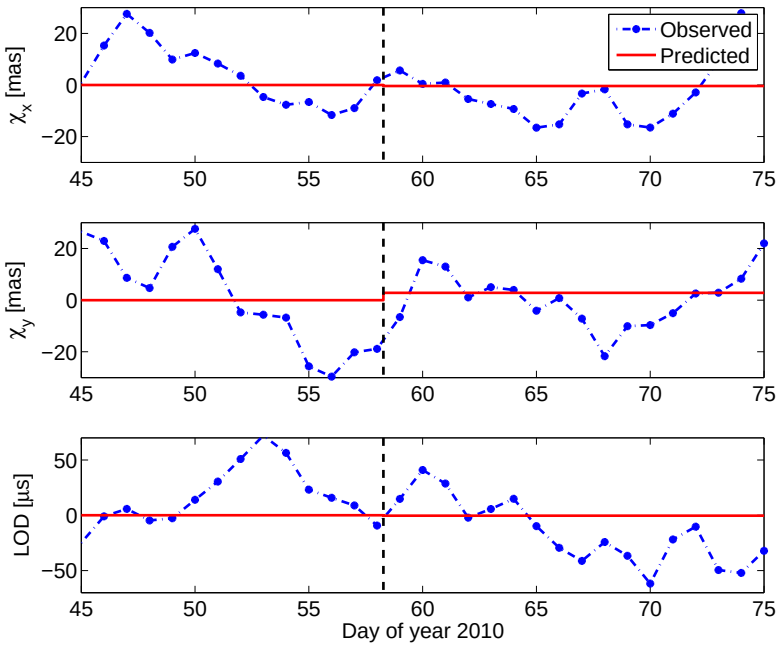

Figure 2: Polar motion excitation functions and Length of Day (LOD) observed around the time of the 2010 Chile Earthquake. From the time series the excitations due to the atmosphere, oceans and hydrology have been removed (see text). The red lines show the predicted changes due to the Earthquake (from table 1).

For explicit expressions of the functions Γ and g, see Dahlen (1973) or Lambeck (1980).

Table 1 gives the predicted changes in the polar motion excitation functions and in the LOD caused by the 2010 Chile Earthquake. The seismic parameters for the Earthquake were obtained from two sources: the Global CMT (Centroid Moment Tensor) Catalogue (`http://www.globalcmt.org/`) and from the USGS (US Geological Survey) CMT solution (`http://earthquake.usgs.gov/`). As seen the predictions obtained using the two CMT solutions agree relatively well.

4. CAN THE EFFECT BE OBSERVED?

There are mainly two problems with observing the change in Earth rotation caused by the Earthquake. The first problem is that the accuracy of the Earth rotation measurements is limited. Currently, space geodetic techniques like VLBI and GPS can measure LOD with and accuracy of 5–10 μs and polar motion excitation functions with an accuracy of about 5 mas (Gross and Chao, 2006), i.e. the predicted changes (table 1) are smaller than the measurement accuracies. The other problem is that there are processes in e.g. the atmosphere and the oceans causing variations in Earth rotation which are much larger than the predicted change due to the Earthquake. For example, variations caused by the atmosphere over one day can be 100 μs in LOD and several tens of mas in the polar motion excitation functions. Clearly, these variations need to be modelled very precisely in order to have any chance to detect the change caused by the Earthquake.

We calculated the LOD and the polar motion excitation functions from the IERS 05 C04 series (Bizouard and Gambis, 2009) for the time period around the 2010 Chile Earthquake. From the time series, we removed the excitations due to the atmosphere, oceans, and hydrology (obtained from `ftp://ftp.gfz-potsdam.de/home/ig/ops/`, Dobslaw et al. (2010)). From the LOD time series we also removed the variations caused by zonal Earth tides (Defraigne and Smits, 1999). The resulting time series are shown in figure 2. We see that the variations from day to day are still much larger than the predicted changes due to the Earthquake. Thus, we are not able to confirm the predicted changes in Earth rotation.

5. CONCLUSIONS

The 2010 Chile Earthquake caused the city of Concepción to move about 310 cm to the West and 65 cm to the South. The Earthquake should also have had an effect on the rotation of the Earth, the LOD should have increased by 0.3-0.5 μs and the polar motion should have changed by 2.5–3 mas (mostly in the y-component). This change currently cannot be confirmed by measurements, the measurement accuracies are too low and all other excitations (due to atmosphere, oceans, hydrology, and other sources) are currently not known with high enough accuracy. For the effect of an Earthquake on Earth rotation to be observable by current techniques, the Earthquake would need to be much stronger than the 2010 Chile Earthquake. For example, the 1960 Chile Earthquake (magnitude 9.5) is predicted to have changed polar motion excitation functions by over 20 mas (Chao and Gross, 1987), and this would most likely be possible to observe if such an Earthquake would happen today.

Acknowledgements. This research was supported by the Deutsche Forschungsgemeinschaft (DFG), project (project SCHUH 1103/3-1).

6. REFERENCES

Bizouard, C., Gambis, D., 2009 "The combined solution C04 for Earth orientation parameters consistent with international terrestial reference frame 2005", In "Geodetic Reference Frames", volume 134 of IAG Symposium, Munich, Germany, Springer, pp. 265–270, doi: 10.1007/978-3-642-00860-3_41.

Böhm, J., Böhm, S., Nilsson, T., Pany, A., Plank, L., Spicakova, H., Teke, K., Schuh, H., 2010, "The new Vienna VLBI software", In IAG Scientific Assembly 2009, Buenos Aires, Argentina, Springer, in press.

Chao, B. F., Gross, R. S., 1987, "Changes in the Earth's rotation and low-degree gravitational field induced by earthquakes", Geophys. J. R. Astr. Soc., 91, pp. 569–596.

Dahlen, F. A., 1971, "The excitation of the Chandler wobble by Earthquakes", Geophys. J. R. Astr. Soc., 25, pp. 157–206.

Dahlen, F. A., 1973 "A correction to the excitation of the Chandler wobble by Earthquakes", Geophys. J. R. Astr. Soc., 32, pp. 203–217.

Defraigne, P., Smits, I., 1999, "Length of day variations due to zonal tides for an elastic Earth in non-hydrostatic equilibrium", Geophys. J. Int., 139, pp. 563–572, doi: 10.1046/j.1365-246x.1999.00966.x.

Dobslaw, H., Dill, R., Grötzsch, A., Brzeziński, A., Thomas, M., 2010, "Seasonal polar motion excitation from numerical models of atmosphere, ocean, and continental hydrosphere", J. Geophys. Res., 115(B10406), doi: 10.1029/2009JB007127.

Dow, J. M., Neilan, R. E., Rizos, C., 2009, "The international GNSS service in a changing landscape of global navigation satellite systems", J. Geodesy, 83, pp. 191–198, doi: 10.1007/s00190-008-0300-3.

Gross, R. S., Chao, B. F., 2006, "The rotational and gravitational signature of the December 26, 2004 Sumatran earthquake", Surv. Geophys., 27, pp. 615–632, doi: 10.1007/s10712-006-9008-1.

Lambeck, K., 1980, "The Earth's Variable Rotation: Geophysical Causes and Consequences", Cambridge Univ. Press, Cambridge, UK.

Mansinha, L., Smylie, D. E., 1967, "Effect of Earthquakes on the Chandler wobble and the secular polar shift", J. Geophys. Res., 72(18), pp. 4731–4743, doi: 10.1029/JZ072i018p04731.

Schlüter, W., Behrend, D., 2007, "The International VLBI Service for Geodesy and Astrometry (IVS): current capabilities and future prospects", J. Geodesy, 81(6-8), pp. 379–387, doi: 10.1007/s00190-006-0131-z.

HIGH-RESOLUTION ATMOSPHERIC ANGULAR MOMENTUM FUNCTIONS FROM DIFFERENT ECMWF DATA CLASSES

M. SCHINDELEGGER[1], J. BÖHM[1], H. SCHUH[1], D.A. SALSTEIN[2]

[1] Institute of Geodesy and Geophysics, Vienna University of Technology
27-29 Gußhausstraße, A-1040 Wien, Austria
e-mail: michael.schindelegger@tuwien.ac.at, johannes.boehm@tuwien.ac.at, harald.schuh@tuwien.ac.at

[2] Atmospheric and Environmental Research, Inc.
131, Hartwell Avenue, Lexington, MA 02421-3126, USA
e-mail: salstein@aer.com

ABSTRACT. Atmospheric excitation of Earth rotation at daily and sub-daily periods is routinely inferred from six-hourly atmospheric angular momentum (AAM) functions, which are derived from the operational analysis fields of Numerical Weather Models. The so-called *delayed cut-off stream*, recently introduced by the European Centre for Medium-Range Weather Forecasts (ECMWF), though, produces meteorological data with higher temporal resolution by incorporating short-term forecasts, and thus allows the estimation of three-hourly AAM functions. In detail, we determine six- and three-hourly AAM functions for a time span of five years. Comparisons of the two series reveal differences in amplitude and phase, but also highlight the counteraction of pressure and wind terms at short time scales. Moreover, the three-hourly AAM record represents an opportunity to resolve better the semi-diurnal band of atmosphere-induced variations in polar motion and LOD.

1. INTRODUCTION

By exchanging angular momentum with the solid part of the Earth, large-scale atmospheric processes account for major variations of all Earth Orientation Parameters (EOP), which are precession, nutation, polar motion and changes in length of day (LOD). The atmospheric influence on these parameters is usually studied by employing the angular momentum approach, requiring calculation of the so-called atmospheric angular momentum (AAM) functions from globally gridded meteorological data. The resulting excitation values agree well with the observed EOP variations on time scales of a few days or longer, e.g. Barnes et al. (1983) or Salstein et al. (1993). At daily and sub-daily periods, the AAM functions explain only a fraction of the measured changes in Earth rotation, see Brzeziński and Petrov (2000). However, these high-frequency effects, mainly originating from diurnal and semi-diurnal radiational tides in the atmosphere, are non-negligible, especially in the nutation band (Bizouard et al., 1998).

The aim of this study is to estimate and compare such high-frequency contributions of the atmosphere to EOP variations based on two different meteorological analyses of the European Centre for Medium-Range Weather Forecasts (ECMWF), see Section 2. Since a new, three-hourly AAM dataset is introduced, we seek to complement the recent estimates for atmospheric tides, which, up to now, have been all based on six-hourly analysis fields.

2. DATA DESCRIPTION

The AAM functions used in this study are inferred from two different sets of meteorological data, which are both provided by the ECMWF. The first set comprises data at six-hourly intervals (0, 6, 12, 18 UTC) and is retrieved from the standard analysis, available in the *Atmospheric model* archive. The second set stems from the re-organized ECMWF assimilation system, the so-called *Atmospheric model (delayed cut-off)* analysis, which became operational on 29 June 2004. The cut-off time represents the latest possible arrival time for meteorological observations to be included in an analysis cycle. By combining several analysis cycles and short-term forecasts, it is possible for the ECMWF to delay the cut-off time and achieve a higher temporal resolution of three hours. Both six- and three-hourly analysis

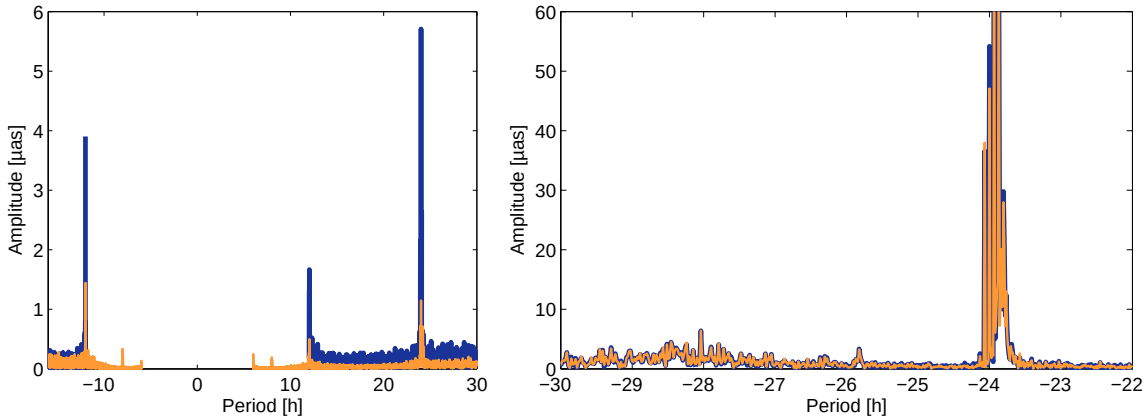

Figure 1: Amplitude spectra of atmosphere-induced variations of polar motion (left figure) and nutation (expressed as motion in the terrestrial reference frame, right figure) calculated from six-hourly AAM functions (*blue line*) and three-hourly AAM functions (*orange line*).

fields, given as 1° by 1° horizontal grids on 21 isobaric levels, are processed for the time span 1 July 2004 to 30 June 2009, yielding two sets of five-year AAM matter and motion time series.

3. ATMOSPHERIC EXCITATION OF EARTH ROTATION

The atmospheric contribution to precession, nutation, polar motion, and changes in LOD can be determined in a similar way for both AAM datasets. Dimensionless AAM functions are calculated from pressure and wind fields, and are subsequently convolved with the corresponding axial and equatorial transfer functions (Brzeziński et al., 2002). The equatorial transfer function comprises the Chandler Wobble and the Free Core Nutation resonance. The resulting amplitude spectra in Figures 1 (left part) and 2 illustrate the daily and sub-daily atmospheric effects in polar motion and LOD, showing that

- the six-hourly AAM functions do not allow resolution of bandwith with higher frequency than semi-diurnal,
- due to the prograde wind term, the six-hourly spectrum contains a lot of noise and
- the three-hourly amplitude estimates are of a significantly lower magnitude level than their six-hourly counterparts.

There is considerably better agreement in the nutation band, which is depicted in Figure 1 (right part).

For all three types of EOP it is of interest to distinguish the specific atmospheric tides in the excitation spectra. The set of $\{\Pi_1, P_1, S_1, K_1, \Psi_1, \Phi_1, T_2, S_2, R_2\}$ comprises the most prominent diurnal and semi-diurnal tides, which can be detected at their corresponding periods, for example in polar motion at $T = -12$ h or in nutation at $T = -24$ h (Figure 3). Naturally, the AAM series sampled at three-hourly intervals are superior in the semi-diurnal band, revealing S_2 plus its side-lobes. This detection is rather qualitative and can be replaced by a simple least squares adjustment of amplitude and phase at each tidal frequency. For this purpose, the axial excitation

$$l(t) = \sum_{j=1}^{9} a_j \cos(\omega_j t) + b_j \sin(\omega_j t) \tag{1}$$

is modeled as harmonic series containing the nine tides with unknown coefficients $\{a_j, b_j\}$ and the given frequencies ω_j with $j = 1, ..., 9$. The coefficients determine amplitude and phase of each tidal wave. Similar to Equation 1, $\{a_j, b_j\}$ are estimated separately for the real and imaginary parts of the equatorial excitation. This procedure yields real pro- and retrograde as well as imaginary pro- and retrograde amplitudes, which can be converted to pro- and retrograde phase and mean amplitude of every single tidal wave. The resulting mean amplitudes for the three-hourly AAM functions are summarized in Table 1.

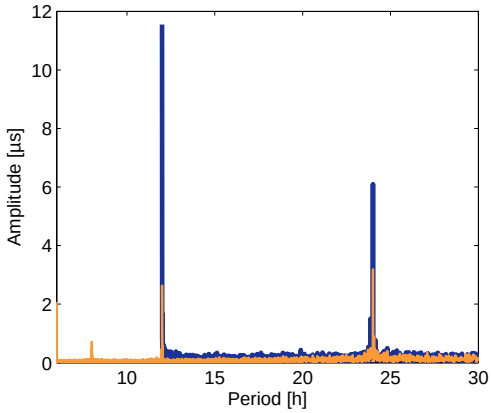

Figure 2: Amplitude spectrum of high-frequency LOD from six-hourly AAM functions (*blue line*) and three-hourly AAM functions (*orange line*).

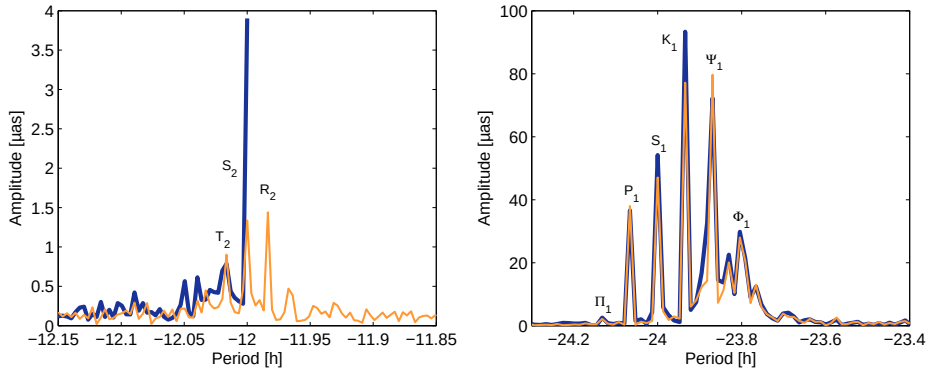

Figure 3: Amplitude spectra of polar motion (left figure) and nutation (right figure) calculated from six-hourly AAM functions (*blue line*) and three-hourly AAM functions (*orange line*).

As already indicated in Figures 1 and 2, the three-hourly amplitude estimates suggest very small atmospheric contributions to high-frequency EOP. The obtained values appear to be several times smaller compared to the results of Brzeziński and Petrov (2000) from six-hourly data from the U.S. National Centers for Environmental Prediction (NCEP) or to the six-hourly estimates of this study, which are 5.7 μas (S_1), 1.9 μas (S_2) for polar motion and 6.1 μs (S_1), 11.6 μs (S_2) for LOD. To a large extent, these discrepancies can be attributed to a distinct feature of the delayed cut-off series, which is a counteraction of pressure and wind terms. Both for the axial as well as the equatorial component, pressure and wind contributions to atmospheric excitation are of comparable size but likely to cancel out each other when their corresponding spectra are added. (This summation is carried out separately for real and imaginary parts.) Figure 4 gives a detailed look at the real prograde part of polar motion excitation, highlighting the phase shift of about 180° between pressure and wind signals.

4. CONCLUSIONS

Two sets of five-years AAM matter and motion terms with different temporal resolutions of three and six-hours, respectively, have been used to study the atmospheric contribution to daily and sub-daily EOP variations. The mean amplitudes and phases of the most important atmospheric tides, estimated by a simple least squares adjustment on both AAM datasets, differ significantly for polar motion and changes in LOD, but are in good agreement for the nutation band. The advantage of the three-hourly series is the ability to resolve the spectral structure in the semi-diurnal band. The small amplitudes of atmospheric effects calculated from this dataset can be ascribed to a counteraction of pressure and wind terms, which could originate from atmospheric circulation on short time scales. Detailed investigations concerning the time evolution and the physical reasoning of this phenomenon are in progress.

	Period [h]	**equatorial exc., prograde** [μas]	**equatorial exc., retrograde** [μas]	**axial exc.** [μs]
Π_1	24.13214	0.4	2.1	0.5
P_1	24.06589	0.4	37.9	0.9
$\boldsymbol{S_1}$	**24.00000**	**1.1**	**47.0**	**3.2**
K_1	23.93447	0.7	77.0	0.3
Ψ_1	23.86930	0.2	79.8	0.5
Φ_1	23.80448	0.0	27.9	0.2
T_2	12.01645	0.5	0.9	0.6
$\boldsymbol{S_2}$	**12.00000**	**0.2**	**1.3**	**2.6**
R_2	11.98360	0.3	1.4	0.5

Table 1: Atmospheric excitation: mean amplitudes of polar motion [μas] (prograde band and retrograde band at $T = -12$ h), nutation [μas] (retrograde band at $T = -24$ h) and LOD [μs], calculated from five-years AAM matter and motion terms with a temporal resolution of three hours.

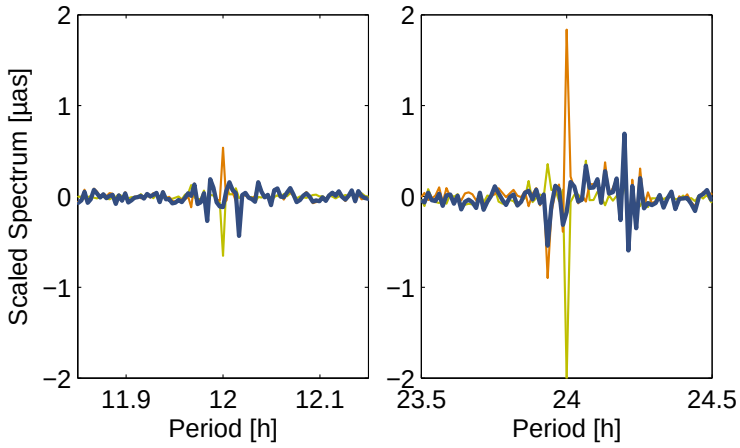

Figure 4: Real part of the discrete Fourier transform of polar motion from three-hourly AAM functions at $T = +12, +24$ h. *Bold blue line*: pressure plus wind terms, *olive line*: pressure term, *orange line*: wind term. The scale factor of the corresponding amplitude spectrum has been applied.

Acknowledgements. This study was carried out within project P20902-N10 of the Austrian Science Fund.

5. REFERENCES

Barnes, R., Hide, R., White, A., Wilson, C., 1983. Atmospheric angular momentum fluctuations, length-of-day changes and polar motion. Proc. R. Soc. Lond, A 387, 31-73.

Bizouard, C., Brzeziński, A., Petrov, S., 1998. Diurnal atmospheric forcing and temporal variations of the nutation amplitudes. J. Geod., 72, 561-577.

Brzeziński, A., Bizouard, C., Petrov, S.D., 2002. Influence of the atmosphere on Earth rotation: What new can be learned from the recent atmospheric angular momentum estimates? Surveys in Geophysics, 23, 33-69.

Brzeziński, A., Petrov, S., 2000. High frequency atmospheric excitation of Earth rotation. IERS Technical Note, 28, 53-60.

Salstein, D.A., Kann, D.M., Miller, A.J., Rosen, R.D, 1993. The sub-bureau for atmospheric angular momentum of the International Earth Rotation Service: A meteorological data center with geodetic applications. Bulletin American Meteorological Society, 74, 67-80.

RECENT IMPROVEMENTS IN IERS RAPID SERVICE/PREDICTION CENTER PRODUCTS

N. STAMATAKOS[1], B. LUZUM[2], B. STETZLER[3], N. SHUMATE[4], M. S. CARTER[5]

[1 2 3 4] USNO
3450 Massachusetts Avenue, N. W.
Washington, D. C. 20392

[5] NOFS
10391 West Naval Observatory Road
Flagstaff, Arizona 86001-8521

e-mail: [1] Stamatakos.Nick@usno.navy.mil [2] Brian.Luzum@.usno.navy.mil
[3] Beth.Stetzler@usno.navy.mil [4] Nathan.Shumate@usno.navy.mil [5] MSC@nofs.navy.mil

ABSTRACT. The International Earth Rotation and Reference Systems Service (IERS) Rapid Service/Prediction Center (RS/PC) has made several improvements to its products and has also developed a web-based Earth Rotation matrix calculator. The improvements include a correction to the Universal Time Atmospheric Angular Momentum (UTAAM) implementation in the combination. Also, use of the International GNSS Service (IGS) Ultras for UT1-UTC and a twice daily Earth Orientation Parameter (EOP) solution are being investigated on testing computers. The web-based calculator returns the Earth rotation matrix at specified user input times based on the IERS 2003 Conventions models.

1. OVERVIEW OF RS/PC SOLUTION AND IMPROVEMENTS

The daily EOP combination and prediction (CP) solution (finals.daily) is produced at approximately 1700 UTC each day; the weekly version (Bulletin A) is produced on Thursday at approximately 1700 UTC. Both provide EOP values which include polar motion, UT1-UTC, and celestial pole offsets, with results located at `http://maia.usno.navy.mil`. These EOP values are used in determining the terrestrial to celestial transformation matrix. Data from Very Long Baseline Interferometry (VLBI), Global Positioning System (GPS), Satellite Laser Ranging (SLR), and AAM are used in these solutions. Observations from the past are combined with appropriate weighting factors and used, along with AAM forecast data, to predict EOP values into the future. It is estimated there are 700 users who receive IERS RS/PC data each week, and roughly 60000 ftp downloads are made per month. Most uses of the data are for practical, non-research purposes with many users — *85 to 90%* — having limited EOP knowledge. Details on the inputs, processes, and results of the RS/PC solution can be found in Stamatakos et al. (2008).

A change in the UTAAM processing within the EOP combination has resulted in improved UT1-UTC short-term predictions. Test computer runs which a) use the IGS Ultra-Rapid observed data (also known as the IGS Ultras) for UT1-UTC and b) generate a twice daily EOP solution are discussed. Lastly, a web-based Earth rotation matrix calculator developed at the RS/PC is presented.

2. UTAAM PROCESSING CHANGE

One of the users of EOP data reported systematic errors in the 1 to 10 day UT1-UTC predictions, and EOP personnel had previously observed a related issue with the last combination day. These errors are shown for the year 2009 in Figure 1 and were computed by differencing the finals.daily with the finals.data UT1-UTC solution produced at a much later date. Salient features to observe are the fortnightly and the quasi-annual periodicity. Since predictions are greatly influenced by the last combination value and since the last combination and 1-day prediction errors show a correlation, our investigation quickly focused on the UTAAM because it greatly influences the last day combination and short term predictions. Fifteen days of previous AAM values had been used in the combination; however, the weighting was small since there were other more accurate data sets from VLBI and GPS at those epochs. At the last combination day epoch, the AAM influence grows rapidly since only Universal Time-like GPS (UTGPS), integrated IGS Rapids, and occasional e-VLBI results were available on the same day. For short term UT1 predictions, the AAM influence grows even more rapidly since the USNO UT1 predictions out to 7 days are based on AAM forecasts.

In the past, Johnson et al. (2005), observed an occasional and possibly erroneous low-frequency signal in the combination results caused by the AAM input, and so this input had been modified and

down-weighted to reduce the problem. However, the implemented down-weighting method might not have worked as intended, and it was discovered, in early 2010, that simply removing the AAM from the combination (but not from the predictions) greatly improved the results. In Figure 2, one can observe the improvement in the 1-day prediction error obtained over the range of dates from July 28, 2009 through January 20, 2010, when the AAM was removed from the combination. The green curve is the 1-day prediction error using the AAM in the combination and the red curve is the prediction error with the AAM removed (on a test computer), and the resulting reduction in error was approximately 20 to 30%.

When one examines Figure 3, the rationale for removing the AAM from the combination becomes clear. The error in the operational combination which uses AAM in both the combination and prediction (blue), the UTGPS (cyan), a test version of the combination which used AAM only in prediction (green), and another test version of the combination which used no AAM in combination or prediction (black) are plotted together from August 9 to September 28, 2010. Also included in the plot are vertical line markers (red) which indicate the epochs in which e-VLBI results were available to the combination on the same day as the observation. For most days shown, the combination with AAM only in predictions results in a reduced error. Even for the days when both e-VLBI and UTGPS results are available, one would have expected a very low error in the blue curve; however, on days 270, 278 and 298, the error is larger than expected. However, once the AAM was removed (green) from the combination, the errors on these dates decreased significantly — indicating even when the more accurate e-VLBI data were available, the AAM errors and weights were large enough to cause large combination errors. Note that although only 50 days of 2009 are shown in Figure 3, it is representative of what was seen throughout 2009.

The removal of the AAM from the operational combination (but not prediction) was implemented on February 25, 2010. Figure 4 is a comparison of the 1-day UT1-UTC prediction results from January 1, 2009 to February 24, 2010 with results from February 25, 2010 through August 24, 2010, and one can clearly see the reduction in error after the change. Before the change, the mean was -1.30 μsec and standard deviation was 112.34 μsec; after the change, the mean was -18.20 μsec and standard deviation was 71.14 μsec. Thus, so far, there has been a 25 to 30% reduction in 1-day prediction error due to using the AAM input data only in the predictions, and not in the combination.

3. EOP SOLUTION MULTIPLE TIMES PER DAY

A second, automatic, EOP CP solution is run at 03:00 UTC each day on a test computer, and additional manual runs can be made at most other times. Currently this solution can accommodate updates to any VLBI and IGS input data. With some additional effort, the software could be made to accommodate multiple-times-per-day updates to SLR, UTGPS, and AAM once more frequent updates are available. So far, only multiple-times-per-day updates to the IGS Ultras have been available. Once the Wettzell and Tsukuba radio antennas come back on-line in late 2010, it is hoped that multiple-times-per-day updates to VLBI will be available.

4. USE OF IGS ULTRA DATA IN THE UT1-UTC COMBINATION

Another test case EOP CP solution, running since early September 2010, includes the IGS Ultra data in the UT1-UTC combination, which provide additional useful UT1-UTC estimates beyond the last available VLBI intensive and UTGPS data. These ultras provide LOD and UT1-UTC information for the 0, 6, 12, and 18-hour UTC observations each day with only a few hours of latency between the observations and processing. When the daily solution is run at 17:00 UTC, the previous day 18-hour and current day 0-hour observations (beyond the last IGS Rapid) are available. This additional data could provide a reduction in the last combination and short-term prediction errors for UT1-UTC.

When the 03:00 UTC second EOP CP solution (discussed in section 3 above) is run, the 6 and 12-hour IGS Ultras from the previous day are available to the combination — providing two additional epochs. It is anticipated that if one could use the EOP CP solution produced at this time, instead of waiting for the next daily run at 17:00 UTC, then there would be an additional reduction in last combination and short term prediction errors.

5. EO MATRIX WEB-BASED CALCULATOR

A transformation matrix calculator was added at the USNO EOP server, located at `http://maia.usno.navy.mil/t2crequest/t2crequest.html`; although, a dedicated server for the calculator may be

coming soon to USNO. The calculator is based on the IERS Conventions (2003), Technical Note 32 using the equinox-based International Terrestrial Reference Frame (ITRF) to Geocentric Celestial Reference System (GCRS) transformation. The code is written in FORTRAN and relies heavily on code provided at `http://tai.bipm.org/iers/conv2003/conv2003_c5.html` and by the Standards of Fundamental Astronomy (SOFA) organization. Observable quantities are from a version of the finals2000A.data or finals.daily files provided at the EO Department server listed above. Polar motion and UT1 observables are interpolated when needed, with long-period tidal terms removed before the interpolation and then, long-period tidal, diurnal, and sub-diurnal tidal terms are added back into the observables. Adding sub-diurnal and diurnal tides is a user option, which provides additional accuracy. Outputs include the ITRF to GCRS and several intermediate transformation quantities.

Figure 5 contains a picture of the user interface to the calculator. The user chooses date and time intervals. The code produces an output page containing the ITRF to GCRS transformation and desired intermediate quantities. The user is restricted to 100 intervals or less; however, once the dedicated server is available, this restriction limit will be raised considerably. The standard output, observed in Figure 6, is the transformation and requested intermediate matrices at the epochs corresponding to the user specified start and stop time intervals. Optional quaternion (also known as Euler parameters) output can be chosen. The available intermediate quantities are polar motion, Greenwich Mean Sidereal Time (GMST), equation of the equinoxes, precession, nutation, and combined bias-precession-nutation.

6. FUTURE DIRECTIONS

The 2x-daily EOP solution will be evaluated in 2010 and then made operational in early 2011. Eventually, an Nx-daily solution will be made to re-evaluate a new EOP solution any time a new input data series is detected. Also, Celestial Pole Offsets published by the IERS RS/PC will be with respect to the P03 series. The use of the Geospatial Information Authority (GSI) of Japan VLBI intensives in the operational EOP CP solution has begun recently and is being evaluated. Finally, the use of the IGS Ultra data in the UT1-UTC CP solution on a test computer will be evaluated.

7. REFERENCES

Johnson T.J., Luzum B.L., Ray J.R., "Improved near-term Earth rotation predictions using atmospheric angular momentum analysis and forecasts", Journal of Geodynamics 39 2005, pp 209-221.

Stamatakos N., Luzum B., Wooden W., (2008) "Recent improvements in the IERS Rapid Service/Prediction Center Products", Journées Systèmes de référence spatio-temporels 2007, pp 163-166.

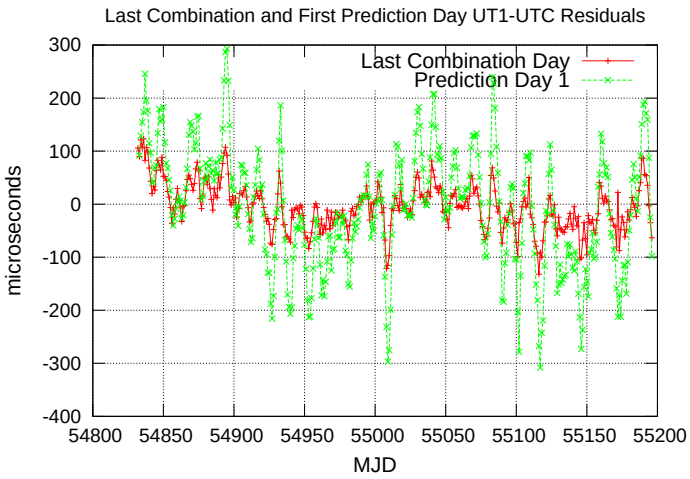

Figure 1: Last Combination and 1-Day Prediction Errors

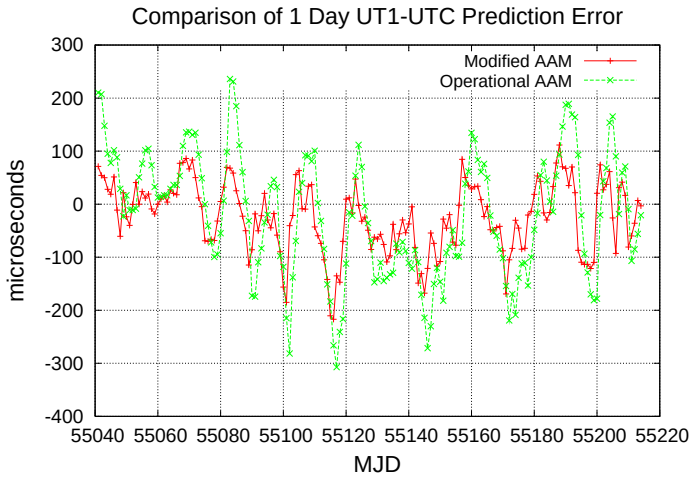

Figure 2: 1-Day prediction error with (green) and without (red) AAM in the Combination

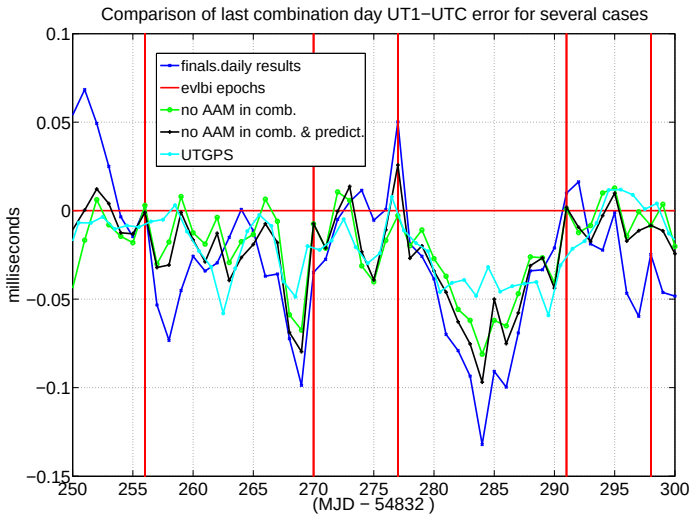

Figure 3: Comparison of Input Data Sets to finals.data for UT1-UTC

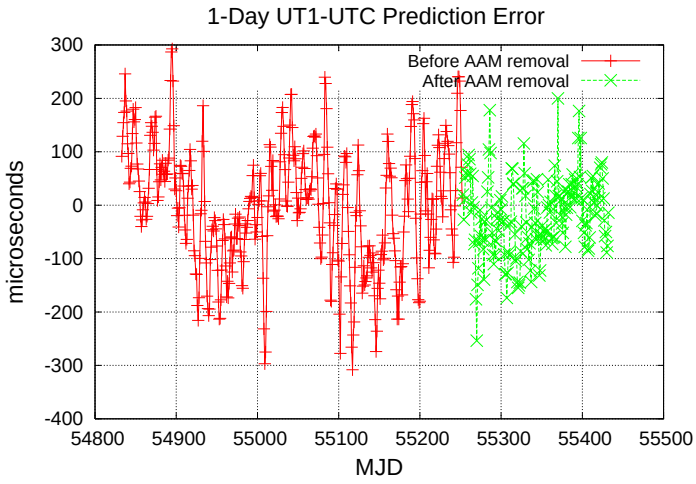

Figure 4: 1-Day UT1-UTC Prediction Error before and after AAM Removal from the Combination

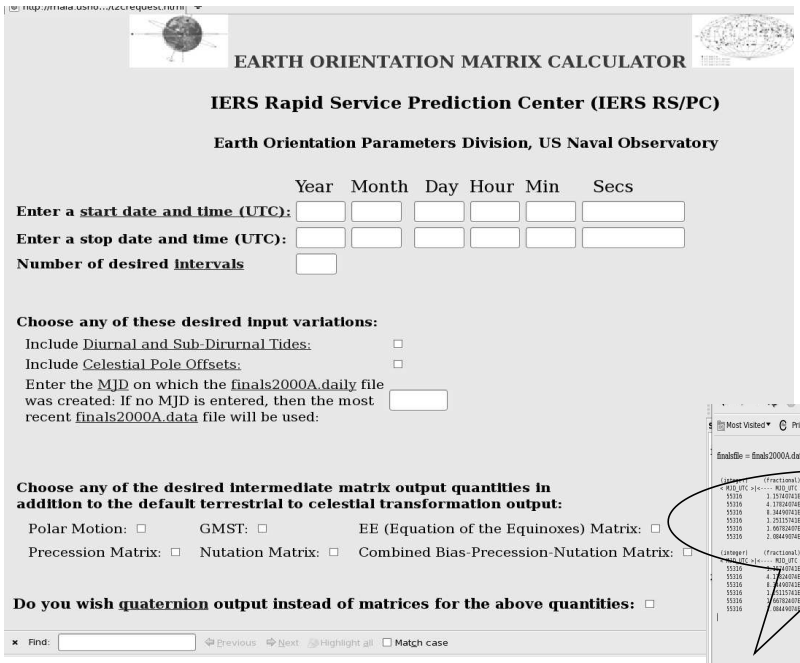

Figure 5: EO Matrix Calculator: User Interface

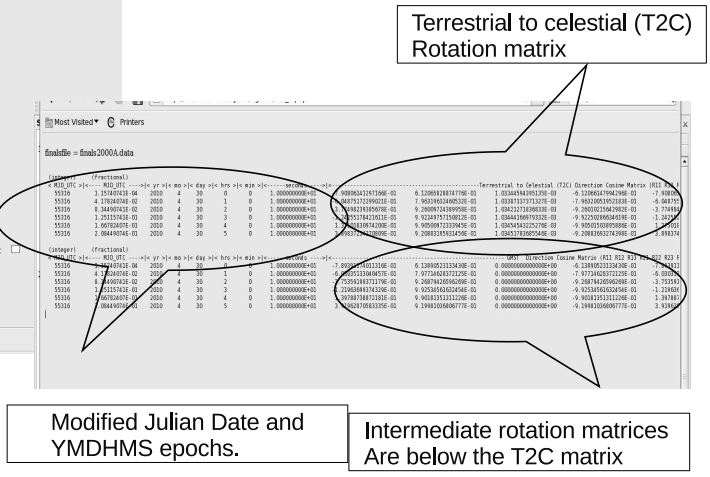

Figure 6: EO Matrix Calculator: Output

ANALYSIS OF CHANDLER WOBBLE EXCITATION, RECONSTRUCTED FROM OBSERVATIONS OF THE POLAR MOTION OF THE EARTH

L.V. ZOTOV
Sternberg Astronomical Institute of Moscow State University, Russia

ABSTRACT Chandler excitation was reconstructed since 1846 yr. from EOP C01 by three methods: complex Singular Spectrum Analysis (SSA) with Wilson filter, least squares adjustment (LSA) with Tikhonov regularization, Panteleev smoothing. The aim was to damp annual component and side frequencies and to obtain excitation only for chandler wobble. Results of different methods are in agreement with each other. Modulation of Chandler excitation of ∼18.6 yr period, synchronous with Saros tidal effects in the length of the day (LOD) was found. It means that Chandler wobble swings under the influence of Luni-Solar tide. Amplitude and phase evolution in time was analyzed with use of Gabor transform. Phase changes in Chandler excitation found to have ∼37 yr period. It explains, why 18.6 yr modulation is not seen in the Chandler component itself, but only in its excitation.

1. INTRODUCTION

More than a century has passed since S.C. Chandler discovered in 1891 the periodicity, named in his honor [4,5]. Despite this, its final explanation still has not been found [16]. It's not clear what causes the modulation of the Chandler oscillation, what process makes a major contribution to this resonance phenomenon. As it is shown in [1,2,3,7,9,11] most of the energy can be explained by oceanic and atmospheric excitation, as well as changes in the ocean bottom pressure. But it's hard to show, that Chandler excitation behaves in time like these noisy processes on the long periodic scale. Additionally the longest observational time series of Atmospheric Angular Momentum (AAM) starts only in 1940-th. In this paper we offer a variety of approaches for the excitation functions (EF) reconstruction, in particular, looking for the Chandler oscillation physical causes.

Among the first H. Jeffreys raised the question about reconstruction of the polar motion (PM) causes [8]. EF reconstruction from the geodetic observations of the PM is an ill-posed problem. Wilson filter [15] is a standard procedure of reconstruction, but it does not include stabilization of solution. We suggest to use Panteleev corrective smoothing [10] or Phillips-Tikhonov regularization [12]. Chandler excitation reconstruction is complicated because of its resonance nature and strong annual component presents nearby in frequency band. We need to develop filter, which would damp annual oscillation together with low and high frequency components.

2. EXCITATION RECONSTRUCTION TECHNIQUES

Powerful method, which allows to separate PM trend, Chandler, annual components and noise is Singular Spectrum Analysis (SSA) [6]. We applied SSA to the complex PM coordinates time series $m = x - iy$ obtained from the IERS EOP C01 bulletin since 1846 yr. up to now (2010), brought to a time step of 0.05 yr. Figure 1a shows a plot of SSA-separated components. We illustrate the results on the example of x-coordinate of the pole, the picture for the y-component is similar. The main parameter of SSA is lag L, it was chosen to be 240 points, i.e. 12 years, almost equal to the double beat period of the annual and Chandler oscillations. Figure 1b shows spectrum of the annual and Chandler components, separated by means of SSA. The spectrum of the original PM series is represented as a background.

The dynamical system of the rotating Earth can be written in form

$$\frac{i}{\sigma_c}\frac{dm(t)}{dt} + m(t) = \chi(t), \tag{1}$$

with a complex parameter $\sigma_c = 2\pi f_c(1 + i/2Q)$, where Q is a quality-factor, f_c is a Chandler frequency. This first order equation is based on the linearization of the original Euler-Liouville equation and is a simple but an adequate approximation of the real system [2, 14]. Q and f_c are not known precisely,

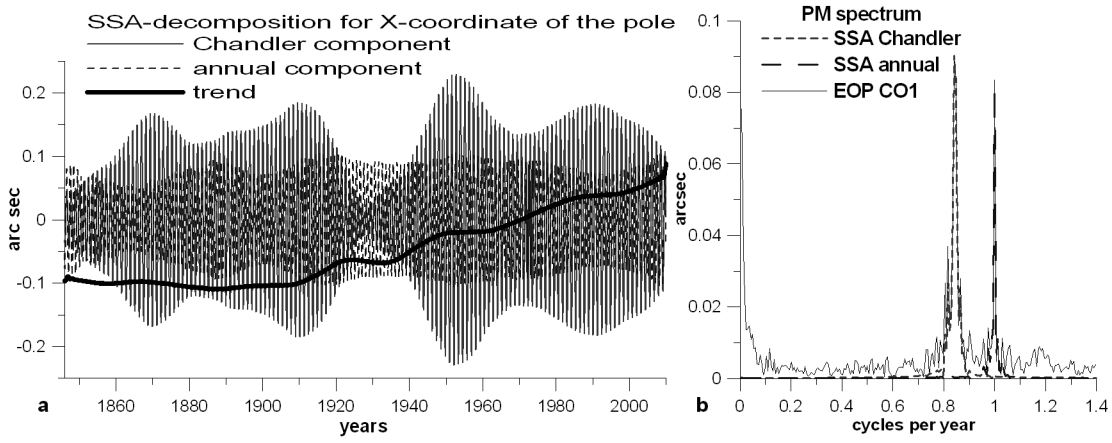

Figure 1: SSA-decomposition of PM (a) and it's spectrum (b).

what introduces uncertainty into the corresponding operator (1). In this research we use values $Q = 175$, $f_c = 0.843$ (Chandler period $T_c \approx 433$ days), as estimated in [13]. To obtain $\chi(t)$ trajectory of the pole $m(t)$ should be differentiated. This is a typical ill-posed problem.

The transfer function of equation (1) has the form

$$L(f) = \frac{\sigma_c}{\sigma_c - 2\pi f.} \tag{2}$$

Reconstruction of $\chi(t)$ from $m(t)$ can be represented in the frequency domain by multiplication of the PM spectrum by inverse operator

$$\hat{\chi}(f) = L^{-1}(f)\hat{m}(f),$$

here hat represents Fourier transform. AFR of the operator $L^{-1}(f)$ is represented on figure 2a by the solid line. It strengthen the side-frequency components in comparison with Chandler one. The Wilson filter

$$\chi(t) = \frac{ie^{-i\pi f_c \Delta t}}{\sigma_c \Delta t}\left[m_{t+\frac{\Delta t}{2}} - e^{i\sigma_c \Delta t} m_{t-\frac{\Delta t}{2}}\right], \tag{3}$$

where $\Delta t/2$ is a time interval between the equidistant observation samples, can be used as approximation of L^{-1} [14,15], at least near the Chandler frequency. It does not contain any procedure to stabilize the inverse solution. We applied filter (3) to the Chandler component, separated by SSA. So that annual component, trend and noises were removed, SSA together with Wilson filter could be consider as inversion with stabilization. Similar to Moore-Penrose inversion with cut-off of singular numbers, used for ill-conditioned linear systems.

The result of the Chandler excitation reconstruction, separated by means of SSA through Wilson filtering, is shown on Figure 2b by a solid line. For greater confidence, we shall try to prove the result by other methods, independent of SSA.

To solve the ill-posed problems regularization can be used [12]. Reconstruction of $\chi(t)$ can be regularized, so that the inverse operator will be written as

$$L^{-1}_{reg}(f) = \frac{L^*(f)}{L^*(f)L(f) + \alpha}, \tag{4}$$

where α is a regularization parameter. When $\alpha \to 0$, $L^{-1}_{reg}(f)$ tends to the inverse operator $L^{-1}(f)$. On the Figure 2a, together with AFR of $L^{-1}(f)$ operator, the AFR of $L^{-1}_{reg}(f)$ operator (4) with parameter $\alpha = 500$ is represented. This value was chosen to make the results more or less consistent with SSA results. Regularized operator is a filter, which suppresses those frequencies, where $|L(f)|$ is small. However, its AFR has very slowly decreasing slopes. It is hard to make annual component not to pass. Instead, we estimated the parameters of annual component by means of LSA and subtracted it from the original EOP C01 series (Table 1). The result of regularization in frequency domain is represented on Figure 2b by dot-dashed curve. Finally we used Panteleev corrective smoothing technique [10], based on the additional

	amplitude	phase for 1846.0
x-coordinate	0.088" ± 0.005"	231° ± 3°
y-coordinate	0.078" ± 0.006"	148° ± 4°

Table 1: Annual harmonic parameters, adjusted by LSM.

filtering of the inverse solution to suppress noise and annual component. The operator of the corrective smoothing is built in the frequency domain according to the expression

$$L_{corr}^{-1}(f) = \frac{L_{filter}(f)}{L(f)}, \tag{5}$$

here $L_{filter}(f)$ is a transfer function of the additional smoothing filter. We used Panteleev filter [16] with a frequency response centered at the Chandler frequency

$$L_{filter}(f) = \frac{f_0^4}{(f - f_c)^4 + f_0^4}. \tag{6}$$

The parameter $f_0 = 0.04$ was chosen to suppress low and high frequencies, including the annual. Such filter does not introduce phase distortion. The result of the corrective smoothing, performed in spectral domain, is also represented on Figure 3b. The phase change of Chandler excitation, obtained from the

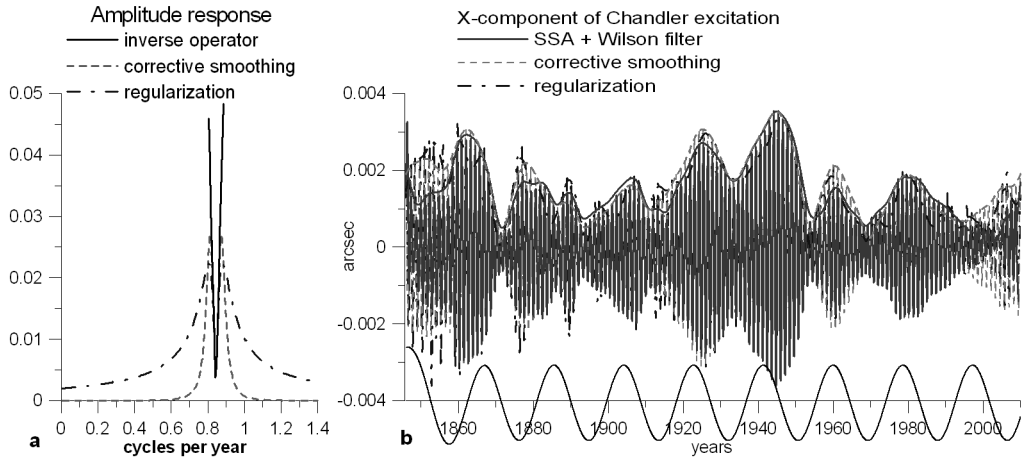

Figure 2: Impulse response of inverse operators (a) and reconstructed Chandler excitation (b).

Gabor transform argument, is shown on Figure 3 together with the phase evolution of the SSA-separated Chandler PM component [17]. Phase changes of Chandler EF, obtained by three different methods are in good agreement with each other.

3. DISCUSSION

Chandler excitation, as seen on Figure 2b has an amplitude modulation. It's amplitude changes and is quite large in the 1930-th, when the observed amplitude of Chandler PM component is small (Fig. 1a). Along the abscissa on Figure 2b the 18.6-yr oscillation is plotted, calculated as the mean of the IERS model of zonal tides for the length of day (LOD). This harmonic, associated with Saros cycle, has the behavior, synchronous with modulation of the Chandler excitation in most cases. The correlation is not observed in the 1990-th, probably, because of the boundary-effects and for early astronomical observations, obtained before the establishing of the International Latitude Service (ILS) in 1899. However, during the XX cent. there are 5 synchronous peaks. Thus, when the rotation of the Earth slows down, during the peak tides, the Chandler excitation amplitude increases. This leads us to the hypothesis that the same factor governs both rotational velocity of the Earth and the Chandler motion of the pole on this time

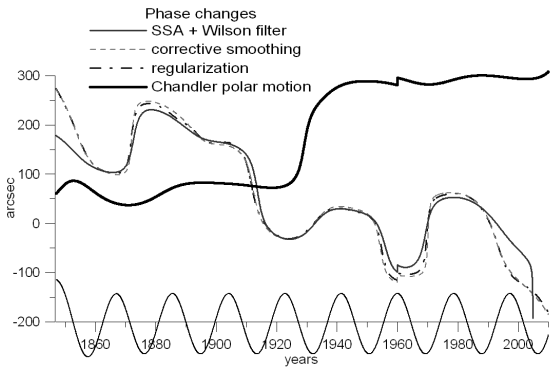

Figure 3: Phase changes of Chandler PM and excitation function.

scale. It is possible that tidal perturbations make the energy transfer to the Chandler oscillation. The mechanism is not clear, perhaps, the atmosphere and the ocean are the mediators.

Speaking about the phase, Fig. 3, the well-known $\sim 3\pi/2$ phase jump in the Chandler PM around 1930-th, almost disappears in EF. So that filter (6) does not change phase, this can be explained only by the influence of the dynamical system (1) and constricting of frequency band. At the same time phase changes of $\sim 37 \approx 2 * 18.6$ yr period are seen in the EF. This phase changes do not allow us to see in the Chandler PM component (Fig. 1a) such amplitude changes, as in it's excitation (Fig. 2b).

Acknowledgments. This work is supported by the President of Russia grant MK-4234.2009.5 and RFBA grant No 10-05-00215. We are thankful to V.L. Panteleev for the method.

4. REFERENCES

[1] Bizouard C., Lambert S., Remus F., Seoane L., Gambis D., "The source of the variable Chandler wobble", Proceedings of Journees 2010.

[2] Bizouard C., L. Seoane, 2010, Atmospheric and oceanic forcing of the rapid polar motion J Geod., Vol. 84, pp.19-30, doi: 10.1007/s00190-009-0341-2.

[3] Brzezinski A., and J. Nastula, 2002 "Oceanic excitation of the Chandler wobble", Adv. Space Res., Vol. 30, pp. 195-200, doi: 10.1016/S0273- 1177(02)00284-3.

[4] Carter M.S., Carter W.E., 2000, "Setho Carlo Chandler Jr.: the discovery of variation of latitude", ASP conference series, Vol. 208, p. 109.

[5] Chandler S.C., 1891, "On the variation of latitude I, II", AJ , Vol. 248, 59, Vol. 249, 65.

[6] Ghil, M., R. M. Allen, M. D. Dettinger, K. Ide, D. Kondrashov, et al., 2002, "Advanced spectral methods for climatic time series", Rev. Geophys. 40(1), 3.13.41, doi: 10.1029/2000RG000092.

[7] Gross R. S., 2000, "The excitation of the Chandler wobble", Geophysical Research Letters, Vol. 27, No. 15, pp. 2329-2332.

[8] Jeffreys H., 1940, "The variation of latitude", Mon Not Roy Astr. Soc., Vol. 100, pp. 139-155.

[9] Liao D., Xinhao Liao and Yonghong Zhou, 2003, "Oceanic and atmospheric excitation of the Chandler wobble", Geophys. J. Int. , Vol. 152, pp. 215-227.

[10] Panteleev V.L.,Chesnokova, T.S., 2011, Problem deconvolution in inertial gravimetry, Moscow University Physics Bulletin, Vol. 66, N 1.

[11] Salstein D., 2000, "Atmospheric excitation of polar motion", ASP Conference Series, Vol. 208, pp. 437-446.

[12] Tikhonov A.N., Arsenin V.Y., 1977, "Solution of ill-posed problems", John Wiley and Soc.

[13] Vicente R., Wilson C., 1997, "On the variability of the Chandler frequency", J. Geophys. Res., Vol. 102(B9), pp. 20439-20445.

[14] Vicente R., Wilson C., 2002, "On long-period polar motion", J. of Geod., Vol. 76, No. 4, pp. 199-208.

[15] Wilson C., 1985, "Discrete polar motion equations", Geophys J. Roy. Astr. Soc., Vol. 80, pp. 551-554.

[16] Yatskiv Y., 2000, "Chandler Motion Observatios", ASP Conference Series, Vol. 208, 383.

[17] Zotov L., 2010, "Dynamical modeling and excitation reconstruction as fundamental of Earth rotation prediction", Artificial satellites, Vol. 45, N 2, pp. 95-106.

ON CORRELATION BETWEEN VARIATIONS IN EARTH ROTATION AND FREQUENCY OF EARTHQUAKES

E.Yu. ALESHKINA

Main (Pulkovo) Astronomical Observatory of the Russian Academy of Sciences
Pulkovskoye ave., 65-1, 196140 Saint-Petersburg, RUSSIA
e-mail: aek3@list.ru

1. INTRODUCTION

The behavior of the Universal time UT describes the axis rotation of the Earth and provides the data for investigating the constitution of the Earth and an interaction between its main components such as the core, the shell, an atmosphere and oceans. It is in fact the longest experimental sets of observations used for the study of geophysical processes. On the other hand regularly earthquakes are very considerable and important geophysical processes and information about them are collecting for centuries. Attempts for searching correlations between Earth rotation irregularities and the frequency of earthquakes were carried out starting from the work of Brown (1926). The present paper is devoted to this problem.

2. IRREGULARITIES IN EARTH ROTATION 1700 - 1955

The correction $\Delta T = TD - UT$ connects the observational Universal time UT and the theoretically uniform time-argument in the motion theories TD. Before the atomic time-scale was established these corrections were the only way for comparison observations with theories. In the early papers (Aleshkina E.Yu., 1994) the system of time-correction $\Delta T = TD - UT$ characterized irregularities in Earth rotation for the time span 1700-1955 was obtained from analysis of the transits of Mercury and Venus and lunar observations. Table 1 presents this system ΔT.

Year	ΔT **(s)**	**Year**	ΔT **(s)**	**Year**	ΔT **(s)**	**Year**	ΔT **(s)**	**Year**	ΔT **(s)**	**Year**	ΔT **(s)**
1700	55.8	1745	29.1	1790	23.2	1835	16.6	1880	2.5	1925	27.5
1705	49.1	1750	28.4	1795	22.6	1840	15.5	1885	2.3	1930	27.4
1710	44.0	1755	27.6	1800	22.2	1845	15.7	1890	2.4	1935	26.8
1715	38.1	1760	26.9	1805	22.0	1850	17.4	1895	1.9	1940	27.1
1720	34.9	1765	26.4	1810	21.6	1855	17.4	1900	4.3	1945	29.0
1725	32.9	1770	25.8	1815	21.3	1860	17.7	1905	10.6	1950	30.8
1730	31.9	1775	24.9	1820	21.6	1865	14.1	1910	17.1	1955	32.0
1735	30.8	1780	24.3	1825	20.4	1870	10.2	1915	22.1	1960	33.9
1740	29.9	1785	23.8	1830	19.7	1875	4.1	1920	25.4		

Table 1: The system of time-corrections $\Delta T = TD - UT$

The first derivative of ΔT gives the changes in the length of day (LOD) during the 250-years time-span. To uncover the possible periodic components in irregularities of Earth rotation we have performed frequency analysis (Aleshkina et al., 2010) of changes in LOD for this period. Three different techniques were employed: the CLEAN method (Vityazev V.V., 2001a), Lomb-Scargle method (Scargle J.D., 1982), and technique involving wavelets (Vityazev V.V., 2001b). All these methods have different mathematical grounds. CLEAN involves Fourier transform. Lomb-Scargle method is based on least-squares adjustment. The last technique exploits the special form of three-dimensional wavelet function. Hence one may consider these three methods as complementing each other. Results obtained by all methods described above both for changes in LOD and frequency of earthquakes is presented in Table 2 (see Section 4).

3. DATABASE OF POWERFUL EARTHQUAKES 1500 - 1955

On the basis of cross-identification of several databases and sources catalogue CPE2010 of powerful earthquakes of 1490-1960 with magnitudes exceeding 7.5 was carried out.

1. http://www.intute.ac.uk/hazards/Earthquakes-database.html
2. http://earthquake.usgs.gov/earthquakes/eqarchives/epic/
3. http://www.ngdc.noaa.gov/nndc/struts/
4. http://www.magicbaikal.ru/info/earthquake.htm

The fullest database about the earthquakes in direct access is the base NOAA of National Geophysical Data Center [3]. The database [1] repeats above mentioned in many respects. Unfortunately, they are

not full, there are numerous recurrences of the same events and different estimations of earthquake's magnitudes in them. In such cases we used the maximal value of magnitude in sources. The following information is included in a database: calendar date, magnitude under the Richter scale (from 7.5 up to 9.9), region of an epicentre. The catalogue CPE2010 includes 689 powerful earthquakes and is available on www.ad-astra.len.su/bd/cpe2010.html.

4. CORRELATION BETWEEN ASTRONOMICAL AND GEOPHYSICAL DATA

Attempts for searching correlations between LOD changes and the frequency of earthquakes were carried out starting from the work of Brown (1926) where he tried to analyze such correlation on the basis of statistic of earthquakes in England. According to analysis of connection between earthquakes in China region and fluctuations in Earth rotation it is shown in (Du P., 1993) that the number of earthquakes with M ¿ 8 increases with increase in the rate of Earth rotation. Variations in Earth rotation can be one of the major factors for modulation of global seismic activity (Liao, Jin, Zheng, 1993). However the main difficulty is that earthquakes in general have local character. So that for the purpose of the present paper the most powerful earthquakes have a significant interest. The comparison of the frequency of such earthquakes and secular and long-periodic changes in LOD for 250 years was carried out. We carried out the same frequency analysis as it described in Section 2. Results are presented in Table 2.

As it can be seen from Table 2 LOD is likely to contain the several periods about 48, 70 and 100 years. Number of earthquakes contains the same periods about 45 and 75 - 80 years. There are other possible periods of 200 and 300 years. All these values are detected by all techniques used, which suggests that they are rather reliable. The periods of 45 - 48 years and 70 - 80 years are in good agreement and presented in both phenomena. In LOD changes there is an additional period of 100 years that is in agreement with so called Newcomb's empirical terms that are likely to be caused by changes in Earth moments of inertia. The value of 0.77 for coefficient of correlation between 250-years behavior of LOD and global earthquakes was obtained.

Series	**CLEAN**	Lomb-Scargle	**Wavelets**
LOD	P1 = 48 P2 = 68 P3 = 102	P1 = 57 P2 = 97	P1 = 48 P2 = 72 P3 = 99
Frequency of earthquakes	P1 = 44 P2 = 80 P3 = 203 P4 = 305 P5 = 610	P1 = 251 P2 = 603	P1 = 46 P2 = 75 P3 = 200 P4 = 298

Table 2: Frequency analysis for changes in LOD and frequency of earthquakes. Periods are given in years.

5. CONCLUSIONS

The following conclusions can be drawn from this analysis of the data about long-period variability of the Earth's rate of rotation and global earthquakes in the period 1500 - 1960. There are fluctuations in LOD in the period of 250 years with periods of 48, 70 and 100 years. Changes in number of powerful earthquakes in the period of 450 years have periods of 45, 75 - 80, 200 and 300 years. It is likely that periods of 45 - 48 and 70 - 80 years for earthquakes frequency and changes in LOD are connected each other. Coefficient of correlation between 250-years behavior of LOD and global earthquakes is significant and equal 0.77. Period of 100 years in LOD changes is in agreement with so called Newcomb's empirical terms that are likely to be caused by changes in Earth moments of inertia.

6. REFERENCES

Aleshkina, E.Yu., 1994, Analysis of the lunar optical observations XVIII-XX centuries, Proc.of the Conf. on Astrometry and Celestial Mechanics, Poznan, Poland, 13-17 Sept. 1993, pp.139–143

Aleshkina, E.Yu. et al., 2010, Analysis of impacted object 2008 TC3 observations, Proc. of "ACH-2010", September 21 - 25, 2009, St. Petersburg, pp.37–42

Brown, E., 1926, Transactions of Yale Univ.Obs., v.3, part.6, 205

Du, P., 1993, Northwest Seismol.J., v.15, N2, pp.36–41

Liao, Jin, Zheng, 1993, Int.Assoc.Geod.Ged.Meet., Beijing, 8 - 13 Aug. 1993, Abstr. Book, pp.342-343

Scargle, J.D., 1982, Studies in astronomical time series analysis, Ap.J., 263, pp.835–853.

Vityazev, V.V., 2001a, Analysis of irregular time series , SPb University press, 67 p. (in Russian).

Vityazev, V.V., 2001b, Wavelets analysis, SPb University press, 58 p. (in Russian).

REVISITING A POSSIBLE RELATIONSHIP BETWEEN SOLAR ACTIVITY AND EARTH ROTATION VARIABILITY

R. ABARCA DEL RIO[1], D. GAMBIS[2]

[1] Departamento de Geofisica (DGEO), Facultad de Ciencias Fisicas y Matematicas Universidad de Concepcion, Casilla 160-C, Concepcion, Chile

[2] Observatoire de Paris, CNRS, UPMC
61 Av de l'Observatoire, Paris, France

ABSTRACT. A variety of studies have searched to establish a possible relationship between the solar activity and earth variations (Danjon, 1958-1962; Challinor, 1971; Currie, 1980, Gambis, 1990). We are revisiting previous studies (Bourget et al, 1992, Abarca del Rio et al, 2003, Marris et al, 2004) concerning the possible relationship between solar activity variability and length of day (LOD) variations at decadal time scales. Assuming that changes in AAM for the entire atmosphere are accompanied by equal, but opposite, changes in the angular momentum of the earth it is possible to infer changes in LOD from global AAM time series, through the relation : delta (LOD) $(ms) = 1.68\,10^{-29}$ delta(AAM) $(kg\,m^2/s)$ (Rosen and Salstein, 1983), where delta(LOD) is given in milliseconds. Given the close relationship at seasonal to interannual time's scales between LOD and the Atmospheric Angular Momentum (AAM) (see Abarca del Rio et al., 2003) it is possible to infer from century long atmospheric simulations what may have been the variability in the associated LOD variability throughout the last century. In the absence of a homogeneous century long LOD time series, we take advantage of the recent atmospheric reanalyzes extending since 1871 (Compo, Whitaker and Sardeshmukh, 2006). The atmospheric data (winds) of these reanalyzes allow computing AAM up to the top of the atmosphere; though here only troposphere data (up to 100 hPa) was taken into account.

1. RESULTS AND DISCUSSION

Both the low frequency term of AAM (LF AAM), as the annual and semiannual amplitude modulation (AN-A AAM and SA-A AAM) present power at interannual, decadal and interdecadal time scales. Some analyses are described. We show on the following figures the decadal band pass filtered times series of each of the signals. The decadal cycle of Semi Annual amplitude is inverted (-SA-A). The comparison between the decadal oscillation in Solar Activity (SUN) and these in the LF AAM and AN-A terms (Fig A and Fig B) show that both series appears to phase shift through times. Clearly in phase opposition to the solar activity forcing at the turn of 19th to 20th century in phase from 1955-1985 and out of phase since then (at the turn of the 20th to 21th century) when the decadal signal in AAM lengthens (see Abarca del Rio et al., 2003). Interestingly the comparison with the inverted decadal modulation of the semiannual cycle (Fig C), show that both signals appears to be somehow in phase or varies accordingly from roughly 1920 to 1990, extending herein precedent findings (Bourget et al, 1992)

2. CONCLUSION

The analysis performed here shows that both the low frequency signals in AAM as the annual and semiannual amplitude modulation present interannual to secular time scales. We concentrate our study particularly in the so-called Schwabe cycle (9-13 yr periods) in solar activity where the different terms in AAM, low frequency, the modulation of the annual and semiannual cycle do also presents a cycle at these times scales. The comparison with the decadal cycle in the SUN shows that only the decadal cycle in the semiannual cycle modulation presents an homogeneous phase shift with the SUN for almost 70 years (1920-1990), therefore extending precedent findings (see Bourget et al, 1992). We will finally conclude as on our precedent paper (Abarca del Rio et al., 2003) in this field: "The present results indicate the need for better understanding of atmospheric dynamics at decadal time scales. It seems that the coming years will be fruitful in this regard, given the advent of extended and improved atmospheric and solar data".

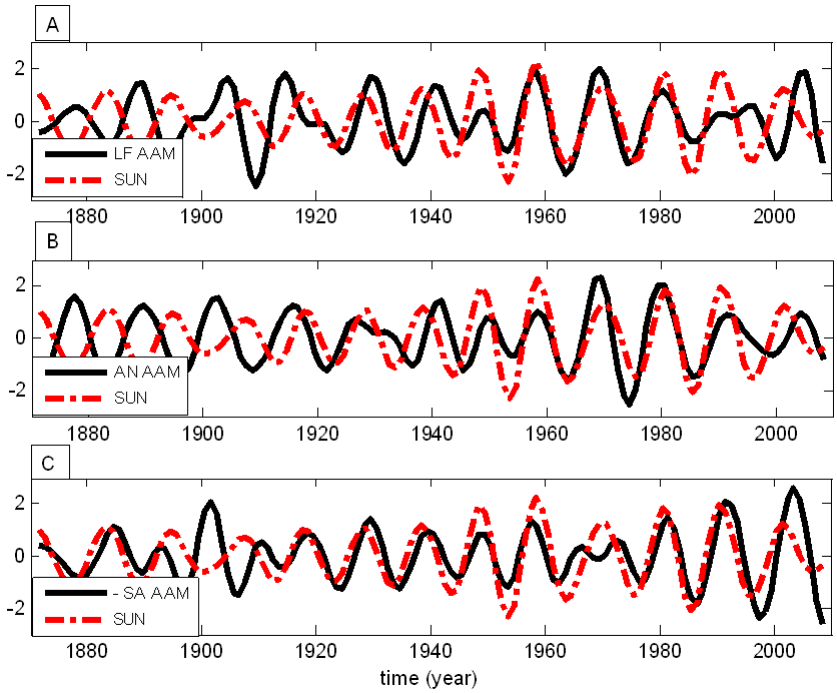

Figure 1: Decadal band pass filtered times series, from up to bottom of: Solar Activity (SUN; as represented by the Sunspots number), the Low Frequency AAM (LF AAM) Annual and Semiannual amplitude modulation (AN AAM and SA AAM respectively. The decadal cycle of Semi Annual amplitude is inverted (-SA-A).

3. REFERENCES

Abarca del Rio R., Gambis D., Salstein D., P. Nelson P., Dai A., 2003, "Solar Activity and Earth rotation variability", J. of Geodynamics, 36, 3, 423-443

Bourget P., Gambis D. and D. Salstein, 1992, "Possible relationships between Solar activity, atmospheric variations and Earth Rotation", Journes 1992 Systmes de rfrence spatio-temporels, Capitaine (ed.), 172-176.

Challinor, R.A., 1971, "Variations in the rate of rotation of the Earth", Science 172, 1022-1024

Compo,G.P., J.S. Whitaker, and P.D. Sardeshmukh, 2006, "Feasibility of a 100 year reanalysis using only surface pressure", data. Bull. Amer. Met. Soc., 87, 175-190.

Currie, R.G., 1980, "Detection of the 11-yr sunspot cycle signal in Earth rotation", Geophys. J. R. Astr. Soc. 61, 131-140.

Danjon, 1958-1962, C.R. Acad. Sciences, Paris.

Gambis D., 1990, "A. Danjon, Variations de la rotation de la Terre et activit solaire", Actes du Colloque A. Danjon, JSR1990, N. Capitaine (ed.), 177-182.

Gambis D. and M. Bourget, 1993, "Correlation between the 11-year solar cycle, the atmosphere angular momentum and the Earth rotation", Ann. Geophys., Space and Planetary Sciences, supp. III to vol 11, C368.

Maris G., Mioc V., Oncica A., Stavinschi M.and D. Gambis, 2004, "Common periodicities in solar activity and earth rotation", romanian Astronomical journal, 14,2, 157-167.

Rosen, R. D., Salstein, D. A., 1983, "Variations in atmospheric angular momentum on global and regional scales and the length of day", J. of Geophys. Res., 88, 5451-5470.

THE SOURCE OF THE VARIABLE CHANDLER WOBBLE

C. BIZOUARD, S. LAMBERT, F. REMUS, L. SEOANE, D. GAMBIS
Observatoire de Paris, SYRTE, CNRS, UPMC
61, av. de l'Observatoire 75014 Paris FRANCE
e-mail: christian.bizouard@obspm.fr

In the absence of forcing, the Chandler wobble (CW) would have a period of 430.3 days, and would lose most of its energy after a few decades because of dissipation in the mantle and in the oceans. Observation of the Earth's polar motion, however, reveals a prograde oscillation of which pseudo period can be as far as 20 days from the above value (Vondrak 1988). It gains energy at some epochs (Danjon & Guinot 1954) so that it never disappears. The CW excitation is accounted for, on average, by the atmosphere and oceans (Gross 2000, Brzeziński & Nastula 2002), but its variability is so far poorly explained. We attempt to interpret it as consequence of the hydro-meteorological forcing, as suggested by Plag (1997), Celaya et al. (1999), and Seitz & Schmidt (2005). At periods larger than 2 days and for a deformable Earth surrounded by fluid layers, the time evolution of the complex pole coordinates $p = x - iy$ is given by Barnes et al. (1983):

$$p + i\frac{\dot{p}}{\sigma_c} = \frac{1.02c}{(C-A)\Omega} + \frac{1.43h}{(C-A)\Omega} \tag{1}$$

where $\sigma_\mathrm{c} = \sigma_0(1 + i/2Q)$ is the Chandler frequency, $c = c_{13} + ic_{23}$ and $h = h_1 + ih_2$ are respectively the off-diagonal moment of inertia and the equatorial relative angular momentum of the fluid layer, and A and C are respectively the mean equatorial and axial moments of inertia of the Earth. The LHS of (1) is referred to as the geodetic excitation χ_g, while the RHS χ_f is referred to as the geophysical (or fluid) excitation. The theoretical computation of σ_c leads to a period of 430.3 days and a quality factor of $Q = 88$ (Mathews et al. 2002). Those values are consistent with estimates based on analyses of polar motion time series.

The most common approach to explain the Chandler wobble excitation by external fluid layers consists in computing χ_g from observed pole coordinates, and comparing it against χ_f directly given by fluid layer angular momentum time series. Conversely a modeled polar motion obtained by time integration of (1) can be directly compared with the observed pole coordinates:

$$p_\mathrm{f}(t) = p_0(t_0)\mathrm{e}^{i\sigma_\mathrm{c}(t-t_0)} - i\sigma_\mathrm{c}\mathrm{e}^{i\sigma_\mathrm{c}t}\int_{t_0}^{t}\chi_\mathrm{f}(t')\mathrm{e}^{-i\sigma_\mathrm{c}t'}\mathrm{d}t', \tag{2}$$

where t_0 is the time origin of the integration. The first term represents a damped, free wobble of relaxation time $2Q/\sigma_0 \sim 40$ years for $Q = 100$. This progressive damping is not observed, but balanced by the integral expressing the forced polar motion. The latter term mainly contains the effects of the seasonal forcing and an oscillation emerging in the Chandler signal.

We used the pole coordinates of the combined C 01 series, computed at the International Earth Rotation and Reference Systems Service Earth Orientation Parameter Product Center (EOP PC 2010). We considered the geophysical forcing made up of (i) atmospheric angular momentum (AAM) as given by the National Center for Environmental Prediction/National Center for Atmospheric Research (NCEP/NCAR) reanalysis project (SBA 2010), and (ii) oceanic angular momentum (OAM) output from the ECCO model in a near-global domain (SBO 2010). The model is forced by NCEP/NCAR reanalysis products.

Using (2), we computed the modeled polar motion $p_\mathrm{f}(t)$ from the geophysical excitation by a trapezoidal integration. The value of the observed CW at t_0 was taken as initial condition. Doing so, we assumed that the atmosphere and the oceans are the only sources of the observed CW, thus neglecting the contribution of continental waters. The CW was extracted from the observed and modeled polar motions by singular spectrum analysis, a technique that allows one to isolate quasi periodic modes without any assumption on their periods. We chose a covariance lag close to 6.4 years in order to separate the CW from the annual oscillation of which amplitude is of the same order of magnitude (Fig. 1a). We repeated the integration of the geophysical data sets and the comparison with observed polar motion using different values for Q and computed the regression coefficient between the observed and modeled

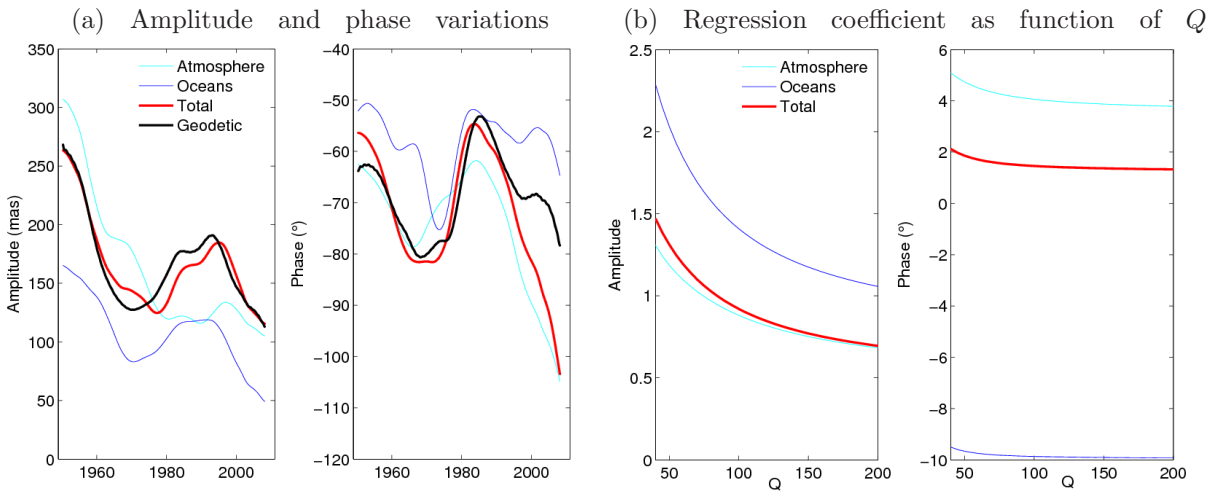

Figure 1: Variability of the observed and modeled Chandler mode: (a) amplitude and phase variations (b) regression coefficient as a function of Q

Chandler modes (Fig. 1b). The value $Q \sim 84$ produces an optimal regression. The amplitude and phase of the observed and modeled CW obtained with $Q = 84$ are displayed in Fig. 1. The regression coefficient between the observed and modeled CW is $1.001 + 0.027\,i$. The atmosphere alone poorly accounts for the CW irregularities. Though it explains the large amplitude before 1960, the minimum around 1970 and the bump in 1980–1990 is mainly due to the oceans. The atmospheric contribution remains stable within the same period. Similar remarks can be made for the phase variations before 1995. Around 2000, the phase of the observed CW presents a bump around $-70°$. The phase shifts of the CW are equivalent to variations of the observed Chandler period that can reach 33 days, corresponding to the period for which the forcing exhibits maximal energy in the vicinity of the eigenperiod. We repeated the integration using different starting epochs t_0, and we computed the regression coefficient between the observed and modeled Chandler modes. The combination of the atmosphere with the oceans generally drew the amplitude of the regression coefficient towards unity and the phase closer to zero.

Our results show that the integration of the NCEP/NCAR reanalysis project's atmospheric data, combined with the ECCO oceanic data, explain most of the observed variations in the CW amplitude and phase since the middle of the twentieth century. The integration approach therefore constitutes a valuable alternative method, which has the advantage of being more intuitive from the point of view of the astronomer who directly observes the position of the pole.

REFERENCES

Barnes, R. T. H., Hide, R., White, A. A., & Wilson C. A., 1983, Proc. R. Soc. London A, 387, p. 31
Bizouard, C., Remus, F., Lambert, S.B., Seoane, L., & Gambis D., 2011, A&A 526, A106. DOI 10.1051/0004-6361/201015894
Brzeziński, A., & Nastula, J. 2002, Adv. Sp. Res., 30, 195
Celaya, M., Wahr, J. M., & Bryan, F. O. 1999, J. Geophys. Res., 104, 12813
Danjon, A., & Guinot, B., 1954, C. R. Acad. Sci., 238, 1081
EOP PC 2010, http://hpiers.obspm.fr/eop-pc
Gross, R. S., 2000, Geophys. Res. Lett., 27, 2329
Mathews, P. M., Herring, T. A., & Buffett B. A., 2002, J. Geophys. Res., 107, B4, 10.1029/2001JB000390
Plag, H. P., 1997, In: Tidal Phenomena, Lecture Notes in Earth Sciences 66, Springer, 183
SBA 2010, IERS Special Bureau for the Atmosphere,http://geophy.uni.lu/ggfc-atmosphere.html
SBO 2010, IERS Special Bureau for the Oceans, http://geophy.uni.lu/ggfc-oceans.html
Seitz, F., & Schmidt, M., 2005, J. Geophys. Res., 110, doi:10.1029/2005JB003826
Vondrák, J. 1988, in: A. Kay & G. A. Wilkins (Eds.), International Astronomical Union Symposium 128, Kluwer Academic Publishers, Dordrecht, 359

VARIATIONS OF THE EARTH PRINCIPAL MOMENTS OF INERTIA DUE TO GLACIAL CYCLES FOR THE LAST 800KA

Ya. CHAPANOV[1], D. GAMBIS[2]

[1] National Institute of Geophysics, Geodesy and Geography of Bulgarian Academy of Sciences
Acad. G. Bonchev Str., Bl.1, Sofia 1113, Bulgaria, e-mail: chapanov@clg.bas.bg

[2] SYRTE, Observatoire de Paris, CNRS, UPMC
61, Avenue de l'Observatoire, 75014 Paris, France, e-mail: daniel.gambis@obspm.fr

The Earth shape, gravity and rotation are highly affected by climatic variations associated with the glacial cycles in the late Pleistocene. The processes of glaciation, followed by ice melting, are connected with significant changes of the mean sea level. These processes redistribute great amount of water masses between oceans and ice sheets, which lead to changes of the main moments of inertia. Let consider a homogeneous sphere with radius $R = 6371km$, density $4.9g/cm^3$ which corresponds to equivalent inertial moment of the real earth (the mean Earth density is $5.519g/cm^3$), inertial moment C, mean angular velocity ω_0 and constant mass M. From the conservation of angular momentum, the small changes of the radius R are connected with a corresponding change of the Length of Day (LOD) by the expressions $\Delta LOD = 2\Delta R\omega_0/(\omega_1 R)$, where $\omega_1 = 0.843994809prad/s$. The transfer from homogeneous elastic sphere to the real Earth need to replace the variations of radius R by equivalent changes of the mean sea level ΔMSL. It is necessary to determine transfer coefficient $k = \Delta MSL/\Delta R$ between the homogeneous elastic sphere and the real Earth. Involving coefficient q of ice sheets influence on the moment of inertia, and coefficient p of elastic Earth deformation due to ice loading effect we obtain $\Delta LOD = 2\omega_0(1-p)(1-q)\Delta MSL/(k\omega_1 R)$, $\Delta C = 0.8(1-p)(1-q)MR\Delta MSL/k$. By comparing of the observed amplitudes of 11-year oscillations of the MSL and UT1 we determine p= 0.58 and corresponding effectiveness of MSL on C and LOD variations $1 - p = 0.42$. The value of the coefficient k depends on the mean density of sea water at the ocean surface, total ocean surface and the moment of inertia of the thin ellipsoidal shell over the ocean with thickness equal to ΔMSL. In the case of small MSL variations (significantly less than 1m), the water lost occur from all Earth surface, more intensive from the free water surfaces and less intensive from the ground. The coefficient k is approximately equal to 5 in this case (Chapanov and Gambis, 2010). The MSL changes are more than 100m during the glaciations, the level of the water lost from the ground is neglectful, so $k = D_E S_E I_{ES}/D_O S_O I_{OS}$, where D_E is the mean Earth density ($4.9g/cm^3$), D_O - the mean sea water density at the ocean surface, S_E - the total Earth surface, S_O - the global ocean surface, I_{ES} - the moment of inertia of the thin ellipsoidal shell over the Earth, I_{OS} - the moment of inertia of the thin ellipsoidal shell over the ocean. The mean sea surface water density is $1.025g/cm^3$, so $D_E/D_O = 4.78$. The total Earth surface is 510 106 km^2, the global ocean surface - 361 106 km^2, and their ratio - 1.414. The continental ice sheets influence with surface S_{IC} on the axial moment of inertia is $q = S_O I_{IC}/S_{IC} I_{OC}$, where I_{IC} is the total moment of inertia of thin ellipsoidal shell over the continental ice sheets. The sea ice does not affect the moment of inertia changes, due to its hydrostatical equilibrium with the ocean water. Let the surface glacial data is represented over a grid with size $\alpha \times \alpha$ degrees and the geocentric coordinates of the center of the n-th grid element are geocentric distance r_n, longitude λ_n and latitude θ_n. If a and b denote Earth equatorial and polar radii ($a = 6478.137km$, $b = 6356.572km$), then $r_n = \sqrt{a^2b^2(a^2 sin^2\theta_n + b^2 cos^2\theta_n)}$ and the distance from the center of the n-th grid element to the Earth axis of rotation is $h_n = r_n cos\theta_n$. The surface of the n-th grid element is approximately $s_n = 4\pi^2(\alpha/360)^2 r_n h_n$ and the axial moment of inertia of thin ellipsoidal shell with unit density and thickness over a given area is $I = \sum_n s_n h_n^2$. The axial moment of inertia of ellipsoidal shell with unit density and thickness over the Earth is 1.38×10^{14} km^4 and over the ocean - $1.0\times10^{14} km^4$. Their ratio is 1.38, and the transfer coefficient k in the case of great MSL changes is k=9.3. The continental ice sheets during the last glacial maximum reach latitudes between 40° and 50° in the North America and between 50° and 60° in Euro-Asia. Roughly, this area is almost circular with radius 4400km (corresponding to 40° over the meridian). The center of this area is shifted by 10° from the North Pole to the Greenland direction. The South Pole ice sheet cover almost circular area with latitude above 50° (Paul and Schfer-Neth, 2003; Schfer-Neth and Paul, 2003), thus its radius is approximately the same as the North Pole ice sheet. It is possible to determine coefficient q by means of reconstructed data

of global sea surface temperature and salinity during the last glacial maximum (available in the World Data Center for Paleoclimatology, Boulder). A linear $S_O/S_{IC} = 0.084\Delta MSL + 12.45$ and a parabolic $I_{IC}/I_{OC} = 0.0019 + 5 \times 10^{-5}\Delta MSL + 5.71 \times 10^{-6}\Delta MSL^2$ dependencies exist (MSL is expressed in meters), so the coefficient q varies non-linearly between 0.022 and 0.2. The relative glacial steric sea level variations are 0.004 only and therefor it is possible to neglect. Finally the dependencies between LOD in ms (Fig.1, a), inertial moment C in $kg\,m^2$ (Fig.1, c) and glacial MSL variations in meters are

$$\Delta LOD = 2.29(1-p)(1-q)\Delta MSL, \qquad \Delta C = 1.025 \times 10^{12}(1-p)(1-q)I_{OS}\Delta MSL. \tag{1}$$

The moments of inertia of thin ellipsoidal shell with unit density and thickness over the ocean area I_A relative to the x axis and I_B relative to the y axis are $I_A = \sum_n s_n r_n^2(sin^2\theta_n + sin^2\lambda_n cos^2\theta_n)$, $I_B = \sum_n s_n r_n^2(sin^2\theta_n + cos^2\lambda_n cos^2\theta_n)$. The influence of the polar ice on the variations of the axial moments of inertia A and B is $I_P = 1.025(1-p)S_O\Delta MSL\, b'^2$, where b' is the polar Earth radius, corrected with the half mean polar ice hight. Let $I_{H(A,B)}$ denotes the corrections for Himalaya ice, then the variations ΔA and ΔB of the axial moments of inertia A and B (Fig.1, b) are

$$\Delta A = 1.025 \times 10^{12}(1-p)I_A\Delta MSL - I_P - I_{HA},\ \Delta B = 1.025 \times 10^{12}(1-p)I_B\Delta MSL - I_P - I_{HB}. \tag{2}$$

The MSL data for the last $800Ka$ are composed by the reconstructed MSL for the last $380Ka$, determined by the sediments from the Red sea (Siddall et al., 2003) and variations for the period $380Ka - 800Ka$ before present (BP), based on the temperature changes, determined by deuterium data from Antarctica ice core (Jouzel et al., 2007).

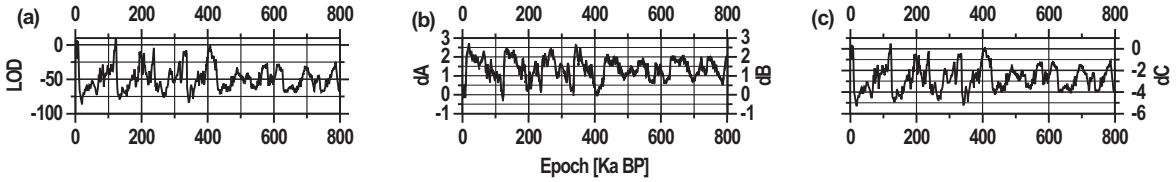

Figure 1: Variations of LOD in ms - (a), inertial moments A (solid line), B (dashed line) in $kg\,m^2 \times 10^{17}$ - (b) and axial moment C in $kg\,m^2 \times 10^{29}$ - (c).

The reconstructed glacial variations of the sea level for the last 800Ka give good opportunity for studying the millennial scale variations of the Earth rotation, shape and axial moments of inertia and to determine long-periodical oscillations of the Length of Day LOD and the Universal Time UT1. The changes of the Earth axial moments of inertia are due to global water redistribution between the ocean and continental ice, which is connected with the sea level variations. The variations of the axial moment of inertia C are synchronized with MSL variations with maximal value $-5.35 \times 10^{29} kg\,m^2$. The variations of the principal moments of inertia A and B are opposite to the MSL variations, due to dominating effect of the polar ice. Their maximal values during the glacial maxima are about $2.54 \times 10^{17} kg\,m^2$. The variations of the principal moment of inertia A are grater by 7% of the variations of the principal moment of inertia B. The periodical part of principal moments of inertia consists of frequencies similar to the frequencies of the Earth orbital variations with periods around $20Ka$, $40Ka$ and $100Ka$.

Acknowledgement. The paper was supported by the contract DO02-275 with the Bulgarian NSF.

REFERENCES

Chapanov, Ya., D. Gambis, 2010, "A model of global water redistribution during solar cycles, derived by astronomical data", Proc. BALWOIS 2010, Ohrid.

Jouzel, J., and 31 coauthors, 2007, "Orbital and Millennial Antarctic Climate Variability over the Past 800,000 Years". Science, Vol. 317, No. 5839, pp.793-797.

Paul, A., C. Schfer-Neth, 2003, "Modeling the water masses of the Atlantic Ocean at the Last Glacial Maximum", Paleoceanography, 18, No. 3, 1058.

Schfer-Neth, C., A. Paul, 2003, "The Atlantic Ocean at the last glacial maximum: 1. Objective mapping of the GLAMAP sea-surface conditions", in: G. Wefer, et al. (eds) "The South Atlantic in the Late Quaternary: Material Budget and Current Systems", Springer-Verlag, Berlin, Heidelberg, 531-548.

Siddall, M., E.J. Rohling, A. Almogi-Labin, C. Hemleben, D. Meischner, I. Schmelzer, and D.A. Smeed, 2003, "Sea-level fluctuations during the last glacial cycle", Nature, Vol. 423, pp. 853-858.

COMBINATION OF GPS AND GLONASS IN PPP ALGORITHMS AND ITS EFFECT ON SITE COORDINATES DETERMINATION

J. HEFTY[1], L. GERHATOVA[1], J. BURGAN[1]

[1] Department of Theoretical Geodesy, Slovak University of Technology
Radlinskeho 11, 813 68 Bratislava, Slovakia
e-mail: jan.hefty@stuba.sk, lubomira.gerhatova@stuba.sk, juraj.burgan@stuba.sk

ABSTRACT. Precise Point Positioning (PPP) approach using the un-differenced code and phase GPS observations, precise orbits and satellite clocks is an important alternative to the analyses based on double differences. We examine the extension of the PPP method by introducing the GLONASS satellites into the processing algorithms. The procedures are demonstrated on the software package ABSOLUTE developed at the Slovak University of Technology. Partial results, like ambiguities and receiver clocks obtained from separate solutions of the two GNSS are mutually compared. Finally, the coordinate time series from combination of GPS and GLONASS observations are compared with GPS-only solutions.

1. INTRODUCTION

The PPP processing enables direct determination of geocentric coordinates using the Global Navigation Satellite System (GNSS) observations without necessity of connection to reference stations. The attachment to the geocentric reference frame is achieved by application of precise satellite orbits and satellite clocks provided by IGS. Principal information about PPP is given by Kouba and Heroux (2001). The necessary reduction procedures and adjustment algorithms were developed for GPS observations. As the European Space Operation Centre (ESOC) produces besides GPS based data also orbits and clocks for GLONASS there is a chance to modify the PPP procedures also for other GNSS. The aim of this paper is to demonstrate experiences from introducing GLONASS into the PPP processing scheme and to discuss some partial result. The final effect of inclusion of GLONASS will be examined by inspection of geocentric coordinates. Coordinates obtained by application of the PPP software ABSOLUTE will be compared to products estimated by Bernese GPS Software Version 5.0 (Dach et al., 2007).

2. ADJUSTMENT STRATEGY

Principal steps of processing of GPS and GLONASS in the ABSOLUTE software package are: (1) Pre-processing of continuous simultaneous dual frequency phase and code observations resulting in the iono-free pseudoranges and approximate real valued phase ambiguities. (2) Interpolation of precise orbits and satellite clocks. (3) Reduction of observed ranges for systematic phenomena and computation of $o-c$ (observed minus calculated) values. (4) Forming of adjustment model and estimation of site coordinates, receiver clocks, corrections to approximate ambiguities, troposphere zenith delays and other optional parameters. Processing starts with iterative separate GPS and GLONASS adjustment and is followed by the combination of observations from both GNSS in one batch. In the ABSOLUTE software package we applied models for following range corrections: satellite clocks offsets, special relativity effect, satellite antenna offsets and differential code biases, Sagnac effect due to Earth rotation, troposphere correction, site displacement due to solid Earth tides, effects of sub-daily polar motion, Earth rotation variations and receiver antenna offsets. The theoretical background for the utilized reductions is given e.g. in (Kouba and Heroux, 2001) and (Xu, 2007). The main differences in PPP processing of GPS and GLONASS are: (1) Different orbital parameter, (2) Different signal modulations, (3) Carrier frequencies: GPS unique for all satellites, GLONASS satellite dependent. (4) Used GNSS receiver code observables: GPS C/A and P2, GLONASS P1 and P2. (5) Maximum number of operational satellites: GPS 31, GLONASS 21.

3. EXPERIMENTAL RESULTS

We will demonstrate some results related to the GPS and GLONASS PPP processing on the basis of the one-month interval (DOY 001-DOY 031 of 2010) of 24-hour sessions at the IGS and EUREF GNSS

permanent station Ganovce (GANP), Slovakia, equipped with Trimble NETR8 receiver. The accuracy of L3 ambiguities resolution obtained in the first step of processing is shown in Fig. 1a. We emphasize that no orbit or clock information was used in this case and the RMS errors reflect the internal consistency of code and phase observations. The generally larger uncertainties for GLONASS are clearly visible. Fig. 1b shows independent GPS and GLONASS receiver clock estimates. Besides the constant bias of 240 ns between the two solutions we point to the sub-daily variability of their difference. Finally, in Fig. 1c are shown RMS residuals of phase observations for GPS and GLONASS estimated from one-month interval of PPP processing. It is evident that the GLONASS values are more variable than the GPS ones, especially the GLONASS PRN 7, 14 and 15 systematically manifest extremely large phase residuals. Time series of coordinate estimates of one-month period of 24-hour PPP solutions resulting from ABSOLUTE application for GPS-only and for GPS+GLONASS are in Fig. 2. The Bernese software based PPP solutions restricted to GPS observations are shown for comparison. The introduction of GLONASS into the combined adjustment decreased the coordinate repeatability.

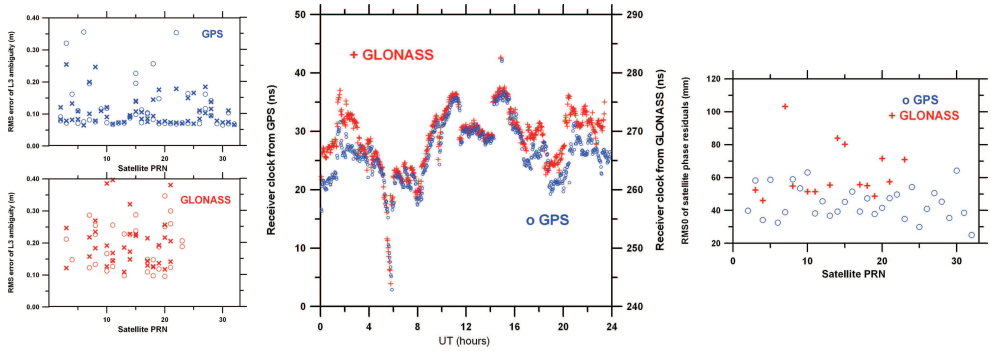

Figure 1: a) RMS errors of L3 ambiguities estimates, x-DOY 002, o-DOY 028 (left), b) Receiver clock estimates (middle), c) RMS phase residuals (right).

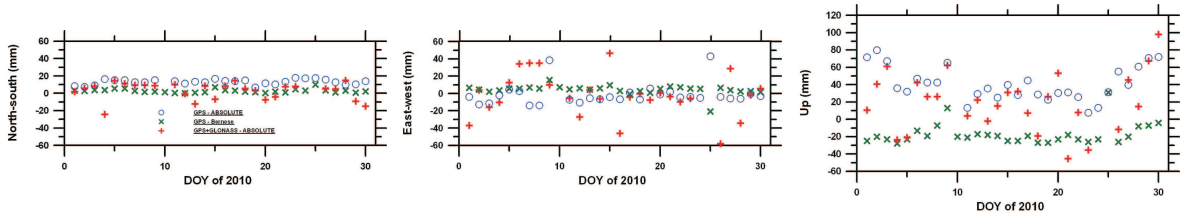

Figure 2: Local coordinate variations from PPP solutions using ABSOLUTE and the Bernese software

4. CONCLUSIONS

We demonstrated the possibilities and limitations of inclusion of GLONASS into the PPP processing. The GLONASS observations, ESOC GLONASS orbits and satellite clocks are suitable for PPP positioning. However, the accuracy of GLONASS phase and code observations as well as the reduction process yields less stabile $o - c$ values and does not improve the GPS-only PPP adjustment. The possibilities of enhancement the models for application of GLONASS in PPP are in progress.

Acknowledgement. This work was supported by Grant No. 1/0569/10 of the VEGA Grant Agency.

5. REFERENCES

Dach, R., Hugentobler, U., Fridez, P. and Meindl, M. (eds), 2007, "Bernese GPS Software Version 5.0", Astronomical Institute, University of Berne, 2007, 612 p.

Kouba, J. and Heroux, P., 2001, "Precise Point Positioning Using IGS Orbit and Clocks Products", GPS Solutions, Vol. 5, No. 2, pp. 12-28.

Xu, G., 2007, "GPS Theory, Algorithms and Applications", Springer, Berlin - Heidelberg, 340 p.

DETERMINATION OF NUTATION OFFSETS BY COMBINING VLBI/GPS-PRODUCED NORMAL EQUATIONS

M. KUDRYASHOVA[1], S. LAMBERT[2], V. DEHANT[1], C. BRUYNINX[1], P. DEFRAIGNE[1]

[1] Royal Observatory of Belgium
3, av. Circulaire, 1180, Brussels
e-mail: mariak@oma.be

[2] Paris Observatory
61 avenue de l'Observatoire, F-75014 Paris, France

ABSTRACT. Long standing routing operation of individual geodetic space- and ground-based techniques (like, for instance, VLBI, GNSS, LLR, etc.) revealed their strong and weak aspects. More effective use of these strengths as well as reduction of their weaknesses is possible by incorporating of the information collected by each individual technique into combined products. Such a consistent combination can be performed either by combination at the observational level or at the level of normal equations (NEQ's). We concentrate on the combination of normal equations gathered during VLBI/GPS-data processing. The main goal of this combination is to construct a time series of nutation offsets in the most consistent way. The objective of this presentation is to describe the developed strategy of combination and to present the current status of its implementation and first results. Combination presented here is based on the normal equations stemmed from the processing of VLBI and GPS observations during a continuous VLBI campaign CONT08. Earth orientation parameter determination will, in our procedure, benefit from angle and rate observation for a unique estimation.

1. GPS AND VLBI SOLUTIONS

In order to generate both GPS and VLBI normal equations we took observations gathered during campaign CONT08. CALC/SOLVE software (Paris Observatory) is used to produce VLBI solution. GPS observations are processed with Bernese v.5.0 software at the Royal Observatory of Belgium. During the processing of observations site coordinates are constrained to the ITRF2005 values. We used IAU2000A nutation model as a reference for both solutions. Diurnal and semidiurnal variations in the EOP are modeled according to the IERS 2003 conventions. Niell mapping function (MF) have been chosen for the troposphere modeling. There are two main reasons for such a choice: 1. we pre-eliminate troposphere parameters before NEQ saving and thus, this a priori model cannot be changed during the combination process; 2. more modern MF are not implemented into CALC/SOLVE package.

2. RIGOROUS COMBINATION OF NUTATION OFFSETS AND RATES (PRELIMINARILY RESULTS)

For a combination of Earth orientation parameters and site coordinates at the level of normal equations (with the primary goal of combining nutation offsets and rates) we used Bernese v.5.0 software [1]. For this purpose an implementation of some additional procedures like calculation of weighting factors and introduction of local ties have been perforemed. In order to find an appropriate weights for individual data sets we used the procedure described in the work of Thaller, 2008. The obtained re-weighting factors are summirized in Table 1. They are in a good agreement with re-weighting factors obtained in other studies for VLBI/GPS combination performed by means of Bernese software [2],[3]. In this study all available local ties have been taken into consideration (in spite of qualities of individual ties).

Fig. 1 represents the difference between our combined solution and IERS C04 time series. The comparison shows rather good agreement between our combined estimation for polar motion and the values from IERS C04. For the nutation offsets the correspondence is worse probably due to: 1. the systematic errors introduced by GPS orbits missmodeling which are shifting away the nutation rates; 2. nutation values given by IERS C04 are interpolated values and thus do not suit very well for comparison purpose.

	this work		Thaller(2008)		Thaller,Rothaher(2003)	
	GPS	VLBI	GPS	VLBI	GPS	VLBI
data used	dayly solutions (CONT08)		dayly solutions (CONT02)		1 yr of weekly solutions IERS comb campaign	
weighting factor	$2.5648 * 10^{-5}$	1.0	$3.7636 * 10^{-6}$	1.0	$5.1321 * 10^{-6}$	1.0

Table 1: The comparison of the weighting factors, which have been calculated for this work, with the values used in the work of Thaller [1] and IERS SINEX Combination campaign [2]. Since we use Bernese software to process GPS observations and also for further combination of GPS/VLBI normal equations, we are keeping GPS NEQ's in the Bernese's internal format. In it's internal manipulations, Bernese software multiply GPS-based normal equations with the weighting factor $\sigma^2 = 10^{-6}$. Thus, the difference of 5-6 orders in weighting factors for VLBI and GPS Neq matrices is not real.

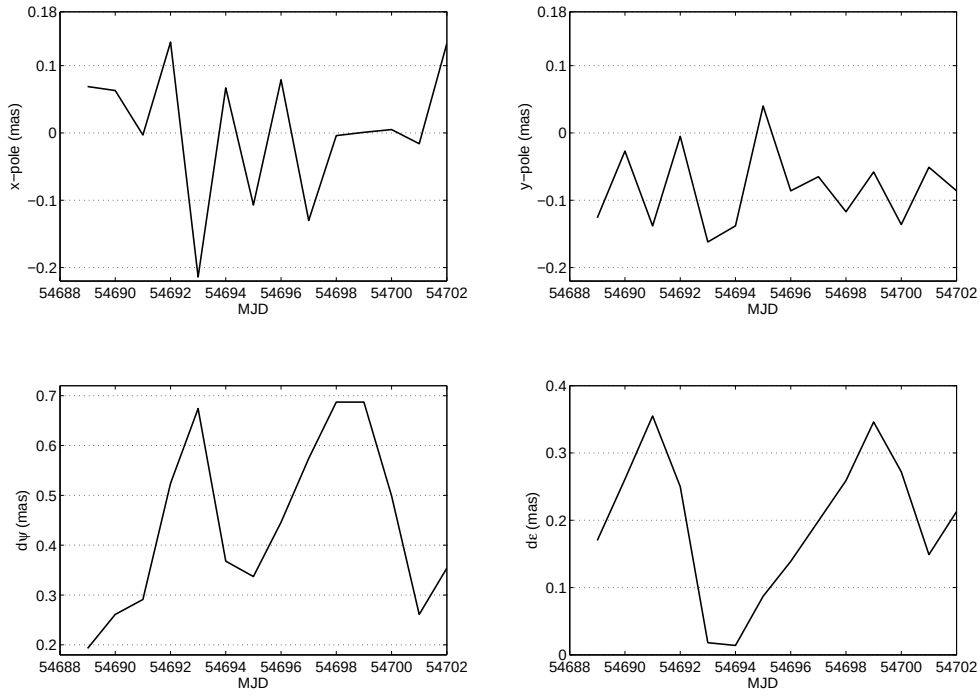

Figure 1: Difference between combined solution and IERS C04 time series. Upper panel: x- and y-pole coordinates (left and right, respectively) over two weeks. The total scales on the two graphs are 0.4 and 0.25 mas for the x- and y-pole coordinates, respectively. Bottom panel: nutation offsets in longitude and obliquity (left and right, respectively) over two weeks. The total scales on the two graphs are 0.4-0.5 mas.

3. REFERENCES

Bernese GPS Software v. 5.0, U.Hugentobler, R. Dach, P.Fridez (eds.), 2007.

Thaller, D., 2008, "Inter-technique combination based on homogeneous normal equation systems including station coordinates, Earth orientation and troposphere parameters"; Dissertation, Scientific Technical Report STR 08/15, Deutsches GeoForschungsZentrum, ISSN 1610-0956, doi: 10.2312/GFZ.b103-08153.

Thaller, D., Rothacher, M., 2003, "Comparison and Combination of GPS, VLBI and SLR Solution Series", in: A. Rudloff, L. Stroink, (eds.) Observation of the System Earth from Space, GEOTECHNOLOGIEN Science Report, Nr. 3, pp. 176-180.

OPERATIONAL AND RESEARCH ACTIVITY AT OPAR

S. B. LAMBERT, A.-M. GONTIER, C. BARACHE
Observatoire de Paris/SYRTE/CNRS/UPMC
61 av. de l'Observatoire 75014 Paris
http://ivsopar.obspm.fr
ftp://ivsopar.obspm.fr

ABSTRACT. The IVS analysis center of the Paris Observatory (OPAR) was born in 1999 when the IVS was created. In the early years, the operational activity was mainly focused on the production of UT1 from intensive sessions. The activity was renewed in 2007 with the submission of a new long term solution to the IVS. OPAR now proposes a larger number of VLBI products.

1. THE ANALYSIS SERVICE

The base solutions provide up-to-date TRF and CRF data together with consistent EOP series. They are generally released on or about the first day of January, April, July and October. The analysis configuration includes all EOP and rates as session parameters, most of radio source and station coordinates as global parameters, a wise modeling of station non linear motions, and clock offsets and troposphere gradients as segmented parameters. The geophysical modeling includes the Vienna mapping functions (Böhm et al. 2006) for a priori zenith delay, and the APLO data (Petrov & Boy 2004) the FES 2004 model (Lyard et al. 2006) for atmospheric and oceanic loading, respectively. The latest solution (opa2010d) processed more than 5,000 sessions back to 1979 (7.3 million ionosphere-free group delays).

In a specific analysis configuration, we regularly estimate station and radio source coordinates per session. In addition, our web pages propose follow-ups of various physical phenomena like the free core nutation, the unmodeled tidal nutation terms, and the post-seismic displacement of the TIGO station at Concepción, Chile.

As soon as new observations are delivered at the IVS data center, an automated script launches a the rapid solution to process them. EOP, station and source coordinates are aligned to the current base solution. The updated EOP series (i.e., base + rapid, starting in 1979) are posted at

`ftp://ivsopar.obspm.fr/vlbi/ivsproducts/eops/opa*`

The intensive solution estimates UT1 from VLBI intensive sessions (short duration, about 1 hour). Up-to-date UT1 series are posted at

`ftp://ivsopar.obspm.fr/vlbi/ivsproducts/eopi/opa*`

SINEX files are routinely produced for diurnal and intensive experiments to participate in the IVS combination made at the Analysis Coordinator office. The files are made available at

`ftp://ivsopar.obspm.fr/vlbi/ivsproducts/daily_sinex/opa*`
`ftp://ivsopar.obspm.fr/vlbi/ivsproducts/int_sinex/opa*`

To better match the IERS requirements in terms of latency, the rapid and intensive operational solutions and the production of SINEX files have been running automatically since early 2010. The incoming new observations posted at one of the IVS primary data centers are analyzed at OPAR within a few hours.

2. THE DATA CENTER

OPAR is one of the three IVS primary data centers. Their activities are done in close collaboration for collecting files, and making them available to the community as soon as they are submitted. The access

protocol gives to the IVS community a transparent access to a data center through the same directory, and a permanent access to files in case of a data center breakdown. The OPAR data center is operated on a PowerEdge 2800 - Xeron 3.0 GHz server located at Paris Observatory, and running a Fedora Linux operating system. The server is equipped with a RAID 3 TB disk extensible up to 4.7 TB. The OPAR server is accessible 24/7 through a 2 Mb/s Internet connection. In 2009, 13 distinct users submitted data to OPAR.

3. RESEARCH AND DEVELOPMENT

OPAR personnel contributes to research in the fields of astrometry and geosciences. Some of the topics are directly related to VLBI analysis and take benefit from the OPAR analysis center facilities.

3.1 CONTRIBUTION TO THE ICRF2

Various schemes to select the most suitable radio sources to realize a stable celestial reference frames were investigated (e.g., Lambert & Gontier 2009) to prepare the next ICRF. OPAR personnel was involved in the ICRF2 project for selecting the defining sources and aligning the new frame to the ICRS. This work was done in collaboration with P. Charlot (Bordeaux Observatory) and E. F. Arias (BIPM). See more details in Fey et al. (2010).

3.2 DISSIPATION IN THE EARTH'S CORE REGIONS

We investigated the nutation offsets derived from VLBI measurements in order to improve the current determination of the outer core parameters, especially the quality factor (i.e., imaginary part of the free core nutation frequency) that expresses the energy dissipation at the core-mantle boundary due to viscosity and other dissipative processes (Rosat & Lambert 2009).

3.3 LIGHT DEFLECTION BY THE SUN

The post-Newtonian parameter γ was determined by a global inversion of the full VLBI observational database in Lambert & Le Poncin-Lafitte (2009), yielding a value close to unity with an error of less than 2×10^{-4}. Recent new determinations with improved geophysical and astronomical models and an increased number of observations gave $|\gamma - 1|$ less than 10^{-4} with an error of 1.2×10^{-4} (Lambert & Le Poncin-Lafitte 2010).

3.4 MEASUREMENT OF THE SECULAR ABERRATION DRIFT

We detected the effect of the Galactocentric acceleration of the Solar system barycenter in quasar proper motions at the level of $\sim$6 mas/yr oriented within $\sim 8^\circ$ around the Galactic center, in fair agreement with theoretical predictions from recent determinations of the Galactic parameters (Titov et al. 2010).

4. REFERENCES

Böhm, J., Werl, B., & Schuh, H. 2006, J. Geophys. Res., 111, 10.1029/2005JB003629

Fey, A. L., Gordon, D. G., & Jacobs, C. S. (Eds.) 2009, The Second Realization of the International Celestial Reference Frame by Very Long Baseline Interferometry, Presented on behalf of the IERS / IVS Working Group, International Earth Rotation and Reference Systems Service (IERS) Technical Note 35, Frankfurt am Main: Verlag des Bundesamts für Kartographie und Geodäsie

Lambert, S. B., & Gontier, A.-M. 2009, A&A, 493, 317

Lambert, S. B., & Le Poncin-Lafitte, C. 2009, A&A, 499, 331

Lambert, S. B., & Le Poncin-Lafitte, C. 2010, A&A, submitted

Lambert, S. B., Dehant, V., & Gontier, A.-M. 2008, A&A, 481, 535

Lyard, F., Lefèvre, F., Letellier, T., & Francis, O. 2006, Ocean Dyn., 56, 394

Petrov, L., & Boy, J.-P. 2004, J. Geophys. Res., 109, 3405

Rosat, S. & Lambert, S. B. 2009, A&A, 503, 287

Titov, O., Lambert, S. B., & Gontier, A.-M. 2010, A&A, in revision

PHYSICAL CHARACTERISTICS OF THE ICRF2 SOURCES

A.-M. GONTIER, S. B. LAMBERT
Observatoire de Paris/SYRTE/CNRS/UPMC
61 av. de l'Observatoire 75014 Paris

1. INTRODUCTION

This paper summarizes the way we obtained the physical information on the ICRF2 radio sources. This information includes the object type, redshift, 8.4 GHz and 2.3 GHz fluxes, spectral index, visual magnitude, a classification of spectrum, and comments. The physical characteristics are made available in ASCII format at the International Celestial Reference System Product Center (ICRS-PC) of the International Earth rotation and Reference systems Service (IERS) at:

`http://hpiers.obspm.fr/icrs-pc`

under the section "Information on radio sources".

2. INFORMATION RETRIEVAL FROM CATALOGUES AND DATA BASES

The physical characteristic were obtained from the following primary catalogues or compilations:

- The Large Quasar Astrometric Catalogue (LQAC, Souchay et al. 2009) is a compilation of 12 of the largest quasar catalogues (4 from radio interferometry programs, 8 from optical surveys). It contains 113,666 quasars, providing information when available on: u, b, v, g, r, i, z, J, K photometry as well as redshift, radio fluxes at 1.4 GHz, 2.3 GHz, 5.0 GHz, 8.4 GHz, 24 GHz, and redshift references,
- Malkin & Titov (2008, hereafter referred to as MT08) includes 4,261 radio sources with J2000.0 coordinates, redshift, V magnitude, object type and comments,
- Véron-Cetty & Véron (2006, hereafter referred to as VV06) provides a list of 85,221 quasars, 1,122 BL Lac objects and 21,737 active galaxies together with known lensed quasars and double quasars,
- Healey et al. (2007, hereafter referred to as H07) publishes precise positions, sub arc second structures, and spectral indices for some 11,000 sources, and
- Stickel et al. (1989–1993), referred to as S89, provides position, magnitude, type of the optical identification, flux at 5 GHz and two-point spectral index between 2.7 GHz and 5 GHz.

Essentially, the table of radio source physical characteristics has been derived by sequentially obtaining data using these five references. The steps were as follows:

1. The LQAC was used to provide information on flux at 8.4 GHz and 2.3 GHz and initial information for the redshift and the magnitude.
2. A comparison was made with the MT08 catalogue. Matches were done by IERS name. In this comparison, information on object type and comments was brought in. The redshift and the magnitude were checked and such data were provided for some sources. Most of the found discrepancies are explained by the comments.
3. The VCV06 data were merged in a similar fashion. At this stage, the object type was refined and the classification of spectrum was added.
4. Spectral index data between low frequency and 8.4 GHz were taken from the H07 catalogue and completed for 7 sources by the S89 catalogue.

Table 1: Table giving the number of ICRF2 sources for which physical informations are available.

	Redshift	Magnitude	Spectral Index	Flux
Redshift	1,571			
Magnitude	1,354	2,012		
Spectral Index	1,292	1,682	2,543	
Flux	1,459	1,840	2,317	3,051

This research has made use of the NASA/IPAC Extragalactic Database (NED) which is operated by the Jet Propulsion Laboratory, Caltech, under contract with the National Aeronautics and Space Administration. This research has also made use of the Virtual Observatory tool TOPCAT.

3. CONCLUDING REMARKS

An important part of the redshifts, magnitudes and spectral indices is still missing and observation programs must be undertaken to complete the ICRF2 information. The permanently updated database of MT08 and the upcoming version 2 of the LQAC will be of interest for an update in a near future. Regular VLBI monitoring of sources with poor observational history must also be scheduled.

4. REFERENCES

Souchay, J., Andrei, A. H., Barache, C., et al. 2009, The Large Quasar Astrometric Catalog (LQAC), A&A, 494, 799

Malkin, Z., & Titov, O. 2008, Optical Characteristics of Astrometric Radio Sources, In: A. Finkelstein and D. Behrend (Eds.), Measuring the Future, Proc. Fifth IVS General Meeting, 183

Véron-Cetty, M.-P., Véron, P.2006, Quasars and Active Galactic Nuclei (12th Ed.), A&A, 455, 773

Healey, S. E., Romani, R. W., Taylor, G. B., et al. 2007, CRATES: An All-Sky Survey of Flat-Spectrum Radio Sources, ApJ Suppl. Ser., 171, 61

Stickel, M., Fried, J. W., & Kuehr, H. 1989, Optical spectroscopy of 1 Jy BL Lacertae objects and flat spectrum radio sources, A&A Suppl. Ser., 80, 103

Stickel, M., Kuehr, H., & Fried, J. W. 1993, Spectroscopy of 1 Jy and S5 radio source identifications, A&A Suppl. Ser., 97, 483

Stickel, M., Fried, J. W., & Kuehr, H. 1993, The complete sample of 1 Jy BL Lac objects. II - Observational data, A&A Suppl. Ser., 98, 393

AMPLITUDE AND PHASE VARIATIONS OF THE CHANDLER WOBBLE FROM 164-YR POLAR MOTION SERIES

Z.M. MALKIN, N.O.MILLER

Central Astronomical Observatory at Pulkovo of RAS
Pulkovskoe Ch. 65, St. Petersburg 196140, Russia
e-mail: malkin@gao.spb.ru, natm@gao.spb.ru

ABSTRACT. This paper is aimed at investigation of the Chandler wobble (CW) at the 164-year interval to search for the major CW amplitude and phase variations. The CW signal was extracted from the IERS polar motion series using digital filtering. The CW amplitude and phase variations were examined by means of several methods which yield very similar results. Results of our analysis have shown that, besides the well-known CW phase jump in the 1920s, two other large phase jumps have been found in the 1850s and 2000s, all three contemporarily with a sharp decrease in the CW amplitude.

1. INTRODUCTION

The Chandler wobble (CW) is one of the principal eigenmodes of the Earth rotation, and investigation of its properties such as period, amplitude and phase variations is very important for the understanding of the physical processes in the Earth. Among other interesting CW peculiarities, the phase jump of about 180° with simultaneous drastic decreasing of the CW amplitude occurred in the 1920s and supposed to be an unique event is a subject of intensive investigation by many authors. However recent work of Miller (2008) has shown clear evidence of two other large CW phase jumps that occurred in the beginning and the end of the IERS C01 PM series used for the analysis. In this paper, we performed more detailed investigation of the 164-year PM series to confirm that preliminary finding. Our study consists of three steps: forming the longest available IERS PM time series joining C01 and C04 series, extracting CW signal, and analyzing this signal. To improve reliability of our conclusions, several methods of analysis were used, and their results corroborate each other. This work is similar to our previous study (Malkin & Miller 2009) with more data added to the end of the interval.

2. DATA PROCESSING AND RESULTS

To extract the CW signal from the PM series one have to separate it from trends and all periodic and quasi-periodic terms out of the CW frequency band. This was done by means of using Fourier and Singular Spectrum Analysis (SSA) filtering. To extract the CW amplitude and phase variations from the filtered PM series two different techniques were used. First, we used the method previously developed for study of the Free Core Nutation, which allows us to find the CW amplitude and phase variations using wavelet technique (Malkin 2007). Secondly, we used the SSA and the Hilbert transform (HT) to compute an independent time series of the CW amplitude and phase.

The CW amplitude variations are shown in Fig. 1 for two methods used. One can see that both methods show very similar behavior of the CW amplitude, with some differences near the ends of the interval. In both CW series, three deep minima of the amplitude below 0.05 mas around 1850, 1925 and 2005 are unambiguously detected.

The results of the computation of the CW phase variations using Hilbert transform after removing the linear trend are shown in Fig. 2. Using wavelet transform yields very similar results (Malkin & Miller 2009). One can see similar behavior of the CW phase obtained in two variants, with some differences near the ends of the interval. However, substantial phase jumps in the the 1850s and 2000s are clearly visible in all the cases, and their epochs are contemporary with the minima of the CW amplitude as shown in Fig. 1. So, we can conclude that the well-known event in the 1920s of the simultaneous deep minimum of the CW amplitude and the large phase jump in the 1920s may be not unique.

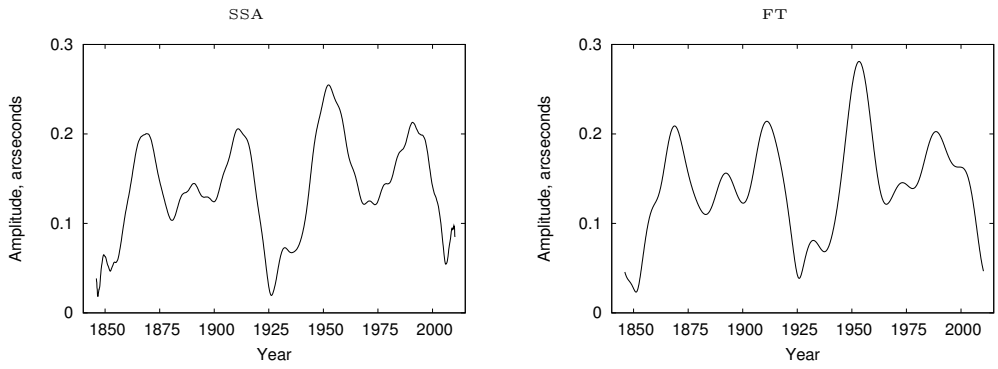

Figure 1: The CW amplitude computed for SSA-filtered and FT-filtered CW time series. Unit: mas.

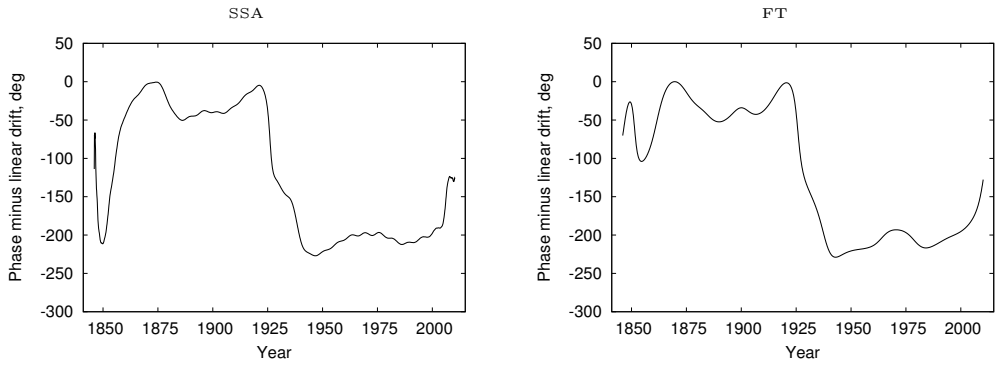

Figure 2: The CW phase variations computed for SSA-filtered and FT-filtered CW series. Unit: degrees.

3. CONCLUSIONS

In this paper, we have investigated the whole 164-year PM series available from the IERS with the main goal to reveal and evaluate the major CW phase jumps. To improve the reliability of the results we used several analysis methods. All the methods gave very similar results, with some differences at the ends of the interval. These discrepancies can be most probably explained by different edge effects of the methods used, but they can hardly discredit the final conclusion that can be made from this study about existence of two epochs of deep CW amplitude decrease around 1850 and 2005, which are also accompanied by a large phase jump, like the well-known event in the 1920s. Thus, the latter seems to be not unique anymore.

Unfortunately, both periods of the phase disturbances found in this paper are located at the edges of the interval covered by the IERS EOP series. As for the end of the interval, the next decade will allow us to quantify the phase jump in the beginning of the 21st century more accurately. On the other hand, a supplement study seems to be extremely important to try improve our knowledge of the PM in the 19th century, including an extension of the PM series in the past.

Acknowledgements. One of the authors (ZM) is grateful to the organizers of the conference for the travel support.

4. REFERENCES

Malkin, Z.M., 2007, "Empiric Models of the Earth's Free Core Nutation", Solar System Research, 41, pp. 492–497.

Malkin, Z., Miller, N., 2009, "Chandler wobble: two more large phase jumps revealed", Earth, Planets and Space, accepted (preprint is available in arXiv: 0908.3732).

Miller, N., 2008, "On the Chandler wobble amplitude and phase variations", Izvestiya Vysshikh Uchebnykh Zavedeniy: Geodeziya i Aerofotos'emka, No. 5, 48–49. (in Russian)

METHOD FOR PREDICTION OF ΔT BASED ON LONG-PERIODIC TERMS IN THE EARTH'S RATE OF ROTATION

D. MARČETA[1], S. ŠEGAN[2]

[1] Faculty of Mathematics, Belgrade University
Studentski trg 16, Belgrade, Serbia
e-mail: dmarceta@matf.bg.ac.rs

[2] Faculty of Mathematics, Belgrade University
Studentski trg 16, Belgrade, Serbia
e-mail: ssegan@matf.bg.ac.rs

ABSTRACT. In this paper we have examined possibilities for prediction of ΔT by searching for similarities in variations of the Earth's rate of rotation and solar activity for the past 250 years. Some results indicate that solar activity, directly or indirectly, has a significant influence on the changes in the Earth's rate of rotation.

1. ANALYSIS

By analyzing variation in the length of day (LOD) and variation in the Solar activity, namely number of Sun spots (NSS), some interesting relations were noticed. If Figure 1 are shown 11 years moving averages of these two variations from 1761. to 1997.

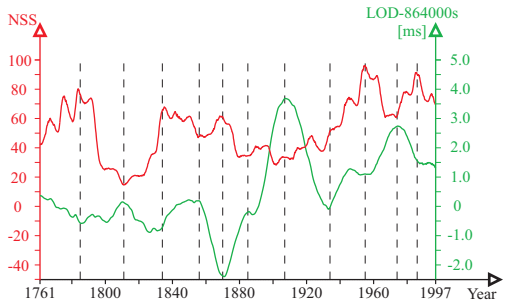

Figure 1: Variation of NSS and LOD

Vertical lines in Figure 1 show that local extremes of both variations are coupled in such a way that maxima in Solar activity match minima in LOD and vice versa, which indicates that the Earths rate of rotation is somehow connected with the solar activity.

In order to find out if there are some mutual periodical changes in these two parameters, we applied different types of spectral analysis on the data shown in the Figure 1. We assumed that these two sets of data can be approximated with polyharmonic function of the form:

$$y = C_0 + \sum_{i=1}^{n} C_i \cos\left(\frac{2\pi}{T_i}t + \varphi_i\right) \tag{1}$$

Where C_0 is a free term, $C_i s$ are amplitudes, $T_i s$ periods, $\varphi_i s$ phases and n is a number of the assumed harmonics.

2. RESULTS

The data from the Figure 1 are approximated with the equation (1) with 9 harmonics and their periods in years, amplitudes and phases are shown in Table 1.

LOD	T_i	20	23	28	33	40	54	80	86	230	$C_0 = 0.54$
	C_i	0.11	0.24	0.24	0.44	0.27	0.94	1.32	0.46	1.33	
	φ_i	296.2	231.2	221.7	164.8	167.7	108.8	37.9	202.5	65.5	
NSS	T_i	21	22	27	30	41	56	86	167	224	$C_0 = 48.56$
	C_i	3.22	2.56	3.27	3.82	5.29	8.40	12.77	22.18	29.51	
	φ_i	211.1	241.9	346.5	172.4	111.4	197.6	308.5	151.3	18.8	

Table 1: Periods in years, free terms, amplitudes and phases of the harmonics

From the Table 1, it can be seen that LOD and NSS can be approximated with polyharmonic functions with 9 harmonics, from which 8 are with same or nearly same periods.

According to Stephenson and Morrison, for a very near future, mathematical modelling can be used to project values of ΔT with great confidence. Accepting their suggestion, we made a mathematical approximation of the form:

$$\Delta T = C^0 + C^1 t + \sum_{i=1}^{n} C_i \cos\left(\frac{2\pi}{T_i} t + \varphi_i\right) \tag{2}$$

Periods in years of the harmonics in the approximation (2) are given in Table 2.

T_i	222.2	46.0	22.2	19.5	12.5	9.3	7.9	6.5	5.8	5.3	4.6	4.1	3.6	1.1	1.0	0.5

Table 2: Periods in years of the harmonics in the approximation (2)

Comparing Tables 1 and 2, it can be seen that there are three terms in approximations of ΔT, LOD and NSS that have almost same periods. In Figure 2 is shown this approximation and extrapolation to 2025.

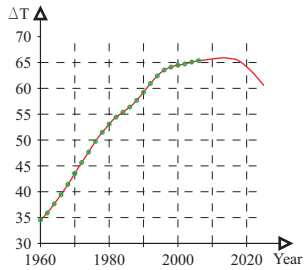

Figure 2: Approximation of ΔT from 1962. to 2025. (points are IERS data)

3. CONCLUSION

The above analysis shows that solar activity, directly or indirectly, has a significant influence on the changes in the Earth's rate of rotation. This allows us to use changes in the solar activity to predict changes in LOD and thus ΔT. This could also be done backward in time to estimate solar activity based on historical data of ΔT.

4. REFERENCES

Morrison, L. V., Stephenson, F. R., 2004, "Historical values of the Earth's clock error ΔT and the calculation of eclipses" Journal for the History of Astronomy, Vol. 35, Part 3, No. 120, pp. 327-336

Hide, R., Dickey, J. O., 1991, "Earth's Variable Rotation", Science, Vol. 253, No. 5020, pp. 629–637

Vondrák, J, Čepek, A, 2001, "On the use of the method of combined smoothing to combine EOP data from different techniques", Journées 2000 Systèmes de référence spatio-temporels, Paris

APPLICATIONS OF SIMULTANEOUS GROUND-BASED AND SATELLITE OBSERVATIONS

F.J. MARCO[1], M.J. MARTINEZ[2]

[1] Universidad Jaume I
Dept. Matematicas. Institut de Matematiques I Aplicacions de Castello. Catellon. Spain
e-mail: marco@mat.uji.es

[2] Universidad Politecnica de Valencia
Dept. Matematica Aplicada. Valencia. Spain
e-mail: mjmartin@mat.upv.es

ABSTRACT. Simultaneous ground-based and satellite observations either of a body of the solar system or an external source, together with mutual observations between satellite and Earth observational sites could be used to monitor different reference systems.

1. GENERAL DESCRIPTION OF THE METHOD

We consider F and f, the functionals to optimize, where f depends on the following set of parameters: the terrestrial physical π_ϕ, the geometrical of the terrestrial system π_E and the geometrical of the considered system (for example, a net of artificial satellites) π_S . Analogously, the functional F also includes, implicitly, parameters related to the terrestrial motion in the inertial system Π_E, geometrical of the terrestrial system π_E and also physical π_ϕ. From the initial values $\pi^0_\phi, \pi^0_E, \pi^0_S$ we can obtain increments $\delta\pi^0_\phi, \delta\pi^0_E, \delta\pi^0_S$ minimizing the functional f. The previous process provides values, which we denote as $\pi^1_\phi, \pi^1_E, \pi^1_S$ which are the result of adding to the initial values the obtained increments.
These new parameters are included in the functional F where, in addition, we should consider the increments $\delta\pi^1_\phi, \delta\pi^1_E, \delta\Pi^0_E + \delta\Pi^1_E$ where we have usually a relationship between $\delta\pi^0_\phi$ and $\delta\Pi^0_E$, through a expression $g(\delta\Pi^0_E) = \delta\pi^0_\phi$. Then, we optimize the other functional F to obtain the corresponding corrections and then we return to the functional f until we obtain stationary values in the parameters.
To summarize, we consider a precision previously fixed, $\varepsilon > 0$ and the process may be described as:

Opt $F(\Pi^{[i]}_E + \delta\Pi^{i+1}_E, \pi^{i+1}_E + \delta\pi^{i+1}_E, \pi^{i+1}_\phi)$ subject to
Opt $f(\pi^i_\phi + \delta\pi^i_\phi, \pi^i_E + \delta\pi^i_E, \pi^i_S + \delta\pi^i_S)$
$g(\delta\pi^i_\phi) = \delta\Pi^i_E$
$\Pi^{[i]}_E = \Pi^i_E + \delta\Pi^i_E$
Stop if $\left\|(\delta\pi^i_\phi, \delta\pi^i_E, \delta\pi^i_S, \delta\Pi^i_E)\right\|_\infty < \varepsilon$
on the contrary
put $\Pi^{i+1}_E = \Pi^{[i]}_E, \pi^{i+1}_E = \pi^i_E + \delta\pi^i_E, \pi^{i+1}_\phi = \pi^i_\phi + \delta\pi^i_\phi$ and
Continue

We should remark that each problem usually includes the optimization (generally minimization) of a different discrete either continuous functional, defined by means of a succession of temporal data either a spatial distribution either both cases. In any case, the traditional methods of optimization (quadratic minimization) do not necessary work. We should pay a special attention to the distribution of the available data. Some particular cases are now been studied by the authors.

Acknowledgements. Part of this work was supported by grant P1-1B2009-07 from Fundacio Caixa Castello BANCAIXA and a grant GV/2009/027 from Generalitat Valenciana

ΔT AND TIDAL ACCELERATION VALUES FROM THREE EUROPEAN MEDIEVAL ECLIPSES

M.J. MARTINEZ[1], F.J. MARCO[2]

[1] Universidad Politecnica de Valencia
Dept. Matematica Aplicada, Valencia, Spain
e-mail: mjmartin@mat.upv.es

[2] Universidad Jaume I
Dept. Matematicas, Institut de Matematiques I, Aplicacions de Castello, Catellon, Spain
e-mail: marco@mat.uji.es

ABSTRACT. There are many possible reasons for the fact that the rate of rotation of the Earth is slowly decreasing in time, being the most important the tidal friction. Since Universal Time (UT) is a time scale based on the rotation of the Earth and ΔT is defined as the difference between the uniform time-scale (Dynamical Time), and the Universal Time, clearly that ΔT will vary with time. The problem is that this variation is not uniform, existing irregular fluctuations. In addition, it is not possible to predict exact values for ΔT, being the only possibility its deduction a posteriori from observations. ΔT is strongly related with occultations and eclipses, because it is used for the calculation of exact times of the event, and for determining the position of the central line or the zone of visibility. In this sense, a value ΔT =3600s is roughly equivalent to a shift of 15° in longitude. Past values of ΔT can be deduced from historical astronomical observations such as ancient eclipses which have been widely studied by F.R. Stephenson [3] and [4] who has even obtained an approximation fitted with cubic splines for ΔT from -500 to +1950. This approximation is nowadays widely used in astronomical calculations. The derived relative error from ΔT obtained from ancient eclipsed is quite large, mainly because of the large width of the totality zone and the inaccuracy in the definition of the observational place. A possibility to partially solve these former problems is the analysis of total eclipse records from multiple sites, which could provide a narrow parameter range. In addition, The conjunct analysis of these astronomical phenomena is useful for determining a range of ΔT in function of the tidal acceleration of the Moon. Further discussion about these eclipses in under review.

1. THE ECLIPSES OF 3^{RD} JUNE 1239, 6^{TH} OCTOBER 1241 AND 17^{TH} SEPTEMBER 1354

The eclipse to 3th June 1239 is one of the most recorded in the history [2]. As an example, we shall only make reference to one record from [1] (chap. 305) of King Jaume I which makes reference to the eclipse as seen from the city of Montpellier: "(...) I went to Montpellier. One Friday, between midday and nones, there was the greatest eclipse seen in the memory of men now living, for the moon covered the whole of the sun, and one could see seven stars in the sky". The AD1241 eclipse was also recorded twice in the city of Soria: in the Concatedral of San Pedro is written "OBSCVRATVS E(st) SOL(s)T(i)CIO IV" and not further, in the San Nicols church (in ruins) a fragment remains with the following inscription: CVRAT(us) EST SOL(sticio) ER(a) MCCLX(xvii). The word "Era" refers to the Spanish era (38 years must be subtracted to transform it into the Julian date). All the other observation records for this eclipse are taken from [4]. Finally, the AD1354 eclipse was hybrid. Stephenson records only one account in the city of Perugia, where the eclipse was partial, although very large. We will use data obtained from Sos del Rey Catolico [2] to improve the wide range of ΔT obtained using Perugias observation. The former reference shows a pair of inscriptions sited in the arc of middle point of the arcade overlooking the Council place. In one of them it reads: Anno domini MCCC: L: IIII XVII die septembris: hora prima: Obscura uit sol. The translation will be: "In the first hour of the 17 September in the year of God 1354 the sun got dark."

2. DETERMINATION OF ΔT AND THE TIDAL ACCELERATION

In the study of the variation of the Earth rotation using untimed observations of total eclipses, the

precision of the ΔT obtained values depends mainly on the width of the totality band and on the precise definition of the observational place (See Fig. 1, for the AD1239 eclipse), it follows that the analysis of the eclipse observed from multiple sites provides more precise measures. There is the possibility of including also the conjunct determination of ΔT and the variation of the tidal acceleration of the Lunar Motion following [5]. To this aim, we have chosen three eclipses observed in Europe in the XIIIth and XIVth centuries, and we have obtained the ranges of ΔT for different values of the tidal acceleration (see Fig. 2). The inclusion of other almost contemporary eclipses could provide a narrower range of ΔT for each value of the tidal acceleration and help to identify redundant or inconsistent observations.

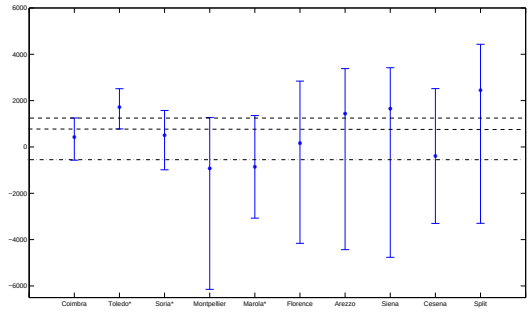

Figure 1: Values for ΔT at the observational sites. The mean value is 618 s. The dashed-lined interval represents the ΔT considering all sites, the dotted-solid line is the former value without Toledo.

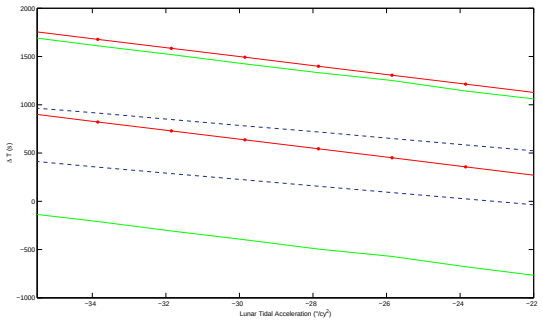

Figure 2: Total eclipse regions in the (ΔT, $\Delta\dot{n}$)-plane. We represent the data from the eclipse in AD1239 (solid line), AD1241 (solid-pointed line) and AD1354 (dashed line). If $\Delta\dot{n} = 0$ the range is 451 s< ΔT <650 s. For the two contemporary eclipses (AD1239 and AD1241) we obtain 451 s< ΔT <1251 s.

Acknowledgements. Part of this work was supported by grant P1-1B2009-07 from Fundacio Caixa Castello BANCAIXA and a grant GV/2009/027 from Generalitat Valenciana

3. REFERENCES

[1] Ferrando A., V.J. Escart, "Llibre dels Fets" Ed. Afers. 1995.
[2] Ibaez L & Dominguez P.: 2005, Momentos en Sos, Ayuntamiento de Sos del Rey Catolico.
[3] Morrison, L. and Stephenson, F. R., J. Hist. Astron., Vol. 35 Part 3, No. 120, pp 327-336, 2004.
[4] Stephenson, F.R. Historical Eclipses and Earth Rotation, Cambridge: Cambridge University Press, 1997.
[5] Tanikawa K., Soma M. Publ. Astron. Soc. Japan. 56. 879-885. 2004.

ABOUT THE CONFIGURATION OF THE GEOID UNDULATIONS AND THEIR KINEMATICS

G. MORCOV

Faculty of Geodesy, Technical University of Civil Engineering of Bucharest
Bulevardul Lacul Tei, nr. 124, sector 2, Bucharest, Romania
e-mail: georgemorcov@yahoo.com

ABSTRACT. The paper aims to underline the continuity of the geoid undulation positions of same frequency, on the terrestrial surface, which are the result of some possible movements in ratio with Earth rotation. In order to reach this theory, one must carry out the configuration of the geoid undulations in parallel sections, after which it is used the animation method. The results demonstrate the following: the continuity of the same frequency undulations; kinematic vectors that are parallel with the rotation movement; an advance of equatorial section's undulation.

1. METHOD

Creating the undulations configuration in some sections, at the same scale, resulting in specific figures. Kinematic running (animation) of these figures.

2. RESULTS

By kinematic unfolding of the undulation's configuration is found that: - there is a continuity of the same frequency undulations from a parallel to another; - there are kinematic vectors in two directions: a) in east-west direction; b) in north-south direction in the Boreal Hemisphere and in south-north direction in the Southern Hemisphere; - there is an advance of the same frequency undulations in equatorial section, in progressively relation with the undulations placed in the parallels sections. The size and the orientation of the arrows demonstrate the trend of the undulation configuration from the sections of the latitudes in relation to the undulation configuration from the equator's section (Fig. 7). This trend is much more visible, using the animation method.

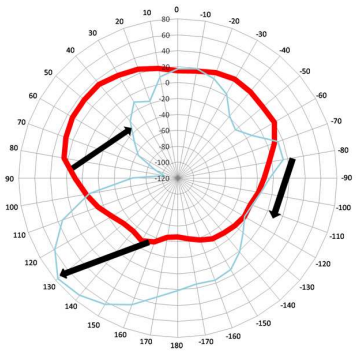

Fig. 1. Section 60^0 S - Latitude

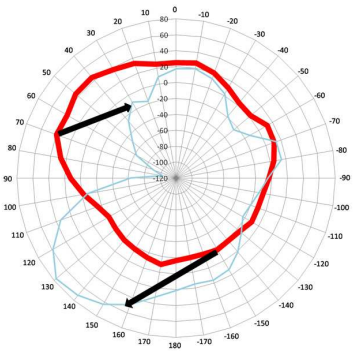

Fig. 2. Section 50^0 S - Latitude

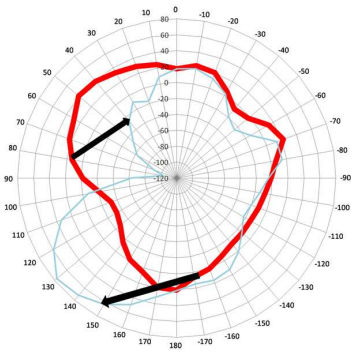

Fig. 3. Section 40^0 S – Latitude

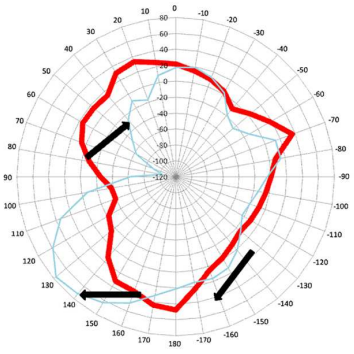

Fig. 4. Section 30^0 S - Latitude

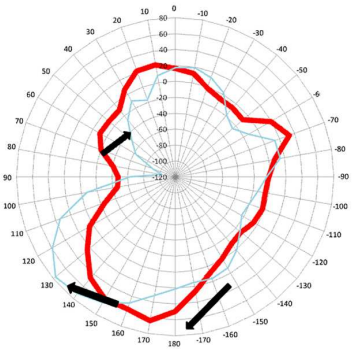

Fig. 5. Section 20^0 S - Latitude

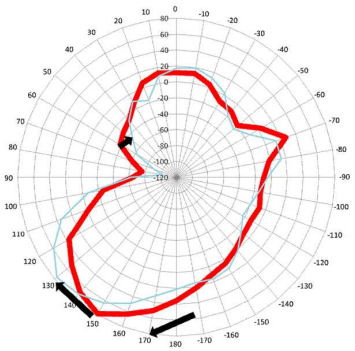

Fig. 6. Section 10^0 S – Latitude

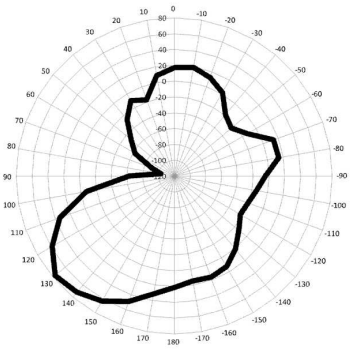

Fig. 7. Section 0^0 - Latitude

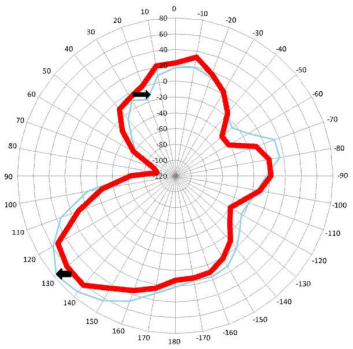

Fig. 8. Section 10^0 N - Latitude

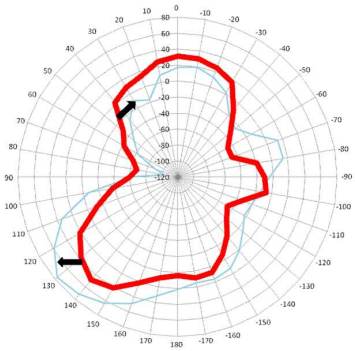

Fig. 9. Section 20^0 N – Latitude

3. CONCLUSIONS

- Using the undulations animation globally highlights the Coriolis effect, emphasizing possible progressive stages in undulation's translation from west to east and from the equator to the poles.

- If the apparent path of the undulations in some directions, can be explained as a product of continental drift, there may be clarifications, for the principle of the terrestrial reference frame, no net rotation (NNR) with regard to the Earth's lithosphere.

4. REFERENCES

NGA : (U) NGA EGM Geoid Calculator (UNCLASSIFIED), 11 Apr 2008 NGA : (U) WGS 84 Earth Gravitational Model 96 (EGM 96) Metadata, released by the Federal Geographic Data Committee, June 8, 1994. Science Product Suport - Geoid Height Calculator, UNAVCO Facility, 2 Mar 2009.

NONLINEAR SEA LEVEL VARIATIONS IN THE EQUATORIAL PACIFIC DUE TO ENSO

T. NIEDZIELSKI[1,2], W. KOSEK[1,3]

[1] Space Research Centre, Polish Academy of Sciences
ul. Bartycka 18A, 00-716 Warsaw, Poland
e-mails: niedzielski@cbk.waw.pl, kosek@cbk.waw.pl

[2] Oceanlab, University of Aberdeen
Main Street, Newburgh, Aberdeenshire AB41 6AA, UK

[3] Environmental Engineering and Land Surveying, University of Agriculture in Kraków
ul. Balicka 253A, 30-198 Kraków, Poland

ABSTRACT. Gridded sea level anomaly time series from TOPEX/Poseidon and Jason-1 satellite altimetry have been processed in order to detect nonlinearity of sea level change in the period 1993-2003. Basic statistics, such as standard deviation, skewness and kurtosis, along with testing hypothesis served well the purpose of statistical evaluation. The data obtained by both satellites have been merged by applying the offset between two time series, separately for each location grid. In order to infer nonlinear features of sea level variation, four specific terms (linear trend, annual oscillation, semiannual component and alias-type 62-days oscillation) have been removed from the merged time series for each grid. It has been shown that the particularly meaningful departures from the normal distribution of sea level change are present within the equatorial zone in the Pacific and Indian Oceans. This finding has been associated with the asymmetry between strengths of El Niño and La Niña episodes. The interpretation of the results has been based on geophysics of Kelvin and Rossby ocean waves which drive the ocean part of the ocean-atmosphere coupling in the El Niño/Southern Oscillation (ENSO). It has been argued that the nonlinear heating, occurring only during strong ENSO episodes, can be responsible for local nonlinear sea level change during such considerable ENSO events.

1. RECENT RESULTS

There is a wealth of observational evidence that the El Niño/Southern Oscillation (ENSO) phenomenon is somehow controlled by nonlinear processes. This is due to the nonlinear dynamical heating of the sea surface of the tropical Pacific which is the case during strong warm and cold ENSO episodes (Jin et al., 2003; An and Jin, 2004). There are also statistical investigations which show that both sea surface temperature and sea level anomalies in the equatorial Pacific depart from the normal distribution (Burgers and Stephenson, 1999; Niedzielski and Kosek, 2010a; Niedzielski, 2010). When the deviation from the normal distribution is linked to the asymmetry between El Niño and La Niña, one may infer that certain nonlinear processes are driving the oscillation in question (Hannachi et al., 2003). The asymmetry between warm and cold ENSO episodes has also been found in secular changes of ENSO, as inferred from simulated data (Hunt and Elliot, 2003).

However, recent studies indicate that linear models serve as reasonable tools for modelling and prediction of sea level anomalies from TOPEX/Poseidon and Jason-1 satellite altimetry (Niedzielski and Kosek, 2009; Niedzielski and Kosek, 2010b). This paper summarizes the results already published by the authors and provides a coherent picture of the current state-of-art in linear/nonlinear modeling of sea level fluctuations.

For the purpose of the exercises, the gridded data on sea level anomalies from TOPEX/Poseidon and Jason-1 – obtained courtesy of the Center for Space Research, University of Texas at Austin, USA – have been processed. The temporal coverage of the merged times series (TOPEX/Poseidon and Jason-1 data combined by taking into account the offset between the two) is 10.01.1993-14.07.2003 whereas the area is spatially limited by 65° S and 65° N parallels. There have been a few types of residuals calculated for the purpose of the analysis. Basically, they have been obtained be subtracting various trend and seasonal components from the input data (combinations of the following terms: linear trend, annual oscillation,

semiannual component and alias-type 62-days oscillation). The aforementioned data pre-processing and statistical evaluation of nonlinearity have been performed gridwise.

The analysis focuses on two spatial extents: the east equatorial Pacific and the global ocean. The first area plays a key role in ENSO dynamics whereas the global approach allows one to evaluate if nonlinearities of sea level change are intrinsic only for the equatorial Pacific or have wider spatial occurrence.

The areas of the east equatorial Pacific with significant departures of sea level anomalies from the normal distribution correspond to four specific zones, i.e. the equatorial zone, the Intertropical Convergence Zone, the eastern Pacific warm pool and the continental shelf (Niedzielski, 2010). The results for coastal areas are rather uncertain due to inaccuracy of radar altimetry. However, all four zones are linked to ENSO forcing and it seems to be inevitably a key reason of the detected nonlinearities. The interpretation of deviations from a linear variability is based on the paper by Jin et al. (2003) who link the asymmetry of El Niño and La Niña episodes with the nonlinear heating of the sea surface. These four zones quite precisely fit the areas where linear predictions of sea level anomalies fail (Niedzielski and Kosek, 2009). This specific correspondence implies an intrinsic recommendation for using the nonlinear time series approach to anticipate future sea level change at different lead times.

A similar exercise has been performed for the global ocean (Niedzielski and Kosek, 2010a). It has been found that the equatorial Pacific and the tropical Indian Ocean are the main zones where the probability law of sea level anomalies departs from the normal distribution. This serves as a confirmation for the aforementioned asymmetry, the interpretation of which is probably of the same origin. The spatial pattern of the nonlinear signal in sea level anomalies has been shown to correspond to shapes typical for Kelvin and Rossby waves. The natural recommendation for modelling with nonlinear approaches has been formulated. However, as subsequently shown by Niedzielski and Kosek (2010b), it is tough to implement such an advice because – inferring simple low-order time series models – the goodness-of-fit is better for linear techniques than for the nonlinear ones. It should be noted that the prediction performance of such models has not been checked in this exercise.

2. CONCLUSIONS

Recent investigations carried out by the authors of this paper and published elsewhere show that it is rather difficult to unequivocally recommend particular models capable to describe the nonlinear sea level anomalies present in the equatorial Pacific and the tropical Indian Ocean. In the light of the comparison between the prediction accuracy of sea level anomalies and the nonlinear variability of sea level change it appears to be crucial to implement nonlinear time series models for forecasting purposes. However, at this stage of the analysis, the structure of such models is rather tough to find. Low-order generalised autoregressive conditional heteroscedastic models have been shown to be inadequate, even though they offer time-varying variance modelling. The explanation of the correspondence between the nonlinear sea level changes and the optimal models for them remains to be ambiguous. Thus, a further research in this field seems to be highly recommended.

3. REFERENCES

An, S.-I., Jin, F.-F., 2004, "Nonlinearity and Asymmetry of ENSO", Journal of Climate 17, 2399–2412.

Burgers, G., Stephenson, D.B., 1999, "The Normality of El Niño", Geophysical Research Letters 26(8), 1027–1030.

Hannachi, A., Stephenson, D.B., Sperber, K.R., 2003, "Probability-based methods for quantifying nonlinearity in the ENSO", Climate Dynamics 20, 241–256.

Hunt, B.G., Elliot, T.I., 2003, "Secular variability of ENSO events in a 1000-year climatic simulation", Climate Dynamics 20, 689–703.

Jin, F.-F., An, S.-I., Timmermann, A., Zhao, J., 2003, "Strong El Niño events and nonlinear dynamical heating", Geophysical Research Letters 30(3), 1120, doi:10.1029/2002GL016356.

Niedzielski, T., Kosek, W., 2009, "Forecasting sea level anomalies from TOPEX/Poseidon and Jason-1 satellite altimetry", Journal of Geodesy 83, 469–476.

Niedzielski, T., 2010, Non-linear sea level variations in the eastern tropical Pacific, Artificial Satellites 45(1), 1–10.

Niedzielski, T., Kosek, W., 2010a, "El Niño's impact on the probability distribution of sea level anomaly fields", Polish Journal of Environmental Studies 19(3), 611–620.

Niedzielski, T., Kosek, W., 2010b, "An application of low-order ARMA and GARCH models for sea level fluctuations", Artificial Satellites 45(1), 27–39.

EARTH ROTATION PARAMETERS DETERMINED OVER CONT08 FROM THE COMBINATION OF SPACE GEODETIC TECHNIQUES

J.Y. RICHARD , D. GAMBIS , C. BIZOUARD
Observatoire de Paris, SYRTE UMR8630, GRGS
61 av. de l'Observatoire, 75014 Paris
e-mail: jean-yves.richard@obspm.fr

A IERS Working Group on Combination at the Observation Level (COL-WG) was set up in the course of 2009 [http://www.iers.org/IERS/EN/Organization/WorkingGroups/]. Its main objective is to enhance techniques at the observation level. The period relative to the continuous VLBI campaign CONT08 extending from 10 to 30th August 2008 was selected to inter compare multi-technique combinations. We present the first analyzes.

1. PROJECT

We produced EOP solutions with a time resolution of 6h for pole coordinates and universal time and 12h for nutation offset parameters. The file exchange format is SINEX delivering normal equations (NEQ) per week. VLBI NEQ were obtained by the Bordeaux Observatory, SLR NEQ by the Côte d'Azur Observatory, GPS NEQ and DORIS NEQ by CNES-CLS and combination is processed at Paris Observatory.

2. ANALYSIS

We first analyze pole coordinates with respect to the a-priori C04 series in which the ocean tidal model is included. These parameters are estimated at 6h intervals by individual techniques and combined. For the polar motion estimation nutation offsets and space stations coordinates were held fixed to their a-priori (Figure 1)
We secondly determine celestial pole offsets with respect to the IAU 1980 precession nutation model. Pole and space stations coordinates were held fixed to their a-priori values for the nutation estimation (Figure 2). The a-priori EOP series is C04, interpolated at 6h intervals for pole series and at 12h intervals for nutation offsets series, the a-priori space station coordinates are those of the ITRF2005 and the a-priori quasar coordinates are issued from ICRF2.

3. RESULTS and CONCLUSIONS

When Terrestrial (TRF) and Celestial (CRF) reference frames are held fixed, pole coordinates are unbiased for all techniques. The combination of the four techniques (Comb) using the variance component analysis for weighting techniques exhibits the smallest mean and RMS values. When the TRF is simultaneously estimated with polar motion (Comb+TRF), we obtain a bias of a few hundred μas revealing a disagreement between the combined and terrestrial reference frame [table 1].
Considering celestial pole offsets estimated by VLBI, the continuity constraints have no effect. When combined with GPS and DORIS (Comb), and simultaneously estimated with TRF, the smallest mean and RMS values are observed. Nutation parameters estimated with TRF and CRF (Comb+TRF+CRF), exhibit a bias of 400 μas due to the disagreement of the estimated CRF and the a-priori ICRF2 [table 2].

Technique	**X-Pole** mean	**X-Pole** WRMS	**Y-Pole** mean	**Y-Pole** WRMS
GPS	-10.3	160	-60.3	117
VLBI	-17.2	189	-91.7	174
DORIS	31.5	1485	262	1098
SLR	-25.7	855	-193	800
Comb	-10	165	-66.8	106
Comb+TRF	298	185	-794	211

Table 1: Weighted mean and RMS values of daily pole corrections versus C04 series in μas

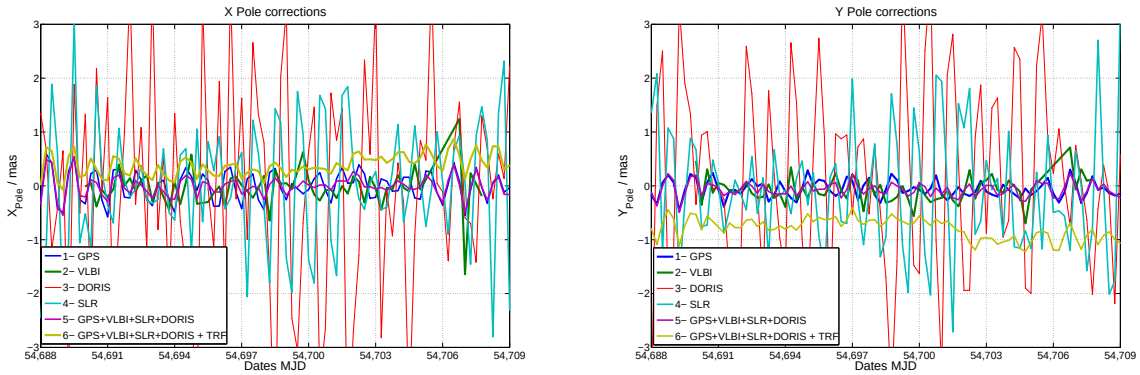

Figure 1: X and Y pole corrections at 6h interval. *1)GPS with TRF fixed, UT removed, 2)VLBI with TRF fixed, quasars removed, tropospheric zenithal bias substituted, 3)DORIS with TRF fixed, 4)SLR with TRF fixed, 5)Weighted Combination GPS+VLBI+SLR+DORIS with TRF fixed, 6)Weighted Combination GPS+VLBI+SLR+DORIS + TRF estimated, with continuity constraints of 3cm for polar motion, minimal constraints and co-located ties for space stations coordinates*

.

Technique	**d**ψ mean	**d**ψ WRMS	**d**ϵ mean	**d**ϵ WRMS
VLBI	-26.2	183	77.9	132
VLBI const.	-6.5	190	91	133
VLBI+CRF	-81.7	192	-688	229
Comb+TRF	-1.2	261	41.4	256
Comb+TRF+CRF	-388	313	322	279

Table 2: Weighted mean and RMS values of daily celestial pole offset versus C04 series in μas

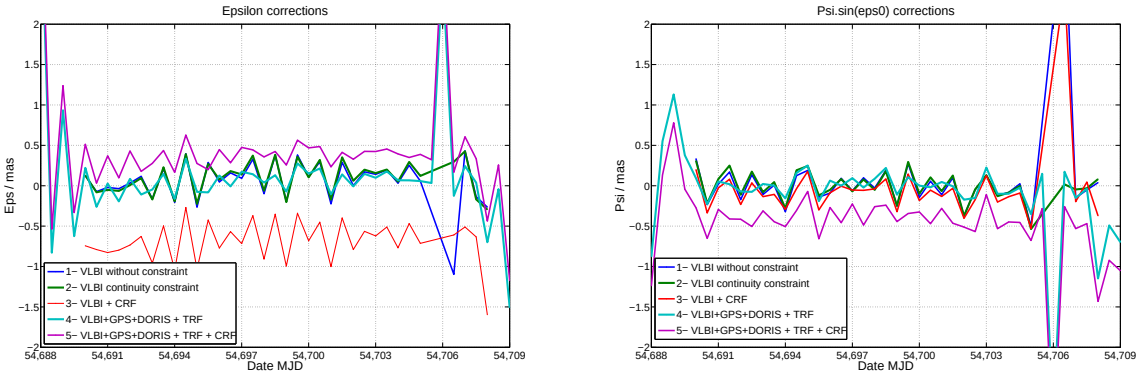

Figure 2: dϵ and dψ corrections at 12h intervals. *1)VLBI with TRF fixed, 2)VLBI with TRF fixed with continuity constraints of 3cm for nutation offsets, 3)VLBI + CRF quasars estimated, nutation and quasars unconstrained, 4)Weighted combination VLBI+GPS+DORIS + TRF estimated, continuity constraints on nutation, 5)Weighted combination VLBI+GPS+DORIS + TRF + CRF estimated, continuity constraints on nutation offsets, minimal constraints, local ties, stability constraints on stations coordinates, stability constraints on quasars coordinates*

COMPARISON OF THE VARIOUS ATMOSPHERIC AND OCEANIC ANGULAR MOMENTUM SERIES

C. RON, J. VONDRÁK, V. ŠTEFKA

Astronomical Institute of AS CR, Prague 4, Czech Republic
e-mail: ron@ig.cas.cz

ABSTRACT. We present here an addition to the recent study of atmospheric and oceanic excitations in the motion of the Earth's spin axis in space (Vondrák & Ron, 2010). Two approaches are used to study the impact of the atmospheric and oceanic excitations on the motion of Earth's spin axis in space. One way consists in the integration of the Brzeziński broad band Liouville equation (Brzeziński, 1994) and second way in the spectral analysis of both the geodetic and geophysical excitation functions. We applied both approaches to the series of the atmospheric and oceanic angular momentum excitation functions. We have used the celestial pole offsets (CPO) from the recent IVS combined solution (Schlüter & Behrend, 2007) `ivs09q3X`, covering the interval 1984.1–2009.7, cleaned and interpolated to 3-day intervals. We used two pairs of the geophysical excitations data. First pair is the pressure and wind terms of atmospheric angular momentum excitation functions (AAMEF) from NCEP/NCAR re-analysis, 1983.0-2009.5 (Salstein, 2005) together with the matter and motion terms of oceanic angular momentum excitation functions (OAMEF) from ECCO model 1993-2009.5. The second pair used is the AAMEF from ERA, 1979.0-2009.0 (Dobslaw & Thomas, 2007), re-analysed model before 2001 and operational model afterwards together with the OAMEF from OMCT model, 1979-2009.0 (Dobslaw & Thomas, 2007) driven by re-analysis atmospheric model before 2001.0 and by operational model afterwards.

The complex AAMEF and OAMEF values χ are given in rotating terrestrial frame, so we have to transform them into the celestial (non-rotating) frame χ' by applying $\chi' = -\chi e^{i\varphi}$, where φ is the Greenwich sidereal time. Because we are interested in only long-periodic motion that is comparable to nutation frequencies we further removed all periods < 10 days using the smoothing after Vondrák (1977). In this way we performed the complex demodulation (Brzeziński et al. 2002) at the retrograde diurnal frequency on the time series χ (in complex form).

We used Brzeziński transfer function (Brzeziński et al., 2002, Eq. 5) to estimate atmospheric and oceanic contribution to annual and semiannual nutation terms shown in Tab. 1 (for more details see Vondrák & Ron, 2010).

	Annual				Semi-annual			
Excitation	Re^+	Im^+	Re^-	Im^-	Re^+	Im^+	Re^-	Im^-
NCEP+ECCO	-58.5	87.9	-78.4	-20.3	-4.0	72.4	13.1	11.8
ERA+OMCT	-130.3	129.2	-52.9	56.5	-39.6	71.9	5.0	-9.9

Table 1: Atmospheric and oceanic contribution in nutation [μas], calculated by convolution with Brzeziński transfer function.

Another possibility to compare the excitations with the observed CPOs is the numerical integration of the broad-band Liouville equations (Brzeziński, 1994)

$$\ddot{P} - i(\sigma'_C + \sigma'_f)\dot{P} - \sigma'_C\sigma'_f P = -\sigma_C \left\{\sigma'_f(\chi'_p + \chi'_w) + \sigma'_C(a_p\chi'_p + a_w\chi'_w) + i[(1+a_p)\dot{\chi}'_p + (1+a_w)\dot{\chi}'_w]\right\},$$

where $P = dX + idY$ is excited motion of Earth's spin axis in celestial frame, σ'_C, σ'_f are the complex Chandler and FCN frequencies in celestial frame, respectively and σ_C in terrestrial frame. The values $a_{p,w}$ are dimensionless constants. To obtain two first-order equations instead of a second-order one, we use the substitution $y_1 = P$ and $y_2 = \dot{P} - i\sigma'_C P$, which leads to differential equations for two complex functions y_1, y_2:

$$\begin{aligned}
\dot{y}_1 &= i\sigma'_C y_1 + y_2 \\
\dot{y}_2 &= i\sigma'_f y_2 - \sigma_C \left\{\sigma'_f(\chi'_p + \chi'_w) + \sigma'_C(a_p\chi'_p + a_w\chi'_w) + +i[(1+a_p)\dot{\chi}'_p + (1+a_w)\dot{\chi}'_w]\right\}
\end{aligned}$$

To integrate the system by the fourth-order Runge-Kutta method with 6-hour steps we need to choose the initial values, $y_1(0) = P_0$, $y_2(0) = i(\sigma'_f - \sigma'_C)P_0$ that are constrained so that the Chandlerian amplitude disappears. The final choice of P_0 was made by two methods. Either until the fit of the integrated motion to VLBI observations reaches a minimum (Vondrák & Ron, 2010) or until the magnitude squared coherence estimate C_{xy} of the input signals of integration and observation is maximum (in this study). The results of both approaches are almost the same for ERA+OMCT and rather different for NCEP+ECCO combination, see the following figure.

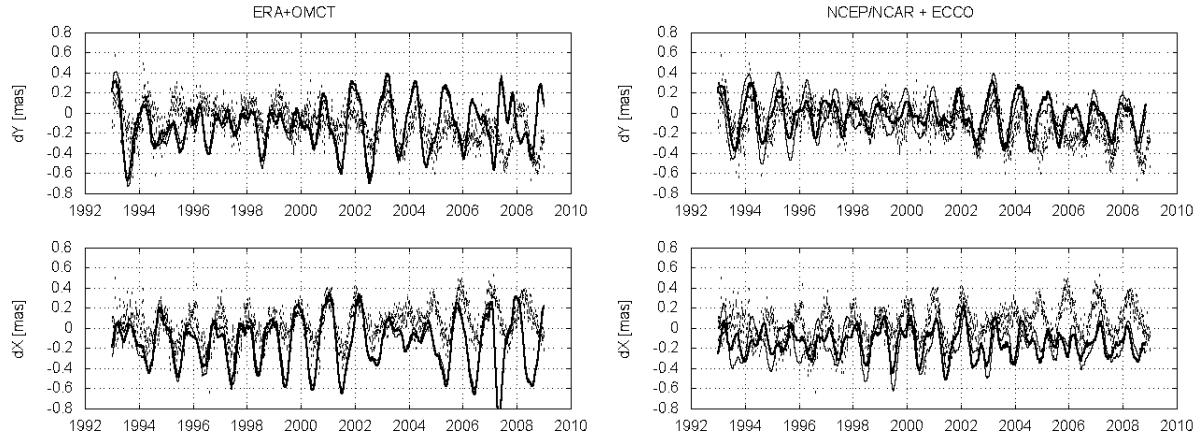

Figure 1: CPO from IVS solution (dots), numerical integration of the excitations fitted to IVS CPO (bold line), numerical integration with maximum coherence with the IVS CPO (thin line). Both series ERA+OMCT (left) and NCEP+ECCO (right) are displayed in the same interval 1993.0–2009.0 for comparison.

We can conclude that the forced nutations due to excitation by the atmosphere and ocean are significant, especially at annual and semi-annual periods. The different models of series of geophysical excitations give slightly different results. The initial values of the integration are close each other for both version of their determination, by the method of the maximum coherence or minimum root mean square differences.

Acknowledgement. This work was supported by the grant No. 205/08/0908 awarded by the Grant Agency of the Czech Republic.

REFERENCES

Brzeziński, A., 1994, "Polar motion excitation by variations of the effective angular momentum function: II. Extended Model", Manuscripta Geodaetica, 19, 157–171.

Brzeziński, A., Bizouard, C., Petrov, S., 2002, "Influence of the atmosphere on Earth rotation: what new can be learned from the recent atmospheric angular momentum estimates?", Surveys in Geophysics 23, pp. 33–69.

Dobslaw, H., Thomas, M., 2007, "Simulation and observation of global ocean mass anomalies", J. Geophys. Res.112, C05040, doi: 10.1029/2006JC004035.

Gross, R. S., Fukumori, I., Menemenlis, D., 2005, "Atmospheric and oceanic excitation of decadal-scale Earth orientation variations", J. Geophys. Res.110, B09405, doi:10.1029/2004JB003565.

Salstein, D., 2005, "Computing atmospheric excitation functions for Earth rotation/polar motion", Cahiers du Centre Europeén de Géodynamique et de Séismologie 24, Luxembourg, pp. 83–88.

Schlüter, W., Behrend, D., 2007, "The International VLBI Service for Geodesy and Astrometry (IVS): Current capabilities and future prospects", J. Geod. 81, pp. 379-387.

Vondrák, J., 1977, "Problem of smoothing of observational data II", Bull. Astron. Inst. Czechosl., 28, pp. 84

Vondrák, J., Ron, C., 2010, "Study of atmospheric and oceanic excitations in the motion of Earth's spin axis in space", Acta Geodyn. Geomater., Vol. 7, No. 1, pp. 19-28

THE RECENT IMPROVEMENT IN NON-RIGOROUS COMBINATION METHOD OF SPACE GEODETIC TECHNIQUES

V. ŠTEFKA

Astronomical Institute, Academy of Sciences of the Czech Republic
Boční II, 14131 Prague 4, Czech Republic
e-mail: stefka@ig.cas.cz

ABSTRACT. Nowadays the orientation of the Earth's body in the space is observed mainly by space geodesy techniques. Each technique has analytical centers that produce highly accurate products, primarily, Earth Orientation parameters (EOP) and station coordinates. This article describes recent progress in the method based on idea (Pešek and Kostelecký, 2006) combining station position vectors in the celestial reference frame in order to obtain representative set of EOP and station coordinates. The new improvement of the method consisted in changing the form of basic observation equation in order to be able to compute station coordinate corrections directly. Final results were compared with the solution of the terrestrial reference frame $ITRF2005$.

1. OUTLINE OF THE COMBINATION METHOD

The transformation from $ITRS$ to $GCRS$, i.e. $x_T \longrightarrow x_C$, in the concept of non-rotating origins, reads (Capitaine at al., 2003):

$$x_C = Q(t)R_3(ERA)R_3(-s)R_1(y_p)R_2(x_p)x_T. \tag{1}$$

Then the partial derivatives of (1) with respect to any unknown, U, yield the observation equations of the form:

$$\sum_j^6 \frac{\delta x_C}{\delta U_j} dU_j = x_{C|obs} - x_{C|0} + v, \tag{2}$$

where the "observed" vectors $x_{C|obs}$ are calculated from the respective input data and $x_{C|0}$ are functions of adopted a priori values of the unknowns (x_T, x_P, y_P and ERA) and v is residual. By contrast to the previous version of this method (Štefka et al., 2010) the station position vectors are solved directly instead of obtaining them through computing seven parameters of the seven-parametric transformation for particular technique.

The EOP are calculated for each individual epoch independently of the others. As a consequence, errors in the input data, including station coordinates, are transferred to the EOP and increase their scatter substantially. The effect can be reduced by including constrains, in the form of additional observation equations, which are based on smoothing method (Vondrák, 1977), and have a form of the third derivative of third-order Lagrange polynomial. The constraints were weighted to retain in the solution as much as 99% of the signal with period greater than 5 days.

To remove singularity of the system (2), three types of additional equations have to be introduced: translation, rotation and scale, all are related to Tisserand condition (Dermanis, 2010) and stabilize calculation of the station coordinates.

1. RESULTS AND CONCLUSIONS

The latter method was applied on the the data covering the period $51549 - 54351$ MJD, which were taken from the $IERS$ Combination Pilot Project database and $ILRS$ analysis center for GPS, $VLBI$ and SLR, respectively.

The results (EOP and station coordinates) were compared with ITRF2005 (Altamimi et. al., 2007): the mean value of station differences is at the level of 1 cm and the rms of differences between computed EOP and ITRF2005 are 0.142 mas, 0.131 mas and 0.117 ms for x_P, y_P and $(UT1 - UTC)$, respectively.

The described improvement in computing station coordinate residuals directly brought substantive benefit to this method so that the solution of station coordinates is closer to the official solution ITRF2005 and might be considered as more real.

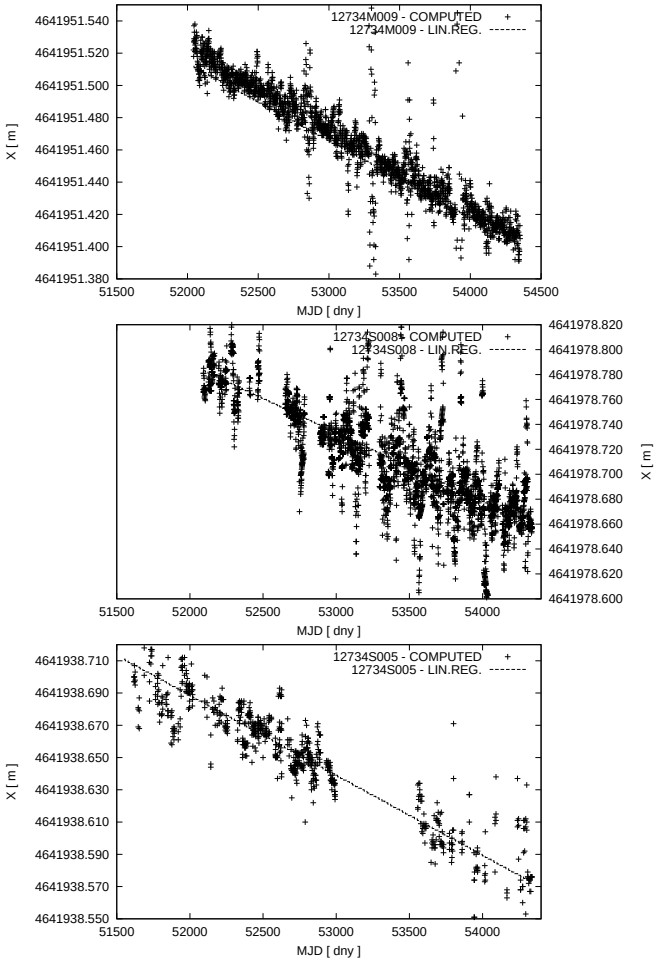

Figure 1: The picture shows corrected station coordinates X as solution of the combination method and lines represent measured data at collocation station 12734, where three geodesy techniques (GPS - top, SLR - center, VLBI - bottom) are present.

3. REFERENCES

Altamimi, Z., X. Collilieux, J. Legrand, B. Garayt, and C. Boucher (2007), ITRF2005: A new release of the International Terrestrial Reference Frame based on time series of station positions and Earth Orientation Parameters , J. Geophys. Res., 112, B09401, doi:10.1029/2007JB004949.

Capitaine, N., Wallace, P., and Chapront, J.: 2003, Expressions for IAU 2000 precession quantities. A&A, 412, 567-586.

Dermanis, A., 2010: Lecture Notes *IAG* School on Reference Frames, June 7-12, Mytilene, Lesvos Island, Greece, `http://www.topo.auth.gr/IAG2010_RefSchool/`.

Pešek, I. and Kostelecký J., 2006: "Simultaneous determination of Earth orientation parameters and station coordinates from combination of results of different observation techniques", Stud. Geophys. Geod., 50, pp. 537–548.

Štefka, V., Pešek, I., Vondrák, J. and Kostelecký, J.: Earth Orientation Parameters ans station coordinates from geodesy techniks, Acta Geodyn. Geomater., Vol. 7, No. 1 (157), 29-33, 2010.

Vondrák, J.: 1977, Problem of smoothing observational data II, Bull. Astron. Inst. Czechosl., 28, 84-89.

THE INTERPRETATION OF HIGH FREQUENCY SIGNALS IN THE G-RING LASER GYROSCOPE

W.TIAN[1], A.BRZEZINSKI[2,3], M.H.SOFFEL[1], A.GEBAUER[4], K.U.SCHREIBER[4], T.KLÜGEL[5]

[1] Lohrmann Observatory, TU Dresden, Dresden, Germany
[2] Faculty of Geodesy and Cartography, Warsaw University of Technology, Warsaw, Poland
[3] Space Research Centre, Polish Academy of Sciences, Warsaw, Poland
[4] Forschungseinrichtung Satellitengeodäsie, TU-München, München, Germany
[5] Bundesamt für Kartographie und Geodäsie, Frankfurt am Main, Germany
e-mail: wei.tian@mailbox.tu-dresden.de

ABSTRACT. As a promising geodetic instrument, the G-RLG(ring laser gyroscope) which is located at the Geodetic Observatory Wettzell (Germany) has been improved over the last several years. Its current sensitivity is around 10^{-9} which makes it possible to detect the variations of the IRP (Instantaneous Rotation Pole) directly and precisely. In this work our aim focuses on modelling and interpreting the diurnal and semi-diurnal signals which are mainly caused by variable rotations of the Earth and orientational variations of the platform.

1. INTRODUCTION

Similar to mechanical gyroscope systems, large RLGs sense its rotational variation with respect to the local inertial system. Their platforms co-move with the Earth with a variable location and orientation on the Earth's surface in the International Terrestrial Reference System (ITRS). By modeling these variations large RLG can provide an observation of the Earth's rotation independent and complementary to VLBI /LLR /SLR observations that refer to quasars, the Moon or satellites as reference objects.

In this work, 72 days of RLG data from "G" are analyzed. Its temporal resolution of 30 minutes allows us to investigate high frequency signals. Here only the diurnal and semi-diurnal signals are considered, and three main contributing sources will be discussed: Oppolzer terms, solid Earth and ocean tides.

2. REDUCED GEOPHYSICAL EFFECTS ON G-RING

The classic Sagnac equation which describes the Sagnac effect in RLG reads:

$$f = \frac{4A}{\bar{\lambda}P}\overrightarrow{n}\cdot\overrightarrow{\Omega}, \tag{1}$$

where, A, P, $\bar{\lambda}$, $\overrightarrow{n}$, $\overrightarrow{\Omega}$ are the enclosed area, perimeter (beam path length), optical wavelength of the RLG, normal vector to A and the instantaneous rotation vector, respectively.

Considering the RLG's orientation $\overrightarrow{n} = [\cos\phi\cos\lambda, \cos\phi\sin\lambda, \sin\phi]$ and the rotation vector of the IRP $\overrightarrow{\Omega} = \Omega[m_1,\ m_2, 1+m_3)]$, the Sagnac equation will turn into a function in terms of orientation and rotation parameters:

$$f = \kappa\{\cos\phi_0\cos\lambda_0 m_1 + \cos\phi_0\sin\lambda_0 m_2 + \sin\phi_0 m_3 + \cos\phi_0 d\phi + \sin\phi_0\}, \tag{2}$$

where $\kappa = \frac{4A\Omega}{\bar{\lambda}P}$, and (ϕ_0, λ_0) is the RLG's geographic latitude and longitude.

The Eq. (2) depicts explicitly how the variations of the Earth's rotation and RLG's orientation affect the performance of RLG. The preliminary result is shown in Fig.1.

The Oppolzer terms driven by the tidal potential are obtained by solving the Earth's rotation dynamical equations in terms of the IRP (Brzezinski, 1986; Mathews et al. 2002).

The variations of polar motion of IRP and LOD driven by ocean tides are derived from Table 8.2 and 8.3 of the IERS Conventions 2003 (McCarthy and Petit, 2004) by a transition from the CIP (Celestial Intermediate Pole; see (*ibid.*) for definition) to IRP in the following form derived by Brzezinski (1992)

$$m = p - i\frac{\dot{p}}{\Omega}, \tag{3}$$

where $i = \sqrt{-1}$ denotes the imaginary unit and $m = m_1 + im_2$, $p = x_p - iy_p$ are the terrestrial coordinates of the IRP and CIP expressed by complex variables.

The tilt of G-RLG platform dominates the semi-diurnal signals in G-RLG data and contributes partly to diurnal and long period signals as well. In this work, the tilt effects are calculated with the second order HW95 tidal potential (Hartmann and Wenzel, 1995) and Wahr's frequency-dependent Love numbers(Wahr, 1981).

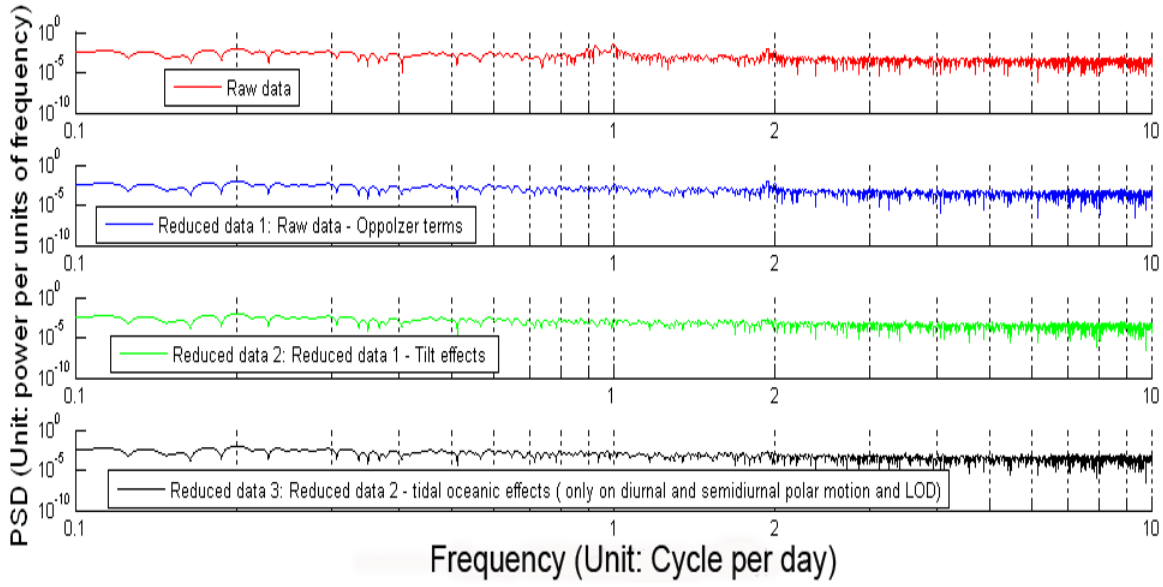

Figure 1: The PSD of high-pass filtered time series

3. CONCLUSIONS

The tidal oceanic effects on RLG are investigated. The retrograde diurnal effect is considered by taking the MBH 2000 into account. The prograde diurnal and semi-diurnal effects are calculated based on the IERS conventions and the kinematical Eq. (3). All these effects contribute only a few μHz to the Sagnac signal and are in the order of the present noise level.

Even though this study does not use the observation of tiltmeters to reduce the RLG's tilt, the tidal tilt signals in RLG are still well removed by our tilt model. When using tiltmeters for tidal correction, one might introduce small attraction model errors in the data. Thus, careful attraction modeling and tiltmeter calibration is required. However, when studying non-periodic signals, the use of measured tilt data is mandatory.

In order to detect signals in the μHz range, further reduction of the noise level by improving the instrument stability and modeling the environmental impact on the Ring Laser Gyroscope are recently in progress.

Acknowledgements. W. Tian would like to acknowledge the financial support from the Chinese Scholarship Council (CSC) for this research.

4. REFERENCES

Brzezinski, A., 1986, Manuscripta Geodetica, 11, pp.226–241.
Brzezinski, A., 1992, Manuscripta Geodaetica, 17, pp.3-20.
Hartmann, T., Wenzel, H.-G., 1995, Geophysical Research Letters, 22, pp. 3553–3556.
McCarthy, D.D., Petit, G. (eds.), 2004, IERS Conventions(2003), IERS Technical Note 32, Verlag des BKG, Frankfurt am Main.
Mathews, P.M., Herring, T.A., Buffett, B.A., 2002, J. Geophys. Res., 107(B4), 2068.
Wahr, J.M., 1981, Geophys. J. R. Astron. Soc. , 64, pp.677-703.

MODELING OF THE EARTH ROTATION AND HIGH PRECISION ASTROMETRY OBSERVATION TECHNIQUES

K. YAO[1], N. CAPITAINE[1]
[1]Observatoire de Paris, SYRTE/UMR8630-CNRS
61, Ave. de l'Observatoire, 75014 Paris, France
e-mail: kunliang.yao@obspm.fr, n.capitaine@obspm.fr

ABSTRACT. Earth Orientation Parameters (EOP) are needed to locate an object in the celestial or terrestrial reference systems. IERS provides EOP series at 1-day interval and standard numerical models for some variations of the EOP. High precision EOP are requested in many research and application domains, i.e. geodesy, satellite orbitography, astronomical observations. Several techniques contribute to estimate the EOP: VLBI, GPS, SLR, LLR, and DORIS. Their contributions vary while their precisions evolve. It is interesting to investigate their potentiality to determine the various components of the Earth's rotation and especially precession-nutation. The purpose of this work is to investigate the potentiality of VLBI and GPS techniques to determine the various components of precession-nutation, and to compare the performance and precision of their results, for long term components and short term components respectively. This paper recalls the IERS modeling of Earth rotation and the method used for estimating the EOP by VLBI and GPS; it also presents a new option to estimate short-period nutations.

1. MODELING EARTH ROTATION

Earth's rotation is described as the sum of following components (see Fig. 1, left):

1. The celestial motion of the Celestial intermediate Pole (CIP), noted (X, Y) in rectangular coordinates in the GCRS; its main component results from the rotation of the Earth's axis around a moving axis perpendicular to the ecliptic plane. It has a polynomial part (precession) and a periodic part (nutation).

2. The terrestrial motion of the CIP (polar motion), noted (x_p, y_p) in rectangular coordinates in the ITRS. Its main components are the Chandler oscillation (period of about 430 days and amplitude lower than 150 mas), annual term (amplitude of about 100 mas), secular motion (4 mas/year towards Canada).

3. Earth's rotation velocity ω, or rotation angle ERA, or length of day (LOD), or UT1.

The IAU 2006/2000A expressions for X, Y (Capitaine et al. 2003, Hilton et al. 2006) and ERA, as well as models for some other variations of the EOP, are available in the IERS Conventions (2003).

The rectangular coordinates in the International Terrestrial Reference System [ITRS] can be transformed into rectangular coordinates in the Geocentric Celestial Reference System [GCRS] by the following equation: [GCRS]= $Q(t) * R(t) * W(t)$*[ITRS], where Q(t) is a matrix determined by (X, Y), R(t) is a matrix determined by the rotation angle ERA, and W(t) is a matrix determined by (x_p, y_p).

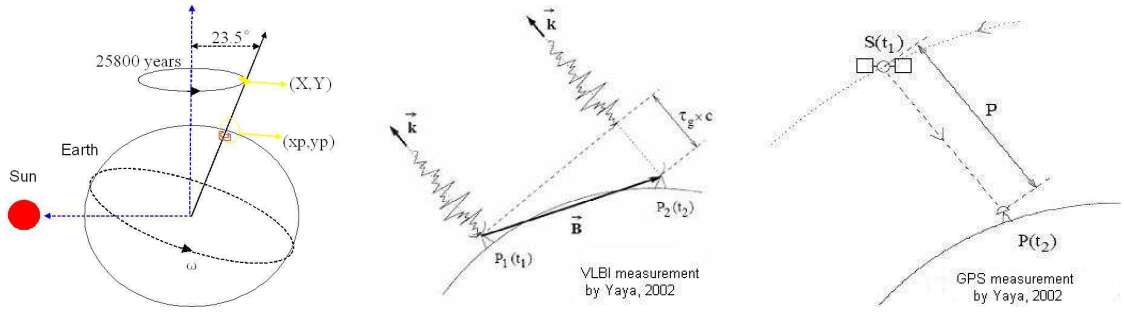

Figure 1: The Earth orientation parameters (left). Techniques for EOP estimation (right): VLBI and GPS

2. EOP DETERMIMATION BY VLBI and GPS

The EOP have been estimated by various techniques, i.e. VLBI, GPS (see Fig. 1), LLR, SLR, DORIS and optical astronomy. VLBI is currently the most important technique to estimate (X, Y) and LOD, while GPS is the most important one to estimate (x_p, y_p).

a) VLBI: the simplified geometric delay function is (see Fig. 1, middle): $\tau_g = ((P_2(t_2) - P_1(t_1)) \cdot \vec{k})/c$. The EOP information are contained in the GCRS stations positions: $P_1(t_1)$ and $P_2(t_2)$. But the troposphere, ionosphere, clock variation contribute to the VLBI delay: $\tau = \tau_g + \tau_{trop} + \tau_{ion} + \tau_{clock}$. These contributions need to be corrected.

Generally, the EOP are estimated by a weighted least squares method based on the normal equations, with a priori values: $\tau_{measured} - \tau_{theoretical} = \sum_i (d\tau_{theoretical}/dp_i) * \Delta p_i$.

The advantage of using VLBI is the accurate realization of the GCRS.

b) GPS: the simplified geometric delay function is (see Fig. 1, right): $\tau_g = t_2 - t_1 = |\vec{S}(t_1) - \vec{P}(t_2)|/c$. The EOP information are contained in the ITRS satellite position $\vec{S}(t_1)$. As it the case of VLBI, corrections for troposphere, ionosphere, clock variation, relativity are needed, as well as linearization, to get a weighted least squares estimation of the EOP. The advantage of using GPS is the accurate realization of the ITRS.

By investigating the satellite position in ITRS, we can obtain the following relation between the rates of the EOP (X, Y, ERA) and those of the satellite orbit parameters (Ω: ascending node, i: inclination, u_0: argument of latitude at the osculation epoch) (see Rothacher & Butler 1999):

$$E\dot{R}A = -\dot{\Omega} - \cos i \cdot \dot{u}_0, \quad \dot{X} = -\sin\Omega \cdot \dot{i} + \sin i \cos\Omega \cdot \dot{u}_0, \quad \dot{Y} = \cos\Omega \cdot \dot{i} + \sin i \sin\Omega \cdot \dot{u}_0.$$

The rates of (X, Y) can thus be derived from the rates of the orbital elements of the satellite and compared with the semi-analytical series for the time derivatives of the IAU 2006/2000 model (see Table 1). This would be a new method to estimate nutation corrections with minimizing the systematic (long-period) errors coming from the correlations between the EOP and the satellite orbit parameters. The estimated values of the rates of (X, Y) can also be combined with VLBI EOP result to get a better estimation of the short term nutations.

	sine coefficient (uas/d)	cosine coefficient (uas/d)	frequency l l' F D Ω	period (days)
1	-51.16	-41648.80	0 0 2 0 2	13.66
2	-22.33	-8249.95	1 0 2 0 2	9.13
3	-6.97	-7100.50	0 0 2 0 1	13.63
4	3.90	-1559.86	1 0 -2 -2 -2	9.56
5	-3.54	-1414.41	1 0 2 0 1	9.12
6	-5.57	-1358.41	0 0 2 2 2	7.10
7	-4.77	-1311.22	2 0 2 0 2	6.86
8	2.54	1072.81	0 0 0 2 0	14.77
9	1.34	530.49	2 0 0 0 0	13.78
10	1.21	475.51	0 0 2 0 0	13.61

Table 1: Series for the development of the time derivative of X (periods less than 23 d)

3. REFERENCES

Capitaine, N., Wallace, P.T. and Chapront, J., 2003, "Expressions for IAU 2000 precession quantities", A&A , 412, pp. 567–586.

Hilton, J., Capitaine, N., Chapront, J., Ferrándiz, J.M., Fienga, A., Fukushima, T., Getino, J., Mathews, P., Simon, J.-L., Soffel, M., Vondrák, J., Wallace, P., Williams, J., 2006, "Report of the International Astronomical Union Division I Working Group on Precession and the Ecliptic", Celest. Mech. Dyn. Astr. , 94, pp. 351-367.

IERS Conventions (2003), IERS Conventions, Verlag des Bundesamts fur Kartographie und Geodasie Frankfurt am Main 2004, D.D. McCarthy and G. Petit (eds).

Rothacher M., Beutler G., Herring T. A., Weber R., 1999, "Estimation of nutation using the Global Positioning System", J. Geophys. Res.104, B3, pp. 4835–4859.

Yaya, Ph., 2002, PhD thesis, Observatoire de Paris.

Session 5

PULSARS TIMING, RELATIVITY AND TIME TRANSFER

CHONOMÉTRAGE DE PULSARS, RELATIVITÉ ET TRANSFERT DE TEMPS

AN EXTENSION OF THE IAU FRAMEWORK FOR REFERENCE SYSTEMS

S.M. KOPEIKIN
Department of Physics & Astronomy, University of Missouri-Columbia
223 Physics Bldg., Columbia, Missouri 65211, USA
e-mail: kopeikins@missouri.edu

ABSTRACT. IAU 2000 resolutions on the reference frames set up a solid theoretical foundation for implementing general relativity in astronomical data processing algorithms and for unambiguous interpretation of measured relativistic effects. We discuss possible directions for further theoretical development of the IAU resolutions aimed to take into account the decadal progress in observational techniques and computer-based technologies. We address the following subjects: 1) space-time transformations and the structure of the metric tensor; -2) PPN parameters and gauge invariance of equations of motion; -3) astronomical reference frames for cosmological applications.

1. INTRODUCTION

Experimental exploration of the nature of space-time demands establishment of a common theoretical platform linking a theory of gravitational field to astronomical observations. This platform should be build on the basis of a complete theory of gravity like general theory of relativity, that describes both the properties of space-time, gravitational field and observables. New generation of microarcsecond astrometry satellites like SIM Lite [1]) did not recommend SIM Lite for development this decade. and a cornerstone mission of ESA - Gaia, require such a novel approach for an unambiguous interpretation of astrometric data obtained from the on-board optical instruments. Advanced inertial reference frame is required for unambiguous physical interpretation of gravitomagnetic precession of LAGEOS satellite and LLR observations [1]. Recent breakthroughs in technology of drag-free satellites, clocks, lasers, optical and radio interferometers and new demands of experimental gravitational physics [1,2] make it necessary to incorporate the parameterized post-Newtonian formalism [4] to the procedure of construction of relativistic local frames around Earth and other bodies of the solar system [5,6]. The domain of applicability of the IAU relativistic theory of reference frames [7] is to be also extended outside the solar system [8] to take into account the impact of the Hubble expansion on the solutions of the gravity field equations and the equations of motion of the bodies.

In what follows, Latin indices takes values 1,2,3; the Greek indices run from 0 to 3. Repeated indices imply the Einstein summation rule. The unit matrix $\delta_{ij} = \mathrm{diag}(1,1,1)$ and the fully anti-symmetric symbol ϵ_{ijk} is subject to $\epsilon_{123} = 1$. The Minkowski metric $\eta_{\alpha\beta} = \mathrm{diag}(-1,1,1,1)$. Greek indices are raised and lowered with the Minkowski metric, Latin indices are raised and lowered with the unit matrix. Bold italic letters $\boldsymbol{a}$, $\boldsymbol{b}$, etc., denote spatial vectors. A dot and a cross between two spatial vectors denote the Euclidean scalar and vector products respectively. Partial derivative with respect to spatial coordinates x^i are denoted as $\partial/\partial x^i$ or $\vec{\nabla}$.

2. STANDARD IAU FRAMEWORK

The IAU resolutions are based on the first post-Newtonian approximation of general relativity which is a conceptual basis of the fundamental astronomy in the solar system [9]. Barycentric Celestial Reference

[1]The Astro2010 Decadal Survey (available at http://sites.nationalacademies.org/bpa/BPA_049810

System (BCRS), $x^\alpha = (ct, \boldsymbol{x})$, is defined in terms of a metric tensor $g_{\alpha\beta}$ with components

$$g_{00} = -1 + \frac{2w}{c^2} - \frac{2w^2}{c^4} + O(c^{-5}) , \quad (1)$$

$$g_{0i} = -\frac{4w^i}{c^3} + O(c^{-5}) , \quad (2)$$

$$g_{ij} = \delta_{ij}\left(1 + \frac{2w}{c^2}\right) + O(c^{-4}) . \quad (3)$$

Here, the post-Newtonian gravitational potentials w and w^i are defined by solving the gravity field equations

$$\Box w = -4\pi G\sigma , \quad (4)$$

$$\Box w^i = -4\pi G\sigma^i , \quad (5)$$

where $\Box \equiv -c^{-2}\partial^2/\partial t^2 + \nabla^2$ is the wave operator, $\sigma = c^{-2}(T^{00} + T^{ss})$, $\sigma^i = c^{-1}T^{0i}$, and $T^{\mu\nu}$ are the components of the stress-energy tensor of the solar system bodies, $T^{ss} = T^{11} + T^{22} + T^{33}$.

Equations (4), (5) are solved by iterations

$$w(t, \boldsymbol{x}) = G\int \frac{\sigma(t, \boldsymbol{x}')d^3x'}{|\boldsymbol{x} - \boldsymbol{x}'|} + \frac{G}{2c^2}\frac{\partial^2}{\partial t^2}\int d^3x'\sigma(t, \boldsymbol{x}')|\boldsymbol{x} - \boldsymbol{x}'| + O(c^{-4}) , \quad (6)$$

$$w^i(t, \boldsymbol{x}) = G\int \frac{\sigma^i(t, \boldsymbol{x}')d^3x'}{|\boldsymbol{x} - \boldsymbol{x}'|} + O(c^{-2}) , \quad (7)$$

which are to be substituted to the metric tensor (1)–(3). Each of the potentials, w and w^i, can be linearly decomposed in two pieces

$$w = w_E + \bar{w} , \quad (8)$$

$$w^i = w^i_E + \bar{w}^i , \quad (9)$$

where w_E and w^i_E are BCRS potentials depending on the distribution of mass and current only inside the Earth, and $\bar{w}_E$ and $\bar{w}^i_E$ are gravitational potentials of external bodies.

Geocentric Celestial Reference System (GCRS) is denoted $X^\alpha = (cT, \boldsymbol{X})$. It has the metric tensor $G_{\alpha\beta}$ with components

$$G_{00} = -1 + \frac{2W}{c^2} - \frac{2W^2}{c^4} + O(c^{-5}) , \quad (10)$$

$$G_{0i} = -\frac{4W^i}{c^3} + O(c^{-5}) , \quad (11)$$

$$G_{ij} = \delta_{ij}\left(1 + \frac{2W}{c^2}\right) + O(c^{-4}) . \quad (12)$$

Here $W = W(T, \boldsymbol{X})$ is the post-Newtonian gravitational potential and $W^i(T, \boldsymbol{X})$ is a vector-potential both expressed in the geocentric coordinates. They satisfy to the same type of the wave equations (4), (5). Planetocentric metric for any planet can be introduced in the same way as the GCRS.

The geocentric potentials, W_E and W^i_E, are split into three parts

$$W(T, \boldsymbol{X}) = W_E(T, \boldsymbol{X}) + W_{\rm kin}(T, \boldsymbol{X}) + W_{\rm dyn}(T, \boldsymbol{X}) , \quad (13)$$

$$W^i(T, \boldsymbol{X}) = W^i_E(T, \boldsymbol{X}) + W^i_{\rm kin}(T, \boldsymbol{X}) + W^i_{\rm dyn}(T, \boldsymbol{X}) . \quad (14)$$

associated respectively with the gravitational field of the Earth, external tidal field and kinematic inertial force. IAU resolutions imply that the external and kinematic parts must vanish at the geocenter and admit an expansion in powers of $\boldsymbol{X}$ [7]. Geopotentials W_E and W^i_E are defined in the same way as w_E and w^i_E in equations (6)-(7) but with σ and σ^i calculated in the GCRS. They are related to the barycentric gravitational potentials w_E and w^i_E by the post-Newtonian transformations [10,7].

The kinematic contributions are linear in the GCRS spatial coordinates $\boldsymbol{X}$

$$W_{\rm kin} = Q_i X^i , \qquad W^i_{\rm kin} = \frac{1}{4}\, c^2\varepsilon_{ipq}(\Omega^p - \Omega^p_{\rm prec})\, X^q , \quad (15)$$

where Q_i characterizes a deviation of the actual world line of the geocenter from a fiducial world line of a hypothetical spherically-symmetric Earth [11]

$$Q_i = \partial_i \bar{w}(\boldsymbol{x}_E) - a^i_E + O(c^{-2}) \,. \tag{16}$$

Here $a^i_E = dv^i_E/dt$ is the barycentric acceleration of the geocenter. Function $\Omega^a_{\rm prec}$ describes the relativistic precession of dynamically non-rotating spatial axes of GCRS with respect to reference quasars

$$\Omega^i_{\rm prec} = \frac{1}{c^2}\,\varepsilon_{ijk}\,\left(-\frac{3}{2}\,v^j_E\,\partial_k \bar{w}(\boldsymbol{x}_E) + 2\,\partial_k \bar{w}^j(\boldsymbol{x}_E) - \frac{1}{2}\,v^j_E\,Q^k\right). \tag{17}$$

The three terms on the right-hand side of this equation represent the geodetic, Lense-Thirring, and Thomas precessions, respectively [11,7]. Dynamic potentials $W_{\rm dyn}$ and $W^i_{\rm dyn}$ are generalizations of the Newtonian tidal potential in the form of a polynomial starting from the quadratic with respect to $\boldsymbol{X}$ terms.

3. IAU SCALING RULES AND THE METRIC TENSOR

The coordinate transformations between the BCRS and GCRS are found by matching the BCRS and GCRS metric tensors in the vicinity of the world line of the Earth by making use of their tensor properties. The transformations are written as [11,7]

$$T = t - \frac{1}{c^2}\,[A + \boldsymbol{v}_E \cdot \boldsymbol{r}_E] + \frac{1}{c^4}\left[B + B^i r^i_E + B^{ij} r^i_E r^j_E\right], \tag{18}$$

$$X^i = r^i_E + \frac{1}{c^2}\left[\frac{1}{2} v^i_E \boldsymbol{v}_E \cdot \boldsymbol{r}_E + \bar{w}(\boldsymbol{x}_E) r^i_E + r^i_E \boldsymbol{a}_E \cdot \boldsymbol{r}_E - \frac{1}{2} a^i_E r^2_E\right], \tag{19}$$

where $\boldsymbol{r}_E = \boldsymbol{x} - \boldsymbol{x}_E$, functions A, B, B^i, B^{ij} obey equations

$$\frac{dA}{dt} = \frac{1}{2}\,v^2_E + \bar{w}(\boldsymbol{x}_E), \tag{20}$$

$$\frac{dB}{dt} = -\frac{1}{8}\,v^4_E - \frac{3}{2}\,v^2_E\,\bar{w}(\boldsymbol{x}_E) + 4\,v^i_E\,\bar{w}^i + \frac{1}{2}\,\bar{w}^2(\boldsymbol{x}_E), \tag{21}$$

$$B^i = -\frac{1}{2}\,v^2_E\,v^i_E + 4\,\bar{w}^i(\boldsymbol{x}_E) - 3\,v^i_E\,\bar{w}(\boldsymbol{x}_E), \tag{22}$$

$$B^{ij} = -v^i_E Q_j + 2\partial_j \bar{w}^i(\boldsymbol{x}_E) - v^i_E \partial_j \bar{w}(\boldsymbol{x}_E) + \frac{1}{2}\,\delta^{ij}\dot{\bar{w}}(\boldsymbol{x}_E)\,, \tag{23}$$

where x^i_E, v^i_E, and a^i_E are the BCRS position, velocity and acceleration vectors of the Earth, the overdot stands for the total derivative with respect to t, and one has neglected all terms of the order $O(r^3_E)$.

Earth's orbit in BCRS is almost circular. This makes the right side of equation (20) looks like

$$\frac{1}{2}\,v^2_E + \bar{w}(\boldsymbol{x}_E) = c^2 L_C + (\text{periodic terms})\,, \tag{24}$$

where the constant L_C and the periodic terms have been calculated with a great precision in [13]. For practical reason the IAU 2000 resolutions recommend to re-scale the BCRS time coordinate t to remove the constant L_C from equation (24). The new time scale is called TDB, and it is defined by equation

$$t_{TDB} = t\,(1 - L_B)\,, \tag{25}$$

where a constant $L_B = L_C + \Delta_C$ is used, instead of L_C, in order to take into account the additional linear drift Δ_C between the GCRS time T and the proper time of clocks on geoid, as explained in [12,13]. Time re-scaling changes the Newtonian equations of motion of planets and light. In order to keep the equations of motion invariant entails re-scaling of spatial coordinates and masses of the solar system bodies. These scaling transformations are included to IAU 2000 resolutions [7]. However, the re-scaling of masses, times and spatial coordinates affects the units of their measurement – the procedure that led to a controversial discussion [14]. The change in units can be avoided if one looks at the scaling laws from the point of view of transformation of the metric tensor.

The thing is that the scaling of time and space coordinates can be viewed as a particular choice of the GCRS metric tensor. Indeed, equation (15) is a solution of the Laplace equation which is defined up to an arbitrary function of time $Q = Q(t)$ that can be incorporated to

$$W_{\rm kin} = Q + Q_i X^i \,, \tag{26}$$

$$\frac{dA(t)}{dt} = \frac{1}{2}\, v_E^2 + \bar{w}(\boldsymbol{x}_E) - Q \,, \tag{27}$$

and, if one chooses $Q = c^2 L_C$, it eliminates the secular drift between times T and t without explicit re-scaling of the time t, which is always measured in SI units. It turns out that Blanchet-Damour [15] relativistic definition of mass depends on function Q and is re-scaled automatically in such a way that the Newtonian equations of motion remain invariant [6]. Introduction of Q to function $W_{\rm kin}$ appropriately transforms the g_{ij} component of the GCRS metric tensor that is formally equivalent to the previously-used re-scaling of the GCRS spatial coordinates. One concludes that introducing the function Q to the GSRC metric tensor without apparent re-scaling of coordinates and masses can be more preferable in updated version of the IAU resolutions as it allows us to keep the SI system of units without changing coordinates and masses. Similar procedure can be developed for the topocentric metric tensor to take into account the linear drift existing between GCRS time T and the atomic clocks on geoid [12,13].

4. PARAMETERIZED COORDINATE TRANSFORMATIONS

The parameterized post-Newtonian (PPN) formalism [4] is not consistent with the IAU resolutions. It limits applicability of the resolutions in testing gravity theories. PPN equations of motion depend on two parameters, β and γ [16] and they are presently compatible with the IAU resolutions only in the case of $\beta = \gamma = 1$. Rapidly growing precision of astronomical observations as well as advent of gravitational-wave detectors urgently demand a PPN theory of relativistic transformations between the local and global coordinate systems.

PPN parameters β and γ are characteristics of a scalar field which makes the metric tensor different from general relativity. In order to extend the IAU 2000 resolutions to PPN formalism one used a general class of Brans-Dicke theories [17] based on the metric tensor $g_{\alpha\beta}$ and a scalar field ϕ that couples with the metric tensor via function $\theta(\phi)$. Both ϕ and $\theta(\phi)$ are analytic functions which can be expanded in a Taylor series about their background values $\bar{\phi}$ and $\bar{\theta}$.

The parameterized theory of relativistic reference frames in the solar system is built in accordance to the same rules as used in the IAU resolutions. The entire procedure is described in papers [5,6]. The PPN transformations between BCRS and GCRS are found by matching the BCRS and GCRS metric tensors and the scalar field in the vicinity of the world line of the Earth. They have the following form

$$T = t - \frac{1}{c^2}\,[A + \boldsymbol{v}_E \cdot \boldsymbol{r}_E] + \frac{1}{c^4}\left[B + B^i\, r_E^i + B^{ij}\, r_E^i\, r_E^j\right] \,, \tag{28}$$

$$X^i = r_E^i + \frac{1}{c^2}\left[\frac{1}{2} v_E^i v_E^j r_E^j + \gamma Q r_E^i + \gamma \bar{w}(\boldsymbol{x}_E) r_E^i + r_E^i a_E^j r_E^j - \frac{1}{2} a_E^i r_E^2\right] \tag{29}$$

where $\boldsymbol{r}_E = \boldsymbol{x} - \boldsymbol{x}_E$, and functions $A(t), B(t), B^i(t), B^{ij}(t)$ obey

$$\frac{dA}{dt} = \frac{1}{2}\, v_E^2 + \bar{w} - Q(\boldsymbol{x}_E), \tag{30}$$

$$\frac{dB}{dt} = -\frac{1}{8}\, v_E^4 - \left(\gamma + \frac{1}{2}\right)\, v_E^2\, \bar{w}(\boldsymbol{x}_E) + 2(1+\gamma)\, v_E^i\, \bar{w}^i + \left(\beta - \frac{1}{2}\right)\, \bar{w}^2(\boldsymbol{x}_E), \tag{31}$$

$$B^i = -\frac{1}{2}\, v_E^2\, v_E^i + 2(1+\gamma)\, \bar{w}^i(\boldsymbol{x}_E) - (1+2\gamma)\, v_E^i\, \bar{w}(\boldsymbol{x}_E), \tag{32}$$

$$B^{ij} = -v_E^i Q_j + (1+\gamma)\partial_j \bar{w}^i(\boldsymbol{x}_E) - \gamma v_E^i \partial_j \bar{w}(\boldsymbol{x}_E) + \frac{1}{2}\,\delta^{ij}\dot{\bar{w}}(\boldsymbol{x}_E)\,. \tag{33}$$

These transformations depends explicitly on the PPN parameters β and γ and the scaling function Q, and should be compared with those (18)-(23) currently adopted in the IAU resolutions.

PPN parameters β and γ have a fundamental physical meaning in the scalar-tensor theory of gravity along with the universal gravitational constant G and the fundamental speed c. It means that if the

parameterized transformations (28)-(33) are adopted by the IAU, the parameters β and γ are to be considered as new astronomical constants which values have to be determined experimentally.

5. MATCHING IAU RESOLUTIONS WITH COSMOLOGY

BCRS assumes that the solar system is isolated and space-time is asymptotically flat. This idealization will not work at some level of accuracy of astronomical observations because the cosmological metric has non-zero Riemannian curvature [18]. It may turn out that some, yet unexplained anomalies in the orbital motion of the solar system bodies are indeed associated with the cosmological expansion [19]. Moreover, astronomical observations of cosmic microwave background radiation and other cosmological effects requires clear understanding of how the solar system is embedded to the cosmological model. Therefore, it seems reasonable to incorporate the cosmological metric to the IAU resolutions.

The gravitational field of the solar system has to approximate the cosmological metric tensor at infinity, not a flat metric. The cosmological metric has a number of parameters depending on visible and dark matter and on the dark energy. One considered a universe, driven by a scalar field imitating the dark energy ϕ, and having a spatial curvature equal to zero [20,21]. The universe is perturbed by a localized distribution of matter of the solar system. The perturbed metric tensor reads

$$g_{\alpha\beta} = a^2(\eta) f_{\alpha\beta} \ , \qquad f_{\alpha\beta} = \eta_{\alpha\beta} + h_{\alpha\beta} \ , \tag{34}$$

where the perturbation $h_{\alpha\beta}$ of the background metric $\bar{g}_{\alpha\beta} = a^2\eta_{\alpha\beta}$ is caused by matter of the solar system, $a(\eta)$ is a 'radius' of the universe depending on the conformal time η related to coordinate time t by simple differential equation $dt = a(\eta)d\eta$. A linear combination of the metric perturbations

$$\gamma^{\alpha\beta} = h^{\alpha\beta} - \frac{1}{2}\eta^{\alpha\beta}h \ , \tag{35}$$

where $h = \eta^{\alpha\beta}h_{\alpha\beta}$, is more convenient for calculations.

One imposes a cosmological gauge given by [20,21]

$$\gamma^{\alpha\beta}{}_{|\beta} = 2H\varphi\delta^{\alpha}_{0} \ , \tag{36}$$

where a vertical bar denotes a covariant derivative with respect to the background metric $\bar{g}_{\alpha\beta}$, $\varphi = \phi/a^2$, $H = \dot{a}/a$ is the Hubble parameter, and the overdot denotes a time derivative with respect to time η. The gauge (36) generalizes the harmonic gauge of the IAU resolutions for the case of the expanding universe. The gauge (36) drastically simplifies the field equations. Introducing notations $\gamma_{00} \equiv 4w/c^2$, $\gamma_{0i} \equiv -4w^i/c^3$, and $\gamma_{ij} \equiv 4w^{ij}/c^4$, and splitting Einstein's equations in components, yield

$$\Box\chi - 2H\partial_\eta\chi + \frac{5}{2}H^2\chi = -4\pi G\sigma \ , \tag{37}$$

$$\Box w - 2H\partial_\eta w = -4\pi G\sigma - 4H^2\chi \ , \tag{38}$$

$$\Box w^i - 2H\partial_\eta w^i + H^2 w^i = -4\pi G\sigma^i \ , \tag{39}$$

$$\Box w^{ij} - 2H\partial_\eta w^{ij} = -4\pi G T^{ij} \ , \tag{40}$$

where $\partial_\eta \equiv \partial/\partial\eta$, $\Box \equiv -c^{-2}\partial^2_\eta + \boldsymbol{\nabla}^2$, $\chi \equiv w - \varphi/2$, the Hubble parameter $H = \dot{a}/a = 2/\eta$, densities $\sigma = c^{-2}(T^{00} + T^{ss})$, $\sigma^i = c^{-1}T^{0i}$ with $T^{\alpha\beta}$ being the tensor of energy-momentum of matter of the solar system defined with respect to the metric $f_{\alpha\beta}$. These equations extend the equations (4), (5) of the IAU resolutions to the case of expanding universe.

Equation (37) describes evolution of the scalar field ϕ while equation (38) describes evolution of the scalar perturbation w of the metric tensor. Equation (39) yields evolution of vector perturbations of the metric tensor, and equation (40) describes TT gravitational waves emitted by the solar system. Equations (37)–(40) depend on the Hubble parameter and can be solved analytically. The Green functions for these equations have been found in [20,21] and solutions can be smoothly matched with the BCRS metric (6), (7) of the IAU resolutions.

Acknowledgements. This work was promoted by the Research Council Grant FIT-11-020 of the University of Missouri-Columbia. The author is thankful to N. Capitaine and the LOC of Journées 2010 for travel support.

6. REFERENCES

[1] Ciufolini, I. & Matzner, R. (eds.) 2010, "General Relativity and John Archibald Wheeler", Astrophysics and Space Science Library, 367

[2] Lämmerzahl, C., Everitt, C.W.F. & Hehl, F.W. (eds.) 2001, "Gyros, Clocks, Interferometers: Testing Relativistic Gravity in Space", Lecture Notes in Physics, 562

[3] Dittus, H., Lämmerzahl, C., Ni, W.-T. & Turyshev, S. (eds.) 2008, "Lasers, Clocks and Drag-Free: Technologies for Future Exploration in Space and Tests of Gravity", Springer: Berlin

[4] Will, C.M. 1993, "Theory and Experiment in Gravitational Physics", Cambridge University Press: Cambridge

[5] Kopeikin, S. & Vlasov, I. 2004, "Parametrized post-Newtonian theory of reference frames, multipolar expansions and equations of motion in the N-body problem", Phys. Reports, 400, pp. 209-318

[6] Xie, Y., & Kopeikin, S. 2010, "Post-Newtonian Reference Frames for Advanced Theory of the Lunar Motion and a New Generation of Lunar Laser Ranging", Acta Physica Slovaca, 60, pp. 393-495

[7] Soffel, M., Klioner, S. A., Petit, G., Wolf, P., Kopeikin, S. M., Bretagnon, P., Brumberg, V. A., Capitaine, N., Damour, T., Fukushima, T., Guinot, B., Huang, T.-Y., Lindegren, L., Ma, C., Nordtvedt, K., Ries, J. C., Seidelmann, P. K., Vokrouhlický, D., Will, C. M. & Xu, C. 2003, "The IAU 2000 Resolutions for Astrometry, Celestial Mechanics, and Metrology in the Relativistic Framework: Explanatory Supplement", Astron. J. (USA), 126, pp. 2687-2706

[8] Kopeikin, S.M. & Gwinn, C.R. 2000, "Sub-Microarcsecond Astrometry and New Horizons in Relativistic Gravitational Physics", IAU Colloquium, 180, pp. 303–307

[9] Capitaine, N., Andrei, A. H., Calabretta, M., Dehant, V., Fukushima, T., Guinot, B., Hohenkerk, C., Kaplan, G., Klioner, S., Kovalevsky, J., Kumkova, I., Ma, C., McCarthy, D. D., Seidelmann, K. & Wallace, P. T. 2007, "Proposed terminology in fundamental astronomy based on IAU 2000 resolutions", Highlights of Astronomy, 14, pp. 474-475

[10] Brumberg, V. A. & Kopejkin, S. M. 1989, "Relativistic reference systems and motion of test bodies in the vicinity of the Earth", Nuovo Cim. B, 103, pp. 63-98

[11] Kopeikin, S. M. 1988, "Celestial coordinate reference systems in curved space-time", Cel. Mech., 44, pp. 87-115

[12] Brumberg, V. A. & Kopeikin, S. M. 1990, "Relativistic time scales in the solar system", Cel. Mech. Dyn. Astron., 48, pp. 23-44

[13] Irwin, A. W. & Fukushima, T. 1999, "A numerical time ephemeris of the Earth", Astron. Astrophys., 348, pp. 642-652

[14] Klioner, S., Capitaine, N., Folkner, W., Guinot, B., Huang, T. Y., Kopeikin, S., Petit, G., Pitjeva, E., Seidelmann, P. K. & Soffel, M. 2009, "Units of Relativistic Time Scales and Associated Quantities", IAU Symposium, 261, pp. 79-84

[15] Blanchet, L. & Damour, T. 1989, "Post-Newtonian generation of gravitational waves", Ann. Inst. H. Poincare, Phys. Theor., 50, pp. 377-408

[16] Seidelmann, P. K. 1992, "Explanatory Supplement to the Astronomical Almanac", University Science Books: Mill Valley, California, pp. 281–282

[17] Brans, C.H. & Dicke, R.H. 1961, "Mach's Principle and a Relativistic Theory of Gravitation", Phys. Rev. D, 124, pp. 925-935

[18] Mukhanov, V. 2005, "Physical Foundations of Cosmology", Cambridge University Press: Cambridge

[19] Anderson, J. D. & Nieto, M. M. 2010, "Astrometric Solar-System Anomalies", IAU Symposium, 261, pp. 189-197

[20] Kopeikin, S. M., Ramirez, J., Mashhoon, B. & Sazhin, M. V. 2001, "Cosmological perturbations: a new gauge-invariant approach", Phys. Lett. A, 292, pp. 173-180

[21] Ramirez, J. & Kopeikin, S. 2002, "A decoupled system of hyperbolic equations for linearized cosmological perturbations", Phys. Lett. B, 532, pp. 1-7

DEVELOPING A PULSAR-BASED TIMESCALE

G. HOBBS[1], W. COLES[2], R. MANCHESTER[3], D. CHEN[4]

[1] CSIRO Astronomy and Space Science
PO Box 76, Epping, NSW 1710, Australia
george.hobbs@csiro.au

[2] Electrical and Computer Engineering, University of California
La Jolla, California, U.S.A.
bcoles@ucsd.edu

[3] CSIRO Astronomy and Space Science
PO Box 76, Epping, NSW 1710, Australia
dick.manchester@csiro.au

[4] National Time Service Center
CAS, Xian, China
ding@ntsc.ac.cn

ABSTRACT. We show how pulsar observations may be used to construct a time standard that is independent of terrestrial time standards. The pulsar time scale provides a method to determine the stability of terrestrial time standards over years to decades. Here, we summarise the method, provide initial results and discuss the possibilities and limitations of our pulsar time scale.

1. INTRODUCTION

Almost 2000 rapidly rotating neutron stars, known as pulsars, have now been discovered (Manchester et al. 2005)[1]. Pulses of radiation from these pulsars are detected using large radio telescopes. The pulses are thought to be caused by a beam of radiation that sweeps across the Earth as the star rotates. As pulsars are very stable rotators, the pulse arrival times (ToAs) can be predicted very accurately over many years. Recent work (Hobbs, Lyne & Kramer 2010a) has shown that, for some pulsars, every rotation of the neutron star over the previous ~ 40 yr can be accounted for. That work also confirmed the existence of unexplained irregularities in the rotation rate of many pulsars. Such irregularities are generally divided into "glitch events" (e.g., Wang et al. 2000) during which the pulsar suddenly increases its spin rate and "timing noise" where gradual variations are observed in the pulse arrival times (e.g., Lyne et al. 2010, Shannon & Cordes 2010). A subset of pulsars, the millisecond pulsars, have rotational periods of a few milliseconds and are extremely stable. This allows ToAs to be measured with high precision (to within $\sim$50 ns for some pulsars) and can be accurately predicted over many years using a simple model of the pulsar spin.

Studies of individual pulsars discovered the first extra-Solar planetary systems (Wolszczan & Frail 1992), provided tests of the theory of general relativity (Kramer et al. 2006) and have allowed the magnetic field of our Galaxy to be mapped (Han et al. 2006). In contrast, Foster & Backer (1990) developed the concept of a "pulsar timing array" in which many pulsars are observed and phenomena that affect all the pulsar signals are studied. For instance, the irregular rotation of a pulsar will be uncorrelated with the rotation of a different pulsar. However, the presence of a gravitational wave passing the Earth will lead to variations in pulse arrival times that are dependent upon the angle between the Earth, pulsar and gravitational-wave source (e.g., Detweiler 1979). By searching for such correlated signals, an unambiguous detection of gravitational waves may be made. As described in this paper, irregularities in terrestrial time standards will lead to correlated pulse ToAs (for instance, if the observatory clock is running fast then the pulse arrival times for all pulsars observed will be later than predicted).

The International Pulsar Timing Array (IPTA) project (Hobbs et al. 2010b) has been developed to search for correlated signals in pulsar data with the main goals of 1) detecting low-frequency gravitational waves, 2) improving the Solar System ephemeris and 3) developing a pulsar-based time scale. The IPTA

[1] http://www.atnf.csiro.au/research/pulsar/psrcat

project includes data from various observatories. In this paper we use observations obtained from the Parkes observatory as part of the Parkes Pulsar Timing Array project (PPTA; Verbiest et al. 2010 and references therein).

In §2 we provide background information relevant to this work. In §3 we describe the observations obtained from the PPTA project. In §4 we overview the method and present our results in §5. In §6 we discuss the implications of a pulsar time scale. This paper provides an overview; full details of the method and results will be published elsewhere.

2. BACKGROUND

Atomic frequency standards have been the basis of time keeping since 1955. Individual countries publish local atomic scales. These are combined by the Bureau International des Poids et Mesures (BIPM) to form International Atomic Time (TAI). TAI is a realisation of a theoretical time scale known as terrestrial time (TT). Once published, TAI is never revised, but corrections are published via other realisations of TT. For instance, TT(BIPM2010) is the most recent post-corrected realisation of TT available. The difference between this time scale and TAI is shown in Figure 1 from MJD 44000 (the year 1979) to the current date and clearly shows a drift of $\sim 20\,\mu$s over $\sim$30 yr. As TT(BIPM2010) is a post-corrected version of TT(TAI), it is expected that this drift is caused by inaccuracies in TT(TAI). However, as TT(BIPM2010) is the world's best time standard, there is no existing method by which a similar figure can be produced to measure inaccuracies in this realisation of TT.

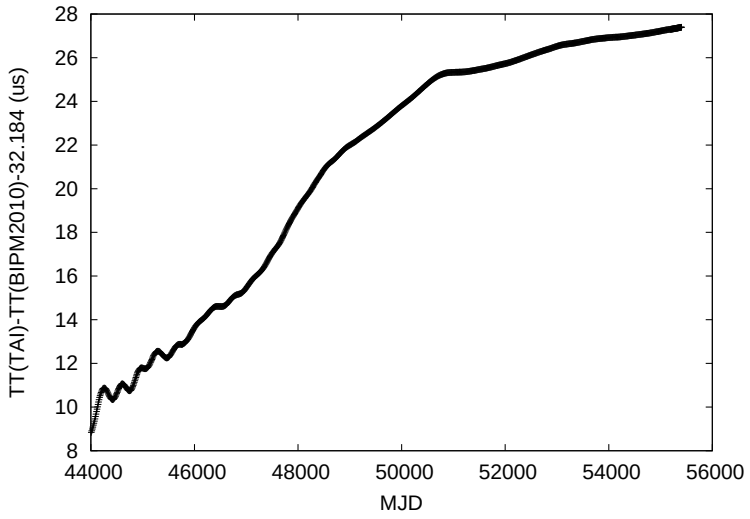

Figure 1: The difference between TT(TAI) and TT(BIPM2010).

Pulsars, being macroscopic astrophysical objects, are completely unrelated to atomic clocks and are governed largely by unrelated physical principles. Thus a time standard based upon the rotation of pulsars should be independent of one based on atomic clocks[2]. The rotation of millisecond pulsars is expected to remain stable for billions of years, so they can provide a very long-term standard. Matsakis et al. (1997) developed a statistic to compare the stability of pulsar rotation with the stability of various time standards. A summary of this work is shown in Figure 2 which shows that the two pulsars studied (PSRs B1855+09 and B1937+21) are significantly less stable than atomic time standards on timescales up to a few years. On longer timescales the stability of PSR B1937+21 decreases because of timing noise dominating the spin-down of the pulsar. However, for PSR B1855+09 the stability continues to improve and becomes comparable or better than the time standards.

Since the publication of Matsakis et al. (1997) significant improvements have occurred that have allowed many pulsars to be observed with much higher precision. Such improvements have included new observing instrumentation, the use of higher observing frequencies, the discovery of more stable pulsars and improved calibration procedures. It is, therefore, now possible to make a pulsar-based time scale that significantly improves on previous attempts.

[2]Note that the atomic time scale is used in observing pulsars; this "contradiction" is discussed in section 6.

Various methods have been published describing how to use the pulsar ToAs to form a pulsar time scale (e.g., Guinot & Petit 1991, Petit & Tavella 1996, Foster & Backer 1990 and Rodin 2008). The initial stage of all these methods is to form "pulsar timing residuals" which are the difference between the measured arrival times and predictions of these times given a model of the pulsar (see, e.g., Edwards, Hobbs & Manchester 2006). If the model for the pulsar is "perfect" then there will be no statistically significant timing residuals. However, if the Earth-based time scale is incorrect then the pulse arrival times measured using this time scale will deviate from the predicted arrival times resulting in significant timing residuals. Previous pulsar time scales all involved taking a suitably weighted linear combination of the timing residuals from the various pulsars, exactly as one determines a time scale from an array of atomic clocks. However these methods are not optimal for pulsars because they do not take into account the irregular nature of pulsar observations and the interaction between fitting the timing model and taking a weighted sum of the residuals. In fact the problem is best expressed statistically as recovering a signal which all the ToAs have in common.

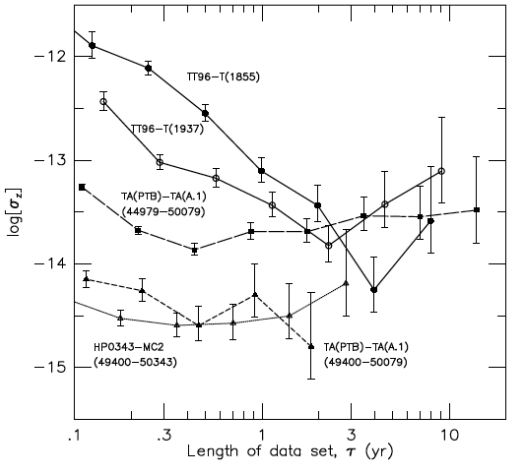

Figure 2: Figure taken from Matsakis et al. (1997) comparing the stability of PSRs B1855+09 and B1937+21 with various atomic clock differences.

3. OBSERVATIONS

Here we make use of observations from the Parkes telescope. These observations, of 19 millisecond pulsars, were presented in Verbiest et al. (2008) and Verbiest et al. (2009). For this paper we do not make use of PSR J1939+2134, which was also published in Verbiest et al. (2009) as its timing residuals are dominated by timing noise and our algorithm gives it essentially zero weight. All observations were carried out in the 20 cm band except for PSR J0613−0200 for which 50 cm observations have been used. Most of the processing was identical to that described in Verbiest et al. (2008/2009). However, we have now measured the majority of the timing offsets between the different instruments. Timing residuals were formed using the TEMPO2 software package (Hobbs, Edwards & Manchester 2006) using the JPL DE414 ephemeris and referred to TT(TAI).

The timing residuals for two pulsars, PSRs J0437−4715 and J1909−3744 are shown in Figure 3. This figure highlights various issues that need to be considered when developing a pulsar time scale:

- The observations of different pulsars cover different ranges and do not necessarily overlap.
- The ToA uncertainties vary by several orders of magnitude in time because of different observing durations, scintillation and improvements in observing systems. The precision with which ToAs can be determined can vary by many orders of magnitude between different pulsars.
- The observations are unevenly sampled and large gaps (of many months or years) exist for some pulsars.

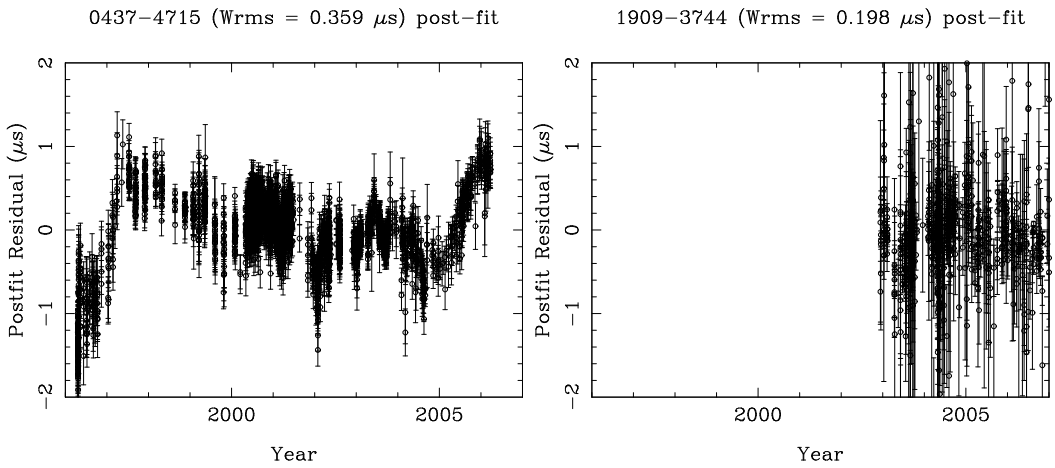

Figure 3: Timing residuals for PSRs J0437−4715 (left) and J1909−3744 (right) displayed with the same axis scaling.

- The pulsar timing model is formed by least-square-fitting to the timing residuals. This process will always fit and remove a quadratic polynomial from the timing residuals.
- Unmodelled timing noise is apparent for some pulsars. It is uncorrelated between pulsars.

We emphasise that the fit and subsequent removal of the quadratic polynomial implies that we can never detect linear or quadratic drifts in terrestrial time standards (the long-term drift in Figure 1 could not be detected using pulsars, however the smaller, faster variations are detectable).

4. METHOD

We have developed a method for comparing the timing residuals from multiple pulsars and determining the correlated signal. Details of the method and the tests undertaken to confirm its validity will be described in a separate paper. Here we provide an overview.

We choose to model the correlated signal (i.e., the clock error) as a Fourier series to provide some control of the covariance between the quadratic in the timing model and the clock error:

$$x_c(t) = \sum_{k=1}^{n} A_k \cos(k\omega_0 t) + B_k \sin(k\omega_0 t) \quad (1)$$

where $2\pi/\omega_0$ is chosen to be close to the total span of the observations. The total number of harmonics n is dependent upon the exact data being analysed. The parameters A_k and B_k are fitted as part of the standard TEMPO2 procedure which has been updated to include multiple pulsars simultaneously. We whiten and normalise the residuals for each pulsar using the Cholesky method which has recently been implemented in TEMPO2 (Coles et al., submitted to MNRAS). The fitting process provides the covariance matrix for the parameters A_k and B_k from which we calculate the uncertainty of $x_c(t)$. The resulting correlated signal is referred to TT(TAI) so the correlated signal, $x_c(t)$, can be regarded as TT(PSR)-TT(TAI).

5. RESULTS

The sampling and data spans for the 19 pulsars included in this analysis are shown in the top panel of Figure 4. The dashed line connecting the error bars in the bottom panel is $x_c(t)$ and the solid line is TT(BIPM2010)-TT(TAI) with a best-fit quadratic removed. If the observations were equally spaced and the observational errors were equal our procedure would be equivalent to a spectral analysis and the error bars would be independent. In practice the error bars are correlated, but we have spaced them such that the correlation is not too high. It is clear that the pulsar timescale is very similar to TT(BIPM2010);

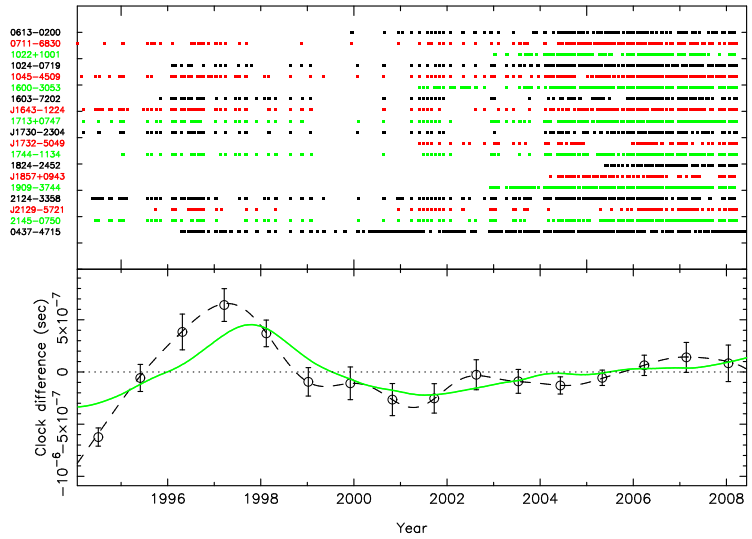

Figure 4: The top panel shows the data sampling for the different pulsars in the sample. The bottom panel shows the pulsar time scale with respect to TT(TAI). The solid line indicates TT(TAI)-TT(BIPM2010) with a quadratic polynomial fitted and removed.

they show similar deviations from TT(TAI) around 1997 and a similar linear trend more recently. There is a marginally significant difference between $x_c(t)$ and TT(BIPM2010) between 1996 and 1998.

6. DISCUSSION AND CONCLUSIONS

Here we outline and summarise the discussion that followed the presentation of this paper.

- *Can any phenomena mimic a terrestrial time standard error?* We have detected significant correlations in the pulsar timing residuals and have attributed these correlations to the terrestrial time standard. Errors in the time transfer to the Parkes observatory would appear in $x_c(t)$, but these are thought to be <20 ns. The possible effects of gravitational waves are also partially correlated, but these are expected to be <100 ns (Yardley et al., in preparation).

- *Can a weighted average approach be used to form the pulsar based time standard?* We do not believe that a weighted average approach is a reliable technique. Step errors will occur at the beginning and end of shorter data sets and these will require smoothing. Some of the variations will be spuriously reduced by the independent quadratic removal.

- *Is the pulsar time scale independent of atomic clocks and is the pulsar time a realisation of terrestrial time?* In order to form pulsar timing residuals it is necessary that a precise time is recorded with each observation and that this time can be converted to Barycentric Coordinated Time (TCB) via a realisation of terrestrial time. However, assuming that both the conversion from TT to TCB and the transfer from the observatory time to TT are known to within a few nanoseconds then any induced correlated timing residuals will be caused by irregularities in the realisation of TT. Subtracting these correlated residuals from the realisation of TT produces a new, improved realisation, TT(PSR). TT(PSR) is presented in the form of corrections to TT(TAI) exactly as is TT(BIPM2010).

- *What is the effect of correcting TAI?* The difference between TT(TAI) and TT(BIPM2010), shown in Figure 1, is a result of a deliberate correction of the primary standard frequencies. Around 1993 the frequency of TAI was found to be too low (Petit 2004) which resulted in the decision in 1995 to correct the primary frequency. This correction was phased in over three years (Petit, 2004) which resulting in the obvious "bump" in Figure 1. Around the year 2000, when caesium fountains began to contribute significantly to TAI, further steering has been necessary. These corrections should be reflected in TT(BIPM2010) so it should agree with TT(PSR). However, it is possible that the

corrections in TT(BIPM2010) were not perfect and some of the difference between TT(BIPM2010) and the pulsar time scale may be real.

Pulsar timing precision is continuing to improve as new pulsars are discovered, new telescopes built and new instrumentation installed. Combining data from observatories world-wide will lead to a large increase in the number of pulsars and the data span compared with our PPTA observations. Comparing data from different observatories also provides a means by which irregularities in the time transfer from the observatory clock to TT can be determined and removed. Within a few decades it is likely that the Square Kilometre Array (SKA) telescope will revolutionise pulsar timing. We therefore believe that pulsar timing will continue to advance in step with the expected improvements in atomic clocks and continue to provide a valuable independent time reference.

Acknowledgements. The Parkes Pulsar Timing Array project is a collaboration between numerous institutes in Australia and overseas and we thank our collaborators on this project. The Parkes radio telescope is part of the Australia Telescope which is funded by the Commonwealth of Australia for operation as a National Facility managed by CSIRO. GH acknowledges support from the Chinese Academy of Sciences #CAS KJCX2-YW-T09, NSFC 10803006 and from the Australian Research Council (project #DP0878388).

7. REFERENCES

Detweiler, S., 1979, "Pulsar timing measurements and the search for gravitational waves", ApJ, 234, 1100

Edwards, R., Hobbs. G, Manchester, R. N., 2006, "TEMPO2, a new pulsar timing package - II. The timing model and precision estimates", MNRAS, 372, 1549

Foster, R. S., Backer, D., C., 1990, "Constructing a pulsar timing array", ApJ, 361, 300

Guinot, B., Petit, G., 1191, "Atomic time and the rotation of pulsars", A&A, 248, 292

Han, J. L., et al., 2006, "Pulsar Rotation Measures and the Large-Scale Structure of the Galactic Magnetic Field", ApJ, 642, 868

Hobbs, G., Lyne, A. G., Kramer., M., 2010a, "An analysis of the timing irregularities for 366 pulsars", MNRAS , 402, 1027

Hobbs, G., et al., 2010b, "The International Pulsar Timing Array project: using pulsars as a gravitational wave detector", CQGra, 27, 4013

Hobbs, G., Edwards, R. T., Manchester, R. N., 2006, "TEMPO, a new pulsar-timing package - I. An overview", MNRAS, 369, 655

Kramer, M., et al. 2006, "Tests of General Relativity from Timing the Double Pulsar", Science, 314, 97

Lyne et al., 2010, "Switched Magnetospheric Regulation of Pulsar Spin-Down", Science, 329, 408

Matsakis, D. N., Taylor, J. H., Eubanks, T. M., 1997, "A statistic for describing pulsar and clock stabilities", A&A, 326, 924

Manchester, R. N., Hobbs, G. B., Teoh, A., Hobbs, M., 2005, "The Australia Telescope National Facility Pulsar Catalogue", AJ 129, 1993

Petit, G., 2004, www.bipm.org/cc/CCTF/Allowed/16/cctf04-17.pdf

Petit, G., Tavella, P., 1996, "Pulsars and time scales", A&A, 308, 290

Rodin, A. E., 2008, "Optimal filters for the construction of the ensemble pulsar time", MNRAS, 387, 1583

Shannon, R., Cordes, J. M., 2010, "Assessing the Role of Spin Noise in the Precision Timing of Millisecond Pulsars", arXiV, 1010, 4794

Verbiest, J. P. W. et al., 2010, "Status update of the Parkes pulsar timing array", CQGra, 27, 4015

Verbiest, J. P. W. et al. 2009, "Timing stability of millisecond pulsars and prospects for gravitational-wave detection", MNRAS, 400, 951

Verbiest, J. P. W. et al. 2008, "Precision timing of PSR J0437-4715: An accurate pulsar distance, a high pulsar mass, and a limit on the variation of Newton's Gravitational constant", ApJ, 679, 675

Wang et al., 2000 "Glitches in Southern Pulsars", MNRAS, 317, 843

Wolszczan, A., Frail, D. A., 1992, "A planetary system around the millisecond pulsar PSR1257+12", Nature, 355, 145

ENSEMBLE PULSAR TIME SCALE

A.E. RODIN
Pushchino Radio Astronomy Observatory of the Lebedev Physical Institute RAS
Russia, 142290, Moscow region, Pushchino, PRAO
e-mail: rodin@prao.ru

ABSTRACT. The algorithm of the ensemble pulsar time scale (PT_{ens}) based on the optimal Wiener filtration method has been proposed. This algorithm allows the separation of the contributions to the post-fit pulsar timing residuals of the atomic clock and pulsar itself. Filters were designed with the use of the cross-spectra of the timing residuals. The method has been applied to the timing data of six millisecond pulsars. Direct comparison with the classical method of the weighted average showed that use of the optimal Wiener filters before averaging allows noticeably to improve the fractional instability of the ensemble time scale. Application of the proposed method to the most stable millisecond pulsars with the fractional instability $\sigma_z < 10^{-15}$ may improve the fractional instability of PT_{ens} up to the level $\sim 10^{-16}$.

1. INTRODUCTION

Despite the algorithms of construction of the ensemble time scales are well established and the fractional instability of the TAI and TT(BIPM) scales currently is at level of a few 10^{-16} (Petit, 2010), development of new methods and approaches of the ensemble scales construction, including pulsar ones, presents an interest (Rodin, 2008), (Hobbs et al, 2010). In this paper the method of the optimal Wiener filtration is developed for construction of the ensemble pulsar time scale as applied to pulsar timing data. This method is compared with the classical algorithm based on the computation of the weighted average of time scales. From the general reasoning one can expect increasing of the signal estimation accuracy in comparison with the weighted average method since an additional information is used in form of the covariance function or spectrum of the estimated signal. The paper (Rodin, 2008) on the basis of computer simulation confirms the above statement.

In this paper PT_{ens} is considered primary as an independent basement for calculation of variations of the terrestrial time scales rather than an independent realisation of the barycentric time.

Section 2 of the paper contains basic formulae of the optimal Wiener filtration. Section 3 tells about pulsar observations used in this paper. In section 4 the method of optimal filtration is applied to timing data of six millisecond pulsars. The fractional instability σ_z is computed for time scales averaged with the different methods.

2. BASIC FORMALAE

Let us assume that we have M time series of the length n ${}^k r(t_i) = {}^k r_i(t)$ $(i = 1, 2, \ldots, n, k = 1, 2, \ldots, M)$. In our case ${}^k r_i$ are post-fit timing residuals of time of arrivals (TOAs) of pulsar pulses observed relative to the same time scale and with the same registering equipment. This paper uses so called square root Wiener filter which expressed by the following formula (Terebizh, 1993)

$$ {}^k H(\omega) = \sqrt{\frac{S(\omega)}{S(\omega) + {}^k N(\omega)}},\ k = 1, 2, \ldots, M, \tag{1} $$

where $S(\omega)$ is spectrum of the signal, ${}^k N(\omega)$ is spectrum of the noise of the kth pulsar.

In this paper the problem of stochastic signal estimation is solved under condition of lack of apriori information, since the covariance matrix and spectrum of the signal are apriori unknown and estimated from the data itself in the assumption that the clock variations (estimated signal) and variations of the rotational pulsar phase (additive noise) are uncorrelated. Spectrum $S(\omega)$ of the signal were calculated as

an average of all cross-spectra by the formula ($k \neq l$)

$$S(\omega) = \frac{1}{2\pi} \left| {}^{k}R(\omega)^{l}R^{*}(\omega) \right|, \; k, l = 1, 2, \ldots, M, \tag{2}$$

where $(\cdot)^{*}$ denominates complex conjugation, ${}^{k}R(\omega) = \mathcal{F}[{}^{k}r(t)]$ is Fourier transform of the input data.

The optimal filter is used according to the following formula

$${}^{k}\hat{R}(\omega) = {}^{k}H(\omega){}^{k}R(\omega), \; k = 1, 2, \ldots, M. \tag{3}$$

The filtered signal is obtained with the inverse Fourier transform ${}^{k}s(t) = \mathcal{F}^{-1}[{}^{k}\hat{R}(\omega)]$.

The averaged signal (the ensemble scale) is calculated by the weighted average formula

$$\mathbf{s} = \sum_{k=1}^{M} {}^{k}w\,{}^{k}s(t), \; \sum_{k} {}^{k}w = 1. \tag{4}$$

Weight ${}^{k}w \sim {}^{k}\mathrm{rms}^{-2}$, rms is the root mean square of the kth time series.

3. OBSERVATIONS

The pulsars PSR J0613-0200, J1640+2224, J1643-1224, J1713+0747, J1939+2134 and J2145-0750 were observed with the fully steerable RT-64 radio telescope of the Kalyazin Radio Astronomy Observatory (KRAO) (Potapov et al., 2003) (Ilyasov et al., 2004), (Ilyasov et al., 2005) (fig. 1). The AS-600 instrumental facility of the Pushchino Radio Astronomy Observatory (Astro Space Center, Lebedev Physical Institute) was used for the registration (Oreshko, 2000). The pulsar pulses were accumulated by a spectrum analyzer in two circular polarizations, 80 channels in each, with a channel frequency band 40 kHz. The observing sessions were conducted, on average, once every two weeks. The total signal integration time in each session was about 2 hours.

The topocentric TOAs were determined by fitting the session-summed pulsar pulse profile into a reference template with a hight signal to noise ratio. We computed the barycentric TOAs, determined the TOA residuals and refined the pulsar timing parameters by minimizing the residuals by the least-squares method using the software Tempo (Taylor, Weisberg, 1989). The DD model (Damour, Deruelle, 1986) was used to refine and compute the pulsar orbital parameters. The astrometric, spin and orbital parameters of all six pulsars can be found in the paper (Rodin, 2011).

4. RESULTS

For the purpose of unification all pulsar data were binned and averaged at the interval 30 days. Gaps were filled with the linear interpolation of adjacent values. The common part of the data in the interval MJD=51000–53490 were used. Since all observations were carried out with the same registering system, no data matching was applied.

Fig. 2a shows the binned pulsar residuals and their weighted average (solid line). Fig. 2b shows the same data passed through the optimal filter (1) and their weighted average.

The stability of a time scale is characterised by so-called Allan variance numerically expressed as a second-order difference of the clock phase variations. Since timing analysis usually includes determination of the pulsar spin parameters up to at least the first derivative of the rotational frequency, it is equivalent to excluding the second order derivative from pulsar TOA residuals and therefore there is no sense in the Allan variance. For this reason, for calculation of the fractional instability of a pulsar as a clock, another statistic σ_z has been proposed (Taylor, 1991).

Fig. 3 shows the fractional instability of the ensemble pulsar time scale constructed on the basis of six millisecond pulsars observed at KRAO. From the fig. 3 one can see that the optimal filter applied to data before weighted average improves the fractional instability almost two times along all time interval τ. On the basis of visual analysis of the fig. 2 one can conclude that the common signal presented in all pulsar data and caused by behavior of the registering equipment and by variations of the local frequency standard is better determined in data passed through the filter.

At the present time at least five pulsars display the fractional instability at the level $\leq 10^{-15}$ (Verbiest et al, 2009). One can expect that application to them of the optimal filter method will allow to obtain the

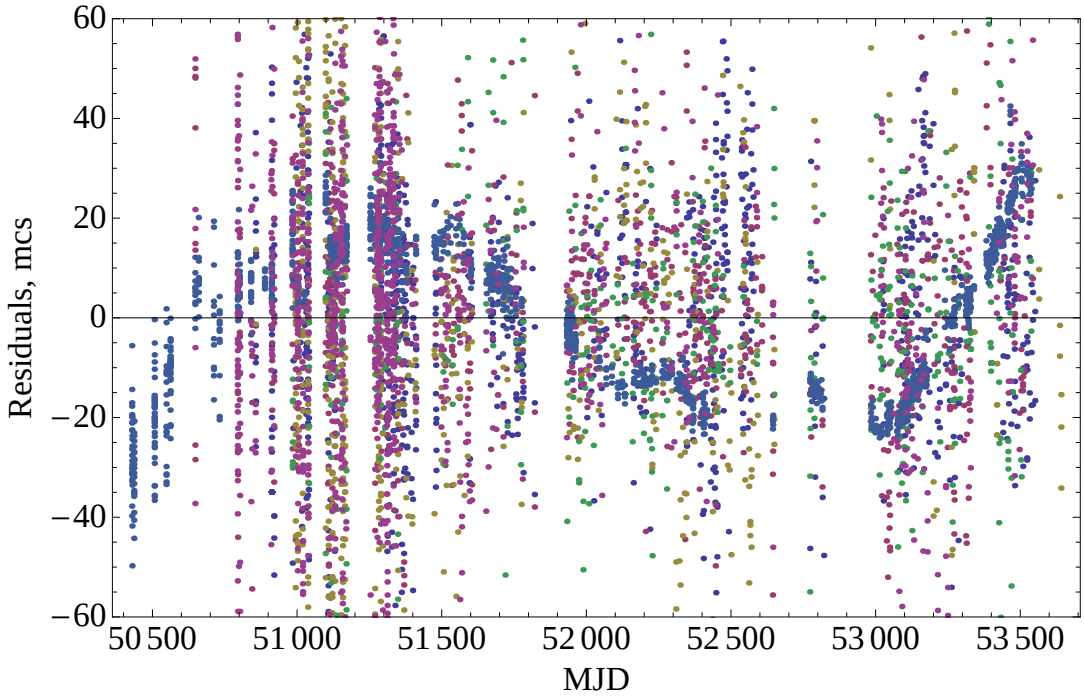

Figure 1: Post-fit timing residuals of six millisecond pulsars observed at the Kalyazin Radio Astronomy Observatory.

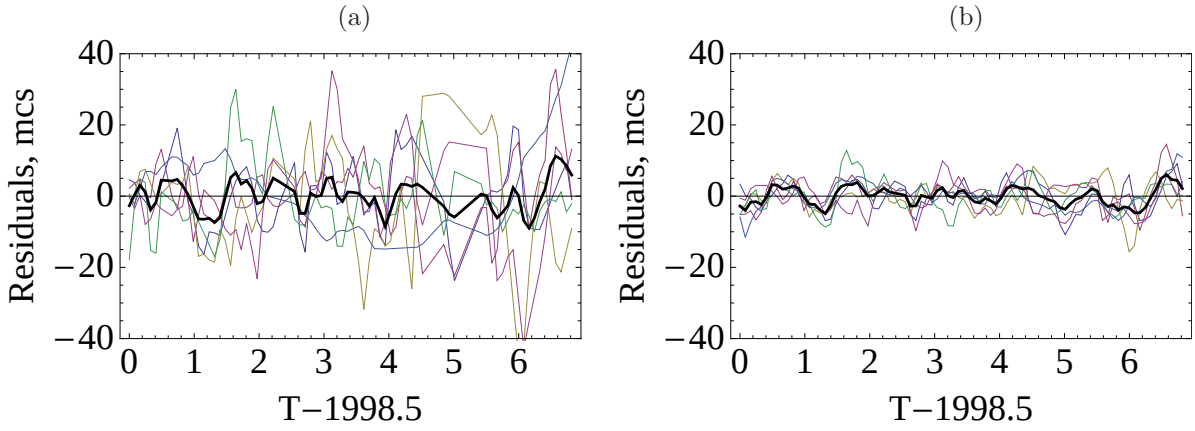

Figure 2: The binned post-fit timing residuals of six millisecond pulsars observed at the Kalyazin Radio Astronomy Observatory before (a) and after (b) applying Wiener optimal filter. Solid line indicates weighted average.

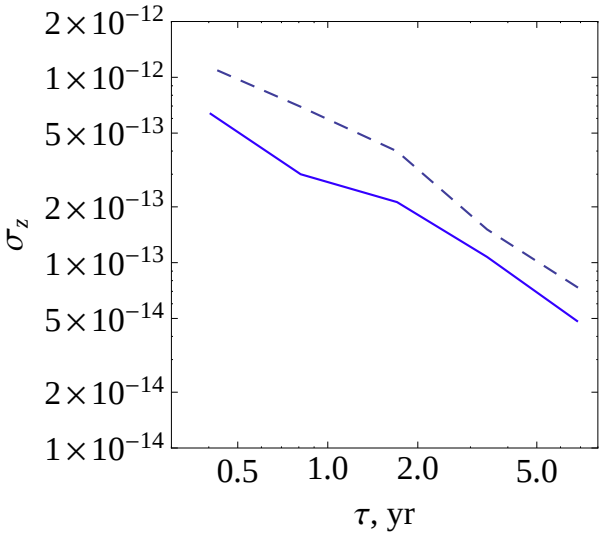

Figure 3: Fractional instability σ_z of the ensemble pulsar time scale in dependence on the observation interval τ. Dashed line indicates weighted average method, solid line indicates optimal filters method.

fractional instability of the ensemble pulsar time scale at the level of a few units of 10^{-16} , i.e. comparable with the instability of the best terrestrial frequency standards.

5. REFERENCES

Damour D., Deruelle N, 1986, "General relativistic celestial mechanics of binary systems. II. The post-Newtonian timing formula", Ann. Inst. Henri Poincaré, Physique théorique, 44, 263 (1986).

Hobbs, G.; Coles, W.; Manchester, R.; Chen, D., 2010, "Developing a pulsar-based timescale", this issue.

Ilyasov Yu., Oreshko V., Potapov V., Rodin A., 2004, "Timing of Binary Pulsars at Kalyazin, Russia", IAU Symposium no.218, (Ed. F. Camilo and B. M. Gaensler, ASP Series, San Francisco, 2004), p. 433.

Ilyasov Yu., Imae M., Hanado Y., Oreshko V., Potapov V., Rodin A., Sekido M., 2005, "Two-frequency timing of the pulsar B1937+21 in Kalyazin and Kashima in 1997-2002", Astron Lett., 31, 33.

Oreshko.V.V., 2000, "Pulsar timing instrumental errors. AC-600/1600 facility". Proceedings of the Lebedev Physical Institute.,(Ed. O.Krokhin and N.Kardashev, Moscow, 2000) v. 229, p. 110 (in Russian).

Petit G., 2010, "Atomic time scales TAI and TT(BIPM): present performances and prospects", Highlights of Astr., 15, p. 220.

Potapov, V. A.; Ilyasov, Yu. P.; Oreshko, V. V.; Rodin, A. E., 2003, "Timing Results for the Binary Millisecond Pulsar J1640+2224", Astronomy Letters, 29, p. 241.

Rodin A.E., 2008, "Optimal filters for the construction of the ensemble pulsar time", MNRAS , 387, 1583.

Rodin A.E., 2011, "Detection of the gravitational waves by observations of several pulsars", Astr.Lett., v.88, No.2, p.1.

Taylor J. H. and Weisberg J. M., 1989, "Further experimental tests of relativistic gravity using the binary pulsar PSR 1913 + 16", ApJ345, 434.

Taylor J.H., 1991, "Millisecond pulsars - Nature's most stable clocks", Proc.IEEE 79, 1054.

Terebizh V.Yu., 1992, "Analysis of time series in astrophisics", Moscow: Nauka (in Russian).

Verbiest, J. P. W.; Bailes, M.; Coles, W. A.; Hobbs, G. B.; van Straten, W.; Champion, D. J.; Jenet, F. A.; Manchester, R. N.; Bhat, N. D. R.; Sarkissian, J. M.; Yardley, D.; Burke-Spolaor, S.; Hotan, A. W.; You, X. P., 2009, "Timing stability of millisecond pulsars and prospects for gravitational-wave detection", MNRAS , 400, Issue 2, p. 951.

HIGH PRECISION PULSAR TIMING: NANCAY AND THE EUROPEAN PULSAR TIMING ARRAY

I. COGNARD[1], G. DESVIGNES[1,2], G. THEUREAU[1,3], and the EPTA consortium

[1] LPC2E, Université d'Orléans-CNRS
3A, Av de la Recherche Scientifique - 45071 ORLEANS CEDEX2 - FRANCE
e-mail: icognard@cnrs-orleans.fr

[2] Astronomy Dept, University of California
CA 94705 BERKELEY - USA

[3] Station de radioastronomie de Nançay
18330 NANCAY - FRANCE

ABSTRACT. Pulsars are highly stable celestial rotators used in many different applications, from tests of the theories describing the gravitation to the search for a Gravitational Waves background. They could even play a role in time scales definition and those point sources are also used to link the different reference frames. Nancay radiotelescope is involved in high precision timing since 20 years. Since 2004, a coherent dedispersion instrumentation enables numerous routine observations on more than 200 pulsars using half of the time of this 100-meters class radiotelescope. Two main programs are currently conducted. A large set of young and old pulsars is timed for a multi-wavelength approach, complementary to the very successful high energy observations of pulsars done by the instrument FERMI/LAT (Abdo et al., 2009). A set of highly stable millisecond pulsars is monitored as our contribution to the European Pulsar Timing Array in order to probe any kind of Gravitational Waves background.

1. INTRODUCTION

Highly magnetized neutron stars are called pulsars when we receive collimated radio beams from them on every rotation. The most stable pulsars are used as clocks for many different kind of studies. Such pulsars located in a relativistic binary are used to put constrains on the theories of gravitation (Kramer et al., 2006). An array of highly stable pulsars distributed over the sky is used to search for a gravitational waves background (Jenet et al., 2006). An effort towards an international Pulsar Timing Array is taking place in every large telescope in the world in order to share all the observations and set the best limit on a gravitational waves background coming from the early Universe.

With a collecting area corresponding to a 100m dish, the Nançay radiotelescope is a centimetric telescope among the largest in the world. Based on a Kraus design, the telescope has two receivers providing a continuous coverage from 1.1 to 3.5GHz. The 1.4 to 2GHz range is a good choice to observe pulsars between embarrassing interstellar effects at the lower frequencies and faint emission received from pulsars at higher ones.

2. A COHERENT PULSAR DEDISPERSION INSTRUMENTATION

A quasi-perfect way to remove the dispersion introduced by the ionized part of the interstellar medium, called the coherent dedispersion, is to apply a transfer inverse function in the complex Fourier domain of the data time series (Hankins & Rickett, 1975). This operation needs a huge computing power since we need to do direct and inverse Fast Fourier Transforms in real-time on the Nyquist sampled data stream. At Nançay, we were among the very first in June 2008 to routinely use the Graphical Processing Units (GPU) instead of standard processors (CPU) to dedisperse pulsar data (Figure 1). With the now fairly old Nvidia GeForce 8800GTX, we are able to coherently dedisperse a 128MHz bandwidth having 2 computers hosting 2 GPU units each. The two GPUs we put in each computer are water-cooled to increase their lifetime. Presently the folding of the data in phase with the pulsar rotation is done in the CPUs. and the overall load of each computer during observations is around 60%. We are already testing the next generation which is able to coherently dedisperse a 512MHz bandwith (Figure 1), the maximum

currently available at the Nançay telescope. While the current version is based on a Serendip5 board, we are now using a ROACH board also designed by the CASPER group (http://casper.berkeley.edu/).

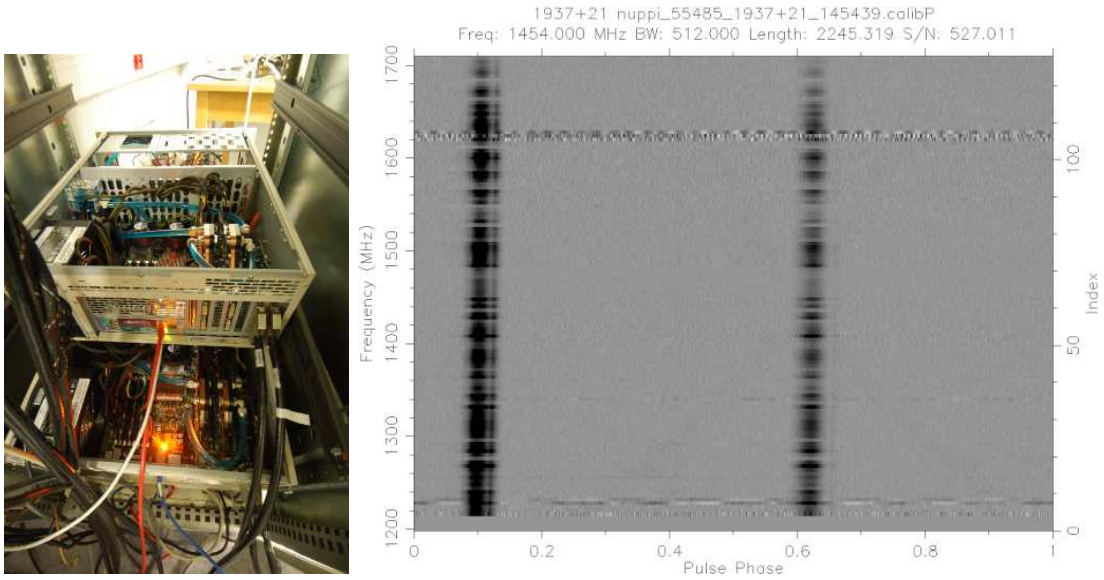

Figure 1: View of the 128MHz coherent dedispersion instrumentation based on GPUs. Profiles from the pulsar B1937+21 shown as function of the frequency and integrated for more than half an hour with the new 512MHz version of the instrumentation.

3. AN INTERNATIONAL EFFORT

The Nançay radiotelescope is part of an European consortium called the European Pulsar Timing Array (EPTA) which gather people from the five main radiotelescopes in Europe (Janssen et al. 2008): Cagliari (IT), Effelsberg (G), Jodrell Bank(GB), Nançay (F) and Westerbork (NL). The 64 meters antenna in Sicilia (Cagliari) is still under construction. We do have regular short workshops, usually at one of the radiotelescopes. During a few days, we closely interact to make progress on the different actions we planned together : coordinations of project and publications for students and post-docs, coordinations of source lists and joined observing sessions, sharing among partners of Time of Arrival (ToAs) and templates (used to derive ToAs), building a library of common synthetic multi-frequency templates. We are also open to international collaboration to share ToAs for joined goals, and we are presently preparing a Memorandum of Understanding being signed with the Australian Parkes Pulsar Timing Array (PPTA). We hope to reach the same level of agreement with the US NanoGrav consortium.

Lead by Michael Kramer (MPIfR, Bonn and University of Manchester), an advanced grant from the European Research Council called LEAP (for Large European Array for Pulsars) was obtained to coherently add the pulsar signal from the five large European radiotelescopes. Based on the high concentration of large antennae in central Europe, the aim is to get an Arecibo-like radiotelescope able to observe all the Northern sky.

4. THE NANCAY CONTRIBUTION

The Nançay pulsar coherent dedispersor is producing high quality timing data on a number of stable millisecond pulsars. Figure 2 shows an example of a daily profile and a template obtained on the ultra-stable pulsar PSR J1909-3744. From the coherently dedispersed profiles, we derive a ToA using a χ^2 fit in the Fourier domain (Taylor, 1992). A fit for the pulsar parameters (period and derivatives, position, proper motion and potentially several orbital parameters) is done from the ToAs using the code 'tempo2' (Hobbs et al., 2006) producing ToA residuals (differences between calculated and measured ToAs). We then carefully inspect them to make sure all the needed parameters are included in the analysis. A set of ToAs residuals is shown Figure 3 for pulsar J1909-3744. A summary of the ToAs residuals rms obtained at Nançay are shown in Table 1 (Desvignes, 2009). The excellent quality of the Nançay data can be

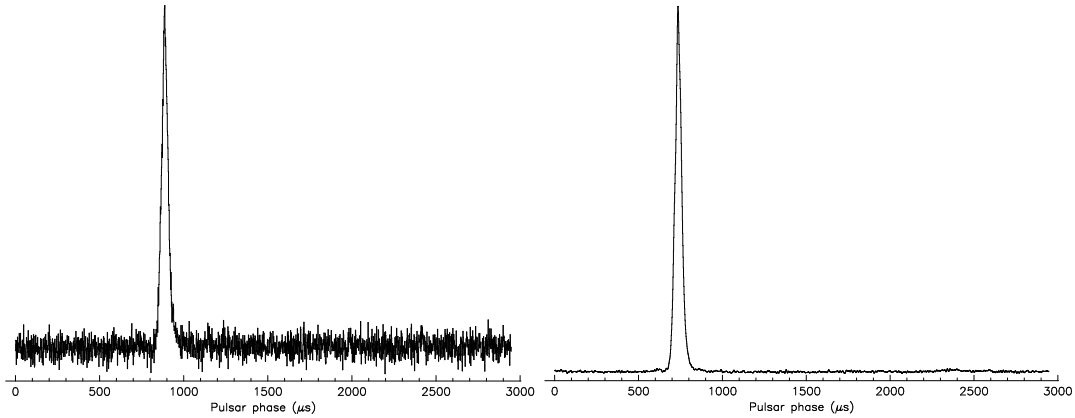

Figure 2: Exemple of a daily profile for pulsar J1909-3744, along with the template used to accurately determine the Times of Arrivals.

emphasized observing that half of the residuals are characterized by an rms below 1 μs and few of them are even below 500ns. Nançay is now an important partner to build a Pulsar Timing Array, within the EPTA first, and then the EPTA being part of the International Pulsar Timing Array.

5. AN EPTA LIMIT ON A GRAVITATIONAL WAVES BACKGROUND

As already mentioned, the direct detection of low-frequency gravitational waves (in the range $10^{-9} - 10^{-8}$Hz) is the main goal of the different Pulsar Timing Array projects around the world. High precision timing measurements will be processed to measure the stochastic background of gravitational waves (GWB) whose characteristic strain is expected to approximately follow a power-law of the form $h_c(f) = A(f/yr^{-1})^{\alpha}$, where f is the gravitational-wave frequency. A recent work (van Haasteren et al., 2010), used the current data from the European PTA along with a Bayesian algorithm to determine an upper limit on the GWB amplitude A as a function of the unknown spectral slope. For the case $\alpha = 2/3$, which is expected if the GWB is produced by supermassive black- hole binaries, a 95% confidence upper limit on A of 6×10^{-15} was obtained, which is 1.8 times lower than the 95% confidence GWB limit obtained by the Parkes PTA in 2006.

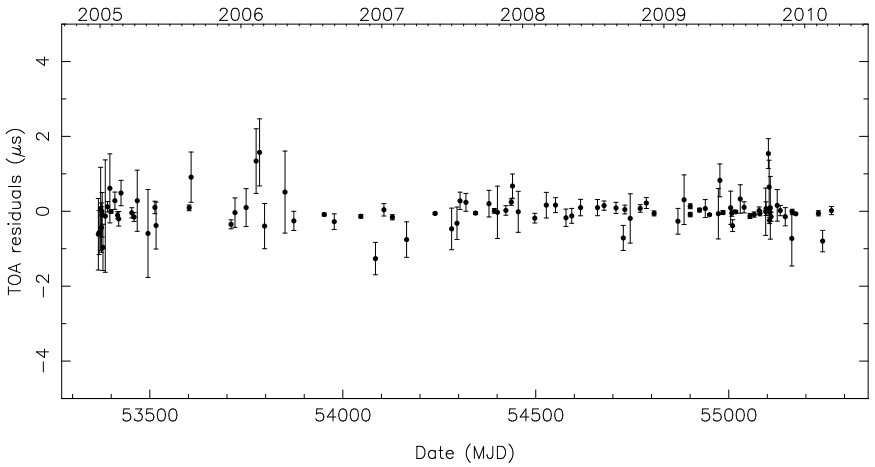

Figure 3: Timing residuals for the pulsar J1909-3744 observed with the Nançay radiotelescope. The residuals are characterized by a weighted rms of only ∼120ns.

Acknowledgments. The Nançay Radio Observatory is operated by the Paris Observatory, associated with

Pulsar	Period (ms)	P_{orb} (jours)	Span (yr)	N_{toa}	σ (μs)
J0030+0451	4.87	–	4.6	402	1.84
J0613−0200	3.06	1.2	4.5	280	0.913
J0751+1807	3.48	0.26	4.5	158	1.73
J0900−3144	11.10	18.7	2.0	199	2.87
J1012+5397	5.25	0.6	4.3	107	0.771
J1022+1001	16.45	7.8	4.5	136	1.97
J1024−0719	5.16	–	3.6	128	1.23
J1455−3330	7.99	76.2	4.5	139	2.33
J1600−3053	3.60	14.3	2.8	211	0.576
J1643−1224	4.62	147	4.5	271	1.7
J1713+0747	4.57	67.8	4.5	260	0.350
J1730−2304	8.12	–	4.5	85	1.55
J1744−1134	4.07	–	4.5	87	0.343
J1751−2857	3.91	110.7	3.5	36	0.948
J1824−2452	3.05	–	4.5	313	2.63
J1857+0943	5.36	12.3	4.5	51	0.860
J1909−3744	2.95	1.53	4.5	109	0.119
J1910+1256	4.98	58.4	3.5	31	1.04
J1939+2134	1.55	–	4.5	277	0.483
J2145−0750	16.05	6.84	4.5	159	0.993

Table 1: Timing residuals rms for different pulsars monitored with the Nançay radiotelescope. Columns are pulsar's name, period, orbital period if binary, data span, number of ToAs and ToA residuals rms.

the French Centre National de la Recherche Scientifique (CNRS).

6. REFERENCES

Abdo et al. 2009, "A Population of Gamma-Ray Millisecond Pulsars Seen with the Fermi Large Area Telescope", Science 325, 848

Desvignes, G. 2009, PhD Thesis, Université d'Orléans

van Haasteren, R., Levin, Y., Janssen, G. H., Lazaridis, K., Kramer, M., Stappers, B. W., Desvignes, G., Purver, M. B., Lyne, A.G., Ferdman, R.D., Jessner, A., Cognard, I., Theureau, G., D'Amico, N., Possenti, A., Burgay, M., Corongiu, A., Hessels, J., Smits, R., 2010, "Placing limits on the stochastic gravitational-wave background using European Pulsar Timing Array data", submitted

Hankins, T. H., & Rickett, B. J. 1975, Methods in Computational Physics, 14, 55

Hobbs, G. B., Edwards, R. T., & Manchester, R. N. 2006, "TEMPO2, a new pulsar-timing package - I. An overview", MNRAS, 369, 655

Janssen, G. H., Stappers, B. W., Kramer, M., Nice, D. J., Jessner, A., Cognard, I., & Purver, M. B. 2008, "Multi-telescope timing of PSR J1518+4904", A&A, 490, 753

Jenet, F. A., et al. 2006, "Upper Bounds on the Low-Frequency Stochastic Gravitational Wave Background from Pulsar Timing Observations: Current Limits and Future Prospects", ApJ, 653, 1571

Kramer, M., et al. 2006, "Tests of General Relativity from Timing the Double Pulsar", Science 314, 97

Taylor, J. H. 1992, "Pulsar Timing and Relativistic Gravity", Philosophical Transactions of the Royal Society of London, 341, 117-134

CHANDLER WOBBLE AND FREE CORE NUTATION OF SINGLE PULSAR

A. GUSEV
Kazan Federal University
18, Kremlevskaya, Kazan, 420008, Russia
e-mail: Alexander.Gusev@ksu.ru

ABSTRACT. PSR B1828-11 has long-term, highly periodic and correlated variations pulse shape and of the rate of slow-down with period variations approximately 1000, 500 and 250 days (Stairs et al., 2000). There are three potential explanations of pulses time-of-arrival from pulsar concerned with the interior of the neutron star, planetary bodies, free precession and nutation. We use the Hamiltonian canonical method of Getino et al., (1999) for the dynamically symmetrical pulsar consisting of the rigid crust, elliptical liquid outer core and solid inner core of PSR B1828-11. Correctly extending theory of differential rotation of a pulsar, we investigated dependence on Chandler wobble period, Inner Chandler Wobble, retrograde Free Core Nutation and prograde Free Inner Core Nutation from ellipticity of inner crystal core, outer liquid core and total pulsar.

1. INTRODUCTION

Observation of pulsars is a powerful source of the information for research of dynamics and internal structure of neutron stars. It's known, that innate feature of pulsar radiation is high stability of time-of-arrival (TOA) of pulses, and therefore the analysis of the TOA fluctuations can be reflection of thin effects of neutron stars dynamics. A small number of neutron stars also exhibit long-term cyclical but not precisely oscillatory variations in their spin (Sedrakian et al., 1999 and references there). For example, the Crab pulsar has very systematically phase residuals with peak-to-peak range of order ± 10 ms and characteristic cycle duration of about 20 months (Gusev,Kitiashvili, 2004). Observation of Vela pulsar's glitch in 1988 showed suppressing of oscillatory phase residuals with a period of order 25 days (Alpar et al., 1990); evidence for oscillations (Tkachenko oscillation) in the frequency derivative of the pulsar both before and after the glitch with a period about 25 days was also reported (Gusev, Kitiashvili, 2005); the evidence of frequency derivative oscillations (Tkachenko oscillation) of the pulsar both before and after the glitch with a period about 25 days was also reported (Gusev,Kitiashvili, 2008). The long-term variations (correlation times 100 days) in the pulse shape of the Vela pulsar has been found in data spanning approximately 4 yr (Sedrakian et al., 1999). The analysis of the pulse shape of PSR 1642-03 has allowed picking out the evidence of cyclical pulse shape variations with a period about 1000 days (Sedrakian et al., 1999). TOA variations of pulsars can be interpreted by three reasons: gravitational

Table 1: Some parameters of PSR B1828-11.

Period, ms	405.039883158(8)	
Dispersion measure, $cm^{-3}pc$	159.7(10)	
Characteristic age, Myr	0.11	
Long-term variation	167	250
in the pulse shape, days	500	1000

perturbation by planetary bodies, peculiarities of a pulsar interior like Tkachenko oscillations and free precession motion, when axis of rotation do not coincide with vectors of the angular moment of solid crust, liquid outer core and crystal core.

The radial velocity of a star is obtained by measuring the magnitude of the Doppler effect in its spectrum. Stars showing a small amplitude variation of the radial velocity can be interpreted as systems having planetary companions. Assuming that the pulsar has a mass of $1.35M_{\odot}$, the Keplerian orbital

radii identified with the three harmonically related sinusoids are 0.9, 1.4 and 2.1 AU and with masses are $3.1M_{\oplus}/sin(i)$, $10.2M_{\oplus}/sin(i)$, $4.6M_{\oplus}/sin(i)$, where i is the orbital inclination.

The second explanation are the periods of Tkachenko oscillations (Tkachenko, 1966) of the neutron superfluid vortex array, which carries much of the angular momentum of the neutron star, depends on the size of the star and the square root of the pulse period. Tkachenko oscillations for the Crab pulsar (PSR 0531+21) are expected 4 months; the period of the Tkachenko oscillations for the PSR B1828-11 are waited 13 months (Ruderman, 1970). Unfortunately, the theory of the Tkachenko oscillations does not easily explain the existence of multiple harmonics in the PSR B1828-11 timing residuals. The Crab pulsar has quasi-periodical variations from 15 to 30 months (Lyne & Graham-Smith, 1998).

The third case, more possible interpretation of TOA variations is a free precession of the pulsar. The time scale for the precession depends on the pulsar deformation degree. The wobble angle θ between the star's symmetry axis and its angular momentum can be estimated by the pulse profile changes. The difference in widths between the "wide" and "narrow" beam profiles is 20 (Link & Epstein, 2001). Interpretation of TOA variations by free precession gives a wobble angle 0.3^0 for the PSR B1828-11 (Stairs et al., 2000) and $0.3^0 - 0.8^0$ for the PSR B1642-03 (Shabanova, 2000; Shabanova et al., 2001). Using observed variations some authors calculated estimates of oblateness for different periods of PSR B1828-11 by: 1000 days $\sim 5 \cdot 10^{-9}$ (Stairs et al., 2000); 500 days $\sim 10^{-8}$ (Link & Cutler, 2002); 511 days - $\epsilon = 9 \cdot 10^{-9}$ (Link & Epstein, 2001).

We propose the explanation for all harmonics of TOA pulses variations as precession of a neutron star owing to differential rotation of crust, outer liquid core and inner crystal core of the pulsar.

2. HAMILTON APPROXIMATION

2.1 Two-layer model

At present time there are investigations of precession and nutation for very different celestial bodies: the Earth (Getino, 1995), Moon (Gusev, 2010), planets of Solar system (Gusev, 2010) and pulsars (Sedrakian et al., 1999; Link & Epstein, 2001; Wasserman, 2003; Cutler et al., 2003).

A correct application of the Hamiltonian method to the problem of the non-rigid Earth (Kinoshita, 1977; Getino, 1995) is a natural way for obtaining an analytical theory of the rotation pulsar which is more appropriate to the real neutron star. Rotation of the Earth-like planets of the Solar system, which have rigid mantle and elliptic liquid core, is characterized by free core nutation (Van Hoolst, 2000).

According to Getino approximation (Getino, 1995), core-mantle interaction can be presented as deformation of inertia tensor of the core (inertional deformation) and free motion of rigid crust and liquid core; interaction can be detected for a definite coordinate frame.

2.2 Three-layer model

The next step in the investigation of rotational variation of the pulsar is the research of the three-layer model. Different authors described rotational variations in the frame of the three-layer model for planets of the Solar system (Dehant et al., 2003; Getino et al., 1999) that have a rigid mantle, a liquid outer core and a solid inner core. The three-layer model is more complicated than the previous case therefore classical methods fail. Getino and Ferrandiz (Getino et al., 1999) developed a canonical formulation for an Earth model, which includes three layers: an axis symmetrical rigid mantle, a fluid outer core (FOC) and a solid inner core (SIC). Flattened of the pulsar, core, FOC and SIC are

$$e = \frac{C-A}{A} - Totalpulsar, \qquad e_f = \frac{C_f - A_f}{A_f} - FOC$$
$$e_c = \frac{C_c - A_c}{A_c} - Core, \qquad e_s = \frac{C_s - A_s}{A_s} - SIC \tag{1}$$

Here $A, C, A_f, C_f, A_s, C_s, A_c, C_c$ are moments of inertia of the pulsar, fluid outer, solid inner and total cores and of the neutron star accordingly.

$$P_{CW} = P_{PSR}\frac{A_{cr}}{C-A} = P_{PSR}\frac{A_{cr}}{A}\left(\frac{C}{A}-1\right)^{-1} P_{FCN} = -P_{PSR}\frac{A_{cr}}{A}\left(\frac{C_c}{A_c}-1\right)^{-1} \tag{2}$$

We are used four models of pulsar (tabl. 4) for modelling obligates of inner and outer cores and total pulsar (tabl. 5) with mass $\sim 1.4M_{\odot}$ and moment inertia $\sim 10^{44}$ g cm^2. Getino's investigation (Getino et al., 1999) showed that interaction between rigid mantle, FOC and SIC can be characterized by

Table 2: Four models of inner structure for PSR B1828-11

	R_{PSR}, km	h_{cr} km	A_{cr}, g cm^2	h_f, km	A_f, g cm^2	h_s, km	A_s, g cm^2
Model 1	10	0,1	$9 \cdot 10^{39}$	8,9	10^{44}	1	$2 \cdot 10^{40}$
Model 2	11	0,5	$7 \cdot 10^{40}$	10,5	$2,6 \cdot 10^{44}$	1	$2 \cdot 10^{40}$
Model 3	11	1	$9 \cdot 10^{39}$	9	10^{44}	1	10^{41}
Model 4	11	2	$2 \cdot 10^{40}$	8	10^{44}	1	$2 \cdot 10^{41}$

Table 3: Estimates of dynamic ellipticities of crust, mantle and core for PSR B1828-11.

	Model 1	Model 2	Model 3	Model 4
$P_{CW} = 167$ days	$\epsilon = 5,8 \cdot 10^{-12}$	$2 \cdot 10^{-11}$	$4,5 \cdot 10^{-11}$	$6 \cdot 10^{-11}$
$P_{RFCN} = 250$ days	$\epsilon_f = 2 \cdot 10^{-8}$	$2 \cdot 10^{-11}$	$2 \cdot 10^{-11}$	$3,75 \cdot 10^{-11}$
$P_{PFCN} = 500$ days	$\epsilon_s = 1,5 \cdot 10^{-8}$	$1,5 \cdot 10^{-8}$	$1,5 \cdot 10^{-8}$	$1,5 \cdot 10^{-8}$
$P_{ICW} = 1000$ days	$\delta = -9,4 \cdot 10^{-9}$	-10^{-8}	-10^{-8}	-10^{-8}

four modes of periodic variations of rotation pole: Chandler wobble (CW), retrograde free core nutation (FCN), prograde free core nutation (FICN) and inner Chandler wobble (ICW). Thus we can explain all four TOA periodic variations of the PSR B1828-11. In case rotation of a three-layer neutron star we have variations of next types:

- The *Chandler Wobble* (CW) is a motion of the pulsar rotation axis around its dynamical figure due to the bulges of the pulsar. It is the only global rotational mode for completely solid pulsar.
- The *Free Core Nutation* (FCN) is a differential rotation of the liquid core relatively the crust rotation. This mode does exist only if the core is liquid.
- The *Free Inner Core Nutation* (FICN) is a mode related to the differential rotation of the inner core with respect to the other layers of the pulsar. The mode exists only if the pulsar has two-layer core contains outer liquid and inner solid components.
- The *Inner Core Wobble* (ICW) is a differential rotation of the figure axis of the pulsar core with respect to the rotation axis of the pulsar and is due to the flattened of the inner core, having an excess of density with respect to the liquid core. This mode does exist only if there is an ellipsoidal solid inner core inside a liquid core in the pulsar.

2.3 Application of three-layer model for PSR B1828-11

In the frame of the three-layer model we investigate the free rotation of dynamically-symmetrical PSR B1828-11 by Hamilton methods proposed Getino (Getino et al., 1999). Thus, according to our model, the neutron star has rigid the crust, the fluid outer core and the solid inner core. The model explains generation of four modes in the rotation of the pulsar: two modes of Chandler wobble (CW, ICW) and two modes connecting with free core nutation (FCN, FICN) (Gusev & Kitiashvili, 2008). The periods of the described variations can be described in the next way

$$P_{CW} = P_{PSR}\left(\frac{A}{A_{cr}}e - \frac{A_s}{A_{cr}}e_s\right)^{-1}, \qquad P_{RFCN} = P_{PSR}\left(\frac{A}{A_{cr}}e_f\right)^{-1},$$

$$P_{PFCN} = P_{PSR}\left(\delta + \frac{A_s}{A_{cr}}e_f\right)^{-1}, \qquad P_{ICW} = P_{PSR}\left(e_s + \delta\right)^{-1} \tag{3}$$

where P_{PSR} is the period of PSR B1828-11 rotation; $,_{cr}, _f, _s$ are moments of inertia of the total pulsar, fluid outer and solid inner cores; e_{PSR}, e_f, e_s are dynamical flattening of the pulsar, the fluid outer and the solid inner cores; δ is a small parameter

$$e = \frac{A_{cr}}{A}\left(\frac{P_{PSR}}{P_{CW}} + \frac{A_s}{A_{cr}}e_s\right), \; e_f = \frac{P_{PSR}}{P_{RFCN}}\frac{A_{cr}}{A}, \quad e_s = \frac{P_{PSR}}{P_{ICW}} - \delta, \quad \delta = -\left(\frac{P_{PSR}}{P_{PFCN}} + \frac{A_s}{A_{cr}}e_f\right) \tag{4}$$

We have got the estimates of dynamical flattening of the crust, the outer liquid and the inner solid cores of the pulsar for known periodic variations of the TOA pulse from PSR B1828-11: 1000, 500, 250, 167 days. Numerical results of the TOA pulse fluctuations are shown in the table 4 for different models of the neutron star interior.

3. CONCLUSION

The observation of PSR B1828-11 has revealed the existence of four periodic variations TOA pulses. In the frame of the three-layer model we proposed the explanation for all pulse fluctuations by differential rotation crust, outer core and inner core of the neutron star and received estimations of dynamical flattening of the pulsar inner and outer cores. We have offered the realistic model of the dynamical pulsar structure and the feature of flattened of the crust, the outer core and the inner core of the pulsar.

4. REFERENCES

Alpar, M.A., Pines, D. & Cheng, K.S. 1990, "The fast recovery of the Vela pulsar from its Christmas 1988 glitch" Nature, 348, pp. 707-708.

Bisnovatyi-Kogan, G.S., Mersov, G.A. & Sheffer, E.K., 1989, "Can we expect a freely precessing neutron satr in Her-X1"? A&A 221, pp. L7-L9.

Bisnovatyi-Kogan, G.S. & Kahabka, P., 1993, "Period variations and phase residuals in freely precessing stars". A&A 267, L43-L46.

Cutler, C., Ushomirsky, G. & Link, B., 2003, "The crustal rigidity of a neutron star and implications for PSR 1828-11 and other precession candidates". ApJ, 588, 975-991.

Dehant, V., Van Hoolst, T. & de Viron, O. et al., 2003, "Can a solid inner core of Mars be detected from observations of polar motion and nutation of Mars?", J.Geoph.Res., 108, E12, 1.1-1.12.

Getino, J., Farto, J.M. & Ferrandiz, J.M., 1999, Obtaining the free frequencies of the non-rigid Earth. Celest. Mech. & Dyn. Astr., 71, pp. 95-108.

Getino, J., 1995, "An interpretation of the core-mantle interaction problem". Geop. J. Int., 120, pp. 693-705.

Gusev A. & Kitiashvili I., 2004, Modelling of pulsar rotation for three layers model of PSR B1828-11. Proc. of Int. Conf. "Modern direction of astronomical evolution in Russia", Kazan university, Russia, Sept. 21-25, 2004, Kazan, Russia. pp. 219-223. 2004.

Gusev, A. & Kitiashvili, I., 2005, Chandler wobble and free core nutation of pulsar. Georesources, 9, pp. 41-43, 2005.

Gusev,& Kitiashvili, 2008, "Rotation evolution of extra-solar planet systems and pulsars", Kazan Univ.Press, 261pp.

Gusev A., 2010, "Spin-orbital evolution, physical libration and interior structure of multi-layer celestial bodies", Kazan Univ.Press, 512 pp.

Kinoshita, H., 1977, "Theory of the rotation of the rigid Earth". Celest. Mech., 15, pp. 277-326.

Link B. & Cutler C., 2002, "Vortex unpinning in precessing neutron stars". MNRAS, 336, 1, pp. 211-216.

Link & Epstein, 2001, "Precession interpretation of the isolated pulsar B1828-11". ApJ, 556, 1, pp.392-398.

Lyne & Graham-Smith, 1998, "Pulsar Astronomy", Cambridge, Univ. Press, UK. pp. 14-22.

Ruderman, M., 1970, "Pulsar wobble and neutron starquakes". Nature, 225, pp. 838-839.

Sedrakian, A., Wasserman, I., & Cordes, J.M., 1999, "Precession of isolated neutron stars. I. Effects of imperfect pinning". ApJ, 524, pp. 341-360.

Stairs I.H., Lyne A.G. & Shemar S.L., 2000, "Evidence for free precession in a pulsar". Nature, 406, pp. 484-486.

Shabanova, T.V. & Urama, J.O., 2000, "Evidence for free precession in the pulsar B1642-03", ASR Conf. Series, 202, pp. 99-100.

Shabanova T.V., Lyne, A.G. & Urama J.O., 2001, "Evidence for free precession in the pulsar B1642-03". ApJ , 552, 1, p. 321.

Tkachenko, K., 1966, "Stability of vortex lattices". Sov. Phys. JETP, 23, 1049-1056. (In Russian).

Van Hoolst, T., Dehant, V. & Defraigne, P.,2000, "Sensitivity of the free core nutation and the Chandler wobble to changes in the interior structure of Mars", PEPI 117, 1-4, pp. 397-405.

Wasserman, I.,2003, "Precession of isolated neutron stars - II. Magnetic fields and type II super-conductivity". MNRAS, 341, 3, 1020.

ABOUT THE MACCULLAGH RELATIONS IN RELATIVITY

M.H. SOFFEL, S.A. KLIONER and E. GERLACH
Lohrmann Observatory,
Dresden Technical University,
01062 Dresden, Germany

ABSTRACT. The Newtonian MacCullagh relations relate two different aspects of the global Earth: its rotational motion and its external gravitational field. They relate components of the tensor of inertia with $l = 2$ potential coefficients.These two concepts can be generalized to the first post-Newtonian approximation to Einstein's theory of gravity and one can ask if the usual form of the MacCullagh relation still holds if $1/c^2$ are taken into account. To answer this question a simple Newtonian model for the Earth was employed: a uniformly rotating homogenous oblate spheroid. For this model a violation of the usual MacCullagh relations was found. Implications for a post-Newtonian nutation model are shown to be negligible.

1. THE NEWTONIAN MACCULLAGH RELATIONS

The Newtonian MacCullagh relations relate two different aspects of the global Earth: its rotational motion and its external gravitational field. More precisely they relate the components of the tensor of inertia tensor with $l = 2$ potential coefficients. If the external gravity field of the Earth is expanded in terms of spherical harmonics in the form

$$U(\mathbf{x}) = \left(\frac{GM}{r}\right) \sum_{l=0}^{\infty} \sum_{m=0}^{l} \left(\frac{a}{r}\right)^l P_{lm}(\cos\theta)\big(C_{lm}\cos m\phi + S_{lm}\sin m\phi\big)$$

the Newtonian MacCullagh relations read

$$\begin{aligned} C_{21} &= -\frac{I_{13}}{Ma^2}\,, \qquad S_{21} = -\frac{I_{23}}{Ma^2}\,, \\ C_{22} &= \frac{I_{22}-I_{11}}{4Ma^2}\,, \qquad S_{22} = -\frac{I_{12}}{2Ma^2}\,, \\ C_{20} &= \frac{1}{Ma^2}\left(\frac{I_{11}+I_{22}}{2} - I_{33}\right)\,, \end{aligned}$$

where I_{ij} are the components of the moment of inertia tensor

$$I_{ij} = \int_B (\mathbf{x}^2\delta_{ij} - x^i x^j)\rho\, d^3x\,.$$

If the external gravitational field is expanded in terms of Cartesian symmetric and trace-free (STF) tensors all five MacCullagh relations are contained in the relation ($I_{kk} = I_{11} + I_{22} + I_{33}$)

$$M_{ij} = -\mathrm{STF}(I_{ij}) = \frac{1}{3}\delta_{ij}I_{kk} - I_{ij}\,, \tag{1}$$

i.e., the Cartesian mass quadrupole tensor M_{ij} equals minus the (symmetric) trace-free part of the moment of inertia tensor. In the STF language the external gravity field is expanded as

$$U(\mathbf{x}) = G\sum_{l=0}^{\infty}\frac{(2l-1)!!}{l!}M_L\frac{\hat{n}_L}{r^{l+1}}$$

with

$$\hat{n}_L \equiv \frac{\hat{x}^L}{r^l}\,, \qquad \hat{x}^L \equiv \hat{x}^{i_1\ldots i_l} = \mathrm{STF}_{i_1\ldots i_l}\left(x^{i_1}\cdots x^{i_l}\right)$$

and every index i runs over 1,2,3 corresponding to x, y, z. E.g., $\hat{x}^{ij} = \mathrm{STF}_{i,j}(x^i x^j) = x^i x^j - \delta_{ij}\,\mathbf{x}^2/3$.

2. RELATIVITY AND THE MACCULLAGH RELATIONS

With respect to some relativistic precession/nutation theory (e.g., Klioner et al., 2001, 2010) we now want to ask about relations that might generalize the Newtonian MacCullagh relations in Relativity. Unfortunately in Einstein's theory of gravity neither a mass quadrupole tensor nor some moment of inertia tensor can be defined for a real astronomical body. However, if one resorts to the first post-Newtonian approximation to Einstein's theory of gravity both concepts can be defined. As for the mass quadrupole tensor the Blanchet-Damour quadrupole mass moment (Damour et al., 1991)

$$M_{ij} = \int_B d^3x\hat{x}_{ij}\sigma + \frac{1}{14c^2}\frac{d^2}{dt^2}\int_B d^3x\hat{x}_{ij}\mathbf{x}^2\sigma - \frac{20}{21c^2}\frac{d}{dt}\int_B d^3x\hat{x}^{ijk}\sigma^k$$

generalizes the $l = 2$ potential coefficients. Here, $\sigma = (T^{00} + T^{ss})/c^2$, $\sigma^i = T^{0i}/c$ and $T^{\alpha\beta}$ are the components of the energy-momentum tensor (generalizing the density ρ). In Damour et al., (1993) a post-Newtonian spin vector was defined for the Earth from which a post-Newtonian moment of inertia tensor can be derived (see also Klioner 1995).

One can then ask if relation (1) is still valid for the corresponding post-Newtonian quantities. In the general case of a gravitational N-body problem this question is not so easy to answer since gravitational fields from external bodies (Moon, Sun, etc.) enter the mass quadrupole and moment of inertia tensors of the Earth. We have stated to answer our basic question by considering a simplified situation: we employed a specific Newtonian model for the $1/c^2$ terms, a uniformly rotating homogeneous oblate spheroid with semi-major axis a, semi-minor axis b (pointing in z-direction) and eccentricity e given by $e^2 = 1 - b^2/a^2$. The internal gravity field that is needed to compute various integrals can be found in Chandrasekhar (1987). For our model a violation of the usual MacCullagh relations was found. Instead we have

$$M_{ij} = -\mathrm{STF}(I_{ij}) - (Ma^2)\delta\mathrm{diag}(1,1,-2) + \mathcal{O}(e^4)\,, \tag{2}$$

where

$$\delta = \frac{418}{875}\,\frac{GM}{c^2 a}\,e^2\,.$$

For the Earth $\delta = 0.787\times10^{-12}$. To assess the consequences of the δ-term for a relativistic nutation theory we employed the numerical code that solves for the three Euler angles ϕ, ψ and ω (the obliquity) for the post-Newtonian model of rigidly rotating multipoles (Klioner et al., 2010) including the relativistic torques from Moon, Sun and planets. We found that effects from the δ-term do not exceed $10^{-6}\,\mu$as for all three Euler angles (see Fig. 1). At least for our simple model the detected violation of the usual MacCullagh relations can be neglected in the post-Newtonian precession/nutation model in the near future. For the real Earth additional aspects come into play: deviations from axial symmetry or gravitational fields from external bodies. Such effects are presently under investigations. Details will be published elsewhere.

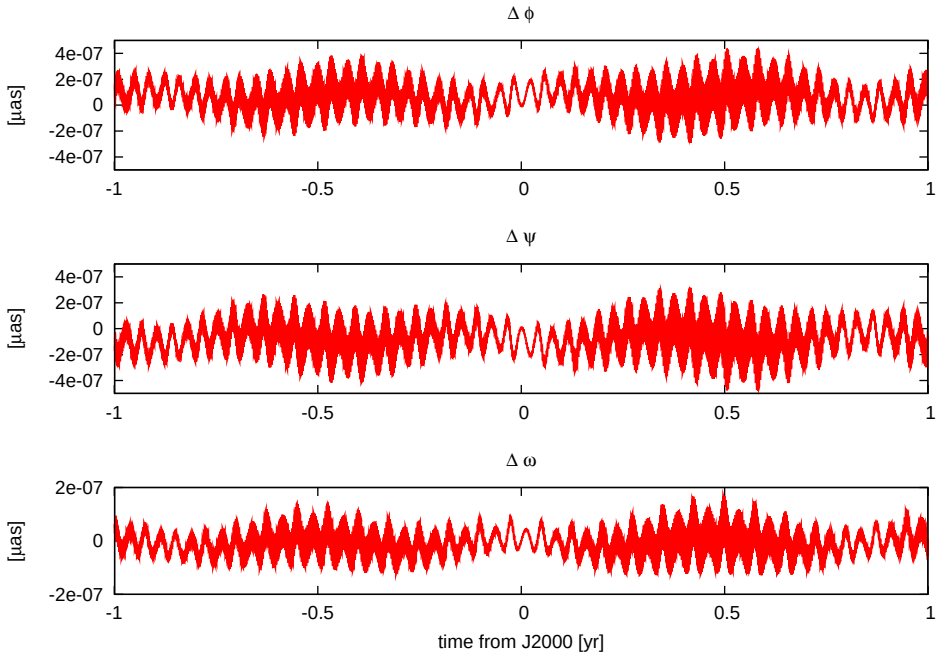

Figure 1: The effect of the relativistic violation of the MacCullagh relations over 2 years as differences in the Euler angles describing the orientation of the Earth. The main periods are 1 year and 0.5 months. The maximal amplitudes of the effect over a few hundred years around J2000 does not exceed $5 \cdot 10^{-7} \mu$as for phi and psi and $2 \cdot 10^{-7} \mu$as for omega.

3. REFERENCES

Chandrasekhar, S.: 1987, Ellipsoidal Figures of Equilibrium, Dover Publications, New York

Damour, T., Soffel, M., Xu, C: 1991, Phys. Rev. D, 43, 3273

Damour, T., Soffel, M., Xu, C: 1993, Phys. Rev. D, 47, 3124

Klioner, S: 1995, in: S.Ferraz-Mello, B.Morando, J.Arlot (eds.), Dynamics, ephemerides and astrometry in the solar system, Kluwer, Dordrecht, 309-320

Klioner, S., Soffel, M., Xu, C., Wu, X: 2003, Proc. Journées 2001 "Systèmes de référence spatio-temporels", N. Capitaine (ed), pp. 232–238

Klioner, S., Gerlach, E., Soffel, M: 2010, Proc. of IAU Symposium 261 (Virginia Beach), Klioner, S., Seidelmann, K., Soffel, M. (eds.), Cambridge University Press, Cambridge

POST-NEWTONIAN MECHANICS OF THE EARTH-MOON SYSTEM

Yi XIE[1], Sergei KOPEIKIN[2]

[1] Astronomy Department, Nanjing University
Nanjing, Jiangsu 210093, China
yixie@nju.edu.cn

[2] Department of Physics and Astronomy, University of Missouri-Columbia
Columbia, Missouri 65211, USA
kopeikins@missouri.edu

ABSTRACT. We introduce the Jacobi coordinates adopted to the advanced theoretical analysis of the relativistic celestial mechanics of the Earth-Moon system. Theoretical derivation utilizes the relativistic resolutions on the local reference frames adopted by the International Astronomical Union in 2000. The advantage of the local frames is in a more simple mathematical description of the metric tensor and equations of motion. The set of one global and three local frames is introduced in order to decouple physical effects of gravity from the gauge-dependent effects in the equations of relative motion of the Moon with respect to Earth. We pay particular attention to a unique opportunity to detect the gravitomagnetic tidal field in the orbital motion of the Moon with the advanced LLR technology.

The tremendous progress in technology, which we have witnessed during the last 30 years, has led to enormous improvements of precision in the measuring time and distances within the boundaries of the solar system. Observational techniques like lunar and satellite laser ranging, radar and Doppler ranging, very long baseline interferometry, high-precision atomic clocks, gyroscopes, etc. have made it possible to start probing the kinematic and dynamic effects in motion of celestial bodies to unprecedented level of fundamental interest. Current accuracy requirements make it inevitable to formulate the most critical astronomical data-processing procedures in the framework of Einstein's general theory of relativity. This is because major relativistic effects are several orders of magnitude larger than the technical threshold of practical observations and in order to interpret the results of such observations, one has to build physically-adequate relativistic models. The future projects will require introduction of higher-order relativistic models supplemented with the corresponding parametrization of the relativistic effects, which will affect the observations.

The dynamical modeling for the solar system (major and minor planets), for deep space navigation, and for the dynamics of Earth's satellites and the Moon must be consistent with general relativity. Lunar laser ranging (LLR) measurements are particularly crucial for testing general relativistic predictions and advanced exploration of other laws of fundamental gravitational physics. Current LLR technologies allow us to arrange the measurement of the distance from a laser on the Earth to a corner-cube reflector (CCR) on the Moon with a precision approaching 1 millimeter [1, 19].

At this precision, the LLR model must take into account all the classical and relativistic effects in the orbital and rotational motion of the Moon and Earth. Although a lot of effort has been made in constructing this model, there are still many controversial issues, which obscure the progress in better understanding of the fundamental principles of the relativistic model of the Earth-Moon system.

Theoretical approach used for construction of the JPL ephemeris accepts that the post-Newtonian description of the planetary motions can be achieved with the Einstein-Infeld-Hoffmann (EIH) equations of motion of point-like masses [9], which have been independently derived by [22, 10] for massive fluid balls as well as by [16] under assumptions that the bodies are spherical, homogeneous and consist of incompressible fluid. These relativistic equations are valid in the barycentric frame of the solar system with time coordinate t and spatial coordinates $x^i \equiv \mathbf{x}$.

However, due to the covariant nature of general theory of relativity the barycentric coordinates are

not unique and are defined up to the space-time transformation [2, 3, 23]

$$t \;\mapsto\; t - \frac{1}{c^4}\sum_B \nu_B \frac{GM_B}{R_B}(\mathbf{R}_B\cdot\mathbf{v}_B)\,, \tag{1}$$

$$\mathbf{x} \;\mapsto\; \mathbf{x} - \frac{1}{c^2}\sum_B \lambda_B \frac{GM_B}{R_B}\mathbf{R}_B\,, \tag{2}$$

where summation goes over all the massive bodies of the solar system ($B = 1, 2, ..., N$); G is the universal gravitational constant; c is the fundamental speed in the Minkowskian space-time; a dot between any spatial vectors, $\mathbf{a}\cdot\mathbf{b}$, denotes an Euclidean dot product of two vectors $\mathbf{a}$ and $\mathbf{b}$; M_B is mass of body B; $\mathbf{x}_B = \mathbf{x}_B(t)$ and $\mathbf{v}_B = \mathbf{v}_B(t)$ are coordinates and velocity of the center of mass of the body B; $\mathbf{R}_B = \mathbf{x} - \mathbf{x}_B$; ν_B and λ_B are constant, but otherwise free parameters being responsible for a particular choice of the barycentric coordinates. These parameters can be chosen arbitrary for each body B of the solar system. Standard textbooks [2, 3, 23, 25] assume that the coordinate parameters are equal for all bodies. These simplifies the choice of coordinates and their transformations, and allows one to identify the coordinates used by different authors. For instance, $\nu = \lambda = 0$ corresponds to harmonic or isotropic coordinates [10], $\lambda = 0$ and $\nu = 1/2$ realizes the standard coordinates used in [15] and in PPN formalism [25]. The case of $\nu = 0, \lambda = 2$ corresponds to the Gullstrand-Painlevé coordinates [21, 11], but they have not been used so far in relativistic celestial mechanics of the solar system. We prefer to have more freedom in transforming EIH equations of motion and do not equate the coordinate parameters for different massive bodies.

If the bodies in N-body problem are numbered by indices B, C, D, etc., and the coordinate freedom is described by equations (1), (2), EIH equations have the following form [2]

$$a^i_B \;=\; F^i_N + \frac{1}{c^2}F^i_{EIH}\,, \tag{3}$$

where the Newtonian force

$$F^i_N \;=\; -\sum_{C\neq B}\frac{GM_C R^i_{BC}}{R^3_{BC}}\,, \tag{4}$$

the post-Newtonian perturbation

$$\begin{aligned}
F^i_{EIH} \;=\; & -\sum_{C\neq B}\frac{GM_C R^i_{BC}}{R^3_{BC}}\Bigg\{(1+\lambda_C)v_B^2 - (4+2\lambda_C)(\mathbf{v}_B\cdot\mathbf{v}_C) + (2+\lambda_C)v_C^2 \\
& -\frac{3}{2}\left(\frac{\mathbf{R}_{BC}\cdot\mathbf{v}_C}{R_{BC}}\right)^2 - 3\lambda_C\left[\frac{\mathbf{R}_{BC}\cdot\mathbf{v}_{BC}}{R_{BC}}\right]^2 - (5-2\lambda_B)\frac{GM_B}{R_{BC}} - (4-2\lambda_C)\frac{GM_C}{R_{BC}} \\
& -\sum_{D\neq B,C} GM_D\left[\frac{1}{R_{CD}} + \frac{4-2\lambda_D}{R_{BD}} - \left(\frac{1+2\lambda_C}{2R^3_{CD}} - \frac{\lambda_C}{R^3_{BD}} + \frac{3\lambda_D}{R_{BD}R^2_{BC}} - \frac{3\lambda_D}{R_{CD}R^2_{BC}}\right)\right. \\
& \left.\times(\mathbf{R}_{BC}\cdot\mathbf{R}_{CD})\right]\Bigg\} - \sum_{C\neq B}\Bigg\{\frac{GM_C v^i_{CB}}{R^3_{BC}}\Big[(4-2\lambda_C)(\mathbf{v}_B\cdot\mathbf{R}_{BC}) - (3-2\lambda_C) \\
& \times(\mathbf{v}_C\cdot\mathbf{R}_{BC})\Big] + \frac{GM_C}{R_{BC}}\sum_{D\neq B,C} GM_D R^i_{CD}\left(\frac{7-2\lambda_C}{2R^3_{CD}} + \frac{\lambda_C}{R^3_{BD}} + \frac{\lambda_D}{R_{CD}R^2_{BC}}\right. \\
& \left.-\frac{\lambda_D}{R_{BD}R^2_{BC}}\right)\Bigg\}\,,
\end{aligned} \tag{5}$$

and $\mathbf{v}_B = \mathbf{v}_B(t)$ is velocity of the body B, $\mathbf{a}_B = \dot{\mathbf{v}}_B(t)$ is its acceleration, $\mathbf{R}_{BC} = \mathbf{x}_B - \mathbf{x}_C$, $\mathbf{R}_{CD} = \mathbf{x}_C - \mathbf{x}_D$ are relative distances between the bodies, and $\mathbf{v}_{CB} = \mathbf{v}_C - \mathbf{v}_B$ is a relative velocity.

Barycentric coordinates $\mathbf{x}_B$ and velocities $\mathbf{v}_B$ of the center of mass of body B are adequate theoretical quantities for description of the world-line of the body with respect to the center of mass of the solar system. However, the barycentric coordinates are global coordinates covering the entire solar system. Therefore, they have little help for efficient physical decoupling of the post-Newtonian effects existing in the description of the local dynamics of the orbital motion of the Moon around Earth [4]. The problem

originates from the covariant nature of EIH equations and the gauge freedom of the general relativity theory. Its resolution requires a novel approach based on introduction of a set of local coordinates associated with the barycenter of the Earth-Moon system, the Earth and the Moon [14, 27].

The gauge freedom is already seen in the post-Newtonian EIH force (5) as it explicitly depends on the choice of spatial coordinates through the gauge-fixing parameters λ_C, λ_D. Each term, depending explicitly on λ_C and λ_D in equation (5), has no direct physical meaning because it can be eliminated after making a specific choice of these parameters. In many works on experimental gravity and applied astronomy (including JPL ephemerides) researches fix parameters $\lambda_C = \lambda_D = 0$, which corresponds to working in harmonic coordinates. Harmonic coordinates simplify EIH equations to large extent but one has to keep in mind that they have no physical privilege anyway, and that a separate term or a limited number of terms from EIH equations of motion can not be measured if they are gauge-dependent [3].

This opinion was recently confronted in publications by [17, 18, 24, 26], who followed [20]. They separated EIH equations (3)-(5) to the form being similar to the Lorentz force in electrodynamics

$$a^i_B = \sum_{C\neq B}\left[E^i_{BC} + \frac{4-2\lambda_C}{c}(\mathbf{v}_B\times\mathbf{H}_{BC})^i - \frac{3-2\lambda_C}{c}(\mathbf{v}_C\times\mathbf{H}_{BC})^i\right] \tag{6}$$

where E^i_{BC} is called the "gravitoelectric" force, and the terms associated with the cross products $(\mathbf{v}_B \times \mathbf{H}_{BC})^i$ and $(\mathbf{v}_C \times \mathbf{H}_{BC})^i$ are referred to as the "gravitomagnetic" force [20]. The "gravitomagnetic" field is given by equation

$$H^i_{BC} = -\frac{1}{c}\left(\mathbf{v}_{BC}\times\mathbf{E}_{BC}\right)^i = \frac{G\mathrm{M}_C}{c}\frac{\left(\mathbf{v}_{BC}\times\mathbf{R}_{BC}\right)^i}{R^3_{BC}}\,, \tag{7}$$

and is proportional to the Newtonian force multiplied by the factor of v_{BC}/c, where v_{BC} is the relative velocity between two gravitating bodies.

Gravitomagnetic field is of paramount importance for theoretical foundation of general relativity [5]. Therefore, it is not surprising that the acute discussion has started about whether LLR can really measure the "gravitomagnetic" field H^i_{BC} [17, 12, 18, 6, 24]. It is evident that equation (6) demonstrates a strong dependence of the "gravitomagnetic" force of each body on the choice of the barycentric coordinates. For this reason, by changing the coordinate parameter λ_C one can eliminate either the term $\left(\mathbf{v}_B \times \mathbf{H}_{BC}\right)^i$ or $\left(\mathbf{v}_C \times \mathbf{H}_{BC}\right)^i$ from EIH equations of motion (6). In particular, the term $(\mathbf{v}_B \times \mathbf{H}_{BC})^i$ vanishes in the Painlevé coordinates, making the statement of [17, 18] about its "measurement" unsupported, because the strength of the factual "gravitomagnetic" force is coordinate-dependent. Hence a great care should be taken in order to properly interpret the LLR "measurement" of such gravitomagnetic terms in consistency with the covariant nature of general theory of relativity and the theory of astronomical measurements in curved space-time. We keep up the point that the "gravitomagnetic" field (7) is unmeasurable with LLR due to its gauge-dependence.

Nevertheless, the observable LLR time delay is gauge invariant. This is because the gauge transformation changes not only the gravitational force but the solution of the equation describing the light ray propagation. For this reason, the gauge parameter λ_C appears in the time delay *explicitly*

$$\begin{aligned} t_2 - t_1 = {} & \frac{R_{12}}{c} + 2\sum_C \frac{G\mathrm{M}_C}{c^3}\ln\left[\frac{R_{1C}+R_{2C}+R_{12}}{R_{1C}+R_{2C}-R_{12}}\right] \\ & + \sum_C \lambda_C \frac{G\mathrm{M}_C}{c^3}\frac{(R_{1C}-R_{2C})^2 - R^2_{12}}{2R_{1C}R_{2C}R_{12}}(R_{1C}+R_{2C}). \end{aligned} \tag{8}$$

At the same time the "Newtonian" distance R_{12} depends on the parameter λ_C *implicitly* through the solution of EIH equations (3)-(5). This implicit dependence of the right side of (8) is exactly compensated by the explicit dependence of (8) on λ_C, making the time delay gauge-invariant.

Papers [17, 18, 26, 24] do not take into account the explicit gauge-dependence of the light time delay on λ_C. If the last term in (8) is omitted but EIH force is taken in form (6), the equations (6) and (8) become theoretically incompatible. In this setting LLR "measures" only the consistency of the EIH equations with the expression for time delay of the laser pulse. However, this is not a test of gravitomagnetism, which actual detection requires more precise measurement of the gauge-invariant components of the Riemann tensor associated directly either with the spin multipoles of the gravitational field of the Earth [7, 8] or with the current-type multipoles of the tidal gravitational field of external bodies [13].

In order to disentangle physical effects from numerous gauge dependent terms in equations of motion of the Moon we need a precise analytic theory of reference frames in the lunar motion that includes several reference frames: Solar System Barycentric Frame, Geocentric Frame, Selenocentric Frame and Earth-Moon Barycentric Frame. This gauge-invariant approach to the lunar motion has been initiated in our paper [14, 27] to which we refer the reader for further particular details.

References

[1] Battat, J., Murphy, T.W., Adelberger, E., et al. 2007, APS Meeting Abstracts, 12.003

[2] Brumberg, V.A. 1972, Relativistic Celestial Mechanics, Moscow: Nauka (in Russian)

[3] Brumberg, V.A. 1991, Essential Relativistic Celestial Mechanics, New York: Adam Hilger

[4] Brumebrg, V.A., Kopeikin, S.M. 1989, Nuovo Cimento B, 103, 63

[5] Ciufolini, I., Wheeler, J.A. 1995, Gravitation and Inertia, NJ: Princeton University Press

[6] Ciufolini, I. 2007, arXiv:0704.3338v2

[7] Ciufolini, I. 2008, arXiv:0809.3219v1

[8] Ciufolini, I., Pavlis, E.C. 2004, Nature, 431, 958

[9] Einstein, A., Infeld, L., Hoffmann, B. 1938, The Annals of Mathematics, 39, 65

[10] Fock, V.A. 1959, The Theory of Space, Time and Gravitation, New York: Pergamon Press

[11] Gullstrand A. 1922, Arkiv. Mat. Astron. Fys., 16, 1

[12] Kopeikin, S.M. 2007, Phys. Rev. Lett., 98, 229001

[13] Kopeikin, S.M. 2008, arXiv:0809.3392v1

[14] Kopeikin, S., Xie, Y. 2010, Cele. Mech. Dyn. Astr, 108, 245

[15] Landau, L.D., Lifshitz, E.M. 1975, The classical theory of fields, Oxford: Pergamon Press

[16] Lorentz, H.A., Droste, J. 1937, Versl. K. Akad. Wet. Amsterdam, 26, 392 (part I) and 649 (part II)

[17] Murphy, Jr., T.W., Nordtvedt, K., Turyshev, S.G. 2007a, Phys. Rev. Lett., 98, 071102

[18] Murphy, Jr., T.W., Nordtvedt, K., Turyshev, S.G. 2007b, Phys. Rev. Lett., 98, 229002

[19] Murphy, T.W., Adelberger, E.G., Battat, J.B.R., et al. 2008, Publ. Astron. Soc. Pacific, 120, 20

[20] Nordtvedt, K. 1988, Int. J. Theor. Phys., 27, 1395

[21] Painlevé, P. 1921, C. R. Acad. Sci. (Paris), 173, 677

[22] Petrova, N.M. 1949, Zh. Exp. Theor. Phys., 19, 989

[23] Soffel, M.H. 1989, Relativity in Astrometry, Celestial Mechanics and Geodesy, Berlin: Springer

[24] Soffel, M., Klioner, S., Müller, J., Biskupek, L. 2008, Phy. Rev. D, 78, 024033

[25] Will, C.M. 1993, Theory and Experiment in Gravitational Physics, Cambridge: Cambridge University Press

[26] Williams, J.G., Turyshev, S.G., Murphy, T.W. 2004, IJMPD, 13, 567

[27] Xie, Y., Kopeikin, S., 2010, Acta Phys. Slovaca, 60, 393

POST-POST-NEWTONIAN LIGHT PROPAGATION WITHOUT INTEGRATING THE GEODESIC EQUATIONS

P. TEYSSANDIER

SYRTE, Observatoire de Paris, CNRS, UPMC
61 avenue de l'Observatoire, F-75014 Paris, France
e-mail: Pierre.Teyssandier@obspm.fr

ABSTRACT. A new derivation of the propagation direction of light is given for a 3-parameter family of static, spherically symmetric space-times within the post-post-Newtonian framework. The emitter and the observer are both located at a finite distance. The case of a ray emitted at infinity is also treated.

1. INTRODUCTION

The aim of this work is to present a new calculation of the propagation direction of light rays in a 3-parameter family of static, spherically symmetric space-times within the post-post-Newtonian framework. Rather than deriving the results from an integration of the geodesic equations, we obtain the desired expressions by a straightforward differentiation of the time delay function (see, e. g., Teyssandier & Le Poncin-Lafitte 2008 and Refs. therein). This study is motivated by the fact that any in-depth discussion of the highest accuracy tests of gravitational theories requires to evaluate the corrections of order higher than one in powers of the Schwarzschild radius (see, e.g., Ashby & Bertotti 2010 for the Cassini experiment). Even for the Gaia mission, a discrepancy between the analytical post-Newtonian solution and a computational estimate has recently necessitated a thorough analysis of the post-post-Newtonian propagation of light (see Klioner & Zschocke 2010 and Refs. therein).

2. LIGHT DIRECTION IN SPHERICALLY SYMMETRIC SPACE-TIMES

The gravitational field is assumed to be generated by an isolated spherically symmetric body of mass M. Setting $m = GM/c^2$, the metric is supposed to be of the form

$$ds^2 = \left(1 - \frac{2m}{r} + 2\beta\frac{m^2}{r^2} + \cdots\right)\left(dx^0\right)^2 - \left(1 + 2\gamma\frac{m}{r} + \frac{3}{2}\epsilon\frac{m^2}{r^2} + \cdots\right)\delta_{ij}dx^i dx^j, \tag{1}$$

where $r = \sqrt{\delta_{ij}x^i x^j}$, β and γ are the usual post-Newtonian parameters, and ϵ is a post-post-Newtonian parameter ($\beta = \gamma = \epsilon = 1$ in general relativity). We put $x^0 = ct$ and $\boldsymbol{x} = (x^i)$, with $i = 1, 2, 3$.

Consider a photon emitted at a point $\boldsymbol{x}_A$ at an instant t_A and received at a point $\boldsymbol{x}_B$ at an instant t_B. The propagation direction of this photon at any point x of its path is characterized by the triple

$$\widehat{\underline{\boldsymbol{l}}} = (l_i/l_0) = (l_1/l_0, l_2/l_0, l_3/l_0)\,, \tag{2}$$

where l_0 and l_i are the covariant components of the vector tangent to the ray, i.e. the quantities defined by $l_\alpha = g_{\alpha\beta}dx^\beta/d\lambda$, $g_{\alpha\beta}$ denoting the metric components and λ an arbitrary parameter along the ray.

Denote by $\widehat{\underline{\boldsymbol{l}}}_A$ and $\widehat{\underline{\boldsymbol{l}}}_B$ the expressions of $\widehat{\underline{\boldsymbol{l}}}$ at points $\boldsymbol{x}_A$ and $\boldsymbol{x}_B$, respectively. In any stationary space-time, these triples can be derived from the relations (see Le Poncin-Lafitte et al. 2004)

$$\left(\frac{l_i}{l_0}\right)_A = c\frac{\partial\mathcal{T}(\boldsymbol{x}_A, \boldsymbol{x}_B)}{\partial x^i_A}, \qquad \left(\frac{l_i}{l_0}\right)_B = -c\frac{\partial\mathcal{T}(\boldsymbol{x}_A, \boldsymbol{x}_B)}{\partial x^i_B}, \tag{3}$$

where $\mathcal{T}(\boldsymbol{x}_A, \boldsymbol{x}_B)$ is the expression giving the travel time of a photon as a function of $\boldsymbol{x}_A$ and $\boldsymbol{x}_B$:

$$t_B - t_A = \mathcal{T}(\boldsymbol{x}_A, \boldsymbol{x}_B). \tag{4}$$

For the metric (1), $\mathcal{T}(\boldsymbol{x}_A, \boldsymbol{x}_B)$ is given by (see, e.g., Teyssandier & Le Poncin-Lafitte 2008):

$$\mathcal{T}(\boldsymbol{x}_A, \boldsymbol{x}_B) = \frac{|\boldsymbol{x}_B - \boldsymbol{x}_A|}{c} + \frac{(\gamma+1)m}{c} \ln\left(\frac{r_A + r_B + |\boldsymbol{x}_B - \boldsymbol{x}_A|}{r_A + r_B - |\boldsymbol{x}_B - \boldsymbol{x}_A|}\right) + m^2 \frac{|\boldsymbol{x}_B - \boldsymbol{x}_A|}{c}\left[\kappa \frac{\arccos(\boldsymbol{n}_A.\boldsymbol{n}_B)}{|\boldsymbol{x}_A \times \boldsymbol{x}_B|} - \frac{(\gamma+1)^2}{r_A r_B + \boldsymbol{x}_A.\boldsymbol{x}_B}\right] + \cdots, \tag{5}$$

where

$$\boldsymbol{n}_A = \frac{\boldsymbol{x}_A}{r_A}, \quad \boldsymbol{n}_B = \frac{\boldsymbol{x}_B}{r_B}, \quad \kappa = \frac{8 - 4\beta + 8\gamma + 3\epsilon}{4}. \tag{6}$$

Substituting for $\mathcal{T}(\boldsymbol{x}_A, \boldsymbol{x}_B)$ from Eq. (5) into Eqs. (3) yields $\widehat{\underline{\boldsymbol{l}}}_A$ and $\widehat{\underline{\boldsymbol{l}}}_B$ as linear combinations of $\boldsymbol{n}_A$ and $\boldsymbol{n}_B$. However, it is more convenient to introduce the unit vector $\boldsymbol{N}_{AB}$ defined by

$$\boldsymbol{N}_{AB} = \frac{\boldsymbol{x}_B - \boldsymbol{x}_A}{|\boldsymbol{x}_B - \boldsymbol{x}_A|} \tag{7}$$

and the unit vector $\boldsymbol{P}_{AB}$ orthogonal to $\boldsymbol{N}_{AB}$ defined as $\boldsymbol{OH}/|\boldsymbol{OH}|$, H being the orthogonal projection of the center O of the mass M on the straight line passing through $\boldsymbol{x}_A$ and $\boldsymbol{x}_B$, that is

$$\boldsymbol{P}_{AB} = \boldsymbol{N}_{AB} \times \left(\frac{\boldsymbol{n}_A \times \boldsymbol{n}_B}{|\boldsymbol{n}_A \times \boldsymbol{n}_B|}\right). \tag{8}$$

Using Eqs. (5)-(8), we deduce the following proposition from Eqs. (3).

Proposition 1. *The triples $\widehat{\underline{\boldsymbol{l}}}_A$ and $\widehat{\underline{\boldsymbol{l}}}_B$ are given by*

$$\widehat{\underline{\boldsymbol{l}}}_A = -\boldsymbol{N}_{AB} - \frac{m}{r_A}\left\{(\gamma+1) + \frac{m}{r_A}\left[\kappa - \frac{(\gamma+1)^2}{1 + \boldsymbol{n}_A.\boldsymbol{n}_B}\right]\right\}\boldsymbol{N}_{AB} - \frac{m}{r_A}\left\{(\gamma+1)\frac{|\boldsymbol{n}_A \times \boldsymbol{n}_B|}{1 + \boldsymbol{n}_A.\boldsymbol{n}_B} + \frac{m}{r_A}\frac{1}{|\boldsymbol{n}_A \times \boldsymbol{n}_B|}\left\{\kappa\left[\frac{\arccos(\boldsymbol{n}_A.\boldsymbol{n}_B)}{|\boldsymbol{n}_A \times \boldsymbol{n}_B|}\left(1 - \frac{r_A}{r_B}\boldsymbol{n}_A.\boldsymbol{n}_B\right) + \frac{r_A}{r_B} - \boldsymbol{n}_A.\boldsymbol{n}_B\right] - (\gamma+1)^2\left(1 + \frac{r_A}{r_B}\right)\frac{1 - \boldsymbol{n}_A.\boldsymbol{n}_B}{1 + \boldsymbol{n}_A.\boldsymbol{n}_B}\right\}\right\}\boldsymbol{P}_{AB} \tag{9}$$

and

$$\widehat{\underline{\boldsymbol{l}}}_B = -\boldsymbol{N}_{AB} - \frac{m}{r_B}\left\{\gamma + 1 + \frac{m}{r_B}\left[\kappa - \frac{(\gamma+1)^2}{1 + \boldsymbol{n}_A.\boldsymbol{n}_B}\right]\right\}\boldsymbol{N}_{AB} + \frac{m}{r_B}\left\{(\gamma+1)\frac{|\boldsymbol{n}_A \times \boldsymbol{n}_B|}{1 + \boldsymbol{n}_A.\boldsymbol{n}_B} + \frac{m}{r_B}\frac{1}{|\boldsymbol{n}_A \times \boldsymbol{n}_B|}\left\{\kappa\left[\frac{\arccos(\boldsymbol{n}_A.\boldsymbol{n}_B)}{|\boldsymbol{n}_A \times \boldsymbol{n}_B|}\left(1 - \frac{r_B}{r_A}\boldsymbol{n}_A.\boldsymbol{n}_B\right) + \frac{r_B}{r_A} - \boldsymbol{n}_A.\boldsymbol{n}_B\right] - (\gamma+1)^2\left(1 + \frac{r_B}{r_A}\right)\frac{1 - \boldsymbol{n}_A.\boldsymbol{n}_B}{1 + \boldsymbol{n}_A.\boldsymbol{n}_B}\right\}\right\}\boldsymbol{P}_{AB}, \tag{10}$$

respectively.

In any static, spherically symmetric space-time the geodesic equations imply that the vector $\boldsymbol{L}$ defined as $\boldsymbol{L} = -\boldsymbol{x} \times \widehat{\underline{\boldsymbol{l}}}$ is a constant of the motion. The null geodesics considered here are assumed to be unbound. Consequently the magnitude of $\boldsymbol{L}$ is such that $|\boldsymbol{L}| = lim_{|\boldsymbol{x}|\to\infty} |\boldsymbol{x} \times d\boldsymbol{x}/cdt|$ since $\widehat{\underline{\boldsymbol{l}}} \longrightarrow -(d\boldsymbol{x}/cdt)_\infty$ when $|\boldsymbol{x}| \longrightarrow \infty$. So the quantity b defined by

$$b = |-\boldsymbol{x} \times \widehat{\underline{\boldsymbol{l}}}| \tag{11}$$

is the Euclidean distance between the asymptote to the ray and the line parallel to this asymptote passing through the center O as measured by an inertial observer at rest at infinity. Hence b may be considered as *the impact parameter* of the ray (see, e.g., Chandrasekhar 1983). Besides its geometric meaning, b presents the interest to be *intrinsic*, since it corresponds to a quantity which could be really measured.

Substituting for $\widehat{\underline{\boldsymbol{l}}}_B$ from Eq. (10) into Eq. (11), introducing the zeroth-order distance of closest approach r_c defined as

$$r_c = \frac{r_A r_B}{|\boldsymbol{x}_B - \boldsymbol{x}_A|}|\boldsymbol{n}_A \times \boldsymbol{n}_B|, \tag{12}$$

and then using $(r_A + r_B)|\boldsymbol{n}_A \times \boldsymbol{n}_B|/|\boldsymbol{x}_B - \boldsymbol{x}_A| = |\boldsymbol{N}_{AB} \times \boldsymbol{n}_A| + |\boldsymbol{N}_{AB} \times \boldsymbol{n}_B|$, we get

$$b = r_c \left[1 + \frac{(\gamma+1)m}{r_c}\frac{|\boldsymbol{N}_{AB} \times \boldsymbol{n}_A| + |\boldsymbol{N}_{AB} \times \boldsymbol{n}_B|}{1 + \boldsymbol{n}_A.\boldsymbol{n}_B} + \cdots\right]. \tag{13}$$

Using this expansion of b, we obtain the proposition which follows.

Proposition 2. *In terms of the impact parameter b, the triples $\widehat{\underline{\boldsymbol{l}}}_A$ and $\widehat{\underline{\boldsymbol{l}}}_B$ may be written as*

$$\begin{aligned}\widehat{\underline{\boldsymbol{l}}}_A = -\boldsymbol{N}_{AB} &- \frac{m|\boldsymbol{N}_{AB} \times \boldsymbol{n}_A|}{b}\left\{\gamma + 1 + \frac{m}{b}\left[\kappa|\boldsymbol{N}_{AB} \times \boldsymbol{n}_A| + (\gamma+1)^2\frac{|\boldsymbol{N}_{AB} \times \boldsymbol{n}_B|}{1 + \boldsymbol{n}_A.\boldsymbol{n}_B}\right]\right\}\boldsymbol{N}_{AB} \\ &- \frac{m|\boldsymbol{N}_{AB} \times \boldsymbol{n}_A|}{b}\left\{(\gamma+1)\frac{|\boldsymbol{n}_A \times \boldsymbol{n}_B|}{1 + \boldsymbol{n}_A.\boldsymbol{n}_B}\right. \\ &\left. + \frac{\kappa m}{b}\left[\frac{\arccos(\boldsymbol{n}_A.\boldsymbol{n}_B)}{|\boldsymbol{n}_A \times \boldsymbol{n}_B|}\boldsymbol{N}_{AB}.\boldsymbol{n}_B - \boldsymbol{N}_{AB}.\boldsymbol{n}_A\right]\right\}\boldsymbol{P}_{AB},\end{aligned} \tag{14}$$

$$\begin{aligned}\widehat{\underline{\boldsymbol{l}}}_B = -\boldsymbol{N}_{AB} &- \frac{m|\boldsymbol{N}_{AB} \times \boldsymbol{n}_B|}{b}\left\{\gamma + 1 + \frac{m}{b}\left[\kappa|\boldsymbol{N}_{AB} \times \boldsymbol{n}_B| + (\gamma+1)^2\frac{|\boldsymbol{N}_{AB} \times \boldsymbol{n}_A|}{1 + \boldsymbol{n}_A.\boldsymbol{n}_B}\right]\right\}\boldsymbol{N}_{AB} \\ &+ \frac{m|\boldsymbol{N}_{AB} \times \boldsymbol{n}_B|}{b}\left\{(\gamma+1)\frac{|\boldsymbol{n}_A \times \boldsymbol{n}_B|}{1 + \boldsymbol{n}_A.\boldsymbol{n}_B}\right. \\ &\left. - \frac{\kappa m}{b}\left[\frac{\arccos(\boldsymbol{n}_A.\boldsymbol{n}_B)}{|\boldsymbol{n}_A \times \boldsymbol{n}_B|}\boldsymbol{N}_{AB}.\boldsymbol{n}_A - \boldsymbol{N}_{AB}.\boldsymbol{n}_B\right]\right\}\boldsymbol{P}_{AB}.\end{aligned} \tag{15}$$

3. DEFLECTION OF A LIGHT RAY EMITTED AT INFINITY

Assume now that the ray arriving at $\boldsymbol{x}_B$ is emitted at infinity in a direction defined by a unit vector $\boldsymbol{N}_e$. Substituting $\boldsymbol{N}_e$ for $\boldsymbol{N}_{AB}$ and $-\boldsymbol{N}_e$ for $\boldsymbol{n}_A$ in Eq. (15) yields the expression of $\widehat{\boldsymbol{l}}_B$, where b is furnished by the limit of Eqs. (12) and (13) when $r_A \to \infty$ and $\boldsymbol{n}_A \to -\boldsymbol{N}_e$. We can set a proposition as follows.

Proposition 3. *For a light ray emitted at infinity in a direction $\boldsymbol{N}_e$ and arriving at $\boldsymbol{x}_B$, $\widehat{\underline{\boldsymbol{l}}}_B$ is given by*

$$\begin{aligned}\widehat{\underline{\boldsymbol{l}}}_B = -\boldsymbol{N}_e &- \frac{m|\boldsymbol{N}_e \times \boldsymbol{n}_B|}{b}\left[\gamma + 1 + \frac{\kappa m|\boldsymbol{N}_e \times \boldsymbol{n}_B|}{b}\right]\boldsymbol{N}_e \\ &+ \frac{m}{b}\left\{(\gamma+1)(1 + \boldsymbol{N}_e.\boldsymbol{n}_B) + \frac{\kappa m}{b}\left[\pi - \arccos(\boldsymbol{N}_e.\boldsymbol{n}_B)\right.\right. \\ &\left.\left. + |\boldsymbol{N}_e \times \boldsymbol{n}_B|\boldsymbol{N}_e.\boldsymbol{n}_B\right]\right\}\boldsymbol{P}_B(\boldsymbol{N}_e),\end{aligned} \tag{16}$$

where $\boldsymbol{P}_B(\boldsymbol{N}_e)$ is the unit vector orthogonal to $\boldsymbol{N}_e$ defined as

$$\boldsymbol{P}_B(\boldsymbol{N}_e) = -\boldsymbol{N}_e \times \frac{\boldsymbol{N}_e \times \boldsymbol{n}_B}{|\boldsymbol{N}_e \times \boldsymbol{n}_B|} \tag{17}$$

and b is the impact parameter of the ray, namely

$$b = r_c\left[1 + \frac{(\gamma+1)m}{r_c}\frac{|\boldsymbol{N}_e \times \boldsymbol{n}_B|}{1 - \boldsymbol{N}_e.\boldsymbol{n}_B} + \cdots\right], \tag{18}$$

with $r_c = r_B|\boldsymbol{N}_e \times \boldsymbol{n}_B|$.

The deflection of the ray at point $\boldsymbol{x}_B$ may be characterized by the angle $\Delta\chi_B$ made by the vector $\boldsymbol{N}_e$ and a vector tangent to the ray at $\boldsymbol{x}_B$. We have

$$\Delta\chi_B = \frac{|\boldsymbol{N}_e \times \widehat{\underline{\boldsymbol{l}}}_B|}{|\widehat{\underline{\boldsymbol{l}}}_B|} + O(1/c^6). \tag{19}$$

Substituting for $\widehat{\underline{\boldsymbol{l}}}_B$ from Eq. (16) into Eq. (19), and then introducing the angle ϕ_B between $\boldsymbol{N}_e$ and $\boldsymbol{n}_B$ defined by

$$\boldsymbol{N}_e.\boldsymbol{n}_B = \cos\phi_B, \qquad 0 \leq \phi_B \leq \pi, \tag{20}$$

we get

$$\Delta\chi_B = \frac{(\gamma+1)GM}{c^2 b}(1+\cos\phi_B) + \frac{G^2M^2}{c^4b^2}\left[\kappa\left(\pi-\phi_B+\frac{1}{2}\sin 2\phi_B\right)-(\gamma+1)^2(1+\cos\phi_B)\sin\phi_B\right], \tag{21}$$

where the impact parameter given by Eq. (18) may be rewritten as

$$b = r_c\left[1+\frac{(\gamma+1)GM}{c^2 r_c}\frac{\sin\phi_B}{1-\cos\phi_B}+\cdots\right], \qquad r_c = r_B\sin\phi_B. \tag{22}$$

It may be seen from the formulas given in Teyssandier & Le Poncin-Lafitte 2006 that $\phi_B + \Delta\chi_B$ is the angular distance between the center O and the source at infinity as measured at $\boldsymbol{x}_B$ by a static observer, i.e. an observer at rest with respect to the coordinates x^i. It will be shown in a subsequent paper that this property implies that $\Delta\chi_B$ can be regarded as an *intrinsic* quantity.

The $1/c^2$ term in Eq. (21) is currently used in VLBI astrometry. If b is replaced by its coordinate expression (22), it may be seen that $\Delta\chi_B$ is given by an expression as follows

$$\Delta\chi_B = \frac{(\gamma+1)GM}{c^2 r_c}(1+\cos\phi_B) + \frac{G^2M^2}{c^4r_c^2}\left[\kappa\left(\pi-\phi_B+\frac{1}{2}\sin 2\phi_B\right)-(\gamma+1)^2(1+\cos\phi_B)\sin\phi_B \right.$$
$$\left. \underbrace{-(\gamma+1)^2\frac{(1+\cos\phi_B)^2}{\sin\phi_B}}\right]. \tag{23}$$

For a ray grazing a mass M of radius r_0, the underbraced term in the r.h.s. of Eq. (23) generates a post-post-Newtonian contribution $(\Delta\chi_B^{(2)})_{grazing} \approx -4(\gamma+1)^2(GM/c^2r_0)^2(r_B/r_0)$ which can be great if $r_B \gg r_0$. For Jupiter, $(\Delta\chi_B^{(2)})_{grazing} = 16.1\,\mu$as if the observer is located at a distance from Jupiter $r_B = 6$ AU: this value is appreciably greater than the level of accuracy expected for Gaia. However, this 'enhanced' term is due to the use of the coordinate-dependent quantity r_c instead of the intrinsic impact parameter b. This result confirms the conclusion recently drawn in Klioner & Zschocke 2010.

4. CONCLUSION

Deriving the second-order terms in the propagation direction of light from the time transfer function rather than from the null geodesic equations is a very elegant and powerful procedure. The application of this method to a ray emitted at infinity and received by a static observer located at a finite distance from the central mass is easy and yields an intrinsic characterization of the gravitational bending of light.

5. REFERENCES

Ashby, N., Bertotti, B., 2010, Class. Quantum Grav. 27, 145013 (27pp).
Chandrasekhar, S., 1983, "The Mathematical Theory of Black Holes", Clarendon Press.
Klioner, S. A., Zschocke, S., 2010, Class. Quantum Grav. 27, 075015 (25pp).
Le Poncin-Lafitte, C., Linet, B., Teyssandier, P., 2004, Class. Quantum Grav. 21, 4463 (20pp).
Teyssandier, P., Le Poncin-Lafitte, C., 2006, arXiv:gr-qc/0611078v1.
Teyssandier, P., Le Poncin-Lafitte, C., 2008, Class. Quantum Grav. 25, 145020 (12pp).

TESTS OF FUNDAMENTAL PHYSICS WITH THE GAIA MISSION

S. MOURET[1,2]

[1] Lohrmann Observatory, Dresden Technical University
Institute for Planetary Geodesy, 01062 Dresden, Germany
e-mail: serge.mouret@tu-dresden.de

[2] IMCCE, UMR CNRS 8028, Paris Observatory
77 av. Denfert-Rochereau, 75014 Paris, France
e-mail: mouret@imcce.fr

ABSTRACT. With a launch scheduled in late 2012, the ESA Gaia mission will perform a systematic survey of the whole sky several times during its operational five years. It will provide high-accurate data of solar-system objects including the positions of about 250,000 asteroids with an unprecedented precision (at the sub-milliarcsecond level). Opportunities are thus arisen in carrying out various tests of fundamental physics from the dynamics of minor planets. Here we present the future performance of Gaia in estimating a set of global parameters which are, the PPN parameters β and γ, the dynamic solar quadrupole $J_{2\odot}$, the variation of the gravitational constant $\dot{G}/G$, and the Nordtvedt parameter η (test of the Strong Equivalence Principle). The expected precisions were obtained from simulations taking into account the time sequences and geometry of the observations peculiar to Gaia as well as the astrometric precision of the future measurements for about 230,000 asteroids.

1. INTRODUCTION

The theory of General Relativity (GR) put forward by Einstein in 1915 allowed to explain many noticeable deviations from the Newton's law of gravitation. The "anomalous" perihelion precession of Mercury is one classical test of GR which contributed to the wide adoption of this theory. The idea of analysing asteroid motions to test the GR theory arose in 1953 from Gilvarry [1], who suggested to base an observational test of the relativistic perihelion precession from high-eccentric minor planets, and in particular, (1566) Icarus [2] discovered 4 years before. This experiment was performed several times [3]-[4] reaching at best a precision of a few percent on the estimation of a relativistic parameter. Nevertheless, the measurement accuracy was strongly limited by large observational stochastic errors and an incomplete dynamical model (e.g. unmodeled non-gravitational forces), and did not allow to fully use the potential of minor planets: By reason of their various orbital characteristics, asteroids allow to disentangle relativistic effects from other perturbations. However, recent advances in high-accuracy astrometry from the ground (radar) or from space (Hipparcos) and those to come such as the Gaia mission [5] will enable us to perform GR experiments competing with the best present ones.

The ESA second-generation astrometric mission Gaia is on its way to the launch (2012). It will make a breakthrough in astrometry by performing observations at the sub-milliarcsecond level. The satellite will observe about 250,000 minor planets down to V magnitude 20 with a precision ranging from a few milli-arcsecond (mas) to a hundred micro-arcsecond (μas) or so. Furthermore, the Gaia stellar catalogue—positions of about one billion stars with a precision of a few hundreds μas at the lowest detectable magnitude—will drastically improve the reduction accuracy of ground-based observations. The huge number of high-accuracy data will thus boost our knowledge in the dynamics of the Solar System and allow us to perform clean tests of fundamental physics.

Here we evaluate the performance of Gaia in fitting a set of global parameters: the PPN parameters β and γ, the solar oblateness $J_{2\odot}$, the variation in time of the gravitational constant $\dot{G}/G$, the Nordtvedt parameter η (test of the Strong Equivalence Principle) and the Jovian GM_j (product of the gravitational constant G and the mass of Jupiter M_j) by reason of a possible strong correlation with η. The expected precisions on their measurements are given in Section 3 from a variance analysis using realistic simulated data (Section 2).

2. SIMULATIONS

From simulated data, a variance analysis was performed from the formulation of observed minus calculated position (O-C) linearised with respect to the position and velocity vectors of each asteroid and the set of global parameters (β or γ, $J_{2\odot}$, $\dot{G}/G$, η, GM_j) at the initial epoch T_0. The latter is taken at the half of the Gaia observational timespan (2012-2017), that is T_0 = JD 2456841.125 (3.07.2014). The matrix giving the partial derivatives with respect to the unknown parameters is computed by numerical integration of the variational equations simultaneously with the equations of motion. A precise description of the Gaia fitting process can be read in [6]. From a software developed for the mission by F. Mignard and caring for the updated observational characteristics of the satellite, a systematic exploration of the Gaia transit times was thus performed from 01/01/2012 over a period of five years for 509,550 asteroids. The orbital elements and absolute magnitudes—necessary to apply the filter on the apparent magnitude—were taken from the ASTORB catalog of Bowell [7]. Thus, at least 229,657 asteroids are expected to be observed by Gaia and considered in the estimation of the expected precisions on the global parameters. The astrometric precision of each simulated observation (necessary to weight the equations of observation) is derived from a function depending on the apparent magnitude and velocity of the asteroid [8].

3. RESULTS AND DISCUSSIONS

In Table 1, we yield, for the above set of parameters, the Gaia expected precisions, the best current ones as a comparison and those by other future missions. The correlation coefficients are given in Table 2. The parameter β and γ were separated in the variance analysis: as they are very strongly correlated, it is more relevant to fit only one and to hold the other one at an estimated value from another method. In our case, fitting β turns out to be the best solution given that the PPN parameter γ can be derived more precisely: the bending of light experiment by Gaia should allow us to achieve a precision of about 10^{-6} [9] instead of 8×10^{-4} from the Gaia asteroid observations.

Testing the Nordtvedt effect is important. The latter is a violation of the Strong Equivalence Principle (SEP)—one of bases of General Relativity—, which states the inequality between the inertial and gravitational masses, respectively, m_i and m_g. This effect can be generalised in the PPN formalism by the expression $m_g/m_i = 1 + \eta\Omega$, where η is the dimensionless Nordtvedt parameter and Ω a term depending on the gravitational self-energy of the astronomical body. In our case, the Nordtvedt effect is considered only for the Sun whereupon it would produce for $\eta \neq 0$ an "anomalous" indirect perturbation on the asteroid motion through the other solar-system objects, and mainly through the most massive planet. The formal precision on η is thus estimated through the Jovian perturbations.

The fit of all these parameters by Gaia will be the most accurate ever achieved from the dynamics of asteroids, and even if the expected precisions are not better than the best current ones (see Tab. 1), they remains in general though competitive and valuable. Besides, the astrometric precision used in the simulations were underestimated [8]. The Gaia data should thus provide a new accurate constrain on these parameters: the systematic errors will be limited because the accurate observations will span a short period of time (five years) and the dynamical model will be very complete taking into account the perturbations from many massive asteroids, relativistic effects from the Sun, and the planets for certain asteroids as well as non-gravitational forces. The correlations between the adjusted parameters are low excepted between $J_{2\odot}$ and β as expected with a correlation coefficient of 0.672. However, the estimation of the solar quadrupole $J_{2\odot}$ by Gaia does not turn to be relevant, the standard deviation being similar to current estimates. Thus, holding $J_{2\odot}$ at a nominal value from future mission like BepiColombo appears to be a wise solution to fit the other global parameters.

An interesting point to note is that the more accurate estimations expected for these parameters from other missions and methods, will inform us about the correctness of the dynamical model used for the Gaia mission: for example, a precision of 10^{-5} is predicted from the LLR experiments with the APACHE telescope [15], and a deviation between the LLR measurement and those from Gaia could highlight inadequacies of the dynamical model.

For the sake of curiosity, a variance analysis for the simultaneous fit of the GM of the eight planets and Pluto was carried out. The Gaia expected precisions and comparison to other derivations are compiled in Table 3. We can notice that only one estimation is interesting: the formal precision on the Jovian GM is similar to the current one and should be better by reason of the underestimated simulated Gaia precision.

Table 1: Overview of the Gaia expected formal precisions on the estimation of the PPN parameters β and γ, the solar quadrupole $J_{2\odot}$, the variation in time of the gravitational constant $\dot{G}/G$, the Nordtvedt parameter η and the GM of Jupiter.

Parameter	Initial value	Best Current		Precision Gaia	Future other missions	
β	1 †	$\sim 10^{-4}$	Planetry ephem.	$\mathbf{1.48\times10^{-3}}$	2×10^{-6}	BepiColombo[10]
γ	1 †	2.3×10^{-5}	Cassini[11]	$\mathbf{8.08\times10^{-4}}$	10^{-9}	ASTROD[12]
$J_{2\odot}$	2×10^{-7}	$\sim 5\times10^{-8}$	Planetry ephem.	$\mathbf{2.53\times10^{-7}}$	10^{-8}	BepiColombo[13]
$\dot{G}/G$ $[year^{-1}]$	0†	9×10^{-13}	LLR[14]	$\mathbf{2.99\times10^{-12}}$	$\sim 7.3\times10^{-14}$	LLR[15]
η	0†	4.5×10^{-4}	LLR[14]	$\mathbf{2.86\times10^{-3}}$††	$\sim 10^{-5}$	LLR[15]
GM_j $[AU^3/d^2]$	2.82×10^{-7}	3.35×10^{-15}	Jovian satellites[16]	$\mathbf{2.78\times10^{-15}}$		

† Theoretical value, †† $\Omega \sim -3.52\times10^{-6}$ was used [17].

Table 2: Correlation matrix for the fit of the global parameters listed in Tab. 1.

	β	$J_{2\odot}$	η	GM_j	$\dot{G}$
β	-				
$J_{2\odot}$	**0.672**	-			
η	-0.035	-0.015	-		
GM_j	-0.040	-0.037	0.097	-	
$\dot{G}/G$	-0.008	-0.008	0.217	0.049	-

Table 3: Gaia formal precisions on the GM estimates of the planets and Pluto.

Body j	GM_j $[AU^3/d^2]$	Gaia precision $[AU^3/d^2]$	Current precision $[AU^3/d^2]$	Estimation method—references
Mercury	4.91×10^{-11}	1.33×10^{-15}	8.919×10^{-17}	Space probe [18]
Venus	7.24×10^{-10}	6.48×10^{-16}	1.338×10^{-17}	Space probe [19]
Earth	8.89×10^{-10}	2.41×10^{-16}	3.122×10^{-18}	Moon (LLR) [20]
Mars	9.55×10^{-11}	3.17×10^{-16}	6.243×10^{-19}	Space probes [21]
Jupiter	2.82×10^{-07}	3.76×10^{-15}	3.345×10^{-15}	Natural satellites [22]
Saturn	8.46×10^{-08}	6.84×10^{-14}	2.453×10^{-15}	Natural Satellites and Space probes [23]
Uranus	1.29×10^{-08}	1.04×10^{-12}	1.338×10^{-14}	Natural satellites [24]
Neptune	1.52×10^{-08}	2.90×10^{-12}	2.230×10^{-14}	Space probe and Natural satellites [25]
Pluto	1.95×10^{-12}	3.43×10^{-12}	2.163×10^{-14}	Natural satellites [26]

3. REFERENCES

[1] Gilvarry, J. J., 1953, "Relativity Advances of the Perihelia of Minor Planets", PASP, 65, 173

[2] Gilvarry, J. J., 1953, "Relativity Precession of the Asteroid Icarus", Physical Review, 89, 1046

[3] Shapiro, I. I., Smith, W. B., Ash, M. E., & Herrick, S., 1971, "General Relativity and the Orbit of Icarus", AJ , 76, 588

[4] Sitarski, G. 1992, "On the relativistic motion of (1566) Icarus", AJ , 104, 1226

[5] Mignard, F., et al., 2007, "The Gaia Mission: Expected Applications to Asteroid Science", EM&Planets, 101, 97

[6] Mouret, S., Hestroffer, D., & Mignard, F., 2007, "Asteroid masses and improvement with Gaia", A&A, 472, 1017

[7] Bowell, E., 2001, "Asteroid Orbital Elements Database", http://www.lowell.edu/users/elgb/

[8] Mouret, S., & Mignard, F., 2010, "Detecting the Yarkovsky effect with the Gaia mission: list of the most promising candidates", MNRAS , submitted

[9]Hobbs, D., Holl, B., Lindegren, L., Raison, F., Klioner, S., & Butkevich, A., 2010, "Determining PPN γ with Gaia's astrometric core solution", IAU Symposium, 261, 315

[10] Milani, A., Vokrouhlický, D., Villani, D., Bonanno, C., Rossi, A., 2002, "Testing general relativity

with the BepiColombo radio science experiment", Phys. Rev. D, 66, pp. 082001.
[11] Bertotti, B., Iess, L., & Tortora, P., 2003, "A test of general relativity using radio links with the Cassini spacecraft", Nature, 425, 374
[12] Ni, W.-T., 2008, Astrod and Astrod i — Overview and Progress", International Journal of Modern Physics, D 17, 921
[13] Benkhoff, J., et al., 2010, "BepiColombo—Comprehensive exploration of Mercury: Mission overview and science goals", Planet. Space Sci., 58, 2
[14] Williams, J. G., Turyshev, S. G., & Boggs, D. H., 2004, "Progress in Lunar Laser Ranging Tests of Relativistic Gravity", Physical Review Letters, 93, 261101
[15] Williams, J. G., Turyshev, S. G., & Murphy, T. W., 2004, "Improving LLR Tests of Gravitational Theory", International Journal of Modern Physics D, 13, 567
[16] Jacobson, R.A., 2005, "Jovian Satellite ephemeris - JUP230", private communication.
[17] Anderson, J. D., Gross, M., Nordtvedt, K. L., & Turyshev, S. G., 1996, "The Solar Test of the Equivalence Principle", ApJ, 459, 365
[18] Smith, D. E., et al., 2010, "The equatorial shape and gravity field of Mercury from MESSENGER flybys 1 and 2", Icarus, 209, 88
[19] Konopliv, A. S., Banerdt, W. B., & Sjogren, W. L., 1999, "Venus Gravity: 180th Degree and Order Model", Icarus, 139, 3
[20] Folkner, W.M. and Williams, J.G., 2008, "GM parameters and uncertainties in planetary ephemeris DE421." Inter. Memo. 343R-08-004 (internal document), Jet Propulsion Laboratory, Pasadena, CA.
[21] Konopliv, A. S., Yoder, C. F., Standish, E. M., Yuan, D.-N., & Sjogren, W. L., 2006, "A global solution for the Mars static and seasonal gravity, Mars orientation, Phobos and Deimos masses, and Mars ephemeris", Icarus, 182, 23
[22] Jacobson, R. A., 2005, "Jovian Satellite ephemeris - JUP230" private communication.
[23] Jacobson, R. A., et al., 2006, "The Gravity Field of the Saturnian System from Satellite Observations and Spacecraft Tracking Data", AJ , 132, 2520
[24] Jacobson, R. A., 2007, "The Gravity Field of the Uranian System and the Orbits of the Uranian Satellites and Rings", Bulletin of the American Astronomical Society, 38, 453
[25] Jacobson, R. A., 2009, "The Orbits of the Neptunian Satellites and the Orientation of the Pole of Neptune", AJ , 137, 4322
[26] Jacobson, R. A., 2007, "The orbits of the satellites of Pluto - Ephemeris PLU017", private communication.

TESTING GRAVITY LAW IN THE SOLAR SYSTEM

B. LAMINE[1], J.-M. COURTY[1], S. REYNAUD[1], M.-T. JAEKEL[2]

[1] Laboratoire Kastler Brossel
CNRS : UMR8552 - UPMC Univ Paris 06 - École Normale Supérieure de Paris - ENS Paris
Case 74 - 4 place Jussieu, F-75252 Paris CEDEX 05
e-mail: brahim.lamine@upmc.fr, jean-michel.courty@upmc.fr and serge.reynaud@upmc.fr

[2] Laboratoire de Physique Théorique
CNRS : UMR8549 - UPMC Univ Paris 06 - École Normale Supérieure de Paris - ENS Paris
24 rue Lhomond, 75231 Paris CEDEX 05
e-mail: jaekel@lpt.ens.fr

ABSTRACT. The predictions of General relativity (GR) are in good agreement with observations in the solar system. Nevertheless, unexpected anomalies appeared during the last decades, along with the increasing precision of measurements. Those anomalies are present in spacecraft tracking data (Pioneer and flyby anomalies) as well as ephemerides. In addition, the whole theory is challenged at galactic and cosmic scales with the dark matter and dark energy issues. Finally, the unification in the framework of quantum field theories remains an open question, whose solution will certainly lead to modifications of the theory, even at large distances. As long as those "dark sides" of the universe have no universally accepted interpretation nor are they observed through other means than the gravitational anomalies they have been designed to cure, these anomalies may as well be interpreted as deviations from GR. In this context, there is a strong motivation for improved and more systematic tests of GR inside the solar system, with the aim to bridge the gap between gravity experiments in the solar system and observations at much larger scales. We review a family of metric extensions of GR which preserve the equivalence principle but modify the coupling between energy and curvature and provide a phenomenological framework which generalizes the PPN framework and "fifth force" extensions of GR. We briefly discuss some possible observational consequences in relation with highly accurate ephemerides.

1. TESTS OF GENERAL RELATIVITY (GR) IN THE SOLAR SYSTEM

The foundations of GR rely on two main pillars. The first one is the equivalence principle which states the universality of free fall and gives gravitation its geometric nature. This principle is tested in modern experiments at the 10^{-12} level, which makes it one of the best tested properties of nature. The validity of the equivalence principle has also been tested very accurately in the solar system using Lunar Laser Ranging [1] or the Sun-Mars orbit [2]. The resulting bound is too small to allow the comparatively large anomalies observed in the solar system. Therefore, even if a violation of the equivalence principle is nevertheless possible, this strongly indicates that the anomalies, if of gravitational origin, should find an explanation in the framework of metric extensions of GR. We focus on theories which describe gravity by a tensor metric field $g_{\mu\nu}$. Let us mention at this point that the general static and isotropic metric, which can be used as a preliminary description of the solar system, essentially reduces to two functions $g_{00}(r)$ and $g_{rr}(r)$ such that

$$\mathrm{d}s^2 \equiv g_{\mu\nu}\mathrm{d}x^\mu \mathrm{d}x^\nu = g_{00}(c\mathrm{d}t)^2 + g_{rr}\mathbf{d}\boldsymbol{r}^2 \tag{1}$$

The Einstein curvature tensor $G_{\mu\nu}$, built upon the Ricci curvature, has a null covariant divergence (Bianchi identity)

$$G_{\mu\nu} \equiv R_{\mu\nu} - \frac{1}{2}\, g_{\mu\nu} R \qquad , \qquad D^\mu G_{\mu\nu} = 0 \tag{2}$$

This geometrical identity is often put in correlation with the conservation of the stress tensor, $D^\mu T_{\mu\nu} = 0$. This remark leads to the second pillar of GR which are the equations relating the curvature of spacetime to the energy-momentum content. Those equations allow one to determine the metric tensor from the distribution of energy-momentum in spacetime through the Einstein-Hilbert equation which involves a

unique Newton gravitational constant G_N

$$G_{\mu\nu} = \frac{8\pi G_N}{c^4} T_{\mu\nu} \tag{3}$$

Note that this form is not imposed by any geometrical argument, so that GR has to be selected out from a large variety of metric theories by comparing the predictions drawn from the Einstein-Hilbert equation to the results of observations or experiments. When performed in the solar system, the tests effectively show a good agreement with the solutions of (3), which means that the metric tensor $g_{\mu\nu}$ has a form close to its GR prediction given, for a static point-like mass M by

$$g_{00} = 1 + 2\phi + 2\phi^2 + \dots \quad , \quad -g_{rr} = 1 - 2\phi + \dots \quad \text{with} \quad \phi = -\frac{GM}{rc^2} \tag{4}$$

More precisely, the predictions of the Einstein-Hilbert equation in the solar system are often tested in the PPN framework or a Yukawa fifth force framework. The simplest PPN framework is characterized by two constant parameters β and γ inserted in the previous Taylor expansion (4)

$$g_{00} = 1 + 2\phi + 2\beta\phi^2 + \dots \quad , \quad -g_{rr} = 1 - 2\gamma\phi + \dots \tag{5}$$

It turns out that 30 years of tests have put stringent bounds on the parameters β and γ and selected a vicinity of GR when analyzed in the PPN framework, namely $\gamma - 1 = (2.1 \pm 2.3) \times 10^{-5}$ and $\beta - 1 = (-2.5 \pm 7.5) \times 10^{-5}$. Concerning γ, the current bound is essentially given by the experiment performed through radar ranging of the Cassini probe during its 2002 solar occultation [3], while the bound on β is obtained via analysis of ephemerides [4].

It is important to note that the previous observations have also been tested in other frameworks. For example the so-called "fifth force" tests which focus on a possible scale-dependent deviation from the gravity force law. Such a deviation, corresponding to an additional massive scalar gravity field, reduces to a modification of the Newtonian potential by an additional Yukawa potential

$$g_{00} = [g_{00}]_{\rm GR} + 2\phi(r)\alpha \exp\left(-\frac{r}{\lambda}\right) \tag{6}$$

with an amplitude α measured with respect to Newton potential and a range λ related to the mass scale of the hypothetical new particle which would mediate the "fifth force". The presence of such a correction has been looked for on a large range of distances and it turns out that the Yukawa term is excluded with a high accuracy at some ranges, for example $\alpha < 10^{-10}$ at $\lambda \simeq$ Earth-Moon distance and $\alpha < 10^{-9}$ at $\lambda \simeq$ Sun-Mars distance. These bounds, again deduced from Lunar Laser Ranging and tracking of planetary probes, correspond to a remarkable result which approaches the accuracy of equivalence principle tests.

2. NEW FRAMEWORK OF METRIC EXTENSION OF GR

We now present a more general framework, which extends the two previously discussed frameworks. As already emphasized, the form of the coupling between energy-momentum and curvature can still be discussed so that we can generalize Einstein-Hilbert equation (3) such that it takes the form of a non local response relation between Einstein curvature and the energy-momentum tensor (see [5,6] for details)

$$G_{\mu\nu}(x) = \int \mathrm{d}^4x' \chi_{\mu\nu}{}^{\rho\sigma}(x - x') T_{\rho\sigma}(x') \tag{7}$$

As an example, we retrieve GR with the following local expression of the susceptibility $\chi_{\mu\nu}{}^{\rho\sigma}$

$$\left[\chi_{\mu\nu}{}^{\rho\sigma}(x - x')\right]_{\rm GR} = \frac{4\pi G_N}{c^4} \left(\delta^\rho_\mu \delta^\sigma_\nu + \delta^\rho_\nu \delta^\sigma_\mu\right) \delta^{(4)}(x - x') \tag{8}$$

Let us note at this point that generalized response equations naturally arise from radiative corrections of GR [5,6]. Radiative corrections may induce modifications of GR not only at high energies, but also at large distances [7]. In our simple model of solar system, the stress tensor reads $T_{\rho\sigma}(x) = \delta_{\rho 0}\delta_{\sigma 0} M c^2 \delta^{(3)}(\boldsymbol{x})$ so that the modified Einstein tensor reads

$$\delta G_{\mu\nu}(x) = Mc^2 \int c\mathrm{d}t' \, \delta\chi_{\mu\nu}{}^{00}(x - x') \quad , \quad x' = (ct', \mathbf{0}) \tag{9}$$

An important feature of this framework is that the Einstein tensor $G_{\mu\nu}$, and therefore the Ricci curvature $R_{\mu\nu}$ do no longer vanish outside the sources, as it is the case in GR. Nevertheless, because GR is in good accordance with observations, it is expected that $\delta G_{\mu\nu}$ should stay small. Within a linear approximation, the Bianchi identity can be used to extract the two degrees of freedom $\delta G^{(0)}$ and $\delta G^{(1)}$ which are present :

$$\delta G_{\mu\nu}(r) = \delta G^{(0)}_{\mu\nu}(r) + \delta G^{(1)}_{\mu\nu}(r) = \pi^{(0)}_{\mu\nu 00}\frac{8\pi M \delta G^{(0)}(r)}{c^2} + \pi^{(1)}_{\mu\nu 00}\frac{8\pi M \delta G^{(1)}(r)}{c^2} \tag{10}$$

where $\pi^{(0)}_{\mu\nu 00}$ and $\pi^{(1)}_{\mu\nu 00}$ are operators of projection on the two sectors of different conformal weights, that is to say the traceless and traced part (see [5] for their expression). It has been shown in [6] how these two functions $\delta G^{(0)}$ and $\delta G^{(1)}$ are related to a modification δw of $w \equiv \frac{1}{2}\ln|g_{rr}/g_{00}|$ (which is equivalent to a modification of the Weyl tensor), and a modification δR of the Ricci scalar R

$$\delta G^{(0)}(r) = -\frac{c^2}{8\pi M}\left(\partial_r^2 + \frac{2}{r}\partial_r\right)\delta w(r) \qquad , \qquad \delta G^{(1)}(r) = -\frac{c^2}{8\pi M}\delta R(r) \tag{11}$$

Generally speaking, in the present framework, the gravitational constant G_N is replaced by a non local susceptibility tensor of rank 4 which reduces to only two functions $\delta G^{(0)}$ and $\delta G^{(1)}$. Those two functions correspond to two different sectors for gravitation which, in the simplified situation considered here, can be exactly matched to the two degree of freedom g_{00} and g_{rr} with the help of (11).

$$g_{00} = [g_{00}]_{\rm GR} + \delta g_{00} \qquad , \qquad g_{rr} = [g_{rr}]_{\rm GR} + \delta g_{rr} \tag{12}$$

The functions $\delta g_{00}(r)$ and $\delta g_{rr}(r)$ can have a general r-dependence. As a pedagogical example, we will focus in the following on simplified phenomenological models obtained as a Taylor expansion of δg_{00} and δg_{rr} in a vicinity of the Solar system ($\alpha_n r^n \ll 1$ and $\chi_n r^n \ll 1$)

$$\delta g_{00} = 2\sum_{n>0}\alpha_n r^n \qquad , \qquad \delta g_{rr} = 2\sum_{n>0}\chi_n r^n \tag{13}$$

More elaborated models can be obtained by adding a cutoff to allow the perturbation to start from a given distance from the sun. The previous models can be viewed equivalently as distance-dependent PPN parameters

$$\beta(r) - 1 = \left(\frac{c^2}{GM}\right)^2 \sum_{n>0}\alpha_n r^{n+2} \qquad , \qquad \gamma(r) - 1 = -\frac{c^2}{GM}\sum_{n>0}\chi_n r^{n+1} \tag{14}$$

3. PHENOMENOLOGICAL CONSEQUENCES ON A SIMPLIFIED MODEL

As emphasized in the previous section, modifications of g_{00} are heavily constrained. Therefore, we will consider in the following a modification of the spatial part g_{rr} alone. Then, even if we can deal with the general case, we further restrict ourselves to the following simple modification

$$\delta g_{rr} = 2\chi_2 r^2 \tag{15}$$

This specific model corresponds to a constant Ricci curvature $R_{rr} = 8\chi_2$, so that χ_2 represents the amount of Ricci curvature outside the source. The geodesic equation is modified, as well as the Shapiro time delay, leading to anomalies in spacecraft tracking and ephemerides. For example, a test particle (spacecraft or planet) is submitted to the following anomalous coordinate acceleration

$$\delta a_r = 2\chi_2\left(rv_r^2 - rv_\theta^2 - GM\right) \quad , \quad \delta a_\theta = 4\chi_2\, r v_r v_\theta \tag{16}$$

It is easy to verify that if $\chi_2 > 0$, a purely radial escape trajectory suffers a positive radial acceleration (towards the outside of the solar system) while a circular orbit suffers a negative radial acceleration (towards the sun). Moreover, the orthoradial acceleration δa_θ vanishes for circular orbits and radial escape trajectories. The order of magnitude of the anomalous acceleration is given by

$$\delta a \sim \chi_2 GM \tag{17}$$

This anomalous coordinate acceleration is of course not the observable that is deduced from measurement. Indeed, one has to take into account the effect on light propagation. The modification $\delta\mathcal{T}$ of the one-way light-time $\mathcal{T} = t_2 - t_1$ from position $\boldsymbol{r}_1(t_1)$ to position $\boldsymbol{r}_2(t_2)$ can be computed by integrating $\mathrm{d}s^2 = 0$ along the path, giving

$$c\mathcal{T} = R_{12} + c\delta\mathcal{T}_{\rm Shapiro} + c\delta\mathcal{T} \quad , \quad c\delta\mathcal{T} = -\frac{1}{3}\,\chi_2 R_{12}\left(r_1^2 + r_2^2 + \boldsymbol{r}_1\cdot\boldsymbol{r}_2\right) \tag{18}$$

where $r_i = |\boldsymbol{r}_i| = [r_i]_{\rm GR} + \delta r_i$ and $R_{12} = |\boldsymbol{r}_2 - \boldsymbol{r}_1| = [R_{12}]_{\rm GR} + \delta R_{12}$ are modified when compared with their GR values due to the anomalous coordinate acceleration (16). The tracking observables can then be computed from the knowledge of the two-way light-time (a sum of two one-way light-time connected at the level of the spacecraft). For example, up to small relativistic corrections, the Doppler signal is obtained by the time derivative of the light-time while the position in the sky (right ascension and declination) is obtained through spatial derivatives.

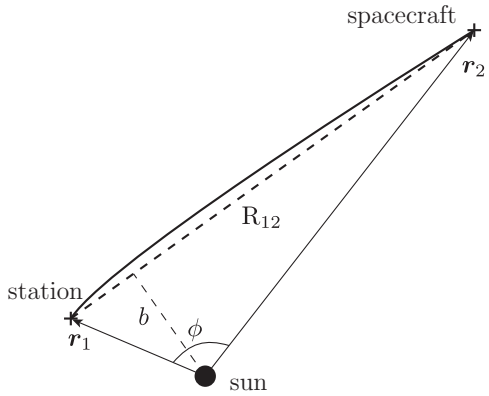

Figure 1: Geometry of spacecraft tracking.

An important feature is that the light-time correction naturally produces daily and semi-annual modulations, due to the geometry of the triangle sun-station-spacecraft. Those modulations will show up in all observables, in particular in ranging. Therefore, correlated anomalies should be observed in ephemerides and analyzed within this framework. As a matter of fact, only a careful comparison of observations in the outer solar system, within the post-Einsteinian phenomenological framework, could allow one to determine whether all gravity tests can be compatible with the anomalies seen in the solar system. This comparison will have to account for the presence of the two sectors as well as for their r-dependences.

4. REFERENCES

[1] J.G. Williams, X.X. Newhall and J.O. Dickey, Phys. Rev. D 53, 6730 (1996).

[2] R.W. Hellings et al, Phys. Rev. Lett. 51, 1609 (1983); J. D. Anderson et al., Astrophys. J. 459, 365 (1996).

[3] Bertotti B., Iess L. and Tortora P., Nature 425 374 (2003).

[4] Fienga A. et al, published in this proceeding; Folkner W.-M, IAU symposium, volume 261, 155 (2010); Pitjeva E., IAU symposium, volume 261, 170 (2010).

[5] M.-T. Jaekel and S. Reynaud, Annalen der Physik 4, 68 (1995).

[6] M.-T. Jaekel and S. Reynaud, Class. Quantum Grav. 23, 777 (2006); Class. Quantum Grav. 22 (2005) 2135-2157.

[7] G. t'Hooft and M. Veltman, Ann. Inst. H. Poincaré A 20, 69 (1974); E.S. Fradkin and A.A. Tseytlin, Nucl. Phys. B 201, 469 (1982); O. Lauscher and M. Reuter, Class. Quantum Grav. 19, 483 (2002); H.W. Hamber and R.M. Williams, Phys. Rev. D 75, 084014 (2007).

2PN LIGHT PROPAGATION AND MEASUREMENT IN THE SOLAR SYSTEM

X.-M. DENG[1], T.-Y. HUANG[2]

[1] Purple Mountain Observatory, Chinese Academy of Sciences
No. 2 Beijing West Road, Nanjing 210008, China
e-mail: xmd@pmo.ac.cn

[2] Department of Astronomy, Nanjing University
No. 22 Hankou Road, Nanjing 210093, China
e-mail: tyhuang@nju.edu.cn

ABSTRACT. As a sensitive and useful tool in gravitational physics, especially for some high order effects, the propagation of light carries lots of information about the nature of spacetime and plays an important role in high-precision experiments and measurements. Three methods can be used in this issue. First is mainly developed by Kopeikin & Schäfer (1999) and Kopeikin & Makarov (2007) and so on. Second is mainly developed by Brumberg (1991) and Klioner & Kopeikin (1992) and so on. Recently, Linet & Teyssandier (2002) and Le Poncin-Lafitte & Teyssandier (2008) and others used Synge's world function to investigate the light propagation avoiding the integration of geodesic equations. We adopt the second one. In this paper, the second post-Newtonian (2PN) framework for light propagation is developed with two additional parameters ς and η besides the two parameterized post-Newtonian (PPN) parameters γ and β. For a precision level of a few microarcsecond for space astrometry missions in the near future, started from the definition of a measurable quantity, a gauge-invariant angle between the directions of two incoming photons for a differential measurement in astrometric observation is discussed.

1. SECOND POST-NEWTONIAN FRAMEWORK FOR LIGHT PROPAGATION

We parameterize the 2PN metric of Klioner & Kopeikin (1992) in BCRS (Soffel et al., 2003) as follows

$$g_{00} = -1+\epsilon^2 2\sum_A\left(\frac{Gm_A}{r_A}+\frac{3}{2}\frac{G}{r_A^5}J_A^{<ik>}r_A^i r_A^k\right)-\epsilon^4 2\beta\frac{G^2m_\odot^2}{r_\odot^2}+\mathcal{O}(5), \quad (1)$$

$$g_{0i} = -\epsilon^3 2(1+\gamma)\sum_A\frac{Gm_A}{r_A}v_A^i-\epsilon^3 2(1+\gamma)\sum_A\frac{G}{r_A^3}\varepsilon_{jk}^i S_A^j r_A^k+\mathcal{O}(5), \quad (2)$$

$$g_{ij} = \delta_{ij}+\epsilon^2\delta_{ij}2\gamma\sum_A\left(\frac{Gm_A}{r_A}+\frac{3}{2}\frac{G}{r_A^5}J_A^{<kl>}r_A^k r_A^l\right) +\epsilon^4\left\{\delta_{ij}\varsigma\frac{G^2m_\odot^2}{r_\odot^2}+\eta\frac{G^2m_\odot^2}{r_\odot^4}r_\odot^i r_\odot^j\right\}+\mathcal{O}(5), \quad (3)$$

where $\epsilon = 1/c$ and $\mathcal{O}(n)$ means of order ϵ^n, ς and η are two 2PN parameters and have different values and dependences in different gravitational theories (see Table below).

Parameter	General Relativity	Scalar-Tensor theory Damour & Esposito-Farèse (1996)	Einstein-aether theory Xie & Huang (2008)
ς	1	$2\gamma^2-\frac{1}{2}\gamma+2\beta-\frac{5}{2}$	$1+\frac{1}{2}c_{14}$
η	1	$\frac{1}{2}(1+\gamma)$	$1-\frac{1}{2}c_{14}$

For a photon propagating in a spacetime in which Einstein Equivalence Principle (EEP) is valid, we obtain the equations of light propagation (ELP) based on the basic equations of light. ELP includes four parts: the 1PN monopole components coupled with orbital motions, the influences of quadrupole moments of the bodies, the effects from their spins which are also called by gravitomagnetic fields, and the 2PN monopole component of the Sun. The trajectory of a light ray in BCRS can then be obtained

through integrating ELP by adopting an iterative method used by Brumberg (1991), Klioner & Kopeikin (1992) and Klioner (2003).

2. ANGULAR MEASUREMENT

Now, we construct a gauge-invariant angle θ between the directions of two incoming photons based on Brumberg (1991) and Will (1993). Then, we obtain

$$\begin{aligned}\theta(t) &= \vartheta_0 + \overset{(1)}{\vartheta}_{obs} + \left(\overset{(2)}{\vartheta}_{obs} + \overset{(2)}{\vartheta}_{1PN} + \overset{(2)}{\vartheta}_{Q}\right) + \left(\overset{(3)}{\vartheta}_{obs} + \overset{(3)}{\vartheta}_{OM} + \overset{(3)}{\vartheta}_{S}\right) \\ &\quad + \left(\overset{(4)}{\vartheta}_{obs} + \overset{(4)}{\vartheta}_{2PN}\right), \end{aligned} \tag{4}$$

where $\vartheta_0 \in (0, \pi)$ is the angle between the unperturbed light paths from two given sources

$$\vartheta_0 = \arccos(\hat{\mathbf{n}}_1 \cdot \hat{\mathbf{n}}_2), \tag{5}$$

and $\overset{(n)}{\vartheta}_{obs}$ is the deflection angle due to the observer's motion in terms of order ϵ^n, $\overset{(2)}{\vartheta}_{1PN}$ is the 1PN deflection angle due to the spherically symmetric field of each body, $\overset{(2)}{\vartheta}_{Q}$ is the deflection angle due to quadrupole moment, $\overset{(3)}{\vartheta}_{OM}$ is the deflection angle due to the orbital motions of N-body, $\overset{(3)}{\vartheta}_{S}$ is the deflection angle due to the spin of the bodies and $\overset{(4)}{\vartheta}_{2PN}$ is the 2PN deflection angle due to the spherically symmetric field of the Sun.

2. DISCUSSION

For LATOR-like missions, with the angle between the initial emitting directions of two light signals 1 and 2

$$\vartheta_0 = \hat{\mathbf{n}}_1 \cdot \hat{\mathbf{n}}_2 \approx 1^\circ, \tag{6}$$

it means that the distance between these two spacecrafts is about 5.22×10^9 m. With the cut-off precision of ~ 1 μas: the 1PN monopole moment of the Sun causes $1.75''$ and $0.47''$ deflections for two light rays respectively; the 1PN monopole moment of Mercury causes 83.06 μas; the deflections caused by the 1PN monopole of Venus are 492.76 μas and 4.13 μas . If we assume that the velocity of the observer in BCRS is the same as the orbital velocity of the Earth. The first order aberration is about 3.14 mas. The second and the third ones are respectively 18.2 μas and 3.05 μas. The coupling term of solar monopole and aberration leads to 1.53 μas. The 2PN solar monopole causes 11.32 μas and 7.44 μas. However, for the Sun, quadrupole moments ($J_2 \approx 10^{-7}$)and its spin lead to light deflection are beyond 1 microarcsecond. They are respectively 0.35 μas and 0.72 μas. It needs further analytical and numerical studies.

3. REFERENCES

Brumberg, V. A., 1991, Essential Relativistic Celestial Mechanics, Bristol: Hilger
Damour, T. & Esposito-Farèse, G., 1996, Phys. Rev. D 53, 5541
Klioner, S. A. & Kopeikin, S. M., 1992, AJ 104, 897
Klioner, S. A., 2003, AJ 125, 1580
Kopeikin, S. M. & Schäfer, G., 1999, Phys. Rev. D 60, 124002
Kopeikin, S. M. & Makarov, V. V., 2007, Phys. Rev. D 75, 062002
Le Poncin-Lafitte, C., & Teyssandier, P., 2008, Phys. Rev. D 77, 044029
Linet B., & Teyssandier, P., 2002, Phys. Rev. D, 66, 024045
Soffel, M., et al. 2003, AJ 126, 2687
Will, C. M., 1993, Theory and Experiment in Gravitational Physics, Cambridge: Cambridge
Xie, Y. & Huang, T.-Y., 2008, Phys. Rev. D 77, 124049

PERTURBATION OF A PLANETARY ORBIT BY THE LAMBDA-TERM (DARK ENERGY) IN EINSTEIN EQUATIONS

Yu.V. DUMIN
IZMIRAN, Russian Academy of Sciences
Troitsk, Moscow reg., 142190 Russia
e-mail: dumin@yahoo.com

1. INTRODUCTION

The problem of cosmological influences at small (e.g. interplanetary) scales is discussed for many decades, starting from the early 1930's, but still remains unsolved definitively by now (Bonnor 2000). It became especially topical in the context of the "dark-energy"-dominated cosmology, because the usual arguments against the local Hubble expansion, such as Einstein–Straus (1945) theorem, are no longer applicable when the most contribution to the energy density of the Universe comes from the perfectly-uniform dark energy (Λ-term). Moreover, there are some empirical evidences in favor of the local cosmological influences. For example, assumption of the local Hubble expansion in the dynamics of the Earth–Moon system is a promising way to resolve a long-standing discrepancy in the rates of secular increase of the lunar semi-major axis measured by the lunar laser ranging, on the one hand, and derived from astrometric observations of the Earth's rotation deceleration, on the other hand (Dumin 2003, 2008, 2009). The aim of the present report is to provide a further support for this idea by a rigorous mathematical treatment of the two-body problem against the cosmological background formed by the Λ-term.

2. MATHEMATICAL FORMULATION OF THE PROBLEM

The starting point of our consideration is Kottler metric for a point-like mass embedded in the background formed by the Λ-term, which should be transformed to the Robertson–Walker coordinates to provide the adequate cosmological asymptotics at infinity (Dumin 2007). Keeping only the first-order terms of the Schwarzschild radius $r_g = 2GM/c^2$ and the inverse de Sitter radius $1/r_0 = \sqrt{\Lambda/3}$, we get:

$$\begin{aligned}
&\mathrm{d}s^2 = g_{tt}\,c^2\mathrm{d}t^2 + 2\,g_{tr}\,c\,\mathrm{d}t\,\mathrm{d}r + g_{rr}\,\mathrm{d}r^2 + g_{\theta\theta}\,\mathrm{d}\theta^2 + g_{\varphi\varphi}\,\mathrm{d}\varphi^2\,,\\
&g_{tt} \approx -\Big[1 - \frac{2GM}{c^2 r}\Big(1 - \frac{c\sqrt{\Lambda}\,t}{\sqrt{3}}\Big)\Big]\,, \qquad g_{tr} \approx \frac{4\,GM\sqrt{\Lambda}}{\sqrt{3}\,c^2}\,,\\
&g_{rr} \approx \Big[1 + \frac{2GM}{c^2 r}\Big(1 - \frac{c\sqrt{\Lambda}\,t}{\sqrt{3}}\Big)\Big]\Big(1 + \frac{2c\sqrt{\Lambda}\,t}{\sqrt{3}}\Big)\,, \quad g_{\theta\theta} = g_{\varphi\varphi}/\sin^2\theta \approx r^2\Big(1 + \frac{2c\sqrt{\Lambda}\,t}{\sqrt{3}}\Big)\,.
\end{aligned} \tag{1}$$

The equations of motion of a test particle of infinitely small mass in this metric are (for conciseness, we put $c \equiv 1$, use the quantities r_g and r_0 defined above, and the coordinate system is oriented so that the particle moves in its equatorial plane $\theta = \pi/2 = \mathrm{const}$):

$$\begin{aligned}
&2\Big[1 - \frac{r_g}{r}\Big(1 - \frac{t}{r_0}\Big)\Big]\,\ddot{t} - 4\,\frac{r_g}{r_0}\,\ddot{r} + \frac{r_g}{r_0}\,\frac{1}{r}\,\dot{t}^{\,2} + 2\,\frac{r_g}{r^2}\Big(1 - \frac{t}{r_0}\Big)\,\dot{t}\,\dot{r} + \frac{1}{r_0}\Big(2 + \frac{r_g}{r}\Big)\,\dot{r}^{\,2} + 2\,\frac{r^2}{r_0}\,\dot{\varphi}^{\,2} = 0\,,\\
&4\,\frac{r_g}{r_0}\,\ddot{t} + 2\Big[1 + 2\,\frac{t}{r_0} + \frac{r_g}{r}\Big(1 + \frac{t}{r_0}\Big)\Big]\,\ddot{r} + \frac{r_g}{r^2}\Big(1 - \frac{t}{r_0}\Big)\,\dot{t}^{\,2}\\
&\qquad\qquad + \frac{2}{r_0}\Big(2 + \frac{r_g}{r}\Big)\,\dot{t}\,\dot{r} - \frac{r_g}{r^2}\Big(1 + \frac{t}{r_0}\Big)\,\dot{r}^{\,2} - 2\,r\Big(1 + 2\,\frac{t}{r_0}\Big)\,\dot{\varphi}^{\,2} = 0\,,\\
&r\Big(1 + 2\,\frac{t}{r_0}\Big)\,\ddot{\varphi} + 2\,\frac{r}{r_0}\,\dot{t}\dot{\varphi} + 2\Big(1 + 2\,\frac{t}{r_0}\Big)\,\dot{r}\dot{\varphi} = 0\,,
\end{aligned} \tag{2}$$

where dot denotes a derivative with respect to the proper time of the moving particle.

3. RESULTS OF NUMERICAL SOLUTION

Since analytical treatment of the above-written equations is very hard, we shall use here only numerical solutions for the test-particle orbits. Besides, a serious obstacle in the numerical computation is a very

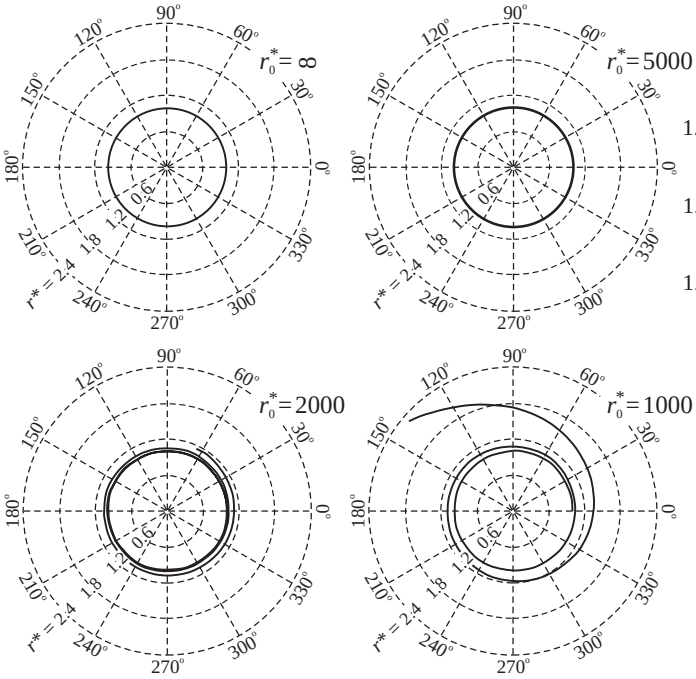

Figure 1: Orbits of the test particles at the specified Schwarzschild radius $r_g^* = 0.01$ and various de Sitter radii r_0^* (i.e., various values of the Λ-term).

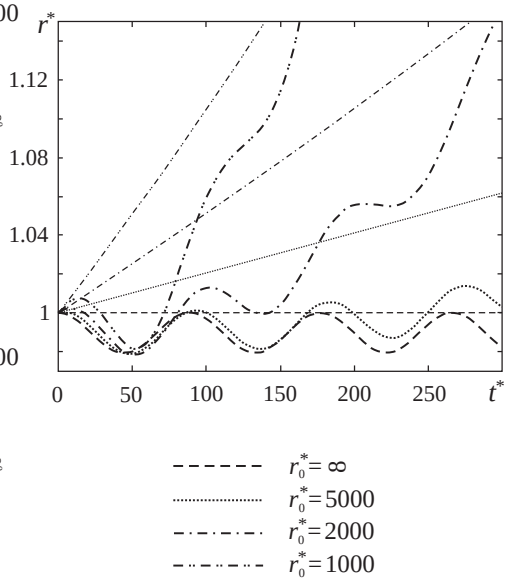

Figure 2: Radii of the orbits as functions of time at the specified Schwarzschild radius of the central body $r_g^* = 0.01$.

much difference in the three characteristic scales of the problem – Schwarzschild radius (e.g., for the Earth as a central body, $\sim 10^{-2}$ m), typical radius of the planetary orbit (e.g., for the Moon, $\sim 10^9$ m), and de Sitter radius ($\sim 10^{27}$ m). So, we present here the results of numerical integration only for a toy model, when difference between the characteristic scales is not so much as in reality. Namely, we take the dimensionless Schwarzschild radius $r_g^* = 0.01$ and de Sitter radii r_0^* about a few thousand. (Here, the quantities with asterisks are normalized to the initial radius of the orbit.)

As is seen in Figure 1, the orbits are almost circular during the first few revolutions if $r_0^* \gtrsim 5000$, but they take a spiral form at $r_0^* \lesssim 2000$ (i.e., when Λ-term is sufficiently large). Figure 2 represents a temporal dependence of radii for the same orbits. (The curves are wavy because the initial unperturbed orbit was chosen to be slightly elliptic.) The almost straight lines in this figure represent the pure Hubble flows (without a massive central body) for the same values of Λ. It is evident that under certain circumstances (depending on the ratio between the above-mentioned characteristic parameters) the orbital radii tend to approach the rates of the Hubble flows. In our opinion, this points to the potential importance of the local Hubble effect for the planetary dynamics, although a more careful analysis (with realistic Earth–Moon parameters and the additional factors affecting the planetary dynamics) is still to be done.

An opposite point of view, that cosmological influences are totally negligible in the Solar system, was put forward by some other authors, e.g., Klioner & Soffel (2005).

4. REFERENCES

Bonnor, W.B., 2000, Gen. Rel. Grav., vol. 32, p. 1005.

Dumin, Yu.V., 2003, Adv. Space Res., vol. 31, p. 2461.

Dumin, Yu.V., 2007, Phys. Rev. Lett., vol. 98, p. 059001.

Dumin, Yu.V., 2008, Proc. 11th Marcel Grossmann Meeting on Gen. Rel. (World Sci., Singapore), p. 1752.

Dumin, Yu.V., 2009, Proc. "Journées 2008: Systèmes de référence spatio-temporels", p. 31.

Einstein, A., Straus, E.G., 1945, Rev. Mod. Phys., vol. 17, p. 120.

Klioner, S.A., Soffel, M.H., 2005, Proc. Symp. "The Three-Dimensional Universe with Gaia, 2004" (ESA SP-576, ESA Publ. Div., Noordwijk), p. 305.

USE OF MILLISECOND PULSARS TO TEST AND LINK PLANETARY EPHEMERIDE REFERENCE FRAMES TO ICRF

A. FIENGA[1,2], G. DESVIGNES[(3)], I. COGNARD[(3)], G. THEUREAU[(3)]

[1] Institut UTINAM-CNRS 6213
41 bis avenue de l'observatoire, 25000 Besançon, France
e-mail: agnes.fienga@obs-besancon.fr

[2] Astronomie et Systèmes Dynamiques, IMCCE-CNRS UMR8028
77 avenue Denfert-Rochereau, 75014 Paris

[3] LPCE-CNRS 6115, Orléans, France

ABSTRACT. We describe here the method used to test the links between INPOP and DE reference frames to ICRF in using radio timing and VLBI astrometry of millisecond pulsars. The obtained rotation matrices are consistent with estimations done previously for DE405 and DE200 and confirm the efficiency of such procedures in waiting for a densification of millisecond pulsars with a mas-level VLBI and radio-timing astrometry.

1. METHOD

Space missions need more and more accurate positions and velocities of solar system objects and especially the earth. It is then important to check the planetary ephemerides accuracy in using very accurate observations of objects close from the earth (in order to be sensitive to the earth orbit) but not used in the fit process of the ephemerides. If the same object is also directly connected to ICRF sources, we can also test the link between the planetary ephemeride frame and ICRF.

VLBI-derived positions of millisecond pulsars (MSP) can provide a tie between the extragalactic (earth-rotation based) reference frame in which VLBI "operates" and the dynamic (earth-orbit based) reference frame in which MSP timing positions are derived.

If (α_{PE1},δ_{PE1}) are positions of a MSP deduced from TOA in using Planetary Ephemerides 1 (PE1) and (α_{PE2},δ_{PE2}) are positions of the same MSP deduced either from VLBI observations and then in ICRF either from TOA in using Planetary Ephemerides 2, the differences(α_{PE1},δ_{PE1}) and (α_{PE2},δ_{PE2}) can be seen as residual rotations $R_x(\theta)$,$R_y(\eta)$ and $R_z(\zeta)$ about the x,y and z axis of PE1 reference frame such as $\alpha_{PE1} = R_x(\theta)R_y(\eta)R_z(\zeta)\alpha_{PE2}$ and $\delta_{PE1} = R_x(\theta)R_y(\eta)R_z(\zeta)\delta_{PE2}$. The angles θ, η and ζ can then be deduced by least square fitting.

2. MILLISECOND PULSARS USED FOR THIS STUDY

From the radio timing profiles obtained at the NRT (Desvignes 2010), we selected 18 MSPs with radio timing astrometry better than 10 mas. These 18 MSPs are used for the estimation of the rotation matrices between DE414, INPOP08, DE405 and DE200 presented in figure 1. For the second step, we collected in the literature positions and velocities of millisecond pulsars obtained by VLBI astrometry (Chatterjee et al. 2009, Deller et al. 2009) and observed by the NRT. 4 MSPs have a mas-level accuracy in both techniques, VLBI and radio timing, and are used to test the link between planetary frames and ICRF. The obtained rotation matrices are presented in this volume in (Fienga et al. 2010).

3. RESULTS

We have first estimate the impact of using different planetary ephemerides (with different set of planet masses) on the analysis of radio timing data. For the 18 MSP used for this study, no specific trend remains in the postfit residuals of the radio timing despite the change in planet masses and initial conditions brought by each different ephemerides. Among the parameters fitted during the radio timing data analysis, the positions and the proper motions of the pulsars are sightly modified. No other parameters related to the distance, the rotation or the orbit of the companion are affected by the change of planetary ephemerides.

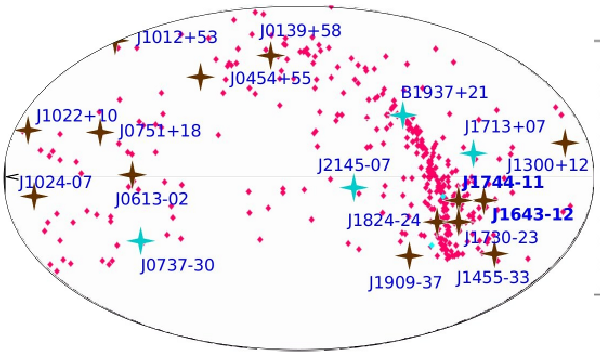

	θ mas	η mas	ζ mas
18 MSPs with TOA $(\sigma_\alpha,\sigma_\delta) < 10$ mas			
DE405 → DE200	-0.4 ± 0.3	-13 ± 0.4	-13 ± 0.3
(Standish 1998)	-1 ± 2	-14 ± 3	-10 ± 3
DE414 → DE405	1.5 ± 0.3	-1.0 ± 0.4	-0.9 ± 0.3
INPOP08 → DE405	1.3 ± 0.3	-0.3 ± 0.4	-1.1 ± 0.3
INPOP10A → DE405	1.6 ± 0.3	-0.7 ± 0.4	-0.7 ± 0.3
Only 4 MSPs with TOA $(\sigma_\alpha,\sigma_\delta) < 10$ mas			
DE405 → DE200	-0.5 ± 0.2	-12 ± 0.3	-13 ± 0.18
INPOP08 → DE405	1.4 ± 0.03	-0.03 ± 0.05	-1.4 ± 0.03
INPOP10A → DE405	1.7 ± 0.01	-0.03 ± 0.02	-1.0 ± 0.01

Figure 1: On the left hand side, distribution in (α,δ) of MSPs on an Aitoff equatorial map centered on (0,0). The small stars are (Hobbs et al. 2004) PSR catalogue positions. The big stars are the MSP used in this study, the light gray ones are the one selected for the link between INPOP and DE reference frames to ICRF. On the right hand side, angles of rotation deduced from adjustment of rotation matrices defined in the text. The angles are given in mas and the uncertainties are the formal 1-sigma deduced from the least squares.

Based only on radio timing observations, the angles presented in figure 1 and obtained in using the 18 selected pulsars are quite compatible with previous determinations of rotation matrices between planetary frames. In (Fienga et al. 2010) are given the rotations obtained between planetary ephemerides frames and ICRF as deduced from pulsar timing and VLBI astrometry. None of these rotations are statistically significant except the one between DE200 and the ICRF. The obtained matrices are consistent with results obtained by (Folkner et al. 1994) and (Standish 1998). This is also consistent with the fact that DE200 was not directly linked to ICRF. VLBI tracking data of spacecraft were not used for the DE200 construction and only optical observations of planets with an accuracy of about 100 mas were used to link the planetary frame to the ICRF.

This study shows the efficiency of using radio timing and VLBI astrometry of millisecond pulsars to estimate the rotation matrices between the planetary frames and between the DE and INPOP frames with the ICRF. We checked that the procedures give similar angles as the one already deduced by other methods (Standish 1998, Folkner et al. 1994) and confirmed the mas level internal accuracy of the planetary ephemerides. More MSPs should be observed in VLBI in order to increase the sample to directly link planetary frames and ICRF.

4. REFERENCES

Chatterjee, S.,Brisken, W.F.,Vlemmings, W. H. T., Goss, W. M., Lazio, T. J. W., Cordes, J. M., Thorsett, S. E., Fomalont, E. B., Lyne, A. G., Kramer, M., 2009, "Precision Astrometry with the Very Long Baseline Array: Parallaxes and Proper Motions for 14 Pulsars", The Astrophysical Journal, Volume 698.

Deller, A. T.; Tingay, S. J.; Bailes, M.; Reynolds, J. E., 2009, "Precision Southern Hemisphere VLBI Pulsar Astrometry. II. Measurement of Seven Parallaxes", The Astrophysical Journal, Volume 701.

Desvignes, G., 2009, private communication.

Hobbs, G. et al. 2004, MNRAS , 353, 1311.

Fienga, A., Manche, M., Kuchynka, P., Laskar, J., Gastineau, M., 2010, "Planetary and lunar ephemerides INPOP10a", this volume.

Folkner, W.B., Charlot, P., Finger, M. H., Williams, J. G., Sovers, O. J., Newhall, Xx, Standish, E. M., Jr., 1994, "Determination of the extragalactic-planetary frame tie from joint analysis of radio interferometric and lunar laser ranging measurements", A&A 287, 279.

Standish, E.M., 1998, "Linking the Dynamical Reference Frame to the ICRF", Hightlights of Astronomy, 11, 37.

DEVELOPMENT OF THE TWSTFT CARRIER-PHASE TECHNIQUE AT LNE-SYRTE*

A. KANJ, J. ACHKAR
LNE-SYRTE
Observatoire de Paris, LNE, CNRS, UPMC
77 avenue Denfert Rochereau,75014 Paris, France
e-mail: amale.kanj@obspm.fr
* This work is funded by LNE and CNES.

ABSTRACT. The Two-Way Satellite Time and Frequency Transfer (TWSTFT) method (Achkar at al. 2006) permits to compare two remote atomic clocks by using a microwave link through a geostationary satellite. The best performance reachable today at OP is achieved on the Ku band link with a frequency stability of 8.10^{-16} at one day (Zhang et al. 2009). In order to improve stability of the two-way links in the short term, the TWSTFT carrier-phase is the most appropriate method. The work proposed here is limited to the development of the TWSTFT carrier-phase method. The main idea is to calculate the offset between the frequencies of the two clocks located each one in a different station. The Doppler's effect is taken into consideration regarding the spread of the signal between each station and the satellite and vice versa. Note that, one Doppler coefficient corresponds to each Station-Satellite link in both directions. The same hardware is used in the two methods. We establish the equation system of the TWSTFT carrier-phase technique composed by four nonlinear equations with four unknown values which are : the first Doppler coefficients, the satellite's local oscillator frequency and the frequency offset of the distant clocks. This system cannot be solved directly (Fonville et al. 2004). As a first approach, we use the Newton-Raphson method to transform the nonlinear system to a linear one. Then, the singular value decomposition technique is used to solve the resulting linear system.

1. INTRODUCTION

The national metrology institute LNE-SYRTE has developed on the site of the Observatoire de Paris a TWSTFT earth station using a microwave link through a geo-stationary telecommunication satellite. The station is equipped with a SATRE modem which applies the spread spectrum method over a generated pseudo random noise code sequence at 1 MChips/s, carrying the clock signal. The main goal is to improve the contribution of the French atomic clocks to the international atomic time TAI calculated by the BIPM and to have an accurate system to compare primary frequency standards which are developed through the national laboratories.

2. TWSTFT CARRIER-PHASE

The most equipment used in the standard method (Achkar at al. 2006) is required. The reference station is the station 1. Considering that the frequency of the clock 1 is f_{sys}, the frequency of clock 2 is then shifted from f_{sys} by a value df. As shown in Figure 1, F_{11} and F_{22} are the ranging frequencies, F_{12} is the frequency of the signal transmitted from to station 2 to the station 1 and F_{21} is the frequency of the signal transmitted from the station 1 to the station 2. The ranging and two-way signals are subject to the Doppler effect.

3. THE EQUATION SYSTEM

$$\begin{cases} F_{11} = f_{tx}(1+k_1)^2 - f_{slo}(1+k_1) \\ F_{22} = f_{tx}(1+k_2)^2 - f_{slo}(\frac{f_{sys}}{f_{sys}+df})(1+k_2) \\ F_{12} = f_{tx}(\frac{f_{sys}+df}{f_{sys}})(1+k_1)(1+k_2) - f_{slo}(1+k_1) \\ F_{21} = f_{tx}(\frac{f_{sys}}{f_{sys}+df})(1+k_1)(1+k_2) - f_{slo}(\frac{f_{sys}}{f_{sys}+df})(1+k_2) \end{cases}$$

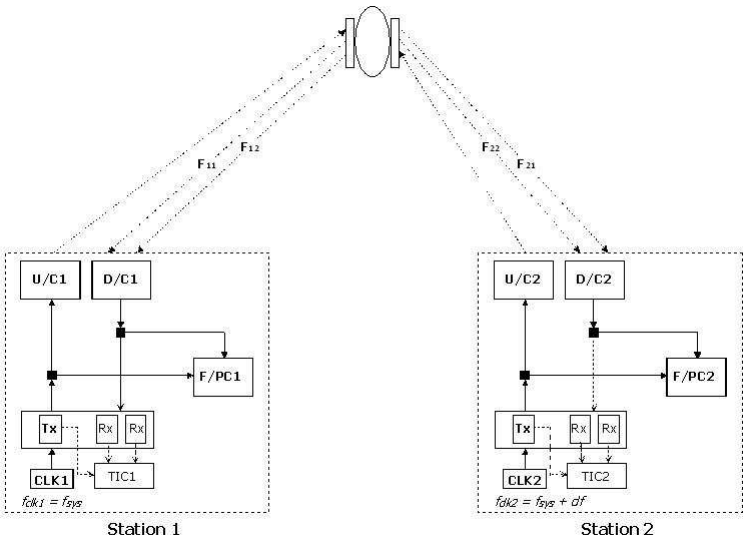

Figure 1: TWSTFT carrier-phase technique

4. SOLVING THE EQUATION SYSTEM

The Newton-Raphson method is the most appropriate method for solving non linear equation systems (Press et al. 1992). We start from an initial estimation vector for the system's unknowns. The Taylor development is applied to each system's function. Therefore, the non linear system is transformed to a linear system with a singular Jacobian matrix thus the system cannot be solved directly. The singular value decomposition is used to find the inverse of the matrix. The solution vector is then updated and we continue the iterations in order to reach the most suitable solution.

5. CONCLUSION

The TWSTFT carrier-phase allows to improve the short term stability of the TWSTFT method. In this paper, we have established the equation system of this technique. Then, we have applied the Newton Raphson method combined with the singular value decomposition to solve the obtained system. For the method's implementation, routines from numerical recipes in C language are used (Press et al. 1992).

6. REFERENCES

Achkar, J., Merck, P., 2006, "Comparaisons d'horloges atomiques au sol par liasons micro-ondes deux voies avec satellite de telecommunication", Revue francaise de metrologie, volume 2006-2.

Zhang, V., Parker, T., Achkar, J., Bauch, A., Lorini, L., Matsakis, D., Piester, D.,Rovera, G.D., 2009, "Two-way satellite time and frequency transfer using 1 MCHIP/S codes ", 41st Annual Precise Time and Time Interval (PTTI) Meeting.

Fonville, B., Schaefer, W., 2004, "Development of carrier-phase two-way satellite time and frequency transfer (TWSTFT)", 36th Annual Precise Time and Time Interval (PTTI) Meeting.

Press, W., Flannery, B., Teukolsky, S., Vetterling, W., 1992, "Numerical recipes in C : The art of scientific computing ".

LIGHT TIME CALCULATIONS FOR DEEP SPACE NAVIGATION

S. BERTONE[1], C. LE PONCIN-LAFITTE[1], V. LAINEY[2]
[1]SYRTE, Observatoire de Paris, CNRS, UPMC
61 avenue de l'Observatoire, 75014 – Paris, France
[2]IMCCE, Observatoire de Paris, CNRS, UPMC
77 avenue Denfert-Rochereau, 75014 – Paris, France

ABSTRACT. With the recent discovery of few astrometric anomalies derived from the tracking of spacecrafts, such as the Pioneer and Earth flyby anomalies, we propose to reconsider the light time calculation used by Deep Space Navigation. In particular, we show that some traditional approximations can lead to neglect tiny terms that may produce instability in the orbit determination of a probe during Earth flyby.

1. INTRODUCTION

Deep space data processing during the last decade has revealed the presence of some anomalies in the trajectory of probes. Lots of hypothesis have been made trying to solve this puzzle, but they can be summarized in two main approaches : whether these anomalies are the manifestation of some new physics, or something is incorrectly modeled in the data processing. We investigated Moyer's book, which describes the relativistic framework used by space agencies for data processing, and came to the conclusion that the modeling is correct up to the first post-Newtonian approximation of General Relativity. However, some terms, a priori of very small amplitude, have been neglected in the light time calculation. In section 2, we give a brief overview of light time computation as described by the Moyer's book; we show that the transponder's delay, *i.e.* the time delay between the reception and retransmission of the light signal on board the satellite, is not correctly taken into account. In section 3 we present an alternative modeling that corrects this. Finally in section 4 we compare these modelings to highlight the differences and we give some conclusions in section 5. Throughout this work we will suppose that space-time is covered by some global barycentric coordinates system $x^\alpha = (x^0, \boldsymbol{x})$, with $x^0 = ct$, c being the speed of light in vacuum, t a time coordinate and $\boldsymbol{x} = (x^i, i = 1, 2, 3)$. Greek indices run from 0 to 3, and Latin indices from 1 to 3. Here $\boldsymbol{x}_t^b/\boldsymbol{v}_t^b$ represents the position/velocity of b at time t, where b can take the value GS (ground station) or SC (spacecraft). Primed values are related to the *Moyer's modeling*, while we will use non-primed values for the alternative modeling.

2. MOYER NAVIGATION MODEL

Deep space navigation is based on the exchange of light signals between a probe and at least one observing ground station. The calculation of a light time is quite simple : a clock starts counting as an uplink signal is emitted from ground at $\boldsymbol{x}_{1'}^{GS}$. The signal is received by the probe at $\boldsymbol{x}_{2'}^{SC}$ and then reemitted immediately towards the Earth where it is received by a ground station at $\boldsymbol{x}_{3'}^{GS}$. The clock stops counting and gives the round-trip light time ρ', referred to as "two-ways light time" or simply "light time". ρ' can be computed as follow:

$$\rho' = \frac{1}{c}|\boldsymbol{x}_{3'}^{GS} - \boldsymbol{x}_{2'}^{SC}| + \frac{1}{c}|\boldsymbol{x}_{2'}^{SC} - \boldsymbol{x}_{1'}^{GS}| + Shapiro + \delta TS, \tag{1}$$

where $Shapiro$ and δTS are the Shapiro delay and other corrections described by Moyer, respectively. Then the light time is used to compute two physical quantities: the *Ranging*, describing the distance between the probe and the ground station, and the *Doppler* related to the radial velocity of the probe with respect to the Earth. *Ranging* signal almost coincides with ρ' when one simply adds a calibrated transponder's delay δt. *Doppler* signal, F, is obtained by differentiating two successive light-time measurements, $\rho'_s = t_{3s} - t_{1s}$ and $\rho'_e = t_{3e} - t_{1e}$, during a given count interval $T_c = t_{3e} - t_{3s}$. Moyer showed

that $F = M_2 f_T(t_1)\left(\rho'_e - \rho'_s\right)/T_c$ where M_2 is a transponder's ratio applied to the downlink signal when it is reemitted towards the Earth.

3. ALTERNATIVE NAVIGATION MODEL

In the Moyer's model, the uplink signal is received at $\boldsymbol{x}_{2'}^{SC}$ and immediately transponded towards the Earth : no transponder delay is taken into account. Nevertheless, an electronic delay of some microseconds due to on board processing of the incoming signal is present and we have studied its influence on light time modeling for *Ranging* and *Doppler* calculations. To do that we introduce an alternative model taking into account four events: the emission from the ground station at $\boldsymbol{x}_1^{GS}$, the reception by the probe at $\boldsymbol{x}_2^{SC}$, the reemission at $\boldsymbol{x}_3^{SC}$ and the reception at ground at $\boldsymbol{x}_4^{GS}$. The additional event $\boldsymbol{x}_3^{SC} = \boldsymbol{x}_{2+\delta t_{23}}^{SC}$ accounts for this small delay of δt_{23}=2.5 μs (for modern spacecrafts) :

$$\rho = \frac{1}{c}|\boldsymbol{x}_4^{GS} - \boldsymbol{x}_3^{SC}| + \delta t_{23} + \frac{1}{c}|\boldsymbol{x}_2^{SC} - \boldsymbol{x}_1^{GS}| + Shapiro + \delta TS. \tag{2}$$

4. COMPARISON OF THE TWO MODELINGS

One main difference between the two modelings consists in considering different numbers of epochs. Indeed we introduced the event $\boldsymbol{x}_3^{SC} = \boldsymbol{x}_{2+\delta t_{23}}^{SC}$; this term is implicitly related to δt_{23} by the approximation $\boldsymbol{x}_3^{SC} = \boldsymbol{x}_2^{SC} + \delta t_{23}\boldsymbol{v}_2^{SC} + O(\delta_{23}^2)$. In practice, this delay is calibrated by space agencies; it is added to ρ when computing *Ranging* and has no consequence on the differential *Doppler* F since δ_{23} is a calibrated constant quantity. However, as δ_{23} appears in the expression of $\boldsymbol{x}_3^{SC}$, we can compute the difference between ρ and ρ' by developing to the first order in δt_{23}. We found that this difference is given by:

$$\Delta\rho = \rho - \rho' = \delta t_{23}\frac{1 - \frac{\boldsymbol{v}_2^{SC}\cdot\boldsymbol{N}_{12}}{c}}{1 - \frac{\boldsymbol{v}_1^{GS}\cdot\boldsymbol{N}_{12}}{c}}\,, \tag{3}$$

where $\boldsymbol{N}_{12} = \frac{\boldsymbol{x}_2^{SC} - \boldsymbol{x}_1^{GS}}{\|\boldsymbol{x}_2^{SC} - \boldsymbol{x}_1^{GS}\|}$.

The last equation highlights the presence of an extra non-constant term directly linked to the transponder delay. It depends also on positions and velocities of both probe and ground station. Neglecting it would actually lead to a wrong determination of the epoch t_1 and to an error in both *Ranging* and *Doppler*. In fact, extracting the downlink signal, we get $|\boldsymbol{x}_{2'}^{SC} - \boldsymbol{x}_{1'}^{GS}| \neq |\boldsymbol{x}_2^{SC} - \boldsymbol{x}_1^{GS}|$ since $t_2 \neq t'_2$ and $t_1 \neq t'_1$.

5. CONCLUSIONS

It is obvious that the influence of the transponder delay has no reason to be only calibrated. It is responsible of a tiny effect on the computation of light time and has an impact on both *Ranging* and *Doppler* determination. Mainly, to summarize, it leads to consider four epochs instead of three. In order to test the amplitude and variability of this effect on real data, we calculated its influence on some real probe-ground station configurations during recent Earth flybys (NEAR, Rosetta, Cassini and Galileo) and we computed the alternative orbit fitted to *Ranging* and *Doppler* data from our light time model. The results showed an amplitude of some mm (*Ranging*) and mm/s (*Doppler*), but also a variability of the signal for different orbital configurations. A more detailed version of these calculations will be presented in a forthcoming article.

6. REFERENCES

T.D. Moyer, 2000, "Formulation for Observed and Computed Values of Deep Space Network Data Types for Navigation", JPL Publications.

J. Anderson et al., 2008, "Anomalous Orbital-Energy Changes Observed during Spacecraft Flybys of Earth", Physical Review Letters, 100, 9, 091102.

POSTFACE

JOURNÉES 2011 SYSTÈMES DE RÉFÉRENCE SPATIO-TEMPORELS

"Earth rotation, reference systems and celestial mechanics: Synergies of geodesy and astronomy"

organized by Vienna University of Technology (Austria), 19-21 September 2011

Scientific Organizing Committee

N. Capitaine, France (Chair); H. Schuh (Co-Chair), Austria; A. Brzeziński, Poland; V. Dehant, Belgium; C. Hohenkerk, UK; I. Kumkova, Russian Federation; D.D. McCarthy, USA; M. Soffel, Germany; J. Souchay, France; J. Vondrák, Czech R.; Ya. Yatskiv, Ukraine

Local Organizing Committee

H. Schuh (Chair), J. Böhm, S. Böhm, R. Dvorak, S. Linsmayer, T. Nilsson, M. Schindelegger, R. Weber

Conference location : Bundesamt für Eich- und Vermessungswesen (BEV), Vienna, Austria

Scientific objectives

The Journées 2011 "Systèmes de référence spatio-temporels", with the sub-title "Earth rotation, reference systems and celestial mechanics: Synergies of geodesy and astronomy"', will be organized by the Institute of Geodesy and Geophysics of the Vienna University of Technology (TU Vienna) from 19 to 21 September 2011. The venue of the scientific sessions will be at Bundesamt fr Eich- und Vermessungswesen (BEV), Vienna. It will be the twenty-first meeting in these Journées conference series which provide an international forum for advanced discussion in the fields of space and time reference systems, Earth rotation, dynamics of the solar system, astrometry and time. In 2011, the Journées will be focused on issues related to recent developments in fundamental astronomy, time and relativity, plans for the next generation of space-time reference systems, Earth rotation and global geodynamics, celestial mechanics of solar system bodies, space observations and dedicated missions for geodesy and astronomy. There will be a discussion devoted to several IAU questions.

The Journées 2011 are co-sponsored by the International Astronomical Union (IAU) and the International Association of Geodesy (IAG).

Scientific programme

The scientific programme of the Journées 2011 will include the following sessions:

Session 1 - Fundamental astronomy, time and relativity
Session 2 - Towards the next generation of space-time reference systems
Session 3 - Modelling, observation and prediction of Earth rotation and global geodynamics
Session 4 - Celestial mechanics of solar system bodies
Session 5 - Space observations and dedicated missions for geodesy and astronomy
Discussion - On future IAU recommendations and organization

Contact

For information related to the scientific program, Nicole Capitaine: n.capitaine@obspm.fr,
for questions related to the local organisation, Sigrid Böhm: sigrid.boehm@tuwien.ac.at,
and for questions or suggestions about the website, Michael Schindelegger: michael.schindelegger@tuwien.ac.at.

See also the web page at: `http://info.tuwien.ac.at/hg/meetings/journees11/index.html` (that will be regularly updated).